AAPS Advances in the Pharmaceutical Sciences Series 14

Stephan Schmidt
Hartmut Derendorf
Editors

Applied Pharmacometrics

aapspress
Springer

AAPS Advances in the Pharmaceutical Sciences Series

The AAPS Advances in the Pharmaceutical Sciences Series, published in partnership with the American Association of Pharmaceutical Scientists, is designed to deliver well written volumes authored by opinion leaders and authorities from around the globe, addressing innovations in drug research and development, and best practice for scientists and industry professionals in the pharma and biotech industries. For more details and to see a list of titles in the Series please visit http://www.springer.com/series/8825

Stephan Schmidt • Hartmut Derendorf
Editors

Applied Pharmacometrics

aapspress

Springer

Editors
Stephan Schmidt
Center for Pharmacometrics & Systems Pharmacology
Department of Pharmaceutics
University of Florida
Orlando, Florida, USA

Hartmut Derendorf
Department of Pharmaceutics
College of Pharmacy
University of Florida
Gainesville, Florida, USA

ISSN 2210-7371 ISSN 2210-738X (electronics)
ISBN 978-1-4939-1303-9 ISBN 978-1-4939-1304-6 (eBook)
DOI 10.1007/978-1-4939-1304-6
Springer New York Heidelberg Dordrecht London

Library of Congress Control Number: 2014955076

Printed on acid-free paper

Springer is part of Springer Science+Business Media (www.springer.com)

Preface

Modeling and simulation tools have long been used in engineering and aerospace industries to develop products that would be prohibitively expensive to optimize through iterative improvement of prototypes. Modern drug development is now adapting and integrating analogous tools based on information from all phases of the development process. This integrative approach is now recognized as the discipline of pharmacometrics. With the increased regulatory burden and high expectations from prescribers and patients, it is neither cost-effective nor time-efficient to tackle all open questions experimentally. An increasing number of decisions are now based on appropriate modeling and simulation, which allows integration of all available knowledge in a quantitative and objective way.

This book provides an update on the current state of pharmacometrics in drug development. After an introduction of the basic and underlying pharmacokinetic and pharmacodynamic concepts of pharmacometrics in drug development, the book presents numerous specific applications as examples that utilize pharmacometrics with modeling and simulations over a variety of therapeutic areas. These chapters were contributed and written by leading scientists from academia, the pharmaceutical industry, and regulatory agencies. The examples illustrate how results from all phases of drug development can be integrated in a more timely and cost-effective process. The process of applying pharmacometric decision tools during drug development can allow data-based objective decision making. At the same time, the process can identify redundant or unnecessary experiments as well as some costly clinical trials that can be avoided. In addition to cost savings by the expedited development of successful drug candidates, pharmacometrics has an important economic impact in drug product selection. Unsuccessful drug candidates can be identified early and discontinued without expending efforts required for additional studies and allocating limited resources. Hence, pharmacometric modeling and simulation has become a powerful tool to bring new and better medications to the patients at a faster pace and with greater probability of success. We hope that this book will help to spread modeling and simulation activities in drug development and that it will initiate many more applications in the future.

We thank all of our colleagues who contributed to this book and were most generous in devoting their time and effort to make this envisioned project a reality. We

deeply appreciate the priority given to this project by these leaders in their field who have numerous demands on their professional expertise. Prof. Daan Crommelin provided the initial seed for this book and deserves a special thanks. We also thank the team at Springer Science+Business Media for the pleasant, professional, and uncomplicated collaboration on this project. And finally, we thank our families for their patience and understanding.

Orlando, FL, USA Stephan Schmidt, PhD
Gainesville, FL, USA Hartmut Derendorf, PhD

Contents

Contributors

Jeffrey Barrett Interdisciplinary Pharmacometrics Program, Pediatric Clinical Pharmacology, Sanofi Pharmaceuticals, 55 Corporate Drive, Bridgewater, NJ 08807, USA

Margreke J. E. Brill Department of Clinical Pharmacy, St. Antonius Hospital, Nieuwegein, The Netherlands

Ashley N. Brown Research and Academic Center, Institute for Therapeutic Innovation, University of Florida, Orlando, FL, USA

Antonio Cabal Quantitative Pharmacology & Pharmacometrics, Merck, Sharpe & Dohme Corp., Oss, The Netherlands

Anne S. Y. Chain Modeling and Simulation, Merck Research Laboratories, Merck & Co., Inc., Rahway, NJ, USA

Jenny Y. Chien Lilly Research Laboratories, Eli Lilly & Company, Indianapolis, IN, USA

Cornelius Joseph Clancy Department of Medicine, Division of Infectious Diseases, University of Pittsburgh, Pittsburgh, PA, USA

Brian Corrigan Department of Neuroscience, Pfizer, Groton, CT, USA

Elizabeth C. M. de Lange Target Site Equilibration Group, Division of Pharmacology, Leiden Academic Centre of Drug Research, Leiden University, Leiden, The Netherlands

Hartmut Derendorf Department of Pharmaceutics, College of Pharmacy, University of Florida, Gainesville, FL, USA

Jeroen Diepstraten Department of Clinical Pharmacy, St. Antonius Hospital, Nieuwegein, The Netherlands

George L. Drusano Research and Academic Center, Institute for Therapeutic Innovation, University of Florida, Orlando, FL, USA

Maurice G. Emery Department of Pharmacokinetics and Drug Metabolism, Amgen, Inc, Seattle, WA, USA

Ghassan N. Fayad Quantitative Pharmacology & Pharmacometrics, Merck, Sharpe & Dohme Corp., Oss, The Netherlands

Parag Garhyan Global PK/PD & Pharmacometrics, Eli Lilly & Company, Indianapolis, IN, USA

Anna Georgieva Kondic Quantitative Pharmacology & Pharmacometrics, Merck, Sharpe & Dohme Corp., Oss, The Netherlands

John P. Gibbs Department of Pharmacokinetics and Drug Metabolism, Amgen Inc, Thousand Oaks, CA, USA

Pankaj Gupta Department of Clinical Pharmacology, Global Innovative Pharma Business, Pfizer, Groton, CT, USA

Peter C. Haughney Department of Pharmacokinetics and Drug Metabolism, Amgen Inc., Seattle, WA, USA

Günther Hochhaus College of Pharmacy, University of Florida, Gainesville, FL, USA

Kaori Ito Department of Neuroscience, Pfizer, Groton, CT, USA

Ping Ji Office of Clinical Pharmacology, Center for Drug Evaluation and Research, US Food and Drug Administration, Silver Spring, MD, USA

Bhargava Kandala College of Pharmacy, University of Florida, Gainesville, FL, USA

Thomas Kerbusch Quantitative Pharmacology & Pharmacometrics, Merck, Sharpe & Dohme Corp., Oss, The Netherlands

Catherijne A. J. Knibbe Department of Clinical Pharmacy, St. Antonius Hospital, Nieuwegein, The Netherlands

Sriram Krishnaswami Department of Clinical Pharmacology, Pfizer, Groton, CT, USA

Manisha Lamba Department of Clinical Pharmacology, Global Innovative Pharma Business, Pfizer, Groton, CT, USA

Lawrence J. Lesko Center for Pharmacometrics and Systems Pharmacology, University of Florida, Orlando, FL, USA

Jiang Liu Office of Clinical Pharmacology, Center for Drug Evaluation and Research, US Food and Drug Administration, Silver Spring, MD, USA

Khamir Mehta Quantitative Pharmacology & Pharmacometrics, Merck, Sharpe & Dohme Corp., Oss, The Netherlands

Sujatha Menon Department of Clinical Pharmacology, Pfizer, Groton, CT, USA

Diane R. Mould Projections Research, Phoenixville, PA, USA

Joanna Parkinson Computational Toxicology, Global Safety Assessment, AstraZeneca R&D Innovative Medicines, Mölndal, Sweden

Charles A. Peloquin College of Pharmacy and Emerging Pathogens Institute, University of Florida, Gainesville, FL, USA

Marc Pfister University Children's Hospital Basel (UKBB), Basel, Switzerland

Quantitative Solutions, Bridgewater, USA

Daniel Polhamus Department of Medical-Science, Metrum Research Group LLC, Tariffville, CT, USA

Teun M. Post Quantitative Pharmacology & Pharmacometrics, Merck, Sharpe & Dohme Corp., Oss, The Netherlands

Vivek S. Purohit Department of Clinical Pharmacology, Global Innovative Pharma Business, Pfizer, Groton, CT, USA

James Rogers Department of Medical-Science, Metrum Research Group LLC, Tariffville, CT, USA

Klaus Romero Department Clinical Pharmacology, Critical Path Institute, Tucson, AZ, USA

Amit Roy Clinical Pharmacology & Pharmacometrics, Bristol-Myers Squibb, Princeton, NJ, USA

Stephan Schmidt Department of Pharmaceutics, Center for Pharmacometrics & Systems Pharmacology, University of Florida, Orlando, FL, USA

Vikram P. Sinha Division of Pharmacometrics, Office of Clinical Pharmacology/ Translational Sciences, U.S. Food and Drug Administration, Indianapolis, IN, USA

Diane Stephenson Coalition Against Major Diseases, Critical Path Institute, Tucson, AZ, USA

Sherwin K. B. Sy Department of Pharmaceutics, University of Florida, Gainesville, FL, USA

Brian Gregory Topp Lilly Research Laboratories, Eli Lilly & Company, Indianapolis, IN, USA

Piet H. van der Graaf Leiden Academic Centre for Drug Research (LACDR), Gorlaeus Laboratories, Leiden, The Netherlands

Anne van Rongen Department of Clinical Pharmacy, St. Antonius Hospital, Nieuwegein, The Netherlands

Sandra A. G. Visser Modeling & Simulation, Early Stage Development, Merck Research Labs, Merck & Co., Inc., North Wales, Pennsylvania, USA

Xiaofeng Wang Clinical Pharmacology, Otsuka Pharmaceuticals, Princeton, NJ, USA

Yaning Wang Office of Clinical Pharmacology, Center for Drug Evaluation and Research, US Food and Drug Administration, Silver Spring, MD, USA

Liping Zhang Model Based Drug Development Group, Janssen Pharmaceutical Research and Development, Titusville, NJ, USA

Hao Zhu Office of Clinical Pharmacology, Center for Drug Evaluation and Research, US Food and Drug Administration, Silver Spring, MD, USA

About the Editors

Stephan Schmidt PhD is an Assistant Professor at the University of Florida's Center for Pharmacometrics and Systems Pharmacology in Lake Nona, Orlando, Florida. Prof. Schmidt's research focuses on the application of quantitative analysis (pharmacometrics and systems pharmacology) tools to address clinically relevant research questions in the area of antimicrobial chemotherapy, pediatrics, diabetes, cardiovascular safety, and postmenopausal osteoporosis. Prof. Schmidt received his PhD in Pharmaceutics from the University of Florida in Gainesville, Florida. He has published his work in more than ten peer reviewed scientific journals and received the Paul Ehrlich Society Thesis Award as well as the University of Florida's Excellence Award for assistant professors. Prof. Schmidt is an active member of the International Society of Pharmacometrics (ISoP), the American Society for Clinical Pharmacology and Therapeutics (ASCPT), the American Association of Pharmaceutical Scientists (AAPS), the American College of Clinical Pharmacology (ACCP), and the Paul-Ehrlich Society for Chemotherapy (PEG).

Hartmut Derendorf PhD is Distinguished Professor, V. Ravi Chandran Professor of Pharmaceutical Sciences and Chairman of the Department of Pharmaceutics at the University of Florida College of Pharmacy in Gainesville, Florida. He received his PhD in Pharmaceutics at the University of Münster in Germany. Prof. Derendorf has published more than 400 scientific publications and seven textbooks in English and German. He is editor or associate editor of five journals including *The Journal of Clinical Pharmacology.* Prof. Derendorf has served as President of the American College of Clinical Pharmacology (ACCP) and President of the International Society of Antiinfective Pharmacology (ISAP). He was awarded the Distinguished Research Award and the Nathaniel T. Kwit Distinguished Service Award of ACCP, the Research Achievement Award in Clinical Science of the American Association of Pharmaceutical Scientists (AAPS), the Leadership Award of the International Society of Pharmacometrics (ISOP), and the Volwiler Award of the American Association of Colleges of Pharmacy (AACP).

Chapter 1
Introduction to Pharmacometrics and Quantitative Pharmacology with an Emphasis on Physiologically Based Pharmacokinetics

Sherwin K. B. Sy, Xiaofeng Wang and Hartmut Derendorf

1.1 Introduction

Pharmacometrics has become a term that encompasses modeling and simulation for pharmacokinetics (PK), exposure–response relationship, and disease progression. Mechanistic models that describe the biochemical processes involved in a physiological system have become more utilized in drug development. The models of complex systems are generally classified as systems pharmacology. A quote from William Jusko describes the role of pharmacometrics in drug development: "Pharmacometrics lies at the heart of what drug companies do: collecting data from animals, normal volunteers, and patients; quantifying it, and then being able to determine what that data mean for optimizing drug efficacy and minimizing toxicity" (Nielsen and Friberg 2013). Pharmaceutical and biotech companies have invested heavily in establishing pharmacometrics expertise to utilize the preclinical, clinical, as well as human genomic data to understand the disease progression, the drug behavior, and its effect on individual patients and to personalize medicine to specific groups of patient population. The purpose of this chapter is to provide an overview of different approaches that were used in pharmacometrics in the context of pharmaceutical drug development.

H. Derendorf (✉)
Department of Pharmaceutics, College of Pharmacy, University of Florida, Gainesville, FL, USA
e-mail: hartmut@ufl.edu

S. K. B. Sy
Department of Pharmaceutics, University of Florida, Gainesville, FL, USA

X. Wang
Clinical Pharmacology, Otsuka Pharmaceuticals, Princeton, NJ, USA

S. Schmidt, H. Derendorf (eds.), *Applied Pharmacometrics,* AAPS Advances in the Pharmaceutical Sciences Series 14, DOI 10.1007/978-1-4939-1304-6_1

1.2 Classical PK Analysis

There are two primary approaches in the classical PK analysis: the compartmental modeling and the noncompartmental analysis. Compartmental modeling is based on the mass balance equations on the compartment and the noncompartmental modeling is based on the statistical moments derived from the time course of the drug concentration data.

Compartmental PK models are widely used to characterize the disposition of a drug using its concentration–time profiles sampled from body fluid such as plasma, serum, or whole blood following an administered dose. The general expression of the compartmental model is given in Eq. 1.1, where a series of exponential terms are used to fit to the drug concentration–time profile:

$$C(t) = \sum_{i}^{n} A_i e^{-\alpha_i t} \tag{1.1}$$

where i indicates each compartment, n is the total number of compartment, and A_i and α_i are called macroconstants reflecting the amount of the drug administered, the mass transfer between the compartments, and the elimination of the drug from the body. The number of compartments (n) determined by curve fitting is a rather abstract mathematical construct. The interpretation of Eq. 1.1 is that the body is a series of compartments; the drug is distributed between compartments, and is eliminated from the body. It was recognized that Eq. 1.1 was the solution of a series of ordinary differential equations derived by mass balance of each compartment.

The simplest compartmental model has one compartment with a bolus injection. The differential equation for the one-compartment model can be derived from mass balance; that is, the rate of change of the drug amount in the compartment equals the rate of the input minus the rate of output:

$$\frac{dVC}{dt} = rate\ of\ input - k_e VC, \quad \text{at } t = 0, C = C_0 \tag{1.2}$$

where V is the volume of the compartment, C is the drug concentration of the compartment, and k_e is the first-order elimination rate constant. C_0 is the initial condition of the differential equation, which is the drug concentration prior to drug administration. For a bolus injection, when using the delta function to represent the rate of input, the solution to the above equation, assuming V is a constant, is:

$$C(t) = \frac{Dose}{V} e^{-k_e t} \tag{1.3}$$

where $Dose$ is the input amount of the drug. Comparing Eq. 1.1 with Eq. 1.3, it is obvious that $A = Dose/V$, $\alpha = k_e$, and $n = 1$.

Because Eq. 1.1 is first-order kinetics, the half-life ($t_{1/2}$) can be estimated as $t_{1/2} = \frac{\ln(2)}{k_e}$. Keep in mind that only for first-order kinetics, the half-life is a constant. Equation 3 is often reparameterized to

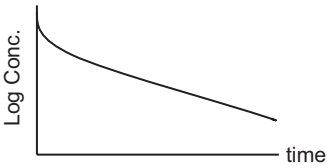

Fig. 1.1 Log concentration–time profile that follows a bi-exponential decline

$$C(t) = \frac{Dose}{V} e^{-\frac{CL}{V}t} \tag{1.4}$$

where $k_e = CL/V$ and CL refers to clearance. Clearance is one of the most important concepts introduced in PK. Additional information on clearance will be discussed in the section on the clearance definition.

In many cases, the disposition of a drug in the body follows a multi-exponential decline, which shows as multi-linear phases in the log concentration versus time profile shown in Fig. 1.1. This type of drug concentration profile is often characterized by two or more compartments. For a two-compartmental model with a bolus injection, Eq. 1.1 becomes

$$C(t) = Ae^{-\propto t} + Be^{-\propto t} \tag{1.5}$$

The half-life of the α phase and the β phase (or called the terminal phase) of the drug can be estimated as

$$t_{1/2,\alpha} = \frac{\ln(2)}{\alpha}, \quad t_{1/2,\beta} = \frac{\ln(2)}{\beta} \tag{1.6}$$

To estimate the overall half-life of a drug in the body following multi-exponential decline, the concept of "effective half-life" was introduced and the calculation is given in Eq. 1.7, e.g. for a two-compartment model:

$$effective\ t_{1/2} = \frac{1}{AUC}\left(\frac{A}{\alpha} t_{\frac{1}{2},\alpha} + \frac{B}{\beta} t_{\frac{1}{2},\beta}\right), \tag{1.7}$$

where AUC is the area under the concentration–time profile.

The differential equations for a two-compartmental model can be derived through mass balance on each compartment:

$$\begin{aligned} \frac{dA_c}{dt} &= Input\ rate - k_{12}A_c - k_e A_c + k_{21}A_p \\ \frac{dA_p}{dt} &= k_{12}A_c - k_{21}A_p \end{aligned} \tag{1.8}$$

where A_c and A_p refer to the drug amounts in the central and peripheral compartments, respectively; k_{12} and k_{21} are the mass transfer rate constants between the

central and the peripheral compartments, also called microconstants. The analytical solution to Eq. 1.8 for a bolus injection can be expressed in the same manner as Eq. 1.5, with the following micro- and macroconstant conversion:

$$\alpha + \beta = k_e + k_{12} + k_{21}$$

$$\alpha \times \beta = k_e \cdot k_{21}$$

$$A = \frac{Dose(\propto - k_{21})}{V_c(\propto - \beta)}$$

$$B = \frac{Dose(k_{21} - \beta)}{V_c(\propto - \beta)}.$$

Re-parameterization for a two-compartment model in terms of CL, intercompartmental clearance (Q), V_c, and V_p can be expressed as $k_e = \frac{CL}{V_c}$, $k_{12} = \frac{Q}{V_c}$, $k_{21} = \frac{Q}{V_p}$. For more detailed discussions of commonly used PK models including intravenous infusion and extravascular routes, the reader may refer to the textbooks on PK and pharmacodynamic (PD) analysis (Derendorf and Hochhaus 1995; Gabrielsson and Weiner 2000; Gibaldi and Perrier 1999; Rowland and Tozer 1989).

The compartmental models are often used to simulate concentration profiles from one dosing regimen to another, or from a single dose to a steady-state concentration profile. The compartmental model has its limitation, however. First, the number of compartments and the property of the compartments are rather abstract mathematical constructs. The underlying physiology of the model and the resulting model representation is subject to the analyst's interpretation. Second, the parameters do not have a clear physiological meaning, and so the source of the variability of the parameters cannot be clearly identified and be correlated to physiological reality.

A noncompartmental model is based on statistical moments of the concentration–time data (Dunne 1993; Yamaoka et al. 1978). The *n*th-order statistical moment has the following mathematical form:

$$\int_0^\infty t^n C(t) dt, \tag{1.9}$$

where t is time, n is the order of moment, and $C(t)$ is the drug concentration as a function of time. The area under the concentration–time curve (AUC), the moment curve (AUMC), and subsequently the mean residence time (MRT) can then be computed through integrating the concentration–time profile:

$$AUC = \int_0^\infty t^0 C(t) dt = \int_0^\infty C(t) dt \tag{1.10}$$

$$AUMC = \int_0^\infty t^1 C(t)dt = \int_0^\infty tC(t)dt \tag{1.11}$$

$$MRT = \frac{\int_0^\infty tC(t)dt}{\int_0^\infty C(t)dt} = \frac{AUMC}{AUC}. \tag{1.12}$$

In practice, the computations of the above parameters are carried out using numerical integrators such as the linear or log-linear trapezoidal rule on the discrete concentration–time data. PK parameters such as CL, V_{ss}, and $t_{1/2}$ can be derived from those statistical moments:

$$CL = \frac{Dose}{AUC} \tag{1.13}$$

$$V_{SS} = CL * MRT. \tag{1.14}$$

The terminal half-life can be calculated using the slope, λ_z, of the log concentration curve, $t_{1/2} = \frac{\ln(2)}{\lambda_z}$. If the concentration profile shows mono-exponential decline, the terminal half-life can also be calculated using the $t_{1/2} = \ln(2) * MRT$. If the concentration profile shows multi-exponential decline, the half-life calculated using $t_{1/2} = \ln(2) * MRT$ will be the "effective half-life," the same as the solution using Eq. 1.7 in the compartmental modeling approach. The underlying assumption of the noncompartmental modeling is that the PK of a drug is linear (Gibaldi and Perrier 1999). A special case is that the noncompartmental model is equivalent to a one-compartment PK model, where the PK parameters derived through noncompartmental analysis can also be obtained from a one-compartment model through integration of Eq. 1.2.

The advantage of a noncompartmental method compared to the compartmental model is that the results from the moment approach are less subjective on the analysts' bias of their model of choice (Yamaoka et al. 1978). From a numerical analysis point of view, noncompartmental analysis is using numerical integration over the time course of drug concentration to derive PK parameters rather than optimization on either algebraic or differential equations. Thus, the "noise" in the drug concentration–time profile has less impact on the PK parameters than that of compartmental modeling. For example, when calculating the effective half-life using Eq. 1.7, an unrealistically long effective half-life could be generated when the terminal phase slope cannot be accurately estimated. In that situation, the effective half-life estimated using $\ln(2) * MRT$ is more reliable. The noncompartmental analysis is often the choice for computing PK parameters of a drug for regulatory submission.

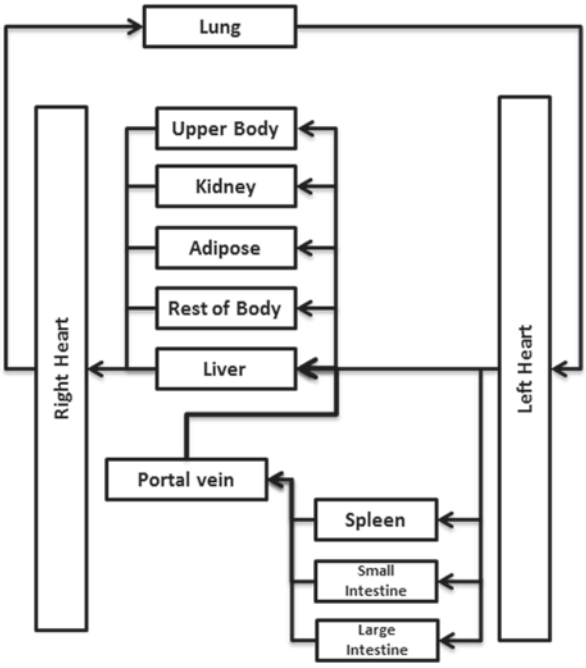

Fig. 1.2 An illustration of a PBPK model for a mammalian circulation system

1.3 Physiologically Based PK Modeling

The physiologically based pharmacokinetic (PBPK) model was developed to overcome the limitations of the compartmental modeling. The structure of the model, the property of the compartments, and the parameters are based on the underlying physiological and biological processes that are responsible for drug disposition.

1.3.1 History and Methodology of PBPK Approach

The concept of predicting the effect of a xenobiotic on a living organism based on mathematical models that incorporate real physiological parameters such as organ functions and flow rates was initially proposed by Teorell in (1937a, b). No progress was made in PBPK since Teorell's postulation of using mathematical models to describe xenobiotic disposition until the late 1950s, possibly due to the limitation in computational power. The most comprehensive development was made by Bellman and colleagues in the early 1960s (Bellman et al. 1963). The depiction of a PBPK model proposed by Bellman and his colleagues is shown in Fig. 1.2 with modifications. In the model, the tissue or lumped tissue was connected through blood flow. Blood flow through the main arteries and veins was assumed to be similar to a plug flow, that is, the drug concentration during the circulation was changing

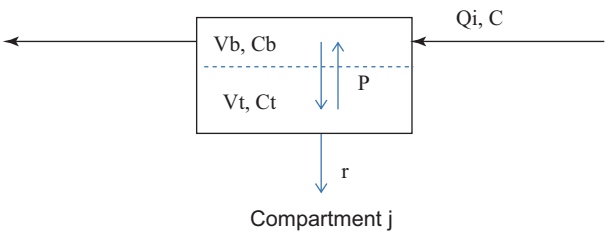

Fig. 1.3 A representative compartment with lumped interstitial and cellular regions

with time and longitude. The interstitial fluid and intracellular region were treated as perfectly mixed compartments. Based on those assumptions, the mathematical expression for the model was a set of difference-differential equations. The assumption of the plug flow leads to computational difficulties, as the entire past history of the drug concentration at each region of the body needs to be retained for the calculation of the successive time interval. Their work was discussed in detail and summarized by Bischoff and Brown in 1966 (Bischoff 1966). In the same publication, Bischoff and Brown discussed the application of mass transfer concept at great length at the levels of capillary, interstitial, and intracellular region. They also discussed the time needed for "mixed" drug concentration in the blood circulation versus the transient time of a typical human (~1 min). Based on the physiological reality and transport phenomena, the compartment property including the capillary, interstitial, and cellular region in Fig. 1.2 was characterized without accounting for every detail. They turned a set of difference-differential equations into differential equations such as Eqs. 1.15 and 1.16. Using a delta function to represent a bolus injection, the drug concentration profiles in different regions of the body were simulated.

To illustrate the mathematical expression and the parameters of a general PBPK model, for simplicity, if we assume that the interstitial and cellular regions are at equilibrium, a compartment in Fig. 1.2 can be illustrated as shown in Fig. 1.3. The differential equations describing the compartment were given in Eqs. 1.15 and 1.16:

$$\frac{V_{b,j}dC_{b,j}}{dt} = Q_j(C - C_{b,j}) - PA(C_{bf,j} - C_{tf,j}) \tag{1.15}$$

$$\frac{V_{t,j}dC_{t,j}}{dt} = PA(C_{bf,j} - C_{tf,j}) - r_j, \tag{1.16}$$

where Q_j is the blood flow rate for the j compartment, PA is the product of the membrane permeability and the membrane area; subscript b is for blood, t for tissue, and f for free drug concentration. The free and the total drug concentration can be correlated based on linear or nonlinear binding. The term r_j represents the elimination rate (metabolism and/or excretion) of the drug from compartment j; it can occur at different regions of the compartment. The drug can be administered through oral, intravenous, or intramuscular routes. The route of administration can be incorporated to the PBPK model.

As shown in Eqs. 1.15 and 1.16, there are three types of information required to solve a PBPK model: (1) the anatomy and physiology of a specific species; (2) the physicochemical properties, such as binding and membrane permeability, that are drug specific; (3) metabolism and excretion that are both drug- and species-specific. The anatomical and physiological parameters are usually available. Extensive data such as weight and blood flow rate through each tissue for different species were provided by Brown et al. (1997). However, physicochemical data and metabolism information are limited and often rely on *in vitro* studies or *in vivo* tests that were carried out in different species.

1.3.2 Number of Compartments in a PBPK Model

The two questions that an analyst needs to ask himself/herself when developing a PBPK model are: (1) how many compartments are needed and (2) how much detail is required for that compartment? Extensive work from a typical four-compartment model with flow-limited assumption with or without extensive details for a particular targeted organ to more than ten compartments describing the whole body can be found in the literature (Andersen et al. 1984, 1987; Bischoff et al. 1968, 1970, 1975; Liu et al. 2005; Peters 2008; Peters and Hultin 2008; Ramsey and Andersen 1984; Wang et al. 1997). A general consideration of the number of compartments to choose from and the details of the model depend on these information: the target organ, the physicochemical and pharmacologic properties of the drug that determine the drug transfer in the body, and the PK time scale (Bischoff 1975).

1.3.3 Target Organ

The structure of a PBPK model starts with the anatomy of the body. As the drug concentration in a target organ or at the site of action is of interest, single compartment is often used to represent the target organ. A significant amount of work using the PBPK approach has been done for anticancer drugs, central nervous system, hepatic metabolism and xenobiotic inhalation (Andersen et al. 1984, 1987; Baxter et al. 1994; Chen and Gross 1979; Collins and Dedrick 1983; Pang and Durk 2010; Ramsey and Andersen 1984; Reddy et al. 2005).

1.3.4 Mass Transfer Phenomenon

Lumping is often used for PBPK model reduction. There are two levels of lumping: (1) at the organ level and (2) at the cellular level. Lumping at the cellular level was originally discussed in details by Bischoff and Brown in their work mentioned above (Bischoff 1966). Lumping at the organ level was extensively discussed from

the late 1960s to the 1990s (Bischoff 1987; Bischoff and Dedrick 1968; Coxson and Bischoff 1987a, b; Gerlowski and Jain 1983; Nestorov et al. 1998). The basis for lumping is dependent on the mass transfer process and the physicochemical properties of a drug. The following section discusses the types of mass transfer function and the conditions for their applications.

1.3.4.1 Flow-Limited Assumption

The flow-limited assumption was made primarily due to the lack of information on membrane permeability. The criterion of flow limited was given as $\frac{PA_j}{Q_j} \gg 1$ (Bischoff 1975), that is, the membrane transfer is much faster than convection (from blood flow). Under this assumption, the free drug concentration in the tissue and in the blood is at equilibrium, $C_{tf,j} = C_{bf,j}$. Therefore,

$$C_{t,j} = C_{bf,j} + \frac{R_{\text{tot},j} C_{bf,j}}{K_{d,j} + C_{bf,j}}. \tag{1.17}$$

For linear binding, Eq. 1.16 can be simplified as $C_t = R * C_b$, where R is called the tissue to blood partition coefficient. Under flow-limited assumption, Eqs. 1.15 and 1.16 become

$$\left(V_{t,j} + \frac{V_{b,j}}{R_j}\right)\frac{dC_{t,j}}{dt} = Q_j\left(C - \frac{C_{t,j}}{R_j}\right) - r_j \tag{1.18}$$

Or if it is expressed using C_b, Eq. 1.18 becomes

$$(V_{b,j} + R_j V_{t,j})\frac{dC_{b,j}}{dt} = Q_j(C - C_{b,j}) - r_j \tag{1.19}$$

Equations 1.18 and 1.19 demonstrate that the concentration of a drug in a particular organ, $C_{b,j}$ or $C_{t,j}$, is determined by the value of $\frac{Q_j}{V_{b,j} + R_j V_{t,j}}$ and the elimination of that organ, $\frac{r_j}{V_{b,j} + R_j V_{t,j}}$. As such, lumping different organs or body regions depends on the blood flow rate through the organ, the partitioning of the drug between the blood and the tissue levels, and the elimination process of the organ (for an eliminating organ).

For noneliminating organs connected in parallel, the blood concentration entering those organs, C, is the same. Therefore, the blood concentration leaving the organ, $C_{b,j}$, and the concentration of the tissue, is determined by the ratio of $\frac{Q_j}{V_{b,j} + R_j V_{t,j}}$. The richly perfused organs with similar partition coefficient of the

drug are usually lumped into a single compartment. The blood flow rate through the compartment is $\sum_{j=1}^{n} Q_j$, and the volume of the compartment is $\sum_{j=1}^{n} V_{b,j} + R_j V_{t,j}$. The same principle can be applied to poorly perfused organs with similar partition coefficient. For a lipophilic compound, higher partition coefficient in the adipose versus the lean tissue resulted in different profiles of the concentration of the drug in the tissue, and therefore, a separate compartment for the lean tissue or the adipose tissue is often required. In addition, an organ or a body region with significantly low blood flow rate and low partition coefficient of the drug in those regions can be omitted in the PBPK model. Whether an eliminating organ can be lumped with a noneliminating organ depends on the ratio of the blood flow rate to the clearance of that organ (Bischoff 1975; Nestorov et al. 1998).

For organs that are connected in series, such as the venous–lung–artery channel or the splanchnic organs, the blood concentration profile leaving the channel and returning to the vein is determined by the organ that has the longest transient time, or the organ that eliminates the xenobiotics. If the partition coefficient between the plasma and the lung tissue is small, the transient time of the lung is much smaller than those of the vein and the artery. The vein and the artery often can be lumped to one compartment without including the lung, $V = V_{artery} + V_{vein}$, if the lung is not an eliminating organ. In the splanchnic channel, the splanchnic organs are often omitted, since the liver is the primary eliminating organ and the blood concentration leaving the channel is approximately represented by the liver. The gastrointestinal tract (GI) tract may be included to describe the absorption and/or reabsorption of the drug.

In general, a four-compartment lumped PBPK model, consisting of the blood compartment, the richly perfused compartment such as liver or kidney, the poorly perfused compartment such as the muscle, and a compartment representing the adipose tissue can adequately describe the drug disposition in the body. Other compartments may be added to describe the specific target organ as in the PBPK model to study tumor, wherein a separate compartment was incorporated to represent that organ where the tumor resides.

If the drug transfer across the membrane is fast enough compared to the mass transfer through convection (blood flow), the entire body can be modeled as a single-compartment model assuming that the blood concentration is at equilibrium with tissues at different regions. See the elimination-limited case below for the mathematical expression.

1.3.4.2 Membrane Limited

The opposite situation contrasting to the flow-limited mass transfer is the case wherein the membrane transfer is slow enough compared to the rate of the drug supply by blood flow, $\frac{PA_j}{Q_j} \ll 1$, so that the gradient of the drug concentration in the blood entering and leaving the compartment is negligible (Bischoff 1975). Therefore, $C_{b,j} \approx C$. Equations 1.15 and 1.16 for the compartment with membrane-limited transfer can be simplified as:

$$V_{t,j}\frac{dC_{t,j}}{dt} = PA(C - C_{tf,j}) - r_j. \tag{1.20}$$

If the drug transfer across the membrane of all regions of the body is slow enough that it can be considered negligible, the entire body can be modeled as a single-compartment model by only including the blood pool:

$$V_b\frac{dC}{dt} = Input - r_j. \tag{1.21}$$

1.3.4.3 Elimination Limited

In their publication on the general solution of a two-compartment model, Bischoff and Dedrick introduced the concept of the elimination-limited assumption, where the mass transfer is much more rapid than the total elimination rate (Bischoff et al. 1970). The importance of introducing the elimination-limited concept is to simplify a PBPK model to a one-compartment model. The criteria for when a system follows the elimination-limited profile is given in their study through a two-compartment open model under a flow-limited assumption, that is, the drug distribution to the tissue through the blood flow rate (mass transfer through convection) is much faster than the rate of elimination. In the elimination-limited situation, the entire body can be lumped into a one-compartment model:

$$\left(V_b + \sum_j^n R_j V_{tj}\right)\frac{dC_b}{dt} = Input - r_j. \tag{1.22}$$

Equation 1.21 has the same mathematical expression as the one-compartment model in classical compartmental modeling. The difference is that Eq. 1.5 derived from PBPK model gives the meaning to V_d, which is equivalent to $V_b + \sum_j^n R_j V_{t,j}$. In fact, the elimination-limited case does not necessary require flow-limited assumption. As long as the elimination rate is slow enough compared to both convection and membrane transfer, the elimination-limited case stands. This also explains why in covariate analysis in the population PK modeling, the volume of distribution often is related to body weight, as tissue volume is proportional to the body weight. The tissue concentration then can be easily calculated as $\frac{C_b}{R_{t,j}}$, where C_b is the blood concentration and $R_{t,j}$ is the partition coefficient of the organ. A typical example can be found for 2,3,7,8-tetrachlorodibenzo-*p*-dioxin (TCDD), since TCDD is known to remain in the biological system for a very long time. The half-life in human is around 5–10 years. Table 1.1 lists the physiological data for a standard human with body weight of 70 kg and the estimated value of $\frac{1}{\lambda}$ with $\lambda_i \approx \frac{Q_i}{k_{el}}\frac{V_{lip,b}}{V_b V_{lip}}$ for a

Table 1.1 Physiological parameters of TCDD for a standard 70-kg human

	Weight (kg)	Blood flow (L/day)	Partition coefficient	PA (mL/h)	Lipid content (kg)	$\frac{1}{\lambda}$
Lung	1.17	8064	6	Flow-limited	0.057	4.03×10^{-10}
Spleen	0.182	111	5	Flow-limited	0.0089	2.93×10^{-8}
Kidney	0.308	1786	6	9	0.015	3.49×10^{-7}
Adipose	14.994	374	100	30	12.9	1.08×10^{-7}
Liver	1.799	2088	6	731	0.088	4.45×10^{-9}
Skin	2.597	432	10	39	0.52	8.36×10^{-8}
Rest of the body	44.388	3273	1.5	98	2.84	3.31×10^{-8}

flow-limited case, or $\lambda_i \approx \frac{PA_i}{k_{el}} \frac{V_{lip,b}}{V_b V_{lip}}$ for a membrane-limited case, where the subscript lip refers to lipid content.

The lipid contents of each organ in Table 1.1 were calculated based upon the values from the literature (van der Molen et al. 1996). The elimination rate constant k_{el} was estimated conservatively assuming a half-life of 5 years. The values shown in Table 1.1 suggested that the elimination-limited assumption was satisfied for TCDD. This one-compartment model through PBPK reduction was adopted in human risk assessment in the environmental toxicology (Thomaseth and Salvan 1998; van der Molen et al. 1996).

1.3.5 PK Time Scale

The PK time scale plays an important role in PBPK model development (Bischoff 1975; Dedrick and Bischoff 1980; Nestorov et al. 1998; Oliver et al. 2001). For a standard male or female, the time it takes to complete one blood circulation is about 1 min. For most of the drug acting in the scale of several minutes, hours, days or longer, it can be assumed that the blood in the circulation is a uniform pool. However, more details are required in the model for the rapidly eliminated drug, in a time scale of minutes. The sampling site could also be important. The following example illustrates the methodology in the selection of the number of compartments to use for building a PBPK model for a short-acting drug.

1.3.6 Example 1: A PBPK Model for a Contrast Agent for Ultrasound Imaging

The PBPK model developed for a contrast agent for ultrasound imaging (Wang et al. in preparation) is shown in Fig. 1.4. The model has detailed information on the cardiovascular circulation and pulmonary circulation, which included the vena cava, right heart, pulmonary vein, lungs, pulmonary artery, left heart, and aorta. The actual sampling site and the administration site had to be specified in the model to

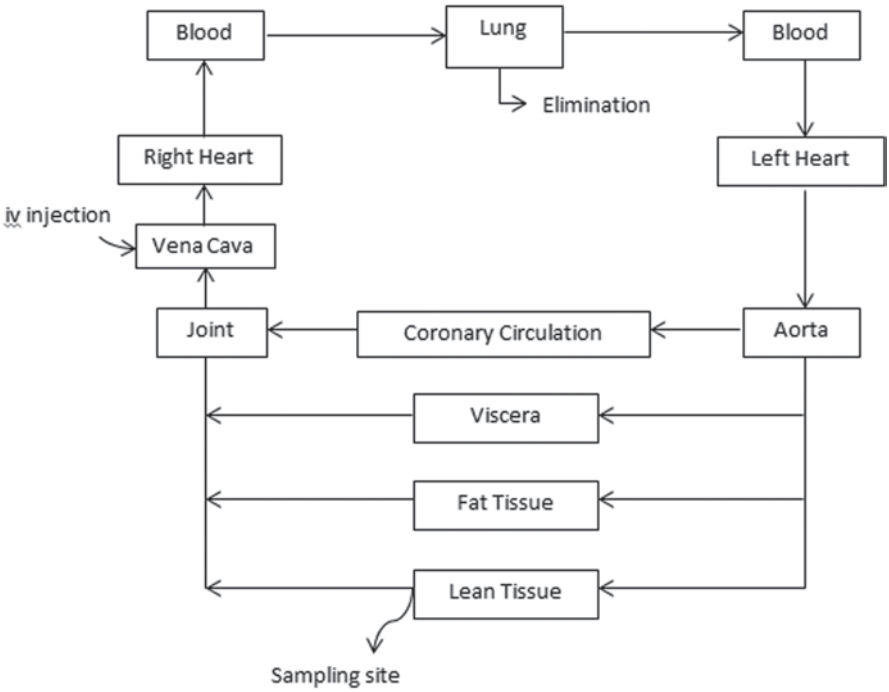

Fig. 1.4 Illustration of the PBPK model of the human body for a contrast agent used in ultrasound imaging

accurately describe the concentration of the agent in the blood circulation, the left and the right heart. Such detailed information became necessary due to the short time scale in its PK profile. For example, within 3 min following injection, blood concentration of the agent dropped tenfold. The left and the right sides of the heart are the target tissues for this contrasting agent. The lung is the eliminating organ. The adipose tissue and the lean tissue compartments were specified in the model, as the agent is a lipophilic compound. Coronary circulation was included in the model to evaluate whether coronary artery disease would have an impact on the PK of this agent. The viscera tissues consist of the kidney, the brain, the liver, etc. The blood flow rate per volume in these tissues is much faster than those of either adipose or lean tissues. Except for the lung, each compartment includes vascular and extravascular sub-compartments.

The lung is the primary eliminating organ for this compound. A heterogeneous compartment for the agent based on the anatomy of the lung and mass transfer is depicted in Fig. 1.5. As a static homogeneous lung compartment overpredicted the concentration in the alveolar gas phase during the absorption and under-predicted the concentrations during the elimination phase (Hutter et al. 1999), a heterogeneous lung model developed by Liguras and Bischoff (unpublished data), Frank (1982), and Bernards (1986) was adopted instead, as the one shown in Fig. 1.5.

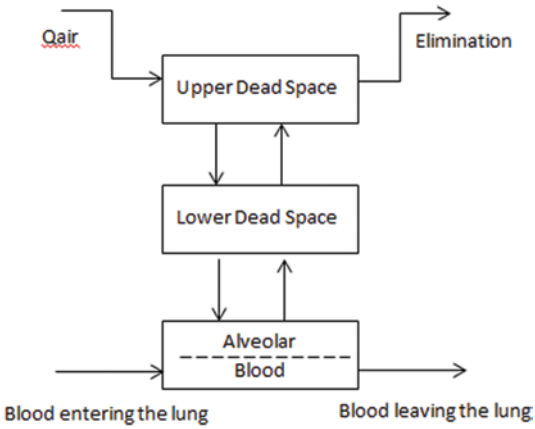

Fig. 1.5 Structure of the physiological model of the lung

The lung was modeled using three compartments based on the physiology of the lungs, consisting of an upper dead space plus a lower dead space in series and a perfectly mixed alveolar region. The dead space is taken to be that of the large bronchial vessels, such that there is no mass transfer between the air in the lung and the capillary blood. The volume of the alveolar compartment changes with inhalation and exhalation. The mass transfer between the air in the lung and the capillary blood occurs across the alveolar-capillary membrane. Mathematical equations describing the PBPK model including the lung compartment are given in Eqs. 1.23–1.32.

1.3.6.1 Whole-Body PBPK Model

For the left and right sides of the heart, and other compartments except the lung, the mass balance equations have the following form:

$$V_{b,j}\frac{dC_{tb,j}}{dt} = Q_j(C_a - C_{tb,j}), \tag{1.23}$$

where $V_{b,j}$ is the tissue blood volume, $C_{tb,j}$ refers to the concentration in the tissue blood, and C_a is the drug concentration in the blood entering the tissue. For other tissues, the mass balance equations take the form of a flow-limited case.

1.3.6.2 Lung Compartment

The breathing pattern is described by the following equation:

$$Q_{\text{air}} = 0.5 \cdot \omega\, TV \sin(\omega t), \tag{1.24}$$

where $Q_{\text{air}} > 0$ indicates an inhalation process, $Q_{\text{air}} < 0$ represents exhalation. In the following equations, all Q_{air} are absolute values, and the inhalation and exhalation

processes are identified by either a positive or a negative sign, respectively. The total dead space was modeled using two compartments.

For the upper dead space of the lung, the inhalation and exhalation processes were described by Eqs. 1.25 and 1.26, respectively, and the elimination rate for the lung was characterized by Eq. 1.27.

Inhalation:

$$V_{UPD}\frac{dC_{\mathrm{UPD}}}{dt} = -Q_{air}C_{UPD} \tag{1.25}$$

Exhalation:

$$V_{UPD}\frac{dC_{UPD}}{dt} = Q_{air}(C_{LPD} - C_{UPD}) \tag{1.26}$$

$$rex_{LU} = Q_{air}C_{UPD}. \tag{1.27}$$

For the lower dead space of the lung, the inhalation and exhalation processes were also described separately using Eqs. 1.28 and 1.29, respectively:

Inhalation:

$$V_{LWD}\frac{dC_{LWD}}{dt} = Q_{air}(C_{UPD} - C_{LWD}) \tag{1.28}$$

Exhalation:

$$V_{LWD}\frac{dC_{UPD}}{dt} = Q_{air}(C_{alv} - C_{LWD}). \tag{1.29}$$

For the alveolar region, the volume of the alveoli is described by a sinusoidal function, given that the volume of the alveoli changes with the breathing pattern:

$$V_{alv} = V_{alv,0} + 0.5 \cdot TV(1 - \cos(\omega t)). \tag{1.30}$$

And the corresponding inhalation process was characterized by coupled differential Eqs. 1.31 and 1.32:

$$\frac{dV_{alv}C_{alv}}{dt} = Q_{air}C_{LWD} + PA\left(C_{b,out} - \frac{C_{alv}}{P_{air}}\right) \tag{1.31}$$

$$V_{bLu}\frac{dC_{b,out}}{dt} = Q(C_{b,in} - C_{b,out}) - PA\left(C_{b,out} - \frac{C_{alv}}{P_{air}}\right). \tag{1.32}$$

The exhalation process was also defined by coupled differential Eqs. 1.33 and 1.34:

$$\frac{dV_{alv}C_{alv}}{dt} = -Q_{air}C_{alv} + PA\left(C_{b,\text{out}} - \frac{C_{alv}}{P_{air}}\right) \tag{1.33}$$

$$V_{bLu}\frac{dC_{b,out}}{dt} = Q(C_{b,in} - C_{b,out}) - PA\left(C_{b,out} - \frac{C_{alv}}{P_{\text{air}}}\right). \tag{1.34}$$

The breathing frequency is $\omega = 2\pi f$, where, f is the number of breaths/per minute. $V_{alv,0}$ is the functional residual capacity of alveoli; Q is the cardiac output; PA is the product of membrane permeability and area of membrane transfer. The subscripts refer to the following: UPD—upper dead space; LWD—lower dead space; alv—alveolar; b,in—blood entering the lung; b,out—blood leaving the lung; and V_{bLu} is the blood volume in the lung tissue.

1.3.7 Sensitivity Analysis in PBPK Modeling

As shown in the example above, there are several different types of parameters in a PBPK model. Parameter values for tissue volume, blood volume, and blood flow rates were obtained from published results (Brown et al. 1997). These values usually represent a typical male or female individual. Other parameters such as partition coefficient of a compound between blood and the tissue are often estimated based on *in vitro* or scaled-up studies from animals to human. The remaining unknown parameters are then estimated by fitting the model to the observed data. Given the large number of parameters, it is critical to evaluate the impact of the uncertainty of those parameters on the disposition of the compound in the body. This is often done through a local (derivative) and global (Monte Carlo method) sensitivity analysis. We used the first example to illustrate the importance of this analysis.

In Example 1, the anatomical and physiological parameters related to the lung such as the volume of the alveoli, the dead space inside the lung, the functional residual capacity, the tidal volume, and the breathing frequency were obtained from Guyton's textbook of physiology (Guyton and Hall 1996; Hall and Guyton 2011). The partition coefficient, $P_{\text{ft}} = C_{\text{fat}}/C_{\text{blood}}$, of 50, was estimated based on the oil/water partition ratio of the compound. According to the results reported for other lipophilic compounds such as dioxin or thiopental (Bischoff and Dedrick 1968; Wang et al. 1997), the partition coefficient for nonfatty tissue is approximately 10% of that of the fat tissue. Therefore, the partition coefficients of other nonfatty tissue were assumed to be $P_t = 5$. Table 1.2 listed the parameter values for a typical 70-kg healthy subject.

There are three remaining unknown parameters, the partition coefficient between air and blood, P_{air}, and the two permeability values, PA_{air} and PA_t. Both individual fitting and mean value fitting were conducted. Figs. 1.6 and 1.7 present the fitting of the mean values at 0.3 mg/kg dose level. The fitted parameter values are given below:

$$\text{PA}_{\text{air,}} = 42.0 \pm 4.2\ (\text{m}^3/\text{min})$$

$$\text{P}_{\text{air}} = \text{C}_{\text{gas}}/\text{C}_{\text{blood}} = 106 \pm 50.$$

Table 1.2 PBPK model parameters for a 70-kg healthy subject. (Parameter values from Guyton and Hall 1996)

Body weight = 70,000 g Male: cardiac output = 1.3 × Body weight$^{0.75}$ (mL/min) Coronary blood flow = 0.0455 × cardiac output (mL/min) Total blood volume = 6.3 L Blood volume in pulmonary circulation and cardiac circulation = 30 % of the total Blood volume Rest of the blood = 70 % of the total blood volume			
Blood volume in pulmonary circulation and cardiac circulation (mL)		*Parameters for the lung model*	
Pulmonary vein = 315 Lung capillary = 150 Pulmonary artery = 290 Right heart chamber = 340 Left heart chamber = 340 Vena cava = 340 Aorta = 100		Breathing frequency = 15 (No/min) Tidal volume (excluding dead space) = 350 mL Total dead space = 150 mL Upper dead space[a] = 50 mL Lower dead space[a] = 100 mL Functional residual capacity = 2300 mL	
Compartments[b]	*Tissue volume as fraction of body weight*[b]	*Tissue blood volume as fraction of the total blood volume*[b]	*Blood flow rate as fraction of cardiac output*[b]
Lung	0.0105	As shown above	1
Heart	0.0103		1
Viscera	0.05	0.0051/VBc	0.56
Adipose	0.214	0.0043/Vbc	0.065
Lean	Rest of the part	Rest of the part	Rest of the part

[a] Parameter values were obtained from Liguras and Bischoff (unpublished data), Frank (1982), and Bernards (1986)
[b] Values from Brown et al. (1997)

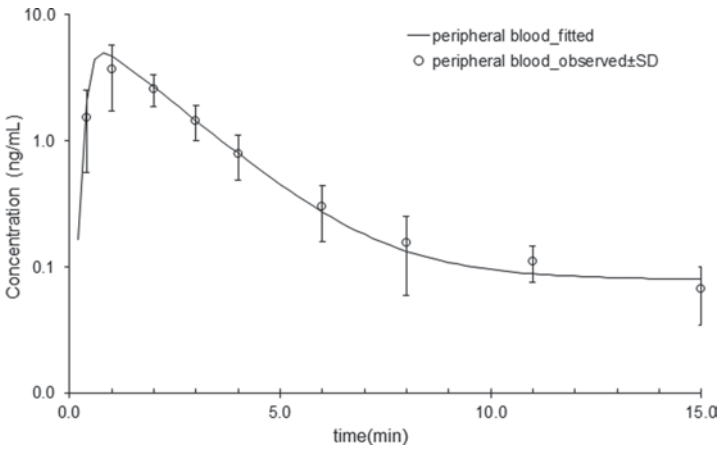

Fig. 1.6 Mean observed and fitted blood concentrations following bolus injection (dose of 0.3 mL/kg; *solid line* is model-fitted values, *symbols* are observed concentrations, *error bars* represent SD)

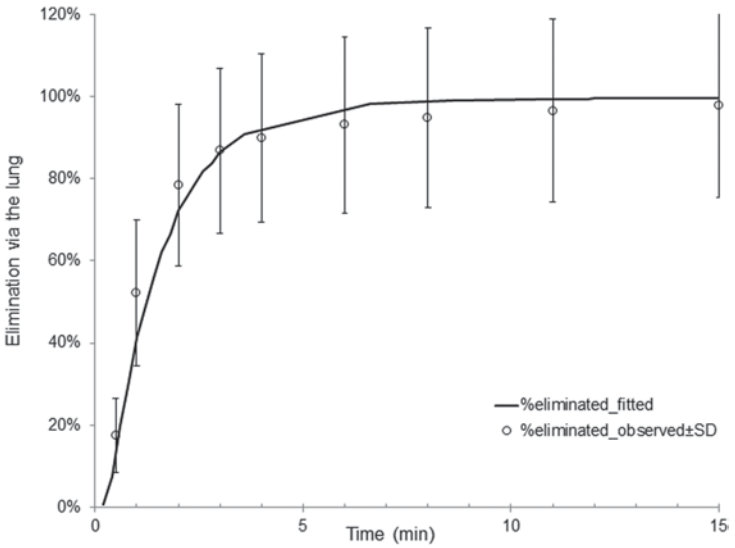

Fig. 1.7 Mean cumulative lung elimination (%) following bolus administration (dose of 0.3 mL/kg; *solid line* is model-fitted values, *symbols* are observed values of the elimination via the lung, *error bars* represent SD)

The ratio of PA to the blood flow rate through that tissue were such that

$PA_t/Q = 0.53 \pm 0.15$ (for the heart, the lung, and the viscera compartment)

$PA_t/Q = 1.80 \pm 0.22$ (for the lean compartment and the fat tissue).

To assess the impact of parameters on the PK of the agent, Monte Carlo simulation was conducted. The low, median, and high values of a parameter based on physiological reality were selected. For example, the total cardiac output range of 0.975–1.625 indicates that the low value of the total cardiac output is 0.975 with a median value of 1.3 and an upper range of 1.625. The results of Monte Carlo simulation demonstrated that only cardiac output, tidal volume of the lung and permeability have a significant impact on the concentration in the left heart of the agent. Other parameters such as the coronary blood flow rate, the fat content (though it is a lipophilic compound), the total blood volume, the breathing frequency, and functional residual volume have negligible effects on the concentration in the left heart. This analysis suggested that fixing a large number of parameter values using published data would have little impact on the fitted values of those three parameters (Table 1.3). This sensitivity analysis also provided information on potential source of interindividual variability.

1.3.8 Application of PBPK Modeling

There are many similarities in the anatomy and physiology of mammalian species; for example, many physiological processes vary as the 0.7–0.8 power of body weight and the anatomic variables are proportional to the body weight (Hu and

Table 1.3 Parameter effect of the contrasting agent disposition after sensitivity analysis

Parameters having significant effect	Parameters having negligible effect
Cardiac output (QTOTC)	Coronary blood flow rate (QCORC)
Permeability (PA)	Fraction of the fat (Wfc)
Tidal volume (TVC)	Total blood volume (VBTOTC)
	Breath No/min (BN)
	Functional residual volume (VAV0C)

Hayton 2001; Peters 1986; Savage et al. 2004; West et al. 1997, 1999). As such, the physiological process per unit body weight or organ weight tends to decrease as body size increases. Physicochemical parameters, such as blood-to-tissue partition coefficient and plasma protein binding, are not expected to have a great variation across species. Hence, a major application of PBPK model was in the field of species scaling (Boxenbaum 1982; Boxenbaum and Ronfeld 1983; Dedrick 1973; Dedrick and Bischoff 1980; Mordenti and Chappell 1989). One of the main limitations in the extrapolation of a PBPK model, from one species to another, is when significant difference in metabolic pathways and enzyme activities exist. Since the first PBPK model with flow-limited assumption for thiopental (Bischoff and Dedrick 1968), extensive application has been seen in drug development and environmental toxicology (Dedrick 1973; Peters 2012; Reddy et al. 2005; Rowland et al. 1973).

Peters presented a generic 14-compartment PBPK model that includes one compartment for the stomach, seven compartments to describe the absorption of a substance from the small intestine, and another compartment for the colon (Peters 2008). The dissolution of an orally administered substance from the GI tract is dependent on the product of the dissolution parameter and the difference between the solubility of the drug and its concentration. The model, being used for the *in vivo* prediction based on *in vitro* measurements, requires parameter for solubility, the pH of the buffer that was used for solubility measurement, and the in vitro absorption rate constant from Caco-2 permeability. For the estimation of drug concentration leaving a specific organ, the model utilizes plasma protein-binding information and tissue: plasma partition coefficients based on the work by Poulin and Theil (Poulin et al. 2001; Poulin and Theil 2000, 2002a, b; Theil et al. 2003). Peters used the model to predict the PK parameters of several compounds (Peters 2008; Peters and Hultin 2008). The measure to assess the quality of fitting was based on the reduced χ^2 -statistics and mean fold error. The author concluded that a "generic and integrative PBPK approach of drug disposition as a tool for a priori simulations and mechanistic evaluations of pharmacokinetics has the potential to improve the selection and optimization of new drug candidates" (Peters 2008).

In recent years, PBPK modeling has been applied to drug development and regulation (Zhao et al. 2009, 2011, 2012). A comprehensive review on the application of PBPK modeling in drug development and regulatory review/submission was provided in a number of articles from the Food and Drug Administration (FDA; Huang 2012; Huang and Rowland 2012; Leong et al. 2012; Rowland et al. 2011; Zhao et al. 2011, 2012). The articles summarized the major advances in the predictability of key PK parameters in human from *in vitro* data, the availability of dedicated

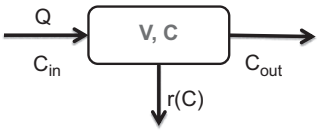

Fig. 1.8 Schematic representation of an eliminating organ

software platforms, and associated databases. Specific advances and contemporary challenges with respect to predicting the processes of drug absorption, distribution and clearance were reviewed, together with the ability to anticipate drug–drug interactions and the impact of age, genetics, diseases, and formulations on the PK of a drug. The value of this capability in selecting and designing appropriate clinical studies, its implications for cost-effective strategies, and a more holistic view of the application of PK across the preclinical and clinical drug development processes are considered. Finally, there is a greater focus on positioning PBPK within the drug development and approval paradigm, as well as its future application in personalized medicine.

1.4 Relationship Between Systemic and Tissue Clearance with PBPK Modeling Approach

1.4.1 Clearance Definition

Clearance is one of the most important concepts in PK. As Benet stated, "it allowed the field to develop a basic understanding and to make predictions as to how pathological and physiological changes would influence drug kinetics and drug dosing" (Benet 2010). By October 2009, there were more than 47,827 references found in PubMed under "drug clearance" (Benet 2010). The clearance concept was originally developed to quantify the functional efficiency of the kidney in the removal of urea (Grehant 1904a, b) and was then extended to describe the elimination of xenobiotics through the liver (Lewis 1948). Early contributions on developing the clearance concept for the whole body were made by Benet, Rowland, and Wilkinson (Benet and Galeazzi 1979; Rowland 1972; Rowland et al. 1973; Wilkinson 1987; Wilkinson and Shand 1975).

Using the definition provided by Wilkinson (1987), "the most general definition of clearance is that it is a proportionality constant describing the relationship between a substance's rate of transfer in amount per unit time, and its concentration, in an appropriate reference fluid." This is illustrated in Fig. 1.8 for an elimination organ.

The mathematical expression for clearance (CL) is given as follows:

$$CL = \frac{r(C)}{C_{in}}. \tag{1.35}$$

The extraction ratio reflecting the efficiency of an organ to remove a drug was defined as:

$$E = \frac{CL}{Q}, \tag{1.36}$$

where $r(C)$ is the elimination rate, C is the drug concentration inside the compartment, C_{in} is the drug concentration entering the organ, and Q is the blood flow rate through the organ.

The instantaneous clearance and extraction ratio from a blood or plasma concentration–time profile can be derived by applying mass balance to the eliminating organ, as in Fig. 1.8. Assuming that the organ is a homogeneous compartment such that $C_{out} = C$, where C_{out} is the drug concentration leaving the organ, the mass balance equation is then

$$V\frac{dC}{dt} = Q \cdot C_{in} - Q \cdot C - r(C) \tag{1.37}$$

given that $C = 0$ at $t = 0$.

By dividing Eq. 1.37 by $Q \cdot C_{in}$, the resulting expression is

$$\frac{V}{Q \cdot C_{in}}\frac{dC}{dt} = 1 - \frac{C}{C_{in}} - \frac{r(C)}{Q \cdot C_{in}}. \tag{1.38}$$

The third term on the right side of Eq. 1.38 is the definition of extraction ratio. The expression for instantaneous extraction ratio and clearance can be derived as follows:

$$E = 1 - \frac{C}{C_{in}} - \frac{V}{Q \cdot C_{in}}\frac{dC}{dt} \tag{1.39}$$

$$CL = Q\left(1 - \frac{C}{C_{in}}\right) - \frac{V}{C_{in}}\frac{dC}{dt} \tag{1.40}$$

Both Eqs. 1.39 and 1.40 show that, in general, instantaneous extraction ratio and organ clearance are time-dependent variables. Therefore, they have no definitive meaning unless the time when clearance is estimated is specified, or steady state is achieved.

At steady state, both C and C_{in} are constant, such that $\frac{dC}{dt} = 0$. The steady-state extraction ratio and clearance can be derived from Eqs. 1.39 and 1.40:

$$E_{ss} = 1 - \frac{C}{C_{in}} \tag{1.41}$$

$$CL_{ss} = Q\left(1 - \frac{C}{C_{in}}\right). \tag{1.42}$$

Since instantaneous clearance is of not much value for nonsteady-state situation, the mean clearance over time is more useful and can be derived by rearranging Eqs. 1.35 and 1.36 and integrating from 0 to infinity with respect to time:

$$\int_0^\infty E \cdot C_{in} dt = \int_0^\infty \frac{r(C)}{Q} dt$$

$$\int_0^\infty CL \cdot C_{\text{in}} dt = \int_0^\infty r(C) dt.$$

Applying the mean integration theorem to the equations above, there exists a value θ for clearance such that $\int_0^\infty CL \cdot C_{in} dt = \theta \int_0^\infty C_{in} dt$. The value θ is the mean clearance over time from 0 to infinity. Equations for the computation of mean clearance and mean extraction ratio are shown in Eqs. 1.43 and 1.44:

$$\overline{CL} = \frac{\int_0^\infty r(C) dt}{\int_0^\infty C_{in} dt} \tag{1.43}$$

$$\overline{E} = \frac{\int_0^\infty r(C) dt}{Q \int_0^\infty C_{in} dt}. \tag{1.44}$$

Using the example of an eliminating organ in Fig. 1.8, integration of the mass balance Eq. 1.37 from $t=0$ to infinity,

$$V \int_0^\infty dC = \int_0^\infty \left[Q \cdot C_{in} - Q \cdot C - r(C) \right] dt. \tag{1.45}$$

For limited dosage regimens, if $t \to \infty$, $C_{in} \to 0$ and therefore $C \to 0$. Together with the initial condition that $C = 0$ at $t = 0$, the left side of Eq. 1.45 is 0. Thus,

$$0 = \int_0^\infty \left[Q \cdot C_{in} - Q \cdot C - r(C) \right] dt. \tag{1.46}$$

By rearranging and dividing Eq. 1.46 by $\int_0^\infty Q \cdot C_{in} dt$, we obtain

$$\frac{\int_0^\infty r(C) dt}{\int_0^\infty Q \cdot C_{in} dt} = 1 - \frac{\int_0^\infty C \, dt}{\int_0^\infty C_{in} dt}. \tag{1.47}$$

The left side of Eq. 1.47 is the term for the mean extraction ratio (see Eq. 1.44). From Eq. 1.47, one can derive the relationship between mean extraction ratio and clearance:

$$\bar{E} = \frac{\overline{CL}}{Q} = 1 - \frac{\int_0^\infty C\,dt}{\int_0^\infty C_{in}\,dt} \tag{1.48}$$

$$\overline{CL} = Q\left(1 - \frac{\int_0^\infty C\,dt}{\int_0^\infty C_{in}\,dt}\right). \tag{1.49}$$

For an eliminating organ, $\int_0^\infty C\ dt < \int_0^\infty C_{in} dt$ holds true. One can deduce that the mean clearance is always smaller than the blood flow rate and the extraction ratio is smaller than one.

It has been observed that for some xenobiotics, the estimated extraction is greater than one, which is impossible as the amount of drug being removed cannot be greater than the amount supplied to the organ. Using the same eliminating organ shown in Fig. 1.8, if clearance is calculated using the blood samples leaving the specific organ, we would divide Eq. 1.46 by $\int_0^\infty Q \cdot C\ dt$, where C is the drug concentration in the blood stream leaving the elimination organ. Following the same steps to derive Eq. 1.48, we obtain Eq. 1.50:

$$\frac{\overline{CL}_{out}}{Q} = \frac{\int_0^\infty C_{in}\,dt}{\int_0^\infty C\,dt} - 1. \tag{1.50}$$

As one can see that for a high extraction drug, it is possible that $\frac{\int_0^\infty C_{in}\,dt}{\int_0^\infty C\,dt} - 1$ is greater than 1. And if $\frac{\int_0^\infty C_{in}\,dt}{\int_0^\infty C\,dt} - 1 > 1$, the extraction ratio defined in Eq. 1.48 is larger than 1, and the estimated clearance will exceed the blood flow rate. The conversion between $\overline{CL}_{\text{out}}$ and $\overline{CL}$ can be derived from Eqs. 1.48 and 1.50, such that

$$\frac{\overline{CL}}{Q} = \frac{\overline{CL}_{out}}{Q + \overline{CL}_{out}}, \tag{1.51}$$

where $\overline{CL}_{out}$ refers to the clearance computed from the blood samples taken from the blood leaving the organ and $\overline{CL}$ is the clearance estimated from the blood entering

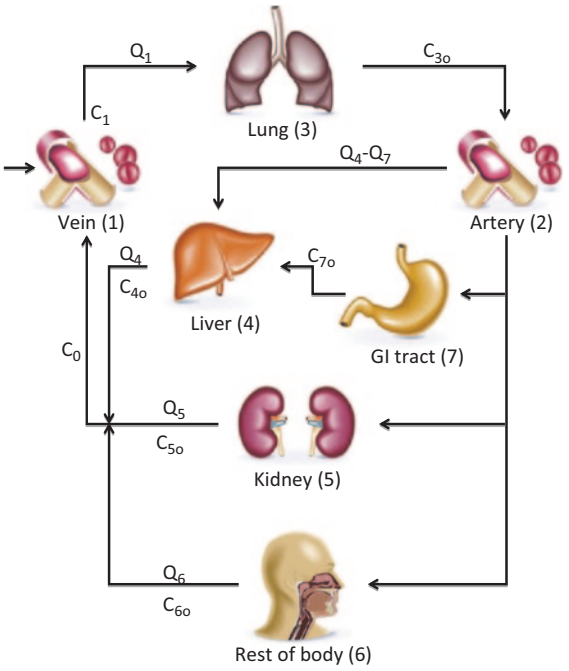

Fig. 1.9 A representative PBPK model used to illustrate total body clearance and organ clearance

the organ. The equation for extraction ratio, which is the left-hand side of Eq. 1.51, can be rearranged to obtain $\overline{CL}_{out}$ such that

$$\overline{CL}_{out} = \frac{\overline{CL}}{1-\overline{E}}. \tag{1.52}$$

We can extrapolate the result to total body clearance (TBC) in relation to cardiac output. The TBC, in this case, can also be greater than cardiac output for a compound that is rapidly eliminated through the lungs.

1.4.2 Establishing a General Relationship between TBC and Organ Clearance

It is often misunderstood that TBC is the sum of the individual organ clearance. The contribution of the organ clearance to the TBC depends on the anatomy of the body. In this section, we derived a general mathematical expression of the TBC with the individual organ clearance through PBPK modeling (Wang, Lam and Bischoff, unpublished work).

Figure 1.9 illustrates a representative PBPK model. This model consists of seven tissues, namely vein, artery, lung, GI tract, liver, kidney, and the rest of the body.

The first compartment C_1 represents the vein, second C_2 for the artery, third C_3 the lung, fourth C_4 the liver, fifth C_5 the kidney, sixth C_6 for the rest of the body, and seventh C_7 for the GI tract. In this example, an intravenous administration was utilized for the simplicity of the mathematical derivation. Assuming a flow-limited mass transfer, the equations representing the model based on mass balance are as shown in Eq. 1.53.

$$
\begin{aligned}
V_1 \frac{dC_{1(vein)}}{dt} &= Q_1 \cdot C_0 - Q_1 \cdot C_1 + K_I(t) \\
V_2 \frac{dC_{2(artery)}}{dt} &= Q_1 \cdot C_{3o} - Q_1 \cdot C_2 \\
V_3 \frac{dC_{3(lung)}}{dt} &= Q_1 \cdot C_1 - Q_1 \cdot C_{3o} - r_3(C_3) \\
V_4 \frac{dC_{4(liver)}}{dt} &= Q_7 \cdot C_{7o} + (Q_4 - Q_7) \cdot C_2 - Q_4 \cdot C_{4o} - r_4(C_4) \\
V_5 \frac{dC_{5(kidney)}}{dt} &= Q_5 \cdot C_2 - Q_5 \cdot C_{5o} - r_5(C_5) \\
V_6 \frac{dC_{6(rest\ of\ body)}}{dt} &= Q_6 \cdot C_2 - Q_6 \cdot C_{6o} \\
V_7 \frac{dC_{7(GI\ tract)}}{dt} &= Q_7 \cdot C_2 - Q_7 \cdot C_{7o} - r_7(C_7)
\end{aligned}
\tag{1.53}
$$

where $K_I(t)$ is the drug input function, $r_i(C_i)$ represents the rate of elimination from an eliminating organ, and the subscript o for out symbolizes the concentration leaving the organ. The initial conditions were assumed such that $C_i = 0$ at $t = 0$. The drug concentration at the joint point where the blood stream leaves the organ is represented by Eq. 1.54:

$$
Q_1 \cdot C_0 = Q_4 \cdot C_{4o} + Q_5 \cdot C_{5o} + Q_6 \cdot C_{6o}. \tag{1.54}
$$

Given the relationship above, we solve for the venous compartment C_1 (see Appendix for details), assuming that the input function $K_I(t) = 0$ and $C_i \to 0$ as $t \to \infty$:

$$
\begin{aligned}
&\int_0^\infty Q_1(C_1 - C_{3o})dt + \int_0^\infty Q_4(C_p - C_{4o})dt + \int_0^\infty Q_5(C_2 - C_{5o})dt \\
&\quad + \int_0^\infty Q_7(C_2 - C_{7o})dt = \int_0^\infty K_I(t)dt,
\end{aligned}
\tag{1.55}
$$

where $Q_4 \cdot C_p = Q_7 \cdot C_{7o} + (Q_4 - Q_7)C_2$.

Using Eq. 1.49 to compute the mean organ clearance, the generalized expression, except for the lung and liver, is shown in Eq. 1.56:

$$\overline{CL_i} = \frac{Q_i \int_0^\infty (C_2 - C_{io})dt}{\int_0^\infty C_2 dt} \in i \neq 3,4. \tag{1.56}$$

For the lung and liver compartments (C_3 and C_4), the resulting expressions for mean organ clearance are as follows:

$$\overline{CL_3} = \frac{Q_1 \int_0^\infty (C_1 - C_{3o})dt}{\int_0^\infty C_1 dt} \tag{1.57}$$

$$\overline{CL_4} = \frac{Q_4 \int_0^\infty (C_p - C_{4o})dt}{\int_0^\infty C_p dt}. \tag{1.58}$$

The total amount of drug elimination from the body, derived from solving the mass balance equations over the entire body, is $\int_0^\infty \sum_i r_i(t)dt = Q_1 \int_0^\infty (C_1 - C_0)dt = \int_0^\infty K_I(t)dt$. Following the expression in Eq. 1.43 for mean clearance, TBC or systemic clearance is derived as

$$\overline{CL}_{\text{total}} = \frac{Q_1 \int_0^\infty (C_1 - C_0)dt}{\int_0^\infty C_1 dt} = \frac{\int_0^\infty K_I(t)dt}{AUC} = \frac{Dose}{AUC}. \tag{1.59}$$

By substituting Eqs. 1.56–1.58 into Eq. 1.55, the relationship between TBC and organ clearance can be obtained as shown in Eq. 1.60 (see Appendix for derivation of Eq. 1.60):

$$\overline{CL_{total}} = \overline{CL_{lung}} + (1 - \bar{E}_{lung})\left[\overline{CL_{liver}} + (1 - \bar{E}_{liver})\overline{CL_{GI}} + \overline{CL_{kidney}}\right], \tag{1.60}$$

where $\bar{E}_i = \frac{\overline{CL_i}}{Q_i}$. A generalized relationship between TBC and organ clearance can then be established by extrapolating Eq. 1.60 to multiple eliminating organs:

$$\overline{CL_{systemic}} = \overline{CL_{lung}} + (1 - \bar{E}_{lung})\left[\overline{CL_{liver\_channel}} + \sum_i \overline{CL_i}\right], \tag{1.61}$$

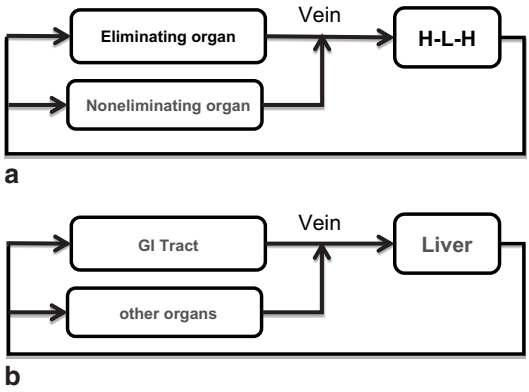

Fig. 1.10 Schematic illustration of **a** the left heart–lung–right heart (*H–L–H*) circulatory system and **b** the liver channel

where $\overline{CL}_{liver\_channel} = \overline{CL}_{liver} + (1-\bar{E}_{liver})\sum_j \overline{CL}_j$, and j indicates other organs except the liver in the liver channel. The subscript i in Eq. 1.61 includes all other body organs except the lungs and organs in the liver channel.

The mathematical equation in Eq. 1.61 is broadly applicable not only to the linear systems but also to the nonlinear systems because the assumption made in the derivation of Eq. 1.61 was flow-limited mass transfer. From Eq. 1.61, one can deduce that the contribution of organ clearance to the systemic clearance can be derived by following the circulation scheme starting from the arteries. For those organs connected in parallel, the contribution of organ clearance to systemic clearance is additive. For the organs connected in series, the contribution of the *i*th organ clearance to systemic clearance needs to be corrected by a factor of $(1-\bar{E}_{next\ organ})$. For example, following the blood circulation starting from the artery, the whole body can be viewed as consisting of two components connected in series, the rest of the body and the lung. Hence, in Eq. 1.61, the clearance of the portion that represents the rest of the body needs a correction factor of $(1-\bar{E}_{lung})$, as illustrated in Fig. 1.10a. The same is true for the liver channel such that the clearance of the GI tract or spleen also requires a correction factor $(1-\bar{E}_{liver})$, as represented in Fig. 1.10b.

The PBPK model used in this discussion is a lumped total body model but represents a rather general description of the anatomical structure of the mammalian system. The expression describing TBC and the individual organ clearances can be easily derived based on the location of the eliminating organ by following the circulation starting from the arteries. For these organs that are connected in series, the contribution of the first organ clearance to TBC equals $(1-\bar{E}_{i+1})\overline{CL}_i$, whereas for organs connected in parallel, the contribution of organ clearance to TBC is additive. Even though the current discussion only considered the example of an intravenous administration, the conclusions derived from this scenario are broadly applicable to other routes of administration.

1.5 Population PK

PBPK models provide the quantitative information between the dose and the concentration of the xenobiotic agent at different regions of the body. Interindividual variability in PK can be quantified based on the physiological/biological difference among the target population. However, it is often impractical to apply PBPK models directly to humans. The nonlinear mixed effect model (also commonly referred to as population PK) incorporating both fixed effect (identified covariates representing the known source of variability) and random effect (unidentified source of variability) was introduced in the 1970s by Sheiner et al. (1977). This approach adopts the simplicity of the classical PK models but correlates the PK parameters to covariates such as body weight, age, gender, etc. to quantify the source of variability in PK. For example, the volume of distribution is often correlated to the body size, and clearance to body weight, creatinine clearance, and enzyme activities. Covariate analysis is primarily performed through statistical analysis, together with the information on physiology, pathology, metabolism, and clinical relevance. The population PK modeling has been widely applied to the analysis of clinical PK data, especially to the sparse PK samples from phase 2/3 trials. With this approach, the source of variability in PK can be identified using large pooled datasets. More importantly, population PK modeling has innovated the drug development through model-based approach (Bhattaram et al. 2005). From what used to be an unusable sparsely sampled blood concentration from phase 2/3 trials, population PK modeling made it possible to identify the PK characteristics in patients based on their demographic information, metabolic status, liver/kidney function, and disease status to support labeling. This ability to hone into a specific factor responsible for drug response is what makes population PK a valuable tool for personalized medicine. In a survey from the US FDA between 2000 and 2004, they reported that pharmacometric analyses were pivotal in regulatory decision making in more than half of the 42 new drug applications (NDA; Bhattaram et al. 2005). In the case of a failed trial of nesiritide, they concluded that “dose selection based on pharmacometric analysis could have saved 3 years of drug development time and 1 clinical trial.”

1.5.1 Population PK Model Development

A population PK model consists of the structural model and the covariate models. The structural model takes the form of the classical compartment model to describe the concentration profile for a typical subject, whereas the covariate model quantifies the sources of intersubject variability: the known (covariates) and unknown (first level random effect term) source of variability (Sheiner and Ludden 1992; Sheiner et al. 1977). The second level of variability is within-subject variability that is often described by additive or proportional error model. Sometimes, a third level variability, called inter-occasion variability, is introduced to describe the variability for the same individual when replicate samples were taken following different dosing occasions.

Population PK model development and key considerations were clearly discussed in Meibohm et al. (2005) and regulatory documents (EMA 2007; FDA 1999), which include base model and covariate model development, internal and/or external model validation. The base model development follows the same principles as classical compartmental PK model development. Covariate model development and model validation will be described briefly in the following sections.

1.5.2 Covariate Models

Covariate models quantify the source of intersubject variability contributing to a PK parameter. For continuous covariates, the covariate model usually takes the form of a linear or power function, which probably originated from the allometric scaling concept. Different ways of parameterization of the covariate model are often done using the reference value of the covariate such as the median value, as shown in Eqs. 1.62 and 1.63:

$$TVP = \theta_0 + \sum_{i=1}^{m} \theta_i (Cov_i - Ref_i) \tag{1.62}$$

$$TVP = \theta_0 \prod_{i=1}^{m} \left(\frac{Cov_i}{Ref_i} \right)^{\theta_i} \tag{1.63}$$

where TVP is the typical value of a model parameter, Cov represents the covariates, m is the number of covariates, and θ_i is the coefficient.

For categorical covariates such as binary, ordered, or nonordered, an indicator function $I_i(Cov_i)$ is introduced such that if the covariate has a specific dummy variable value, a separate coefficient is designated:

$$TVP = \theta_0 + \sum_{i=1}^{m} \theta_i I_i (Cov_i) \tag{1.64}$$

$$TVP = \theta_0 \prod_{i=1}^{m} I_i (Cov_i)^{\theta_i} \tag{1.65}$$

and

$$I_i(Cov_i) = \begin{cases} 1, \text{if } i = i \\ 0, \text{otherwise} \end{cases} \tag{1.66}$$

Random effect is usually assumed to be log-normally or normally distributed, as given in Eq. 1.67, where n_j follows a normal distribution with mean 0 and covariance matrix Ω:

$$P_j = TVP \times \exp(\eta_j) \quad \text{or} \quad P_j = TVP + \eta_j. \tag{1.67}$$

1.5.2.1 Allometric Scaling

One of the approaches for covariate model development is by applying allometric scaling principle. Thus, the body weight often contributes to clearance to the power of 0.75 and to the volume of distribution to the power of 1. The allometric scaling is also often used for scaling PK parameters obtained from the adult to the pediatric population.

1.5.2.2 Stepwise Regression

Stepwise regression is a common statistical method used in covariate model building. The algorithm includes forward addition, backward elimination, or combination of forward addition and backward deletion in stepwise fashion. This process is automated in Perl-Speaks-NONMEM. Each step of the model building process in the forward inclusion involves testing the effect of each covariate on the appropriate model parameter in a separate model run, such that the statistical significance of each covariate–parameter relationship is screened individually (univariate analysis). Covariates that reduce the objective function above a predefined significance level are added to the PK model. The backward elimination step starts with the final model from the forward inclusion step; the subsequent removal of each covariate is also based on a predefined difference in the objective function. The hypothesis testing to discriminate alternative hierarchical models is based on the likelihood ratio test, often at preset *p*-values for the forward inclusion and backward elimination of, e.g., 0.05 and 0.01, respectively. The differences in the objective function values of two alternative models is equivalent to −2 log-likelihood, which follows a chi-squared distribution with *n* degrees of freedom, where *n* is the difference in the number of parameters in the hierarchical models. A difference of 3.84 and 6.64, for example, in the value of the objective function is considered significant under the likelihood-ratio test for $n = 1$ and *p*-values of 0.05 and 0.01, respectively.

1.5.2.3 Full Covariate Model

Because covariates often have collinearity and depending on the degree of correlation between covariates, the statistical inference approach such as stepwise methods could include a covariate that is not preferential. An algorithm of using full covariate model approach was proposed as an alternative for covariate model building (Agoram et al. 2006; Ravva et al. 2009). The decision on which covariate to include is based on exploratory graphics, scientific and clinical interest, mechanistic plausibility, or previous knowledge of these relationships. Covariates that are both statistically insignificant and clinically irrelevant can be dropped during covariate model development. The inferences on which covariate has clinical importance are then based on the magnitude of the estimated effect and the precision (Agoram et al. 2006). This approach is a simplification of the global model approach (Burnham

and Anderson 2002) and is claimed to be the preferred choice when the goal is to estimate the magnitude of an effect (Harrell 2001). A hybrid approach can also be implemented, starting with a full covariate model from which covariates are tested using stepwise backward deletion.

1.5.2.4 Case Deletion to Determine Influential Individual

The statistical inferences based on maximum likelihood or likelihood ratio test are easily influenced by outliers or a few individuals (not necessarily outliers) in the data. Influential individual or a group of influential individuals can be evaluated using case-deletion diagnostics. The jackknife method evaluates how removing a specific individual affects the objective function values of the base model and the one with covariate, both models with all the data versus the one with the specific individual removed (Sadray et al. 1999):

$$\Delta OFV_{jackknife,i} = (OFV_{final,n} - OFV_{basic,n}) - (OFV_{final,n-1} - OFV_{basic,n-1}). \quad (1.68)$$

The algorithm fits both the covariate model and the base model to the dataset containing all the individuals and the dataset with the specific individual removed. The $\Delta OFV_{jackknife,i}$ value in Eq. 1.72 is obtained for each individual of the dataset. The "shark" plot with the number of subjects removed on the *x*-axis and the change in OFV on the *y*-axis and curves showing both positive and negative ΔOFV_i can be used as visual inspection for case-deletion diagnostics.

1.5.2.5 Covariate Identification Through PBPK Modeling

As mentioned in the section of PBPK modeling, lumping has been used to simplify the complicity of a PBPK model without losing the key physiological reality of the model. During the lumping process, covariates having impact on the PK can be identified. This approach requires a PBPK model that can be developed using preclinical data. Sensitivity analysis of the PBPK model can also assist in identifying the factors that could have significant impact on the disposition of a xenobiotic.

The example below demonstrating the advantage of using PBPK modeling to identify the covariate was from a collaboration between Bischoff and Stanski in the early 1990s (Bischoff 1992). It was observed that the amount of thiopental needed to be administered to elderly patients (about 70–80 years old) was much less than that used for a standard 30-year-old healthy male. Therefore, age could be considered as a covariate for dose adjustment for thiopental based on the classical PK and population PK models. To investigate the age effect on thiopental PK, a PBPK model (Bischoff and Dedrick 1968) was applied to the PK data obtained from clinical studies. An adipose tissue compartment was included in the PBPK model for thiopental, as this compound is highly lipophilic. The differences in cardiac outputs between young adult subjects at 30 years of age versus the geriatric patients at 70 years

were taken into account in the PBPK model. By incorporating the physiological difference in cardiac output between the two age groups, the PBPK model captured well the difference in the exposure of thiopental for patients at age 30 versus those at 70 years, without having to incorporate age as a covariate of the model. This work was continued by Wada and colleagues to demonstrate the underlying mechanism behind the observed age effect in thiopental PK (Wada et al. 1997). Their results showed that the difference were due to the decline in cardiac output, followed by the increase in fat content with age. Since the cardiac output starts to decline at approximately 40 years of age, a nonlinear covariate equation to link clearance with age would be necessary. However, using the known data of age and gender differences in cardiac output and BMI (Brandfonbrener et al. 1955; Freedson et al. 1979; Guyton and Hall 1996), the change in clearance and volume of distribution of thiopental with age can be derived from these relationships.

1.5.2.6 Clinical Relevance in Covariate Model Development

Clinical relevance is a key consideration in covariate model assessment. In general, if the contribution of a covariate to the PK parameters resulted in less than 20% difference in systemic exposure using the bioequivalence (BE) criteria, this covariate can be ignored or dropped even though it is shown to be statistically significant. Sometimes, if a drug has a large therapeutic window and the influential covariate determined from the PK analysis does not have any significant impact on clinical endpoints, this covariate can be removed. In contrasting situations, the lack of statistical significance does not necessarily indicate that the covariate tested is lacking impact on the clinical endpoints. For example, due to limited sample size (< 10% of the subjects with a specific co-medication) or limited range of the covariate tested such as age, the impact of co-medication or age effect on the PK may not be statistically significant.

1.5.2.7 Power and Sample Size Calculation

Sample size (the total number of subjects and the sampling time per subject) is critical for population PK development. To be able to detect the interindividual and intraindividual variability, a minimum of two PK samples per subject is necessary. Ogungbenro and Aaron have demonstrated the minimal samples size requirement for a one- or two-compartmental PK model (Ogungbenro and Aarons 2008) based on the confidence interval of the PK parameters estimated.

Another statistical methodology called the Monte Carlo Mapped Power (MCMP) to determine the power and sample size calculation for covariate model development was introduced by Vong et al. (2012). Using the difference in individual's objective function values between the reduced and full models ($\Delta iOFV = iOFV_{reduced} - iOFV_{full}$), the MCMP analysis tests for drug or covariate effect by the summation of the individual's contribution to the overall objective

function value in the likelihood ratio test (Vong et al. 2012). The MCMP uses the sum of the n $\Delta iOFV$ instead of the overall ΔOFV to base its statistical inference. The algorithm maps the statistical power over a specified sample size range. The MCMP method is simple to run without the need for correcting for type I error that is associated with stochastic simulations and estimations (Ette et al. 1998; Kowalski and Hutmacher 2001; Lee 2001).

1.5.2.8 Model Evaluation

Model evaluation is a key step in population PK model development. Diagnostic plots, bootstrap, shrinkage in the η (Savic and Karlsson 2009), prediction-corrected visual predictive check, internal validation through dataset split are often used to evaluate the model. In addition to those approaches, external validation with additional datasets is a preferable method when feasible.

1.5.3 Application of Population PK Model

Since Sheiner's first and subsequent publications that established the population PK model methodology, population PK modeling and simulation together with information on disease progression, placebo response, dropout rates, as well as exposure–response (ER) of drug treatment, have been used in regulatory decision making, clinical trial waiver, as well as identification of design flaws and trial implementation problems prior to running a trial. These strategies have shown to decrease costs, improve the likelihood of achieving the trial goals, and generate conclusive findings (Brindley and Dunn 2009; Holford et al. 2010). Kimko and Peck recently edited a textbook on clinical trial simulation that encompasses diverse areas relevant to drug development such as metabolic disease, cardiovascular, infectious disease, oncology, and many other fields (Kimko and Peck 2011).

Yang et al. took an approach of incorporating a case–control comparison in the ER analysis to reduce the bias introduced by confounding risk factors when evaluating the recommended dosing regimen for trastuzumab in a registration trial (Yang et al. 2012). Their analysis suggested that patients with the lowest quartile of trastuzumab exposure did not benefit from addition of trastuzumab treatment to chemotherapy. However, contrary to the nonresponder hypothesis for this subgroup with the lowest quartile of tratuzumab, this subgroup appeared to be more sensitive to a higher trastuzumab exposure than the remaining 75 % population, suggesting that increasing trastuzumab exposure in the low-exposure subgroup may result in better overall survival (OS) benefit. This analysis justified the FDA recommendation of conducting postmarketing clinical trials to investigate a dosing regimen with higher exposure and acceptable safety in the identified subgroup and to prospectively evaluate whether this regime will result in acceptable OS benefit.

Other examples can be found from the approval of the 0.8 mg/kg once-weekly regimen of etanerceptin pediatric patients with juvenile rheumatoid arthritis. The clinical trial simulation confirmed that the 0.8 mg/kg once weekly yielded overlapping steady-state time–concentration profiles with that of 0.4 mg/kg SC twice weekly, leading to equivalent clinical outcomes (Yim et al. 2005).

The author (Wang) utilized model-based approach to apply for waiver of clinical pharmacology trial for a novel tyrosine kinases inhibitor that was under development in oncology. The absolute bioavailability of the tablet was required in the NDA submission. However, to conduct a clinical trial to obtain the absolute bioavailability was difficult, since the intravenous dosage formulation needed to be developed, and the study can only be conducted in cancer patients due to genotoxicity. A population PK model of the PK datasets obtained from several phase I dose escalation trials with either oral solution or tablet was developed with the formulation as one of the covariates. Covariate model test demonstrated that the formulation was not a statistically significant covariate. The health authority accepted this approach and a standalone absolute bioavailability trial was no longer required. The example listed above demonstrates how the model-based approach can cut development costs, as well as improve trial designs to come to conclusive findings.

1.6 PD Models for Continuous Response Variables

PD often refers to as the body's response to drug. Derendorf et al. defined PD as "a broad term that is intended to include all pharmacological actions, pathophysiological effects and therapeutic responses, both beneficial and adverse, of an active drug ingredient, therapeutic moiety, and/or its metabolite(s) on the various systems of the body from subcellular effects to clinical outcomes. Pharmacodynamic studies can provide information about a drug's mechanism of action or about its dose-response relationship where response can be expressed as a direct or indirect measure of efficacy and/or safety of the drug" (Derendorf et al. 2000). As collecting biomarker information is becoming common in clinical trials, modeling the exposure and biomarker responses has become critical in model-based drug development.

PK/PD studies intend to link the dose–exposure profile relationship with the PD response, in particular, the time course of the pharmacological/pathophysiological effects (Derendorf et al. 2000). Integrated PKPD models are categorized according to the manner in which the PK and PD data are related. The two types of basic PD models that are often used to establish PKPD relationships are the direct and indirect response models. Based on receptor theory, the response of a drug is triggered by the free drug concentration at the site of action. Since the systemic blood or plasma drug concentration samples were collected during a trial, while the effect or response is dependent on the concentration at the effect site, a delay in response might be observed when linking the blood/plasma concentration to the drug response. If the effect is further downstream in the process, a longer delay in response could be observed.

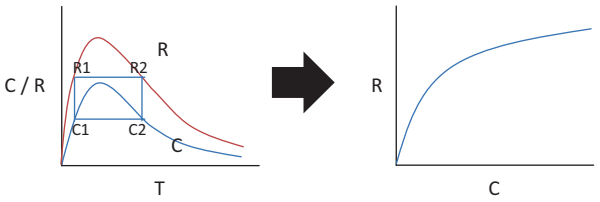

Fig. 1.11 Relationship between drug concentration and response in a direct response relationship

1.6.1 Direct response PD Model

In the direct response model, the linear, E_{max}, or sigmoidal E_{max} models are often used. Equation 1.69 is the expression for the sigmoidal E_{max} model. When γ equals 1, it is the called the E_{max} model:

$$E(C) = E_0 \pm \frac{E_{max} C(t)^{\gamma}}{EC_{50}^{\gamma} + C(t)^{\gamma}}, \tag{1.69}$$

where E_0 is the baseline of the response and E_{max} is the maximum response. C is the concentration of drug and $C(t) = \frac{\text{Dose}}{V} e^{-\frac{CL}{V}t}$ is the drug concentration at which 50% of the maximum response is achieved and γ is the sigmoidicity factor that determines the steepness in the linear portion of the curve. The direct response relationship assumes that the processes involved in the drug transfer to the site of action and eliciting the response is rapid enough compared to the disposition of a drug. Thus, for the same drug concentration, the response elicited by the drug is the same, regardless of the time to reach that drug concentration. As shown in the left panel of Fig. 1.11, the concentration $C1$ in the ascending phase of the concentration–time profile with the equivalent concentration level at $C2$ in the descending phase has a corresponding response $R1$ in the ascending phase of the response profile and the equivalent response level $R2$ in the descending phase. In other words, there is only one value for the response corresponding to one value for the drug concentration, as shown in the right panel of Fig. 1.11.

1.6.2 Indirect Response Model

It is often the case in pharmacology that the effect of the pharmacological agent is lagging behind the drug concentration–time course, where, the response versus concentration does not exhibit a one-to-one relationship, often called a hysteresis loop (counterclockwise hysteresis), as shown in the right panel of Fig. 1.12. The temporal dissociation between the time courses of drug concentration and effect results in the hysteresis pattern and is likely caused by a distributional delay between the drug concentrations in the plasma and the effect site (Derendorf et al. 2000).

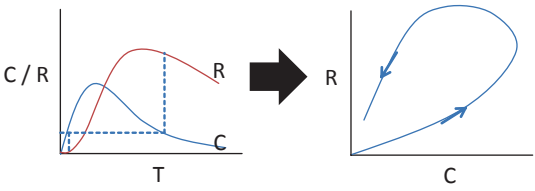

Fig. 1.12 Relationship between drug concentration and response in an indirect response relationship

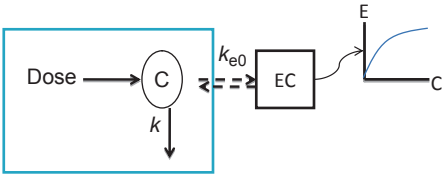

Fig. 1.13 Schematic representation of the effect compartment linking to a pharmacodynamic model

The two different approaches often used to describe the observed delay in the plasma concentration and drug response are the effect compartment model originally proposed by Sheiner et al. (1979) and the indirect response model with differential equation by Jusko (Dayneka et al. 1993; Jusko and Ko 1994).

1.6.2.1 Effect-Compartment PD Model

The effect-compartment model links the drug effect to the drug concentration of a hypothetical effect compartment (Sheiner et al. 1979), instead of the drug concentration in the systemic circulation. In the effect-compartment model, it was assumed that the drug amount entering the effect compartment is negligible, so that the plasma concentration of the central compartment can be described without the mass transfer between the central compartment and the effect compartment. The drug concentration in the effect compartment is at equilibrium with that of the central compartment. The equilibration process between the plasma drug concentration and the effect site is determined by the first-order rate constant k_{e0} that also describes the loss of drug from the effect compartment (Derendorf et al. 2000). The illustration in Fig. 1.13 shows a schematic representation of the link model, where EC refers to the effect compartment. When the drug response links to the drug concentration of the effect compartment, the hysteresis observed will be collapsed.

Equations for calculating the effect compartment concentration can be found in Gabrielsson and Weiner (2000). For example, for a one-compartment model with bolus injection, the plasma concentration can be calculated using Eq. 1.4, and the effect compartment concentration can be expresses as:

$$C_e = \frac{Dose \cdot k_{e0}}{V_e\left(k_{e0} - \frac{CL}{V}\right)}\left(\exp\left(-\frac{CL}{V}\cdot t\right) - \exp(-k_{e0}\cdot t)\right), \tag{1.70}$$

where C_e is the drug concentration in the effect compartment, V_e is the volume of the effect compartment.

1.6.2.2 Indirect Response Models

The indirect response models was developed based on the receptor theory and signal transduction, where a series of delay could occur during those processes caused by indirect-response mechanism such as a synthesis or dissipation of an endogenous substance or response mediator. Dayneka et al. proposed four basic models for indirect PD response (Dayneka et al. 1993; Jusko and Ko 1994). The generalized form of the indirect response models in the absence of drug is described as follows:

$$\frac{dR}{dt} = k_{in} - k_{out}R, \tag{1.71}$$

where k_{in} is the zero-order constant for the production of the response, and k_{out} refers to the first-order rate constant for the dissipation of response. A biological system should stay at steady state under normal condition when no drug intervention is applied. Therefore, at baseline $R_o = \frac{k_{in}}{k_{out}}$.

The four indirect response models under drug intervention are shown below:

$$\frac{dR}{dt} = k_{in}I(C_p) - k_{out}R \tag{1.72}$$

$$\frac{dR}{dt} = k_{in} - k_{out}I(C_p)R \tag{1.73}$$

$$\frac{dR}{dt} = k_{in}S(C_p) - k_{out}R \tag{1.74}$$

$$\frac{dR}{dt} = k_{in} - k_{out}S(C_p)R, \tag{1.75}$$

where $I(C_p) = 1 - \frac{C_p}{C_p + IC_{50}}$ represents the classical inhibitory function and $S(C_p) = 1 + \frac{E_{\max} \cdot C_p}{EC_{50} + C_p}$ is the stimulation process using an $E_{\max}$ model. The schematic representations of the indirect response models showing effect on the synthesis and dissipation processes are presented in Fig. 1.14.

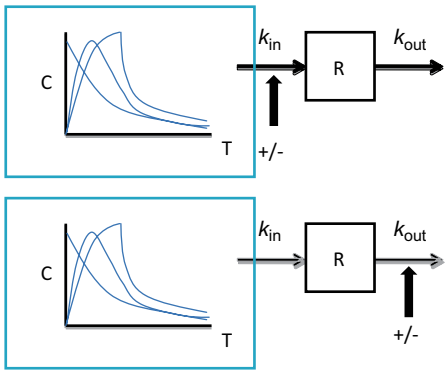

Fig. 1.14 Schematic representation of an indirect response—stimulation or inhibition of synthesis (*top*) and dissipation rates (*bottom*)

The indirect response model was used to fit to the data of the inhibition of prothrombin complex activity by warfarin, an oral anticoagulant used in thrombophlebities and pulmonary embolism (Jusko and Ko 1994). It blocks the vitamin K epoxide reductase, an enzyme that reduces vitamin K epoxide to vitamin K, which is a cofactor for carboxylation of the clotting factor such as factor II, VII, IX, and X. The blockade of the reductase activity by warfarin leads to the inhibition of coagulation, measured by the prothrombin time. It is assumed that the clotting factors are synthesized with a zero-order rate constant, k_{in}, and degraded with a first-order rate constant, k_{out}.

1.7 PD Models for Noncontinuous Response

Data collected from clinical trials, which are not continuous but categorical variables, can be dichotomous, ordinal scaled (e.g., none/mild/moderate/severe), or censored data (e.g., time to recurrence of a disease). Logistic regression and survival models are usually applied to describe the probability of events. Recently, Markov chain models to estimate event probability were also applied in pharmacometrics (Bizzotto et al. 2011; Lacroix et al. 2009; Sy et al. 2013a).

1.7.1 Time to Event

In the time to event analysis, the time of origin in pharmacometric analysis is usually the start of treatment. If the endpoint is some events, such as the occurrence of an adverse event, relapse of a disease, death, etc., the observations, which are the difference between the time of the specific event and the time from the origin, are referred to as time to event data or survival times. The distribution of time to event data is usually not normal and the data are often "censored." Right censoring refers to data that the specific event of interest has not yet occurred when the subjects

leave the study. Left censoring can occur in clinical studies when we know that the event of interest has already occurred at the observation time, but it is not known exactly when. For example, a patient may be tested positive for a specific disease but the exact time of the disease onset is unknown.

The survivor function, $S(t)$, is defined as the probability that the event of interest has not occurred by duration t, such that

$$S(t) = \Pr\{\mathrm{T} > t\} \tag{1.76}$$

where T denotes the time of an event; Pr stands for probability. The probability that the event has occurred by duration t, $F(t)$, is defined as the complement of the survivor function, which is 1-$S(t)$. The survivor function is related to the hazard function $h(t)$ and the cumulative hazard $H(t)$, as defined in Eqs. 1.77–1.79 (Collett 1994). One can obtain the hazard function by dividing the event density function $f(t)$ by the survivor function.

$$S(t) = \exp\left[-H(t)\right] \tag{1.77}$$

$$h(t) = \lim_{\Delta \to 0} \frac{\Pr\{t < T \le t + \Delta \mid T > t\}}{\Delta} = \frac{f(t)}{S(t)} = -\frac{\partial \log S(t)}{\partial t} \tag{1.78}$$

$$H(t) = -\log S(t). \tag{1.79}$$

Figure 1.15 shows representative examples of cumulative distribution, probability density, survival, and hazard functions.

With nonparametric and semi-parametric methods, namely the Kaplan–Meier estimate of the survivor function and the Cox proportional hazard model, which is an extension of the Kaplan–Meier method, the form of the baseline hazard is not specified. The form of the covariate relationship, however, is specified in the Cox proportional hazard model.

With parametric models, both the hazard function and the effect of covariates are explicitly defined. Holford argued for using a parametric model for the hazard function because "hazard is the way to introduce biological mechanism to the survival model and understanding the variability of time to event distributions" (Holford 2013). Table 1.4 lists the density, hazard, and survivor functions for the commonly used parametric models. Figure 1.15 shows the example of the probability density function and the corresponding hazard function for the exponential and Weibull distributions. In the exponential example, the hazard is a constant over time. This may not be the case in most clinical situations.

The Weibull model is more flexible as well as more generalized than the exponential model; the hazard rates are monotonic in the sense that the hazard is either increasing, decreasing, or constant over time. The hazard for a Weibull cannot be

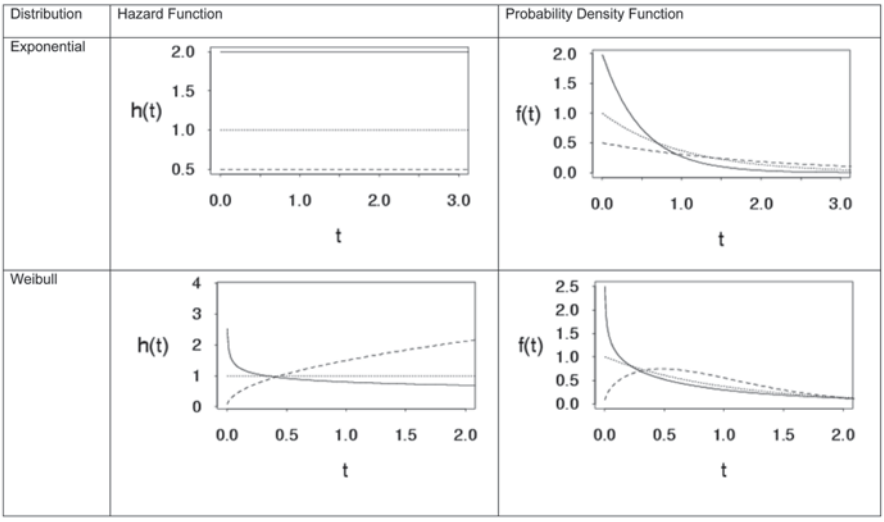

Fig. 1.15 Example of baseline hazard and the corresponding probability density functions for exponential and Weibull distribution

a combination of increasing and decreasing trends. The shape parameter, p, determines the trend. When $p<1$, the hazard is decreasing monotonically. For $p>1$, the hazard is increasing with time. With $p=1$, the Weibull becomes an exponential function and the hazard is constant. The log-logistic model allows for nonmonotonic hazards. The shape parameter, p, determines the trend such that if $p>1$, then the hazard increases and then declines whereas if $p<1$, the hazard has a decreasing trend.

The Kaplan–Meier type estimate is useful for determining the appropriate hazard function to use. The ratio of the number of events (δ_j) and the number of individuals at risk at the time ($n_j\tau_j$) is the hazard in the time interval from t_j to t_{j+1}:

$$h(t)=\frac{\delta_j}{n_j\tau_j}, \tag{1.80}$$

where n_j is the number of individual who has not had the event and therefore at risk of the event and τ_j is the time interval computed as $t_{j+1}-t_j$. The plot of time versus $h(t)$ provides a visual inspection of the trend of the hazard function.

The proportional hazard is one of the methodologies to introduce and evaluate a nontime-varying covariate effect, the other being accelerated failure time, which will not be discussed. Assuming a set of nontime-varying covariate vector $X=\left[X_1,X_2,\cdots,X_n\right]$, the proportional hazard function can be setup as

$$h(t,X)=h_0(t)\exp(\beta^T X), \tag{1.81}$$

Table 1.4 Relationship between density, survival, hazard, and likelihood functions for exponential, Weibull, and log-logistic parametric models

Parametric model	Density, f(t)	Survival,S(t)	Hazard, h(t)	Likelihood, L
Exponential	$\lambda \exp(-\lambda t)$	$\exp(-\lambda t)$	λ	$\prod_{i=1}^{N}\left\{\lambda \exp(-\lambda t)\right\}^{e_i}\left\{\exp(-\lambda t)\right\}^{1-\delta_i}$
Weibull	$\lambda p(\lambda t)^{p-1}\exp(-\lambda t)^{p}$	$\exp(-\lambda t)^{p}$	$\lambda p(\lambda t)^{p-1}$	$\prod_{i=1}^{N}\left\{\lambda p(\lambda t)^{p-1}\exp(-\lambda t)^{p}\right\}^{\delta_i}\left\{\exp(-\lambda t)^{p}\right\}^{1-\delta_i}$
Log-logistic	$\dfrac{\lambda^{p}t^{p-1}}{\left\{\frac{1}{p}\left[1+(\lambda t)^{p}\right]\right\}^{2}}$	$\dfrac{1}{1+(\lambda t)^{p}}$	$\dfrac{\lambda^{p}t^{p-1}}{\frac{1}{p}\left[1+(\lambda t)^{p}\right]}$	$\prod_{i=1}^{N}\left\{\dfrac{\lambda^{p}t^{p-1}}{\left\{\frac{1}{p}\left[1+(\lambda t)^{p}\right]\right\}^{2}}\times\dfrac{1}{1+(\lambda t)^{p}}\right\}^{\delta_i}\left\{\dfrac{1}{1+(\lambda t)^{p}}\right\}^{1-\delta_i}$

where $h_0(t)$ is the baseline hazard that depends on t but not X and $\beta^T X$ is $\beta_1 X_1 + \beta_2 X_2 + \cdots + \beta_n X_n$. A covariate, for example the presence of a specific disease, has an effect on the hazard and the coefficient, $\beta_{disease} = 1.39$. The relative risk for individuals with the disease is approximately fourfold (since $\exp(1.39) = 4$) that of the healthy individual. We recently applied the proportional hazard model in pharmacogenomics to evaluate the influence of *CYP3A5* and *ABCB1* polymorphisms on the renal transplant patient's relative risks for adverse events associated with tacrolimus (Sy et al. 2013b). The study used a marginal proportional hazard model with common baseline hazard to adjust for possible correlations between multiple incidents of adverse events, given that each patient can have multiple adverse events which were considered competing risks (Sy et al. 2013b; Wei et al. 1989; Wei and Glidden 1997). The marginal semi-parametric model is not without its criticism. The most frequent concern being raised is its assumption that each individual is considered to be at risk of all recurrent events from the start (Metcalfe and Thompson 2007). This assumption apparently would result in estimates that exceed those provided by alternative approaches. However, the marginal approach is considered to be the lesser of the two evils, with the alternative being one that does not consider a marginal model for repeated events from the same individual. For the parametric approach, the frailty model where the random effect has a multiplicative effect on the hazard can be used to handle recurrent events coming from the same individual. As pointed out by Hougaard, the limitation of the frailty model is the standard assumption of using a gamma distribution for frailty which puts more importance on late events (Hougaard 1995).

One can treat frailty as multiplicative of the hazard term such that

$$h(t_{ij} \mid \boldsymbol{X}_{ij}, \nu_i) = h_0(t_{ij})\nu_i \exp(\beta \boldsymbol{X}_{ij}), \tag{1.82}$$

where j refers the individual and i is the subgroup, and the frailty term is $\nu_i = \exp(W_j \psi)$. W_j is the "frailty" sampled from a distribution with mean 0 and a variance 1. If ψ is 0, we have a standard proportional hazard. The hazard rate above is conditional on both the covariates and the frailty term and so is the survivor function,

$$S\left(t_{ij} | \boldsymbol{X}_{ij}, \nu_i\right) = \exp\left(-\int_0^t h(u \mid \nu) du\right) = \exp\left(-\nu \int_0^t h(u)\, du\right). \tag{1.83}$$

Before we obtain the marginal survivor function, we shall introduce the gamma distribution. The density for the gamma distribution is given by

$$g(\nu, \alpha, \beta) = \frac{1}{\beta^{\alpha} \Gamma(\propto)} \nu^{\propto -1} e^{-\nu/\beta}, \tag{1.84}$$

where $\propto = \frac{1}{\theta}$, $\beta = \theta$, and the gamma integral is given by $\Gamma(\propto) = \int_0^{\infty} \nu^{\propto -1} e^{-\nu}$. By adopting the gamma distribution, $g(\nu)$, the expected survivor function can be derived:

$$S(t) = E\left[S\left(t_{ij} \mid \boldsymbol{X}_{ij}, \nu_i\right)\right] = E\left[\exp\left(-\int_0^t h(u \mid \nu) du\right)\right] = \mathrm{L}\left[\exp\left(\int_0^t h(u)\, du\right)\right], \quad (1.85)$$

where L is the Laplace transformation to integrate out the distribution of the frailty term.

Using the Weibull model as an example, the marginal Weibull survivor function with gamma frailty is such that

$$S(t) = \left[1 + \theta(\lambda t)^p\right]^{-1/\theta} \quad (1.86)$$

and the Weibull hazard with gamma frailty is equal to

$$h(t) = \lambda p(\lambda t)^{p-1}\left[S(t)\right]^{\theta}. \quad (1.87)$$

The frailty model is applicable in the clinical setting. For example, when a population is heterogeneous, it is likely that the population composition over time will consist of the more robust individuals as the frail ones failed. In such case, the overall population hazard is declining while individual hazards increase. The frailty term allows for the overall population hazard to decrease regardless of the individual hazard shape. The frailty model is more suited for the population approach in this respect.

For time-varying covariates, which are very applicable in the pharmacometric setting wherein the effect of drug concentration on the risk or hazard is a dynamic variable, the hazard should vary over time. Holford provided a tutorial explaining how the treatment effect can be incorporated to the hazard function to evaluate the dynamic drug time course on the hazard over time (Holford 2013).

1.7.2 Logistic Regression

A logistic regression is suitable for establishing relationship between the outcome of binary response data and explanatory variables (predictors). The probability of having an event is defined as:

$$\pi(x) = \frac{\exp(L(x))}{1 + \exp(L(x))} \quad (1.88)$$

where $\pi(x)$ is called logistic function with values between 0 and 1. $L(x)$ is a linear function of predictors, $L(x) = \beta_0 + \beta_1 x + \cdots + \beta_i x_i$, where β_0 is the intercept and $\beta_1, \ldots \beta_i$ are the coefficients, and x represents the predictors, such as drug concentration (Heiberger and Holland 2004; Venables et al. 1994).

We take the probability of no event, which is one subtract the previous probability, $\pi(x)$:

$$1-\pi(x)=\frac{1+\exp(L(x))-\exp(L(x))}{1+\exp(L(x))}=\frac{1}{1+\exp(L(x))}. \tag{1.89}$$

The odds describe the relative risk such that:

$$\frac{\pi(x)}{1-\pi(x)}=\frac{\exp(L(x))/\left[1+\exp(L(x))\right]}{1/\left[1+\exp(L(x))\right]}=\exp(L(x)). \tag{1.90}$$

Taking the natural logarithm of the odds above gives the $logit(L)$:

$$logit(L)=\log\left(\frac{\pi(x)}{1-\pi(x)}\right)=L(x). \tag{1.91}$$

The logit is no longer bounded and its value can take from $-\infty$ to $+\infty$. It is important to note that the error around the logit follows a binomial distribution rather than a normal distribution.

The generalized logistic regression model extends the analysis to multiple categorical response data or multinomial responses (Agresti 1999). The approach is to model cumulative logits by comparing each response category with baseline such that

$$\log\frac{\pi_i(\boldsymbol{x})}{\pi_{baseline}(\boldsymbol{x})}=\beta_{i0}+\boldsymbol{\beta}'_i\boldsymbol{x}, \tag{1.92}$$

where the subscript i represents the $i-1$ levels of response categories plus the baseline, $\pi_i(\boldsymbol{x})=P(Y=i|\boldsymbol{x})$ and $\sum_i\pi_i(\boldsymbol{x})=1$. This approach is often called the proportional odds assumption (McCullagh 1980; Peterson and Harrell 1990):

$$\text{logit}\left[P(Y\le i|\boldsymbol{x}\right]=\beta_{i0}+\boldsymbol{\beta}'\boldsymbol{x} \tag{1.93}$$

The comparison between two responses is then

$$\log\frac{\pi_a(\boldsymbol{x})}{\pi_b(\boldsymbol{x})}=\log\frac{\pi_a(\boldsymbol{x})}{\pi_{baseline}(\boldsymbol{x})}-\log\frac{\pi_b(\boldsymbol{x})}{\pi_{baseline}(\boldsymbol{x})}. \tag{1.94}$$

Sheiner in 1994 used the proportional odds model with individual specified random effects for the analysis of a 4-degree pain scale. The nonlinear mixed-effects model of ordered categorical PD data is mostly based on the proportional odds model and has been widely used for the evaluation of both efficacy and adverse events (Cullberg et al. 2005; Gomeni et al. 2001; Gupta et al. 1999; Johnston et al. 2003; Knibbe et al. 2002; Kowalski et al. 2003; Lunn et al. 2001; Mandema and Stanski 1996; Mould et al. 2001, 2002; Olofsen et al. 2005; Xie et al. 2002; Zingmark et al. 2003).

Kjellsson et al. presented a differential odds model to circumvent the assumption with the proportional odds model that the size of the predictor effect is the

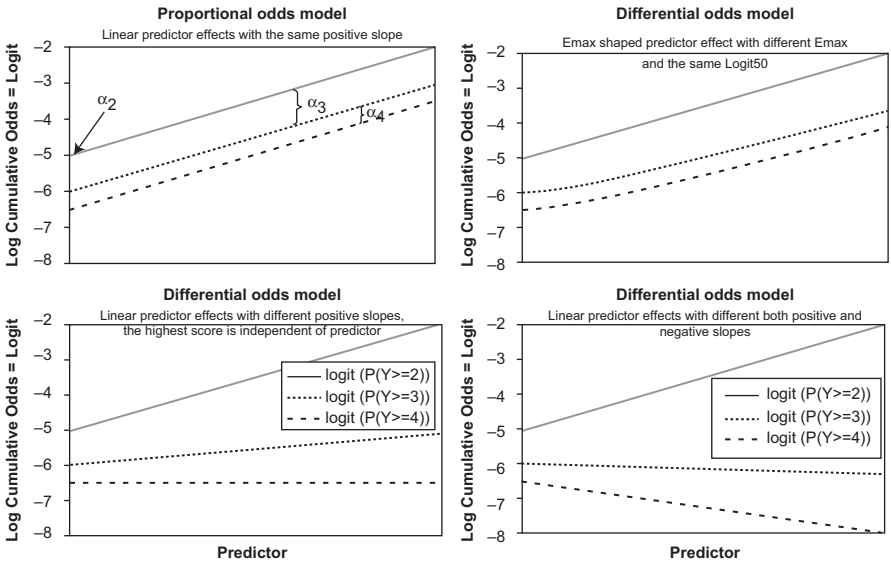

Fig. 1.16 Logit functions based on proportional odds versus differential odds models and their effects on the cumulative log odds. Examples include proportional odds model with linear predictor effects of the same slope (*upper left*), differential odds model using E_{max}-shaped predictor with variable E_{max} values (*upper right*), linear predictor with variable but positive slopes (*lower left*), and linear function with both positive and negative slopes (*lower right*). α_2 for baseline logit with score ≥ 2, α_3 and α_2 for baseline-shifted logit with score ≥ 3 and ≥ 4, respectively. (Image from Kjellsson et al. 2008, used with permission)

same for the log odds for all categories (Kjellsson et al. 2008). They argued that the assumption is valid for categories on a continuous scale but would not hold for categories based on ranking scale. Even though historically, the partial proportional odds model has been used to allow for variable sizes of predictor effect, some of the categories within the model have odds that are proportional to each other. While the predictor function is identical for the proportional odds model, the differential odds model allowed this function to vary. The model was implemented using cumulative probabilities so that the correct probability value can be allocated to a specific score or category (for example, mild score is more likely than severe score for a response such as sedation). Figure 1.16 illustrates the predictor versus log cumulative odds in proportional and differential odds model. In the upper left-hand corner, the slopes of the log cumulative odds versus the predictor graph are the same for the proportional odds model. The remaining graphs illustrate the log-cumulative odds versus predictor trend with differential odds model. The E_{max}-shaped predictor effects in the upper right all had positive slopes whereas mixtures of positive and negative slopes are possible with the alternative implementation.

1.7.3 Markov Chain

Another methodology in pharmacometrics that is gaining popularity for the analysis of categorical response variable is the Markov chain model, which has been applied in clinical studies. A Markov chain process is a probability model in which the distribution of future outcomes depends only on the current state and not on the whole history; this is often referred to as the memoryless property of a Markov chain (Bass 2011). In other words, the probability of a certain state to occur in the following time interval is only dependent on the state in the current time frame. With this definition, we suppose that a process in state i has a fixed probability P_{ij} that it will be in the next state j, such that

$$P\left\{X_{n+1} = j \middle| X_n = i\right\} = P_{ij}, \tag{1.95}$$

where the set $\left\{X_n, n = 0,1,2,\cdots\right\}$ is a stochastic process of finite possible outcomes and P_{ij} is often referred to as transition probability.

For this discussion, we shall use the example of early and late tacrolimus-related adverse event occurrence in stable pediatric renal allograft recipients after transplantation (Sy et al. 2013a). The transition probabilities were defined based on two states: without (state 0) and with (state 1) adverse event. A Markov chain model was chosen in that study because the observations may not be independent since it was assumed that the occurrence of an adverse event is related to the drug concentration. The current state of the patient was conditioned on his previous visit. The transition probabilities were: P_{00} for those who did not report an adverse event at a particular visit given no adverse event in the previous visit; P_{01} if the patient without adverse event in the previous visit reported an adverse event in the current visit; P_{10} for patients with an adverse event in the previous visit but no adverse event in the current one; and P_{11} if an adverse event occurred on both visits. The transition probabilities adhered to Markov properties such that the sum of the transition probabilities from the specific state is 1:

$$\sum_{j=0}^{1} P_{ij} = 1. \tag{1.96}$$

The function that is utilized for the estimation of the transition probabilities varies depending on the study needs. Kemp and Kamphuisen simulated human hypnograms using a Markov chain model (Kemp and Kamphuisen 1986). Karlsson et al. parameterized the transition probabilities through binary logistic function to describe sleep data (Karlsson et al. 2000). Bizzotto et al. utilized a multinomial logistic function to characterize the time course of transition probabilities between sleep stages in insomniac patients (Bizzotto et al. 2010, 2011). Ouellet et al. used a logistic regression wherein the logit function is linear to estimate the transition probability of having an adverse event due to dizziness in subjects who were administered a selective glycine transporter 1 inhibitor (Ouellet et al. 2011). An example in Ross

probability textbook adopted Poisson probability density function (pdf) for counting process in the estimation of transition probability (Ross 2006). The Poisson pdf assumes that the magnitude of the variance is identical to its mean. However, many counting processes show greater variability than that predicted by the Poisson model. Troconiz et al. explored mixed Markov elements and Poisson distribution to evaluate overdispersion in the variance of a Poisson distribution (Troconiz et al. 2009). There are numerous other implementations of the transition probability which we cannot possibly list all of them in this introductory chapter. When selecting whether or not to use a Markov model, Karlsson suggested that the Markov model is more suitable for consecutive same-state observations, which are typical for sleep patterns, as an example (Karlsson et al. 2000).

1.8 Disease Progression Model

The natural time course of a disease is often not one that is static but becomes progressively worse if left untreated. The disease trajectory is not constant, unlike the common assumption that is taken when using the E_{max} model wherein the baseline E_0 is static. Even as early as the 1970s, investigators reported longitudinal studies of the natural history of non-Hodgkin's lymphoma stages and coronary artery stenosis (Fuller et al. 1975; Rosch et al. 1976). A disease progression model describes how an indicator for the disease or a clinically relevant endpoint changes in time. For the purpose of modeling disease progression, the approach has been applied in degenerative diseases such as Alzheimer's disease (Holford and Peace 1992a, b), schizophrenia (Kimko et al. 2000), and diabetic neuropathy (Bakris et al. 1996; Bjorck et al. 1992; Crepaldi et al. 1998; Gall et al. 1993; Lewis et al. 1993; Parving et al. 1995).

Most of the disease progression models are empirical that describe the disease trajectory rather than its physiological background. The linear model has the following general form of equation that characterizes the disease as changing linearly with time:

$$S(t) = S_0 + \alpha t, \tag{1.97}$$

where $S(t)$ represents the disease status at a specific time t, S_0 is the baseline that can be constant or a time-dependent function (e.g., sinusoidal function to characterize circadian rhythm), and $\propto$ is the slope of the linear process. Therapeutic interventions, including placebo, can change the trajectory of a disease process. Interventions are generally classified as either symptomatic or disease modifying. Let $f(T)$ be the function to characterize the effect of treatment or intervention. In the case of symptomatic treatment, the effect of intervention would shift the disease baseline but not change the slope whereas disease-modifying interventions would change the rate of disease progression, as shown in Eqs. 1.98 and 1.99, respectively (Mould 2007; Mould et al. 2007; Schmidt et al. 2011):

$$S(t) = S_0 + f(T) + \alpha t \tag{1.98}$$

$$S(t) = S_0 + (f(T) + \alpha)t \tag{1.99}$$

From the two equations above, the symptomatic interventions have different effect on the disease status from disease-modifying interventions. The disease trajectory will revert to its natural progression rate α once the treatment is discontinued, regardless of the type of treatment. A third type of intervention is one that exerts completely cure and reverses the disease status back to pre-disease state. This type of intervention may best be characterized by a model that incorporates both symptomatic and disease-modifying effect:

$$S(t) = S_0 + f_1(T) + (f_2(T) + \alpha)t \tag{1.100}$$

In the examples listed previously of applications of disease progression modeling approach in specific therapeutic areas, the linear disease progression was used by Kimko et al. to study the effect of quetiapine fumarate, an antischizophrenic agent, on schizophrenia status based on the Brief Psychiatric Rating Scale (Kimko et al. 2000).

Nonlinear functions have also been used as disease progression model. Pors-Nielsen and Friberg used an exponential model to describe the effect of estrogen/progestin treatment on osteoporosis (Pors Nielsen et al. 1994). Grantham et al. also used a similar model to describe the increase in renal volume in autosomal dominant polycystic kidney disease (Grantham et al. 2008). Pillai et al. utilized an indirect response type model to investigate biomarker response to ibandronate (Pillai et al. 2004).

1.9 Systems Pharmacology

Molecular biology evaluates single genes and proteins while systems biology combines the complex interactions at all levels of a biological system. By viewing all levels of biological information in the process, scientists are able to determine important properties of the system. Mathematical models of biological processes help describe time-dependent kinetic behavior and causality. The mechanistic approach to modeling systems' biological processes is based on sound biological principles with prior knowledge about the biochemical network involved. The variables and parameters are related to a physiological or cellular process where the information is obtained from an *in vitro* or physiological experiment. This approach gives the scientist a holistic view of the biological system. The study of mechanism of drug action on the system itself also becomes more precise.

One of the systems level models applied in drug development is that of the regulation of glucose. Landersdorfer and Jusko provided an excellent review of application of modeling in diabetes, with a specific focus on modeling drug effects (Land-

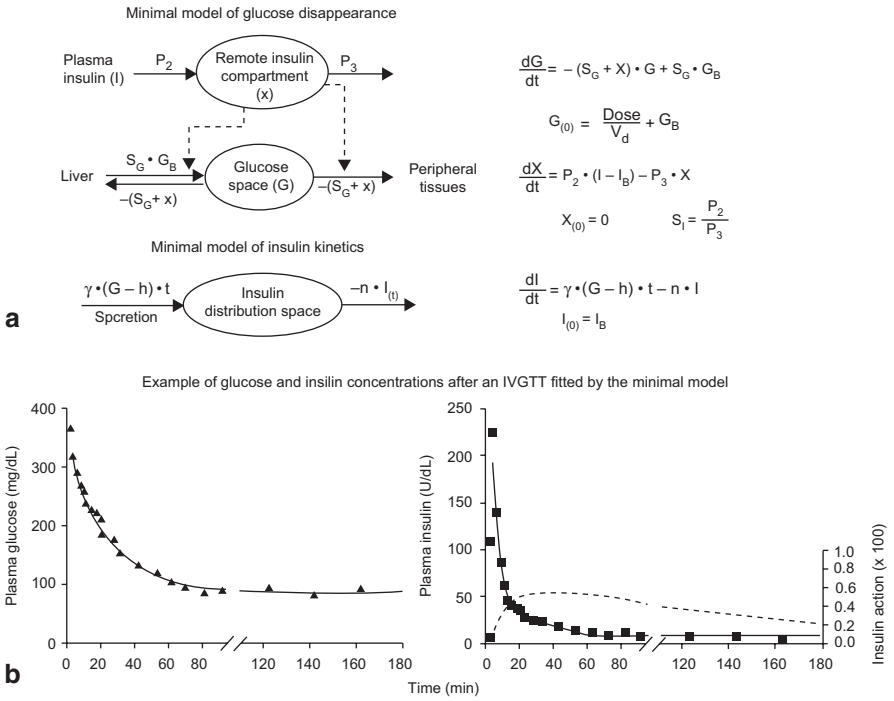

Fig. 1.17 Structure and equations of the minimal model of insulin-glucose feedback and control (*top*) and example of glucose and insulin concentrations after an IV glucose tolerance test fitted by the minimal model. (Image from Landersdorfer and Jusko 2008, used with permission)

ersdorfer and Jusko 2008). In 1979, Bergman et al. developed a minimal model that included three coupled differential equations to describe the intravenous glucose tolerance test (Bergman et al. 1979). Using several feedback control mechanisms, the model couples insulin I and glucose G regulation and also introduces an additional unobserved insulin component X to describe the delay between insulin release and the response characterized by the reduction in blood glucose (Fig. 1.17):

$$\begin{aligned}\frac{dG}{dt} &= -(S_G + X(t)) \cdot G(t) + S_G \cdot G_B \\ \frac{dX}{dt} &= p_2 \cdot (I(t) - I_B) - p_3 \cdot X(t) \\ \frac{dI}{dt} &= \gamma \cdot (G(t) - h)t - n \cdot I(t)\end{aligned} \tag{1.101}$$

The baseline values were h, G_B and I_B and parameters were S_G, p_2, p_3, γ, and n. The initial conditions were such that

$$G(0) = \frac{Dose}{V_d} + G_B$$
$$X(0) = 0$$
$$I(0) = I_B \tag{1.102}$$

Though this model is widely used, it is not without its problems. The model does not allow both insulin and glucose to be fitted simultaneously (Pacini and Bergman 1986). The additional unobserved insulin effect compartment X is unbounded and can increase indefinitely when both glucose and insulin parts of the model were estimated simultaneously (De Gaetano and Arino 2000). Another issue with the model is that it does not take into account the first and second insulin phases (Agerso and Vicini 2003). This model is applicable for diagnostic test but limited for drug evaluation.

In the study of glucagon-like peptide-1 analog NN221, Agerso and Vicini introduced a Gaussian term to describe the first-phase insulin secretion (Agerso and Vicini 2003). The resulting equation for I was such that

$$\frac{dI}{dt} = \beta(t) + \gamma \cdot (G(t) - h)t - n \cdot I(t), \tag{1.103}$$

where $\beta(t)$ is an empirical Gaussian function that accounts for the amplitude of the first-phase insulin as well as duration of this process. Mager et al. (2004) further modified the γ parameter to an $E_{\max}$ model to include a drug effect for another GLP-1 analog, exenatide (Mager et al. 2004). This model was used in the analysis of data from hyperglycemic clamp study in healthy subjects and diabetic patients.

Indirect response type models have been applied to study the effects of various antidiabetic agents on glucose and insulin. Benincosa and Jusko evaluated rosiglitazone effects wherein both fasting plasma glucose (FPG) and hemoglobin A1c (HbA1c) were measured (Benincosa and Jusko 1999). The glycosylation of hemoglobin was described by a second-order process that is proportional to the FPG concentrations and is dependent on the ratio of the steady-state HbA1c and FPG. The elimination of HbA1c is a first-order process. Hamren et al. modified the model for tesaglitazar such that the glycosylation process also takes into account the erythrocyte lifespan and utilizes several transit compartments to describe the aging process of erythrocytes (Hamren et al. 2008).

Given that diabetes is a chronic disease that becomes progressively worse, the models should also examine disease progression for long-term studies of antidiabetic drugs. Frey et al. investigated the effect of sustained-release gliclazide on FPG over 10 weeks to 1 year period (Frey et al. 2003). In patients who responded to the treatment, FPG levels initially declined and then slowly increased whereas the nonresponders' FPG levels continued to increase in the natural disease progression process. The authors utilized an empirical linear model with an intercept and a positive slope to describe the disease progression, measured by FPG over time:

$$FPG(t) = baseline + \alpha \cdot t - E_t, \tag{1.104}$$

where α is the slope of the disease progression process, E_t is the predicted treatment effect at the time when the treatment was administered, and baseline is the predicted baseline FPG. Since gliclazide was assumed to only alleviate the symptoms of the disease without modifying the disease itself, the effect of the drug was to shift the curve without affecting the rate of disease progression that is characterized by the α term.

De Winter et al. modeled the worsening of β cell activity (B) and insulin sensitivity (S) using a different disease progression model approach (de Winter et al. 2006):

$$\begin{aligned} B &= \frac{1}{1+\exp(b_0 + r_b \cdot t)} \\ S &= \frac{1}{1+\exp(s_0 + r_s \cdot t)} \end{aligned} \tag{1.105}$$

where baselines were b_0 and s_0 and rates of disease progression were r_b and r_s. Their investigation also included a model for HbA1c, which was fitted simultaneously along with FPG and insulin levels.

More sophisticated models of the whole body have been developed and focused on tissues and organs that are relevant in diabetes. These models were used to simulate virtual patients and predict clinical trial outcomes. As these complex models are relatively difficult to develop, many assumptions are made and model parameters are often taken from literature. Examples of these models include the Archimedes, the Entelos Metabolism, and T1Dm PhysioLab®. As these models are proprietary, there is a lack of transparency in the model equations and parameter values (Herman 2003).

Another therapeutic area where systems biology and pharmacology models are extensively used is in oncology. Biochemical reactions and signaling pathways are often described by differential equations that characterize a chemical reaction. Most of these processes involve a complex network of chemical and biochemical reactions. The *law of mass action* is the common convention that is used to describe the rate at which chemical entities interact to form a different combination. The computational model for heregulin-induced p-ErBB3 signaling and the effect of antibody inhibitors pertuzumab and lapatinib utilizes such convention (McDonagh et al. 2012; Schoeberl et al. 2009). The following chemical reactions were listed for ErbB2/3-bispecific antibody binding and receptor cross-linking:

$$E2 + BsAb \leftrightarrow E2 : BsAb \tag{1.106}$$

$$BsAb + E3 \leftrightarrow BsAb : E3 \tag{1.107}$$

$$E2 + BsAb : E3 \leftrightarrow E2 : BsAb : E3 \tag{1.108}$$

$$E2:BsAb+E3\leftrightarrow E2:BsAb:E3 \tag{1.109}$$

where E2 and E3 represent ErbB2/3, respectively, and BsAb refers to a bi-specific antibody. The chemical reactions listed in Eqs. 1.106–1.109 are reversible processes and the reaction schema can be generalized:

$$A+B\xrightarrow{k}C\xrightarrow{k'}A+B \tag{1.110}$$

where k is the forward reaction rate and k' is the reversible rate. The rate of change for each of the above species can be written as follows:

$$\begin{aligned}\frac{d[A]}{dt}&=k'[C]-k[A][B]\\ \frac{d[B]}{dt}&=k'[C]-k[A][B]\\ \frac{d[C]}{dt}&=k[A][B]-k'[C]\end{aligned} \tag{1.111}$$

As one can see, writing out the differential equations for the chemical reaction in Eq. 1.111 becomes a tedious effort, especially when the biological system has many players. Some systems biology tools allow user to create reaction processes and will automatically create the corresponding differential equations in the background (Maiwald and Timmer 2008).

In identifying targets, McDonagh et al. utilized computation modeling and cell signaling insights to develop specific targeted antibodies that are capable to destabilize the over expression of ErbB2 by inhibiting ErbB3 signaling (McDonagh et al. 2012). They identified that ErbB3/heregulin activation plays a critical role in ErbB2-positive refractory disease and that the synergy can be achieved in combination therapies involving ErbB3 inhibitor and ErbB2 therapies (McDonagh et al. 2012). System pharmacology models are slowly being adopted in drug development settings and the examples show promising prospect for systems pharmacology to become part of mainstream pharmacometric analyses.

1.10 Software

As software facilitates PKPD modeling and simulation, we will discuss the available software packages that have been used for different types of analyses. For noncompartmental analysis (or statistical moment approach), WinNonlin is most commonly used in the pharmaceutical industry. Alternately, the PK package in R is a basic PK package that performs noncompartmental analysis of PK data as well. A brief description of this tool can be found on the CRAN project website (http://cran.r-project.org/web/views/Pharmacokinetics.html). For nonlinear mixed effect modeling, NONMEM is the most commonly used software in the drug development

setting. The Non-Parametric Adaptive Grid algorithm using NPAG (USC*PACK) is common for modeling population PK data in the therapeutic drug monitoring setting. The other software for mixed effect modeling are ADAPT that is based on important sampling algorithm, MONOLIX with the Markov Chain Monte Carlo (MCMC) stochastic approximation expectation maximization (SAEM). BUGS is a software package for performing Bayesian inference using Gibbs sampling. The user specifies a statistical model by stating the relationships between related variables. The software determines an appropriate MCMC scheme (based on the Gibbs sampler) for analyzing the specified model. The user then controls the execution of the scheme. There are two main versions of BUGS, namely WinBUGS and OpenBUGS. The recent release of NONMEM has incorporated the algorithms in the other software packages mentioned above. SimCyp includes a population-based simulation system using PBPK model.

For systems biology modeling, the Matlab platform and specialized toolboxes that were built on top of the Matlab platform can handle large and complex models that may contain hundreds of coupled differential equations. The large models can be slow in Matlab. Specialized Matlab toolbox such as Potterswheel (URL: potterswheel.de) utilizes chemical reaction scheme and builds the corresponding differential equations in C language to speed up the analysis and fitting processes (Maiwald and Timmer 2008). Curated systems biology models are available from library consortiums that are publicly accessible (e.g., http://www.ebi.ac.uk/biomodels-main) and can be ported to specialized software packages through Systems Biology Markup Language (SBML).

1.11 Conclusion

Over the past decade, pharmacometrics has become a discipline that is frequently utilized in academia, worldwide regulatory agencies, and the biopharmaceutical industry. Cost cutting and improvement in drug development will come from creative application of pharmacometric modeling approach.

The US FDA has emphasized the importance of model-based drug development wherein PK/PD models to characterize drug efficacy and safety are being developed for both preclinical and clinical data. The agency strongly supports this program, “Pharmacometric analyses, we believe, are valuable to gain insights into the data across drugs and to plan future development. The model and simulation approaches should not be viewed as substitutes to conducting clinical trials in all instances. Also, such quantitative analyses should not be primarily used to ‘rescue’ failed trials for seeking approval. Where appropriate, the FDA accepted simulation results” (Bhattaram et al. 2005).

Appendix

Derivation of Eq. 1.55

Implicit in the assumption that the concentration of drug in the system that is being cleared is constant or at steady state, we assumed that the rate of change in the drug concentration is 0 and thus set all the left-hand sides in the list of equations in Eq. 1.53 to 0.

$$0 = V_1 \frac{dC_{1(vein)}}{dt} = Q_1 \cdot C_0 - Q_1 \cdot C_1 + K_I(t) \tag{1.112}$$

$$0 = V_2 \frac{dC_{2(artery)}}{dt} = Q_1 \cdot C_{3o} - Q_1 \cdot C_2 \tag{1.113}$$

$$0 = V_3 \frac{dC_{3(lung)}}{dt} = Q_1 \cdot C_1 - Q_1 \cdot C_{3o} - r_3(C_3) \tag{1.114}$$

$$0 = V_4 \frac{dC_{4(liver)}}{dt} = Q_7 \cdot C_{7o} + (Q_4 - Q_7) \cdot C_2 - Q_4 \cdot C_{4o} - r_4(C_4) \tag{1.115}$$

$$0 = V_5 \frac{dC_{5(kidney)}}{dt} = Q_5 \cdot C_2 - Q_5 \cdot C_{5o} - r_5(C_5) \tag{1.116}$$

$$0 = V_6 \frac{dC_{6(rest\ of\ body)}}{dt} = Q_6 \cdot C_2 - Q_6 \cdot C_{6o} \tag{1.117}$$

$$0 = V_7 \frac{dC_{7(GI\ tract)}}{dt} = Q_7 \cdot C_2 - Q_7 \cdot C_{7o} - r_7(C_7). \tag{1.118}$$

From Eq. 1.112, we integrate

$$\int_0^\infty Q_1 \cdot C_1 \, dt = \int_0^\infty (Q_1 \cdot C_0 + K_I(t)) dt. \tag{1.119}$$

By applying Eq. 1.54 and substituting $Q_1 \cdot C_0$ with $Q_4 \cdot C_{4o} + Q_5 \cdot C_{5o} + Q_6 \cdot C_{6o}$ to Eq. 1.119, the resulting expression is

$$Q_1 \int_0^\infty C_1 \, dt = \int_0^\infty (Q_4 \cdot C_{4o} + Q_5 \cdot C_{5o} + Q_6 \cdot C_{6o}) dt + \int_0^\infty K_I(\mathrm{t}) dt. \tag{1.120}$$

Rearrangement of Eq. 1.120 by adding and subtracting $(Q_7 \cdot C_{7o} + (Q_4 - Q_7) C_2 + Q_5 \cdot C_{5o} + Q_6 \cdot C_2)$ to Eq. 1.120 such that the net result is 0 will yield the following expression:

$$\begin{aligned} Q_1 \int_0^\infty C_1\, dt = \int_0^\infty & \left[(Q_7 \cdot C_{7o} + (Q_4 - Q_7) C_2 + Q_5 \cdot C_{5o} + Q_6 \cdot C_2) \right. \\ & \left. - (Q_7 \cdot C_{7o} + (Q_4 - Q_7) C_2 + Q_5 \cdot C_{5o} + Q_6 \cdot C_2) \right] dt \\ & + \int_0^\infty (Q_4 \cdot C_{4o} + Q_5 \cdot C_{5o} + Q_6 \cdot C_{6o}) dt + \int_0^\infty K_I(t) dt. \end{aligned} \quad (1.121)$$

From Eq. 1.117, $\int_0^\infty (Q_6 \cdot C_2 - Q_6 \cdot C_{6o}) dt = 0$. Given that $Q_7 \cdot C_{7o} + (Q_4 - Q_7) C_2$ represents the total amount of drug entering the liver from the artery and the gut which is also C_p, wherein $Q_4 \cdot C_p = Q_7 \cdot C_{7o} + (Q_4 - Q_7) C_2$, we can then simplify Eq. 1.121 as follows:

$$\begin{aligned} Q_1 \int_0^\infty C_1\, dt = & \int_0^\infty (Q_4 + Q_5 + Q_6) C_2 dt \\ & - \left\{ \int_0^\infty Q_4 (C_p - C_{4o}) dt + \int_0^\infty Q_5 (C_2 - C_{5o}) dt + \int_0^\infty Q_7 (C_2 - C_{7o}) dt \right\} \\ & + \int_0^\infty K_I(t) dt. \end{aligned} \quad (1.122)$$

Furthermore, $\int_0^\infty (Q_4 + Q_5 + Q_6) C_2 dt = Q_1 \int_0^\infty C_2 dt$, since $Q_1 = Q_4 + Q_5 + Q_6$ and from Eq. 1.113, $Q_1 \int_0^\infty C_{3o} dt$, then Eq. 1.122 can be rewritten as Eq. 1.55:

$$\begin{aligned} & \int_0^\infty Q_1 (C_1 - C_{3o}) dt + \int_0^\infty Q_4 (C_p - C_{4o}) dt + \int_0^\infty Q_5 (C_2 - C_{5o}) dt \\ & \qquad + \int_0^\infty Q_7 (C_2 - C_{7o}) dt = \int_0^\infty K_I(t) dt. \end{aligned}$$

Derivation of Eq. 1.60

Using the expression for mean clearance, the rearrangement of Eqs. 1.55 through 1.59 will result in the following:

$$\overline{CL}_{systemic} = \overline{CL}_3 + \left(\frac{\int_0^\infty C_p\, dt}{\int_0^\infty C_1\, dt} \right) \overline{CL}_4 + \left(\frac{\int_0^\infty C_2\, dt}{\int_0^\infty C_1\, dt} \right) (\overline{CL}_5 + \overline{CL}_7). \quad (1.123)$$

We set $Q_4 \cdot C_p = Q_7 C_{7o} + (Q_4 - Q_7) C_2$ to $Q_4 (C_2 - C_p) = Q_7 (C_2 - C_{7o})$. Then integrate the latter expression from 0 to infinity, $Q_4 \int_0^\infty (C_2 - C_p) dt = Q_7 \int_0^\infty (C_2 - C_{7o}) dt$ and divide both sides of the equation by $\int_0^\infty C_2 dt$ to obtain

$\frac{Q_4\int_0^\infty (C_2 - C_p)dt}{\int_0^\infty C_2 dt} = \frac{Q_7\int_0^\infty (C_2 - C_{7o})dt}{\int_0^\infty C_2 dt}$. The previous equation can be rewritten as

$1 - \frac{\int_0^\infty C_p dt}{\int_0^\infty C_2 dt} = \frac{Q_7\int_0^\infty (C_2 - C_{7o})dt}{Q_4\int_0^\infty C_2 dt}$. The ratio consisting the integrating components on the left side of the equation is the expression for the extraction ratio for tissue compartment 7 for the GI tract, $\bar{E}_7 = \frac{\int_0^\infty (C_2 - C_{7o})\mathrm{d}t}{\int_0^\infty C_2 \mathrm{d}t}$. Therefore,

$$\frac{\int_0^\infty C_p dt}{\int_0^\infty C_2 dt} = 1 - \frac{Q_7}{Q_4}\bar{E}_7 \tag{1.124}$$

From Eq. 1.113 above, $Q_1\int_0^\infty C_2 dt = Q_1\int_0^\infty C_3 dt$, and from Eq. 1.57, $\overline{CL}_3 = \frac{Q_1\int_0^\infty (C_1 - C_{3o})dt}{\int_0^\infty C_1 dt} = \frac{Q_1\int_0^\infty (C_1 - C_2)dt}{\int_0^\infty C_1 dt}$. Thus,

$$\frac{\int_0^\infty C_2 dt}{\int_0^\infty C_1 dt} = 1 - \frac{\overline{CL}_3}{Q_1} = 1 - \bar{E}_{lung} \tag{1.125}$$

In the following step, multiply Eq. 1.124 by A125:

$$\frac{\int_0^\infty C_p dt}{\int_0^\infty C_1 dt} = \left(1 - \frac{\overline{CL}_3}{Q_1}\right)\left(1 - \frac{\overline{CL}_7}{Q_4}\right). \tag{1.126}$$

Since $\overline{CL}_7 = Q_7 \cdot \bar{E}_7$. In the following step, we substitute Eqs. 1.126 and 1.125 to Eq. 1.123, $\overline{CL}_{systemic} = \overline{CL}_3 + \left(1 - \frac{\overline{CL}_3}{Q_1}\right)\left(1 - \frac{\overline{CL}_7}{Q_4}\right)\overline{CL}_4 + \left(1 - \frac{\overline{CL}_3}{Q_1}\right)(\overline{CL}_5 + \overline{CL}_7)$

$$= \overline{CL}_3 + (1 - \bar{E}_3)\left[\overline{CL}_4 + (1 - \bar{E}_4)\overline{CL}_7 + \overline{CL}_5\right].$$

References

Agerso H, Vicini P (2003) Pharmacodynamics of NN2211, a novel long acting GLP-1 derivative. Eur J Pharm Sci 19(2–3):141–150

Agoram B, Heatherington AC, Gastonguay MR (2006) Development and evaluation of a population pharmacokinetic-pharmacodynamic model of darbepoetin alfa in patients with nonmyeloid malignancies undergoing multicycle chemotherapy. AAPS J 8(3):E552–E563

Agresti A (1999) Modelling ordered categorical data: recent advances and future challenges. Stat Med 18(17–18):2191–2207

Andersen ME, Gargas ML, Ramsey JC (1984) Inhalation pharmacokinetics: evaluating systemic extraction, total in vivo metabolism, and the time course of enzyme induction for inhaled styrene in rats based on arterial blood:inhaled air concentration ratios. Toxicol Appl Pharmacol 73(1):176–187

Andersen ME, Clewell HJ 3rd, Gargas ML, Smith FA, Reitz RH (1987) Physiologically based pharmacokinetics and the risk assessment process for methylene chloride. Toxicol Appl Pharmacol 87(2):185–205

Bakris GL, Copley JB, Vicknair N, Sadler R, Leurgans S (1996) Calcium channel blockers versus other antihypertensive therapies on progression of NIDDM associated nephropathy. Kidney Int 50(5):1641–1650

Bass RF (2011) Stochastic processes, edn. Cambridge University Press, Cambridge

Baxter LT, Zhu H, Mackensen DG, Jain RK (1994) Physiologically based pharmacokinetic model for specific and nonspecific monoclonal antibodies and fragments in normal tissues and human tumor xenografts in nude mice. Cancer Res 54(6):1517–1528

Bellman RE, Jacquez JA, Kalaba RE, Kotkin B (1963) A mathematical model of drug distribution in the body: implications for cancer chemotherapy. Rand Corporation, Santa Monica, California.

Benet LZ (2010) Clearance (nee Rowland) concepts: a downdate and an update. J Pharmacokinet Pharmacodyn 37(6):529–539

Benet LZ, Galeazzi RL (1979) Noncompartmental determination of the steady-state volume of distribution. J Pharm Sci 68(8):1071–1074

Benincosa L, Jusko W (1999) Novel method of treatment. World Intellectual Property Organization, Geneva, Publ. no. W0/2000/027341

Bergman RN, Ider YZ, Bowden CR, Cobelli C (1979) Quantitative estimation of insulin sensitivity. Am J Physiol 236(6):E667–E677

Bernards JK (1986) A pharmacokinetic model for lung uptake of volatile chemicals. MChE, University of Delaware, Newark, DE (Master's thesis, advisor: K. Bischoff)

Bhattaram VA, Booth BP, Ramchandani RP, Beasley BN, Wang Y, Tandon V et al (2005) Impact of pharmacometrics on drug approval and labeling decisions: a survey of 42 new drug applications. AAPS J 7(3):E503–512

Bischoff KB (1966) Drug distribution in mammals. Chem Eng Med Biol 62(66): 33–45

Bischoff KB (1975) Some fundamental considerations of the applications of pharmacokinetics to cancer chemotherapy. Cancer Chemother Rep Part 1 59(4):777–793

Bischoff KB (1987) Physiologically based pharmacokinetic modeling, edn, Drinking Water and Health, Volume 8: Pharmacokinetics in Risk Assessment. National Academy Press, Washington, DC.

Bischoff KB (1992) PBPK models: what are we really assuming? Presentation at the Chemical Industry Institute of Toxicology Founders Award

Bischoff KB, Dedrick RL (1968) Thiopental pharmacokinetics. J Pharm Sci 57(8):1346–1351

Bischoff KB, Dedrick RL, Zaharko DS (1970) Preliminary model for methotrexate pharmacokinetics. J Pharm Sci 59(2):149–154

Bizzotto R, Zamuner S, De Nicolao G, Karlsson MO, Gomeni R (2010) Multinomial logistic estimation of Markov-chain models for modeling sleep architecture in primary insomnia patients. J Pharmacokinet Pharmacodyn 37(2):137–155

Bizzotto R, Zamuner S, Mezzalana E, De Nicolao G, Gomeni R, Hooker AC et al (2011) Multinomial logistic functions in markov chain models of sleep architecture: internal and external validation and covariate analysis. AAPS J 13(3):445–463

Bjorck S, Mulec H, Johnsen SA, Norden G, Aurell M (1992) Renal protective effect of enalapril in diabetic nephropathy. BMJ 304(6823):339–343

Boxenbaum H (1982) Interspecies scaling, allometry, physiological time, and the ground plan of pharmacokinetics. J Pharmacokinet Biopharm 10(2):201–227

Boxenbaum H, Ronfeld R (1983) Interspecies pharmacokinetic scaling and the Dedrick plots. Am J Physiol 245(6):R768–R775

Brandfonbrener M, Landowne M, Shock NW (1955) Changes in cardiac output with age. Circulation 12(4):557–566

Brindley PG, Dunn WF (2009) Simulation for clinical research trials: a theoretical outline. J Crit Care 24(2):164–167

Brown R, Delp M, Lindstedt S, Rhomberg L, Beliles R (1997) Physiological parameter values for physiologically based pharmacokinetic models. Toxicol Ind Health 13407:484

Burnham KP, Anderson DR (2002) Model selection and multi-model inference: a practical information-theoretic approach, Second edn. Springer

Chen HS, Gross JF (1979) Physiologically based pharmacokinetic models for anticancer drugs. Cancer Chemother Pharmacol 2(2):85–94

Collett D (1994) Modelling survival data in medical research, 1st edn. Chapman & Hall, New York

Collins JM, Dedrick RL (1983) Distributed model for drug delivery to CSF and brain tissue. Am J Physiol 245(3):R303–R310

Coxson PG, Bischoff KB (1987a) Lumping strategy. 1. Introductory techniques and applications of cluster analysis. Ind Eng Chem Res 26(6):1239–1248

Coxson PG, Bischoff KB (1987b) Lumping strategy. 2. System theoretic approach. Ind Eng Chem Res 26(10):2151–2157

Crepaldi G, Carta Q, Deferrari G, Mangili R, Navalesi R, Santeusanio F et al (1998) Effects of lisinopril and nifedipine on the progression to overt albuminuria in IDDM patients with incipient nephropathy and normal blood pressure. The Italian Microalbuminuria Study Group in IDDM. Diabetes Care 21(1):104–110

Cullberg M, Eriksson UG, Wahlander K, Eriksson H, Schulman S, Karlsson MO (2005) Pharmacokinetics of ximelagatran and relationship to clinical response in acute deep vein thrombosis. Clin Pharmacol Ther 77(4):279–290

Dayneka NL, Garg V, Jusko WJ (1993) Comparison of four basic models of indirect pharmacodynamic responses. J Pharmacokinet Biopharma 21(4):457–478

De Gaetano A, Arino O (2000) Mathematical modelling of the intravenous glucose tolerance test. J Math Biol 40(2):136–168

de Winter W, DeJongh, Moules I et al (2006) A mechanism-based disease progression model for comparison of long-term effects of pioglitazone, metformin and gliclazide on disease processes underlying Type 2 Diabetes Mellitus. J Pharmacokinet Pharmacodyn 33(3):313–343

Dedrick RL (1973) Animal scale-up. J Pharmacokinet Biopharma 1(5):435–461

Dedrick RL, Bischoff KB (1980) Species similarities in pharmacokinetics. Fed Proc 39(1):54–59

Derendorf H, Hochhaus G (1995) Handbook of pharmacokinetics/pharmacodynamics correlation, CRC Press, Boca Raton, FL

Derendorf H, Lesko LJ, Chaikin P, Colburn WA, Lee P, Miller R et al (2000) Pharmacokinetic/pharmacodynamic modeling in drug research and development. J Clin Pharmacol 40(12 Pt 2):1399–1418

DiSanto AR, Wagner JG (1972) Pharmacokinetics of highly ionized drugs. 3. Methylene blue–blood levels in the dog and tissue levels in the rat following intravenous administration. J Pharm Sci 61(7):1090–1094

Dunne A (1993) Statistical moments in pharmacokinetics: models and assumptions. J Pharm Pharmacol 45(10):871–875

European agency for the evaluation of medicinal products (2007) Guideline on reporting the results of population pharmacokinetic analyses. CHMP/EWP/185990/06 (available at http://www.ema.europa.eu/docs/en_GB/document_library/Scientific_guideline/2009/09/WC500003067.pdf)

Ette EI, Sun H, Ludden TM (1998) Balanced designs in longitudinal population pharmacokinetic studies. J Clin Pharmacol 38(5):417–423
Frank GT (1982) A physiological pharmacokinetic model of the lung. MChE, University of Delaware, Newark (Master's thesis, advisor: K. Bischoff)
Freedson P, Katch VL, Sady S, Weltman A (1979) Cardiac output differences in males and females during mild cycle ergometer exercise. Med Sci Sports 11(1):16–19
Frey N, Laveille C, Paraire M, Francillard M, Holford NH, Jochemsen R (2003) Population PKPD modelling of the long-term hypoglycaemic effect of gliclazide given as a once-a-day modified release (MR) formulation. Br J Clin Pharmacol 55(2):147–157
Fuller LM, Banker FL, Butler JJ, Gamble JF, Sullivan MP (1975) The natural history of non-Hodgkin's lymphomata stages I and II. Br J Cancer Suppl 2:270–285
Gabrielsson J, Weiner D (2007) Pharmacokinetic and pharmacodynamic data analysis: concepts and applications, Fourth edn. Swedish Pharmaceutical Press
Gall MA, Nielsen FS, Smidt UM, Parving HH (1993) The course of kidney function in type 2 (non-insulin-dependent) diabetic patients with diabetic nephropathy. Diabetologia 36(10):1071–1078
Gerlowski LE, Jain RK (1983) Physiologically based pharmacokinetic modeling: principles and applications. J Pharm Sci 72(10):1103–1127
Gibaldi M, Perrier D (1999) Pharmacokinetics: revised and expanded. Drugs Pharma Sci 92:15–15
Gomeni R, Teneggi V, Iavarone L, Squassante L, Bye A (2001) Population pharmacokinetic-pharmacodynamic model of craving in an enforced smoking cessation population: indirect response and probabilistic modeling. Pharma Res 18(4):537–543
Grantham JJ, Cook LT, Torres VE, Bost JE, Chapman AB, Harris PC et al (2008) Determinants of renal volume in autosomal-dominant polycystic kidney disease. Kidney Int 73(1):108–116
Grehant N (1904a) Mesure de l'activite physio-logique des reins par le dosage de l'ure'e dans le sang et dans l'urine. J Physiol et Path Gen 7:1
Grehant N (1904b) Physiologique des reins par le dosage de l'uree dans le sang et daus l'urine. J physiol (Paris) 6:1–8
Gupta SK, Sathyan G, Lindemulder EA, Ho PL, Sheiner LB, Aarons L (1999) Quantitative characterization of therapeutic index: application of mixed-effects modeling to evaluate oxybutynin dose-efficacy and dose-side effect relationships. Clin Pharmacol Ther 65(6):672–684
Guyton AC, Hall JE (1996) Textbook of medical physiology, 9th edn. Saunders, Philadelphia
Hall JE, Guyton AC (2011) Guyton and hall textbook of medical physiology, 12th edn. Saunders, Philadelphia
Hamren B, Bjork E, Sunzel M, Karlsson M (2008) Models for plasma glucose, HbA1c, and hemoglobin interrelationships in patients with type 2 diabetes following tesaglitazar treatment. Clin Pharmacol Ther 84(2):228–235
Harrell FE (2001) Regression modeling strategies: with applications to linear models, logistic regression, and survival analysis, edn. Springer
Heiberger RM, Holland B (2004) Statistical analysis and data display: an intermediate course with examples in S-plus, R, and SAS, edn. Springer
Herman WH (2003) Diabetes modeling. Diabetes Care 26(11):3182–3183
Holford N (2013) A time to event tutorial for pharmacometricians. CPT Pharmacometrics Syst Pharmacol 2:e43
Holford NH, Peace KE (1992a) Methodologic aspects of a population pharmacodynamic model for cognitive effects in Alzheimer patients treated with tacrine. Proc Natl Acad Sci U S A 89(23):11466–11470
Holford NH, Peace KE (1992b) Results and validation of a population pharmacodynamic model for cognitive effects in Alzheimer patients treated with tacrine. Proc Natl Acad Sci U S A 89(23):11471–11475
Holford N, Ma SC, Ploeger BA (2010) Clinical trial simulation: a review. Clin Pharmacol Ther 88(2):166–182
Hougaard P (1995) Frailty models for survival data. Lifetime Data Anal 1(3):255–273

Hu TM, Hayton WL (2001) Allometric scaling of xenobiotic clearance: uncertainty versus universality. AAPS PharmSci 3(4):E29

Huang SM (2012) PBPK as a tool in regulatory review. Biopharm Drug Dispos 33(2):51–52

Huang SM, Rowland M (2012) The role of physiologically based pharmacokinetic modeling in regulatory review. Clin Pharmacol Ther 91(3):542–549

Hutter JC, Luu HM, Mehlhaff PM, Killam AL, Dittrich HC (1999) Physiologically based pharmacokinetic model for fluorocarbon elimination after the administration of an octafluoropropane-albumin microsphere sonographic contrast agent. J Ultrasound Med 18(1):1–11

Johnston SR, Hickish T, Ellis P, Houston S, Kelland L, Dowsett M et al (2003) Phase II study of the efficacy and tolerability of two dosing regimens of the farnesyl transferase inhibitor, R115777, in advanced breast cancer. J Clin Oncol 21(13):2492–2499

Jusko WJ, Ko HC (1994) Physiologic indirect response models characterize diverse types of pharmacodynamic effects. Clin Pharmacol Ther 56(4):406–419

Karlsson MO, Schoemaker RC, Kemp B, Cohen AF, van Gerven JM, Tuk B et al (2000) A pharmacodynamic Markov mixed-effects model for the effect of temazepam on sleep. Clin Pharmacol Ther 68(2):175–188

Kemp B, Kamphuisen HA (1986) Simulation of human hypnograms using a Markov chain model. Sleep 9(3):405–414

Kimko HC, Peck CC (2011) Clinical trial simulations: applications and trends, edn. Springer, New York

Kimko HC, Reele SS, Holford NH, Peck CC (2000) Prediction of the outcome of a phase 3 clinical trial of an antischizophrenic agent (quetiapine fumarate) by simulation with a population pharmacokinetic and pharmacodynamic model. Clin Pharmacol Ther 68(5):568–577

Kjellsson MC, Zingmark PH, Jonsson EN, Karlsson MO (2008) Comparison of proportional and differential odds models for mixed-effects analysis of categorical data. J Pharmacokinet Pharmacodyn 35(5):483–501

Knibbe CA, Zuideveld KP, DeJongh J, Kuks PF, Aarts LP, Danhof M (2002) Population pharmacokinetic and pharmacodynamic modeling of propofol for long-term sedation in critically ill patients: a comparison between propofol 6% and propofol 1%. Clin Pharmacol Ther 72(6):670–684

Kowalski KG, Hutmacher MM (2001) Design evaluation for a population pharmacokinetic study using clinical trial simulations: a case study. Stat Med 20(1):75–91

Kowalski KG, McFadyen L, Hutmacher MM, Frame B, Miller R (2003) A two-part mixture model for longitudinal adverse event severity data. J Pharmacokinet Pharmacodyn 30(5):315–336

Lacroix BD, Lovern MR, Stockis A, Sargentini-Maier ML, Karlsson MO, Friberg LE (2009) A pharmacodynamic Markov mixed-effects model for determining the effect of exposure to certolizumab pegol on the ACR20 score in patients with rheumatoid arthritis. Clin Pharmacol Ther 86(4):387–395

Landersdorfer CB, Jusko WJ (2008) Pharmacokinetic/pharmacodynamic modelling in diabetes mellitus. Clin Pharmacokinet 47(7):417–448

Lee PI (2001) Design and power of a population pharmacokinetic study. Pharma Res 18(1):75–82

Leong R, Vieira ML, Zhao P, Mulugeta Y, Lee CS, Huang SM et al (2012) Regulatory experience with physiologically based pharmacokinetic modeling for pediatric drug trials. Clin Pharmacol Ther 91(5):926–931

Lewis AE (1948) The concept of hepatic clearance. Am J Clin Pathol 18(10):789–795

Lewis EJ, Hunsicker LG, Bain RP, Rohde RD (1993) The effect of angiotensin-converting-enzyme inhibition on diabetic nephropathy. The Collaborative Study Group. N Engl J Med 329(20):1456–1462

Liu X, Smith BJ, Chen C, Callegari E, Becker SL, Chen X et al (2005) Use of a physiologically based pharmacokinetic model to study the time to reach brain equilibrium: an experimental analysis of the role of blood-brain barrier permeability, plasma protein binding, and brain tissue binding. J Pharmacol Exp Ther 313(3):1254–1262

Lunn DJ, Wakefield J, Racine-Poon A (2001) Cumulative logit models for ordinal data: a case study involving allergic rhinitis severity scores. Stat Med 20(15):2261–2285

Mager DE, Abernethy DR, Egan JM, Elahi D (2004) Exendin-4 pharmacodynamics: insights from the hyperglycemic clamp technique. J Pharmacol Exp Ther 311(2):830–835
Maiwald T, Timmer J (2008) Dynamical modeling and multi-experiment fitting with PottersWheel. Bioinformatics 24(18):2037–2043
Mandema JW, Stanski DR (1996) Population pharmacodynamic model for ketorolac analgesia. Clin Pharmacol Ther 60(6):619–635
McCullagh P (1980) Regression models for ordinal data. J R Stat Soc B 42(2): 109–142
McDonagh CF, Huhalov A, Harms BD, Adams S, Paragas V, Oyama S et al (2012) Antitumor activity of a novel bispecific antibody that targets the ErbB2/ErbB3 oncogenic unit and inhibits heregulin-induced activation of ErbB3. Mol Cancer Ther 11(3):582–593
Meibohm B, Laer S, Panetta JC, Barrett JS (2005) Population pharmacokinetic studies in pediatrics: issues in design and analysis. AAPS J 7(2):E475–E487
Metcalfe C, Thompson SG (2007) Wei, Lin and Weissfeld's marginal analysis of multivariate failure time data: should it be applied to a recurrent events outcome? Stat Methods Med Res 16(2):103–122
Mordenti J, Chappell W (1989) The use of interspecies scaling in toxicokinetics. In: Yacobi A, Skelly JP, Batra V (eds) Toxicokinetics and new drug development, edn. Pergamon, New York, pp 42–96
Mould D, Chapelsky M, Aluri J, Swagzdis J, Samuels R, Granett J (2001) A population pharmacokinetic-pharmacodynamic and logistic regression analysis of lotrafiban in patients. Clin Pharmacol Ther 69(4):210–222
Mould DR (2007) Developing models of disease progression. In: Ette EI, Williams PJ (eds) Pharmacometrics: the science of quantitative pharmacology, edn. Wiley, Hoboken, pp 547–581
Mould DR, Holford NH, Schellens JH, Beijnen JH, Hutson PR, Rosing H et al (2002) Population pharmacokinetic and adverse event analysis of topotecan in patients with solid tumors. Clin Pharmacol Ther 71(5):334–348
Mould DR, Denman NG, Duffull S (2007) Using disease progression models as a tool to detect drug effect. Clin Pharmacol Ther 82(1):81–86
Nestorov IA, Aarons LJ, Arundel PA, Rowland M (1998) Lumping of whole-body physiologically based pharmacokinetic models. J Pharmacokinet Biopharma 26(1):21–46
Nielsen EI, Friberg LE (2013) Pharmacokinetic-pharmacodynamic modeling of antibacterial drugs. Pharmacol Rev 65(3):1053–1090
Ogungbenro K, Aarons L (2008) How many subjects are necessary for population pharmacokinetic experiments? Confidence interval approach. Eur J Clin Pharmacol 64(7):705–713
Oliver RE, Jones AF, Rowland M (2001) A whole-body physiologically based pharmacokinetic model incorporating dispersion concepts: short and long time characteristics. J Pharmacokinet Pharmacodyn 28(1):27–55
Olofsen E, Romberg R, Bijl H, Mooren R, Engbers F, Kest B et al (2005) Alfentanil and placebo analgesia: no sex differences detected in models of experimental pain. Anesthesiology 103(1):130–139
Ouellet D, Sutherland S, Wang T, Griffini P, Murthy V (2011) First-time-in-human study with GSK1018921, a selective GlyT1 inhibitor: relationship between exposure and dizziness. Clin Pharmacol Ther 90(4):597–604
Pacini G, Bergman RN (1986) MINMOD: a computer program to calculate insulin sensitivity and pancreatic responsivity from the frequently sampled intravenous glucose tolerance test. Compute Methods Programs Biomed 23(2):113–122
Pang KS, Durk MR (2010) Physiologically-based pharmacokinetic modeling for absorption, transport, metabolism and excretion. J Pharmacokinet Pharmacodyn 37(6):591–615
Parving HH, Rossing P, Hommel E, Smidt UM (1995) Angiotensin-converting enzyme inhibition in diabetic nephropathy: ten years' experience. Am J Kidney Dis 26(1):99–107
Peters RH (1986) The ecological implications of body size, edn, Cambridge University Press
Peters SA (2008) Evaluation of a generic physiologically based pharmacokinetic model for lineshape analysis. Clin Pharmacokinet 47(4):261–275

Peters SA (2012) Physiologically-based pharmacokinetic (PBPK) modeling and simulations: principles, methods, and applications in the pharmaceutical industry, First edn. Wiley
Peters SA, Hultin L (2008) Early identification of drug-induced impairment of gastric emptying through physiologically based pharmacokinetic (PBPK) simulation of plasma concentration-time profiles in rat. J Pharmacokinet Pharmacodyn 35(1):1–30
Peterson B, Harrell Jr FE (1990) Partial proportional odds models for ordinal response variables. Appl Stat 39(2): 205–217
Pillai G, Gieschke R, Goggin T, Jacqmin P, Schimmer RC, Steimer JL (2004) A semimechanistic and mechanistic population PK-PD model for biomarker response to ibandronate, a new bisphosphonate for the treatment of osteoporosis. Br J Clin Pharmacol 58(6):618–631
Pors Nielsen S, Barenholdt O, Hermansen F, Munk-Jensen N (1994) Magnitude and pattern of skeletal response to long term continuous and cyclic sequential oestrogen/progestin treatment. Br J Obstet Gynaecol 101(4):319–324
Poulin P, Theil FP (2000) A priori prediction of tissue:plasma partition coefficients of drugs to facilitate the use of physiologically-based pharmacokinetic models in drug discovery. J Pharm Sci 89(1):16–35
Poulin P, Theil FP (2002a) Prediction of pharmacokinetics prior to in vivo studies. 1. Mechanism-based prediction of volume of distribution. J Pharm Sci 91(1):129–156
Poulin P, Theil FP (2002b) Prediction of pharmacokinetics prior to in vivo studies. II. Generic physiologically based pharmacokinetic models of drug disposition. J Pharm Sci 91(5):1358–1370
Poulin P, Schoenlein K, Theil FP (2001) Prediction of adipose tissue: plasma partition coefficients for structurally unrelated drugs. J Pharm Sci 90(4):436–447
Ramsey JC, Andersen ME (1984) A physiologically based description of the inhalation pharmacokinetics of styrene in rats and humans. Toxicol Appl Pharmacol 73(1):159–175
Ravva P, Gastonguay MR, Tensfeldt TG, Faessel HM (2009) Population pharmacokinetic analysis of varenicline in adult smokers. Br J Clin Pharmacol 68(5):669–681
Reddy M, Yang R, Andersen ME, Clewell III HJ (2005) Physiologically based pharmacokinetic modeling: science and applications, First edn. Wiley-Interscience
Rosch J, Antonovic R, Trenouth RS, Rahimtoola SH, Sim DN, Dotter CT (1976) The natural history of coronary artery stenosis. A longitudinal angiographic assessment. Radiology 119(3):513–520
Ross SM (2006) Introduction to probability models, edn. Access Online via Elsevier
Rowland M (1972) Application of clearance concepts to some literature data on drug metabolism in the isolated perfused liver preparation and in vivo. Eur J Pharmacol 17(3):352–356
Rowland M, Tozer TN (1989) Clinical pharmacokinetics: concepts and applications, edn, vol. 162. Lea & Febiger, Philadelphia
Rowland M, Benet LZ, Graham GG (1973) Clearance concepts in pharmacokinetics. J Pharmacokinet Biopharma 1(2):123–136
Rowland M, Peck C, Tucker G (2011) Physiologically-based pharmacokinetics in drug development and regulatory science. Annu Rev Pharmacol and Toxicol 51:45–73
Sadray S, Jonsson EN, Karlsson MO (1999) Likelihood-based diagnostics for influential individuals in non-linear mixed effects model selection. Pharm Res 16(8):1260–1265
Savage VM, Gillooly J, Woodruff W, West G, Allen A, Enquist B et al (2004) The predominance of quarter-power scaling in biology. Funct Ecol 18(2):257–282
Savic RM, Karlsson MO (2009) Importance of shrinkage in empirical bayes estimates for diagnostics: problems and solutions. AAPS J 11(3):558–569
Schmidt S, Post TM, Boroujerdi MA, van Kesteren C, Ploeger BA, Della Pasqua OE et al (2011) Disease progression analysis: towards mechanism-based models. In: Kimko HC, Peck CC (eds) Clinical trial simulations, edn. Springer, New York, pp 433–455
Schoeberl B, Pace EA, Fitzgerald JB, Harms BD, Xu L, Nie L et al (2009) Therapeutically targeting ErbB3: a key node in ligand-induced activation of the ErbB receptor-PI3K axis. Sci Signal 2(77):ra31
Sheiner LB, Ludden TM (1992) Population pharmacokinetics/dynamics. Annu Rev Pharmacol Toxicol 32:185–209

Sheiner LB, Rosenberg B, Marathe VV (1977) Estimation of population characteristics of pharmacokinetic parameters from routine clinical data. J Pharmacokinet Biopharma 5(5):445–479
Sheiner LB, Stanski DR, Vozeh S, Miller RD, Ham J (1979) Simultaneous modeling of pharmacokinetics and pharmacodynamics: application to d-tubocurarine. Clin Pharmacol Ther 25(3):358–371
Sy SK, Heuberger J, Shilbayeh S, Conrado DJ, Derendorf H (2013a) A Markov Chain model to evaluate the effect of CYP3A5 and ABCB1 polymorphisms on adverse events associated with tacrolimus in pediatric renal transplantation. AAPS J 15(4):1189–99
Sy SK, Singh RP, Shilbayeh S, Zmeili R, Conrado D, Derendorf H (2013b) Influence of CYP3A5 6986A > G and ABCB1 3435C > T Polymorphisms on Adverse Events Associated With Tacrolimus in Jordanian Pediatric Renal Transplant Patients. Clin Pharmacol Drug Dev 2(1):67–78
Teorell T (1937a) Kinetics of distribution of substances administered to the body, I: the extravascular modes of administration. Arch Int pharmacodyn Ther 57:205–225
Teorell T (1937b) Kinetics of distribution of substances administered to the body, II: the intravascular modes of administration. Arch Int Pharmacodyn Ther 57:226–240
Theil FP, Guentert TW, Haddad S, Poulin P (2003) Utility of physiologically based pharmacokinetic models to drug development and rational drug discovery candidate selection. Toxicol Lett 138(1–2):29–49
Thomaseth K, Salvan A (1998) Estimation of occupational exposure to 2,3,7,8-tetrachlorodibenzo-p-dioxin using a minimal physiologic toxicokinetic model. Environ Health Perspect 106(Suppl 2):743–753
Troconiz IF, Plan EL, Miller R, Karlsson MO (2009) Modelling overdispersion and Markovian features in count data. J Pharmacokinet Pharmacodyn 36(5):461–477
U.S. Department of Health and Human Services, Food and Drug Administration. DA (1999) Guidance for industry: population pharmacokinetics, (available at http://www.fda.gov/downloads/ScienceResearch/SpecialTopics/WomensHealthResearch/UCM133184.pdf)
van der Molen GW, Kooijman SA, Slob W (1996) A generic toxicokinetic model for persistent lipophilic compounds in humans: an application to TCDD. Fundam Appl Toxicol 31(1):83–94
Venables WN, Ripley BD, Venables W (1994) Modern applied statistics with S-PLUS, edn, vol. 250. Springer, New York
Vong C, Bergstrand M, Nyberg J, Karlsson MO (2012) Rapid sample size calculations for a defined likelihood ratio test-based power in mixed-effects models. AAPS J 14(2):176–186
Wada DR, Bjorkman S, Ebling WF, Harashima H, Harapat SR, Stanski DR (1997) Computer simulation of the effects of alterations in blood flows and body composition on thiopental pharmacokinetics in humans. Anesthesiology 87(4):884–899
Wang X, Santostefano MJ, Evans MV, Richardson VM, Diliberto JJ, Birnbaum LS (1997) Determination of parameters responsible for pharmacokinetic behavior of TCDD in female Sprague-Dawley rats. Toxicol Appl Pharmacol 147(1):151–168
Wei L, Glidden DV (1997) An overview of statistical methods for multiple failure time data in clinical trials. Stat Med 16(8):833–839
Wei L-J, Lin DY, Weissfeld L (1989) Regression analysis of multivariate incomplete failure time data by modeling marginal distributions. J Am Stat Assoc 84(408):1065–1073
West GB, Brown JH, Enquist BJ (1997) A general model for the origin of allometric scaling laws in biology. Science 276(5309):122–126
West GB, Brown JH, Enquist BJ (1999) The fourth dimension of life: fractal geometry and allometric scaling of organisms. Science 284(5420):1677–1679
Wilkinson GR (1987) Clearance approaches in pharmacology. Pharmacol Rev 39(1):1–47
Wilkinson GR, Shand DG (1975) Commentary: a physiological approach to hepatic drug clearance. Clin Pharmacol Ther 18(4):377–390
Xie R, Mathijssen RH, Sparreboom A, Verweij J, Karlsson MO (2002) Clinical pharmacokinetics of irinotecan and its metabolites in relation with diarrhea. Clin Pharmacol Ther 72(3):265–275
Yamaoka K, Nakagawa T, Uno T (1978) Statistical moments in pharmacokinetics. J Pharmacokinet Biopharma 6(6):547–558

Yang J, Zhao H, Garnett C, Rahman A, Gobburu JV, Pierce W et al (2012) The combination of exposure-response and case-control analyses in regulatory decision making. J Clin Pharmacol 53(2):160–6

Yim DS, Zhou H, Buckwalter M, Nestorov I, Peck CC, Lee H (2005) Population pharmacokinetic analysis and simulation of the time-concentration profile of etanercept in pediatric patients with juvenile rheumatoid arthritis. J Clin Pharmacol 45(3):246–256

Zhao W, Elie V, Roussey G, Brochard K, Niaudet P, Leroy V et al (2009) Population pharmacokinetics and pharmacogenetics of tacrolimus in de novo pediatric kidney transplant recipients. Clin Pharmacol Ther 86(6):609–618

Zhao P, Zhang L, Grillo JA, Liu Q, Bullock JM, Moon YJ et al (2011) Applications of physiologically based pharmacokinetic (PBPK) modeling and simulation during regulatory review. Clin Pharmacol Ther 89(2):259–267

Zhao P, Rowland M, Huang SM (2012) Best practice in the use of physiologically based pharmacokinetic modeling and simulation to address clinical pharmacology regulatory questions. Clin Pharmacol Ther 92(1):17–20

Zingmark PH, Ekblom M, Odergren T, Ashwood T, Lyden P, Karlsson MO et al (2003) Population pharmacokinetics of clomethiazole and its effect on the natural course of sedation in acute stroke patients. Br J Clin Pharmacol 56(2):173–183

Chapter 2
Personalized Medicine: Integrating Individual Exposure and Response Information at the Bedside

Diane R. Mould and Lawrence J. Lesko

2.1 Introduction

Historically, therapeutic agents were dosed using the same dose for all patients ("flat dosing"), sometimes dosed on body size (weight or body surface area, BSA), or adjusted based on key patient factors (covariates), such as degree of renal impairment. For some agents such as warfarin, the risks associated with both over and underdosing are substantial, and genetic markers can be used to refine the starting dose and the dose increments in order to safely achieve the international normalized ratio (INR) target range and subsequent clinical effect. However, owing to differences in tolerance such as with antineoplastic agents, or effects, such as with antihypertensive agents, adaptive dosing where doses are adjusted based on observed response ("adaptive dosing") is also used. Individualizing drug therapy, or tailoring the selection of both the drug and the dose for a specific patient, has been a long-held objective of physicians and other health-care providers. As stated in a recent review of the history of individualized medicine (Lesko and Schmidt 2012), "personalized medicine is an evolution, not a revolution."

Personalized medicine is expected to optimize the benefit and minimize the harm of medical interventions on a patient-by-patient basis. Thus, the goal of personalized medicine is to identify patient characteristics predictive of response to therapy and to use this information to provide a therapeutically optimal dose for each patient, or patient subgroups, based on their individual characteristics (Conti et al. 2010). Examples of patient characteristics that may affect drug exposure and response, and subsequently require individualization of treatment and dose include age, body weight, race, sex, organ function (e.g., hepatic and renal function), and various types of biomarkers, such as biochemical, disease markers, and genomic

D. R. Mould (✉)
Projections Research, Phoenixville, PA, USA
e-mail: drmould@pri-home.net

L. J. Lesko
Center for Pharmacometrics and Systems Pharmacology, University of Florida, Orlando, FL, USA

S. Schmidt, H. Derendorf (eds.), *Applied Pharmacometrics,* AAPS Advances in the Pharmaceutical Sciences Series 14, DOI 10.1007/978-1-4939-1304-6_2

markers. The goal of personalized medicine aligns well with that of population pharmacokinetic and pharmacodynamic (PK/PD) modeling, which includes identification of covariate factors that are predictive of heterogeneity and uncertainty in drug exposure and/or response.

The utilization of biomarkers for patient care decisions has been limited by the lack of decision-support tools for practitioners to facilitate integration of biomarker data with other patient specific information to generate a treatment recommendation (Zineh and Huang 2011). PK/PD modeling enables integration of multiple patient characteristics in a drug-specific framework, and recently has been combined with web-based applications that provide a user-friendly interface, or "dashboard" for including patient-specific inputs, updating the associated models, and summarizing and visualizing the data and model-based dose predictions (Barrett et al. 2008). Such dashboard systems have the potential to offer an improved and convenient means for health-care provider to tailor treatment for an individual patient, particularly for drugs with high variability in exposure or a narrow therapeutic window.

2.1.1 Current Dosing Paradigms

There are numerous approaches to developing dose regimens for therapeutic agents, but the most common are the "flat" dose (e.g., all patients receive the same dose), with dosing based on body size also being a common dose metric. In addition, dosing is often stratified based on covariates, such as genotype or organ function. Adaptive dosing, where doses are increased or decreased based on observed effect is also used.

One of the issues with the flat dose option is that the exposure and/or response to a given dose is often highly variable. This variability can arise from differences in the PK, such as in genetic subpopulations, that rapidly clear a drug, or can be due to differences in the PD related to a given plasma drug concentration. If there are factors, such as an effect of weight on clearance, then small patients will tend to be overdosed and patients with high weight will be underdosed using this dose adjustment strategy. Figure 2.1 depicts two hypothetical patients' response to the same dose of a drug. Depending on the therapeutically desired response, these patients may need to receive higher (in the case of the patient with a weaker response) or lower (in the case of the patient with a greater response) doses.

Dosing based on body size is a common approach. However dosing on a mg/kg basis often results in subtherapeutic exposures in low weight patients, particularly pediatric patients (Anderson and Holford 2013; Xu et al. 2013) because the relationship between drug clearance and weight (if it exists) is rarely linear due to the differences in the ratio of clearance organ size to overall body weight. This finding has been confirmed for many compounds, including infliximab (Xu et al. 2012; Fasanmade et al. 2011). The US Food and Drug Administration (FDA) has written a guidance document for industry on dose selection for the minimum recommended dose for first time in humans (FTIH) studies (Guidance 2014) that suggests selection of initial doses based on body weight (e.g., mg/kg) in order to scale exposure observed in nonclinical studies to safe levels in humans. While this document is

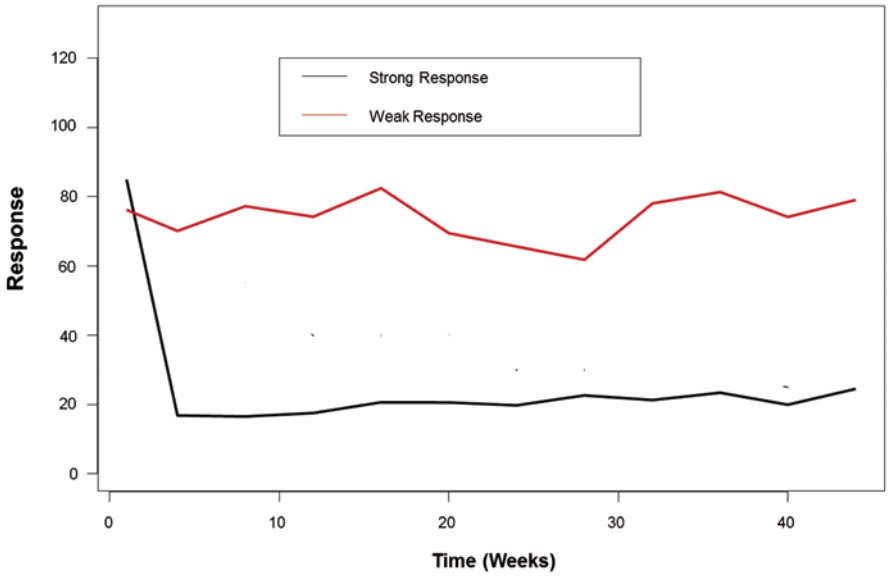

Fig. 2.1 Examples in differences between patients in response to a specific dose. In this figure, two hypothetical patients were administered the same dose of drug with the goal of lowering the measured response indicator. The patient response represented by the *black line* is a patient with a strong response while the patient whose response is represented by the *red line* has a weak response. Thus the latter patient may need a higher dose or a different treatment for their disease

not specifically aimed at providing guidance for dose selection, many marketed monoclonal antibodies (mAbs) are labeled for dosing on a mg/kg basis. A recent review (Mould and Green 2010) found that only three of 26 marketed mAbs had a clearance that was linearly related to weight, eight were dosed on a mg/kg basis and two of these had no weight effect identified on the clearance. Doses based on BSA are similarly problematic. Egorin published a review on BSA-based dosing for antineoplastic agents (Egorin 2003). The variability in exposure with this dosing approach is not always improved as compared to "flat" dosing.

A stratified dose approach where flat doses are administered over specified ranges of body weight, or over and under a given mg/kg weight, is often the best way to ensure appropriate dosing when body size impacts clearance, and may be particularly relevant for pediatric patients (Xu et al. 2013). This approach has the benefit of reducing the overdosing and underdosing seen with flat dosing and dosing based on body size, either weight or BSA.

Some compounds such as epoetin (a biologic agent used to treat anemia) are dosed based on specific hemoglobin measurement. The dose algorithm is complex however, and although the approach works well to control hemoglobin, the complexity of the dose strategy can give rise to dose errors, and dose adjustments takes time to determine. Computer-based dose support has been shown to improve the percentage of patients staying within the target range of hemoglobin, often with a lower dose than the manual adjustment provided (Ho et al. 2010), and with substantially increased staff efficiency without having a negative impact on safety

(Miskulin et al. 2009). Thus, computer-guided dosing may have a substantial impact on optimizing patient management of their therapies.

2.1.2 Definition of a Dashboard

A dashboard is a user interface that, like a dashboard in a car, organizes and presents information so that is easy and quick to read and interpret. Software packages that integrate information from multiple components into a unified display are referred to as dashboards. For example, patient management dashboards might obtain information from electronic medical records, laboratories, and through clinician and patient input and present it as though it all came from the same source. Hewlett Packard (HP) developed the first dashboard system, which began as a tool for customizing Windows desktops. Called "Dashboard," the HP product was later acquired by Borland and then a company called Starfish (Dashboard 2014).

"Dose calculators" have been in existence since the late 1950s, although the majority of these early systems were to calculate radiological doses (Sivyer 1959). Until recently, the computational needs of individualized dosing were limited, although the application of Bayesian forecasting has been shown to result in therapeutic improvements. For example, application of Bayesian-based dosing substantially increased the number of patients whose trough phenytoin levels were within the target range (63.6% of the phenytoin troughs from the Bayesian forecasting group, compared with 34.0% in the conventional dose adjustment group) (Tobler and Mühlebach 2013). One of the earlier dashboard systems in clinical use focused on antineoplastic dosing for pediatrics (Barrett et al. 2008), and the number of dashboard systems has grown over time.

A related topic that will not be covered in detail here is the emergence of computerized clinical decision support systems (CDSS). Papier (2012) defined these as "an interactive system allowing input of patient-specific information and providing customized medical knowledge-based results via automated reasoning, for example, via a set of rules and/or an underlying logic, and associations." These systems generally are not based on an underlying population model but embody collected clinical expertise which is compared to a patient's symptoms using methods such as rule-based or fuzzy logic algorithms (Domínguez Hernández et al. 2013). Like dashboard systems, they are a growing area of research seeking to maximize the use of prior knowledge for an individual patient.

2.1.3 Relationship to Population Models

Dashboard systems are generally built around a population model (Mould and Upton 2012). The population model is essentially an embodiment of the current state of knowledge about the PK or PD of a drug and generally includes three key components:

1. The structural (base) model (e.g., a one-compartment PK model) that provides a (ideally) mechanistic description of the time course of a measured response.

2. Stochastic (probability) models that describe the distribution of unexplained variability in the observed population, such as between-subject variability (BSV) or residual variability (RUV).
3. Covariate models that quantitate the influence of explainable factors such as demographics or disease on individual time course of the response.

The dashboard system is intended to be a user-friendly system for accessing the model to forecast exposure or response for an individual patient, with the predictions of the model refined by incorporating information about each individual patient into the model. The greater the size and diversity of the database used to construct the underlying model, the greater the chance that the model will be able to return useful and accurate individual predictions for most patients. However, it should be recognized that there are limitations to forecasting using population models. The underlying assumption is always that a particular population model will continue to describe data from a patient into the future, and that the model captures all important sources of variability (both explainable and unexplainable). When the underlying assumptions do not apply to a given patient, the model predictions have the potential to be in substantial error. For example, a given model of drug PK may have been appropriate for a patient in the past, but if the patient has a cardiac infarct (with major reductions in cardiac output with a subsequent impact on drug clearance), the forecast concentrations from the model may be substantially underestimated.

2.2 Individualized Forecasts

There are two main mechanisms by which individual data can be used to refine the predictions of a population for a particular patient. These are via covariate relationships identified during the model building process, and by Bayes updating on model parameters based on individual data. Figure 2.2 shows an example of how both methods can work together to improve the forecast for an individual patient.

2.2.1 Covariate Effects

Covariates (e.g., age, sex, renal function) modify the value of a model parameter (e.g., clearance, CL) depending on the value of the covariate (e.g., body weight on CL in Fig. 2.2). The inclusion of a covariate relationship in a model will generally imply that the model provides a better description of the data and that the unexplained BSV of the associated parameter is reduced. Thus, covariate factors effectively convert unexplainable variability to explainable variability at the population level, and reduce the uncertainty in the values of the model parameters for individual patients for whom covariate values are known (Fig. 2.2). However, depending on the drug and the dataset used to develop the model, the contribution of covariates to reductions in unexplainable variability can vary from nothing (i.e., no covariates identified) to modest or substantial contributions. When no covariates are found, this implies that

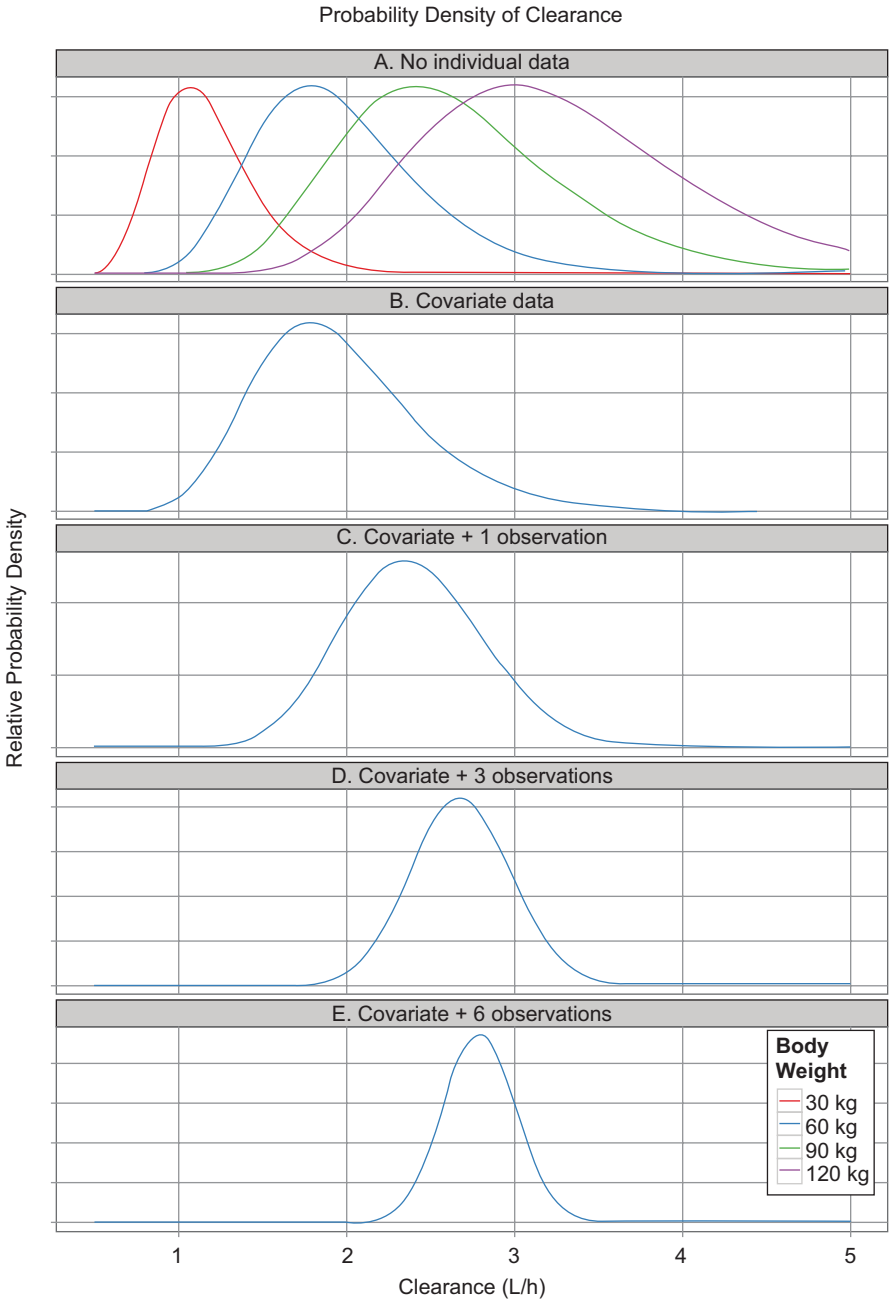

Fig. 2.2 An example of the contribution of individual data to Bayes forecasts. Below is an example model to determine steady-state drug concentration (C_{ss}) of a chronically administered drug: C_{ss} = DoseRate/(CL*(WT/70)$^{0.75}$). CL is a log-normally distributed population parameter with a population value of 2 L/h and BSV of 25%. Patient body weight (WT) is a covariate affecting

the factors causing variability between patients have either not been identified, were not possible to measure in sufficient numbers of individuals, or were not available at all in the analysis dataset. It is important to note that the ability to identify predictive covariates is dependent on both the method used to evaluate the data (Wählby U, Jonsson EN, Karlsson MO. Assessment of actual significance levels for covariate effects in NONMEM. J Pharmacokinet Pharmacodyn. 2001; 28(3):231-52) and the approaches used during modeling (Mould and Upton 2013). However, even when covariates are identified, many agents still have considerable unexplained variability, which limits the use of patient covariates in individualizing dosing.

2.2.2 Bayes Update of Models with Individual Data

Most of the currently available software packages for individualizing therapy utilize Bayesian methods to help predict future response to a given dose regimen. In general, such software packages use a mixture of Bayesian updating, Bayesian forecasting, and Bayesian model averaging. Bayesian inference is a method in which Bayes' rule is used to update the probability estimate for a hypothesis as additional data are obtained. Bayesian updating is particularly important in the dynamic analysis of data collected sequentially over time.

Bayesian updating uses a model that not only describes the time course of exposure and response but also includes terms describing the unexplained (random) variability of exposure and response. It involves applying a "prior" (which is called a prior because it reflects the underlying information derived from previous evaluations) to form the underlying hypothesis. The prior distribution is the distribution of the parameter(s) before any new data are observed and is usually developed in a separate analysis. The prior therefore is the series of mathematical models describing exposure and response following administration of a drug. The sampling distribution is the distribution of the observed data conditional on its parameters. This is also termed the likelihood, especially when viewed as a function of the parameter(s). The marginal likelihood (also called a "posterior") is the distribution

---

CL via an allometric relationship, where the standard body weight is 70 kg. DoseRate is the average steady-state dose rate—set at 10 mg/h, proportional residual error for the model was 20%. We wish to forecast the clearance of the drug (so that individual C_{ss} can be estimated). *Panel A* shows the probability densities for CL for the case where no individual patient information is known (densities are normalized to the same peak value for clarity). There are a variety of possible distributions for CL, depending on the unknown body weight of the patient. *Panel B* shows the distribution of CL with covariate data. The patient has a weight of 60 kg, eliminating other candidate distribution curves. *Panel C* shows the distribution of CL with covariate data and a single observation of C_{ss} in the patient. In this case, C_{ss} was found to be 4 mg/L, which was lower than the expected value of 5.6 mg/L for a 60-kg subject. The distribution therefore moves to the right, reflecting higher individual clearance and becomes narrower, reflecting more certainty about the individual patent value of CL. *Panels D* and E show the distribution of CL with covariate data, and 3 and 6 observations of C_{ss} in the patient, respectively. Note that as more individual data are available, the uncertainty in the distribution of CL reduces (i.e., the distributions are narrower) via Bayesian learning. Adapted from Mould DR, Upton R, Wojciechowski J. Dashboard Systems: Implementing Pharmacometrics from Bench to Bedside. AAPS J ePub June 2014 with permission

Table 2.1 The balance between the prior and the data

Factors that favor the prior	Factors that favor the data
Few data points	Many data points
High residual error	Low residual error
Low population variability	High population variability

of the observed data marginalized over the parameter(s). Thus, Bayes' rule can be applied iteratively. That is, after observing data, the resulting posterior probability can then be treated as a prior probability, and a new posterior probability computed from the next set of new evidence. This procedure is termed Bayesian updating or sometimes "Bayesian learning" (Gill 2008).

However, rather than estimate the parameters for the model based solely on the patients data, Bayes' theorem is implemented to balance the contribution of new data and prior knowledge in the estimation of the model parameters for the individual (see Table. 2.1). Thus, a single data point in an individual is given less weight in the fitting process if it deviates substantially from what has happened before, but is given more weight as additional data points support the finding. Similarly, a parameter value is given less weight in the fitting process if it deviates substantially from the prior values inherent in the population model (see Fig. 2.2). From a Bayes perspective, the interpretation of a data point is seen to have contributions respectively from the truth (the underlying process, described by a model), the errors (intraindividual, interindividual, interstudy, residual, etc.), and the prior knowledge:

$$\text{data} = \text{truth} + \text{error} + \text{prior knowledge}.$$

The updating process involves sampling parameters from the prior distribution and calculating the expected response based on the model, then comparing the difference between the model expectation and the observed data. This difference is referred to as the objective function. The parameters are then adjusted based on the objective function and the new parameters are tested. This process runs iteratively until the objective function is as low as possible (referred to as "minimizing the objective function") suggesting that the parameters are the best to describe the current data. The result of Bayesian updating is a set of parameters conditional to the observed data balanced by the application of the principles of Bayes' theorem.

Bayesian model averaging (Hoeting et al. 1999) offers a systematic method for checking the robustness of one's results to alternative models. The standard practice of selecting a single model from some class of models, and then making inferences based on this model ignores model uncertainty, can impair predictive performance and overestimate the strength of evidence for predicting dose–exposure relationships. Bayesian model averaging allows model uncertainty to be incorporated into inference. The basic idea behind Bayesian model averaging is to make inferences based on a weighted average over model space which includes several models. This approach accounts for model uncertainty in both predictions and parameter estimates. The resulting estimates incorporate model uncertainty and thus may better reflect the true uncertainty in the estimates.

Table 2.2 Overview of selected dashboard systems

Software	Bayesian updating	Bayesian forecasting	Bayesian averaging	Dose	Drugs	Website
Abbottbase (Wong et al. 2013)	Yes	Yes	No	Yes, to an AUC	Aminoglycosides	NA
Drugcalc (García et al. 1994)	Yes	No	No	Yes to an AUC	Aminoglycosides	http://www.testandcalc.com/drugcalc/index.asp
Dosecalc (Mohan et al. 2004)	No	No	No	Yes to an AUC		NA
MW/Pharm (Usman et al. 2013)	Yes	Yes	No	Yes	180 drugs	http://www.mwpharm.nl/main.htm
CHOP Pediatric Knowledgebase Dashboard (Barrett et al. 2008)	Yes	Yes	No	Yes through forecast	Pediatric oncology (methotrexate)	http://pkb.chop.edu/index.php
NZ FirstDose Dashboard (Holford et al.)	No	Yes	No	Yes	Amikacin and vancomycin	http://www.firstdose.org/
TCIworks (Wong et al. 2013)	Yes	No	No	No	Gentamycin and enoxaparin	http://www.tciworks.info/
Warfarin dosing	No	No	No	Yes based on covariates	Warfarin	http://www.warfarindosing.org/Source/Home.aspx
Baysient dose evaluation system (Mould et al. 2013)	Yes	Yes	Yes	Yes, multiple	Any	http://www.baysient.com

NA not applicable

Bayesian forecasting (Elliott et al. 2006) then involves using the updated individual parameters to forecast the likely exposure and response that a given patient will exhibit with varying dose regimens based on the individual parameter estimates obtained via Bayesian model averaging and Bayesian updating. However, when the software does not have the capacity to do Bayesian updating, then the forecasting is generally based on the patient covariates which is generally less precise.

The majority of dashboard systems available are for use with aminoglycoside antibiotics and warfarin although there is one (Knowledgebase) that deals with dosing pediatric oncology. A list of several currently available systems is provided in Table 2.2. As can be seen, these systems utilize varying aspects of Bayesian methods to determine an individualized dose.

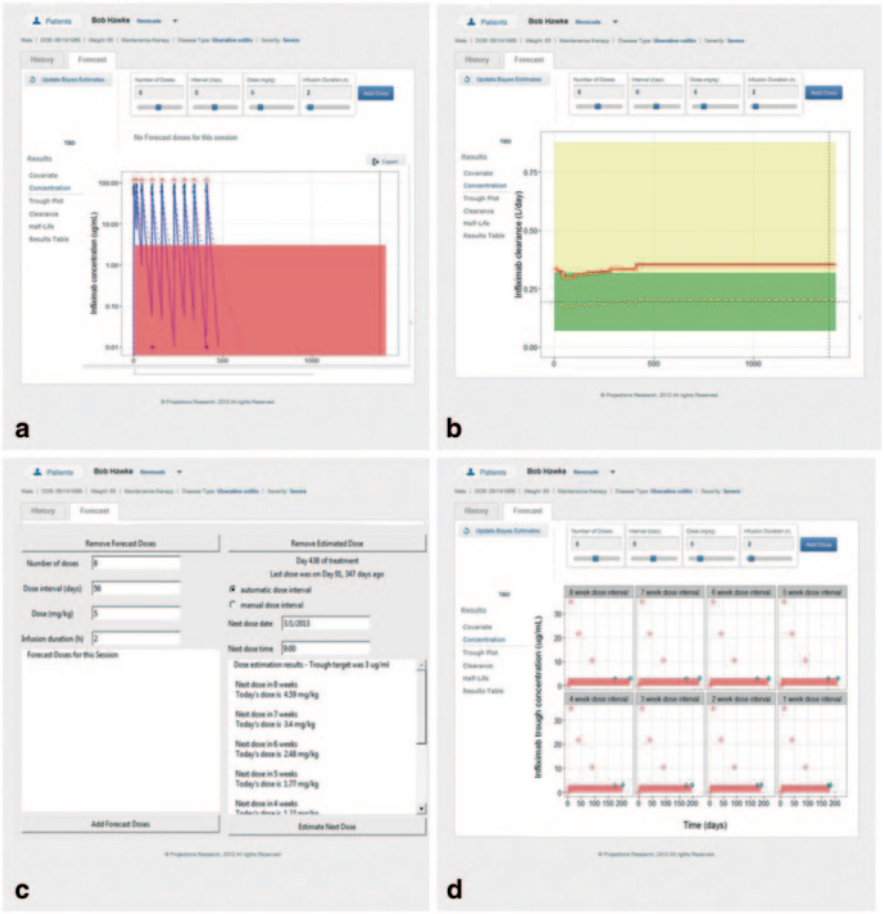

Fig. 2.3 Common dashboard screens. *Panel A* shows the agreement between the model with Bayesian updated parameters (*blue lines*) and the observed data (*blue dots*). Note that the concentrations are within the red shaded region suggesting that this patient is not at or above the target level. *Panel B* shows the patients individually estimated clearance over time. The *green region* is ±3 standard deviations of a typical patient with those covariates. The fact that this patient's clearance is in the *yellow shaded area* suggests that the doses and frequency needed to maintain this patient at the target level will probably exceed the labeled recommendations. *Panel C* shows the dose optimization screen where the clinician can determine either an appropriate regimen (e.g., dose and interval), or can enter the next patient visit to ensure the patient is adequately covered during the interval. *Panel D* shows the expected troughs from all of the recommended dose regimens to ensure they are high enough to achieve a desirable response (https://www.baysient.com)

2.3 Dashboard Systems

In general, dashboard systems have several components including: (1) patient data management, (2) updating/forecasting, and (3) dose recommendations. Figure 2.3 shows screen shots of the results from Bayesian updating and forecasting as well

as the dose recommendation screens. These screens can also be used as a basis for communicating with various health-care providers and patients as the results of delayed or missed doses can be readily shown, potentially improving compliance and an understanding of why medicine responses vary. The output from the Bayesian updating also can be a useful diagnostic for patients whose clearance is so high that maintaining an effective concentration will require very high doses and/or very short dose intervals.

2.3.1 A PK System: Infliximab

In clinical use, infliximab is administered in two "phases": an induction phase where doses are administered frequently (e.g., at weeks 0, 2, and 6) and a maintenance phase where doses are given every 8 weeks. More than one third of patients show no or little response to induction therapy (primary nonresponders) and in up to 50% of responders, tumor necrosis factor (TNF) antagonist therapy becomes ineffective over time (secondary nonresponders; Peyrin-Biroulet et al. 2008). Loss of response to infliximab, which is often due to development of neutralizing antidrug antibodies (ADAs) and subtherapuetic drug concentrations, is an ongoing challenge in managing of patients with chronic inflammatory disease.

There is a strong relationship between serum drug concentrations and response. Studies conducted in both rheumatoid arthritis (RA) and inflammatory bowel disease (IBD), have shown that patients with higher trough drug concentrations achieve superior outcomes without added safety risks (Seow et al. 2010; Maser et al. 2006; Radstake et al. 2009). These findings suggest that therapeutic drug monitoring may be used to direct dose adjustment and support clinical decision making. Infliximab concentrations ≥ 12 μg/ml at 4 weeks after infusion and/or >1.4 μg/ml at dosing trough are considered to be predictive of therapeutic response (Baert et al. 2003). Following dosing, infliximab concentrations have been shown to be highly variable between individuals and differ over time even within an individual patient. The differences in the observed concentration–time profiles can be partially explained by patient covariates and disease characteristics (Nestorov 2005).

The formation of ADAs can profoundly affect drug clearance, resulting in low or nonmeasurable drug concentrations and subsequent loss of therapeutic response. In addition, other factors can affect infliximab PK including concomitant use of immunosuppressive agents, serum albumin concentration, body weight, the degree of systemic inflammation (e.g., serum albumin concentration and TNF burden), and disease pathophysiology (e.g., type of IBD, RA or psoriasis). The effect of weight on infliximab clearance is not linear (Xu et al. 2012) although clearance increases as weight increases. Thus, dosing based on weight (e.g., mg/kg) does not always provide efficacious drug exposure. Consequently, monitoring of serum drug concentrations is particularly important in patients with both low weight and high inflammatory burden. Gender has been shown to influence infliximab, with clearance being higher in males (Ternant et al. 2008; Fasanmade et al. 2009) although the fact that clearance is higher in males may also be related to weight as males

generally have a higher body weight than females. In addition, an inverse relationship exists between serum albumin concentration and infliximab clearance (Fasanmade et al. 2009). The impact of albumin translates to lower response rates (Fasanmade et al. 2010). Patients with a baseline serum albumin concentration below the normal range (a common finding associated with severe inflammation) have lower remission rates following treatment with infliximab.

Recently, a study of patients with rheumatoid arthritis treated with infliximab has shown that a high body mass index (BMI) negatively influences clinical response to anti-TNF agents (Klaasen et al. 2011). Research into the role of mesenteric fat in chronic inflammatory diseases has intersected with investigations into the importance of adipose tissue as a metabolically active source of inflammatory cytokines (e.g., TNF; Coppack 2001) in patients with insulin resistance. Therefore, obese patients would be expected to have higher circulating TNF than patients with normal weight, suggesting that obese patients may require higher drug doses than those currently recommended.

Given the complexity and number of patient factors affecting infliximab PK, together with the large remaining unexplained variability and the high rate of loss of response (Ordás et al. 2012), dashboard systems could provide needed clarity in making dosing decisions (Mould et al. 2013). A retrospective evaluation of a dashboard system (Mould et al. 2013) demonstrated that the dashboard system designed for infliximab was able to accurately predict dose regimens that would provide therapeutically appropriate exposure and that the time of identification of the regimen was substantially shorter than via clinical ("manual") adjustment of the dose (Fig. 2.4).

2.3.2 A PD System: Warfarin

Warfarin is one of the most frequently prescribed oral anticoagulants and is used to prevent thromboembolic events. Warfarin exerts its anticoagulant effect through inhibition of vitamin K epoxide reductase, interfering with the recycling of reduced vitamin K. The time course of warfarin's anticoagulant activity depends on the clearance of vitamin K-dependent clotting factors (e.g., factors II, VII, IX, and X). The earliest changes in the INR, a measure of the sum of the activity of the coagulation factors II, VII, and X, are typically noted at 1–2 days after the administered dose. Warfarin is a racemic mixture; S-warfarin is approximately three to five times more potent than R-warfarin (Breckenridge et al. 1974). S-warfarin is metabolized by CYP2C9, a polymorphic enzyme, which results in large BSV in Pk and subsequent drug exposure (Takahashi and Echizen 2003). Genetic variants in vitamin K epoxide reductase complex 1 (VKORC1) have also been identified (Rost et al. 2004), which further contributes to variability in PD response (INR) to warfarin and thus the dosing. Perlstein et al. (2012) proposed an adaptive dose strategy with starting doses determined on genotype. Hamberg et al. (2007) developed a

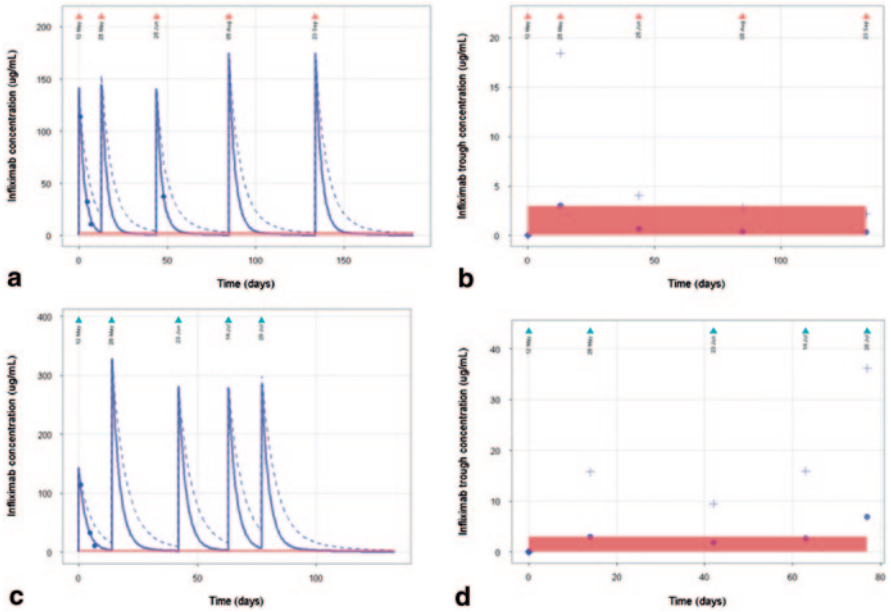

Fig. 2.4 Infliximab dashboard guided dosing. This figure compares conventional and dashboard guided dosing (Mould et al. 2013). The patient is an ulcerative colitis patient with severe disease, managed with infliximab, which is available as 100 mg increments, and dose is typically rounded up to use the entire vial. For conventional dosing: The induction doses (which were started at 6.8 mg/kg (500 mg) owing to the severity of disease), the dose was increased to 8.3 mg/kg (600 mg) every 4 weeks, rather than the labeled 8-week interval. The C-reactive Protein reduced to 30 mg/L and the patient's condition improved to moderate disease activity. A final dose adjustment was made to increase the dose to 11 mg/kg (800 mg). The patient became ADA positive. Plots show the predicted time course of infliximab concentrations (*panel* **a** *solid line, left*) and the concurrent infliximab trough concentrations (*panel* **b** *filled circles right*). For the dashboard guided dosing: The first dose was given as per the conventional dosing scenario, and observed concentration data from that patient's first dose were subjected to Bayesian updating and forecasting. The remaining information is forecast using the dashboard. A dose of 10 mg/kg (700 mg), administered every 4 weeks was found to be likely to maintain therapeutic exposure. The use of a dashboard shortened the time necessary to identify an appropriate dose regimen (2 weeks as compared to 20 weeks for conventional dose selection). Plots show the predicted time course of infliximab concentrations (*panel* **c** *solid line, left*) and the concurrent infliximab trough concentrations (*panel* **d** *filled circles right*)

PK and PD model that took into account patient age and genotype to relate doses, concentrations, and INR. This model was subsequently used to guide dosing in pediatric patients (Hamberg et al. 2013) with generally good success.

Investigating the models proposed by Hamberg et al. (2007) shows the large impact of both age and genotype on the PK and PD of warfarin (Figs. 2.5 and 2.6). Simulated results of model-guided dosing show that INR can be controlled well in a wide range of patients, regardless of age or genotype (Fig. 2.7),

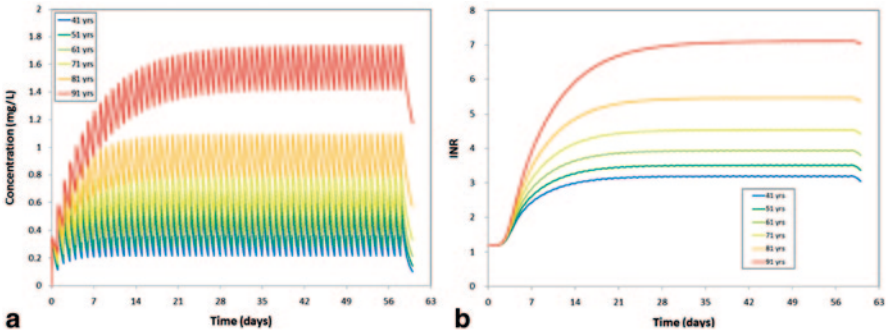

Fig. 2.5 PK and PD of warfarin: CYP2C9 1*1 VKORC1 GG 5 mg QD. *Panel A* shows the long time to steady state following administration of 5 mg daily administration. Patients with advanced age develop very high warfarin concentrations. *Panel B* shows the expected INR, and again the time to reach a stable response is several days. Owing to the very high concentrations in the elderly, the resulting INR is extremely high in this group

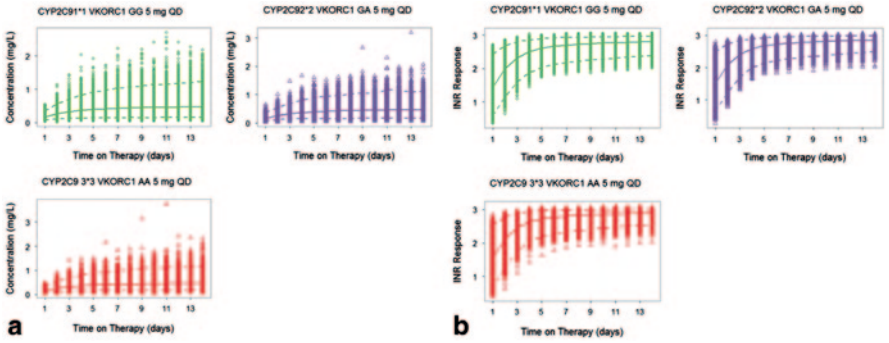

Fig. 2.6 The impact of genotype on warfarin PK and PD. *Panel A* is the range of expected concentrations following a 5 mg QD dose of warfarin in a 50-year-old individual. As can be seen here, there are distinct differences in the CYP2C9 status for concentrations but the remaining variability is high, resulting in substantial overlap between these subpopulations. *Panel B* shows the INR based on VKORC1 genotype. Partly owing to the substantial remaining variability in the INR model and the variability in exposure, the expected range of INR values is quite wide

suggesting that a dashboard approach to warfarin therapy could result in better INR control and fewer bleeding events. There is currently a web application available to improve the safety and efficacy of warfarin developed by Brian F. Gage (Table 2.2). While representing an improvement in safety and efficacy over current dose approaches for warfarin, this application makes use of only the patient factors (genotype and age), there is considerable BSV remaining even after accounting for these factors. Thus, Bayesian-based approaches could further improve safety and efficacy.

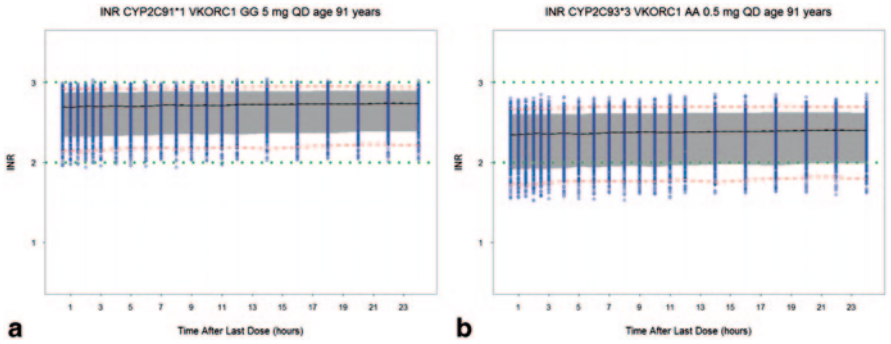

Fig. 2.7 The impact of individualized treatment on international normalized ratio (*INR*) levels. The panels below show the impact on the variability of INR in elderly patients with two different genotype combinations. *Panel A* shows the expected range of INR following individualized warfarin dosing for a 91-year-old subject with CYP2C91*1 and VKROC1 GG. *Panel B* shows the expected range of INR in a 91-year-old subject with CYP2C93*3 and VKORC1 AA. In both panels, the majority of patients are within the target range and the INR values do not exceed 3

2.4 Conclusions

Decision makers in many different fields are increasingly confronted with greater and greater amounts of information from diverse sources, which renders difficult choices when it comes to making the best decisions. Individualizing drug selection and dose choices by health-care providers is no exception. However, dashboard systems for personalized medicine, while still in their infancy, are evolving rapidly and are appealing as evidenced by the first-generation examples discussed in this chapter. Personalized medicine in the future will be characterized by the necessity to have decision support systems to aggregate and clinically interpret next-generation sequencing data, premarketing clinical trial data, and postmarketing clinical research findings in order to tailor medicines to individual patients. Dashboard-based data analytic platforms designed for individual selection of drugs and doses are clearly needed for faster and more informed decision making in therapeutics. The ability to add new patient data to the dashboard, visualize dose-PK/PD-outcome relationships, and drill down into the data to identify patient covariates and explore "what if" scenarios will be critical attributes of effective dashboard systems.

In the future, new drug development programs should consider data collection during the clinical phases that would facilitate development of dashboard software (Mould et al. 2013). This approach would facilitate the use of model-based drug development (MBDD) in the pharmaceutical industry with important benefits. The use of dashboard systems would be analogous to the gathering of information to support the codevelopment of molecular diagnostics and targeted medicines, but it would take the concept of personalized medicine one step further by equipping practitioners with not only the diagnostic–drug pair but also a qualified support

system to deliver individualized treatment for each patient at the point of care. One remaining issue is to what extent the FDA would regulate dashboards as devices, as standalones, or as an accessory for usage with a specific medicine, as a clinical decision support tool.

2.5 Summary

In summary, the following issues have been discussed:

- A description of personalized medicine.
- An outline of current dosing paradigms.
- A brief history of the use of decision support tools in health care.
- A description of the dashboard concept and overview of how they work.
- Potential benefits of using dashboards in clinical care.
- Two example systems (infliximab and warfarin) have been presented.
- Other possible uses of such systems (e.g., drug development).

Acknowledgments The authors are grateful to the many readers of draft versions for their valuable contributions to the manuscript.

Conflict of Interest/Disclosure Dr. Mould is Founder and President of Projections Research Inc., a consulting company working with the pharmaceutical industry; she is also founder of Baysient LLC, a company developing dashboard systems.

Author Contributions The authors contributed equally to the manuscript.

References

Anderson BJ, Holford NH (2013) Understanding dosing: children are small adults, neonates are immature children. Arch Dis Child 98(9):737–744

Baert F, Noman M, Vermeire S, Van Assche G, D'Haens G, Carbonez A, Rutgeerts P (2003) Influence of immunogenicity on the long-term efficacy of infliximab in Crohn's disease. N Engl J Med 348(7):601–608

Barrett JS, Mondick JT, Narayan M, Vijayakumar K, Vijayakumar S (2008) Integration of modeling and simulation into hospital-based decision support systems guiding pediatric pharmacotherapy. BMC Med Inform Decis Mak 8:6

Breckenridge A, Orme M, Wesseling H, Lewis RJ, Gibbons R (1974) Pharmacokinetics and pharmacodynamics of the enantiomers of warfarin in man. Clin Pharmacol Ther 15:424–430

Conti R, Veenstra DL, Armstrong K, Lesko LJ, Grosse SD (2010) Personalized medicine and genomics: challenges and opportunities in assessing effectiveness, cost-effectiveness, and future research priorities. Med Decis Making 30(3):328–340

Coppack SW (2001) Pro-inflammatory cytokines and adipose tissue. Proc Nutr Soc 60(3):349–356

Dashboard development and data visualization tools for effective BI (2014) http://searchcio.techtarget.com/definition/dashboard. Accessed 22 Aug 2014

Domínguez Hernández KR, Aguilar Lasserre AA, Posada Gómez R, Palet Guzmán JA, González Sánchez BE (2013) Development of an expert system as a diagnostic support of cervical cancer in atypical glandular cells, based on fuzzy logics and image interpretation. Comput Math Methods Med 2013:796–387

Egorin MJ (2003) Horseshoes, hand grenades, and body-surface area-based dosing: aiming for a target. J Clin Oncol 21(2):182–183

Elliott G, Granger CWJ, Timmermann AG (2006) Handbook of economic forecasting, vol 1, Chap. 1. Elsevier, Netherlands

Fasanmade AA, Adedokun OJ, Ford J, Hernandez D, Johanns J, Hu C, Davis HM, Zhou H (2009) Population pharmacokinetic analysis of infliximab in patients with ulcerative colitis. Eur J Clin Pharmacol 65(12):1211–1228

Fasanmade AA, Adedokun OJ, Olson A, Strauss R, Davis HM (2010) Serum albumin concentration: a predictive factor of infliximab pharmacokinetics and clinical response in patients with ulcerative colitis. Int J Clin Pharmacol Ther 48(5):297–308

Fasanmade AA, Adedokun OJ, Blank M, Zhou H, Davis HM (2011) Pharmacokinetic properties of infliximab in children and adults with Crohn's disease: a retrospective analysis of data from 2 phase III clinical trials. Clin Ther 33(7):946–964

García MJ, Gavira R, Santos Buelga D, Dominguez-Gil A (1994) Predictive performance of two phenytoin pharmacokinetic dosing programs from nonsteady state data. Ther Drug Monit 16:380–387

Gill J (2008) Bayesian methods: a social and behavioral sciences approach, 2nd edn. Chapman and Hall Boca Raton, Florida, pp. 56–60

Guidance for industry estimating the maximum safe starting dose in initial clinical trials for therapeutics in adult healthy volunteers. http://www.fda.gov/downloads/Drugs/GuidanceComplianceRegulatoryInformation/Guidances/ucm078932.pdf. Accessed 3 Sept 2014

Hamberg AK, Dahl ML, Barban M, Scordo MG, Wadelius M, Pengo V, Padrini R, Jonsson EN (2007) A PK-PD model for predicting the impact of age, CYP2C9, and VKORC1 genotype on individualization of warfarin therapy. Clin Pharmacol Ther 81(4):529–538

Hamberg AK, Friberg LE, Hanséus K, Ekman-Joelsson BM, Sunnegårdh J, Jonzon A, Lundell B, Jonsson EN, Wadelius M (2013) Warfarin dose prediction in children using pharmacometric bridging–comparison with published pharmacogenetic dosing algorithms. Eur J Clin Pharmacol 69(6):1275–1283

Ho WR, Germain MJ, Garb J, Picard S, Mackie MK, Bartlett C, Will EJ (2010) Use of 12x/month haemoglobin monitoring with a computer algorithm reduces haemoglobin variability. Nephrol Dial Transplant 25(8):2710–2714

Hoeting JA, Madigan D, Raftery AE, Volinsky CT (1999) Bayesian model averaging: a tutorial. Stat Sci 14(4):382–417

Holford SD, Holford NHG, Anderson BJ Online dose calculation tool for determining dosing regimens in the very young. http://www.paganz.org/sites/default/files/slides/Admin/Online%20dose%20calculation%20tool%20for%20determining%20dosing%20regimens%20in%20the%20very%20young.pdf. Accessed 23 Aug 2014

Klaasen R, Wijbrandts CA, Gerlag DM, Tak PP (2011) Body mass index and clinical response to infliximab in rheumatoid arthritis. Arthritis Rheum 63(2):359–364

Lesko LJ, Schmidt S (2012) Individualization of drug therapy: history, present state, and opportunities for the future. Clin Pharmacol Ther 92(4):458–466

Maser EA, Villela R, Silverberg MS, Greenberg GR (2006) Association of trough serum infliximab to clinical outcome after scheduled maintenance treatment for Crohn's disease. Clin Gastroenterol Hepatol 4(10):1248–1254

Miskulin DC, Weiner DE, Tighiouart H, Ladik V, Servilla K, Zager PG, Martin A, Johnson HK, Meyer KB (2009) Medical directors of dialysis clinic Inc. Computerized decision support for EPO dosing in hemodialysis patients. Am J Kidney Dis 54(6):1081–1088

Mohan M, Batty KT, Cooper JA, Wojnar-Horton RE, Ilett KF (2004) Comparison of gentamicin dose estimates derived from manual calculations, the Australian 'Therapeutic guidelines: antibiotic' nomogram and the SeBA-GEN and DoseCalc software programs. Br J Clin Pharmacol 58:521–527

Mould DR, Green B (2010) Pharmacokinetics and pharmacodynamics of monoclonal antibodies: concepts and lessons for drug development. Bio Drugs 24(1):23–39

Mould DR, Upton RN (2012) Basic concepts in population modeling, simulation and model based drug development. CPT: Pharmacometrics Syst Pharmacol 1:e6

Mould DR, Moyer B, Amur S, Mukherjee A (2013) The impact of new technologies on the science of clinical care and drug development. AAPS Magazine, December

Mould DR, Upton R, Wojciechowski J (2014) Dashboard Systems: Implementing Pharmacometrics from Bench to Bedside. AAPS J ePub June 2014

Nestorov I (2005) Clinical pharmacokinetics of tumor necrosis factor antagonists. J Rheumatol Suppl 74:13–18

Ordás I, Mould DR, Feagan BG, Sandborn WJ (2012) Monoclonal antibodies in inflammatory bowel disease: pharmacokinetic based dosing paradigms. Clin Pharmacol Ther 91(4):635–646

Papier A (2012) Decision support in dermatology and medicine: history and recent developments. Semin Cutan Med Surg 31(3):153–159

Perlstein TS, Goldhaber SZ, Nelson K, Joshi V, Morgan TV, Lesko LJ, Lee JY, Gobburu J, Schoenfeld D, Kucherlapati R, Freeman MW, Creager MA (2012) The creating an optimal warfarin nomogram (CROWN) study. Thromb Haemost 107(1):59–68

Peyrin-Biroulet L, Deltenre P, de Suray N, Branche J, Sandborn WJ, Colombel JF (2008) Efficacy and safety of tumor necrosis factor antagonists in Crohn's disease: meta-analysis of placebo-controlled trials. Clin Gastroenterol Hepatol 6(6):644–653

Radstake TR, Svenson M, Eijsbouts AM, van den Hoogen FH, Enevold C, van Riel PL et al (2009) Formation of antibodies against infliximab and adalimumab strongly correlates with functional drug levels and clinical responses in rheumatoid arthritis. Ann Rheum Dis 68(11):1739–1745

Rost S, Fregin A, Ivaskevicius V, Conzelmann E, Hörtnagel K, Pelz HJ, Lappegard K, Seifried E, Scharrer I, Tuddenham EG, Müller CR, Strom TM, Oldenburg J (2004) Mutations in VKORC1 cause warfarin resistance and multiple coagulation factor deficiency type 2. Nature 427:537–541

Seow CH, Newman A, Irwin SP, Steinhart AH, Silverberg MS, Greenberg GR (2010) Trough serum infliximab: a predictive factor of clinical outcome for infliximab treatment in acute ulcerative colitis. Gut 59(1):49–54

Sivyer A (1959) A dose-rate calculator. Br J Radiol 32(375):208–209

Takahashi H, Echizen H (2003) Pharmacogenetics of CYP2C9 and interindividual variability in anticoagulant response to warfarin. Pharmacogenomics J 3:202–214

Ternant D, Aubourg A, Magdelaine-Beuzelin C, Degenne D, Watier H, Picon L, Paintaud G (2008) Infliximab pharmacokinetics in inflammatory bowel disease patients. Ther Drug Monit 30(4):523–529

Tobler A, Mühlebach S (2013) Intravenous phenytoin: a retrospective analysis of Bayesian forecasting versus conventional dosing in patients [published online ahead of print 29 June 2013]. Int J Clin Pharm. doi:10.1007/s11096-013-9809-5

Usman M, Ashraf M, Khokhar MI et al (2013) Comparative pharmacokinetics of levofloxacin in healthy volunteers and in patients suffering from typhoid Fever. Iran J Pharm Res 12:147–154

Wong C, Kumar SS, Graham GG, Begg EJ, Chin PK, Brett J, Ray JE, Marriott DJ, Williams KM, Day RO (2013) Comparing dose prediction software used to manage gentamicin dosing. Intern Med J 43:519–525

Xu Z, Mould DR, Hu C, Ford J, Keen M, Davis HM, Zhou H (2012) A population-based pharmacokinetic pooled analysis of infliximab in pediatrics. ACCP national meeting, San Diego CA

Xu Z, Davis HM, Zhou H (2013) Rational development and utilization of antibody-based therapeutic proteins in pediatrics. Pharmacol Ther 137(2):225–247

Zineh I, Huang S-M (2011) Biomarkers in drug development and regulation: a paradigm for clinical implementation of personalized medicine. Biomark Med 5(6):705–713

Chapter 3
Pharmacometrics in Pediatrics

Jeffrey Barrett

3.1 Introduction

Pediatric clinical pharmacology is an essential discipline that facilitates the development of new medicines for children and also the management of pharmacotherapy in children requiring medicine. While many of the challenges in pediatric clinical pharmacology are similar to those faced in adults (e.g., disease progression, dose selection, therapeutic window definition), others are more specific to children and driven to a large extent by the dynamics of the developing child and specifically by changing physiologic processes and conditions that may alter both pharmacokinetics (PK) and pharmacodynamics (PD). Likewise, the application of pharmacometric approaches to these challenges is essential to ensure the appropriate design of pediatric clinical trials, the interpretation of PK/PD data based on sparse sampling, and the recommendations for dosing and dose adjustments in pediatric subpopulations including critically ill children (Zuppa and Barrett 2008). Recent efforts also point to the growing use of pharmacometrics to aid caregivers in the provision of real-time guidance to their patients (Gardner 2002; Barrett et al. 2008b; Dombrowsky et al. 2011). Hence, a new frontier for pharmacometrics facilitating pharmacotherapy in children would seem to be upon us.

The marketplace attests to the economic reality that children are not the "target population" for most new drug development candidates. This reality, in part, guided the assignment of pediatrics as a "special population" in the recent past. The notion that a single study design will be sufficient to extend the data generated in adults to pediatrics is flawed even if the adult and pediatric indications are similar. While opinions differ regarding the upper age boundary, the age window from birth to 17, 18, or 21 years is extremely broad and represents approximately one fourth of the average human life expectancy. Of course, there are subcategories which further differentiate this general classification, but the key notion and the basis for much of

J. Barrett (✉)
Interdisciplinary Pharmacometrics Program, Pediatric Clinical Pharmacology, Sanofi Pharmaceuticals, 55 Corporate Drive, Bridgewater, NJ 08807, USA
e-mail: Jeffrey.Barrett@sanofi.com

S. Schmidt, H. Derendorf (eds.), *Applied Pharmacometrics,* AAPS Advances in the Pharmaceutical Sciences Series 14, DOI 10.1007/978-1-4939-1304-6_3

the current pediatric study design requirements at least from a regulatory perspective are that pediatrics represents a developmental continuum over which younger individuals mature into fully developed adults. While clinical experience over the entire continuum is sought, the value of information collected across this continuum is not equal and pediatric development plans should be guided by both the expected utilization in the various age subgroups, the drug molecule attributes (Laer et al. 2009), and the target attributes (PD) which may individually or in conjunction define age strata where developmental trajectories are nonlinear.

There are several key questions addressed in this chapter as we consider the strategy and implementation of pharmacometrics in the study of pediatric populations. These include the following:

- What are the essential physiologic processes most affected in the developing child?
- How do these processes impact key PK/PD parameters used to describe the dose-exposure and exposure-response relationships?
- How does time affect maturation and ontogeny as well as represent a covariate of interest for key parameters?
- How specifically is pharmacometrics implemented to advance pediatric research?
- How does the choice of appropriate analysis techniques change based on the availability of prior knowledge?

In answering these, we must also answer one additional question that affects all others as well as the underlying assumptions that frame pediatric research in general. If pharmacometrics performed for pediatric trials is fundamentally the same as in adults, what are the key differences (between adults and pediatrics) and how do we address them in the design and implementation of prospective and retrospective analyses?

While there are many recent published examples of pharmacometrics focused in pediatrics (Crom et al. 1994; Shi et al. 2001; Läer et al. 2005; Mondick et al. 2008; Wade et al. 2008), the occasion to consider pharmacometric support of pediatric R&D continues to increase largely motivated by regulatory considerations from the European Medicines Agency (EMA) and the US Food and Drug Administration (FDA). The most common application is the standard PK/safety trial employed when adult and pediatric indications are perceived to be similar and there are information/data to support such assumptions. The primary goal in this setting is to ensure an adequate sample size and an informative sampling scheme that considers the potential shift in PK across age strata or temporal changes in PD response. More uncommon but perhaps increasing is the interest in pediatric efficacy trials.

Drug developers and pediatric caregivers have different objectives when it comes to evaluating the relevant clinical pharmacologic principles that underlie their query. The drug developer ultimately must contend with the dosing of the “typical” pediatric patient, keeping in mind that a recipe for dosing within the usual constraints of an otherwise normal developing child must be provided in the labeling if they expect to market the drug in pediatrics. The caregiver must address the individual

patient, regardless of how the patient presents. Thus, while the typical patient may represent the normal scenario (hopefully) for caregivers, the critically ill child, the child on extracorporeal membrane oxygenation (ECMO), the hypothermic child, the obese child, and the child on multiple medications with some degree of interaction potential must all be treated with the best medical judgment the caregiver can provide. Hence, the availability of source data in these categories is invaluable to the caregiver. When data are not available, some level of extrapolation occurs (usually empirically). Individual patient forecasting (simulation based on prior knowledge and perhaps some individual patient data) is becoming a desirable tool for the caregiver (Barrett et al. 2011).

Differences between children and adults with respect to PK and PD are often influenced by physiologic factors such as changes in body composition, total body water, protein binding, cytochrome P450 ontogeny, gastrointestinal motility and pH, and organ (e.g., renal and hepatic) function all of which can produce significant changes in absorption, distribution, metabolism, and elimination throughout childhood (Kearns et al. 2003a). By overlaying the PK and PD attributes of target drug molecules, we can get a sense of the susceptibility for the underlying PK (absorption, distribution, metabolism, and elimination) and PD (receptor affinities, dissociation, enzyme kinetics, signal transduction, cascade events, etc.) processes to be affected by changes in the aforementioned physiologic factors. Likewise, knowledge of pediatric clinical pharmacology is essential to the design and conduct of informative pediatric trials. More than ever, pharmaceutical sponsors are required to plan for the pediatric investigation as an essential part of their clinical development plans. For older drugs on the market, National Institutes of Health (NIH) and FDA collectively administrate the appropriation of funds that support pediatric research for off-patent drugs through the Best Pharmaceuticals for Children Act (BPCA; Ward and Kauffman 2007). The landscape for support of pediatric research initiatives is thus strongly reliant on pharmacometrics.

3.2 Dosing Considerations in the Developing Child

As children are often not the population in which formal dose-finding studies are conducted, dosing requirements for children are predominantly achieved by extrapolation from the adult clinical experience. Historically, dosing in children has been viewed as a scaling exercise with a simple normalization of bodyweight (BW) for the intended age (or weight) of the child (P, pediatric) applied to the adult (A) dose:

$$\text{Dose}_{\text{P}} = \text{Dose}_{\text{A}} \times \frac{\text{BW}_{\text{P}}}{\text{BW}_{\text{A}}}$$

In this manner, we need not understand the developing child, only trust that the linear scaling of body weight would be a reasonable means to adjust dose. Of course, this approach under-predicts dose requirements across the pediatric continuum though

it is not equally bad in all age/weight ranges. The fatal flaw with this approximation is that it does not acknowledge that the relationship between dose requirement and weight is nonlinear. Substituting body surface area (BSA) for BW in a similar manner is used quite extensively in pediatric oncology settings under the assumption that similar "geometry" can be achieved with this transformation:

$$\text{Dose}_P = \text{Dose}_A \times \frac{\text{BSA}_P}{\text{BSA}_A}$$

While nonlinearity is introduced into the dose relationship through the transformation of BSA with weight and height (e.g., for Mosteller formula, BSA (m^2) = ([Height (cm) × Weight (kg)]/3600)^{½}), there is sufficient experience to know that this expression under-predicts infant and neonate dosing requirements (Johnson 2005, 2008). Allometric or power models are used in various biological settings to adjust for size dependencies of growing/developing systems. The value of the exponent varies with the type of biologic variable and there is certainly no consensus on the numeric validity of these generalized constants:

$$\text{Y} = \text{a} \times \text{BW}^{\text{b}} \begin{cases} \text{b} = 0.25, \text{ time-related variables} \\ \text{b} = 0.75, \text{ metabolic variables} \\ \text{b} = 1, \text{ anatomical variables} \end{cases}$$

It is relevant, however, that we recognize that the adjustments are focused on size and not the more complex biology of a whole living system. If we apply this approach to dose adjustment for children recognizing the relationship among clearance, volume of distribution, and dose, we arrive at the following expression which over-predicts requirements in children less than 1 year of age although it is superior to BSA in this age range (Johnson 2008; Anderson and Lynn 2009):

$$\text{Dose}_P = \text{Dose}_A \times \left(\frac{\text{BW}_P}{\text{BW}_A} \right)^{0.75}$$

The result of this endeavor is the recognition that there is no simple way to generalize dose adjustment in pediatric populations from an adult dosage. This is not surprising given that the adult continuum over which fixed dosing is often recommended typically excludes elderly and obese populations treating them as "special" as well. A PK model is required to serve as the backbone of such consideration. Ultimately, the model for the developing child must span the relevant ages of the target population with the goal being to "match" exposures as close as possible with the adult reference population under the assumption that similar safety and efficacy will be conferred if such matching is achieved. The challenge in the end is to achieve a compromise between the potentially complex and nonlinear model used to describe the PK time course across the target age strata and the desire for simple dosing instructions that do not promote prescribing errors. Simple, in this context refers to (1) the dose in milligram or milliliter (assuming a weight-based (e.g., mg/kg) target

given a liquid formulation or suspension), (2) no calculation requiring a transformation (i.e., no exponent button on a calculator), and (3) the fewest possible changes to dose across age strata (typically not more than three). In the end, we are often left with dose recommendations that vary across two or three age strata essentially approximating the nonlinear relationship between weight and dose. The transition across age strata is better if weight-normalized dosing is possible within the age strata (as will a liquid or suspension) but still can be abrupt on age transition points (e.g., the day your child year turns 12 and requires a 50% increase in dose). As we search for simple dosing instructions, we must reflect that all of the previously mentioned approaches focus on size only, though functional effects (enzyme ontogeny and maturation) are often masked in additional age dependencies requiring further dose adjustments in children less than 2 years and/or neonates.

3.3 Time Considerations

Time is a critical factor in the assessment of pediatric PK/PD relationships. It serves as an index over which response to a dosing event is captured and as an index over which an organism, in this case a child, develops and matures. Coding time for use in a model likewise differs based on the objectives of the modeling and how we intend to express time. For PK purposes, clock time or time-after-dose is defined as an independent variable that tracks exposure or drug actions (PD) to the most recent dosing event and/or cumulative dosing events. The time scale for an organism can be defined as both a time-dependent or time-independent covariate depending on how we will define functions that define maturation. Broadly speaking, then clearance is the primary population parameter for which time considerations are critical. We will start with clearance to see how time-dependent phenomenon in the developing child is defined.

Both maturation (MF) and organ/ontogeny functions (OF) are time-dependent phenomena that require consideration when adjusting for pediatric populations. Maturation is defined as the process of becoming mature; the emergence of personal and behavioral characteristics through growth processes. OF generally refers to the health status of an organ where the fraction of otherwise "normal" function can be quantified as one would have to consider for a critically ill child with, for example, impaired renal function. Consider the generalized population expression for clearance:

$$\mathrm{CL_P} = \mathrm{CL_A} \times \left(\frac{\mathrm{BW}}{70}\right)^{0.75} \times \mathrm{MF} \times \mathrm{OF}.$$

Maturation is generally considered a continuous function which achieves an asymptote at the adult value (MF = 1) at some finite point in development. Usually, the maturation function (MF) is derived from a time index related to birth. Expressions for MF based on postconceptual age (Barker et al. 2005), postmenstrual age

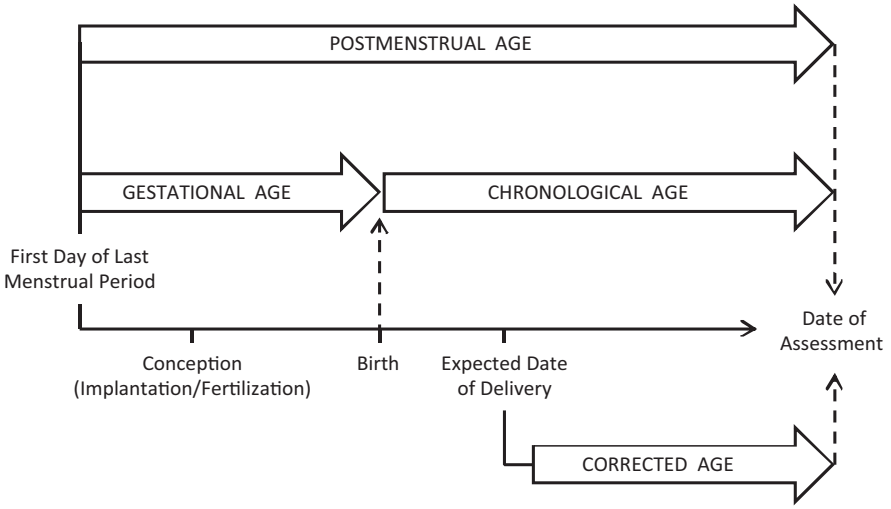

Fig. 3.1 Age terminology during perinatal period adopted from the American Academy of Pediatrics policy statement. (Adapted from data from Engle 2004)

(PMA), postnatal age (PNA), and gestational age (GA) have all been considered (Anderson and Holford 2008). Inconsistent use of terminology has limited the accurate interpretation of data on health outcomes for newborn infants, especially for those born preterm or conceived using assisted reproductive technology (Engle 2004), so one must be careful when trying to derive these relationships from the literature. Figure 3.1 illustrates the relationship between the various age indices. "Gestational age" or "menstrual age" is the time elapsed between the first day of the last normal menstrual period and the day of delivery. The first day of the last menstrual period occurs approximately 2 weeks before ovulation and approximately 3 weeks before implantation. Because most women know when their last period began but not when ovulation occurred, this definition traditionally has been used when estimating the expected date of delivery. "Chronological age" or "postnatal" age is the time elapsed after birth (Fig. 3.1). "Postmenstrual age" is the time elapsed between the first day of the last menstrual period and birth (gestational age) plus the time elapsed after birth (chronological age). "Corrected age" (or "adjusted age") is a term used to describe children up to 3 years of age who were born preterm (Fig. 3.1). This term is preferred to "corrected gestational age" or "gestational age" and represents the age of the child from the expected date of delivery. Corrected age is calculated by subtracting the number of weeks born before 40 weeks of gestation from the chronological age. Corrected age and chronological age are not synonymous in preterm infants. "Conceptional age" is the time elapsed between the day of conception and the day of delivery.

For the purpose of modeling, a key requirement is that the same time index is used when pooling data and that the accurate transformations of time are ensured. MF expressions vary from very simple relationships (Tod et al. 2008) as below:

$$MF = \frac{PCA^s}{PCA_{50}^s + PCA^s}$$

to more complex expressions in which estimate the time to maturation as a parameter (Potts et al. 2009) with a cutoff point that designates a different slope on the MF (Hill_A vs. Hill_B):

$$\begin{cases} MF = \dfrac{1}{1+\left[PMA/TM_{50}\right]^{-Hill\_A}}, PMA \le TM50 \\ MF = \dfrac{1}{1+\left[PMA/TM_{50}\right]^{-Hill\_B}}, PMA > TM50 \end{cases}$$

Based on these expressions it is clear that the most common MFs are empirically and not physiologically defined. As a result, their predictive value is closely linked to range of the observed data from which they are defined. As more of these relationships are reported for various drug attributes, it may be possible to generalize these empirical relationships. An important future consideration will be the extent to which these functions align with more physiologically based relationships (i.e., so-called bottom-up approaches). The shape of the general MF is shown in Fig. 3.2.

OF is typically 1 for healthy children but can be higher or lower for ill children. Again, we are typically expressing these relationships as sigmoidal or hyperbolic functions with a predetermined biomarker for OF (e.g., serum creatinine or creatinine clearance for kidney function) but these factors can also be treated as covariates on clearance as either continuous or dichotomous variables depending on the target population. Often a more immediate consideration is necessary to addressing the age-dependent expression of metabolizing enzyme activity. Much is now know about the ontogeny of many of the cytochrome P450 family of enzymes (Kearns et al. 2003b; Stevens et al. 2008) and recent efforts have incorporated ontologic functions into drug clearance expressions (Johnson et al. 2006, 2008). As complementary data become available for phase-II metabolism and transporters, these too can be considered when relevant. The manner in which ontogeny relationships are accommodated in the clearance expressions is similar to that defining maturation functions. Specifically, age-related functions which define the fraction of adult enzyme expression are factored into the overall clearance expression. Many of these (ontogeny functions, OF) have been defined for the P450 family (Johnson et al. 2006). A generalized expression would look like the following:

$$OF = \frac{a \times Age}{TM_{50} + Age} + b$$

Variations of this generalized expression are used for some enzymes; these typically involve the addition of a power function (exponent) on age. It should be appreciated

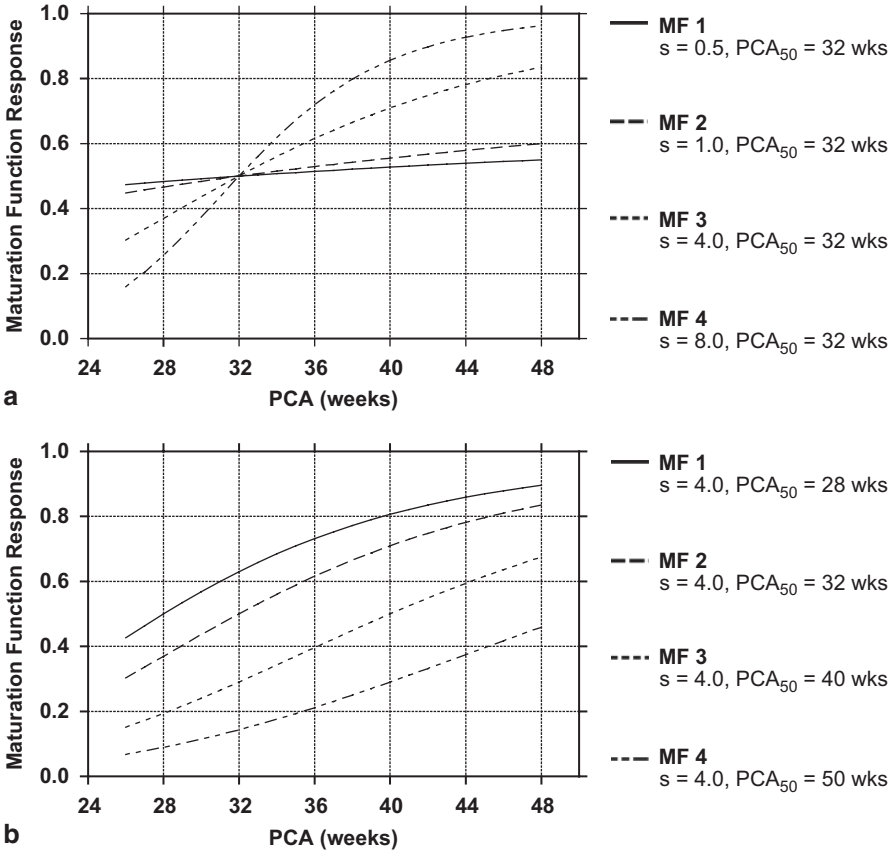

Fig. 3.2 Relationship between Hill coefficient (slope factor) (**a**) and maturation time as estimated by PCA_{50} (**b**) and indices of age (PCA shown) with an MF $\left(\mathrm{MF} = \dfrac{\mathrm{PCA}^{s}}{\mathrm{PCA}_{50}^{s} + \mathrm{PCA}^{s}}\right)$ used to adjust drug clearance in a developmental PK model

that even within the P450 family of enzymes there is great variability in the half-time of adult expression ranging from 3.5 days for hepatic CYP2C9 to 2.4 years for gut CYP3A (Johnson et al. 2006) as well as the functional activity (expression) at birth. This is especially relevant when dealing with drugs that have multiple elimination pathways and/or involve multiple enzymes for drug clearance. Some functional expressions derived by Johnson et al. (2006) are shown in Fig. 3.3.

3.4 Physiologic Considerations for the Developing Child

The appropriate incorporation of developmental considerations is an active area of research for many engaged in pediatric clinical pharmacology research. As the experimental data are generated, it is likewise important that model-based approaches

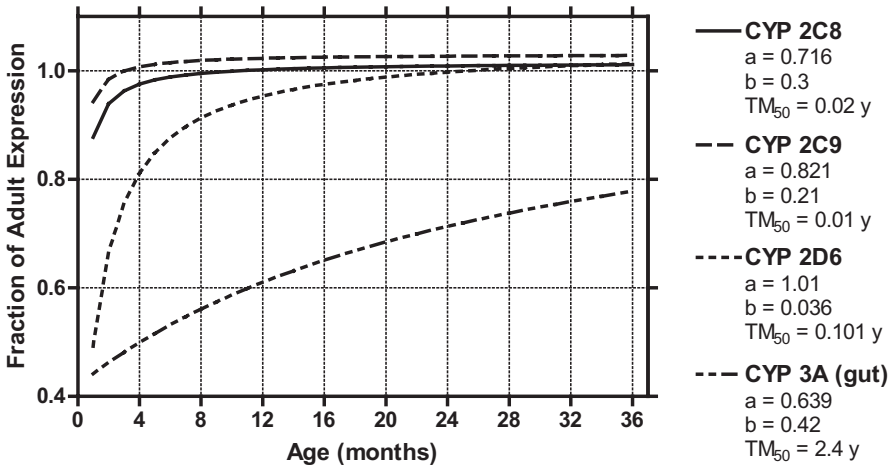

Fig. 3.3 Ontogeny-based functions for common CYP P450 enzymes used to adjust drug clearance in a developmental PK model

evolve to accommodate the new knowledge. Important gaps exist in phase-II metabolic pathways (Blake et al. 2005) and transporter ontogeny considerations although research in these areas look promising (Strolin Benedetti and Baltes 2003; Ge et al. 2007).

An important parallel effort involves the derivation of physiologic relationships that define important developmental considerations. Current physiologically based pharmacokinetic (PBPK) models incorporate age/size dependencies that permit "scaling" of dose in a manner analogous to compartmental approaches. An important milestone in this process has been the development of the underlying physiologic parameter databases that permit such age-dependent projections. The extension of PBPK models beyond adjusting for size likewise must incorporate developmental and age-dependent physiologic factors to further improve their generalizability and utility for individualizing exposure prediction beyond the plasma compartment (Ginsberg et al. 2004; Yang et al. 2006). Table 3.1 lists several known relationships between age-dependent physiologic parameters and PK attributes and parameters. Additional detail is provided in the "Bottom-up Approaches" section.

While the relationship between developing physiology and PK attributes is generally at least qualitatively appreciated, far less emphasis has been placed on the relationships between developmental considerations and pharmacologic pathways. As these represent the target mechanisms of action and/or the off-target affects that govern toxicity, they are often critical in the assessment of the pediatric therapeutic window. These relationships likewise have been absent in the discussion of pediatric development plans and decision trees used to define regulatory expectations for such plans. Table 3.2 shows several examples of systems known to exhibit age-dependent physiologic factors at least theorized to explain differences between pediatric and adult exposure targets or expectations in clinical response.

Table 3.1 Physiologic changes that correlate with the time course of PK attributes (ADME)

Pharmacokinetics		Physiologic considerations	
Attributes	Parameters	Time course	Relationships
Absorption	Ka, F_{abs}, F, MRT_{abs}, C_{max}, T_{max}	Typically occurs rapidly Gastric emptying changes with age	Mucosa changes with age; length/surface area changes with age (Kearns et al. 2003a) Ontogeny of pre-systemic enzymes/transporters
Distribution	Vd (Vd_{ss}, etc.), f_u, BBB, RBC partition	Changes are rapid during the first weeks and months of life	Fat, water partition changes with age/development Change in protein composition and concentration with age Permeability changes with age/developmental status; lung capacity; skin penetration
Metabolism	CL, CL_m, formation rate constants	Varied time to near adult expression ranging from < 1 month (CYPs 2C9 and 2C8) to > 2 years (gut 3A4; Johnson and Thomson 2008)	Ontogeny of systemic and organ-specific enzymes/transporters
Excretion	CL, CL_r	Varied time to adult function (Rodman 1994)	Kidney function maturation and ontogeny of renal transporters

BBB blood–brain barrier, *RBC* red blood cell, *ADME* absorption, distribution, metabolism, and excretion

3.5 Leveraging Adult Data (The Classic Top-Down Approach)

The most common situation envisioned for the modeler when initiating pediatric development program occurs after significant investigation has been completed in adults and the team must assess what pediatric indications are possible, what target populations require clinical investigation to support these indications, whether the PK, PD, and disease progression in adults translates into the potential pediatric population, and what data from the adult program are available to address these questions. Table 3.3 provides a common list of bridging questions to be considered based on the availability of adult data. The utility of the eventual pediatric population pharmacokinetics (PPK), PPK/PD, or trial simulation models derived from the adult data and the experience is that it can be used to examine extrapolation assumptions.

From this stage the next step is usually the construction of adult population-based PK/PD models from which the pediatric situation can be extrapolated. For the modeler, the main challenge is how best to develop a credible model that defines the pediatric condition and how to test assumptions that define the extent of the

Table 3.2 Examples of developmental considerations for physiologic processes that may affect the PD of certain drug classes

Pathway or system	Developmental considerations	Drug classes potentially affected	PD response
Coagulation	Changes in hemostatic response—number and nature of platelet membrane receptors, clotting factors (Revel-Vilk and Chan 2003)	Antithrombotics, antiplatelet agents, vitamin K antagonists	Antifactor-Xa activity, IPA (%), bleeding rate and extent, etc.
Pulmonary system	Vascular wall composition of pulmonary and systemic capacitance vessels and their intravascular pressure changes through development (Belik et al. 2000)	Corticosteroids, calcium channel blockers, prostacyclins, endothelin-1 inhibitors	Collagen, major growth factors (TGF-beta, IGF-2, and bFGF), and cytokine gene expression
Immune system	Development of the immune system is a partial explanation for the increase in the incidence of infectious sequelae (Clapp 2006)	Antibiotics, antiinfectives, antiretrovirals, etc.	MIC determination, cell-kill curves, etc.
Cutaneous system	Newborns have an immature cellular immune defense system that leads to increased susceptibility to infections (Dorschner et al. 2003)	Topical antibacterials	Infection susceptibility
Brain stem	Developmental aspects of phasic sleep parameters, REM density and body movement, and the executive system (Kohyama and Iwakawa 1990)	Drugs which promote loss of sleep as side effect or agents to treat disorders such as ADHD	Correlation of sleep parameters with age likely reflects brainstem maturation

IPA inhibition of platelet aggregation, *MIC* minimum inhibitory concentration, *REM* rapid eye movement, *ADHD* Attention deficit hyperactivity disorder

extrapolation. The steps to achieve a credible pediatric model are typically evaluated against data (perceived or observed) consistent with "bridging" assumptions and the pediatric population relative to the adult reference (e.g., adult to adolescent PK only vs. adult to neonatal PK/PD). The vast majority of applications deal with a PK extrapolation (exposure matching emphasis) under the assumption that the adult and pediatric diseases are similar. Table 3.4 illustrates the progression of modifications made to the adult population PK model to approximate the age continuum. These expressions account for differences in size and maturation or ontogeny. These expressions are likewise used together to account for the various contributions to the overall clearance expression. In addition, the expressions defined in Table 3.4 represent common expressions but are by no means the only relationships available to the modeler to account for age/developmental factors that impact PK behavior (Johnson et al. 2006, 2008; Alcorn and McNamara 2008; Anderson and Holford

Table 3.3 The linkage between the availability of data from an adult drug development program and bridging questions that can be addressed for potential pediatric indications

Adult drug development data	Pediatric bridging challenges
Pre-IND/IND In vitro metabolism, protein binding, absorption studies Animal ADME data	Are the elimination pathways likely to invoke the need to adjust clearance due to maturation?
	Are there CYP P450 enzymes involved that necessitate ontogeny considerations for clearance?
	Any concerns for pediatric formulation development based on absorption in the developing child?
Phase I Single/multiple dose PK/PD Lifestyle effects (e.g., food, DDI, time of day studies) Margin of safety—MTD	Is there a well-defined dose-response for toxicity that can be expected in children?
	Is there a dose threshold that should be avoided?
	Are the safety signals in adults translatable to the proposed pediatric indications?
	What is the likely DDI potential in children? Food effect concerns?
Phase II Dose-finding in patients Therapeutic window Activity measures and surrogate markers linked to efficacy	Do we expect the same therapeutic window in children?
	Is there a likely starting dose or dose range for children based on an exposure matching strategy?
	Do the adult bio/surrogate markers translate to the proposed pediatric indications?
Phase III Proof-of-efficacy/safety Basis for approval Adult indication and target population(s)	Is the adult indication similar to the proposed pediatric indication(s)?
	Are the metrics that demonstrate efficacy for the adult approval reasonable for children?
	Is the duration of treatment in the adult experience reasonable for the pediatric trial?
Phase IV Marketplace performance relative to competitors Medical surveillance—safety/ADR signals	Are there safety considerations from the post marketing adult experience that would be a concern for chronic administration in children?
	Are there concerns regarding switching medications in children within the same class?

ADR adverse drug reactions, *MTD* maximum tolerated dose, *DDI* drug-drug interaction

2008). Developmental factors impacting PD behavior is still really at the frontier of research and there are no published examples of models used for this purpose as of yet. Future investigation will hopefully address this knowledge void.

3.6 In Silico Approaches Reliant on PBPK

The use of PBPK modeling to describe drug disposition in children has become increasingly more utilized. There are many attractive features to this approach but the primary advantage over conventional adult-scaled PPK is the incorporation of physiologic parameters which more appropriately accommodate the developing child and more specifically developing organ systems, metabolic pathways, and

Table 3.4 Progression of parameter descriptions used to convert an adult-defined PPK model to a credible pediatric PPK model (one compartment model reference)

Model/structure	NONMEM syntax	Comments
Adult reference	TVCL=THETA(1) CL=TVCL*EXP(ETA(1)) TVV2=THETA(2) V=TVV2*EXP(ETA(2))	More complex expressions are fine; model can be extended
Allometric scaling of CL and V	TVCL=THETA(1)*(BWT/70)**TH ETA(6) CL=TVCL*EXP(ETA(1)) TVV2=THETA(2)*(BWT/70)**TH ETA(7) V=TVV2*EXP(ETA(2))	Adult reference weight of 70 kg; median of pediatric population also reasonable Similar expressions for V3 and Q used for 2 CPM THETA(6) usually fixed to 0.75; THETA(7) fixed to 1
Maturation function on CL or Enzyme ontogeny on CL	PNA=52; 52 weeks=1- year-old child PMA=PNA+40 MT=46; Maturation time (weeks) HCL=2.5; Hill coefficient MTHCL=MT**HCL PMAHIL=PMA**HCL CLAGE=PMAHIL/ (PMAHIL+MTHCL) CL=THETA(1)*EXP(ETA(1))* (WT/70)**0.75*CLAGE V=THETA(2)*EXP(ETA(2))* (WT/70)**1.0	Code for simulation shown; MT and HCL could be estimated depending on the dataset Other indices of age (e.g., gestational age) could be similarly evaluated Often helpful to bound parameters with such expressions

dynamic pathophysiologic states. The use of the PBPK approach particularly when adult PK/PD data are not available has been increasing over the past few years and improvement in methodologies as well as the incorporation of enzyme ontogeny (Johnson et al. 2006, 2008; Alcorn and McNamara 2008; Anderson and Holford 2008), more systematic workflow (Edginton et al. 2006a, 2006b; Maharaj et al. 2013), and more physiologic consistency with relationships driven by drug physiochemical properties has improved the clinical validity and ultimately the usefulness of recent pediatric applications.

Table 3.5 provides a template for the inputs and outputs needed for a typical PBPK model (Barrett et al. 2012). Schematically, a PBPK model is a multi-compartment model in which the compartments represent actual organs and other physiological spaces. Mass balance equations for each organ describe drug appearance in the organ from arterial blood and its exit into venous blood. The PBPK model is also constructed to incorporate relevant physiological, pharmacogenetic, biochemical, and thermodynamic parameters in a way that organizes much of the knowledge of the drug-body system (Edginton et al. 2006a, 2006b; Barrett et al. 2012).

Thus, PBPK models are more comprehensive than the empirical models used to analyze routine PK data because they not only incorporate drug properties but are built on a system-specific structure that is independent of the drug (Edginton et al. 2006a; Barrett et al. 2012). The model parameters need to include physiological and drug-specific parameters, in vitro predictions for distribution and elimination, and

Table 3.5 Hierarchy of PBPK model inputs and outputs based on intended use in supporting pediatric research and development

Intended use	Model inputs[a]	Outputs
Candidate screening (CS)	User: MW, lipophilicity, solubility, protein binding, pK_a In vitro metabolism data (V_{max}, K_M, etc.) and experimental *details* Database info: organ weight, blood flow, CL ontogeny, f_u ontogeny Study population (healthy volunteers); clearance pathways (CLR and CLH) Dosing (usually single dose but can vary to incorporate simple phase-I designs)	DDI potential (magnitude and shift of C-t profiles relative to a standard (e.g., single agent relative to combination) Dose-exposure relation; evaluation of profiles against TPP expectations
FTIP dose finding (FTP)	CS inputs Pediatric-specific demographics (age, BW, height, etc.) of study population; clearance pathways Dosing (various "rules" can be evaluated)	Dose-exposure relation; evaluation of profiles and PK metrics across age/developmental strata and relative to adult exposures Comparison of exposure from fixed vs. weight-adjusted dosing
Trial design evaluation (CTS)	FTP inputs Design features (e.g., parallel vs. cross-over), sampling scheme, sample size/strata, population, etc. Replication details	Probability of success for scenarios or trial designs to achieve clinical milestones or study objectives
Target organ exposures (TOE)	FTP inputs Species (if comparing animal biodistribution to pediatric predictions) Target organs identified (with data/measured levels) if available	Overlays of observed vs. predicted exposures for animal studies In pediatrics, predicted exposures in target organs; correlation with toxicity or PD measures
Real-time PK-Safety	FTP inputs Measured levels (sampling/observations) Response measures (SAEs, ADRs, PD, etc.)	Overlays of observed vs. predicted exposures with comparisons across age strata and relative to adult data
Targeted drug delivery (TDD)	TOE inputs Delivery inputs (extravascular route, input rate, duration, etc.) Cellular constituent targets Imaging data (if relevant)	Overlays of observed vs. predicted exposures (or equivalent metrics) with comparisons across age strata and relative to adult data

TPP target product profile, *MW* molecular weight, *ADR* adverse drug reactions, *AE* serious adverse effects, *TOE* target organ exposures, *TDD* targeted drug delivery, *DDI* drug-drug interaction, *CLR* renal clearance, *CLH* hepatic clearance, *FTP* first time in pediatrics, *CTS* clinical trial simulation, *SAE* serious adverse events, *PD* pharmacodynamic, *CS* candidate screening

[a]Derived parameters include partition coefficients and permeabilities

perhaps results from in vivo studies in adult animals (Barrett et al. 2012). The common approach in developing a pediatric PBPK model is to modify a PBPK model that has been validated with adult PK data, and then to incorporate the differences

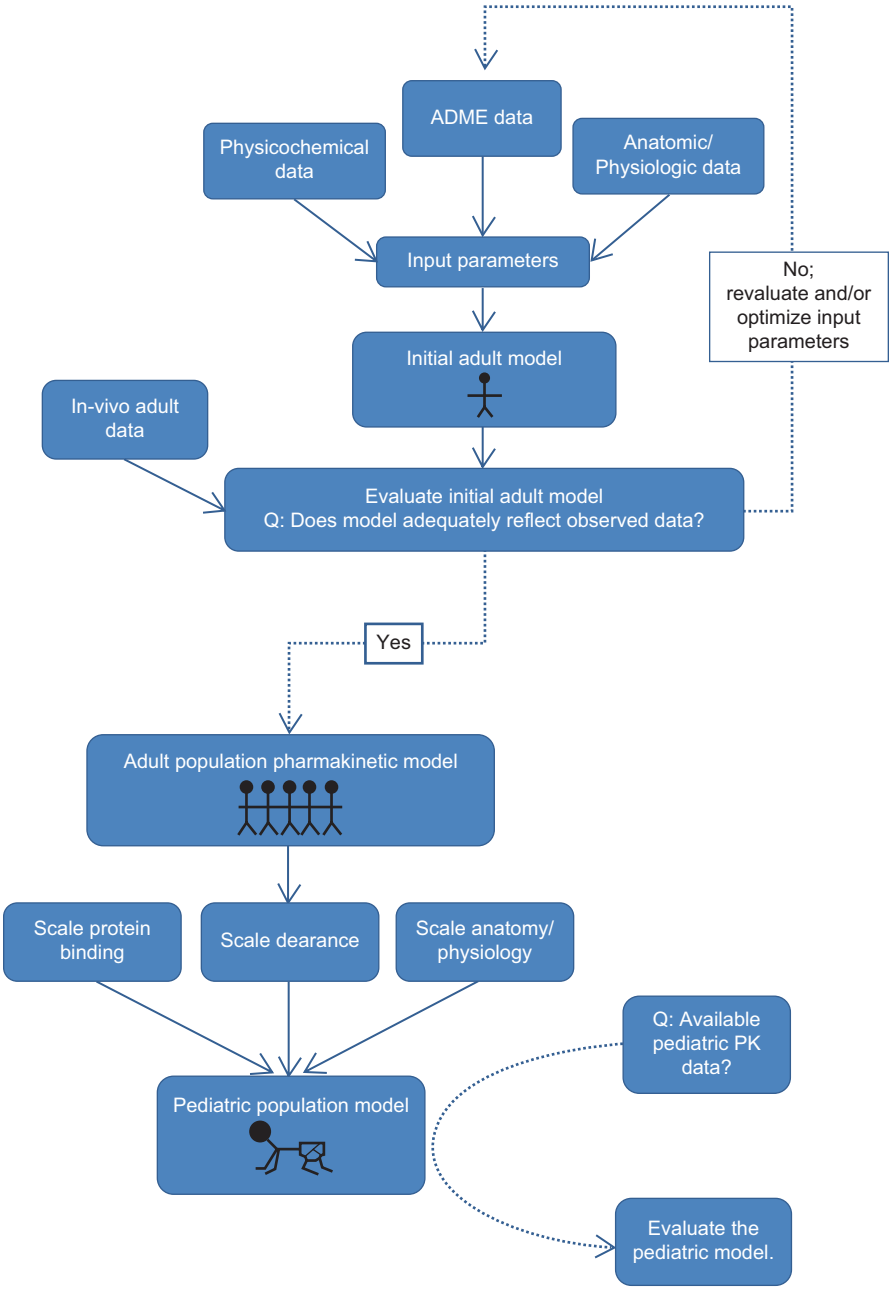

Fig. 3.4 Proposed workflow for scaling adult PBPK models towards children. (Reprinted with permission; Maharaj et al. 2013)

in growth and maturation that can affect all relevant aspects of drug disposition and PD. Figure 3.4 shows a schematic of a typical workflow for converting a PBPK model defined for adults into a credible pediatric PBPK model (Maharaj et al. 2013).

As total clearance of a compound is calculated as the sum of individual clearance pathways, clearance in children can be calculated as the sum of scaled hepatic and renal clearances using a PBPK approach. Physiologic hepatic clearance scaling relies on the following underlying assumptions (Maharaj et al. 2013):

1. Pathways of hepatic clearance in children are the same as those observed in adults.
2. Well-stirred model conditions hold (hepatic uptake of the compound is a function of blood flow—not permeability across cell membranes).
3. Enzyme metabolism follows first order kinetics (concentrations are within linear range—no enzyme saturation).

The effects of maturation and growth on OF can be accommodated using the approach of Hayton (Hayton 2000). For the estimation of renal function parameters as an example (e.g., glomerular filtration rate (GFR) and active secretion), clearance in children can be described as a function of age and weight. Edginton has proposed to scale adult renal clearance values towards pediatric patients with the following equation (Edginton et al. 2006a, 2006b):

$$CL_{GFR(child)} = \frac{GFR_{(child)}}{GFR_{(adult)}} \; x \; \frac{fu_{p(child)}}{fu_{p(adult)}} \; x \; CL_{GFR(adult)}$$

where $CL_{GFR(child)}$ is the child's clearance due to glomerular filtration, $GFR_{(child)}$ is the estimated GFR of the child, $GFR_{(adult)}$ is the GFR in adults (assumed to be 110 ml min^{-1}), and $CL_{GFR(adult)}$ the clearance due to glomerular filtration in adults. Several excellent examples of PBPK approaches applied to pediatrics have been recently published [refs]. While the PBPK approach has great promise for the future, the upfront investment required to refine physiochemical properties via experimentation and parameter "tuning" based on uncertainty in input parameters is not trivial.

3.7 Simulation as a Tool for Design Constructs and Analysis Plans

Any model generated to describe the PK, PD, or outcomes in children is only useful when it is used to examine scenarios, conditions, and subpopulation characteristics that challenge us to adjust medications, dosages or both. Simulation is defined as, "the imitation of the operation of a real-world process or system over time" and is the critical step in this transfer of knowledge. Simulations allow us to explore the validity of our assumptions and provide us with confidence when designing a pediatric trial. There are many levels of simulation and the choice of rigor around the simulations depends on our purpose and value we place on prediction.

A simulation plan allows us to articulate the questions to be explored via the model, the manner in which we answer these questions via a particular simulation scenario and the development of Go/No criteria based on the outcomes of the simulation. The common uses of simulation to support pediatric research and development include the following:

- Determination of acceptable/optimal study design constructs such as dose, sampling scheme (number and timing of blood collections for PK and or PK/PD analyses), and sample size.
- Performance and suitability of study-stopping rules, dosing adjustments, and/or enrollment strategies.
- Sensitivity of screening criteria, population characteristics (demographics, disease status, impairment), drop-outs, compliance, and placebo effect on response and/or outcomes.

The pharmacometrician, in conjunction with the project team, decides the boundaries of each scenario, the degree of replication required and various output (tables and graphs) to convey the interpretation. Each of these is essential to achieve the desired impact. Comparisons between age strata and adults are common but it is also important to evaluate the extremes of the population. While we have the visual predictive check to tell us how well the data fit the model, we use simulation at population extremes or condition boundaries as a further QC that our model performs operationally as expected. A case study which illustrates the iterative nature of modeling and simulation as well as the use of simulation to support pediatric research is provided in the final section.

3.7.1 Case Study: Sample Size and Sampling Scheme in Children

This first example examined the planning of a pediatric trial to examine the successful management of low molecular weight heparin (LMWH) dalteparinin pediatric cancer patients. While multiple disease foci are relevant, LMWH therapy in these patients was judged based on the ability to keep a patient's anti-Xa activity within a perceived therapeutic window. An important objective of this trial was the investigation of the PK/PD behavior in these patients with the goal of characterizing dose-exposure and exposure-response relationships. The ability to define such relationships quantitatively is, of course, governed by both the timing and frequency of sampling as well as the number of samples obtained per patient. Hence, sampling scheme and sample size are important design elements to be considered relative to practical issues of sampling (timing and volume) as well as enrollment (in very young patients) constraints. To this end, modeling and simulation strategies are useful and often recommended by FDA to ensure that the information content of the trial is sufficient.

For the trial in question, a population-based PK/PD model developed from an open-label, dose-finding trial in children (>36 weeks gestational age-16 years) with objectively confirmed thromboembolism (TE) was available as prior information

Table 3.6 Final population PK/PD model parameter estimates generated in 31 pediatric patients with objectively confirmed TE receiving LMWH for prophylaxis (N=31). (Adapted from data from Barrett et al. 2008a)

			Estimate	SE	% RSE	% CV
Final model parameter						
CL	(mL/h)	θ_{CL}	1410	165	11.7	–
V	(mL)	θ_{V}	9470	1310	13.8	–
Q	(mL/h)	θ_{Q}	202	10.7	5.3	–
V2	(mL)	θ_{V2}	42.3	24.8	58.6	–
KA	(IU/mL)	θ_{KA}	0.511	0.127	24.9	–
ENDO	(IU/mL)	θ_{ENDO}	0.0342	0.00226	6.6	–
Inter-individual variance						
ETA1		ω^2_{CL}	0.436	0.106	24.3	66.0
ETA2		ω^2_{V}	0.123	0.0967	78.6	35.1
ETA3		ω^2_{KA}	0.458	0.207	45.2	67.7
ETA4		ω^2_{Q}	7.93	5.96	75.2	281.6
EPS1		ω^2_{prop}	0.0999	0.0166	16.6	31.6

(Barrett et al. 2008a). A total of 31 children contributed PK data to the original analysis data set. The population PK/PD model was based on a two-compartment model (2-CPM) with first order absorption (ADVAN4 TRANS4 used as the NONMEM-specified PREDPP library model) with allometrically scaled clearance (CL) and central compartment volume of distribution (V), a proportional CV error model and endogenous anti-Xa activity. The first-order conditional method (FOCE) with η–ε interaction was used for method/estimation of final parameter estimates. Analysis suggested that the median maintenance dose to achieve the target anti-Xa level varied and correlated with indices of body size (age and weight). The population model parameter estimates from this model are shown in Table 3.6. The diagnostic plots from the final model fit are shown in Fig. 3.5.

The primary assumption relevant to the proposed pediatric oncology trial was that the PK/PD response to LMWH in children with TE was similar to the target population for the prospective trial, principally children with cancer. As the target age range (neonates to 18 years) was similar, demographic alignment was expected as well. Hence, the final population model and parameter estimates from the TE trial were used to construct simulation scenarios to evaluate the impact of sampling scheme (timing of blood sample collection for anti-Xa activity) and sample size within and across age strata in the oncology trial.

There were two primary objectives for the simulation exercise:

1. Evaluate total N of 10, 20, 30, 40, and 50 (2, 4, 6, 8, 10 per age strata) pediatric patients.
2. Evaluate single and two-point sample densities and impact of randomization across strata.

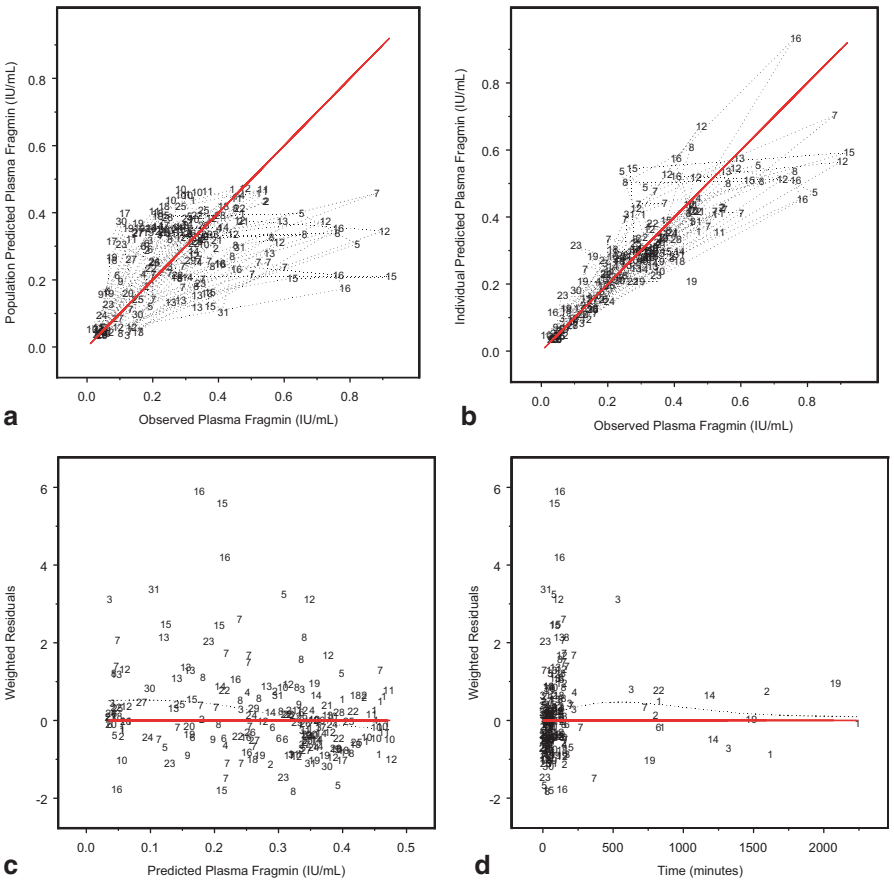

Fig. 3.5 Goodness-of-fit plots for the final model: diagnostic plots confirm the suitability of the model to describe sources of variation in LMWH PK across pediatric subpopulations: **a** PRED vs. DV, **b** IPRED vs. DV, **c** WRES vs. PRED, **d** WRES vs. TIME

Single-point designs were analyzed and performed poorly with an unacceptable number of trial evaluations (based on the simulated sampling) and unable to converge in NONMEM. Two-point designs with patients randomized to different sampling designs (2, 6, and 4, 10 h or 3, 8, and 5, 12 h) were proposed. Each of the ten scenarios (five sample size categories x two sampling schemes) was evaluated with 100 trial simulations per design examined. Each of the ten sampling scheme—sample size combinations required a unique dataset to be created in the NONMEM-required format. Matching population demographics (age, weight, gender, etc.) were obtained from the population dataset of the TE pediatric trial in order to mimic the "to-be-evaluated" target population. Representative file structure for the source simulation datasets is shown in Table 3.7.

The key elements of the source data file are the dosing records denoted by the EVID = 1 records and the "AMT" field which contains the dose in amount admin-

Table 3.7 NONMEM-formatted dataset structure for two-sample design employed to generate 100 replicate datasets with sampled observations generated via simulation

C	SID	ID	Time	DSKG	AMT	DV	EVID	Age	AGID	Sex	Race	WT
.	2	1	0	125	5225	.	1	11.68	4	1	1	41.8
.	2	1	2	.	.	.	0	11.68	4	1	1	41.8
.	2	1	6	.	.	.	0	11.68	4	1	1	41.8
.	4	2	0	125	4287.5	.	1	7.41	4	2	2	34.3
.	4	2	4	.	.	.	0	7.41	4	2	2	34.3
.	4	2	10	.	.	.	0	7.41	4	2	2	34.3
.	6	3	0	125	612.5	.	1	0.3	2	1	4	4.9
.	6	3	2	.	.	.	0	0.3	2	1	4	4.9
.	6	3	7	.	.	.	0	0.3	2	1	4	4.9

istered (International Units or "IU" in the case of LMWH). The DSKG field is the weight-normalized dose in IU per kilogram which is a carry-along variable used for grouping in the post evaluation but not used in the simulation. The DV column with placeholder (temporarily missing) values (coded as ".") indicates that a simulated concentration should be generated at each of the prescribed collection times (denoted in the TIME field). The generation of the 100 replicate datasets is accomplished by the control file. The basic process involves refitting each of the 100 simulated data files in NONMEM using the historical population model. Comparison of the population parameter estimates from the simulated data with the original model parameters used to generate the source data is made to examine if the scheme and sample size is adequate. The calculation of bias is based on these deviations and calculated on a percentage scale. The entire workflow for the simulation analysis is described in Fig. 3.6. Batch processing of the NONMEM simulation jobs is accomplished via PERL scripts (separate.p and databatch.p) and the calculation of bias for key parameters (CL, V, and KA) is performed by a SAS script. The precision of the scenario about each parameter is obtained by examining the distribution of the individual deviations about the expected value of 0 % bias. Box-n-whisker plots of the model prediction error were used to assess bias and precision and were generated using SPLUS (graph.ssc described).

The single-point designs (4, 7, 12, or 24 h) had difficulty with respect to run convergence in NONMEM and yielded unacceptable bias in CL and/or Vd when convergence was attained as previously discussed. It was also suggestive of confounding of effects due to blocking of sample collection within age strata. Box-n-whisker plots showing the precision and bias about key parameters generated from the simulated datasets for each of the two-point, sample size designs were generated for all scenarios. Figure 3.7a–c shows the impact of sample size (total *N* of 20, 30, and 40 patients shown in a, b, and c, respectively) on model prediction error for key PK parameters based on the 3, 8 and 5, 12 h scheme. This result clearly supports increasing the sample size to at least 40 patients (eight per strata) to ensure that re-estimation of the PK parameters is accurate and precise. This assessment is made primarily from the impact on clearance as this is typically the primary parameter of interest with respect to dosing in general.

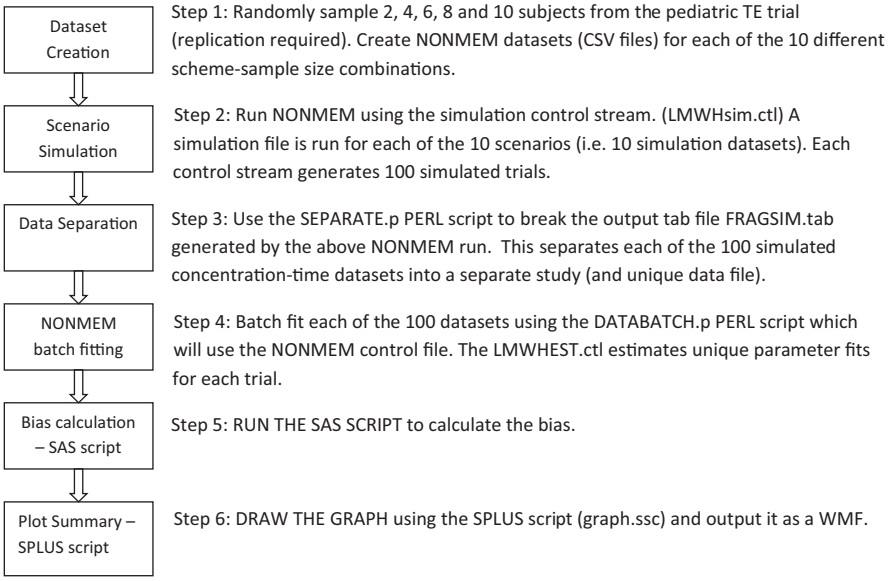

Fig. 3.6 Workflow for simulation execution to evaluate sample size and sampling scheme considerations for the pediatric oncology trial

Figure 3.8a, b illustrates the impact of sampling scheme design on the model prediction error with a 40-patient sample size (n = eight per age strata) shown for illustration purposes. The a and b designation for each of the plots discriminates between the two proposed sampling schemes.

In all cases (sample sizes), when evaluating the 2, 6 and 4, 10 h vs. 3, 8 and 5, 12 h randomized two-sample designs, the 3, 8 and 5, 12 h design performed more efficiently with respect to estimation of CL and V. The 2, 6 and 4, 10 design was better for estimation of Ka. The choice of designs clearly favors the 3, 8 and 5, 12 design reflective of the 3–5 h, 8–12 h sampling windows proposed in the actual protocol. The choice of design and sampling design is easily defended from such an approach. It should also be appreciated that this approach can accommodate the practical negations that occur when planning such trials. It is quite common that the combination of patient convenience, availability and/or cost of staff to draw samples limits the ability to draw samples after say 8 h. This approach allows a data-driven conversation around the "value" of such data in light of study objectives and regulatory recommendations as opposed to more opinion-based discussion.

To complete the example illustrated above, it should be appreciate that in the end the sponsor agreed to a sample size of 50 patients (n = 10/sage strata) based on the simulation results shown in Fig. 3.9. The sample size of 50 would seem to be well supported by the analysis as gains in precision which are evident even from a sample size increment of 40–50 subjects. This analysis was submitted to FDA as a technical appendix supporting the sample size and sampling scheme proposal

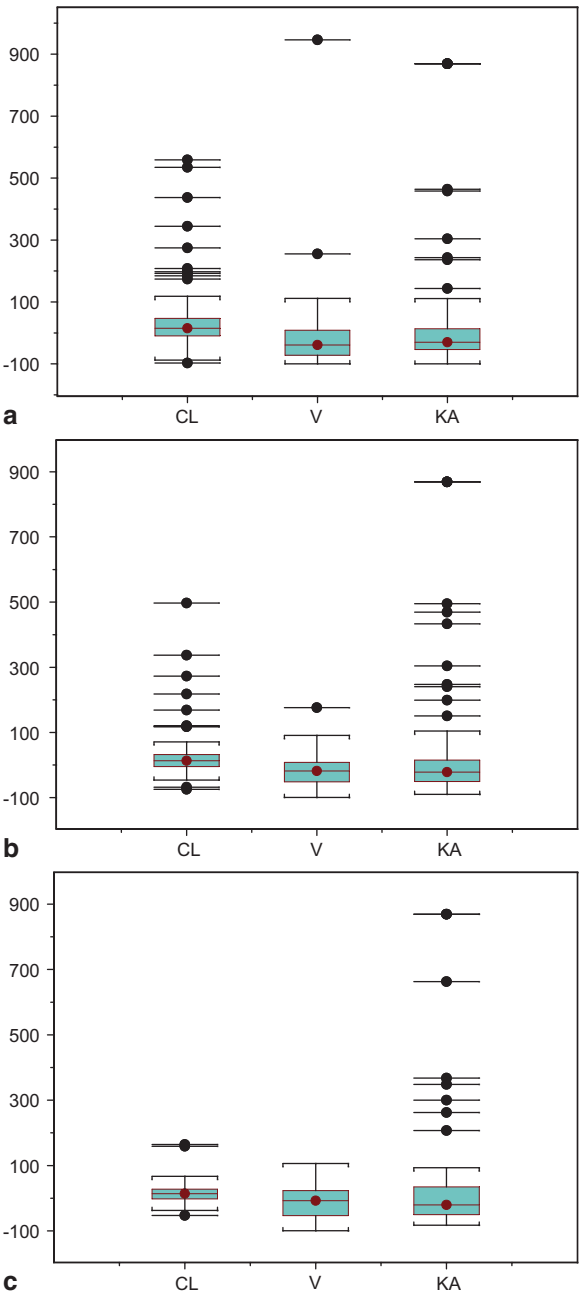

Fig. 3.7 Box-n-whisker plots of MPE for CL, Vd, and Ka based on a 100 trial simulations exploring limited randomized sampling schemes (3, 8 and 5, 12 h design shown) and effect of sample size. Sample sizes of 20, 30, and 40 patients (4, 6, and 8 patients per age strata) shown in Fig. 3.7a, b, and c, respectively

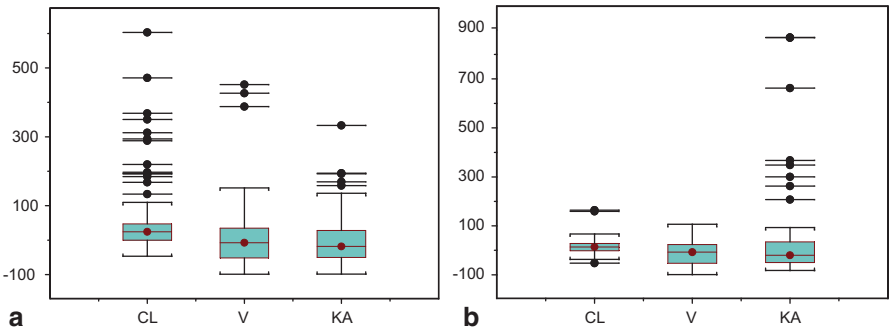

Fig. 3.8 Box-n-whisker plots of MPE for CL, Vd, and Ka based on a 100 trial simulations exploring limited randomized sampling schemes and effect of sample size. The comparison between randomized two-sample designs (a = 2, 6 and 4, 10 h and b = 3, 8 and 5, 12 h) is illustrated at a sample size of 40 patients (eight patients per age strata)

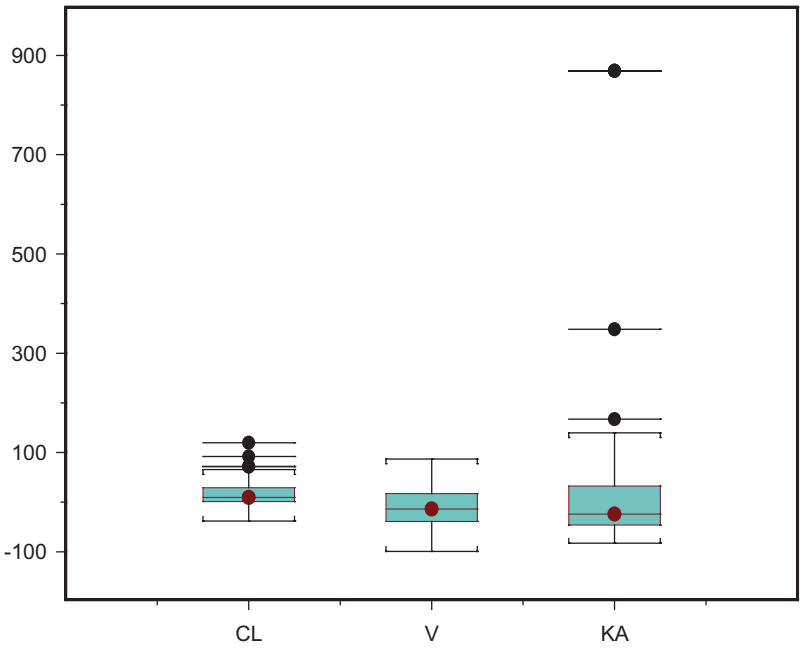

Fig. 3.9 Justification for sampling scheme (3, 8 and 5, 12 h) and sample size ($n = 50$) based on box-n-whisker plots of MPE for CL, Vd, and Ka (100 trial simulations exploring limited randomized sampling schemes and effect of sample size)

and was accepted as an appropriate justification. While recent proposals for sample size seem to focus on more traditional inference testing of adjacent age groups (Wang et al. 2012), the use of simulation from an adult-scaled, allometric (with appropriate adjustments for ontogeny or maturation as needed), or an appropriate

PBPK model would seem to make more sense for the overall support of design constructs. It is seldom possible to decouple dose, sampling scheme, and sampling design. The power of simulations is easily demonstrated in this setting as these factors can be accommodated and specific nuances evaluated via scenario testing.

References

Alcorn J, McNamara PJ (2008) Using ontogeny information to build predictive models for drug elimination. Drug Discov Today 13(11–12):507–512

Anderson BJ, Holford NH (2008) Mechanism-based concepts of size and maturity in pharmacokinetics. Annu Rev Pharmacol Toxicol 48:303–332

Anderson GD, Lynn AM (2009) Optimizing pediatric dosing: a developmental pharmacologic approach. Pharmacotherapy 29(6):680–690

Barker P, Nowak C, King K, Mosca R, Bove E, Goldberg C (2005) Risk factors for cerebrovascular events following Fontan palliation in patients with a functional single ventricle. Am J Cardiol 96:587–591

Barrett JS, Mitchell LG, Patel D, Cox P, Vegh P, Castillo M, Massicotte P (2008a) A population-based analysis of dalteparin pharmacokinetics in pediatric patients at risk for thromboembolic events. J Clin Pharmacol 48(9):1107

Barrett JS, Mondick JT, Narayan M, Vijayakumar K, Vijayakumar S (2008b) Integration of modeling and simulation into hospital-based decision support systems guiding pediatric pharmacotherapy. BMC Med Inform Decis Mak 8:6

Barrett JS, Narayan M, Patel D, Zuppa AF, Adamson PC (2011) Prescribing habits and caregiver satisfaction with resources for dosing children: rationale for more informative dosing guidance. BMC Pediatr 11:25

Barrett JS, Della CAlberighiO, Laer S, Meibohm B (2012) Physiologically based pharmacokinetic (PBPK) modeling in children. Clin Pharmacol Ther 92(1):40–49

Belik J, Karpinka B, Hart DA (2000) Pulmonary and systemic vascular tissue collagen, growth factor, and cytokine gene expression in the rabbit. Can J Physiol Pharmacol 78(5):400–406

Blake MJ, Castro L, Leeder JS, Kearns GL (2005) Ontogeny of drug metabolizing enzymes in the neonate. Semin Fetal Neonatal Med 10(2):123–138

Clapp DW (2006) Developmental regulation of the immune system. Semin Perinatol 30(2):69–72

Crom WR, de Graaf SS, Synold T, Uges DR, Bloemhof H, Rivera G, Christensen ML, Mahmoud H, Evans WE (1994) Pharmacokinetics of vincristine in children and adolescents with acute lymphocytic leukemia. J Pediatr 125(4):642–649

Dombrowsky E, Jayaraman B, Narayan M, Barrett JS (2011) Evaluating performance of a decision support system to improve methotrexate pharmacotherapy in children and young adults with cancer. Ther Drug Monit 33(1):99–107

Dorschner RA, Lin KH, Murakami M, Gallo RL (2003) Neonatal skin in mice and humans expresses increased levels of antimicrobial peptides: innate immunity during development of the adaptive response. Pediatr Res 53(4):566–572

Edginton AN, Schmitt W, Voith B, Willmann S (2006a) A mechanistic approach for the scaling of clearance in children. Clin Pharmacokinet 45(7):683–704

Edginton AN, Schmitt W, Willmann S (2006b) Development and evaluation of a generic physiologically based pharmacokinetic model for children. Clin Pharmacokinet 45(10):1013–1034

Engle WA (2004) Age terminology during the perinatal period. Pediatrics 114(5):1362–1364

Gardner SN (2002) Modeling multi-drug chemotherapy: tailoring treatment to individuals. J Theor Biol 214(2):181–207

Ge Y, Haska CL, LaFiura K, Devidas M, Linda SB, Liu M, Thomas R, Taub JW, Matherly LH (2007) Prognostic role of the reduced folate carrier, the major membrane transporter for meth-

otrexate, in childhood acute lymphoblastic leukemia: a report from the children's oncology group. Clin Cancer Res 13(2 Pt 1):451–457
Ginsberg G, Hattis D, Miller R, Sonawane B (2004) Pediatric pharmacokinetic data: implications for environmental risk assessment for children. Pediatrics 113(4 Suppl):973–983
Hayton WL (2000) Maturation and growth of renal function: dosing renally cleared drugs in children. AAPS Pharm Sci 2(1):E3
Johnson TN (2005) Modelling approaches to dose estimation in children. Br J Clin Pharmacol 59(6):663–669
Johnson TN (2008) The problems in scaling adult drug doses to children. Arch Dis Child 93(3):207–211
Johnson TN, Thomson M (2008) Intestinal metabolism and transport of drugs in children: the effects of age and disease. J Pediatr Gastroenterol Nutr 47(1):3–10
Johnson TN, Rostami-Hodjegan A, Tucker GT (2006) Prediction of the clearance of eleven drugs and associated variability in neonates, infants and children. Clin Pharmacokinet 45(9):931–956
Johnson TN, Tucker GT, Rostami-Hodjegan A (2008) Development of CYP2D6 and CYP3A4 in the first year of life. Clin Pharmacol Ther 83(5):670–671
Kearns GL, Abdel-Rahman SM, Alander SW, Blowey DL, Leeder JS, Kauffman RE (2003a) Developmental pharmacology–drug disposition, action, and therapy in infants and children. N Engl J Med 349(12):1157–1167
Kearns GL, Robinson PK, Wilson JT, Wilson-Costello D, Knight GR, Ward RM, van den Anker JN (2003b) Cisapride disposition in neonates and infants: in vivo reflection of cytochrome P450 3A4 ontogeny. Clin Pharmacol Ther 74(4):312–325
Kohyama J, Iwakawa Y (1990) Developmental changes in phasic sleep parameters as reflections of the brain-stem maturation: polysomnographical examinations of infants, including premature neonates. Electroencephalogr Clin Neurophysiol 76(4):325–330
Läer S, Elshoff JP, Meibohm B, Weil J, Mir TS, Zhang W, Hulpke-Wette M (2005) Development of a safe and effective pediatric dosing regimen for sotalol based on population pharmacokinetics and pharmacodynamics in children with supraventricular tachycardia. J Am Coll Cardiol 46:1322–1330
Laer S, Barrett JS, Meibohm B (2009) The in silico child: using simulation to guide pediatric drug development and manage pediatric pharmacotherapy. J Clin Pharmacol 49(8):889–904
Maharaj AR, Barrett JS, Edginton AN (2013) A workflow example of PBPK modeling to support pediatric research and development: case study with lorazepam. AAPS J 15(2):455–464
Mondick JT, Gibiansky L, Gastonguay MR, Skolnik JM, Cole M, Veal GJ, Boddy AV, Adamson PC, Barrett JS (2008) Population pharmacokinetic investigation of actinomycin-D in children and young adults. J Clin Pharmacol 48(1):35–42
Potts AL, Anderson BJ, Warman GR, Lerman J, Diaz SM, Vilo S (2009) Dexmedetomidine pharmacokinetics in pediatric intensive care—a pooled analysis. Paediatr Anaesth 19(11):1119–1129
Revel-Vilk S, Chan AK (2003) Anticoagulation therapy in children. Semin Thromb Hemost 29(4):425–432
Rodman JH (1994) Pharmacokinetic variability in the adolescent: implications of body size and organ function for dosage regimen design. J Adolesc Health 15(8):654–662
Shi J, Ludden TM, Melikian AP, Gastonguay MR, Hinderling PH (2001) Population pharmacokinetics and pharmacodynamics of sotalol in pediatric patients with supraventricular or ventricular tachyarrhythmia. J Pharmacokinet Pharmacodyn 28:555–575
Stevens JC, Marsh SA, Zaya MJ, Regina KJ, Divakaran K, Le M, Hines RN (2008) Developmental changes in human liver CYP2D6 expression. Drug Metab Dispos 36(8):1587–1593
Strolin Benedetti M, Baltes EL (2003) Drug metabolism and disposition in children. Fundam Clin Pharmacol 17(3):281–299
Tod M, Jullien V, Pons G (2008) Facilitation of drug evaluation in children by population methods and modelling. Clin Pharmacokinet 47(4):231–243

Wade KC, Wu D, Kaufman DA, Ward RM, Benjamin DK Jr, Sullivan JE, Ramey N, Jayaraman B, Hoppu K, Adamson PC, Gastonguay MR, Barrett JS (2008) Population pharmacokinetics of fluconazole in young infants. Antimicrob Agents Chemother 52(11):4043–4049

Wang Y, Jadhav PR, Lala M, Gobburu JV (2012) Clarification on precision criteria to derive sample size when designing pediatric pharmacokinetic studies. J Clin Pharmacol 52(10):1601–1606

Ward RM, Kauffman R (2007) Future of pediatric therapeutics: reauthorization of BPCA and PREA. Clin Pharmacol Ther 81(4):477–479

Yang F, Tong X, McCarver DG, Hines RN, Beard DA (2006) Population-based analysis of methadone distribution and metabolism using an age-dependent physiologically based pharmacokinetic model. J Pharmacokinet Pharmacodyn 33(4):485–518

Zuppa AF, Barrett JS (2008) Pharmacokinetics and pharmacodynamics in the critically ill child. Pediatr Clin North Am 55(3):735–755, xii

Chapter 4
Pharmacometrics in Chronic Kidney Disease

Liping Zhang, Amit Roy and Marc Pfister

4.1 Introduction

Chronic kidney disease (CKD) is a general term for heterogeneous disorders affecting both structure and function of the kidney. Coupled with aging population and higher prevalence of diabetes mellitus and hypertension, CKD has become a leading public health concern worldwide. National Health and Nutrition Examination Survey suggested the prevalence is 38 % in elderly (age ≥ 65 years) and 13 % in the overall US population (Coresh et al. 2007). A similar inexorable increase in the number of patients receiving chronic renal replacement therapy (RRT) by dialysis or transplant is seen in the past decade (Kidney Disease Statistics for the United States [Internet] 2013). CKD is a common and deadly disease (Levey et al. 2007).

The kidney performs endocrine functions (erythropoietin, renin, calcitriol), metabolizes small peptide hormones, produces glucose via gluconeogenesis, maintains homeostasis (solutes, water), and eliminates endogenously produced "waste products" (uremic toxins). Pathophysiologic changes associated with CKD affect other organ systems in the body and have pronounced effects on the pharmacology of many drugs. Rational drug therapy in subjects with CKD must take into account changes in the absorption, distribution, metabolism, and excretion (ADME) of drugs and their active or toxic metabolites due to impaired kidney. To complicate the matter further, a majority of subjects with CKD receive multiple drugs for the treatment of underlying diseases such as hypertension, diabetes mellitus, infection-

M. Pfister (✉)
University Children's Hospital Basel (UKBB), Spitalstrasse 33, CH-4031 Basel, Switzerland
e-mail: Marc.Pfister@ukbb.ch

Quantitative Solutions, Bridgewater, USA

L. Zhang
Model Based Drug Development Group, Janssen Pharmaceutical Research and Development, Titusville, NJ, USA

A. Roy
Clinical Pharmacology & Pharmacometrics, Bristol-Myers Squibb, Princeton, NJ, USA

S. Schmidt, H. Derendorf (eds.), *Applied Pharmacometrics,* AAPS Advances in the Pharmaceutical Sciences Series 14, DOI 10.1007/978-1-4939-1304-6_4

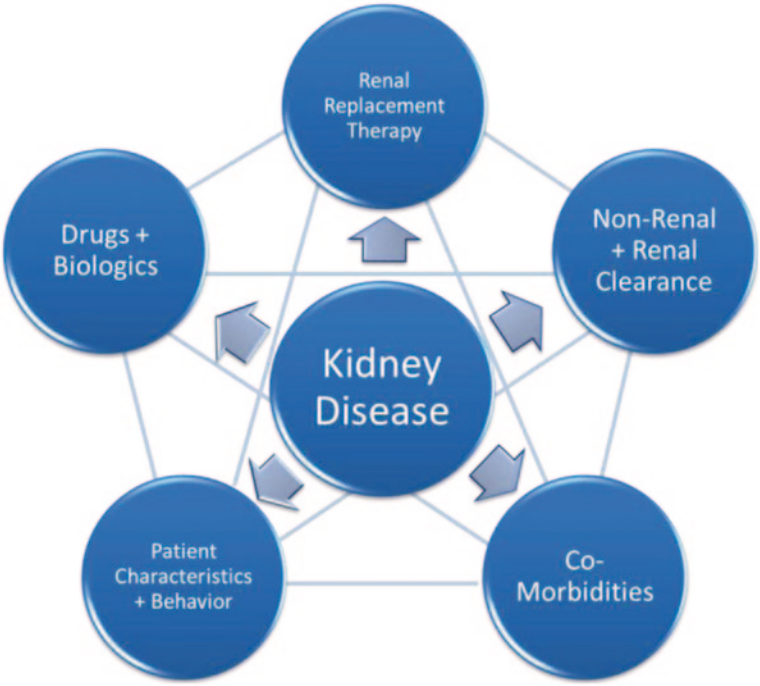

Fig. 4.1 Complex interplay between therapies and CKD

related or autoimmune diseases (e.g., systemic lupus erythematosus). Some of these treatments have renoprotective effects; others are associated with nephrotoxic effects.

The learning for clinical efficacy/safety balance of emerging medicines is vastly based on a general population. Quantitatively extrapolating the knowledge and individualizing such balance for subjects with CKD are not straightforward. Why? The interactions between CKD and treatment are not just unidirectional. Multifaceted factors need to be considered when medicines for subjects with CKD are developed and utilized: (1) altered renal and *non*-renal clearance can affect drug exposure and effects in CKD, (2) drugs for comorbidities or underlying diseases can have nephrotoxic effects and accelerate progression of CKD, (3) progression of CKD requires careful monitoring and frequent adjustments of treatments, (4) RRT by dialysis or transplant can impact drug exposure and effects, and (5) RRT can change a patient's behavior (e.g., drug non-adherence), which in turn can affect drug exposure and clinical outcomes (Fig. 4.1).

This complex interplay between CKD-related multifaceted factors that interact with therapeutics calls for quantitative approaches to optimize therapies for subjects with CKD. Pharmacometrics is a quantitative scientific discipline that uses mathematical models based on biology, pharmacology, physiology, and knowledge in disease for quantifying interactions between disease, drugs, and patients (Zhang et al.

Table 4.1 Five stages of CKD

Stage	Description	GFR (mL/min/1.73 m^2)
1	Kidney damage with normal ↑ GFR	≥90
2	Kidney damage with mild ↓ GFR	60–89
3	Moderate ↓ GFR	30–59
4	Severe ↓ GFR	15–29
5	Kidney failure	<15 (or dialysis)

2008; Pfister and D'Argenio 2010). Pharmacometric approaches have been increasingly applied to understand and characterize interactions between CKD-related factors and therapeutics in the recent years (Pfister et al. 2012).

The goal of this book chapter is to review and discuss opportunities for applying pharmacometrics for facilitating research and development of new drugs in CKD, optimizing development and utilization of medicines in CKD and managing RRT such as dialysis and kidney transplant. A background on CKD and the interactions between CKD, RRT, and therapeutics is given before the introduction of case studies for the application of pharmacometrics in these areas.

4.2 Background on CKD

This section provides an overview of stages, risk factors, and consequences of CKD, assessment of kidney function, effects of CKD on drugs, effects of drugs on CKD, and interactions between drugs and RRT by dialysis or transplant.

4.2.1 Define CKD and its Five Stages

All individuals with kidney damage or a glomerular filtration rate (GFR) < 60 mL/min/1.73 m^2 for 3 months are classified as having CKD. Kidney damage is defined as pathologic abnormalities or markers of damage, including abnormalities in blood or urine tests or imaging studies. Five stages of CKD are classified based on the presence of kidney damage or GFR level (Table 4.1; KDOQI Clinical Practice Guidelines for Chronic Kidney Disease: Evaluation, Classification, and Stratification [Internet] 2013).

4.2.2 Risk Factors and Consequences of CKD

CKD is a silent disease. It is critical to screen for CKD and its risk factors to detect any kidney damage early (Fig. 4.2). Cardiovascular risk factors, such as old age, hypertension, dyslipidemia, smoking, and diabetes mellitus promote the development

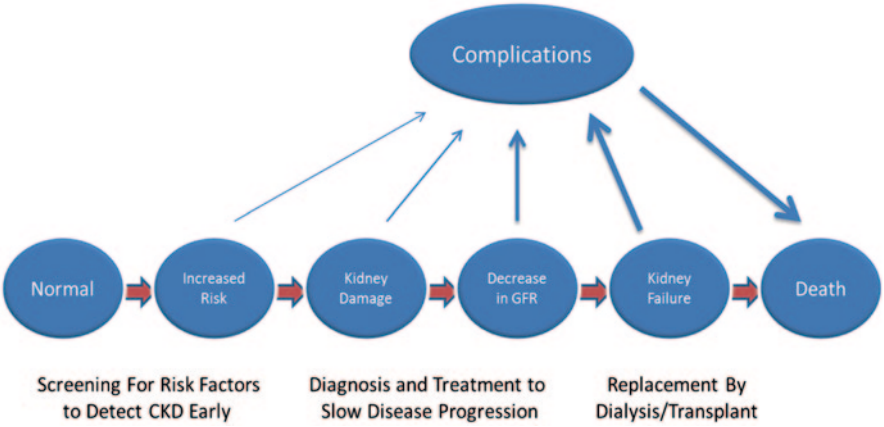

Fig. 4.2 CKD: a silent deadly disease. *GFR* glomerular filtration rate

and progression of both CKD. A direct relationship was observed between the prevalence of CKD and markers of insulin resistance, such as levels of serum insulin, C-peptide, and glycosylated hemoglobin A1c. Family history, low birth weight, race (African Americans), and gender (male) are also shown to be risk factors for CKD. Meanwhile, patients in all stages of CKD are considered at risk for development of cardiovascular disease and CKD is recognized as a cardiovascular risk equivalent. Not only uremic toxins but also homocysteine, lipoproteins, and markers of inflammation and oxidative stress are elevated in CKD.

4.2.3 Assess and Monitor Kidney Function

Filtration markers such as inulin, iohexol, and iothalamate are considered the gold standards for measuring GFR. However, GFR is more commonly estimated using equations for practicality reason. The Cockroft–Gault (C–G) equation was developed in 1976 to estimate urinary creatinine clearance (in units of ml/min) with data from 249 Caucasian men with a mean creatinine clearance of 73 ml/min (Cockcroft and Gault 1976):

$$\mathrm{GFR(ml/min)} = (140 - \mathrm{age}) \times \mathrm{weight}/(72 \times \mathrm{Scr}) \times (0.85 \text{ for female subjects})$$

In 1999, the modification of diet in renal disease (MDRD) study equation was developed to estimate GFR measured with data from 1628 men and women, including African Americans and Caucasians with a mean GFR of 40 ml/min/1.73 m^2 (Levey et al. 1999).

$$\mathrm{GFR(ml/min/1.73\ m^2)} = 186 \times \mathrm{Scr} - 1.154 \times \mathrm{age} - 0.203 \times (0.742 \text{ for female subjects}) \times (1.212 \text{ for African Americans})$$

Comparing with C–G equation, which is a measure of kidney filtration on an absolute scale, the MDRD study equation is normalized to body surface area (BSA) of 1.73 m^2 and is more suitable to judge renal impairment because it adjusts for the expected normal increase in absolute filtration with body size. However, the MDRD study equation underestimates measured GFR at levels > 60 mL/min/1.73 m^2, with variable accuracy among subgroups (Stevens et al. 2010). For this reason, a new GFR-estimating equation, the CKD epidemiology collaboration (CKD-EPI) equation, was developed (Levey et al. 2009). The CKD-EPI equation was found to be more accurate than the MDRD study equation overall and across most subgroups. The CKD-EPI creatinine equation is based on the same four variables as the MDRD study equation, but uses a 2-slope "spline" to model the relationship between estimated GFR (eGFR) and serum creatinine, and a different relationship for age, sex, and race. The CKD-EPI creatinine equation was reported to be more accurate than the MDRD study equation across a wide variety of populations and clinical conditions (Levey et al. 2009; Levey and Stevens 2010; Stevens et al. 2011).

In the future, other GFR estimating equations may be developed that outperform CKD-EPI. The CKD-EPI creatinine equation is:

$$\mathrm{GFR} = 141 \times \min(\mathrm{Scr}/\kappa, 1)^{\alpha} \times \max(\mathrm{Scr}/\kappa, 1)^{-1.209} \times 0.993^{\mathrm{Age}}$$
$$\times 1.018 \text{ if female} \times 1.159 \text{ if black}$$
$$\kappa = 0.7 \text{ if female}$$
$$\kappa = 0.9 \text{ if male}$$
$$\alpha = -0.329 \text{ if female}$$
$$\alpha = -0.411 \text{ if male}$$
$$\min = \text{The minimum of Scr}/\kappa \text{or } 1$$
$$\max = \text{The maximum or Scr}/\kappa \text{or } 1$$

A recent meta-analysis of data from 1.1 million adults (aged≥18 years) indicated that the new CKD-EPI equation classified fewer individuals as having CKD and more accurately categorized the risk for mortality and end-stage renal disease (ESRD) than did the MDRD study equation across a broad range of populations (Matsushita et al. 2012).

Recently, new biomarkers were evaluated to detect and monitor kidney injury/disease, including cystatin C for drug-induced kidney toxicity, urinary β2-microglobulin for earlier and more sensitive measure of kidney tubular toxicity, and kidney injury molecule-1 for detecting early kidney injury in adults and pediatrics (Parikh et al. 2011; Mårtensson et al. 2012). These new biomarkers were additional to the routinely used biomarkers including levels of serum creatinine, BUN, and urinary N-acetyl-glucosamine, glycosuria, and proteinuria. Research, development, and use of new drugs for therapeutic targets associated with diseases associated with deterioration in kidney function, such as diabetes mellitus, hypertension, obesity, heart failure, hyperlipidemia, and transplant rejection may benefit from measuring and modeling such biomarkers.

4.2.4 Understand Impact of CKD on Exposure and Effects of Drugs and Biologics

A progressive decline in kidney function, a hallmark of CKD, often leads to a wide array of the pathophysiologic changes that affect the absorption, distribution, metabolism, and excretion (ADME) characteristics of drugs (Table 4.2), including decreased glomerular filtration and/or renal transport, altered absorption, bioavailability, and/or protein binding (Naud et al. 2012; Joy 2012).

Evidence is also emerging on the impact of CKD on the non-renal clearance of many drugs, specifically affecting uptake and efflux transporters as well as metabolic enzymes in the liver and gastrointestinal tract (Nolin and Unruh 2010). Recent studies suggest that accumulated uremic toxins in subjects with CKD can cause either transcriptional or translational modifications or direct inhibition of these enzymes (e.g., CYP2C11, CYP3A1, CYP3A2) and transporters (e.g., organic anion transporting peptide, OATP; Nolin et al. 2008; Dreisbach 2009). Such pathophysiological changes can explain altered exposure and response of renally and some non-renally eliminated drugs in subjects with CKD.

Protein therapeutics (biologics) are eliminated from the body nearly exclusively by proteolysis. Theoretical considerations and clinical evidence suggest that the kidneys play a relevant role in the catabolism and thus elimination of biologics that have a size below the cutoff for glomerular filtration of approximately 60 kDa. Thus, the effect of CKD on biologics seems to be predictable and only relevant for compounds below this molecular weight cutoff. This is supported by clinical evidence that shows a lack of effect of kidney function on large proteins such as monoclonal antibodies, whereas smaller proteins below the cutoff such as interleukin-10, growth hormone and erythropoietin experience a gradual decrease of their clearance and increase of their systemic exposure with increasing degree of impaired kidney function (Kim et al. 1995; Meibohm and Zhou 2012).

4.2.5 Understand Effects of Drugs on CKD

Much of the differences between drug responses in CKD patients and regular population can be explained by the exposure difference between the two. Altered ADME property of drugs in subjects with CKD leads to different exposure in active drug or metabolites (Table 4.2), which in turn causes difference in responses. Perhaps for this reason, in the *Guidance for Industry Pharmacokinetics in Patients with Impaired Renal Function—Study Design, Data Analysis, and Impact on Dosing and Labeling* issued by Food and Drug Administration (FDA; Tortorici et al. 2012; Draft Guidance: Pharmacokinetics in Patients with Impaired Renal Function—Study Design, Data Analysis, and Impact on Dosing and Labeling [Internet] 2010), the guidance listed detailed instruction for pharmacokinetic (PK) testing but only vaguely mentioned pharmacodynamic (PD) assessment should be included in the testing when appropriate. Dose for subjects with CKD are typically adjusted to produce a comparable range of unbound plasma concentrations of drug of active metabolites in the patients with normal kidney function.

Table 4.2 Impact of CKD on absorption, distribution, metabolism, and excretion (ADME) of drugs

	CKD-related pathophysiological changes	Effect on drugs	Impact
Absorption	Formation of ammonia in the presence of gastric urease and buffers gastric acid	Decreased absorption of drugs that are best absorbed in an acidic environment, prolongs gastric emptying, and delays drug absorption	More variable bioavailability in patients with renal impairment than in patients with normal renal function
	Increase in gastric pH	Increased amounts of active drugs in the systemic circulation and enhanced bioavailability of some drugs	
	Decrease in first-pass hepatic metabolism and biotransformation	More unbounded drugs to be available at the site of hepatic metabolism, thereby increasing the amount of drug removed during the hepatic first pass	
	Decrease in protein binding		
Distribution	Formation of edema and ascites	Increased apparent volume of distribution of highly water soluble or protein bound	Lower plasma concentrations after a given dose
	Decrease in albumin concentration	Decreased affinity for the drug reduces protein binding in patients with uremia, making the unbound fraction of acidic drugs substantially increased	More abundant drug available at the site of drug action or toxicity
	Removal of fluid during dialysis	Altered distribution volume of drugs and change during the dialysis cycle	Different concentration within dialysis cycle
Metabolism	Accumulation of uremic toxins	The rate of reduction and hydrolysis reactions and microsomal oxidation are reduced	Accumulated active drug
		Glucuronidation to polar, water-soluble metabolites is impaired due to decreased clearance of blucuronide from plasma	Slows down the removal of soluble metabolite
		Alternations of intestinal, hepatic, and renal transporters, and metabolic enzymes such as reduced OATP expression and altered CYP expression	Higher incidence of adverse drug reactions
		May also alter the disposition of drugs metabolized by the liver through changes in plasma protein binding while the unbound intrinsic metabolic clearance declines with creatinine clearance	

Table 4.2 (continued)

	CKD-related pathophysiological changes	Effect on drugs	Impact
Excretion	Decrease in GFR	Clearance of drugs eliminated primarily by glomerular filtration	Increased plasma concentration and prolonged half-life in drug that are eliminated primarily by glomerular filtration
	Decrease in protein binding	Decreased filtration of drugs; may also increase the amount secreted by the renal tubule	The excretion of drugs eliminated by active organic ion transport systems in the renal tubules is prolonged in patients with CKD and may become saturated upon multiple drug administration
	Decrease in enzymatic capacity	Decreased metabolism, including many protein and small peptides	Increased concentration and prolonged half life

In epidemiology studies, CKD has been shown to be a risk factor for cardiovascular diseases, hematologic diseases, endocrine diseases, neurologic disease, and may lead to mineral bone disorders (MBDs; Briasoulis and Bakris 2013; Levin 2013). It is foreseeable that the efficacy and safety of these diseases could be different in subjects with CKD and subjects with a different degree of CKD. For drugs that rely on kidney function to exert its effect, the responses in subjects with CKD are expected to be different. Sodium-glucose cotransproter-2 (SGLT2) inhibitors developed for the treatment of type 2 diabetes mellitus (T2DM) by decreasing glucose reabsorption in kidney are shown to rely on a close-to-normal kidney function to exert its full pharmacological effect on glucose (Komoroski et al. 2009; Kasichayanula et al. 2012).

The kidneys are vulnerable to injury due to their high filtration capacity and high metabolic activity, and most drugs, especially hydrophilic drugs and their metabolites, are eliminated largely by kidneys in urine, thus increasing the risk of drug-induced nephrotoxicity (DIN). DIN accounts for approximately 20 % of community- and hospital-acquired episodes of acute kidney injury (AKI), and AKI is a risk factor for the future development or accelerated progression of CKD (Goldstein et al. 2013).

Manifestations of DIN include acid–base abnormalities, electrolyte imbalances, urine sediment abnormalities, proteinuria, pyuria, hematuria, and decrease in GFR. Aminoglycoside antibiotics, nonselective nonsteroidal anti-inflammatory drugs (NSAIDs), and radio-contrast media have been frequently associated with DIN, especially in patients with CKD. Anti-hypertensive drugs such as angiotensin-converting enzyme (ACE) inhibitors and angiotensin II receptor inhibitors (ARBs)

have renoprotective effects by lowering both blood pressure and proteinuria and are the preferred treatment option in CKD with T2DM. At the same time, the use of ACE inhibitors and ARBs can result in adverse effects, which are more common in CKD. The most common side effects-early decrease in GFR, hypotension, and hyperkalemia-require careful monitoring of therapy, but can usually be managed without discontinuation of the agent.

In a recent study in subjects with T2DM and CKD, bardoxolone methyl, an oral antioxidant inflammation modulator, was not lowering proteinuria, but was associated with an increase in eGFR (Pergola et al. 2011).

4.2.6 Understand Effects of Drugs on Kidney Transplants

In transplant medicine, the standard immunosuppressive treatment paradigm for prophylaxis of organ rejection in kidney transplant can be classified into the following three stages (Halloran 2004): (1) induction of immunosuppression (usually with immune-cell-depleting agents), (2) pre-adaptive maintenance therapy (with a combination of a calcinurin inhibitor (CNI; cyclosporin or tacrolimus), an antimetabolite (azothioprene) or nucleotide synthesis inhibitor (mycophenolatemofetil, MMF), and a glucocorticoid), and (3) post-adaptive maintenance therapy with lower dose of the three pre-adaptive therapy drugs. Ironically, CNIs such as cyclosporine are associated with nephrotoxic effects: Acute nephrotoxicity caused by vascular dysfunction and a more chronic fibrotic form. CNIs therefore require therapeutic drug monitoring due to their narrow therapeutic window (Schiff et al. 2007). As noted above, CNIs are often given in combination with MMF, the dose of which is also adjusted based on therapeutic drug monitoring (Kuypers et al. 2010). To complicate matters further, CNIs exhibit time-dependent PK, are eliminated primarily by CYP3A4, and are therefore prone to interactions with other drugs that affect the activity of this enzyme (Lukas et al. 2005; Park et al. 2007), and mycophenolic acid (MPA, the active moiety of MMF) undergoes enterohepatic recycling, the biliary excretion of which is inhibited by cyclosporine A (CsA) (Hesselink et al. 2005). The area under curve (AUC) of MPA for a given dose of MMF can vary by tenfold, and increasingly sophisticated PK models describing the enterohepatic recycling of MPA have been proposed to explain the source of this variability (Sherwin et al. 2011), to enable more precise dose adjustment for this narrow therapeutic window drug.

4.3 Applications of Pharmacometrics in CKD

CKD presents a wide array of treatment-related challenges that are associated with high costs and poor outcomes. Pharmacometric approaches have been frequently applied to understand the interactions between CKD and therapeutics spanning from basic research into disease and mechanisms of drug action to the rational use of medicines in patient care. Innovative and strategic application of quantitative

methods in conjunction with well-designed trials for characterizing drug exposure, efficacy, and toxicity, will benefit patients with CKD. Pharmacometrics provides the foundation for this multidisciplinary effort that involves basic and applied university researchers, industry drug development scientists and decision makers, government regulatory scientists, clinicians, and other health professionals. An appreciation and understanding of opportunities for pharmacometrics in CKD (Table 4.3) call for a sustained collaborative effort between all stakeholders involved in developing and utilizing therapeutics for CKD and related comorbidities.

4.3.1 Quantify the Impact of CKD on Exposure and Effects of Drugs

Pharmacometric approaches are widely used to characterize the impact of CKD on exposure and effects of drugs and biologics. Both mechanism-based and empirical models are developed and applied, given modeling objectives. In the mechanistic models, the function formats of the models are elucidated by the understanding of underlying drug, disease, and CKD physiologic mechanisms. The models include knowledge, data, and scientific perspective from many relevant aspects and are constantly updated. Predictability is the key model performance requirement. In the empirical models, the influence of CKD on drug exposure and effects are typically expressed by including renal function as a covariate on the parameter(s) of the conventional exposure and response models. Treating renal function as a continuous variable, such as using eGFR values in the analysis, is usually preferred to an analysis which treats it as a categorical variable per degree of CKD.

A recently published physiologically based, multi-scale model of calcium homeostasis and bone remodeling describes the impact of progressive loss of kidney function over a typical 10-year course of CKD, including the evolution of secondary hyperparathyroidism, a sequel of which is Mineral Bone Disorder (MBD) (Riggs et al. 2012). This multi-scale physiologic model described CKD-MBD-related clinical changes in phosphate, parathyroid hormone, and calcitriol and linked bone remodeling markers with bone mineral density (BMD) elimination and formation rates. The composite multi-scale model was able to predict lumbar spine BMD losses up to 10 years in various renal function groups (Fig. 4.3) and simulate interventions with a hypothetical calcimimetic agent and calcitriol. This multi-scale mechanism-based model is a quantitative summary on the changes in CKD-MBD from signal to organs and to clinical outcomes. It provided a platform for projecting the CKD disease response and for evaluating therapeutics.

Zhang et al. (2010) provided another example of mechanistic model in CKD, which characterized the exposure and response of the SGLT2 inhibitor, a therapeutic agent developed for the treatment of T2DM. SGLT2 inhibition leads to decreased glucose reabsorption which in turn results in glucose excretion in theurine. This is expected to lower plasma glucose concentrations and urinary loss of excess calories at the same time. The relationship between plasma glucose concentration,

Table 4.3 Opportunities for pharmacometrics in CKD

Opportunities		Approaches
Understand interactions between CKD and Therapeutics	Describe progression of CKD and characterize its effect on other organs	Develop mechanism-based disease models (e.g., model that describes effects of CKD on bone mineralization)
	Facilitate design, conduct, and interpretation of trials in subjects with CKD	Stage kidney function by eGFR (rather than by creatinine clearance)
		Complement trials with integrated pharmacometric analyses
	Investigate impact of drugs on CKD outcomes	Apply model-based meta-analysis to investigate relationships between drugs and CKD outcomes
	Characterize impact of impaired CKD on drugs	Understand impact of CKD on non-renal drug clearance
		Integrate exposure, efficacy, and safety data from phase 1, 2, and/or 3 studies to characterize efficacy/safety in patients with impaired kidney function
		Quantify and understand exposure-efficacy/safety balance (i.e., therapeutic utility) in subjects with CKD
Understand interactions between RRT and Therapeutics	Quantify impact of RRT on drugs	Consider factors that impact removal of drugs in adult and pediatric patients receiving HD
		Apply model-based trial simulation (i.e., pharmacometric approaches) to guide use of drugs in patients receiving HD
	Fine-tune RRT in adults and pediatrics	Explore alternative HD schedules, such as daily short HD or long nocturnal HD
		Define new metrics for assessing and fine-tuning conventional and newer HD modalities
Understand interactions between Kidney Transplant and Therapeutics	Characterize drug effects in kidney transplantation	Utilize pharmacometric approaches to characterize time-dependent drug exposure and effects
	Explore drug non-adherence on kidney transplantation outcomes	Explore patient characteristics (e.g., underlying disease, comorbidities, co-medications) and behavior such as drug adherence

Table 4.3 (continued)

Opportunities		Approaches
Optimize use of Therapeutics in subjects with CKD	Evaluate and optimize dose adjustments in subjects with CKD	Determine relationships between drug exposure and kidney function in order to report renal dosing adjustment recommendations
	Enhance labels for subjects with CKD	Apply pharmacometric approaches to identify safe and efficacious dosing in subjects with CKD

renal glucose excretion threshold, and the amount of glucose in urine can be directly measured in a small number of patients through a well-designed hyperglycemic clamp study (Polidori et al. 2013); however, a modeling approach provided a way to use more data collected in clinical development, sample across a much larger and more heterogeneous population, and link the mechanism-specific biomarkers to long-term disease end points. The model encompassed the factors that could disturb

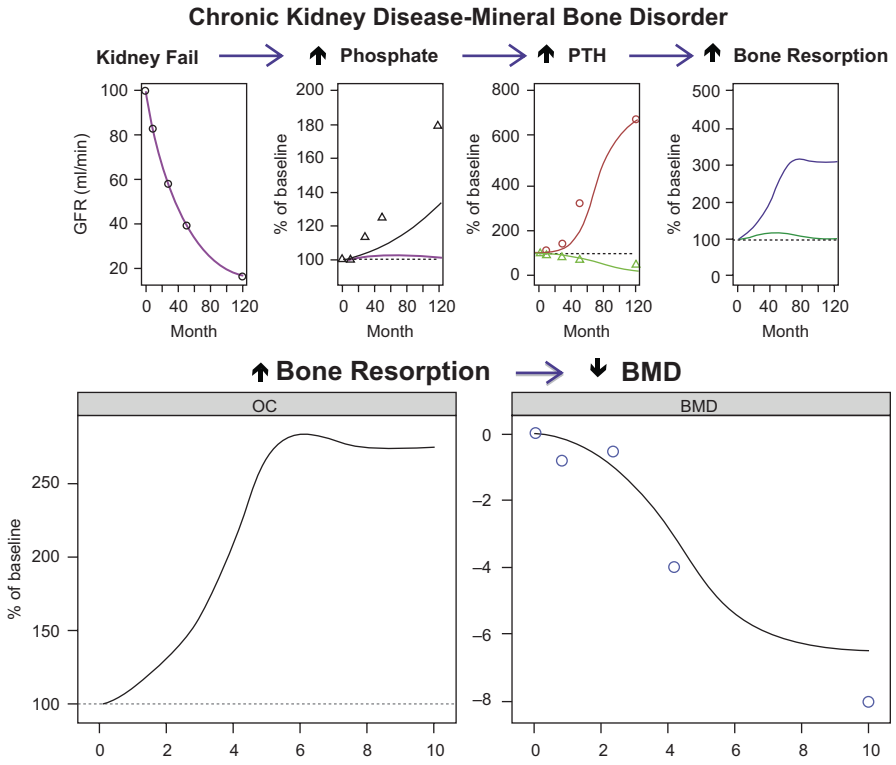

Fig. 4.3 Multi-scale physiology-based modeling of MBD in CKD. *BMD* bone mineral density *PTH* Parathyroidhomone, *MBD* Mineral Bone Disorder

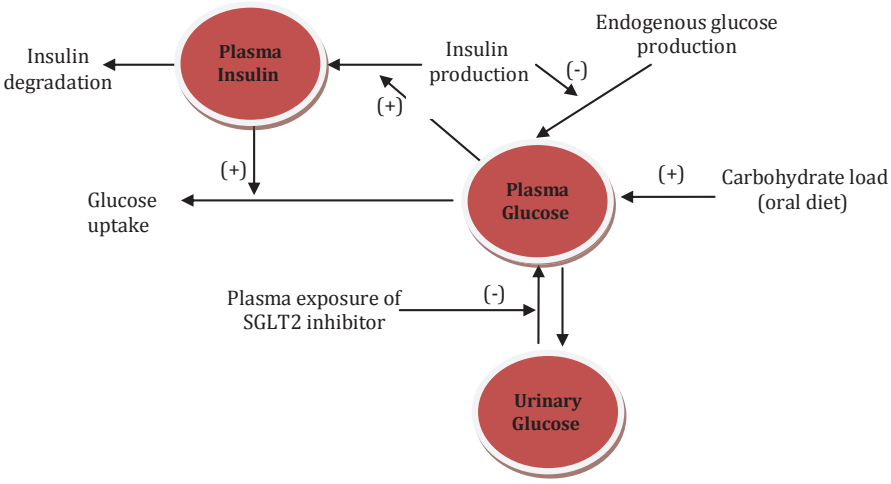

Fig. 4.4 Modeling urinary glucose excretion upon SGLT2 inhibition

the homeostasis of glucose metabolism, including endogenous glucose production, carbohydrate load, and plasma exposure to an SGLT2 inhibitor and predicted glucose amount in urine and glucose concentration and insulin concentration in urine (Fig. 4.4). The projected exposure of SGLT2 inhibitor and the response of glucose excretion at various levels of GFR can also be predicted.

The SGLT2 inhibitor dapagliflozin is metabolized by uridine diphosphate glucuronosyltransferase (UGT) 1A9 to dapagliflozin 3-O-glucuronide. As UGT1A9 is expressed in the kidney and the liver, both impaired hepatic and kidney function may impact the metabolic clearance of dapagliflozin. A semi-mechanistic model was developed for dapagliflozin and its inactive metabolite dapagliflozin 3-O-glucuronide (D3OG) with emphasis on renal and hepatic contribution to dapagliflozin metabolism (van der Walt et al. 2013). Impaired hepatic and kidney function decreased the clearance of dapagliflozin to D3OG and the clearance of D3OG. The fraction of D3OG formed via the renal route decreased from 40 to 55% in subjects with normal kidney function (creatinine clearance CrCL > 80 mL/min) to 10% in subjects with severely impaired kidney function (CrCL = 13 mL/min). Model-based simulations suggested that the increase of systemic exposure (AUCss) of dapagliflozin and D3OG was less than twofold in subjects with mild or moderate impairment of kidney function. This semi-mechanistic model presents a useful approach to evaluate the impact of kidney *and* hepatic function on the PK of dapagliflozin (Fig. 4.5).

Semi-mechanistic models were also applied to quantify non-renally eliminated drugs such as sildenafil, repaglinide, and telithromycin in subjects with CKD (Zhao et al. 2012) or to generate insight into the likely mechanism (inter-conversion) of the increased exposure of tesaglitazar in subjects with CKD (Hamrén et al. 2008).

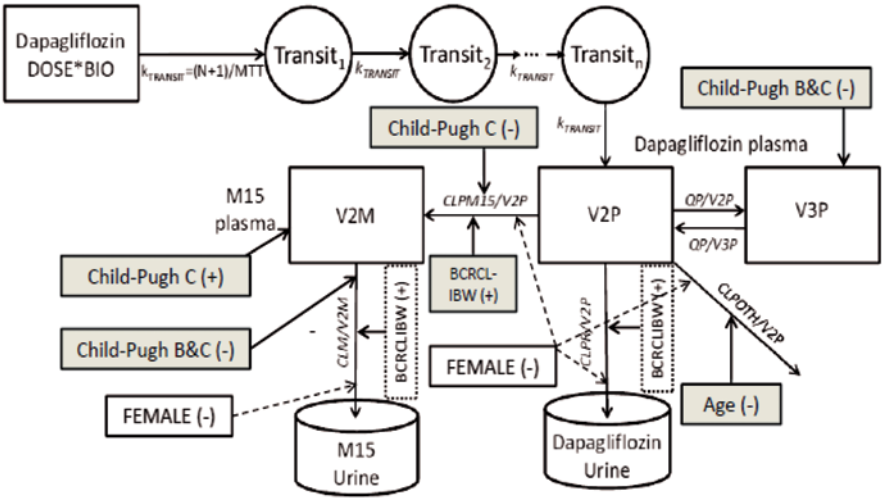

Fig. 4.5 Modeling renal and non-renal elimination of dapagliflozin and D3OG in T2DM subjects with impaired kidney and/or hepatic function (van der Walt et al. 2013). Covariates connected to compartments affect the relevant volume, those connected to pathways affect the relevant clearance. *BCRCLIBW* baseline creatinine clearance calculated using ideal body weight (IBW), *CLM* renal clearance of D3OG, *BIO* bioavailability, CLP_{M15} metabolic clearance of dapagliflozin to D3OG, CLP_{other} metabolic clearance of dapagliflozin to unmeasured metabolites, CLP_{renal} renal clearance of unchanged dapagliflozin to urine, *MTT* mean transit time, *N* number of transit compartments, *QP* inter-compartmental clearance of dapagliflozin, T2DM type 2 diabetes mellitus, *V2P* central volume of distribution of dapagliflozin, *V3P* peripheral volume of distribution of dapagliflozin, *V2M* central volume of distribution of D3OG. *Dashed lines* a priori scaling, *shaded areas* covariates selected during step-wise covariate model building, *unshaded areas* added based on previous modeling experience

4.3.2 Quantify the Impact of Dialysis on Drug Exposure

Treatments for stage V of CKD encompass four types of life-supporting RRT: hemodialysis (HD), peritoneal dialysis, hemofiltration, and kidney transplantation. HD is the most common RRT option. Quantifying the impact of HD on drugs is often a regulatory requirement as well as a clinical practice necessary for optimizing dosing regimen and dialysis prescription. The increased use of more intensive, nonstandard HD regimens other than the conventional three times a week for 3- to 4-h treatments presents additional need for quantification of the impact of dialysis on Drug exposure.

A pharmacometric approach was applied to quantify the impact of CKD and HD on the removal of saxagliptin and its active metabolite 5-hydroxy saxagliptin (Zhang et al. 2012a). Exposures of saxagliptin and its active metabolite 5-hydroxy saxagliptin were predicted at different dose levels during and between HD sessions (Fig. 4.6). A similar approach was used to quantify the dialysis impact on entecavir (Bifano et al. 2010) and candesartan (Pfister et al. 1999). The entecavir work was directly related to the approved label of entecavir for use in subjects with CKD,

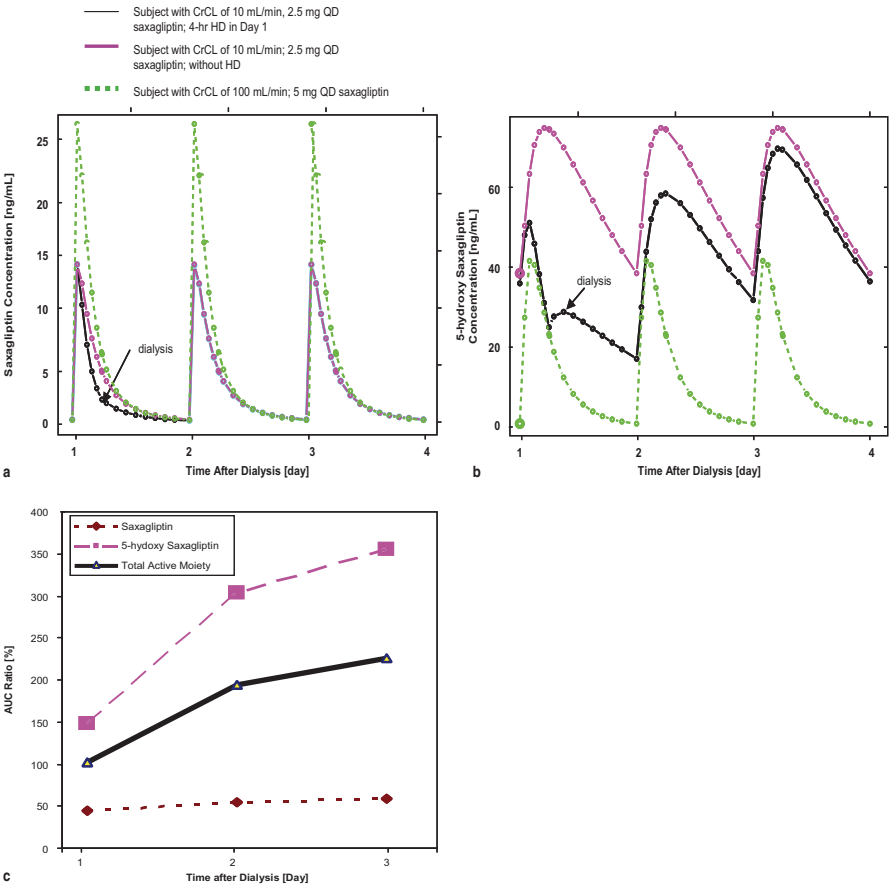

Fig. 4.6 Simulated saxagliptin (*panel a*) and 5-hydroxy saxagliptin (*panel b*) concentrations in subjects with creatinine clearance (CrCL) of 10 mL/min receiving 2.5 mg once daily saxagliptin with or without 4-h HD session starting at 2-h post-dose on day 1, and in subjects with CrCL of 100 mL/min receiving 5 mg once daily saxagliptin. Simulated steady state area under curve (*AUC*) ratio (*panel c*) between subjects with CrCL of 10 mL/min receiving 2.5 mg once daily saxagliptin and 4-h HD session on day 1 vs. subjects with CrCL of 100 mL/min receiving 5 mg once daily saxagliptin. (Zhang et al. 2012a)

including regimens that were never clinically tested. This case study is intensively discussed later in this chapter. In addition to the predictions of dug exposure under conventional HD regimens, simulations can also be performed to predict drug PK profiles under alternative treatment scenarios, such as novel dialysis modalities (e.g., daily short HD instead of three-time weekly dialysis for 4 h each). These successful applications of pharmacometrics to saxagliptin and other drugs demonstrated its utility in the development and review of new therapeutics.

4.3.3 Quantify the Impact of Dialysis on Endogenous Molecules

Similar pharmacometric approaches have also been applied to quantify the impact of dialysis on endogenous molecules and offer the potential of guiding and fine-tuning dialysis prescriptions. Individualized Bayesian urea kinetic modeling (IBKM) has been recently introduced (Pfister et al. 2004). The IBKM method is proposed as a potential method to quantify and predict HD adequacy. The IBKM method can also be used to continuously adjust and optimize individual HD treatment in both adults and children (Marsenic et al. 2010). Based on a Bayesian framework, IBKM is a model-based approach that can predict equilibrated post-rebound BUN concentration using only BUN measures pre-HD and immediately post-HD. In addition, IBKM is able to assess and project individual urea kinetic parameters and profiles for various HD schedules, takes inter-compartmental clearance into account, and can incorporate individual patient data, such as dry weight (Fig. 4.7).

The IBKM method has the potential to be useful at the bedside to inform and guide individual HD prescriptions, particularly when a patient receiving long conventional HD is transitioned to daily ultrashort or nocturnal dialysis (Fissell et al. 2012). Finally, such Bayesian kinetic modeling approach offers the possibility of testing the clearance of solutes other than urea, such as β2-microglobulin and phosphorus.

4.3.4 Evaluate and Fine-Tune Dialysis Treatment in Adults and Pediatrics

Incorporating urea rebound using equilibrated urea concentration (C_{eq}) after a HD session is essential for accurate assessment of HD efficiency. It is impractical to measure C_{eq} in clinical settings, and there are no recommended methodologies to predict C_{eq} in children. The objective of this work is to assess the ability of an IBKM for predicting C_{eq} in children on HD. Developed based on adult HD data, the IBKM is a two-pool urea kinetic model that calculates Bayesian estimates of individual C_{eq}. Blood urea nitrogen (BUN) samples from 30 HD sessions in 13 children (age 12-18 years) were taken at pre-HD, immediately post-HD, and 60 min post-HD (C_{eq}). The IBKM was fitted to the observed data to predict C_{eq}. In comparison with observed C_{eq} (9.5 ± 3.8 mmol/L), the average individual predicted C_{eq} was 9.4 [± 3.8] mmol/L, with absolute individual prediction error of 6.2 ± 4.4%. For a given dialysis goal and desired dialysis duration, the required blood flow rate and dialyzer size are predicted by IBKM (Fig. 4.8) and confirmed by the analysis data. This study suggests that the IBKM can be applied in a pediatric HD setting and accurately predict C_{eq} in children using only pre- and immediately post-HD BUN. The IBKM provides a promising approach to assess HD efficiency and its optimal prescription in adults and children; it would be an obvious choice to forecast the

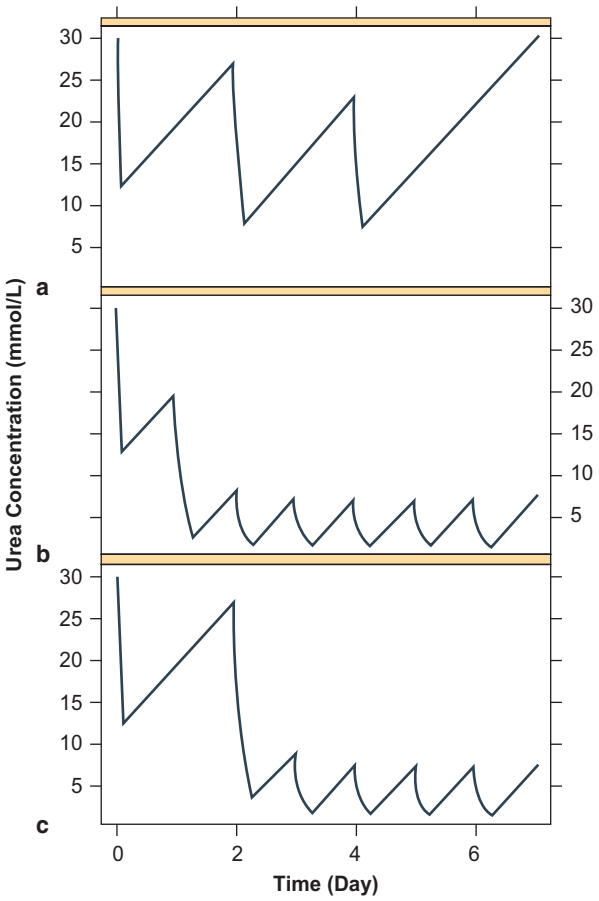

Fig. 4.7 Projected urea kinetic profiles for a patient who is planning to transition from conventional hemodialysis (CHD, three times weekly for 4 h each; *panel a*) to frequent nocturnal HD (five times weekly for 6 h each) 1 day (*panel b*) and 2 days (*panel c*) after the CHD session

removal of solutes other than urea (e.g., creatinine, uric acid) and medications in individual patients as well.

The variables considered are dialyzer size (mass/transfer coefficient, Ko; membrane area, A), blood flow, and treatment time. For an individual with pre-dialysis weight of 40 kg and BUN concentration of 30 mmol/L, the BUN concentrations during the dialysis are simulated with dialyzer mass transfer area coefficient (KoA) KoA ranging from 400 to 800 mL/min, and blood flow ranging from 150 to 300 mL/min. The time to reach 75% urea reduction ratio (% URR) are obtained from the simulation and used in constructing the plot. The lines in the contour plots indicate the time to reach 75% URR for a given combination of dialyzer KoA and blood flow. Dialyzer KoA from three commonly used dialyzers (F4HPS, F5HPS, and Gambro 14S) are indicated in the plot for illustration purpose.

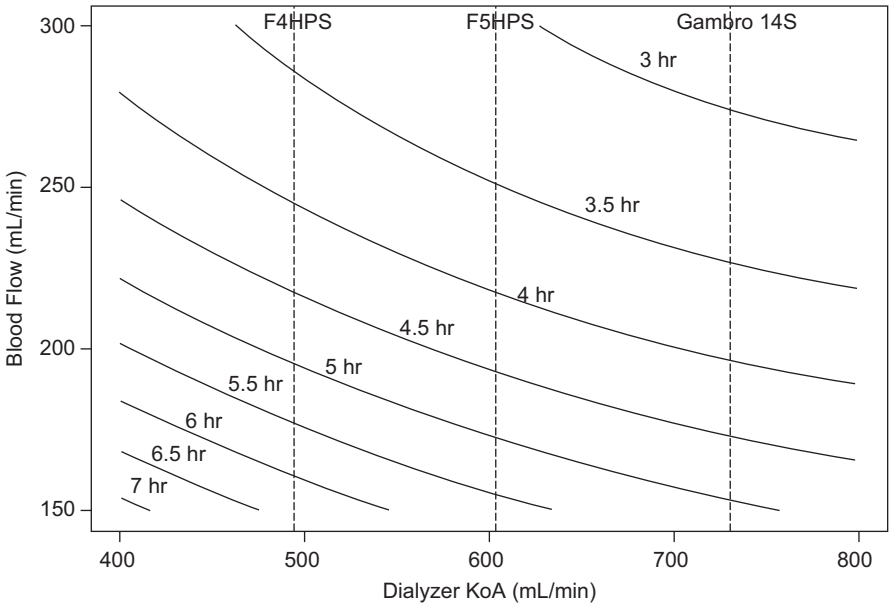

Fig. 4.8 Individual dialysis efficiency as a function of dialysis variables

4.3.5 Characterize Exposure-Response in Kidney Transplant Patients

Given the complexities of Calcineurin inhibitor (CNI)-containing immunosuppressive therapies, there is an increasing interest in CNI-free or sparing-treatment regimens (Giessing et al. 2007), and alternatives to CNI, such as CTLA-4 Ig (El-Charabaty et al. 2012). One of the difficulties of determining a therapeutic window is that it is not ethical to do a true dose-ranging study that includes suboptimal doses. Recently, model-based analyses of pooled data from phase 2 and 3 studies were employed to determine the clinical pharmacology profile of belatacept, a CTLA4-4 fusion protein, and to support dose recommendations based upon exposure-response of efficacy (control of acute rejection) and safety (serious infections and risk of lymphoproliferative events) (Zhou et al. 2012). Belatacept dose amount and frequency are highest during induction of immunosuppression in the peri-transplant period, and the dose intensity is gradually decreased to the currently recommended maintenance dose regimen of 5 mg/kg every 4 weeks, starting at the end of week 16 (Belatacept Prescribing Information (US FDA) [Internet] 2013). Belatacept exposures are therefore highest during the 3 months post-transplantation when the risk of acute rejection is greatest, and steady-state exposures are not reached until after the start of the maintenance period. A time-to-event exposure-response analysis was employed to characterize the efficacy of belatacept, to account for the time-varying nature of the belatacept exposures and of the risk of acute rejection. As shown in

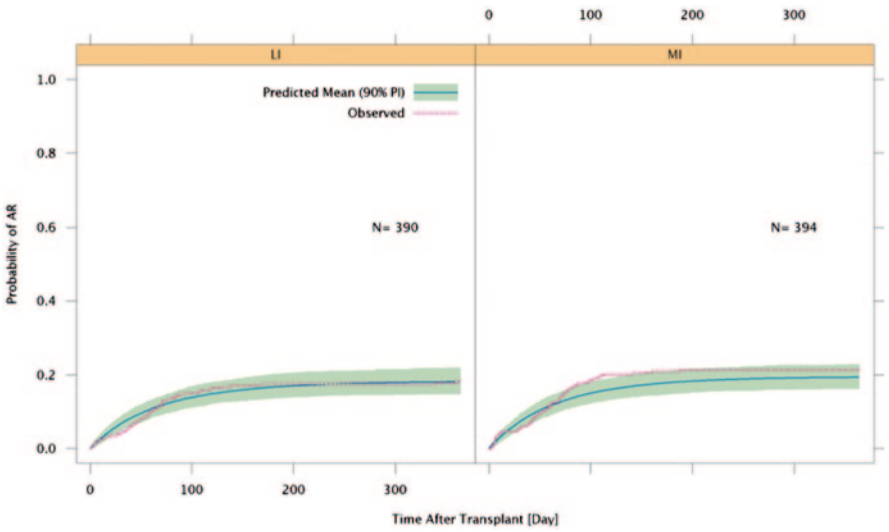

Fig. 4.9 Belatacept exposure-response of efficacy (probability of acute rejection (AR); Zhou et al. 2012). Visual predictive check of the time-to-acute rejection with less intensive (*LI*) and more intensive (*MI*) dosing regimens

Fig. 4.9, the risk of an acute rejection decreases dramatically after 3-months post-transplant, thereby justifying decreased doses of immunosuppressive agents for maintaining prophylaxis of graft rejection.

4.3.6 Quantify Impact of Drug Non-adherence on Kidney Transplant

Lack of adherence to immunosuppressive drugs, given post-transplant, is a serious problem, the prevalence of which does not appear to have changed very much over the past 30 years. A recent study found that approximately 26% of renal transplants were non-adherent to their prescribed immunosuppressive medication (Schmid-Mohler et al. 2010), which is consistent with the median non-adherence of 22% reported in a comprehensive review of the studies published between 1980 and 2001 (Butler et al. 2004). As noted above, therapeutic drug monitoring (TDM) is required for many immunosuppressive drugs due to their narrow therapeutic windows (Schiff et al. 2007; Kuypers et al. 2010). Prolonged exposure to drug levels above or below the therapeutic range is known to be associated with excess toxicity or reduced efficacy. However, the impact of transient deviations from the therapeutic window is less obvious.

A novel model-based analysis was employed to quantify the impact of non-adherence on clinical outcomes by developing and applying a model for non-adherence to CsA to predict variability in drug exposure, which was then linked to outcomes (Maclean et al. 2011). Specifically, a drug adherence model was developed to describe the drug adherence behavior of patients who were categorized according

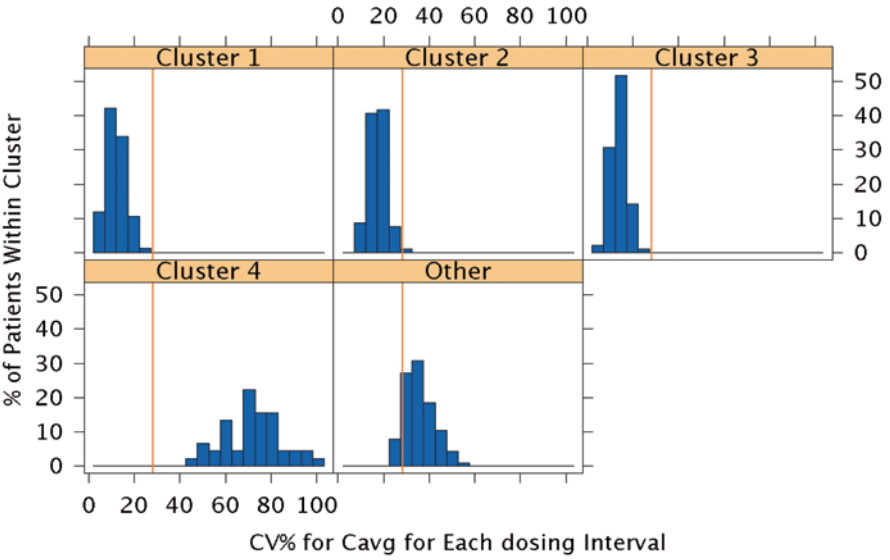

Fig. 4.10 Distribution of cyclosporin time-averaged trough concentration (*Cavg*) variability in kidney transplant patients, by adherence behavior category (**Cluster 1**: patients who almost always took their medication on time; **Cluster 2**: sometimes missed doses or were late, **Cluster 3**: frequently late in taking doses, **Cluster 4**: often missed both doses, and **Cluster 5***:* all other behaviors). The *vertical line* represents the threshold of 28 % CV in *Cavg,* above which chronic rejection rates and health-care costs are higher

to the following five previously reported clusters (Russell et al. 2006): Cluster 1 (32 %), patients who almost always took their medication on time; Cluster 2 (18 %), sometimes missed doses or were late; Cluster 3 (14 %), frequently late in taking doses; Cluster 4 (9 %), often missed both doses; and Cluster 5 (27 %), other. Specifically, the drug adherence model described the frequency with which the morning and evening doses were taken on time, late/early, or missed. The drug adherence model was applied together with a PK model of CsA (Lukas et al. 2005), to predict variability in CsA exposures, which was then linked to clinical outcome based on previously reported associations between variability in CsA exposure and long-term renal function, chronic rejection, and health-care costs based on logistic regression and receiver operating curve analysis (Waiser et al. 2002; Kahan et al. 2000). As shown in Fig. 4.10, the within patient variability in time-averaged trough concentration (Cavg) of patients in Clusters 1, 2, and 3 did not exceed level of variability associated with poor outcomes (30-36 % coefficient of variation CV), and therefore the occasional non-adherence characterized by Clusters 2 and 3 are not expected to have an impact on clinical outcome. In contrast, all patients in Clusters 4 had CV higher than the thresholds associated with poor outcome, and approximately 76 % of the patients in Cluster 5 had a CV greater than 30 %, suggesting that subjects in these groups were at high risk for having poorer outcomes.

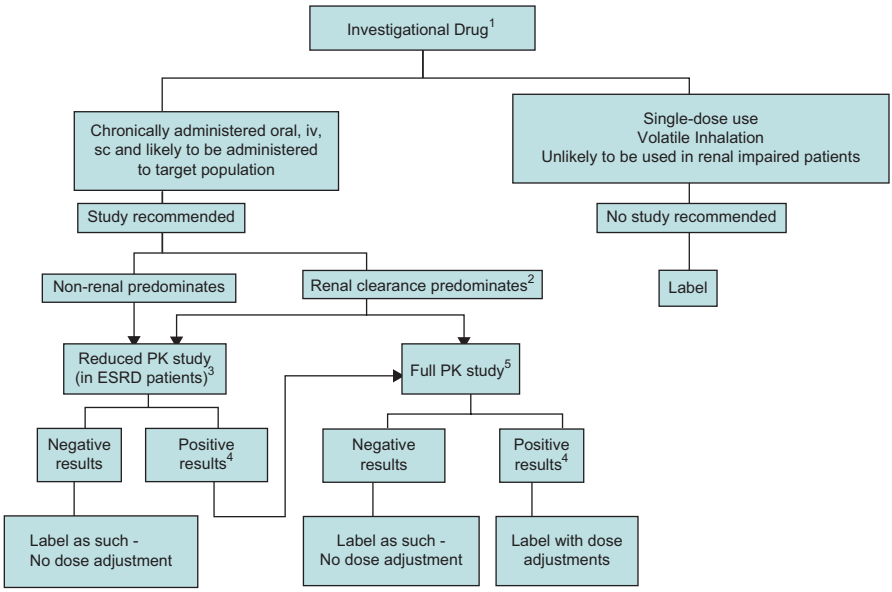

Fig. 4.11 Decision tree for use in determining when a study in subjects with impaired kidney funtion is appropriate (Draft Guidance: Pharmacokinetics in Patients with Impaired Renal Function-Study Design, Data Analysis, and Impact on Dosing and Labeling [Internet] 2010). *1* Metabolites (active/toxic) follow the same decision tree. *2* The sponsor has the option of conducting a reduced study in end-stage renal disease (ESRD) patients or a full study. *3* To be conducted in ESRD patients not yet on dialysis. *4* The results are "positive" when pharmacokinetic (PK) changes are clinically significant based on exposure-response of the drug. *5* See guidance for the full PK study design, or additional studies can be conducted including a population PK evaluation

4.3.7 Evaluate and Fine-Tune Therapeutic Doses for CKD

The FDA encourages to (1) understand multitude of interrelated factors that can affect systemic exposure and response, (2) carefully design trials in subjects with impaired kidney disease, and (3) apply quantitative pharmacometric methods for characterizing drug exposure and evaluating in therapeutic doses in subjects with impaired kidney (Fig. 4.11; Draft Guidance: Pharmacokinetics in Patients with Impaired Renal Function-Study Design, Data Analysis, and Impact on Dosing and Labeling [Internet] 2010; Huang et al. 2009; Zhang et al. 2012b). Compared to the 1998 FDA guidance, there are three new recommendations in the 2010 FDA draft guidance "Pharmacokinetics in Patients with Impaired Renal Function-Study Design, Data Analysis, and Impact on Dosing and Labeling": (1) PK studies in patients with impaired kidney function are conducted for drugs that are eliminated via non-renal route, in addition to those via renal route (Fig. 4.11), (2) staging of kidney function be conducted using the eGFR (e.g., the four-parameter modification of diet in renal disease (MDRD) equation), in addition to the C–G equation, and (3) conduct of studies in HD patients be performed during dialysis (on dialysis) and inter-dialysis (off dialysis) periods.

Table 4.4 Hazard ratio and 95% confidence interval (CI) for stroke/systemic embolic event (SEE) and major bleeds comparing dabigatran etexilate (DE) 150 mg twice daily to warfarin by kidney function. (Hariharan and Madabushi 2012)

Creatinine clearance, mL/min	Fold increase in dabigatran trough plasma concentration in RE-LY	Hazard ratio (95% CI) for stroke/SEE, DE 150 mg vs Warfarin	Hazard ratio (95% CI) for major bleeds, DE 150 mg vs Warfarin
Moderate, 30≤ and <50	2.29	0.46 (0.29–0.73)	0.97 (0.74–1.27)
Mild, 50≤ and <80	1.47	0.67 (0.49–0.91)	0.88 (0.71–1.07)
Healthy, ≥80	1.00	0.71 (0.44–1.15)	0.81 (0.59–1.11)

RE-LY Randomized Evaluation of Long-term Anti-Coagulant Therapy

To optimize drug therapy for individuals and subgroups, it is critical to understand how various intrinsic (e.g., age, gender, race, genetics, organ impairment) and extrinsic factors (e.g., diet, smoking, concomitantly administered drugs) affect drug exposure, dosing, and response. PK data in subjects with impaired kidney function are used to determine appropriate drug dosing in subjects with impaired kidney function in comparison to subjects with normal kidney function. Besides being evaluated in dedicated PK studies, the effect of impaired kidney function on a drug's PK can also be evaluated in phase 2 or phase 3 clinical studies with sparse PK sampling if a sufficient number of patients with various degrees of renal impairment is included in these studies. Pharmacometric analyses can help rationalize a need for dosage adjustment in this specific population based on exposure–response relationship of the drug.

For example, dabigatran represents one of the recent instances where renal function influenced dosing decisions (Hariharan and Madabushi 2012; Lehr et al. 2012). Dabigatran etexilate mesylate, a direct oral thrombin inhibitor, was approved by the FDA in October 2010 for the prevention of stroke and systemic embolism in patients with nonvalvular atrial fibrillation (AF). The pivotal efficacy trial supporting the approval, randomized evaluation of long-term anticoagulant therapy (RE-LY), compared two blinded doses of dabigatran, 110 mg and 150 mg, with open-label warfarin (Table 4.4). Based on the efficacy (reduction in incidence of stroke and systemic embolism) and safety (bleeding risk) findings, the FDA-approved dabigatran 150 mg given orally twice daily in patients with CrCL>30 mL/min. The FDA also approved dabigatran 75 mg administered twice daily in patients with severe renal impairment (defined as CrCL between 15 and 30 mL/min).

To ensure that subgroups with severe impaired kidney function would have access to an appropriate dose of dabigatran, a pharmacometric approach was applied to evaluate dosing regimens of interest in 'virtual' subjects with various levels of kidney function. Results from model-based simulation of various doses of interest indicated that (1) a dosing regimen of 150 mg QD leads to significantly higher average exposures beyond the range studied in RE-LY, (2) a dosing regimen of 75 mg QD regimen results in lower average exposures and was considered to be less effective for stroke reduction, and (3) a dosing regimen of 75 mg twice daily is the preferred dose for subjects with severely impaired kidney function as it provides similar exposures to that expected in subjects with moderately impaired kidney function, for whom a 150-mg twice-daily regimen produced substantial benefit in pivotal clinical trials.

In another case, a pharmacometric approach was applied to quantify apixaban's therapeutic utility in prevention of venous thromboembolism in subjects with normal or moderately impaired kidney function (Leil et al. 2010). A therapeutic utility index (TUI) was assessed by integrating efficacy and safety predictions to quantify apixaban's efficacy/safety balance as a function of steady-state AUC. Of the apixaban dosage regimens tested in phase 2, the 2.5-mg twice-daily dosage regimen had the highest TUI (86.2%). This was also higher than the TUI for either 30-mg twice-daily enoxaparin (82.5%) or for warfarin (71.8%). Difference in apixaban's TUI in subjects with moderately impaired kidney function and those with normal kidney function was marginal indicating that dose adjustment is not needed in subjects with mild or moderate impairment of kidney function.

4.3.8 Enhance Drug Label for CKD

There are several additioned examples where pharmacometric approaches, including physiologically based modeling and simulation (in conjunction with well-designed studies) were used to characterize CKD-related changes in drug exposure and optimize dose selection in CKD: amikacin (De Cock et al. 2012) argatroban (Madabushi et al. 2011), fondaparinux (Turpie et al. 2009), gentamicin (Lanao et al. 1989), panipenem/betamipron (Tajima et al. 2006), pefloxacin (Bruno et al. 1991), piperacillin/tazobactam (Tornøe et al. 2007), ribavirin (Bruchfeld et al. 2002), and telbivudine (Zhou et al. 2009).

Model-based trial simulation can predict drug exposures for alternative dosing regimens, compare simulated drug exposures with a predefined target range (i.e., therapeutic window), and thus identify doses that produce safe and efficacious concentrations in a large portion of patients (i.e., 75% of subjects). This quantitative approach was applied to optimize dosing of entecavir in subjects with CKD (Bifano et al. 2010). Entecavir is predominantly eliminated by the kidney with urinary recovery of unchanged drug at steady state ranging from 62 to 73% of the administered dose. Renal clearance is independent of dose and ranges from 360 to 471 mL/min suggesting that entecavir undergoes both glomerular filtration and net tubular secretion. The PK of entecavir following a single 1-mg dose were studied in 34 subjects (without chronic hepatitis B virus infection) with various degrees of impaired kidney function, including subjects whose CKD was managed by HD or continuous ambulatory peritoneal dialysis (CAPD). In subjects with CKD, the apparent oral clearance of entecavir decreased as creatinine clearance decreased.

A pharmacometric approach was applied to (1) characterize the relationship between a measure of kidney function (CrCL) and apparent oral clearance of entecavir, (2) simulate steady-state exposure of entecavir for various alternative dose regimens, (3) calculate the fraction of subjects with exposure of entecavir within a predefined target range, and (4) identify dose regimens that produce target exposure levels in 75% or more subjects with normal and reduced kidney function. Output from this model-based simulation indicated that the following dose adjustments (percentage of starting dose) provide consistent steady-state exposures in subjects

Table 4.5 Recommended dosage of entecavir (BARACLUDE) in subjects with CKD

Creatinine clearance (mL/min)	Usual dose (0.5 mg)	Lamivudine—refractory or decomposed liver disease (1 mg)
≥50	0.5 mg once daily	1 mg once daily
30-<50	0.25 mg once daily[a] *OR* 0.5 mg every 48 h	0.5 mg once daily *OR* 1 mg every 48 h
10-50<30	0.15 mg once daily[a] *OR* 0.5 mg every 72 h	0.3 mg once daily[a] *OR* 1 mg every 72 h
<10 Hemodialysis[b] or CAPD	0.05 mg once daily[a] *OR* 0.5 mg every 7 days	0.1 mg once daily[a] *OR* 1 mg every 7 days

[a] For doses less than 0.5 mg. BARACLUDE Oral Solution is recommended
[b] If administered on a hemodialysis day. administer BARACLUDE after the hemodialysis session

with impaired kidney function: mild impairment (no adjustment, 100%), moderate impairment (50%), severe impairment four (30%), and subjects on dialysis (20%). These results provided a quantitative rational for a detailed dose recommendation in the drug label (Baraclude Prescribing Information. US Food and Drug Administration [Internet] 2012):

> Dosage adjustment is recommended for patients with creatinine clearance less than 50 mL/min, including patients on hemodialysis or continuous ambulatory peritoneal dialysis (CAPD), as shown in Table 4.5 (Baraclude Prescribing Information. US Food and Drug Administration [Internet] 2012). The once-daily dosing regimens are preferred.

4.4 Opportunities for Pharmacometrics in CKD

Pharmacometric approaches are useful to characterize drug effects on kidneys and effects of kidneys on drugs. Current pharmacometric activities are focused on individual compounds for their search, prevention, and treatment of CKD. Examples of the applications include: (1) assess and compare efficacy/safety profiles of entire drug classes with model-based meta-analyses (e.g., effects of ACE inhibitors, ARBs, and renin inhibitors on hypertension, proteinuria, *and* GFR in CKD), (2) characterize relationships between biomarkers/imaging endpoints and clinical endpoint (e.g., relationships between changes in total kidney volume (TKV) and GFR in polycystic kidney disease), (3) develop disease progression models to project long-term cardiovascular and CKD outcomes (e.g., relationships between proteinuria and GFR and time to RRT in T2DM subjects with CKD), (4) optimize design of clinical trials in subjects with CKD (in conjunction with new regulatory guidance documents), and (5) evaluate new metrics for novel dialysis modalities to further optimize RRT in adults and pediatrics (e.g., use bedside computer models to evaluate, monitor, and fine-tune "dose" of dialysis).

A sustained collaborative effort between key stakeholders involved in research, development, and use of medicines in CKD, is required to bring pharmacometrics to its full potential. Initiatives such as the C-Path consortium (Critical Path Institute [Internet] 2013) and the Drug Disease Model Resources (DDMoRe) consortium (DDMoRe: Innovative Medicines Initiative [Internet] 2013) can advance pharmacometrics and facilitate scientific partnerships between academic institutes, biotech/pharma companies and societies such as the International Society of Nephrology (International Society of Nephrology (ISN) Gateway [Internet] 2013) and the International Society of Pharmacometrics (ISoP International Society of [Internet] 2013).

The Polycystic Kidney Disease (PKD) Outcomes consortium is an example of a successful collaboration between Critical Path Institute (C-Path), the PKD Foundation (PKD Foundation [Internet] 2013), Clinical Data Interchange Standards Consortium (CDISC), and four leading academic medical centers (Tufts University, University of Colorado—Denver, Emory University, and Mayo Clinic). Autosomal dominant PKD (ADPKD) is a debilitating genetic disease affecting more than 600,000 Americans and 12 million people worldwide and for which there is currently no known cure or effective treatment (Helal et al. 2012).

The primary goals of the PKD Outcomes consortium are to use and model clinical data from ADPKD patients to characterize the relationship between early changes in TKV and long-term CKD outcomes, and support the regulatory qualification of TKV as an accepted measure for assessing the progression of ADPKD in clinical trials, with the ultimate goal to facilitate development and approval of new medicines for subjects with ADPKD. Similar efforts are needed for other kidney diseases such as Fabry nephropathy.

Innovative pharmacometric approaches for facilitating research, development, and use of new medicines will help us to fight the silent, deadly kidney disease.

4.5 Take-Home Messages

- Know that CKD is a common and deadly disease
- Use eGFR rather than creatinine clearance to stage CKD
- Understand how drugs can affect kidneys and how kidneys can affect renal and non-renal elimination of drugs and response to drugs
- Apply pharmacometric approaches (including semi-mechanistic models) to characterize relationships between measures of kidney function and drug exposure-response
- Utilize model-based simulations to optimize dose regimens and enhance drug labels for CKD
- Innovate pharmacometric approaches to evaluate and fine-tune RRT by dialysis or transplantation
- Facilitate partnerships between academic institutes, biotech/pharma companies and scientific societies to fight the silent, deadly kidney disease

References

Baraclude Prescribing Information. US Food and Drug Administration [Internet] (2012) http://www.accessdata.fda.gov/scripts/cder/drugsatfda/index.cfm?fuseaction=Search.Overview&DrugName=BARACLUDE. Accessed 27 Jan 2013

Belatacept Prescribing Information (US FDA) [Internet] (2013) http://www.accessdata.fda.gov/scripts/cder/drugsatfda/index.cfm?fuseaction=Search.Label_ApprovalHistory#labelinfo. Accessed 14 March 2013

Bifano M, Grasela D, Pfister, MP (2010) Quantitative modeling and simulation to optimize dosing in renally impaired patients: application to entecavir. Am Soc Nephrol 21:390A

Briasoulis A, Bakris GL (2013) Chronic kidney disease as a coronary artery disease risk equivalent. Curr Cardiol Rep 15(3):340

Bruchfeld A, Lindahl K, Schvarcz R, Ståhle L (2002) Dosage of ribavirin in patients with hepatitis C should be based on renal function: a population pharmacokinetic analysis. Ther Drug Monit 24(6):701–708

Bruno R, Rosier P, Iliadis A, Le Roux Y, Montay G, Frydman A et al (1991) Evaluation of Bayesian estimation to discriminate subpopulations of patients with altered pharmacokinetics using fragmentary data: a pilot study with pefloxacin. Eur J Drug Metab Pharmacokinet Spec No 3:338–345

Butler JA, Peveler RC, Roderick P, Smith PWF, Horne R, Mason JC (2004) Modifiable risk factors for non-adherence to immunosuppressants in renal transplant recipients: a cross-sectional study. Nephrol Dial Transplant 19(12):3144–3149

Cockcroft DW, Gault MH (1976) Prediction of creatinine clearance from serum creatinine. Nephron 16(1):31–41

Coresh J, Selvin E, Stevens LA, Manzi J, Kusek JW, Eggers P, Van Lente F, Levey AS (2007) Prevalence of chronic kidney disease in the United States. JAMA 298(17):2038–2047

Critical Path Institute [Internet] (2013) http://www.c-path.org/. Accessed 15 March 2013

DDMoRe: Innovative Medicines Initiative [Internet] (2013) http://www.ddmore.eu/content/innovative-medicines-initiative. Accessed 15 March 2013

De Cock RF, Allegaert K, Schreuder MF, Sherwin CM, de Hoog M, van den Anker JN, Danhof M, Knibbe CA (2012). Maturation of the glomerular filtration rate in neonates, as reflected by amikacin clearance. Clin Pharmacokinet 51(2):105–117

Draft Guidance: Pharmacokinetics in Patients with Impaired Renal Function—Study Design, Data Analysis, and Impact on Dosing and Labeling [Internet] (2010) FDA. http://www.fda.gov/downloads/Drugs/GuidanceComplianceRegulatoryInformation/Guidances/UCM204959.pdf. Accessed 14 March 2013

Dreisbach AW (2009) The influence of chronic renal failure on drug metabolism and transport. Clin Pharmacol Ther 86(5):553–556

El-Charabaty E, Geara AS, Ting C, El-Sayegh S, Azzi J (2012) Belatacept: a new era of immunosuppression? Expert Rev Clin Immunol 8(6):527–536

Fissell R, Schulman G, Pfister M, Zhang L, Hung AM (2012) Novel dialysis modalities: do we need new metrics to optimize treatment? J Clin Pharmacol 52(1 Suppl):72S–78S

Giessing M, Fuller TF, Tuellmann M, Slowinski T, Budde K, Liefeldt L (2007) Steroid- and calcineurin inhibitor free immunosuppression in kidney transplantation: state of the art and future developments. World J Urol 25(3):325–332

Goldstein SL, Jaber BL, Faubel S, Chawla LS (2013) AKI transition of care: a potential opportunity to detect and prevent CKD. Clin J Am Soc Nephrol 8(3):476–483

Halloran PF (2004) Immunosuppressive drugs for kidney transplantation. N Engl J Med 351(26):2715–2729

Hamrén B, Ericsson H, Samuelsson O, Karlsson MO (2008) Mechanistic modelling of tesaglitazar pharmacokinetic data in subjects with various degrees of renal function–evidence of interconversion. Br J Clin Pharmacol 65(6):855–863

Hariharan S, Madabushi R (2012) Clinical pharmacology basis of deriving dosing recommendations for dabigatran in patients with severe renal impairment. J Clin Pharmacol 52(1 Suppl):119S–125S

Helal I, Reed B, Schrier RW (2012) Emergent early markers of renal progression in autosomal-dominant polycystic kidney disease patients: implications for prevention and treatment. Am J Nephrol 36(2):162–167

Hesselink DA, Van Hest RM, Mathot RAA, Bonthuis F, Weimar W, De Bruin RWF et al (2005) Cyclosporine interacts with mycophenolic acid by inhibiting the multidrug resistance-associated protein 2. Am J Transplant 5(5):987–994

Huang SM, Temple R, Xiao S, Zhang L, Lesko LJ (2009) When to conduct a renal impairment study during drug development: US food and drug administration perspective. Clin Pharmacol Ther 86(5):475–479

International Society of Nephrology (ISN) Gateway [Internet] (2013) http://www.theisn.org/. Accessed 15 March 2013

ISoP International Society of Pharmacometrics [Internet] (2013) http://www.go-isop.org/. Accessed 15 March 2013

Joy MS (2012) Impact of glomerular kidney diseases on the clearance of drugs. J Clin Pharmacol 52(1 Suppl):23S–34S

Kahan BD, Welsh M, Urbauer DL, Mosheim MB, Beusterien KM, Wood MR et al (2000) Low intraindividual variability of cyclosporin A exposure reduces chronic rejection incidence and health care costs. J Am Soc Nephrol 11(6):1122–1131

Kasichayanula S, Liu X, Benito MP, Yao M, Pfister M, Lacreta FP et al (2012) The influence of kidney function on dapagliflozin exposure, metabolism, and efficacy in healthy subjects and in patients with type 2 diabetes mellitus. Br J Clin Pharmacol Dec 4. doi:10.1111/bcp.12056. [Epub ahead of print]

KDOQI Clinical Practice Guidelines for Chronic Kidney Disease: Evaluation, Classification, and Stratification [Internet] (2013) National Kidney Foundation. http://www.kidney.org/professionals/kdoqi/guidelines_ckd/toc.htm. Accessed 14 March 2013

Kidney Disease Statistics for the United States [Internet] (2013) National Kidney and Urologic Diseases Information Clearinghouse (NKUDIC). http://kidney.niddk.nih.gov/kudiseases/pubs/kustats/. Accessed 14 March 2013

Kim DC, Reitz B, Carmichael DF, Bloedow DC (1995) Kidney as a major clearance organ for recombinant human interleukin-1 receptor antagonist. J Pharm Sci 84(5):575–580

Komoroski B, Vachharajani N, Feng Y, Li L, Kornhauser D, Pfister M (2009) Dapagliflozin, a novel, selective SGLT2 inhibitor, improved glycemic control over 2 weeks in patients with type 2 diabetes mellitus. Clin Pharmacol Ther 85(5):513–519

Kuypers DRJ, Le Meur Y, Cantarovich M, Tredger MJ, Tett SE, Cattaneo D et al (2010) Consensus report on therapeutic drug monitoring of mycophenolic acid in solid organ transplantation. Clin J Am Soc Nephrol 5(2):341–358

Lanao JM, Berrocal A, Calvo MV, Perez M, De la Calle B, Domínguez-Gil A (1989) Population pharmacokinetic study of gentamicin and a Bayesian approach in patients with renal impairment. J Clin Pharm Ther 14(3):213–223

Lehr T, Haertter S, Liesenfeld K-H, Staab A, Clemens A, Reilly PA et al (2012) Dabigatran etexilate in atrial fibrillation patients with severe renal impairment: dose identification using pharmacokinetic modeling and simulation. J Clin Pharmacol 52(9):1373–1378

Leil TA, Feng Y, Zhang L, Paccaly A, Mohan P, Pfister M (2010) Quantification of apixaban's therapeutic utility in prevention of venous thromboembolism: selection of phase III trial dose. Clin Pharmacol Ther 88(3):375–382

Levey AS, Stevens LA (2010) Estimating GFR using the CKD Epidemiology Collaboration (CKD-EPI) creatinine equation: more accurate GFR estimates, lower CKD prevalence estimates, and better risk predictions. Am J Kidney Dis 55(4):622–627

Levey AS, Bosch JP, Lewis JB, Greene T, Rogers N, Roth D (1999) A more accurate method to estimate glomerular filtration rate from serum creatinine: a new prediction equation. Modification of diet in renal disease study group. Ann Intern Med 130(6):461–470

Levey AS, Andreoli SP, DuBose T, Provenzano R, Collins AJ (2007) Chronic kidney disease: common, harmful, and treatable–World Kidney Day 2007. Clin J Am Soc Nephrol 2(2):401–405

Levey AS, Stevens LA, Schmid CH, Zhang YL, Castro AF 3rd, Feldman HI et al (2009) A new equation to estimate glomerular filtration rate. Ann Intern Med 150(9):604–612

Levin A (2013) Clinical epidemiology of cardiovascular disease in chronic kidney disease prior to dialysis. Semin Dial 16(2):101–105
Lukas JC, Suárez AM, Valverde MP, Calvo MV, Lanao JM, Calvo R et al (2005) Time-dependent pharmacokinetics of cyclosporine (Neoral) in de novo renal transplant patients. J Clin Pharm Ther 30(6):549–557
Maclean JR, Pfister M, Zhou Z, Roy A, Tuomari VA, Heifets M (2011) Quantifying the impact of nonadherence patterns on exposure to oral immunosuppressants. Ther Clin Risk Manage 7:149–156
Madabushi R, Cox DS, Hossain M, Boyle DA, Patel BR, Young G et al (2011) Pharmacokinetic and pharmacodynamic basis for effective argatroban dosing in pediatrics. J Clin Pharmacol 51(1):19–28
Marsenic O, Zhang L, Zuppa A, Barrett JS, Pfister M (2010) Application of individualized Bayesian urea kinetic modeling to pediatric hemodialysis. ASAIO J 56(3):246–253
Mårtensson J, Martling C-R, Bell M (2012) Novel biomarkers of acute kidney injury and failure: clinical applicability. Br J Anaesth 109(6):843–850
Matsushita K, Mahmoodi BK, Woodward M, Emberson JR, Jafar TH, Jee SH et al (2012) Comparison of risk prediction using the CKD-EPI equation and the MDRD study equation for estimated glomerular filtration rate. JAMA 307(18):1941–1951
Meibohm B, Zhou H (2012) Characterizing the impact of renal impairment on the clinical pharmacology of biologics. J Clin Pharmacol 52(1 Suppl):54S–62S
Naud J, Nolin TD, Leblond FA, Pichette V (2012) Current understanding of drug disposition in kidney disease. J Clin Pharmacol 52(1 Suppl):10S–22S
Nolin TD, Unruh ML (2010) Clinical relevance of impaired nonrenal drug clearance in ESRD. Semin Dial 23(5):482–485
Nolin TD, Naud J, Leblond FA, Pichette V (2008) Emerging evidence of the impact of kidney disease on drug metabolism and transport. Clin Pharmacol Ther 83(6):898–903
Parikh CR, Devarajan P, Zappitelli M, Sint K, Thiessen-Philbrook H, Li S et al (2011) Postoperative biomarkers predict acute kidney injury and poor outcomes after pediatric cardiac surgery. J Am Soc Nephrol 22(9):1737–1747
Park SI, Felipe CR, Pinheiro-Machado PG, Garcia R, Tedesco-Silva H Jr, Medina-Pestana JO (2007) Circadian and time-dependent variability in tacrolimus pharmacokinetics. Fundam Clin Pharmacol 21(2):191–197
Pergola PE, Raskin P, Toto RD, Meyer CJ, Huff JW, Grossman EB et al (2011) Bardoxolone methyl and kidney function in CKD with type 2 diabetes. N Engl J Med 365(4):327–336
Pfister M, D'Argenio DZ (2010) The emerging scientific discipline of pharmacometrics. J Clin Pharmacol 50(9 Suppl):S 6
Pfister M, Schaedeli F, Frey FJ, Uehlinger DE (1999) Pharmacokinetics and haemodynamics of candesartan cilexetil in hypertensive patients on regular haemodialysis. Br J Clin Pharmacol 47(6):645–651
Pfister M, Uehlinger DE, Hung AM, Schaedeli F, Sheiner LB (2004) A new Bayesian method to forecast and fine tune individual hemodialysis dose. Hemodial Int 8(3):244–256
Pfister M, Nolin TD, Arya V (2012) Optimizing drug development and use in patients with kidney disease: opportunities, innovations, and challenges. J Clin Pharmacol 52(1 Suppl):4S–6S
PKD Foundation [Internet] (2013) http://www.pkdcure.org/. Accessed 15 March 2013
Polidori D, Sha S, Mudaliar S, Ciaraldi TP, Ghosh A, Vaccaro N et al (2013) Canagliflozin lowers postprandial glucose and insulin by delaying intestinal glucose absorption in addition to increasing urinary glucose excretion: results of a randomized, placebo-controlled study. Diabetes Care 36(8):2154–2161
Riggs MM, Peterson MC, Gastonguay MR (2012) Multiscale physiology-based modeling of mineral bone disorder in patients with impaired kidney function. J Clin Pharmacol 52(1 Suppl):45S–53S
Russell CL, Conn VS, Ashbaugh C, Madsen R, Hayes K, Ross G (2006) Medication adherence patterns in adult renal transplant recipients. Res Nurs Health 29(6):521–532

Schiff J, Cole E, Cantarovich M (2007) Therapeutic monitoring of calcineurin inhibitors for the nephrologist. Clin J Am Soc Nephrol 2(2):374–384

Schmid-Mohler G, Thut MP, Wüthrich RP, Denhaerynck K, De Geest S (2010) Non-adherence to immunosuppressive medication in renal transplant recipients within the scope of the integrative model of behavioral prediction: a cross-sectional study. Clin Transplant 24(2):213–222

Sherwin CMT, Fukuda T, Brunner HI, Goebel J, Vinks AA (2011) The evolution of population pharmacokinetic models to describe the enterohepatic recycling of mycophenolic acid in solid organ transplantation and autoimmune disease. Clin Pharmacokinet 50(1):1–24

Stevens LA, Schmid CH, Greene T, Zhang YL, Beck GJ, Froissart M et al (2010) Comparative performance of the CKD epidemiology collaboration (CKD-EPI) and the modification of diet in renal disease (MDRD) study equations for estimating GFR levels above 60 mL/min/1.73 m^2. Am J Kidney Dis 56(3):486–495

Stevens LA, Claybon MA, Schmid CH, Chen J, Horio M, Imai E et al (2011) Evaluation of the chronic kidney disease epidemiology collaboration equation for estimating the glomerular filtration rate in multiple ethnicities. Kidney Int 79(5):555–562

Tajima N, Ishizuka H, Naganuma H (2006) Population pharmacokinetic analysis of panipenem/betamipron in patients with various degrees of renal function. Chemotherapy 52(5):245–253

Tornøe CW, Tworzyanski JJ, Imoisili MA, Alexander JJ, Korth-Bradley JM, Gobburu JVS (2007) Optimising piperacillin/tazobactam dosing in paediatrics. Int J Antimicrob Agents 30(4):320–324

Tortorici MA, Cutler D, Zhang L, Pfister M (2012) Design, conduct, analysis, and interpretation of clinical studies in patients with impaired kidney function. J Clin Pharmacol 52(1 Suppl):109S–118S

Turpie AGG, Lensing AWA, Fuji T, Boyle DA (2009) Pharmacokinetic and clinical data supporting the use of fondaparinux 1.5 mg once daily in the prevention of venous thromboembolism in renally impaired patients. Blood Coagul Fibrinolysis 20(2):114–121

Van der Walt JS, Hong Y, Zhang L, Pfister M, Boulton DW, Karlsson MO (2013) A semi-mechanistic non-linear mixed effects model to assess the effects of renal or hepatic impairment on the population pharmacokinetics of dapagliflozin and dapagliflozin 3-O-glucuronide. CPT Pharmacometrics Syst Pharmacol (In press)

Waiser J, Slowinski T, Brinker-Paschke A, Budde K, Schreiber M, Böhler T et al (2002) Impact of the variability of cyclosporin A trough levels on long-term renal allograft function. Nephrol Dial Transplant 17(7):1310–1317

Zhang L, Pfister M, Meibohm B (2008) Concepts and challenges in quantitative pharmacology and model-based drug development. AAPS J 10(4):552–559

Zhang L, Ng CM, List JF, Pfister M (2010) Synergy between scientific advancement and technological innovation, illustrated by a mechanism-based model characterizing sodium-glucose cotransporter-2 inhibition. J Clin Pharmacol 50(9 Suppl):113S–120S

Zhang L, Boulton DW, Pfister M (2012a) A pharmacometric approach to quantify the impact of chronic kidney disease and hemodialysis on systemic drug exposure: application to saxagliptin. J Clin Pharmacol 52(1 Suppl):126S–133S

Zhang L, Xu N, Xiao S, Arya V, Zhao P, Lesko LJ et al (2012b) Regulatory perspectives on designing pharmacokinetic studies and optimizing labeling recommendations for patients with chronic kidney disease. J Clin Pharmacol 52(1 Suppl):79S–90S

Zhao P, Vieira M de LT, Grillo JA, Song P, Wu TC, Zheng JH et al (2012) Evaluation of exposure change of nonrenally eliminated drugs in patients with chronic kidney disease using physiologically based pharmacokinetic modeling and simulation. J Clin Pharmacol 52(1 Suppl):91S–108S

Zhou XJ, Ke J, Sallas WM, Farrell C, Mayers DL, Pentikis HS (2009) Population pharmacokinetics of telbivudine and determination of dose adjustment for patients with renal impairment. J Clin Pharmacol 49(6):725–734

Zhou Z, Shen J, Hong Y, Kaul S, Pfister M, Roy A (2012) Time-varying belatacept exposure and its relationship to efficacy/safety responses in kidney-transplant recipients. Clin Pharmacol Ther 92(2):251–257

Chapter 5
Drug–Disease Model-Based Development of Therapeutic Agents for Treatment of Diabetes

Parag Garhyan, Brian Gregory Topp, Jenny Y. Chien, Vikram P. Sinha, Meindert Danhof and Stephan Schmidt

5.1 Introduction

Diabetes is a chronic, progressive disease that is estimated to be one of the top ten leading causes of death globally (WHO fact sheet number 310). Type 2 diabetes is the most common type of diabetes, affecting 90–95% of the US diabetes population. According to the latest International Diabetes Federation (IDF) report, about 8.3% of the global adult population, or 382 million people, have diabetes. The number of newly diagnosed cases worldwide continues to grow every year and the global figure is expected to rise to 595 million by 2035. The majority of the 382 million people with diabetes are aged between 40 and 59, and 80% of them live in low- and middle-income countries. The economic burden of diabetes is approximately 548 billion US $ in health spending (11% of the total spent worldwide) in 2013 (IDF report 2013). Therefore, improving the treatment and management of diabetes, its comorbidities, and associated complications continue to be an important focus of pharmaceutical research and development (R&D).

Diabetes is a metabolic disease that is rich with quantitative biomarkers and well understood regulatory and counter-regulatory processes. For these reasons, diabetes is one of the therapeutic research areas rapidly gaining R&D efficiencies with the

P. Garhyan (✉)
Global PK/PD and Pharmacometrics, Eli Lilly & Company, Indianapolis, IN, USA
e-mail: pgarhyan@lilly.com

B. G. Topp · J. Y. Chien
Lilly Research Laboratories, Eli Lilly and Company, Indianapolis, IN, USA

V. P. Sinha
Leiden University, Office of Clinical Pharmacology/Translational Sciences,
U.S. Food and Drug Administration, Indianapolis, IN, USA

M. Danhof
Department of Pharmaceutics, Leiden Academic Centre for Drug Research Einsteinweg,
55 P.O. Box 9502 2300 RA Leiden, The Netherlands

S. Schmidt
Department of Pharmaceutics, Center for Pharmacometrics & Systems Pharmacology,
University of Florida, Orlando, FL, USA

S. Schmidt, H. Derendorf (eds.), *Applied Pharmacometrics,* AAPS Advances
in the Pharmaceutical Sciences Series 14, DOI 10.1007/978-1-4939-1304-6_5

use of predictive drug and disease models. The mathematical modeling of glucose–insulin homeostasis has provided significant insights into the underlying mechanisms of the disease and is becoming a critical component of the pharmaceutical R&D program (Ajmera et al. 2013). Driven by the increasing cost of drug development and the high rate of late-stage failures (over 90 % of clinical candidates never make it to market), the scientific leaders and regulators, advocated for the incorporation of model-based approaches into drug development processes (Woodcock and Woosley 2008) to improve the efficiency and the quality of decision-making: to select targets, predictive biomarkers, drug candidates, clinical trial designs, dosing range or regimens, and development programs with high probabilities of success in all the stages of drug discovery and development. Fueled by the recent technical advances in computational power, aided by the arsenal of predictive drug and disease models and study design efficiency-enhancing tools, pharmacometricians have been able to contribute more effectively in the early terminations of the "bad" drugs and the optimization of the development program to expedite the delivery of the "good" drugs to the patient.

All drug-disease models developed should be fit for purpose, specifically, provide answers to the questions of interest. Models should be developed with well-characterized basic physiology and biochemical regulatory aspects of the disease in mind in order to have predictive fidelity. It is consequently important that the pharmacometricians have a basic understanding of the disease, including that the term "diabetes" does not characterize a single, homogenous disease but rather encompasses a group of metabolic disorders, which are all characterized by hyperglycemia that result from defects in insulin secretion, insulin action, or both (American Diabetes Association 2008). It is a condition in which a person has higher than normal blood glucose levels either because the body does not produce enough insulin in response to meal intake (impaired beta cell functions), or because the body does not properly respond to the insulin that is produced (insulin resistance). Insulin is a hormone produced by the beta cells in the Islets of Langerhans located in the pancreas which promotes the uptake of glucose by tissues such as muscles and adipose thereby mediating the clearance of glucose. If there is a diminished uptake of glucose by tissues due to resistance to insulin, the beta cell will compensate by secreting just enough insulin to normalize glucose level (euglycemia). Over time, the acute insulin secretory response to glucose is exhausted and the homeostatic feedback control diminishes progressively, leading to hyperglycemia and ultimately diabetes mellitus. A persistent state of hyperglycemia is associated with complications, including an increased susceptibility to infections, ketoacidosis, microvascular diseases, such as nephropathy or retinopathy and may lead to early macrovascular complications, such as heart attack and stroke (Morghissi et al. 2007). In recent years, there has been a significant emergence of type 2 diabetes driven by lifestyle factors leading to increased body weight and obesity.

Type 2 diabetes can be controlled with various treatment modalities. Regimented treatment of diabetes is important and, generally, a holistic approach that includes blood glucose and blood pressure control, and lifestyle changes, such as maintaining a healthy body weight is recommended. Therefore, the choice of treatments depends on the disease status and often includes more than one antihyperglycemic medication.

5.2 Therapeutic Interventions

An important component in developing drug–disease models of diabetes is that soon after diagnosis, patients with type 2 diabetes mellitus may be able to manage their glucose levels on diet and exercise alone for a few years. However, the disease usually progresses over time requiring multiple drugs to be prescribed concomitantly. Numerous drugs of different mechanisms of action are available by oral or subcutaneous routes of administration. The therapeutic combination for the treatment of type 2 diabetes may include insulin, to provide better glycemic control in combination with the more convenient oral agents. The antihyperglycemic medicines that are available in the market by pharmacologic class include:

- Biguanides for inhibition of hepatic gluconeogenesis (metformin)
- Insulin secretagogues (sulfonylureas)
- Insulin sensitizers (thiazolidinedione)
- Alpha-glucosidase inhibitors for glucose or starch absorption (acarbose)
- Incretin mimetics for glucose-dependent insulin secretion (glucagon-like-peptide-1, or GLP-1 anlogues)
- Dipeptidyl peptidase-4 (DPP-4) inhibitors
- Sodium-dependent glucose co-transporter 2 (SGLT2) inhibitors
- Insulins (including long-acting basal insulins)

In addition, there are many investigational agents in various stages of drug discovery and development, which are targeting different pathways for glucose control (Verspohl 2012), such as glucagon receptor antagonist, glucokinase activator, incretin hormones, sodium-dependent glucose co-transporters, G-protein-coupled receptor agonists, etc. Many newer agents are designed to have pleiotropic effects and have beneficial attributes in addition to glucose lowering to provide the additional benefit in the management of multiple facets of this complex metabolic disorder.

5.3 Biomarkers and Clinical Surrogates

Diabetes disease models are developed using a plethora of quantitatively predictive and clinically relevant biomarkers. The standard biomarker panel is not limited to fasting blood glucose (FBG) and postprandial glucose (PPG). There are numerous biomarkers and pharmacodynamic measurements available to assess glycemic status and pancreatic beta cell health as well as to evaluate the effects of pharmacologic interventions. The pancreas releases insulin which is produced in the pancreatic beta cells, and glucagon is produced in the alpha cells. Glucagon is an antagonist to insulin causing hepatic glucose output to increase either by gluconeogenesis or glycogen breakdown—its effect detectable following prolonged hypoglycemia. In addition, hormones (somatostatin, growth hormone, cortisol, gastrointestinal hormones, etc.), amino and fatty acids also play roles in this complex metabolic system.

The choice of a pharmacodynamic biomarker in model development is dependent on the drug's mechanism of action, the duration of the trial or the stage of development and the objective of the assessment. In addition, during the translational phase of development, the choice of animal models of disease is important and is often dependent on the mechanism of action of the pharmacologic agent and known inter-species differences in the target expression and biomarker response (Shafrir 2007, 2010).

Acute biomarkers (measured in minutes, hours, or days) are measured in preclinical and early clinical phases of drug development in trials of short duration (e.g., in phase 1). The most common biomarkers assessed in early trials are FBG, PPG, C-peptide, or insulin, in response to meals or glucose challenges. Biomarkers of the target engagement may include glucagon, dipeptidyl peptidase-4 [DPPIV] enzyme inhibition, glucagon-like peptide-1 (GLP-1), gastric inhibitory polypeptide (GIP), and other hormones. In addition, complex systems pharmacology models of diabetes may also incorporate information based on biomarkers of pleiotropic effects, such as, cholesterols, free fatty acids and hemodynamic measures (e.g., blood pressure and heart rate) as well as standard laboratory assessment of cardio-renal functions.

Glycosylated hemoglobin (HbA1c) is formed through a nonenzymatic and irreversible reaction between glucose and hemoglobin. HbA1c is a clinical surrogate for long-term disease progression and treatment effects and is, thus, well accepted as an efficacy endpoint in long-term trials (e.g., months to years). Fasting insulin and C-peptide levels, on the other hand, are measures of endogenous insulin production and are used to assess insulin resistance and beta cell function as well as markers of disease progression. Long-term outcomes of diabetes and diabetes complications, such as strokes, coronary heart disease, neuropathy or nephropathy, might take several years to present themselves. Outcomes are often assessed using empirical or Bayesian probability models, rather than drug–disease models.

Each of these biomarkers, whether fast or slow turnover markers, carry importance at different stages of the drug discovery and development process. It is important to have a good understanding of the translatability and reproducibility of these biomarkers such that the use of these biomarkers is reliable and has predictive fidelity.

To evaluate the drug effects, pharmacokinetics-pharmacodynamics relationships are developed in the forms of models linking the concentration of drug to biomarkers of interest or outcomes, as shown in Fig. 5.1.

Diabetes is well known as a risk factor for cardiovascular disease. Despite glucose control, the risk of cardiovascular mortality and morbidity remains high in patients with diabetes. Drug and disease modeling approaches may incorporate cardiovascular biomarkers in combination with glycemic parameters to assess the impact of a new therapeutic intervention on both diabetes and cardiovascular outcomes (Vlasakakis and Pasqua 2013).

Due to increasing awareness in the holistic treatment of the comorbidities of diabetes, namely, obesity and cardiovascular diseases, novel therapies not only treat hyperglycemia but also aim to manage the symptoms of these comorbidities, often

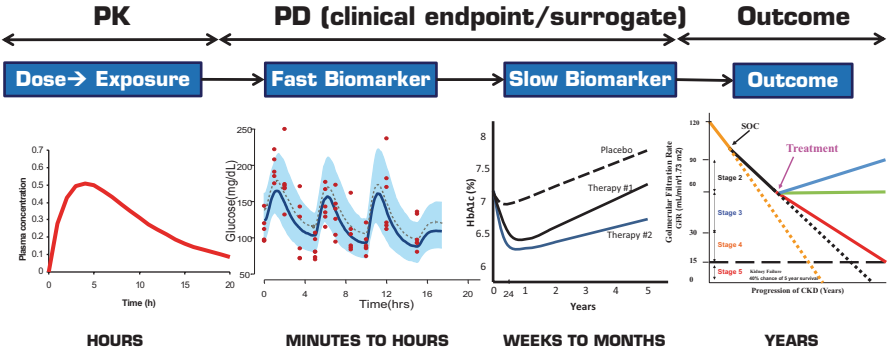

Fig. 5.1 Schematic of the relationship between drug effect, biomarkers, and clinical outcomes

referred to as "diabetes plus". Therefore, the biomarker panels have been expanded to include measures of cardiometabolic health (e.g., body mass index, waist circumference, body fat composition, lipids, triglycerides), assessment of hemodynamics (e.g., blood pressure, heart rate), and risk of arrhythmias (ECG changes). This chapter focuses on the modeling of glycemic parameters; however, similar modeling concepts may be applied to cardiovascular biomarkers.

5.4 Drug–Disease Models of Diabetes

Leveraging the range of available biomarkers, computational models play an increasingly important role in understanding the dynamic behaviors and the mechanisms underlying diverse and complex biological systems, leading to better drug candidate selection, study design, dose and dosing regimen decision, and ultimately, better control and treatment for diabetes.

Computational models of diabetes, either mathematical or statistical, in the published literature can broadly be classified into clinical and nonclinical categories, based on complexity, depth of biological description, and the type of data (individual or population level; Landersdorfer and Jusko 2008; Ajmera et al. 2013). Analysis models of clinical data are mostly empirical in nature and emulate clinical data by considering only essential biological descriptors. Due to the purpose of their uses, these models are useful in understanding effects of dose (concentration) of new treatments, time course in changes of response, understanding disease progression, and predicting risks for complications. Nonclinical physiologically based models are more complex in nature and account for the mechanistic description of the biological systems, eventually, through translational sciences, aimed at being used for simulating clinical scenarios. Recently, semi-mechanistic and mechanistic systems pharmacology models have also been used in clinical setting as described later in this chapter.

As emphasized earlier, the choice of the model really depends on the questions that need to be answered and the nature of available data. For example, simple models without mechanistic understanding that are developed to describe observed clinical data can be used for retrospective hypothesis testing and clinical trial optimization using simulations. On the other hand, a mechanistic model may be necessary to generate prospective hypothesis to be evaluated where changes in biomarkers can be assessed by altering specific biochemical pathways.

In the following section, we summarize key types of models that have to be utilized with nonclinical and clinical data to describe the dynamics of biomarkers of interest. Most of these models can be adequately modified to characterize and predict different biomarkers data and their interactions.

5.4.1 Systems Pharmacology Models

Conceptually, the systems approach is a mathematical representation of the pertinent physiology that comprise of the key pathways or targets of interest. Systems pharmacology models usually employ a "bottom up" modeling approach to represent the physiology and disease states. The approach requires physiological or systems-level information as well as the biological pathways and mechanisms. These physiologically based models aimed to quantitatively integrate relevant biology across the systems, with targets or pathways, are expressed as state variables and parameters. The parameters in these complex models typically include those reported in the literature and those calibrated to match subsystem and/or system-level behaviors. Each unique set of model parameterization represents one "virtual patient," and each virtual patient response is qualified by comparing simulated responses to experimentally observed or published data. This approach focuses on finding biologically feasible parameterizations that reproduce critical behaviors, rather than on exact characterization of numerous difficult-to-measure parameters (Kansal 2004; Klinke 2008; Shoda et al. 2010; Schaller et al. 2013). The PK and PD properties of the drug(s) of interest are subsequently evaluated on specific pathways or targets in a systematic fashion. Together, these integrated drug–disease models are used to simulate the expected physiological and pharmacological responses to a novel therapy or combination of therapies or clinical trial simulations in virtual patient populations (Waters et al. 2009). A detailed case study is presented at the end of this chapter to describe the development and application of systems pharmacology models using a glycogen phosphorylase inhibitor (GPi) for the treatment of type 2 diabetes.

5.4.2 Models for Glucose–Insulin Interaction

An advanced model of glucose–insulin regulation was developed using data from both healthy and type 2 diabetic subjects in glucose provocation experiments (Jauslin et al. 2007, 2011; Silber et al. 2007). Briefly, the glucose model is described

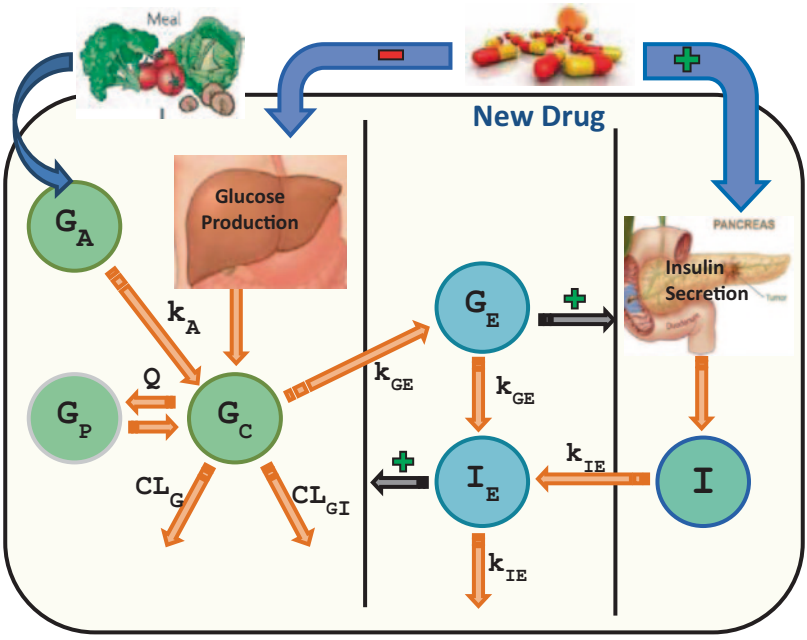

Fig. 5.2 Schematic representation of the integrated insulin–glucose model. *Arrows* indicate flows and control mechanisms

using a two-compartment model with a glucose absorption component. As shown in Fig. 5.2, the glucose model also includes two effect compartments accounting for effects on glucose production and insulin secretion. The model for insulin incorporates both secretion and distribution. Baseline glucose and insulin values are represented as population values with inter-subject variability terms.

One application of this model is for evaluation of combination of treatments with different mechanisms of action. An example of this application is the prediction of glucose response to investigational insulins or incretin mimetics, when added to metformin (a drug that affects hepatic glucose production) in combination with sulfonylurea (a drug that increases insulin secretion). The pharmacokinetic component of drug treatment can be introduced into the model by linking to the site of action. This model characterizes the fast biomarkers, thus the application of this model to predicting long-term steady-state biomarker response is limited. For such an application, the placebo response with respect to inter-occasion glycemic variability and links to HbA1c response will need to be considered. As glucose input is the driver for the biomarker dynamics, this model requires reliable details about the glucose (as OGTT, IVGTT, MGTT or meals) intake.

5.4.3 Models for Glucose–Insulin–Glucagon Interaction

The first models exploring the glucagon counter-regulation (GCR) mechanism were proposed by Farhy and McCall (2009) based on rodent studies. As all the compo-

nents of these models were clinically measurable, these models identify the role of delayed feedback illustrating the relationship between basal glucagon level and different aspects of GCR responses to insulin-induced hypoglycemia in T1DM conditions. Hetherington et al. (2011) and Sumner et al. (2011) developed a composite model for glucagon/insulin driven liver glucose homeostasis by linking a series of sub-system models corresponding to different aspects of physiology. This model has been used further to explore the behavior of glucose homeostasis systems by modulating the liver insulin sensitivity and diet glucose level. Kim et al. (2007) developed a multi-scale model illustrating hormonal control of whole-body glucose homeostasis during exercise and can be envisioned as a roadmap towards achieving a holistic mechanistic view of the glucose homeostasis system from sub-cellular to a "whole-body" level.

Schneck et al. (2013) extended the insulin–glucose interaction model described in previous section to incorporate the key counter-regulatory hormone glucagon; this model was utilized to investigate the effect of a novel glucokinase activator on glycemic control. Baseline glucagon secretion, the inhibitory influence of glucose and insulin, and the stimulatory influence of ingested exogenous protein on glucagon secretion were combined in a differential equation to describe glucagon dynamics. An effect compartment was utilized to represent a delayed effect of glucagon within the system. This model describes the dynamics of fast biomarkers (e.g., glucose, insulin, and glucagon), thus limits the ability to utilize this model for predicting long-term HbA1c effects. As glucose input is the driver for the biomarker dynamics, this model requires reliable details about the glucose intake.

5.4.4 Time Course Models—Fasting Blood Glucose or HbA1c

In clinical trials, glycemic parameters (fasting blood glucose or HbA1c) are measured at intervals during the course of the trial. These time courses of the glycemic parameters are used to evaluate the effects of an intervention relative to placebo or an active comparator. A typical profile of FBG as a function of time is shown in Fig. 5.3. The time course profile of HbA1c or any other biomarker can also be generated and modeled in similar fashion.

At randomization, prior antidiabetic treatments may be washed out to allow better evaluation of the active treatments. Wash-out of prior medication may cause a baseline excursion in fasting glucose. Specifically, trials to evaluate a new agent for a monotherapy indication may include a lead-in phase, during which patients discontinue and washout their previous antidiabetic agents. In these trials, during the lead-in phase, FBG levels will rise as shown by the placebo response curve in Fig. 5.3. Upon treatment, FBG decreases from baseline to reach a maximum possible effect (E_{max}) for the assigned dose. The following model can be used to describe the rise in FBG in the placebo group and the fall in FBG levels with drug treatment.

$$\textit{Change in FBG} = \textit{Placebo effect} + \textit{Drug effect}$$

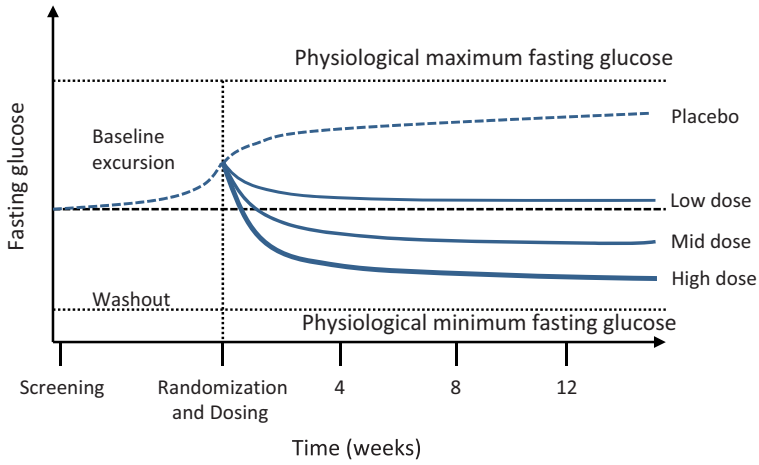

Fig. 5.3 Time course of fasting blood glucose following washout of prior antidiabetic agents. The *dotted curve* indicates glucose profile on placebo from screening to the end of the trial. *Solid lines* show the effects of treatments at three different dose levels

There are various ways of describing the placebo and drug effects. One of the ways we can describe this relationship is by the following equation:

$$Change\ in\ FBG = P_{max} + OAD + E_{max} \cdot FBG_{Base}\left(\frac{exposure^{\gamma}}{exposure^{\gamma} + EC_{50}^{\gamma}}\right)(1 - e^{k_{eff} * time})$$

where P_{max} is the maximum change in FBG for placebo; E_{max} is the maximal drug effect, EC_{50} is the drug exposure that produces half maximal effect. Exposure is the drug exposure (which may be the area-under-curve or average concentration during a doing interval, or dose); FBG_{Base} is the baseline FBG; k_{eff} is a rate constant of glucose turnover in determining the time required to achieve the maximum treatment or placebo effect; γ is a concentration–response steepness parameter (Hill coefficient); OAD stands for oral antidiabetic drug which is the excursion between initiation of washout of antihyperglycemic medications to baseline FBG.

In some cases, when the time-course of biomarker response may not be critical, for example, when the dose (exposure)–response relationship to be evaluated is at steady state, a model describing the changes at a predefined endpoint (for example, at 12 or 26 weeks) may be sufficient. The equation described above may be modified to:

$$Change\ in\ FBG = P_{max} + OAD + E_{max} \cdot FBG_{Base}\left(\frac{exposure^{\gamma}}{exposure^{\gamma} + EC_{50}^{\gamma}}\right)$$

where all the terms are as described earlier. It should be noted that the term that characterized the time course (with k_{eff} and time) has been removed in this equation.

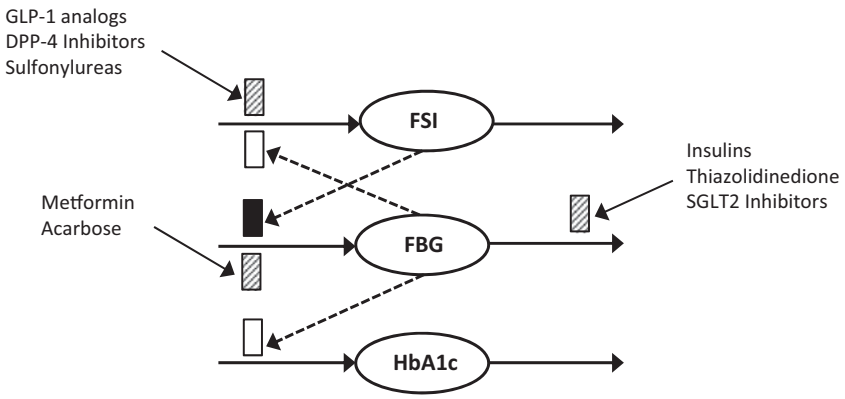

Fig. 5.4 A generalized model structure linking fasting serum insulin, fasting blood glucose, and glycosylated hemoglobin (HbA1c). *Open boxes* show the stimulation and the *solid box* represents suppression of biomarker production rates. *Shaded boxes* represent the rates which are impacted by drugs working via different mechanisms

In longer clinical trials, where HbA1c values are measured to evaluate the effects of a therapeutic intervention, the time course model described in this section for FBG can be easily applied to HbA1c.

In trials of add-on therapy during which patients continue taking their antihyperglycemic medications, without washout, FBG levels are stabilized at baseline.

5.4.5 Indirect Response Models—Insulin, Glucose, and HbA1c

As previously described, the biomarkers that are frequently measured in clinical trials for antidiabetic medications are fasting serum insulin (FSI), FBG, and HbA1c. A generalized approach can be taken to link FSI, FBG, and HbA1c to describe the time courses of these biomarkers. Figure 5.4 shows a representation of the key components and the relationships that can be used in the model.

Møller et al. (2013) used a similar approach of linking glucose to HbA1c where the mean plasma glucose (from 24-h glucose measurements) instead of FBG was used to develop an indirect response model and predict long-term HbA1c changes based on short-term mean plasma glucose data.

5.4.6 Physiological Linked Fasting Glucose and HbA1c Model

Hamrén et al. (2008) published a model that linked fasting glucose and HbA1c using a transit compartment model informed by physiology which is a mechanistically better approach versus using an indirect response relationship between these two biomarkers (as described in Sect. 5.4.5). In this model, a series of four transit compartments describe red blood cell (RBC) aging with a zero-order release of RBCs

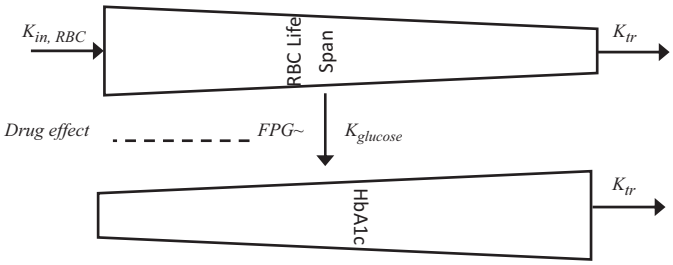

Fig. 5.5 Fasting glucose—glycosylated hemoglobin (HbA1c) transit model using red blood cells (RBCs) lifespan. (Adapted from Hamrén et al. 2008)

into the circulation. A first-order rate constant defines the transition of RBCs from one stage to the next until the cell dies as shown in Fig. 5.5.

5.4.7 Models for Progression

Efforts towards the development of novel antidiabetic agents are directed at the drugs that can alter diabetes progression. In studies of greater than 1 year duration, it is important to include disease progression in the model in order to study the long-term effect of antidiabetic agent at different stages of progression. Disease progression models specific for diabetes incorporating long-term population studies with antidiabetic agents have been developed (Frey et al. 2003; de Winter et al. 2006). De Winter et al. (2006) utilized clinical data with pioglitazone, metformin, and gliclazide to assess the disease progression and drug effect using indirect response model linking FSI, FBG, and HbA1c as described in Sect. 5.4.5 (Fig. 5.6). The model described the rate of disease progression through the drugs effect on beta cell function and insulin sensitivity.

Topp et al. (2000) developed a model of disease progression by considering beta cell mass together with insulin and glucose concentrations. This model was described by three nonlinear ordinary differential equations, where glucose and insulin dynamics were fast relative to beta cell mass dynamics. Extending this model, Ribbing et al. (2010) proposed a semi-mechanistic pharmacokinetic/pharmacodynamic model, illustrating the dynamics of fasting plasma glucose, fasting insulin, insulin sensitivity, and beta-cell function in a heterogeneous population.

5.4.8 Models for Diagnostic Tests

In order to evaluate the diabetic and prediabetic condition in an individual, different glucose tolerance tests, such as intravenous glucose tolerance test (IVGTT), oral glucose tolerance test (OGTT), and mixed meal glucose tolerance test (MMTT) have been devised. The aims of these tests are to obtain estimates of insulin sensitivity

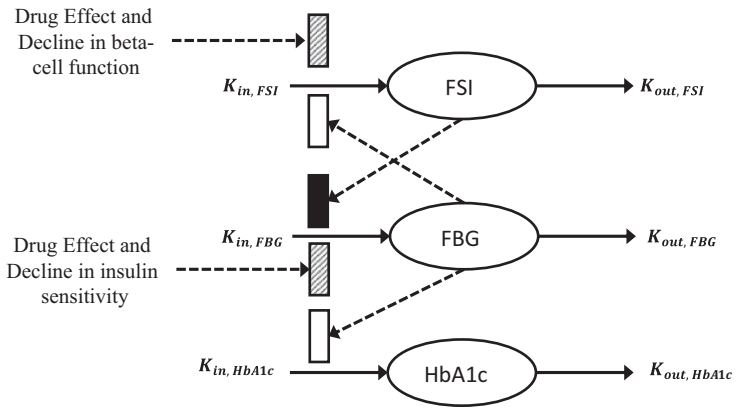

Fig. 5.6 Schematic representation of the structure of the mechanism-based population disease progression model, including the homeostatic feedback between fasting serum insulin (FSI) and fasting blood glucose (FBG) and the feed-forward between FBG and glycosylated hemoglobin (HbA1c). *Open boxes* show the stimulation and the *solid box* represents suppression of biomarker production rates. *Shaded boxes* represent the rates which are impacted by drugs and disease progression

(IS), glucose effectiveness (potency or potentiation), insulin secretion, and beta cell function. Since the liver metabolizes more than half of the secreted insulin before it is utilized by other body tissues, accurate estimation of pre-hepatic insulin secretion, hepatic insulin extraction and clearance are essential for evaluating insulin secretion and beta cell function under normal and diseased conditions. Plasma C-peptide, a part of preproinsulin peptide and therefore secreted in equimolar amounts as insulin by beta cell, acts as an indicator for insulin secretion. However, peripheral C-peptide has a longer half-life and can limit the accurate estimation of insulin secretion. Consequently, a model-based approach may be recommended for greater accuracy.

The assessment of insulin sensitivity has been conducted using either the glucose clamp technique or the minimal models (Bergman et al. 1979, 1989) which had insulin sensitivity and glucose effectiveness as the main parameters. Cobelli et al. (2009) incorporated peripheral compartment for glucose distribution which modeled the glucose and insulin data simultaneously. These models do not take into account dynamic control mechanisms and were not ideal for predictive purposes. Significant improvement over the minimal models was achieved incorporating an additional compartment for glucose kinetics and data from labeled IVGTT experiments. Although these bi-compartment models allow precise estimation of IS and potency, the additional cost and technology involved in using labeled IVGTT make it impractical for application in large clinical trials or patient care settings. Silber et al. (2007, 2010) proposed an integrated insulin–glucose model to describe IVGTT data from healthy as well as diabetic individuals, using an insulin–glucose feedback mechanism. As OGTT closely resembles the physiological condition, this model was extended

further by incorporating the description for glucose absorption and incretin effects following a meal or 24-h glucose and insulin profile following multiple test meals.

5.5 Case Study: Systems Pharmacology Model

A case example of systems pharmacology model aims to assess the therapeutic potential of a glycogen phosphrylase inhibitor (GPi) for treatment of type 2 diabetes. Glycogen phosphorylase is the rate-limiting enzyme in glycogenolysis and thus is responsible for roughly 50 % of hepatic glucose output (HGO). Glycogenolysis is thought to be elevated in type 2 diabetes and several publications have described GPi as a promising therapeutic strategy for type 2 diabetes (Martin et al. 1998; Baker et al. 2005; Torres et al. 2011). The general approach to describe the pertinent physiology is to start with a "core" model of fundamental mechanisms that have been well characterized clinically. An example of such a systems or physiological model that would enable evaluation of various targets of glucose regulation is presented in Fig. 5.7.

As illustrated in Fig. 5.7, glucose enters the blood from the gastrointestinal tract following a meal (SGLT-1 transporter mediated absorption) or through hepatic glucose production (via G6Pase enzyme). The regulation of HGO has been well char-

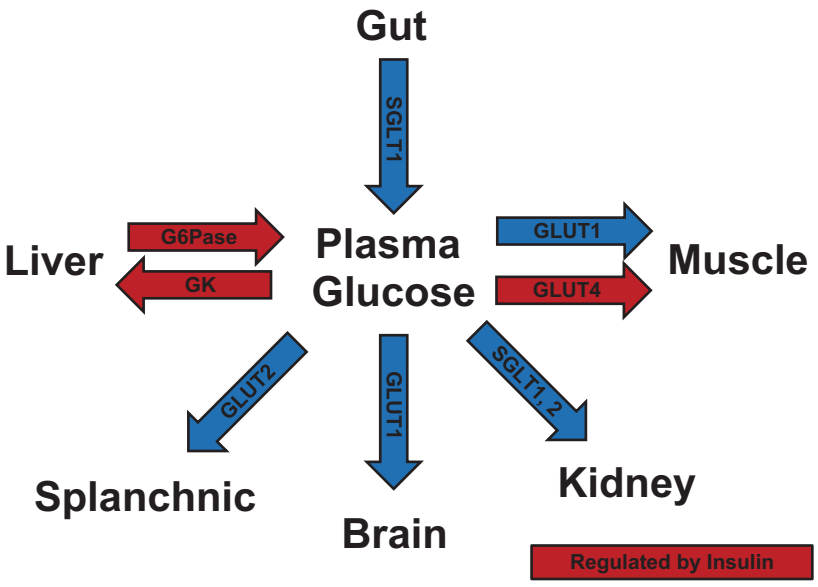

Fig. 5.7 Schematic representation of physiology for glucose processing in various organs in the human body

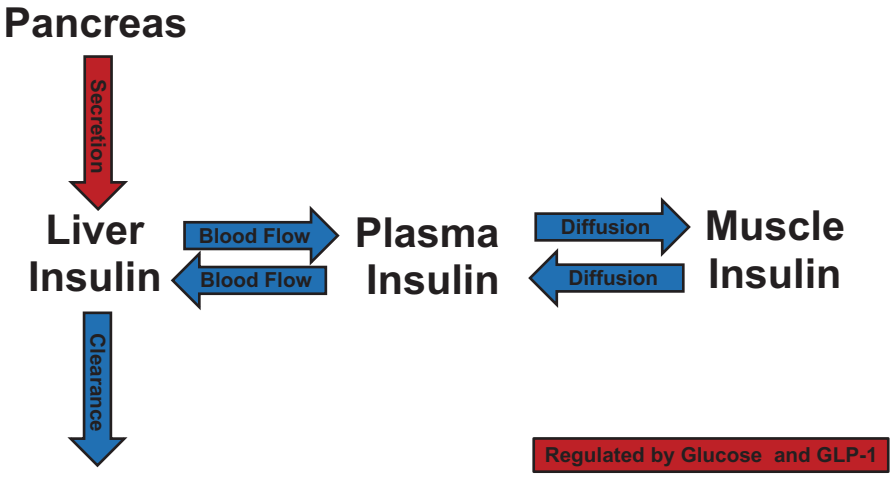

Fig. 5.8 Schematic representation of insulin dynamics

acterized, which can be completely suppressed by high glucose, high insulin, or low glucagon levels. Conversely, low glucose, low insulin, or high glucagon can increase HGO by about fourfold. Glucose is utilized by major tissues of the body, most notably the brain, muscle, and abdominal organs (splanchnic tissue). The brain takes up glucose at a roughly constant rate via GLUT2 transporter. Muscle glucose uptake occurs via GLUT4 and GLUT1 transporters. Splanchnic glucose uptake is thought to be glucose dependent (via GLUT2 transporter). Finally, glucose is filtered, and then reabsorbed at the kidney via SGLT-1 and SGLT-2 transporters. However, the reabsorption process begins to saturate when glucose rises above 180 mg/dl resulting in urinary glucose excretion.

This core model of glucose regulation is coupled to simple models of insulin and glucagon dynamics. Insulin secretion is driven largely by plasma glucose levels and incretin hormones (GLP-1, GIP, etc.). It should also be noted that insulin is secreted directly into the liver via the portal vein where about 50% is cleared on first pass through the liver. Thus, hepatic insulin levels are roughly twice as high as plasma levels. Muscle insulin levels are similar to plasma, but there is a time delay required for insulin to diffuse through the tight capillary junctions. Glucagon is a counter-regulation hormone that increases three- to fourfold during the development of hypoglycemia. A schematic of simple insulin model is represented in Fig. 5.8.

Baseline parameters for this mechanistic model of glucose and insulin dynamics represent the estimated population mean value for healthy volunteers derived from a meta-analysis of public literature. Virtual patients with type 2 diabetes are created by incorporating a real-world distribution of insulin resistance (muscle and liver), and insulin secretory defects. As a specific example, if the therapy of interest targets liver, then the core model can be expanded to include target specific liver

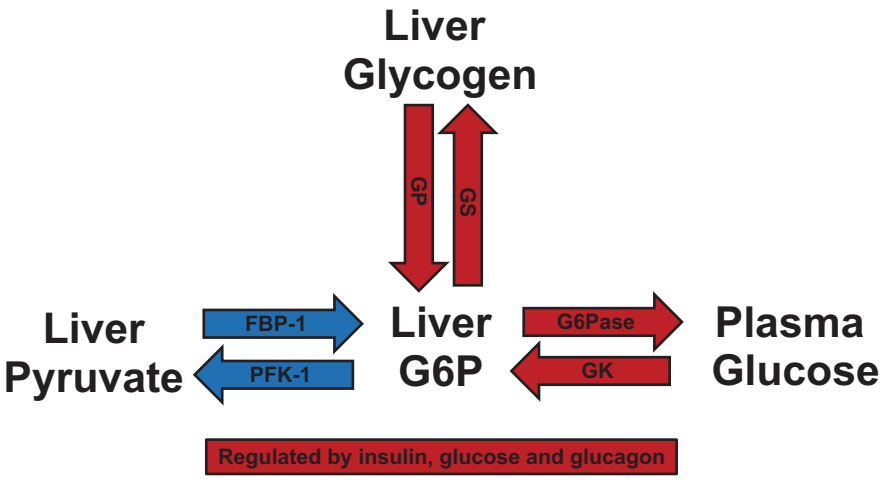

Fig. 5.9 Schematic representation of glucose dynamics in the liver

physiology; in this case the glycogenolysis, glycogen synthesis, gluconeogenesis, and glycolysis (Fig. 5.9).

Available data suggest that glycogenolysis and gluconeogenesis contribute roughly equally to total HGO. Glucose, insulin, glucagon and carbohydrate metabolites (represented in this model by G6Pase process) all contribute to the regulation of glycogenolysis and glycogen synthesis. Glycolysis is thought to be a substrate driven process while gluconeogenesis is thought to be roughly constant throughout the day. However, gluconeogenesis has been shown to increase during prolonged fast and has been linked to glycogenolysis via hepatic auto-regulation.

After representing the physiology mechanistically, the next step is to link the drug effect to a PK/PD model. For representative purpose, we can assume the new drug (GPi) exhibits a 100 % inhibition of GP for the entire 24-h interval in a typical patient. The maximally effective GPi is projected to have a dramatic effect on glycogenolysis (and thus HGO) overnight, but minimal impact during the day (as glycogenolysis is highly inhibited by postprandial glucose and insulin excursions). As a result, GPi is projected to display impressive glucose lowering overnight but little to no effect during the day (Fig. 5.10). Overall, chronic dosing with a maximally effective GPi is projected to result in noncompetitive HbA1c reductions (Fig. 5.10).

In addition to limited efficacy, chronic GPi therapy may be associated with metabolic adverse events. Following an acute dose, glycogen accumulates during the day but does not decrease overnight. Thus, following multiple doses, liver glycogen levels will likely increase to a point where they inhibit glycogen synthesis. At this point, the glucose that is normally converted to glycogen will be redirected to either lactate (risk of lactic-acidosis) or be converted to triglyceride via de novo lipogenesis (risk of hepatic steatosis). These pathways also suggest that GPi may not combine well with metformin (inhibition of gluconeogenesis may exacerbate lactate

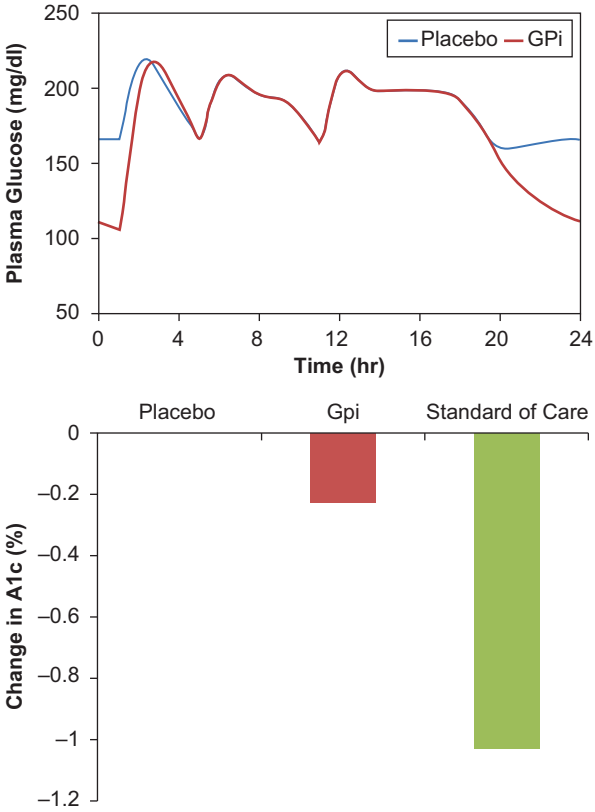

Fig. 5.10 Comparison of simulated 24-h glucose profiles with placebo and glycogen phosphorylase inhibitor (GPi; *upper panel*). Due to the lack of effect on postprandial glucose, GPi is predicted to result in a very modest decrease in HbA1c (*lower panel*)

or triglyceride change) or sulfonylureas (GPi may impede the counter-regulatory response to hypoglycemia). Since these drugs are the two most commonly prescribed diabetes therapies, there is a chance that GPi therapy may be limited to a small subset of the diabetes population.

Overall, this analysis, together with expert knowledge of metabolism and physiology, illustrated using a systems pharmacology model of diabetes, suggests that GPi would be unlikely to become a viable therapy for type 2 diabetes. Thus, detailed mechanistic modeling, although tedious and resource intensive, provides a rigorous methodology for integrating our present knowledge of human pathophysiology and extrapolating to expected clinical outcomes. While the predictions using such complex models may not always have high predictive accuracy, making decisions based on a rigorous analysis of the available data, informed by expert knowledge, is likely to be more effective, and less costly in the long run, than a trial-and-error method of discovery. In addition, mechanistic models can identify key knowledge gaps for strategic expansion of our knowledge.

As described in this case study, mechanistic modeling can effectively inform both efficacy and safety aspects of therapeutic interventions. Lesko et al. (2013) described how systems approaches can be leveraged for understanding adverse drug

events and ability to predict them, thus taking a step towards personalized medicine by enabling better identification of risk factors for an individual or subgroup.

5.6 Applications of Drug–Disease Models

The drug–disease models and the associated simulations that include parameter uncertainty and variability are powerful tools in decision-making in drug discovery and development. After the drug–disease models are developed based on accruing experimental data and informed by expert knowledge, simulations are performed to explore alternative or expanded scenarios of patient populations, clinical trial designs or disease outcome. The common questions or what-if scenarios that can be addressed through model-based analysis or simulations in diabetes R&D may include:

- What is the predicted efficacy in patients based on in vitro or animal data?
- What is the appropriate biomarker of pharmacology, based on variability, sensitivity, and time course of response?
- What is the power or sample size of the study to detect a target response (difference from placebo at endpoint) for a specific biomarker or mechanism of action?
- What is the minimum study duration to demonstrate the target response?
- What is the dose to differentiate or achieve superiority to placebo?
- What is the dose to demonstrate competitive or target response to marketed comparators?
- What is the probability of demonstrating superiority to marketed comparator at the selected dose?
- Are there subpopulations of responders or nonresponders based on the mechanism of action (for efficacy or safety)?
- What is a clinically relevant drug–drug interaction or food effect?

An example application of patient response simulation was illustrated previously using a systems pharmacology model to support compound "go/no-go" decision. Example applications of trial simulations to support design optimization have been extensively published (Chien and Sinha 2010; Zhang et al. 2013). Figure 5.11 shows a conceptual example of application of modeling and simulation to support optimum dose selection.

Based on Fig. 5.11, Table 5.1 shows the probability of each dose meeting the predefined target criteria (superiority to comparator). The dose selected to advance to phase 3 confirmatory trial was selected based on a combination of high probability of competitive success and low probability of safety risk (e.g., cardiovascular or dose-limiting adverse events).

Pharmacometricians have been developing drug–disease models of diabetes to facilitate "rational target selection." This is akin to "rational drug design" where high throughput trial-and-error methods for identifying chemicals that bind to receptors or enzymes have been replaced with methods that use knowledge of target structure to build ideal inhibitors or activators. For target selection, the current strat-

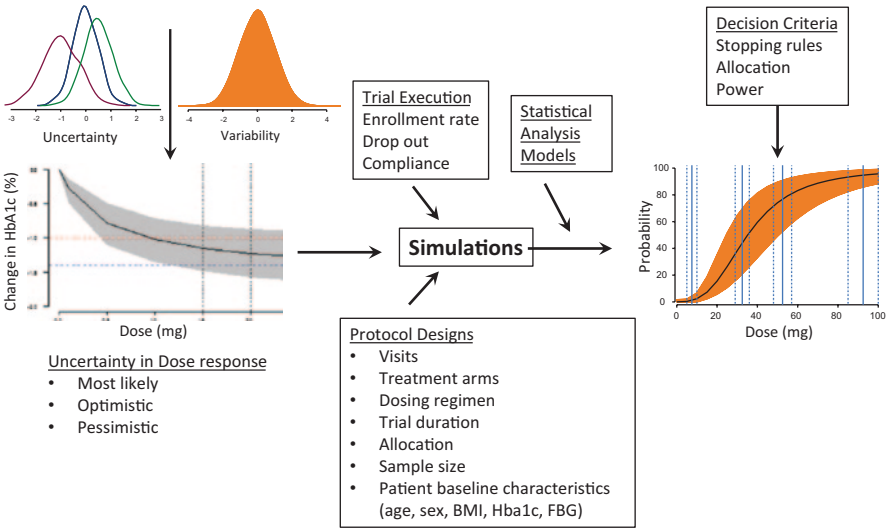

Fig. 5.11 Schematic of application of modeling and simulation for optimum dose selection for an antihyperglycemic agent

Table 5.1 An example statistical analysis output of simulated trial responses

Drug[a]	Predicted HbA1c change from baseline at 12 months (%)	Probability of meeting efficacy target against comparator
Placebo (studied)	−0.08	0.0
Comparator (simulated)	−0.88	NA
Dose 1 (simulated)	−0.26	0.01
Dose 2 (studied)	−0.45	0.2
Dose 3 (simulated)	−0.61	0.38
Dose 4 (studied)	−0.87	0.62
Dose 6 (simulated)[b]	−1.25	0.87
Dose 7 (studied)	−1.5	0.99
Dose 8 (simulated)	−1.9	0.99

HbA1c glycosylated hemoglobin

[a] Indicates if the drug or dose was included in the previous study that generated the data for the model building (studied) or was included only in the simulation exercise (simulated)

[b] Indicates the dose that would be selected for phase 3 confirmatory trial and marketing

egy is to replace trial-and-error methods of testing all reasonable targets preclinically (and many clinically) with an approach that leverages our knowledge of integrated human physiology, and strategically expand our knowledge of physiology, to identify therapeutic strategies that have a higher probability of success. A central part of this approach is mathematical models of human physiology. These ideas can be expanded to include the identification of optimal combination therapy, responder populations, and even personalized medicine (rational drug development). Philo-

sophically, this approach represents a shift from "discovery" to "design." Ultimately, the model-based approaches, through the use of predictive biomarkers, basic science and expert disease knowledge, aim to improve the efficiency and the quality of decision-making in selecting the right targets, drug candidates, dosing range and regimens, optimal clinical trial designs, and a more efficient, more cost-effective development programs with high probabilities of success in drug discovery and development for the treatment and management of diabetes and its comorbidities.

5.7 Key Highlights of the Chapter

- Diabetes is a chronic progressive disease with robust quantitative biomarkers and well understood regulatory/counter-regulatory processes.
- Drug–disease models of varying degrees of complexity can be employed to describe fast biomarkers, slow biomarkers and clinical outcomes with high predictive ability at different stages of drug development.
- Antidiabetic therapies target specific pathways, thus enabling application of mechanistic systems pharmacology models to inform novel therapies.
- Drug–disease models can effectively inform both efficacy and safety aspects of therapeutic interventions.
- Development of drug–disease models should start early in the development program to answer key questions or address uncertainties from early discovery to clinical development in the evaluation of a novel therapy.

References

Ajmera I, Swat M, Laibe C, Le Novère N, Chelliah V (2013) The impact of mathematical modeling on the understanding of diabetes and related complications. CPT: Pharmacometrics Syst Pharmacol 2:e54

American Diabetes Association (2008) Diagnosis and classification of diabetes mellitus. Diabetes Care 31(1):562

Baker DJ, Timmons JA, Greenhaff PL (2005) Glycogen phosphorylase inhibition in type 2 diabetes therapy—a systematic evaluation of metabolic and functional effects in rat skeletal muscle. Diabetes 54:2453–2459

Bergman RN, Ider YZ, Bowden CR, Cobelli C (1979) Quantitative estimation of insulin sensitivity. Am J Physiol 236:E667–E677

Bergman RN, Hope ID, Yang YJ, Watanabe RM, Meador MA, Youn JH, Ader M (1989) Assessment of insulin sensitivity in vivo: a critical review. Diabetes Metab Rev 5:411–429

Chien JY, Sinha VP (2010) The application of drug-disease models in the development of antihyperglycemic agents. In: Kimko HHC, Peck CC (eds) Clinical trial simulations: applications and trends (AAPS advances in the pharmaceutical sciences series) Springer, USA 175–198

Cobelli C, Dalla Man C, Sparacino G, Magni L, De Nicolao G, Kovatchev BP (2009) Diabetes: models, signals, and control. IEEE Rev Biomed Eng 2:54–96

de Winter W, DeJongh J, Post T, Ploeger B, Urquhart R, Moules I, Eckland D, Danhof M (2006) A mechanism-based disease progression model for comparison of long-term effects of piogli-

tazone, metformin and gliclazide on disease processes underlying type 2 diabetes mellitus. J Pharmacokinet Pharmacodyn 33:313–343
Farhy LS, McCall AL (2009) Pancreatic network control of glucagon secretion and counter regulation. Meth Enzymol 467:547–581
Frey N, Laveille C, Paraire M, Francillard M, Holford NH, Jochemsen R (2003) Population PKPD modelling of the long-term hypoglycaemic effect of gliclazide given as a once-a-day modified release (MR) formulation. Br J Clin Pharmacol 55:147–157
Hamrén B, Björk E, Sunzel M, Karlsson MO (2008) Models for plasma glucose, HbA1c, and hemoglobin interrelationships in patients with type 2 diabetes following tesaglitazar treatment. Clin Pharmacol Ther 84(2):228–235
Hetherington J, Sumner T, Seymour RM, Li L, Rey MV, Yamaji S, Saffrey P, Margoninski O, Bogle ID, Finkelstein A, Warner A (2011) A composite computational model of liver glucose homeostasis. I. Building the composite model. J R Soc Interface 9(69):689–700
IDF Report (2013) IDF diabetes atlas, 6th edn. http://www.idf.org/diabetesatlas. Accessed 7 May 2014
Jauslin PM, Silber HE, Frey N, Gieschke R, Simonsson US, Jorga K, Karlsson MO (2007) An integrated glucose-insulin model to describe oral glucose tolerance test data in type 2 diabetics. J Clin Pharmacol 47:1244–1255
Jauslin PM, Frey N, Karlsson MO (2011) Modeling of 24-hour glucose and insulin profiles of patients with type 2 diabetes. J Clin Pharmacol 51:153–164
Kansal AR (2004) Modeling approaches to type 2 diabetes. Diabetes Technol Ther 6(1):39–47
Kim J, Saidel GM, Cabrera ME (2007) Multi-scale computational model of fuel homeostasis during exercise: effect of hormonal control. Ann Biomed Eng 35:69–90
Klinke DJ (2008) Integrating epidemiological data into a mechanistic model of type 2 diabetes: validating the prevalence of virtual patients. Ann Biomed Eng 36(2):321–334
Landersdorfer CB, Jusko WJ (2008) Pharmacokinetic/Pharmacodynamic modelling in diabetes mellitus. Clin Pharmacokin 47(7):417–448
Lesko LJ, Zheng S, Schmidt S (2013) Systems approaches to risk assessment. Clin Pharmacol Ther 93(5):413
Martin WH, Hoover DJ, Armento SJ, Stock IA, McPherson RK, Danley DE, Stevenson RW, Barrett EJ, Treadway JL (1998) Discovery of a human liver glycogen phosphorylase inhibitor that lowers blood glucose in vivo. Proc Natl Acad Sci U S A 95:1776–1781
Møller JB, Overgaard RB, Kjellsson MC, Kristensen NR, Klim S, Ingwersen SH, Karlsson MO (2013) Longitudinal modeling of the relationship between mean plasma glucose and HbA1c following antidiabetic treatments. CPT Pharmacometrics Syst Pharmacol 2:e82
Morghissi ES, Korytkowski MT, DiNardo M, Einhorn D, Hellman R, Hirsch IB, Inzucchi SE, Ismail-Beigi F, Kirkman MS, Umpierez GE (2007) American association of clinical endocrinologists and American diabetes association consensus statement on inpatient glycemic control. Diabetes Care 30(suppl 1):S42–S47
Ribbing J, Hamrén B, Svensson MK, Karlsson MO (2010) A model for glucose, insulin, and beta-cell dynamics in subjects with insulin resistance and patients with type 2 diabetes. J Clin Pharmacol 50:861–872
Schaller S, Willmann S, Lippert J, Schaupp L, Pieber TR, Schuppert A, Eissing T (2013) A generic integrated physiologically based whole-body model of the glucose-insulin-glucagon regulatory system. CPT Pharmacometrics Syst Pharmacol 2(e65):1–10
Schneck KB, Zhang X, Bauer R, Karlsson MO, Sinha VP (2013) Assessment of glycemic response to an oral glucokinase activator in a proof of concept study: application of a semi-mechanistic, integrated glucose-insulin-glucagon model. J Pharmacokinet Pharmacodyn 40:67–80
Shafrir E (2007) Animal models of diabetes, frontiers of research. CRC, Boca Raton, p 365
Shafrir E (2010) Contribution of animal models to the research of the causes of diabetes. World J Diabetes 1(5):137–140
Shoda L, Kreuwel H, Gadkar K, Zheng Y, Whiting C, Atkinson M, Bluestone J, Mathis D, Young D, Ramanujan S (2010) The type 1 diabetes physioLab® platform: a validated physiologically

based mathematical model of pathogenesis in the non-obese diabetic mouse. Clin Exp Immunol 161(2):250–267
Silber HE, Jauslin PM, Frey N, Gieschke R, Simonsson US, Karlsson MO (2007) An integrated model for glucose and insulin regulation in healthy volunteers and type 2 diabetic patients following intravenous glucose provocations. J Clin Pharmacol 47:1159–1171
Silber HE, Frey N, Karlsson MO (2010) An integrated glucose-insulin model to describe oral glucose tolerance test data in healthy volunteers. J Clin Pharmacol 50:246–256
Sumner T, Hetherington J, Seymour RM, Li L, Varela Rey M, Yamaji S, Saffrey P, Margoninski O, Bogle ID, Finkelstein A, Warner A (2011) A composite computational model of liver glucose homeostasis. II. Exploring system behaviour. J R Soc Interface 9(69):701–706
Topp B, Promislow K, deVries G, Miura RM, Finegood DT (2000) A model of beta-cell mass, insulin, and glucose kinetics: pathways to diabetes. J Theor Biol 206:605–619
Torres TP, Sasaki N, Donahue EP, Lacy B, Printz RL, Cherrington AD, Treadway JL, Shiota M (2011) Impact of a glycogen phosphorylase inhibitor and metformin on basal and glucagon-stimulated hepatic glucose flux in conscious dogs. J Pharmacol Exp Ther 337(3):610–620
Verspohl EJ (2012) Novel pharmacological approaches to the treatment of type 2 diabetes. Pharmacol Rev 64(2):188–237
Vlasakakis G, Pasqua OD (2013) Cardiovascular disease: the other face of diabetes. CPT Pharmacometrics Syst Pharmacol 2:e81
Waters SB, Topp BG, Siler SQ, Alexander CM (2009) Treatment with sitagliptin or metformin does not increase body weight despite predicted reductions in urinary glucose excretion. J Diabetes Sci Technol 3(1):68–82
WHO fact sheet number 310. http://www.who.int/mediacentre/factsheets/fs310/en/. Accessed 7 May 2014
Woodcock J, Woosley R (2008) The FDA critical path initiative and its influence on new drug development. Ann Rev Med 59:1–12
Zhang X, Schneck K, Bue-Valleskey J, Yeo KP, Heathman M, Sinha V (2013) Dose selection using a semi-mechanistic integrated glucose-insulin-glucagon model: designing phase 2 trials for a novel oral glucokinase activator. J Pharmacokinet Pharmacodyn 40:53–65

Chapter 6
Applied Pharmacometrics in the Obese Population

Anne van Rongen, Margreke J. E. Brill, Jeroen Diepstraten and Catherijne A. J. Knibbe

6.1 Introduction

Obesity (body mass index, BMI > 30 kg/m^2) and morbid obesity (BMI > 40 kg/m^2) are associated with several (patho)physiological changes, such as increased cardiac output, circulating blood volume and liver blood flow, decreased pulmonary function reflected by forced vital capacity and expiratory volume and an initial increase but later on a decrease in renal function (Lemmens et al. 2006; Maric-Bilkan 2013; Marik and Varon 1998; Wehrmeister et al. 2012). As a result of all these (patho) physiological changes, the pharmacokinetic (PK) and/or pharmacodynamic (PD) profile of drugs in obese individuals may be altered, thereby necessitating adapted dosing algorithms. Until recently, the obese population was hardly studied in pharmacometric analyses. The influence of obesity on PK and PD parameters has received more attention, given the strong rise in obesity incidence and prevalence across the world.

In order to derive evidence-based dosing guidelines for morbidly obese and obese individuals, the influence of obesity on both the PK and PD parameters should be considered. The PK parameter clearance (CL) should especially receive much attention, as clearance determines the maintenance dose. Volume of distribution (V) determines the loading dose and is of interest when peak concentrations are known to be related to efficacy or safety endpoints. Concerning the PD parameters, only a very limited number of studies are available. PD parameters of interest may include drug concentration at half-maximal effect (EC_{50}), maximal effect (E_{max}) and/or baseline (E_0).

PK studies have shown that the impact of obesity on drug clearance differs largely, and is dependent on the metabolic or elimination pathway of the investigated drug (Brill et al. 2012; Kotlyar and Carson 1999). More specifically, CYP3A4-mediated

C. A. J. Knibbe (✉) · A. van Rongen · M. J. E. Brill · J. Diepstraten
Department of Clinical Pharmacy, St. Antonius Hospital, P.O. Box 2500,
3430 EM Nieuwegein, The Netherlands
e-mail: c.knibbe@antoniusziekenhuis.nl

S. Schmidt, H. Derendorf (eds.), *Applied Pharmacometrics,* AAPS Advances in the Pharmaceutical Sciences Series 14, DOI 10.1007/978-1-4939-1304-6_6

drug elimination was found to be consistently lower in obese subjects compared to non-obese subjects, while UGT-, CYP2E1-, arylamine N-acetyltransferase type 2- and xanthine oxidase-mediated drug metabolism was consistently higher among obese subjects as compared with non-obese subjects. Clearance mediated by CYP1A2, CYP2C9, CYP2C19 and CYP2D6 show trends towards higher clearance values in obese individuals. Studies on drug clearance mediated by liver blood flow are somewhat inconclusive, although, on the basis of a few highly extracted drugs, an increase in liver blood flow can be noted in obese patients. Regarding drug elimination, the reviewed studies show an increase of glomerular filtration and tubular secretion in obese patients. The influence of obesity on tubular reabsorption is unknown (Brill et al. 2012; Kotlyar and Carson 1999).

While the impact of obesity on PD parameters has typically received less attention, there are indications that the PD profile of the drug and/or the disorder may be altered in obese individuals. For instance, obese patients showed increased pain experience as compared to non-obese patients (Stone and Broderick 2012), and the relative risk for pulmonary embolism in hospitalized patients was more than two times higher in obese patients compared to non-obese patients (Stein et al. 2011).

Despite a general idea on how the PK and PD profiles of drugs change with obesity, many aspects remain unknown. More specifically, the exact quantification of these changes with increasing body weight is lacking, which is of particular relevance, given the fact that body weights of (morbidly) obese patients are still increasing. Moreover, from the covariates that are often considered, such as BMI, total body weight (TBW) or lean body weight (LBW), it is unknown which covariate is the most predictive for obesity-related changes in PK and PD parameters for a specific drug. As the identification of predictive covariates for variability provides the scientific basis for rational and individualized dosing schemes, studies in which these covariates are identified and quantified are of utmost relevance.

Therefore, in this chapter we aim to provide general information on the currently used body size descriptors for obesity together with a literature overview of currently published equations to quantify obesity-related changes in PK and PD parameters including how they were validated. Finally, future directions are given for the execution of clinical trials in (morbidly) obese patients and the modelling of obesity-related changes in population PK and PD studies.

6.2 Body Size Descriptors

Various body size descriptors are available to characterize the influence of obesity on PK and PD parameters. In Table 6.1, an overview of the different size descriptors can be found including the equation(s) used to calculate the body size descriptor. BMI is the international metric recommended to classify obesity, e.g. BMI higher than 30 kg/m^2 is obese and higher than 40 kg/m^2 is morbidly obese (World Health Organisation 1997). However, as BMI cannot differentiate adipose tissue from muscle mass and has only an approximate relationship to excess body fat, BMI should

Table 6.1 Body size descriptors capturing obesity-related changes in the human body

Abbreviation	Size descriptor	Equation	Reference	Application
TBW	Total body weight (kg)	Kilograms	*Not applicable*	All
BMI	Body mass index (kg/m^2)	BMI=TBW / HT^2(m)	Keys et al. (1972)	Li et al. (2010); Fukuchi et al. (2009); van Kralingen et al. (2011); Cortinez et al. (2010); Barras et al. (2009); Barrett et al. (2001); Schmitt et al. (2009); Ekhart et al. (2009); Pai and Lodise (2011); Thomson et al. (2009); Nguyen et al. (2006); Hall et al. (2011); Bardin et al. (2012); Hall et al. (2012); Slepchenko et al. (2003); Cortinez et al. (2011)
BSA	Body surface area (m^2)	$BSA = TBW^{0.425} \times HT(cm)^{0.725} \times 0.007184$	Dubois and Dubois (1916)	Schmitt et al. (2009)
	Body surface area (m^2)	$BSA = \sqrt{\frac{TBW \times HT(cm)}{3600}}$	Mosteller (1987)	Green and Duffull (2003)
IBW	Ideal body weight (kg)	$IBW(male) = 50 + 0.89 \times (HT(cm) - 152.4)$[a] $IBW(female) = 45.5 + 0.89 \times (HT(cm) - 152.4)$[a]	Devine (1974)	Pai and Lodise (2011); Nguyen et al. (2006)
	Ideal body weight (kg)	$IBW(male) = 50 + \frac{2.3}{2.5} \times (HT - 152)$ (cm) $IBW(female) = 45 + \frac{2.3}{2.5} \times (HT - 152)$ (cm)	Rowland and Tozer (1995)	Barrett et al. (2001)
	Ideal body weight (kg)	$IBW(male) = HT(cm) - 100 - \frac{(HT(cm) - 150)}{4}$ $IBW(female) = HT(cm) - 100 - \frac{(HT(cm) - 150)}{2}$	Lorentz (1929)	Benezet et al. (1997)

Table 6.1 (continued)

Abbreviation	Size descriptor	Equation	Reference	Application
IBW%	Ideal body weight percentage (%)	$PIBW = \frac{TBW - IBW}{IBW} \times 100$	*Not applicable*	Barrett et al. (2001)
LBW	Lean body weight or fat-free mass (kg)	$LBW = FFM(male) = \frac{9.27 \times 10^3 \times TBW}{6.68 \times 10^3 + 216 \times BMI}$ $LBW = FFM(female) = \frac{9.27 \times 10^3 \times TBW}{8.78 \times 10^3 + 244 \times BMI}$	Janmahasatian et al. (2005)	Li et al. (2010); van Kralingen et al. (2011); Barras et al. (2009); Pai and Lodise (2011); Bardin et al. (2012)
FFM	Fat-free mass (kg)	$LBW = FFM(male) = TBW \times (1 - 0.715) + (12.1 \times HT^2(m))$ $LBW = FFM(female) = TBW \times (1 - 0.713) + (9.74 \times HT^2(m))$	Garrow and Webster (1985)	Ekhart et al. (2009)
LBM=LBW	Lean body mass (kg)	$LBW = LBM(male) = 1.1 \times TBW - 0.0128 \times BMI \times TBW$ $LBW = LBM(female) = 1.07 \times TBW - 0.0148 \times BMI \times TBW$	James (1976)	Ekhart et al. (2009); Egan et al. (1998); Cortinez et al. (2010); Green and Duffull (2003)
ABW or AIBW	Adjusted body weight(kg)	$ABW = IBW + corr \times (TBW - IBW)$ ($corr$ =correction factor, e.g. 0.4 for aminoglycoside dosing)	Bauer et al. (1983)	Pai and Lodise (2011); Ekhart et al. (2009); Nguyen et al. (2006)

cm centimeter *HT* height, *kg* kilograms, *m* meter

[a] The factor 0.89 in this equation may also be 0.906

not be considered as measure of *body composition* but rather as descriptor of *body shape* (Green and Duffull 2004). While TBW is mostly used to dose drugs, it is influenced by age, sex, height, muscles and obesity, and therefore should be used with caution as body size descriptor of obesity. LBW is calculated by subtracting body fat weight from TBW and represents the weight of bones, muscles, tendons and organs without body fat (i.e. fat-free mass). To calculate LBW, not only body weight but also height and gender are required. As such, LBW has been suggested as measure of changes in *body composition* (Han et al. 2007). The most recent LBW equation as published by Janmahasatian et al. was reported to provide good predictive performance of the fat-free mass measured with bioelectrical impedance analysis (BIA) or dual-energy x-ray absorptiometry (DXA) (Janmahasatian et al. 2005). Therefore, it is proposed to use the Janmahasatian equation when LBW is considered (Table 6.1). In addition to BMI, TBW and LBW, many more size descriptors, such as ideal body weight (IBW) and adjusted body weight (ABW) have been used in obesity pharmacology, albeit using different definitions. For IBW, the equation of Devine is mainly applied (Table 6.1). The equation to calculate ABW is an empirical formula in which different correction factors can be used and was originally developed for dosing of aminoglycosides (Bauer et al. 1983).

It is emphasized that other covariates such as age and race may interfere with body size descriptors, i.e. elderly and Asians may have lower body weights and heights compared to young adult Caucasians. Therefore, it is important to consider the type of population when using the body size descriptors of Table 6.1.

6.3 Quantification of Obesity-Associated Changes in PK and PD Parameters

6.3.1 Aim

In this paragraph, we aim to provide an overview of reported functions quantifying obesity-related changes in PK and PD parameters of different drugs with specific emphasis on model evaluation in terms of predictive value, internal validation and external validation.

6.3.2 Methods

The PubMed database was used for a literature search for PK/PD modelling in the obese adult population. The following search terms were used:

- Obesity [MeSH Terms] AND population pharmacokinetics [All Fields]. Limits: Humans and English, yielding 167 results on August 6, 2012.

- Obesity [All Fields] AND model [All Fields] and human [All Fields] resulted in 229 hits on November 5, 2012.
- Obesity [All Fields] AND pharmacokinetics [All Fields] AND Nonmem [All Fields] resulted in 17 hits on November 5, 2012.

Individual papers were retrieved from the results and completed with studies referred to in the review by Brill et al. (Brill et al. 2012). Then, the following inclusion and exclusion criteria were applied.

- Inclusion criteria:
  - (Morbidly) obese patients in the studied population
  - Application of population PK–PD software (NONMEM, Monolix, Adapt 5)
  - English language
  - Adult population
- Exclusion criteria:
  - Absence of a covariate analysis quantifying obesity-associated influence on PK and/or PD parameters
  - Children and adolescents

6.3.3 Results

In Tables 6.2 and 6.3 an overview of 20 published studies of which 19 PK analyses, two PK/PD analyses and one PD analysis in obese subjects is presented. The PK studies are divided by the metabolic- or renal-elimination pathway of the studied drug, and separate columns for equations for clearance and volume of distribution are provided. For all models, model evaluation in terms of predictive value, internal validation and external validation are summarized (Tables 6.2 and 6.3).

6.3.3.1 Obesity-Related Changes in Clearance

In this section, the influence of obesity on clearance subdivided by metabolic or elimination pathway (CYP3A, liver blood flow, glomerular filtration rate (GFR) and other metabolic pathways) is discussed. Subsection ‘other metabolic pathways’ consists of studies of drugs metabolized by a pathway for which only one study was available.

CYP3A-mediated Clearance

Clearance of the CYP3A substrate, taranabant, was found to decrease with BMI according to a power function with an exponent of −1.11 in a study evaluating

Table 6.2 Population pharmacokinetic studies with obese patients

Drug	Population (mean±SD (range))[a]	Model and methods	Size descriptors and function (power, linear or allometric)	CL	V	Predictive value	Internal validation	External validation	Comments
CYP3A									
Taranabant (Li et al. 2010)	187 non-obese healthy volunteers TBW 74.3±12.0 kg (50.0–111) BMI 25±3.2 kg/m^2 (18.9–34.3) Age 34±12 y (18–69) 385 obese pts TBW 97.1±14.4 kg (67.5–151) BMI 35.4±3.8 kg/m^2 (28.4–43.4) Age 42±10 y (21–65)	Nonmem Single and multiple oral doses (range 0.5–8 mg) 3-CMT model	CL/F: BMI (power) Vp2/F BMI (power)	CL/F (L/h)=25.4×(BMI/31.5)$^{-1.11}$+0.0668×(CrCL−80.6)	Vp2/F (L)=2130×(BMI/31.5)$^{1.38}$+752×(age/39)$^{2.10}$+643×SEX+1 2.5×(CrCL-80.6) Sex=0 if male Sex=1 if female	DV vs. PRED DV vs. IPRED	VPC	No	Poor performance for peak-plasma concentrations; Adequate performance for simulating 24-h trough concentrations for exposure-response analyses of efficacy and safety; Covariates clinically not relevant;
Amiodarone (also CYP2C8) (Fukuchi et al. 2009	23 Japanese non-obese and obese pts TBW 63.8±10 kg (42.2–79.4) BMI 23.8±2.95 kg/m^2 (17.6–31.4) Age 59±12 y (26–82)	Nonmem V Single and multiple oral doses (mean 2.34 mg/kg/d, range 1.39–8.08) 1-CMT model	CL: TBW (linear) if BMI≥25 22% decrease V: TBW (linear)	CL (L/h)=0.16 s×TBW×0.53$^{age\geq 65}$× 0.78$^{BMI\geq 25}$×DD$^{0.51}$ BMI<25=0 BMI≥25=1 Age< 65=0 Age≥65=1	V (L)=10.2× TBW	DV vs. PRED or IPRED	No	No	Definition of obesity: BMI ≥ 25 and/or pts with body fat percentage (BFP) value of 23 % for males or 28 % for females; V was difficult to estimate due to lack of blood samples directly after administration

Table 6.2 (continued)

Drug	Population (mean±SD (range))[a]	Model and methods	Size descriptors and function (power, linear or allometric)	CL	V	Predictive value	Internal validation	External validation	Comments
Liver blood flow									
Propofol (van Kralingen et al. 2011)	44 non-obese pts TBW 74±11 kg (55–98) BMI 25±4 kg/m^2 Age 52±12 y 20 obese pts TBW 124±20 kg (98–167) BMI 43±6 kg/m^2 Age 45±12 y	Nonmem VI IV bolus and continues infusion 3-CMT model	CL: TBW (power) V: No covariates identified	CL (L/min)=2.22×(TBW/70)$^{0.67}$	–	DV vs. PRED DV vs. IPRED	Bootstrap	No	Size descriptors TBW, IBW, BMI and LBW (Janmahasatian et al. 2005) were tested as covariates for V; Other studies suggest linear and allometric relationships between TBW and V. Larger datasets or different sampling schemes are needed to identify a influence of TBW on V or that factors other than TBW contribute to the large interindividual variability on V
Propofol (Cortinez et al. 2010)	24 non-obese and 27 obese pts TBW 93±24 kg (44–160) BMI 33±9 kg/m^2 (16–52) Age 46±16 y (25–81)	Nonmem VI IV bolus and continues infusion 3-CMT model	CL: TBW (allometric, 0.75 fixed) Vc, Vp_1, Vp_2 TBW (linear, fixed)	CL (L/min)=1.92×(TBW/70)$^{0.75}$	Vc (L)=4.48×(TBW/70) Vp_1 (L)=21.2×(TBW/70)×EXP(−0.0164×(Age-50)) Vp_2 (L)=237× (TBW/70)	No	PC-VPC	No	Vp_2, Vp_1 and Q_2 were difficult to estimate precisely due to relatively short infusion period and post-infusion sampling
Sufentanil (Slepchenko et al. 2003)	11 obese pts TBW 125.4±23.3 kg (82–155) BMI 45±6.5 kg/m^2 (35.0–52.6) Age 39±11 y (24–55)	Nonmem TCI dosing (0.4 ng/ml) 2-CMT model	No covariates identified	(CL: tended to increase with BMI)	–	DV vs. PRED	No	No	Size descriptors TBW and BMI were tested for CL and V

Table 6.2 (continued)

Drug	Population (mean±SD (range))[a]	Model and methods	Size descriptors and function (power, linear or allometric)	CL	V	Predictive value	Internal validation	External validation	Comments
GFR									
Enoxaparin (Barras et al. 2009)	118 non-obese and obese pts Median TBW 77 kg (43–120) Median age 61 y (23–91) 11 pts TBW ≥ 100 kg	Nonmem V FOCE method with interaction Dose according to label or individualized dose according to TBW (pts<100 kg) twice daily 1 mg/kg or LBW (pts ≥ 100 kg) twice daily 1.5 mg/kg 2-CMT model	CL: LBW (linear) (Janmahasatian et al. 2005) Vc: LBW (linear) (Janmahasatian et al. 2005) LBW equation (Janmahasatian 2005)	CL (L/h)=0.3×(CLcr/70) + 0.42×(LBW/55) (Janmahasatian et al. 2005) CLcr: CG equation with LBW (Janmahasatian et al. 2005)	Vc (L)=3.43×(LBW/55) (Janmahasatian et al. 2005)	Eta vs. LBW	VPC Bootstrap	No	Obesity defined as ≥100 kg; Individualized dosing of enoxaparin based upon LBW and renal function reduces the risk of major bruising or bleeding events
Enoxaparin (Green and Duffull 2003)	96 non-obese and obese pts TBW 85.0±20.5 kg (41–160) BMI 28.1±6.27 kg/m^2 (15.0–44.9) Age 56±17 y n=32 BMI<25 n=31 BMI 25–30 n=33 BMI>30	Nonmem V FO estimation method Twice daily SC bolus (100 IU/kg) or once daily (4000 IU) 2-CMT model	CL: LBW (linear) (Morgan and Bray 1994) Vc: TBW (linear) LBW equation (James et al. 1976)	CL (L/h)=1.03×(LBW/70) (Morgan and Bray 1994)	Vc (L)=3.67×(TBW/70)	PRED vs. WRES	No	No	

Table 6.2 (continued)

Drug	Population (mean±SD (range))[a]	Model and methods	Size descriptors and function (power, linear or allometric)	CL	V	Predictive value	Internal validation	External validation	Comments
Tinzaparin (Barrett et al. 2001)	157 non-obese and 30 obese pts TBW 76.6±18.4 kg (37–151) BMI 26.4±6.6 kg/m^2 (14.4–52.1) Age 63±17 y (21–92)	Nonmem VI FO estimation method Single daily SC bolus (175 IU/kg) 2-CMT model	CL: % IBW-median % IBW (power) Vc: No covariates tested IBW equation (ref Rowland and Tozer)	CL(L/h/kg)=0.0176 EXP((Scr-median Scr)×−0.213)×EXP((%IBW-median (Rowland and Tozer 1995) % IBW)×− 0.006)	–	DV vs. PRED DV vs. IPRED IWRES vs. IPRED WRES vs. Time	No	Yes; model building 70 % of dataset. External validation 30 % of dataset	The magnitude of the effect of obesity and renal function on anti-Xa activity seem not significant enough to warrant dose adjustment across the range of body size and renal function studied
Carboplatin (Ekhart et al. 2009)	240 non-obese and obese pts Median TBW 70 kg (46–170) Median BMI 24 kg/m^2 (16–46) Median age 47 y (16–75) n=7 BMI< 18.5 n=146 BMI 18.5–25 n=72 BMI 25–30 n is 15 BMI>30	Nonmem VI FOCE with interaction Varying doses 2-CMT model	CL: no covariates identified V: no covariates tested	–	–	No	No	No	No influence of the size descriptors TBW, IBW (Devine 1974), AIBW (Bauer et al. 1983), FFM (Garrow and Webster 1985), LBM (James et al. 1976), BMI and Benezet equation ((IBW + TBW)/2) on CL, nor CG-equation with these size descriptors

Table 6.2 (continued)

Drug	Population (mean±SD (range))[a]	Model and methods	Size descriptors and function (power, linear or allometric)	CL	V	Predictive value	Internal validation	External validation	Comments
Carboplatin (Schmitt et al. 2009)	357 non-obese and obese pts TBW 65 kg (40–137) Age 60 years (21–87) n=43 BMI ≥ 30 n=285 BMI 18.5–30 n=29 BMI<18.5	Nonmem VI FOCE with interaction IV infusion (30 or 60 min) 2-CMT model	CL: TBW (power) V: no covariates tested	CL (mL/min)=117.8×(Scr/75)$^{0.450}$×(cysC/1.0)$^{-0.385}$×(TBW/65)$^{0.504}$×(age/56)$^{-0.366}$×0.847^{sex} Sex=0 if male Sex=1 if female	–	CWRES vs. Time DV vs. PRED CL values MPE and MAP shrinkage reported	Bootstrap of covariate model (357 pts)	No	Equation for CL was stated as the 'modified Thomas formula' by the authors; V was not estimated, but assumed from PK analysis including extra database with 143 pts, 68 kg (40–112) with rich sampling; volumes were fixed proportional to BSA; Covariate testing only for 357 individuals
Carboplatin (Benezet et al.1997)	25 obese pts TBW range 65–112 kg Age range 23–82 y Pts 120–167 % kg (median 136 %) of IBW (Lorentz 1929)	Nonmem IV IV infusion (1 h) 2-CMT model	CL: IBW (linear) TBW-IBW (linear) V: no covariates tested	CL (mL/min)=(0.134 + (218×(1 − 0.00475×age)×(1 − 0.314×sex))/Scr)×(IBW + 0.512×(TBW-IBW)) Sex=0 if male Sex=1 if female	–	No only: 'Calculated' vs. 'Actual' CL value	No	No	Aim was to determine the best value of substitution for weight in the Chatelut formula for a subpopulation of obese patients defined ≥ 20 % IBW
Ethambutol (Hall et al. 2012)	18 non-obese and obese volunteers Median TBW 90.8 kg (45.6–160.4) Age 36.6±11.3 y n=6 BMI<25 n=6 BMI 25–40 n=6 BMI>40	ADAPT 5 MLEM algorithm Single oral dose (1600 mg) 2-CMT model	IBW equation (ref Lorentz) CL: TBW (allometric, 0.75 fixed) V: no covariates identified	CL (L/h)=42.6×(TBW/45.6)$^{0.75}$	–	DV vs. IPRED (base model only)	No	No	Renal excreted as unchanged drug and converted by alcohol dehydrogenase (ADH) to inactive metabolites; Size descriptors TBW and BMI were tested for V; CrCl was not a significant covariate with any of the PK parameter

Table 6.2 (continued)

Drug	Population (mean±SD (range))[a]	Model and methods	Size descriptors and function (power, linear or allometric)	CL	V	Predictive value	Internal validation	External validation	Comments
Metformin (Bardin et al. 2012)	105 non-obese and obese pts TBW 89.2 kg (49–149 kg) BMI 31.87 kg/m^2 (20.5–51) Age 62 y (34–87) n=15 BMI 20–25 n=34 BMI 25–30 n=24 BMI 30–35 n=20 BMI 35–40 n=6 BMI 40–45 n=5 BMI 45–50 n=1 BMI 50–55	Monolix 3.1 s SAEM algorithm combined with a MCMC procedure Single and multiple oral doses (range 500–3000 mg/day (1000 mg/8 h)) Pts were in steady state Open 1-CMT model	CL/F: LBW (power, 0.75 fixed) V/F: LBW (linear, 1 fixed) LBW equation (ref Janmahasatian)	CL/F (L/h)=56×(LBW/60)$^{0.75}$×(age/60)$^{-1.17}$×(SCr/90)$^{-0.28}$	V/F (L)=558×(LBW/60)[1]	DV vs. PRED	NPDE VPC	No	Sparse sampling (Two blood samples per patient); The design of the study did not allow to distinguish between different allometric exponents for LBW, the 0.75 exponent was retained on basis of a very small difference in the criterion values; Metformin is primarily eliminated via active tubular excretion
Oseltamivir/ oseltamivir carboxylate (Pai and Lodise 2011)	21 healthy obese volunteers Median TBW 122 kg (106–159) Median BMI 43.7 kg/m^2 (40–54.4) Median age 36 y (19–50)	ADAPT 5 MLEM algorithm of Schumitzky and Walker Single and multiple oral dose study (75 mg twice daily for several days) 2-CMT parent model 1-CMT metabolite model	No covariates identified	–	–	DV vs. PRED	Posterior predictive check	No	No influence of size descriptor TBW and CG equation based on LBW (Janmahasatian et al. 2005), IBW (Devine 1974), ABW (Bauer et al. 1983) or TBW for CL/F (parent and active metabolite); No influence of size descriptors TBW, IBW (Devine 1974) or ABW (Bauer et al. 1983) for V/F (parent and active metabolite); Results of this study indicate that oseltamivir dose adjustments are not required for individuals with obesity

Table 6.2 (continued)

Drug	Population (mean±SD (range))[a]	Model and methods	Size descriptors and function (power, linear or allometric)	CL	V	Predictive value	Internal validation	External validation	Comments
Vancomycin (Thomson et al. 2009)	398 non-obese and obese pts Median TBW 72 kg (40–159) Median Age 66 y (16–97) 19 % pts BMI>30	Nonmem VI FOCE with interaction IV infusion 2-CMT model	Vc: TBW Vp: TBW	CL(L/h)=2.99 + (0.0154×Clcr)	Relations not reported	DV vs. PRED	Bootstrap	No	The new dosage guidelines lead to a greater risk of vancomycin trough concentrations accumulating above 15 mg/L, especially after day 3. Monitoring vancomycin concentrations is needed within the first 3 days to avoid excessive accumulation and potential for toxicity.However, troughs of 15–20 mg/L may also simply reflect the flatter profile that the new guidelines aim to achieve
Other metabolic/elimination pathways									
Extrahepatic metabolism in blood and tissue by nonspecific esterases									
Remifentanil (Egan et al. 1998)	12 non-obese pts TBW 64±10 kg (49–82) Age 38±7 y 12 obese pts TBW 113±17 kg (84–140) Age 38±8 y	Nonmem FOCE with interaction IV bolus (over 1 min) 2-CMT model	CL: LBM (linear) Vc: LBM (linear) (Morgan) Vp: LBM (linear) (LBM equation (ref James 1976))	CL(L/min)=1.88 + (0.0185×LBM	Vc (L)=− 0.0731 + (0.121×LBM) Vp (L)=− 0.0713 + (0.165×LBM)	WRES vs. Time	No	No	The model is less accurate as time passes and it slightly under-predicts the measured concentrations (evidenced by slight trend toward an overall positive WRES); The inclusion of LBM is statistically justified, but the clinical relevance is debated by authors

Table 6.2 (continued)

Drug	Population (mean±SD (range))[a]	Model and methods	Size descriptors and function (power, linear or allometric)	CL	V	Predictive value	Internal validation	External validation	Comments
Various metabolic pathways									
Micafungin (Hall et al. 2011)	36 non-obese and obese volunteers Median TBW 97 kg (43–155) Mean age 40±15 y	ADAPT 5 MLEM algorithm IV infusion (over 60 min) 2-CMT model	CL:TBW (allometric) V: no covariates identified	$CL(L/h)=1.04\times(TBW/66)^{0.75}$	–	DV vs. IPRED TBW vs. CL	No	No	Micafungin is metabolized by arylsulfatase and secondarily by COMT (catechol-O-methyltransferase); Volunteers between 43 and 66 kg were left out of covariate model for CL; Size descriptor TBW was tested as covariate for V;
UGT and sulphate conjugation									
Garenoxa cin (Van Wart et al. 2004)	384 non-obese and 196 obese pts TBW 79.3±21.3 kg (34–178) Age 50±17 y (18–88)	Nonmem V FO method Single oral daily dose (400 mg) for 5 to 10 days 1-CMT model	CL: IBW (lineair) V: TBW (power)	$CL(mL/min)=[83.4\times(CrCl/86.9)^{0.436}+0.764\times(IBW-64.2)+10.9\times obese+0.301\times(age-49.5)]\times(1-0.144\times Pseu)$ Obese IBW<130 %=0 IBW>130 %=1 $Pseu_{jk}$ None=0 Use of pseudoephedrine=1	$V(L)=67.1\times(TBW/79.3)^{0.635}+17.7\times sex$ Sex=0 if female Sex=1 if male	DV vs. PRED	No	Yes (n=141)	Low concentrations (< 2 mg/L) were over-predicted and small degree of under-prediction for concentrations>8 mg/L by final model Garenoxacin exposure was 25 % higher for pts with moderate renal function, but does not appear to be clinically significant as exposures in this population were no significant predictors of AE occurrence

Table 6.2 (continued)

Drug	Population (mean±SD (range))[a]	Model and methods	Size descriptors and function (power, linear or allometric)	CL	V	Predictive value	Internal validation	External validation	Comments
GSTA1									
Busulfan (Nguyen et al. 2006)	103 non-obese and obese pts TBW 79.5±18.7 kg (41–125) BMI 26.9±5.83 kg/m^2 (15.3–46.9) Age 39±11 y (47–95)	Nonmem V FOCE method Multiple IV infusion (over 2 h) every 6 h over 4 days 1-CMT model	CL: BSA (linear) V: TBW (linear)	CL (L/h)=5.96×BSA	V (L)=0.870×TBW	DV vs. IPRED or PRED	No	Yes (n=24)	Dosing should be based on BSA or AIBW (Bauer et al. 1983) using these size descriptors, no dose adjustments are needed

% IBW=(TBW−IBW)/IBW×100), *ABW* adjusted body weight, *AIBW* adjusted ideal body weight (kg), *AUC* area under curve, *BMI* body mass index (kg/m2), *BSA* body surface area (m2), *cAUC* cumulative area under the curve, *CG* Cockroft and Gault, *CL* clearance, *CI* confidence interval, *CMT* compartment, *CrCL* creatinine clearance calculated by Cockroft and Gault formula using TBW (or assumed to be TBW when nothing is mentioned in text), unless otherwise stated, *cysC* cystatin C (mg/L), DV dependent variable, *EXP* exponential function, e^x, *F* bioavailability, *FFM* fat-free mass (kg), *FOCE* first-order conditional estimation, *IBW* ideal body weight (kg), *LBW* lean body weight (kg), *LBM* lean body mass (kg), *MCMC* Markov Chain Monte Carlo, *MLEM* maximum-likelihood solution via the expectation-maximization algorithm, *NPDE* normalized prediction distribution error, P probability, *PD* pharmacodynamics, *PK* pharmacokinetics, *Pts* patients, *SAEM* stochastic approximation expectation maximization, *Scr* serum creatinine (μmol/L), *TBW* total body weight (kg), *V* volume of distribution, *Vc* central volume compartment, *Vp* peripheral volume compartment, *VPC* visual predictive check

[a] Unless otherwise stated

Table 6.3 Population pharmacodynamic studies with obese patients

Drug	Population[a]	Model & methods	Covariates	Effect parameter	Predictive value	Internal validation	External validation	Comments
Enoxaprin (Barras et al. 2009)	103 non-obese and obese pts Median TBW 77 kg (43–120) Median age 61 years (23–91)	Nonmem V FOCE method with interaction PD endpoint: bleeding/bruising events 3-category proportional odds model	Age and cAUC (linear)	Logit (P[S=1])=2.83 − 2.75×(Age/61) − 0.536×(cAUC/23) Logit (P[S=2])=Logit (P[S=1]) + 2.05 Event categories S=1 if no event S=2 if minor buising S=3 if major bruising or bleeding	No	Bootstrap	No	Individualized dosing of enoxaparin based upon LBW (Janmahasatian et al. 2005) (for PK) and renal function reduces the risk of major bruising or bleeding events; Traditional binary data analyses require extensive data and a total of 63 events may be considered small to assess confidence bootstrapped PD data
Propofol (van Kralingen et al. 2011)	44 non-obese pts TBW 74±11 kg (55–98) BMI 25±4 kg/m^2 Age 52±12 years20 obese pts TBW 124±20 kg (98–167) BMI 43±6 kg/m^2 Age 45±12 years	Nonmem VI PD endpoint: BIS values Sigmoid E_{max} model	No covariates identified	Effect=92.2 − (62.1×Ce$^{8.76}$)/(2.12 + Ce$^{8.76}$)	DV vs. IPRED BIS DV vs. PRED BIS	Bootstrap	No	
Sevoflurane (Cortinez et al. 2011)	15 non-obese pts TBW 68±7 kg (60–80) BMI 24±0.8 kg/m^2 (23–25) Age 34±8 years (20–47) 15 obese pts TBW 102±13 kg (82–120) BMI 39±4.1 kg/m^2 (35–49) Age 31±7 years (20–44)	Nonmem VI FOCE method with interaction PD endpoint: BIS values PK: sevoflurane end-tidal concentrations Sigmoid E_{max} model	No covariates identified	Effect=62.7 + (33.8 − 62.7)×(Ce$^{5.73}$/(Ce$^{5.73}$ + 1.52$^{5.73}$))	DV vs. PRED or IPRED effect concentration	No	No	To avoid interference with BIS measurements by surgical stimulation, study measurements were performed after the surgery was finished BMI and PEEP tested were tested as covariates

AUC area under (time-concentration) curve; *BIS* bispectral index; *BMI* body mass index; Ce concentration at effect site; *FOCE* first-order conditional estimation; *PD* pharmacodynamics; *PK* pharmacokinetics ; *TBW* total body weight

patients between 50 and 151 kg (Li et al. 2010). However, the covariates found for taranabant clearance and volume of distribution were not considered clinically relevant. Total clearance of amiodarone, which is primarily metabolized through CYP3A but for which CYP2C8 is involved as well, was 22 % lower in overweight patients (BMI >25), while within the same equation a linear increase with total body weight was reported (Fukuchi et al. 2009). It is emphasized, however, that this amiodarone study was performed in obese Japanese patients with substantially lower BMIs than in most obese Caucasian studies (Table 6.2). Even though only two studies were found on the influence of obesity on CYP3A-mediated drug clearance, the results indicate that the clearance of CYP3A substrates may decrease with increasing BMI or TBW.

Liver Blood Flow-Dependent Clearance

Three studies were found on drugs for which clearance is mainly dependent on liver blood flow (Table 6.2). Both reports on propofol identified an increase in propofol clearance with TBW in an allometric manner. Van Kralingen et al. estimated an exponent of 0.67, while Cortinez et al. used a fixed exponent of 0.75 (van Kralingen et al. 2011; Cortinez et al. 2010). Both studies included both non-obese and (morbidly) obese individuals in their analyses.

For sufentanil, only a nonsignificant trend towards a positive influence of BMI on clearance was found in a population with a wide range in TBW (82–155 kg). However, this analysis only included 11 obese subjects.

Clearance Through Glomerular Filtration Rate (GFR)

A total of ten studies on drugs primarily cleared via glomerular filtration were identified and presented in Table 6.2. Seven papers found a significant influence of a body size descriptor on drug clearance of which six identified an increase and one a decrease. For enoxaparin, in two studies a linear increase in clearance with LBW was identified in patients varying in bodyweight between 41 and 160 kg (Barras et al. 2009; Green and Duffull 2003). However, for tinzaparin, a decrease in clearance with percent above IBW (% IBW-median % IBW) was found even though this result was not considered clinically relevant according to the authors (Barrett et al. 2001). For ethambutol, clearance was found to increase with TBW in an allometric manner with a fixed exponent of 0.75. For metformin, which is usually dosed based on GFR even though it is primarily cleared via active tubular secretion (Somogyi et al. 1987), clearance was found to increase with LBW using an allometric function with an exponent of 0.75. It is emphasized, however, that there was only a very small difference in the criterion values, and that the authors did not check whether another value for the exponent would improve the performance of the model. For carboplatin, both an increase of clearance with TBW according to a power equation (apart from age, serum creatinine and cysC) (Schmitt et al. 2009) and a linear

increase of clearance with excess body weight (TBW–IBW) and IBW was reported (Benezet et al. 1997). A third analysis on carboplatin, however, did not find a significant influence of a body size descriptor (Ekhart et al. 2009). Also for vancomycin and oseltamivir, no significant influence of a body size descriptor for clearance was found, even though for vancomycin creatinine clearance calculated using TBW was a significant covariate for vancomycin clearance in a linear function (Pai and Lodise 2011; Thomson et al. 2009).

Other Metabolic Pathways

Clearance of garenoxacin, which is influenced by both glucuronidation and sulphation, showed a linear increase with IBW and a 10.9 mL/min increase in clearance if a patient was obese (defined as IBW >130 %) (Van Wart et al. 2004). Clearance of busulfan which is cleared through glutathione S-transferase A1 was found to increase in a linear manner with body surface area (BSA) (Nguyen et al. 2006). While remifentanil is metabolized in blood and tissue by nonspecific esterases (Egan 1995), clearance was reported to increase in a linear manner with LBM (Egan et al. 1998). Micafungin clearance (various metabolic pathways) was found to increase with TBW using an allometric function with an exponent of 0.75 (Table 6.2) (Hall et al. 2011).

6.3.3.2 Obesity-Related Changes in Volume of Distribution

As depicted in Table 6.2, volume of distribution (V) is reported to increase with various size descriptors for different drugs. In addition, many different relationships between the size descriptor and volume of distribution have been described. Volume of distribution of taranabant, garenoxacin and metformin was shown to increase in a nonlinear manner with BMI (Li et al. 2010), TBW (Van Wart et al. 2004) and LBW (Bardin et al. 2012), respectively. A linear increase with TBW was reported for amiodarone, busulfan and propofol (Fukuchi et al. 2009; Cortinez et al. 2010; Nguyen et al. 2006). Both a linear increase with LBW (Barras et al. 2009) and TBW (Green and Duffull 2003) have been shown for enoxaparin and a linear increase with LBM was seen for remifentanil (Egan et al. 1998). Five PK models, i.e. on propofol, oseltamivir, ethambutol, sufentanil and micafungin found no influence of body size descriptors on the volume of distribution (van Kralingen et al. 2011; Pai and Lodise 2011; Hall et al. 2011, 2012; Slepchenko et al. 2003). In the analysis of four other PK models, volume of distribution was not included due to either uninformative data about initial drug distribution or because the primary aim of the investigation was not related to volume of distribution (Barrett et al. 2001; Benezet et al. 1997; Ekhart et al. 2009; Schmitt et al. 2009). For vancomycin, Thomson et al. reported that TBW was a significant covariate for the central and peripheral volume of distribution; however, the exact relationship was not reported (Thomson et al. 2009).

6.3.3.3 Obesity-Related Changes in Pharmacodynamic Parameters

Only three population PD papers have been reported and are included in Table 6.3. For none of the studied drugs, any of the body size descriptors were reported to influence any of the PD endpoints studied, which may be a result of the small sample size. For sevoflurane, BMI was not of influence on depth of narcosis measured with Bispectral index (BIS) (Cortinez et al. 2011). Also no significant influence of TBW, BMI, LBW or IBW was found for the depth of narcosis for propofol (van Kralingen et al. 2011). For enoxaparin no body size descriptor (TBW, LBW or IBW) was found for the probability of a bleeding event (Barras et al. 2009).

6.3.4 Discussion

Based on the results as presented in Table 6.2, it can be concluded that, to date, many different size descriptors (TBW, BMI, LBW, IBW, %IBW and ABW) in many different equations (linear or nonlinear) have been identified as predictors of the PK parameters clearance and volume of distribution. In addition, the final model equations included also a large number of other covariates, particularly for clearance, resulting in complex equations. It is emphasized that this may increase the risk on correlation between the covariates and on a biased covariate selection process (Han et al. 2009). Sixteen of the 19 PK studies show a change in clearance or volume of distribution with obesity. Except for CYP3A-mediated clearance and tinzaparin clearance, which seem to decrease with obesity, most other elimination pathways seem to increase with obesity or remain unchanged.

Differences in outcome within pathways may in part be explained by the population studied, which varied largely. Some studies did not use the standard definition for obesity (BMI $\geq$30 kg/m^2), but used TBW >100 kg (Barras et al. 2009), IBW >130% (Van Wart et al. 2004), >20% over IBW (Benezet et al. 1997) or BMI $\geq$25 kg/m^2 (Fukuchi et al. 2009) instead. While these differences in definitions may be explained by the relatively new population studied, the variety in definitions highly complicates the comparison between the studies. Furthermore, it raises the question whether the study population as presented in some of the studies (Benezet et al. 1997; Van Wart et al. 2004) are really obese. Moreover, a substantial number of papers included only a small percentage of obese patients, ranging from 6.3% to 19% of the total number of patients (Barras et al. 2009; Barrett et al. 2001; Schmitt et al. 2009; Ekhart et al. 2009; Thomson et al. 2009). In these studies, the majority of the patients had a normal weight and as a result the contribution of obesity to the covariate analyses of size descriptors may be small. Finally, differences in age and race have to be recognised. Some studies also included patients with a high age (Fukuchi et al. 2009; Barras et al. 2009; Barrett et al. 2001; Schmitt et al. 2009; Thomson et al. 2009; Bardin et al. 2012), which may lead to confounding of age with weight, as elderly patients are expected to be less obese than younger patients. In addition, metabolic and elimination pathways may reduce with age.

Also race may be of concern in these analyses, as obese Asian subjects may be less heavy than 'equally obese' Caucasian subjects. It therefore seems that conclusions can only be justified when obesity is either analysed among a non-elderly population of otherwise healthy patients, or obesity is analysed as one of the covariates among other covariates such as age, critical illness or other known covariates in a systematic covariate analysis. In the latter case, the analysis will be complicated by the fact that an a priori relation between age and weight such as described above cannot be excluded. Until more data are available, obesity should be studied across a wide range in bodyweight, preferably within one race and age group to prevent a biased covariate selection process (Han et al. 2009). In addition, it seems that uniformly accepted equations should be used to calculate for instance LBW and IBW, as different equations were used in the described studies of tabel 6.2. For LBW we propose to use the equation of Janmahasatian et al. as this measure was found to correlate well with the fat-free mass measured with BIA or DXA (Janmahasatian et al. 2005). For IBW, we propose to use the equation of Devine (Devine 1974) and for BSA the equation of Dubois and Dubois (DuBois and DuBois 1916).

In some of the studies of Table 6.2, an allometric function with an exponent of 0.75 has been implemented on total body weight (Cortinez et al. 2010; Hall et al. 2011; Hall et al. 2012; Bardin et al. 2012). While this may refer to the frequently debated allometric scaling theory (van Kralingen et al. 2011), from the results in Table 6.2 there seems no basis to a priori apply this 0.75 function in future analyses. Similarly, there is no basis to a priori scale with LBW with an exponent of 2/3 (McLeay et al. 2012).

Besides the identification of predictive covariates for variability in PK and PD parameters, the final model including the covariates should be adequately evaluated and validated. From the 19 PK studies in Table 6.2, only in six papers the predictive value of the models was evaluated and reported by observed values versus population predicted values (DV vs. PRED) plots. From the three PD studies in Table 6.3, one paper reported DV versus PRED and DV versus IPRED plots. Evaluations regarding the appropriateness of the identified covariate (e.g. Eta vs. covariate plots) was solely reported by Barras et al. (enoxaparin; Barras et al. 2009) and Hall et al. (micofungin) (Hall et al. 2011), although Van Kralingen et al. did plot individual post hoc parameters of the simple model against the most predictive covariates (van Kralingen et al. 2011). Regarding internal model validation, only a small number of studies reported visual predictive checks (VPC) (Li et al. 2010; Cortinez et al. 2010; Barras et al. 2009; Bardin et al. 2012) or posterior predictive check (PPC) (Pai and Lodise 2011), while some reported the use of a bootstrap analysis (van Kralingen et al. 2011; Barras et al. 2009; Schmitt et al. 2009; Thomson et al. 2009) and one study used normalised prediction distribution errors (NPDE) as an internal validation method (Bardin et al. 2012). External validation using independent data were conducted in three studies (Barrett et al. 2001; Van Wart et al. 2004; Nguyen et al. 2006). As such, of the 19 PK studies, 11 did not perform an internal validation procedure and 16 did not perform an external validation procedure. Of the three PD studies, one study did not perform an internal validation procedure and none

performed an external validation procedure. Even though it has been reported before that most PK and PD modelling papers do not adequately describe all available evaluation steps (Brendel et al. 2007), model misspecification, if not captured by model validation, may have far-reaching consequences when PK and PD models are used as a basis for dosing algorithms in obese patients. Therefore, the accuracy of the covariate relationships across the entire range in covariate values should be evaluated during model building and evaluation. In line with a previous report in paediatric studies (Krekels et al. 2011), in our opinion at least five evaluation criteria for the covariate model in the obese adult population should be evaluated. These criteria concern objective function value, goodness of fit (in particular DV vs. PRED), uncertainty in parameter estimates, eta distribution versus incorporated covariates of the simple model, and two validation methods (NPDE, VPC and/or bootstrap) and will be explained in more detail in Sect. 6.4.

From Table 6.3, it can be extracted that very few studies have been performed on the PD profile of drugs in obese patients. While it is unknown whether all PD endpoints can be used in the obese population, as they are usually not validated in the obese population, also the disorder or disease status may change as a consequence of obesity. It therefore seems that more future research should concern the PK, PD and disease status in obese patients.

6.4 Future Directions and Conclusions

In this chapter, we have aimed to provide a literature overview of obesity-related body size measures and currently published equations to quantify obesity-related changes in PK and PD parameters including how these equations were validated. The results show that the PK studies vary largely in level of obesity, other covariates such as race and age, and obesity definitions while very little information is available on the PD profile of drugs in the obese population. Depending on the elimination pathway and the available data, a decrease, increase or unchanged clearance was reported as a function of a variety of body size descriptors such as TBW, LBW, IBW or BMI. Given the limited data to identify this parameter, volume of distribution was found to increase or to remain unchanged.

A key issue in obesity population modelling lies in the wide range of body sizes of this population. Obesity as a term may be used for patients and subjects with a BMI ≥ 30 kg/m^2, without a clearly defined upper limit. Because of this wide range, we propose to aim for a large variety of body sizes by means of TBW or BMI stratification of patients in PK/PD studies. In addition to stratification, the inclusion of non-obese patients in the population analysis is highly recommended, as this will put parameter estimates found for the obese population into perspective and may yield a covariate relationship, which includes an even wider range of body sizes. These studies should preferably be performed in a non-elderly population from one race, thereby allowing for exact quantification of the obesity-related changes with clearance while preventing a biased covariate modelling process.

Another important phenomenon in the obesity pharmacology field is the large number of body size descriptors (Table 6.1) while researchers are still coming up with more equations including various factors to explain interindividual variability observed in their model parameters. However, some size descriptors bear some physiologic meaning, which may be relevant for the PK and PD of drugs. LBW (or fat-free mass) represents the mass or organs and other tissue (excluding adipose tissue). As such, it may be a plausible size descriptor of drug clearance, because clearance is, in most cases, mediated by physiologic processes occurring in the lean tissues. The LBW equation presented by Janmahasatian et al. has shown to predict the fat-free mass of obese patients and is currently the most applied LBW equation. However, from Table 6.2, we cannot conclude that there is enough basis to use LBW in obesity, even though this may be explained by the limitations of the studied population in terms of level of obesity, concurrent covariates or other reasons. Therefore, the other body size measures as depicted in Table 6.2, such as TBW or BMI need to be studied as well.

In addition, the current results do not provide any basis to use the recently proposed scaling factor of 2/3 for LBW (McLeay et al. 2012) or the more outdated 0.75 for TBW (Cortinez et al. 2010). In view of the fact that the CYP3A-mediated clearance seemed to decrease instead of increase with obesity, it may be more appropriate to evaluate different 'model' drugs, which represent a specific elimination pathway, in properly designed studies. Potentially, between drugs that share the elimination pathway, similar body size descriptors and equations may be anticipated.

From these results, it seems that more studies on obese individuals should be performed to gather data and that until more results have become available, data should be analysed with an open mind evaluating different covariates, preferably across a wide range of body weights and LBWs. This also applies to the function that is identified, which should be chosen from a variety of linear and nonlinear functions including those with different allometric exponents. A systematic table as depicted in Table 6.4 may be instrumental in this respect.

Ideally, physiologically based PK (and PD) models should be developed for the (morbidly) obese population. Based on body size-dependent alterations in physiologic functions, appropriate clearance and volume of distribution values may be predicted and individual dosing regimens be derived. However, until now, available physiologically based pharmacokinetic models for the obese population are very limited and if available, many assumptions regarding organ size and function are incorporated. Therefore, all empirical population models currently available for drugs in the obese population are still of high value (Table 6.2). Combining knowledge from drugs that were eliminated or metabolised by the same pathway may ultimately lead to development of more physiological models with predictive functions for the whole range of overweight and obese population.

Before models can be used to derive dosing guidelines, the models should be properly evaluated and validated. In line with the published framework for paediatric covariate models (Krekels et al. 2011), we propose the use of five evaluation criteria for covariate modelling in the obese adult population. The first is the objective function value of the covariate model in comparison with the simple model without

Table 6.4 Results of covariate analysis for the pharmacokinetic model of propofol in the dataset of morbidly obese patients and in the combined dataset of morbidly obese and lean patients. (Reproduced from van Kralingen et al. 2011)

Model	Relationship of covariate with CL	No. of structural parameters	OFV	
			Morbidly obese	Morbidly obese and lean patients[a]
Simple	–	6	− 643	− 1557
LBW	$CL_i=CL_{pop}\cdot(LBW_i/55)$	6	− 638	− 1563
IBW	$CL_i=CL_{pop}\cdot(IBW_i/50)$	6	− 640	− 1543
BMI	$CL_i=CL_{pop}\cdot(BMI_i/23)^z$	7	− 651	− 1596
TBW	$CL_i=CL_{pop}\cdot(TBW_i/70)^z$	7	− 653	− 1599

BMI body mass index, BMI_i BMI of the *i*th individual, *CL* clearance from the central compartment, CL_i CL in the *i*th individual, CL_{pop} population mean CL value, *IBW* ideal body weight, IBW_i IBW of the *i*th individual, *LBW* lean body weight, LBW_i LBW of the *i*th individual, *NA* not applicable, *OFV* objective function value, *TBW* total body weight, TBW_i TBW of the *i*th individual, *z* allometric scaling factor

[a] 40 lean patients in whom height data were available

covariates. More specifically, the influence of each covariate on the parameters is examined separately for significance in comparison with the simple model without covariates (Table 6.4). While typically, a significance level of $p<0.05$, corresponding to a decrease of 3.8 in objective function value is considered statistically significant, for a covariate analysis we propose to use more stringent criteria ($p<0.01$ or $p<0.001$) in order to prevent accepting statistically correct but clinically insignificant covariates. In addition to the use of the objective function value, the goodness of fit plots including individual and population-predicted concentrations (or PD endpoint values) plotted versus the concentrations (or PD endpoint values) should improve upon the covariate model versus the simple model. If combined data sets are analysed, for example non-obese and obese data, goodness-of-fit plots should be stratified per data set and evaluated separately. The most important goodness-of-fit plot to evaluate the covariate model is the observed concentrations versus population-predicted concentrations (DV vs. PRED), because it provides information on the ability of the model to predict concentrations for a new individual without considering measured concentrations. As population-predicted concentrations are based on structural parameters solely, Eta values (parameters for interindividual variability), which may suffer from high shrinkage, are excluded and therefore this plot may be more reliable than individual predicted versus observed values. As a third evaluation tool, the uncertainty on parameter estimates should be reported. These uncertainties should also include estimations for inter- and intra-individual variability (eta and residual error estimates). As a fourth evaluation tool, Eta values versus incorporated covariate plots should be evaluated. Incorporated covariates need to describe the relationship with the parameter across the entire range in covariate values. To demonstrate the relationship between the covariate and the structural parameter (e.g. clearance or volume of distribution) the Eta distribution of the structural parameter with covariates should be plotted against this covariate. Figure 6.1 provides an example of post hoc estimates of parameters of the simple

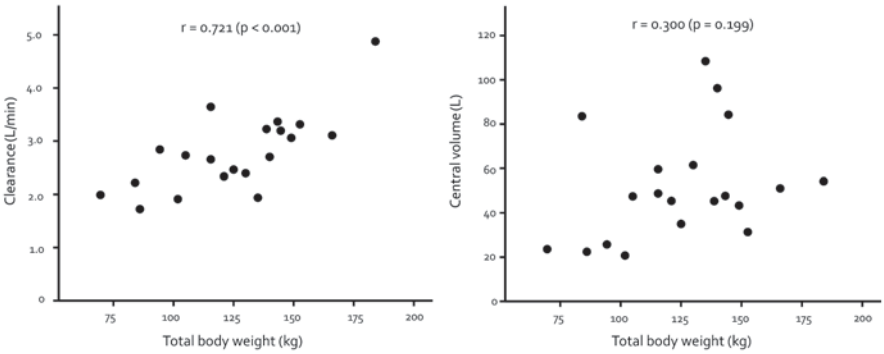

Fig. 6.1 Individual post hoc estimates for clearance and central volume of distribution of propofol versus total body weight in 20 obese and morbidly obese children and adolescents with Pearson's correlation coefficient (*r*). (Reproduced from Diepstraten et al. 2012, with permission from Adis, © Springer International Publishing AG 2011. All Rights reserved)

model without covariates versus the covariate to clearly show whether there is a correlation. Finally, the model should be evaluated using at least one simulation-based validation tool such as VPC (Holford 2005) or NPDE (Brendel et al. 2006), in addition to for example a bootstrap or a jackknife procedure.

In conclusion, many body size descriptors in different functions have been reported for different PK parameters. When subdividing the drugs according to their primary elimination pathway different patterns for different pathways emerge which may provide a basis to derive more physiologically based pharmacokinetic models. Until then, data in obese populations should be gathered and analysed, both on PK and PD of drugs, after which the models are properly validated and used in clinical practice to derive evidence-based dosing guidelines.

6.5 Summary

- A large number of body size descriptors in different equations to characterize the influence of obesity on PK and PD parameters is available
- Depending on the elimination pathway and studied population, a decrease, increase or unchanged clearance was reported as a function of a variety of body size descriptors such as TBW, LBW, IBW or BMI in different functions (linear, power or allometric)
- There is no basis to a priori scale clearance according to TBW or LBW with a fixed exponent (an exponent of 0.75 for TBW (allometric scaling) or an exponent of 2/3 for LBW)
- Even though limited data were available to identify this parameter, volume of distribution was found to increase or remained unchanged
- There is a paucity of studies about the PD of drugs in the obese population

- More PK and PD studies in obesity are needed. Important issues for the design of the study are:
  - Stratification for total bodyweight
  - Restriction to a non-elderly patient group from one race to prevent a biased covariate modelling process
  - Focussing studies on model drugs that are representative for a metabolic or elimination pathway, which may aid the development of more physiologically based PK models for (morbidly) obese populations
- Models should be properly evaluated and validated by use of five evaluation criteria for covariate modelling to avoid model misspecification:
  - Objective function value
  - Goodness of fit (in particular DV vs. PRED)
  - Uncertainty in parameter estimates
  - Eta distribution versus incorporated covariate plots
  - Two validation methods (VPC, NPDE and/or bootstrap)

References

Bardin C, Nobecourt E, Larger E, Chast F, Treluyer JM, Urien S (2012) Population pharmacokinetics of metformin in obese and non-obese patients with type 2 diabetes mellitus. Eur J Clin Pharmacol 68(6):961–968

Barras MA, Duffull SB, Atherton JJ, Green B (2009) Modelling the occurrence and severity of enoxaparin-induced bleeding and bruising events. Br J Clin Pharmacol 68(5):700–711

Barrett JS, Gibiansky E, Hull RD, Planes A, Pentikis H, Hainer JW et al (2001) Population pharmacodynamics in patients receiving tinzaparin for the prevention and treatment of deep vein thrombosis. Int J Clin Pharmacol Ther 39(10):431–446

Bauer LA, Edwards WA, Dellinger EP, Simonowitz DA (1983) Influence of weight on aminoglycoside pharmacokinetics in normal weight and morbidly obese patients. Eur J Clin Pharmacol 24(5):643–647

Benezet S, Guimbaud R, Chatelut E, Chevreau C, Bugat R, Canal P (1997) How to predict carboplatin clearance from standard morphological and biological characteristics in obese patients. Ann Oncol 8(6):607–609

Brendel K, Comets E, Laffont C, Laveille C, Mentre F (2006) Metrics for external model evaluation with an application to the population pharmacokinetics of gliclazide. Pharm Res 23(9):2036–2049

Brendel K, Dartois C, Comets E, Lemenuel-Diot A, Laveille C, Tranchand B et al (2007) Are population pharmacokinetic and/or pharmacodynamic models adequately evaluated? A survey of the literature from 2002 to 2004. Clin Pharmacokinet 46(3):221–234

Brill MJ, Diepstraten J, van Rongen A, van Kralingen S, van den Anker JN, Knibbe CA (2012) Impact of obesity on drug metabolism and elimination in adults and children. Clin Pharmacokinet 51(5):277–304

Cheymol G (2000) Effects of obesity on pharmacokinetics implications for drug therapy. Clin Pharmacokinet 39(3):215–231

Cortinez LI, Anderson BJ, Penna A, Olivares L, Munoz HR, Holford NH et al (2010) Influence of obesity on propofol pharmacokinetics: derivation of a pharmacokinetic model. Br J Anaesth 105(4):448–456

Cortinez LI, Gambus P, Troconiz IF, Echevarria G, Munoz HR (2011) Obesity does not influence the onset and offset of sevoflurane effect as measured by the hysteresis between sevoflurane concentration and bispectral index. Anesth Analg 113(1):70–76

Devine J (1974) Gentamycin therapy. Ann Pharmacother 8:650–655

Diepstraten J, Chidambaran V, Sadhasivam S et al (2012) Propofol clearance in morbidly obese children and adolescents: influence of age and body size. Clin Pharmacokinet 51(8):543–551

DuBois D, DuBois EF (1916) A formula to estimate the approximate surface area if height and weight be known. Arch Intern Med 17:863–871

Egan TD (1995) Remifentanil pharmacokinetics and pharmacodynamics. A preliminary appraisal. Clin Pharmacokinet 29(2):80–94

Egan TD, Huizinga B, Gupta SK, Jaarsma RL, Sperry RJ, Yee JB et al (1998) Remifentanil pharmacokinetics in obese versus lean patients. Anesthesiology 89(3):562–573

Ekhart C, Rodenhuis S, Schellens JH, Beijnen JH, Huitema AD (2009) Carboplatin dosing in overweight and obese patients with normal renal function, does weight matter? Cancer Chemother Pharmacol 64(1):115–122

Fukuchi H, Nakashima M, Araki R, Komiya N, Hayano M, Yano K et al (2009) Effect of obesity on serum amiodarone concentration in Japanese patients: population pharmacokinetic investigation by multiple trough screen analysis. J Clin Pharm Ther 34(3):329–336

Garrow JS, Webster J (1985) Quetelet's index (W/H^2) as a measureof fatness. Int J Obes 9:147–153

Green B, Duffull SB (2003) Development of a dosing strategy for enoxaparin in obese patients. Br J Clin Pharmacol 56(1):96–103

Green B, Duffull SB (2004) What is the best size descriptor to use for pharmacokinetic studies in the obese? Br J Clin Pharmacol 58(2):119–133

Hall RG, Swancutt MA, Gumbo T (2011) Fractal geometry and the pharmacometrics of micafungin in overweight, obese, and extremely obese people. Antimicrob Agents Chemother 55(11):5107–5112

Hall RG 2nd, Swancutt MA, Meek C, Leff RD, Gumbo T (2012) Ethambutol pharmacokinetic variability is linked to body mass in overweight, obese, and extremely obese people. Antimicrob Agents Chemother 56(3):1502–1507

Han PY, Duffull SB, Kirkpatrick CM, Green B (2007) Dosing in obesity: a simple solution to a big problem. Clin Pharmacol Ther 82(5):505–508

Han PY, Kirkpatrick CM, Green B (2009) Informative study designs to identify true parameter-covariate relationships. J Pharmacokinet Pharmacodyn 36(2):147–163

Holford NH (2005) The visual predictive check—superiority to standard diagnostic (Rorschach) plots. Population Approach Group in Europe, Pamplona, Spain. http://www.page-meeting.org/default.asp?abstract=738.

James W (1976) Research on Obesity. London: Her Majesty's Stationery Office

Janmahasatian S, Duffull SB, Ash S, Ward LC, Byrne NM, Green B (2005) Quantification of lean bodyweight. Clin Pharmacokinet 44(10):1051–1065

Keys A, Fidanza F, Karvonen MJ, Kimura N, Taylor HL (1972) Indices of relative weight and obesity. J Chronic Dis 25(6):329–343

Kotlyar M, Carson SW (1999) Effects of obesity on the cytochrome P450 enzyme system. Int J Clin Pharmacol Ther 37(1):8–19

Krekels EH, van Hasselt JG, Tibboel D, Danhof M, Knibbe CA (2011) Systematic evaluation of the descriptive and predictive performance of paediatric morphine population models. Pharm Res 28(4):797–811

Lemmens HJ, Bernstein DP, Brodsky JB (2006) Estimating blood volume in obese and morbidly obese patients. Obes Surg 16(6):773–776

Li XS, Nielsen J, Cirincione B, Li H, Addy C, Wagner J et al (2010) Development of a population pharmacokinetic model for taranabant, a cannibinoid-1 receptor inverse agonist. AAPS J 12(4):537–547

Lorentz F (1929) Ein neuer Konstitutionsindex. Klin Wochenschrift 8:348–351

Maric-Bilkan C (2013) Obesity and diabetic kidney disease. Med Clin North Am 97(1):59–74

Marik P, Varon J (1998) The obese patient in the ICU. Chest 113(2):492–498

McLeay SC, Morrish GA, Kirkpatrick CM, Green B (2012) The relationship between drug clearance and body size: systematic review and meta-analysis of the literature published from 2000 to 2007. Clin Pharmacokinet 51(5):319–330

Morgan DJ, Bray KM (1994) Lean body mass as a predictor of drug dosage. Implications for drug therapy. Clin Pharmacokinet 26(4):292–307

Mosteller RD (1987) Simplified calculation of body-surface area. N Engl J Med 379:1098

Nguyen L, Leger F, Lennon S, Puozzo C (2006) Intravenous busulfan in adults prior to haematopoietic stem cell transplantation: a population pharmacokinetic study. Cancer Chemother Pharmacol 57(2):191–198

Pai MP, Lodise TP Jr (2011) Oseltamivir and oseltamivir carboxylate pharmacokinetics in obese adults: dose modification for weight is not necessary. Antimicrob Agents Chemother 55(12):5640–5645.

Peck CC, Murphy MG (1989) Bedside estimation of ideal body weight. Applied Therapeutics, Inc., Vancouver

Rowland M, Tozer TN (1995) Clinical pharmacokinetics, concepts, and applications, 3rd edn. Williams and Wilkins, Baltimore

Schmitt A, Gladieff L, Lansiaux A, Bobin-Dubigeon C, Etienne-Grimaldi MC, Boisdron-Celle M et al (2009) A universal formula based on cystatin C to perform individual dosing of carboplatin in normal weight, underweight, and obese patients. Clin Cancer Res 15(10):3633–3639

Slepchenko G, Simon N, Goubaux B, Levron JC, Le Moing JP, Raucoules-Aime M (2003) Performance of target-controlled sufentanil infusion in obese patients. Anesthesiology 98(1):65–73

Somogyi A, Stockley C, Keal J, Rolan P, Bochner F (1987) Reduction of metformin renal tubular secretion by cimetidine in man. Br J Clin Pharmacol 23(5):545–551

Stein PD, Matta F, Goldman J (2011) Obesity and pulmonary embolism: the mounting evidence of risk and the mortality paradox. Thromb Res 128(6):518–523

Stone AA, Broderick JE (2012) Obesity and pain are associated in the United States. Obesity (Silver Spring) 20(7):1491–1495

Thomson AH, Staatz CE, Tobin CM, Gall M, Lovering AM (2009) Development and evaluation of vancomycin dosage guidelines designed to achieve new target concentrations. J Antimicrob Chemother 63(5):1050–1057

van Kralingen S, Diepstraten J, Wiezer RJ et al (2011) Population pharmacokinetics and pharmacodynamics of propofol in morbidly obese patients. Clin Pharmacokinet 50(11):739–750

Van Wart S, Phillips L, Bello A et al (2004) Population pharmacokinetics and pharmacodynamics of garenoxacin in patients with community-acquired respiratory tract infections. Antimicrob Agents Chemother 48(12):4766–4777

Wehrmeister FC, Menezes AM, Muniz LC, Martinez-Mesa J, Domingues MR, Horta BL (2012) Waist circumference and pulmonary function: a systematic review and meta-analysis. Syst Rev 1:55

World Health Organisation (1997) Obesity: preventing and managing the global epidemic. World Health Organisation, Geneva

Chapter 7
Pharmacometrics in Cardiovascular Safety

Joanna Parkinson, Anne S.Y. Chain, Piet H. van der Graaf and Sandra A.G. Visser

7.1 Introduction

Approximately one third of all drug discontinuation from preclinical discovery to postapproval stage is caused by drug safety (Kola and Landis 2004; Laverty et al. 2011). Within this category, cardiovascular (CV) safety is a major cause of attrition (Redfern et al. 2010), with drug-induced prolongation of cardiac repolarization and proarrhythmic liabilities being the main reasons for labeling restrictions and drug withdrawals (Darpö 2007; Gwathmey et al. 2009; Redfern et al. 2010). Table 7.1 shows an impact of CV adverse effect throughout the pharmaceutical drug development life cycle. In the case of late-stage adverse events, it can lead to termination of the program, labeling restrictions, prescribing restrictions, requirements for postmarketing studies and in a worst-case scenario, to drug discontinuation or withdrawal. It is therefore not surprising that the assessment of CV liabilities, especially drug-induced prolongation of cardiac repolarization and QT interval have become a primary focus of both pharmaceutical industry and regulatory agencies. These issues were addressed by International Conference on Harmonisation (ICH), which released S7B and E14 documents that address methods of preclinical and clinical assessment of cardiac repolarization (Anon 2005a, b). Table 7.2 shows a list of these

S. A. G. Visser (✉)
Modeling & Simulation, Early Stage Development, Merck Research Labs,
Merck & Co., Inc., North Wales, Pennsylvania, USA
e-mail: Sandra.Visser@merck.com

J. Parkinson
Computational Toxicology, Global Safety Assessment, AstraZeneca R&D Innovative Medicines,
Mölndal, Sweden

A. S. Y. Chain
Modeling and Simulation, Merck Research Laboratories,
Merck & Co., Inc., Rahway, NJ, USA

P. H. van der Graaf
Leiden Academic Centre for Drug Research (LACDR), Gorlaeus Laboratories, Leiden,
The Netherlands

S. Schmidt, H. Derendorf (eds.), *Applied Pharmacometrics,* AAPS Advances
in the Pharmaceutical Sciences Series 14, DOI 10.1007/978-1-4939-1304-6_7

Table 7.1 Relative contributions and frequency of different toxicities by organ function during preclinical and clinical drug development as well as postapproval stage. (Adapted from Redfern et al. 2010)

Phase	"Nonclinical"	Phase I	Phase I–III	Phase III/ marketing	Postmarketing
Impact	Causes of attrition	Serious ADRs	Causes of attrition	ADRs on label	Withdrawal from sale
Source	Car (2006)	Sibille et al. (1998)	Olson et al. (2000)	BioPrint® (2006)	Stevens and Baker (2009)
Number of drugs assessed	88 (stopped)	23	82 (stopped)	1138	47
Cardiovascular	27%	9%	21%	36%	45%
Hepatotoxicity	8%	7%	21%	13%	32%
Haematology/ BM	7%	2%	4%	16%	9%

preclinical and clinical models, which are currently used in evaluation of CV safety during pharmaceutical drug development.

Since CV liabilities, especially drug-induced delayed repolarization and QT interval prolongation, became a great concern for both pharmaceutical industry and regulatory agencies, it also became increasingly important to assess these liabilities early in the drug development process. Ideally, these liabilities should be assessed before the new chemical entity (NCE) is tested in humans for the first time, however, it is also beneficial at other stages of clinical drug development, for example, before the drug is tested in patients or before it is tested in larger population. The main purpose of the assessment in preclinical stages is to select the right compound, i.e., the one that can be safely administered to humans. In the clinical stages, it is important to have the correct quantitative understanding via the right clinical study design to understand the right dose and schedule that are safe to patients. To this end, pharmacometric (model-based) tools have become increasingly beneficial in achieving this goal; they allow making predictions under new circumstances, for example during new dosing regimen or in the alternative patient population, and also allow extrapolating across different systems, for example from in vitro or in vivo to clinical. This is particularly important along the value chain in pharmaceutical industry as it helps to select and progress the best compounds. In addition, it is also beneficial for the regulatory submissions, where pharmacometric tools can be used to describe the observed data and predict risk for a particular compound. Opportunities to use pharmacometric models in various stages of drug life cycle are provided in Table 7.2.

In this chapter, we will review how pharmacometrics can be used to assess the risk of CV liabilities with the main focus on QT interval. We will explain how mathematical models can be used to gain understanding of the drug-induced CV effects using either descriptive or mechanism-based modeling, where underlying mechanisms of action are taken into account, as well as how they can be used for extrapolation and prediction of real-life population and to inform clinical trials.

Table 7.2 Summary of techniques and models used in evaluation as well as opportunities for pharmacometric modeling in cardiovascular safety during pharmaceutical drug development

Technique	Summary	Reference	Opportunities for pharmacometric analysis
QSAR	Quantitative structure–activity relationship (QSAR) models relate physicochemical properties of a compound to its ability to block hERG	(Gavaghan et al. 2007; Inanobe et al. 2008; Clark and Wiseman 2009)	Predictive models of hERG blockage based on fragment descriptors
hERG assay	Measurement of inhibition of the potassium current through hERG; usually few ascending concentrations of NCE and major metabolites are tested to determine a concentration–effect relationship; preparations are made using human cells expressing hERG channel	(Brown 2004; Pollard et al. 2010)	In silico APD models; mechanism-based modeling of QT prolongation, e.g., using operational model of agonism
Other cardiac ion channel assays	Measurement of inhibition of ion channels other than hERG, such as: hNav1.5, hCav1.2, hKv4.3/hKChIP2.2, hKv7.1/hminK, and hKv11.1	For example: Harmer et al. (2008)	In silico APD models; mechanism-based modeling of QT and other CVS parameters, e.g., blood pressure
Purkinje fibers assay	Drug-induced changes in repolarization of action potentials are measured using isolated Purkinje fibers; species used in preparations include dog, rabbit, and guinea pig	(Terrar et al. 2007)	Reverse modeling for predicting ion channel pharmacology
Lagendorff heart model	APD, conduction, triangulation, reverse-use dependency, and instability are measured using isolated, perfused animal heart; species used in preparations include rabbit and guinea pig	(Szilágyi et al. 2004; Valentin et al. 2004; Wu et al. 2004; Suter 2006)	
Ventricular wedge	CVS measurements are taken in the arterially perfused isolated left ventricular wedge preparation; species used in preparations include rabbit and dog	(Chen et al. 2006; Benson et al. 2008)	"Virtual ventricular wedge"
Anaesthetized animal model	ECG measurements and cardiac contractility are measured, while animals are kept under anesthesia (usually to prevent unwanted events such as seizures); it is possible to relate the observed CV effects to the drug concentration using PK/PD modeling; species used in studies include dog and guinea pig	(Ollerstam et al. 2007b; Heath et al. 2011)	PK/PD modeling of CVS parameters such as QT, HR, BP and others for: (1) analysis of preclinical data, (2) optimal preclinical study design, (3) predicting clinical liabilities, and (4) clinical study design

Table 7.2 (continued)

Technique	Summary	Reference	Opportunities for pharmacometric analysis
Conscious animal model	ECG measurement, heart rate, and blood pressure are measured in conscious animals that are free to move; it is possible to relate the observed CV effects to the drug concentration using PK/PD modeling; species used in studies include dog, monkey, and minipig	(Ando et al. 2005; Ollerstam et al. 2006, 2007a, b; Markert et al. 2009; Watson et al. 2011)	
First time in human (FTIH)	ECG measurement, heart rate and blood pressure are measured, usually in healthy males; it is a placebo-controlled trial, with strict inclusion/exclusion criteria (with exclusion of females, elderly and volunteers with underlying CV diseases or those taking additional medications that may interact with the tested drug), where escalating doses of drug are tested	(Patat 2000; Buoen et al. 2005)	Nonlinear mixed-effects PK/PD modeling; Bayesian modeling for (1) analysis of clinical data, (2) clinical trial simulations, (3) "not-in-trial" simulation
Thorough QT study (TQT)	Clinical trial introduced in 2005 by ICH to assess QT prolongation risk; it requires positive control treatment arm (using moxifloxacin) and manually read ECG; QT prolongation risk is assessed using "double-delta" method with a threshold of 10 ms	(Anon 2005b)	
Pharmacovigilance	Postmarketing safety data monitoring, including adverse event reporting	FDA Adverse Event Reporting System (FAERS, http://www.fda.gov/Drugs/GuidanceComplianceRegulatoryInformation/Surveillance/AdverseDrugEffects/default.htm), VigiBase from Uppsala Monitoring Centre (http://whoumc2010.phosdev.se/), (Dumouchel 1999; Clark and Wiseman 2009)	Bayesian data mining; significance analysis using relative reporting ratio

The first section of this chapter provides a summary of CV end points, which are collected during preclinical and clinical studies. The following section is dedicated to the modeling of QT interval and contains a description of modeling and simulation approaches as well as examples of their application in both preclinical and clinical stages of drug life cycle. This will include (1) early discovery phase, where in silico methods are implemented, (2) in vivo studies, where modeling can be beneficial, for example, in optimizing study design as well as (3) in clinical trials, and (4) in large patient populations. The remaining sections of this chapter are dedicated to CV parameters other than QT interval—namely heart rate (HR) and blood pressure (BP), and the application of pharmacometric tools in their assessment.

The work presented here is focused on CV safety; however, there are also numerous examples of the use of pharmacometrics in CV diseases. In this case, changes in CV parameters are treated as a desired effect, rather than unwanted events that need to be avoided, as it is treated here. For more information on the pharmacometrics in CV diseases, we refer readers to the book chapter by Mould et al. (2011).

7.2 CV Parameters

There are various undesired CV effects that can be induced by drugs. These include signs such as palpitations, hypo and hypertension, arrhythmias, stroke or sudden cardiac death, and can range between relatively minor to potentially fatal events. To assess the risk of these effects, it is important to monitor biomarkers that can provide useful information about changes within the CV system. In this chapter, we provide a list of CV biomarkers that are commonly measured during the in vitro, in vivo, and clinical tests as listed in Table 7.2.

7.2.1 QT Interval

QT interval is an index of ventricular cell action potential durations (APD; Fig. 7.1a) in the heart's sinus rhythm (Shah 2002). On the electrocardiogram (ECG), it is defined as a distance between two distinct waves—Q (onset of ventricular excitation) and T (end of repolarization), as can be seen in Fig. 7.1b, and it is usually expressed in milliseconds (ms). Prolongation of QT interval represents a delay in ventricular repolarization and it can lead to a potentially fatal arrhythmia Torsades de Pointes (TdP; Fig. 7.1c; Moss 1999). QT prolongation has been used as a surrogate biomarker of TdP and it is currently mandatory to assess NCE's liability to prolong QT interval in preclinical models (Anon 2005a). TdP is rare; however, it can degenerate into ventricular fibrillation and can cause sudden cardiac death. Risk of drug-induced TdP is one of the major reasons for

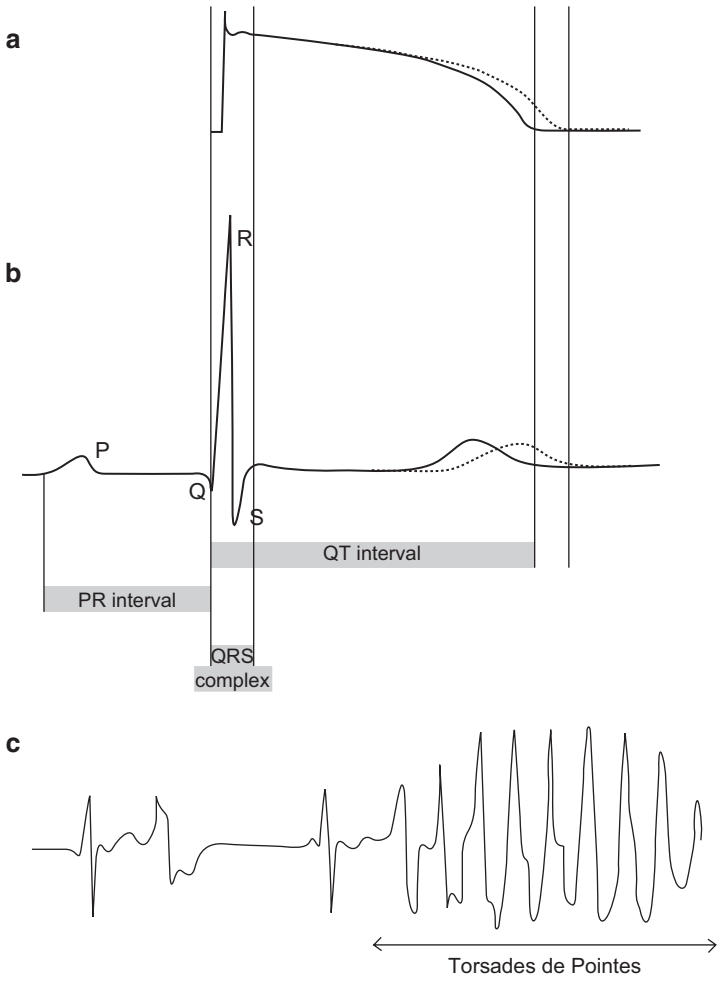

Fig. 7.1 **a** Schematic representation of action potential (*solid line*) and its changes due to hERG inhibition (*dotted line*). **b** ECG with distinct waves (*P*, *Q*, *R*, *S*, *T*), with normal (*solid line*) and prolonged (*dotted line*) QT interval. **c** Electrocardiogram of Torsades de Pointes

drug discontinuation and withdrawals and therefore, a primary concern for the pharmaceutical industry.

Normal QT interval in healthy humans is defined as ≤430 ms for men and ≤450 ms for women. However, it is known that QT interval may be affected by many factors other than drug concentrations, for example, changes in HR, circadian rhythm, potassium levels, glycemia, food intake, and age (Molnar et al. 1996; Nagy et al. 1997; Piotrovsky 2005; Christensen et al. 2010; Chain et al. 2012). It is therefore important to take this into account in order to accurately assess the QT prolongation risk. QT interval is routinely corrected for changes in the HR using standard methods such as Bazzet's (1920), Fridericia's (1920), Van de Water's et al. (1989)

formulae, or individual correction factors (Ollerstam et al. 2007a). Also, circadian rhythm effects can be adjusted for, for example, by including oscillatory component which describes circadian variation in the modeling of drug-induced QT changes (Piotrovsky 2005; Chain et al. 2011).

7.2.2 Heart Rate

HR can be measured from a pulse rate or directly from ECG, as an inverse of a distance between two consecutive R waves. Normal range for resting HR is between 60 and 100 beats per min (defined by the American Heart Association, www.heart.org) and it depends on various factors such as age, body weight, and level of fitness. Rapid increases in HR, for example, induced by drugs can lead to ventricular tachycardia and potentially cause sudden cardiac death; therefore, it is an important parameter measured during safety assessment. Decrease in HR, bradycardia, is also a common clinical problem, although its relevance is poorly understood (Ovsyshcher and Barold 2004).

7.2.3 Blood Pressure

Along with the HR, BP is the main vital sign measurement taken during clinical trials. It is usually measured on the upper arm in humans and expressed as systolic over diastolic pressure, with normal range being less than 120 mmHg for systolic pressure and less than 80 mmHg for diastolic pressure (defined by the American Heart Association, www.heart.org). Increased BP (hypertension) has been associated with an increased risk of age-specific death from a stroke, ischemic heart disease, and other vascular diseases (Prospective Studies Collaboration 2002). Low BP (hypotension) is less dangerous; a common form of hypotension is orthostatic (postural) hypotension, which occurs during sudden changes of position and is often associated with various medications. Although the symptoms are usually limited to dizziness, orthostatic hypotension can lead to falls and injuries, which can be especially hazardous in elderly patients (Tonkin and Wing 1992; Verhaeverbeke and Mets 1997; Shibao et al. 2007).

7.2.4 QRS Complex

Similar to QT, QRS complex can be measured directly from ECG (see Fig. 7.1b) and it includes ventricular activation, depolarization, and contraction (John and Fleisher 2006). Normal duration of QRS complex is usually less than 120 ms (John and Fleisher 2006). Prolongation of QRS interval has been associated with inhibition of Na^+ channel (hNav1.5), which is responsible for the depolarization of cardiomyocytes. Inhibition of this cardiac channel results in a decrease in the rate of

depolarization and consequently slows the velocity of excitation conduction. Although QRS prolongation is not currently addressed in the ICH guidelines, pharmaceutical industry is recognizing its importance and there is an increasing need to better understand drug-induced effects on Na^+ channel (Gintant et al. 2011; Harmer et al. 2011; Erdemli et al. 2012). QRS prolongation is thought to be associated with proarrhythmic risk, especially in patients with underlying cardiac diseases (Kashani and Barold 2005; Adesanya et al. 2008; Sumner et al. 2009). The risk in healthy humans however, is still not fully understood (Seger 2006).

7.2.5 PR Interval

PR interval can be measured on the ECG as the interval between the beginning of the P wave and the beginning of the QRS complex (see Fig. 7.1b) and it represents atrial activity. Normal values range between 120 and 200 ms and prolongation of the interval of more than 200 ms is known as first-degree atrioventricular block (John and Fleisher 2006). It has been suggested that prolongation of PR interval can be linked to an increased risk of atrial fibrillation (Cheng et al. 2009). PR interval prolongation can be caused by inhibition of Na^+ or Ca^{2+} channels (Nav1.5 and hCav1.2, respectively).

7.2.6 Beat-to-Beat Variability

Beat-to-beat variability of the QT interval is a measure of repolarization instability. It has been shown that beat-to-beat variability predicts the risk of TdP well and it was suggested that it can be potentially used as a complementary marker of proarrhythmic risk (Hondeghem et al. 2001; Hinterseer et al. 2008; Jacobson et al. 2011; Varkevisser et al. 2012). New approaches have been developed to assess this temporal variability, for example tangent method (Dota et al. 2002), template matching (Berger et al. 1997), and delta T50 method (Abrahamsson et al. 2011).

7.2.7 Cardiac Contractility

Cardiac contractility represents the capacity of the muscular tissue of the heart to contract (see for example, Mason et al. 1971). Cardiac contractility modifications can lead to clinical signs such as hypo or hypertension, orthostatic deficit or palpitations, which have been reported in 43 % of phase I studies (Moors et al. 2007; Lainee 2009). Currently, there are no defined guidelines for the assessment of cardiac contractility; however, the importance of screening for the potential contractility issues has been recognized by pharmaceutical industry and recently its assessment became a standard within preclinical development (Moors et al. 2007; Norton et al. 2009; Cooper et al. 2011; Bazan et al. 2012).

7.3 Modeling of QT Interval

7.3.1 PK/PD models

QT effects in clinical trials can be quantified in relation to the unbound plasma concentration of the drug through the use of pharmacokinetic and pharmacodynamic (PK/PD) modeling (see for example, Derendorf and Meibohm 1999; Gabrielsson and Weiner 2000; van der Graaf and Gabrielsson 2009). In this approach, QT response is related to the concentration of the drug by describing concentration–QT relationship. Common PD models used to describe QT response include linear (Eq. 7.1), log–linear (Eq. 7.2), simple and sigmoid E_{max} (Eq. 7.3):

$$E = \mathrm{SL} \times C \tag{7.1}$$

$$E = m \times \ln(C + C_0) \tag{7.2}$$

$$E = \frac{E_{max} \times C^{\gamma}}{EC_{50} + C^{\gamma}} \tag{7.3}$$

where E is the effect, C is the concentration of drug, SL is a slope of a linear concentration–effect relationship, m is the slope of the linear segment of the concentration–effect curve, E_{max} is the maximum effect, EC_{50} is the concentration at which the effect is half of E_{max}, and γ is Hill exponent, which in a simple E_{max} model is equal to 1. It is also possible to use alternative parameterization of the E_{max} models (see for example, Gabrielsson and Weiner 2000; Piotrovsky 2005; Groth 2008).

The QT interval can be affected by factors such as changes in HR, circadian rhythm, gender, or age. Therefore, in order to accurately evaluate the effect of the drug, these factors need to be taken into account. An example of a comprehensive PK/PD model, which implements drug effect as well as changes in HR and circadian rhythm is shown in Eq. (7.4) below (Piotrovsky 2005):

$$QT_c = QT_0 \times RR^{\alpha} \times (1 + \mathrm{CIRC} + E) \tag{7.4}$$

where E is a drug-induced effect and can be replaced by any PD models shown in Eqs. (7.1–7.3), QT_0 is a QT baseline parameter, which may differ between males and females, RR^{α} is a correction term for RR change, and CIRC represents the circadian rhythm, which can be described in terms of multiple cosine functions with different periods. An example of circadian rhythm function, which consists of three cosine functions with periods of 24, 12, and 6 h is shown in Eq. (7.5) below (Piotrovsky 2005):

$$CIRC = A_1 \cos\left(\frac{2\pi(t-\phi_1)}{24}\right) + A_2 \cos\left(\frac{2\pi(t-\phi_2)}{12}\right) + A_3 \cos\left(\frac{2\pi(t-\phi_3)}{6}\right) \tag{7.5}$$

where A_x correspond to individual amplitudes and ϕ_x represent phases of the circadian variation component. Similar implementation was also presented recently by Chain et al. and is shown in Eq. (7.6; Chain et al. 2011):

$$QT_c = QT_0 \times RR^{\alpha} + A \times \cos\left(\frac{2\pi}{24}(t - \phi)\right) + E \tag{7.6}$$

where QT_0 is the intercept of the QT–RR relationship and α is the correction factor for HR.

Drug-induced QT response can be instantaneous, i.e., in a situation where a maximum QT effect is observed at the time of maximum drug concentration. In such cases, QT effect can be directly linked to the drug exposure. However, often a time delay between plasma concentration and effect (hysteresis) is observed. It is then necessary to account for this time delay, which can be done by applying effect compartment or indirect response models (Holford and Sheiner 1981; Dayneka et al. 1993; Jusko and Ko 1994; Gabrielsson and Weiner 2000).

In recent years, population PK/PD models have become increasingly popular in the assessment of concentration–effect relationship in CV safety. The advantage of using population models is the ability to estimate the between-subject variability (BSV) i.e., in order to understand how PK and PD parameters may vary across subjects. Additionally, it is also possible to characterize "unexplained" variability in the population, which is the remaining variability, still observed after all other sources have been taken into account. This may include, for example, variability due to the measurement error. In addition to the estimation of various sources of variability, population models also allow to relate covariates such as gender, body weight, renal function, to PK/PD parameters. The approach that is commonly used in population modeling is the nonlinear mixed effect method, which is valuable especially if only sparse data are available. In this method, the population parameters are estimated as well as Bayesian estimates of individual subject parameters. One of the limitations in this method can be lack of identifiability of some parameters, especially if complex models are applied with very sparse data that may not always cover sufficient dynamic range. As a result, it may not be possible to estimate parameters with confidence or alternatively, the analysis may result in parameters that are physically implausible. Detailed information about population modeling and nonlinear mixed effect methods can be found in Sheiner and Beal (1980, 1982), Karlsson et al. (1995), Yano et al. (2001), Tornøe et al. (2004), and Pillai et al. (2005).

Interestingly, the use of Bayesian hierarchical models has been rather limited in the field of PK/PD modeling of QT effects. These methods are computationally intensive and run times may take much longer when compared to the maximum likelihood methods. However, since the introduction of the Markov chain Monte Carlo techniques, they have gained popularity thanks to their many advantages. One of them is the fact that there is no requirement for linearity or normality in the data and so inference is based directly on the desired model. Additionally, the posterior distribution, which is obtained in the form of a random sample, fully reflects all acknowledged sources of uncertainty. In the Bayesian approach, the uncertainty about

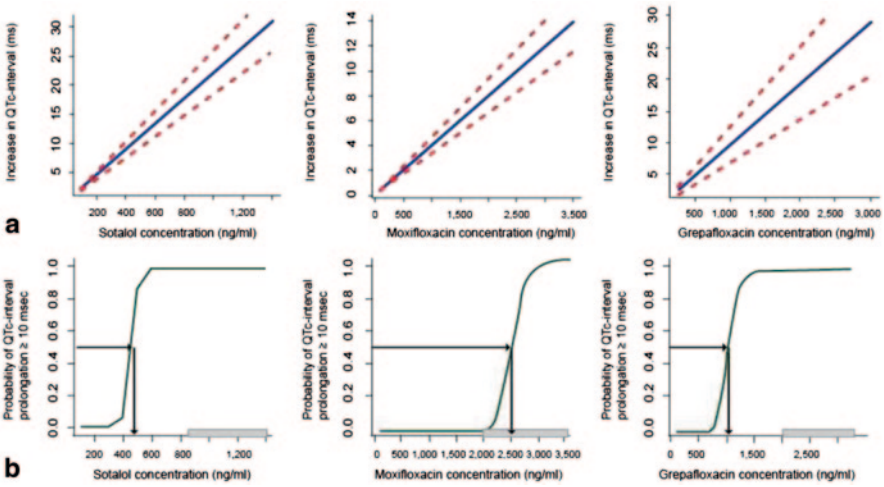

Fig. 7.2 **a** Concentration–QT effect relationships for three QT prolongers: sotalol, moxifloxacin, and grepafloxacin and **b** corresponding probability curves for *QT*c prolongation ≥ 10 ms, obtained through Bayesian modeling. (Reprinted with permission from (Chain et al. 2011)

a parameter is expressed in terms of probability and it can be interpreted in a natural and transparent manner. In the case of QT interval, it can be for example, expressed as a probability of 10 ms increase at a given drug concentration. An example of such probability curves produced using Bayesian modeling of QT prolongation can be found in Fig. 7.2. Another advantage is the ability to incorporate prior information into an analysis. For QT modeling, this can be, for example, prior results from an earlier clinical trial or information about QT–RR relationship and circadian variability. In depth review about the Bayesian approach and its use in PK/PD modeling can be found in Lunn et al. (2002).

7.3.2 Preclinical Models for Predicting Human QT Liability

Since QT prolongation is an important concern in drug development, it is beneficial to detect it as early as possible, ideally before the compound is tested in humans. If a compound is associated with QT prolongation and torsadogenic risk, it would be advantageous to exclude it from the pipeline early and avoid further costly development. Also, most importantly, it would be beneficial from a safety point of view, as it would avoid unnecessary exposure of human volunteers to potentially harmful drugs.

Pharmaceutical companies have employed a range of preclinical assays and tests to eliminate torsadogenic risk and to support the selection of the most appropriate candidate for testing in human trials. The main techniques employed during preclinical development are listed in Table 7.2. In the subsequent paragraphs of this

section, we provide a description of various mathematical methods that utilize data provided during these tests and which can be used to predict human QT liability.

7.3.2.1 In Silico Modeling Using In Vitro Data

The mechanism underlying QT prolongation and the occurrence of TdP is complex at cellular tissue and organ level. QT interval is determined by a balance between inward and outward ion currents, and its prolongation is primarily caused by a blockage of the delayed rectifier potassium current (IKr), encoded by human ether-a-go-go-related gene (hERG; Curran et al. 1995). When hERG is blocked, it causes a reduction in repolarizing currents and hence an increase in the time during which membrane voltage remains at elevated levels. This can be seen as an increase in cell's APD, as it is schematically represented in Fig. 7.1a. Subsequently, an increase in APD gives rise to QT prolongation (Fig. 7.1b). However, the occurrence of TdP cannot be explained purely by an inhibition of a single ion channel. Some drugs can block other channels, in addition to hERG, which may affect QT response (Bril et al. 1996; Martin et al. 2004). For example, if drug inhibits both hERG and other channel that carry currents which oppose repolarization (such as fast sodium channel, I_{Na}), it may result in a situation, where a drug is a hERG blocker; however, it does not cause QT prolongation (Schmitt et al. 2008). For this reason, most pharmaceutical companies include other ion channels, in addition to hERG, in their in vitro high-throughput screens (Harmer et al. 2011; Wible et al. 2008; Chen et al. 2009).

Various mathematical models have been developed to gain an understanding of the underlying processes in ion channel kinetics and action potential (AP) properties. These include models developed by: Winslow et al. (1999), Fox et al. (2002), Hund and Rudy (2004), Mahajan et al. (2008), and Grandi et al. (2010). Figure 7.3 shows a schematic representation of one of the models, a mathematical canine ventricular cell model developed by Hund and Rudy (2004). These mathematical models have been adapted by the pharmaceutical industry to simulate drug-induced effect on AP using experimental in vitro data from various ion channels. For example, Bottino et al. demonstrated how IC_{50} values from five ion channels (hERG, $I_{Na,\ sus}$, I_{CaL}, I_{Ks}, I_{to1}, I_{NaCa}) can be used to simulate canine transmural ECG, which was used as an analog for the human ECG (Bottino et al. 2006). More recently, Davies et al. presented an in silico AP (isAP) model, which was able to predict changes in canine myocyte APD using concentration–effect curve data from five ion channels (hNav1.5, hCav1.2, hKv4.3/hKChIP2.2, hKv7.1/hminK, and hKv11.1). Authors showed that they were able to account for physiological inter-dog variability within the model; they also considerably reduced variation within the dataset by using only one source to generate all ion channel data, IonWorks (Schroeder et al. 2003). The developed isAP model was validated using 53 compounds, which included both ion channel inhibitors and simulators, as well as both single and multi-ion channel blockers. Predictions made by isAP were compared to the experimental measurements of APD performed using canine left ventricular midmyocardial myocytes and the model was found to be 81 % predictive (Davies et al. 2012). A similar approach

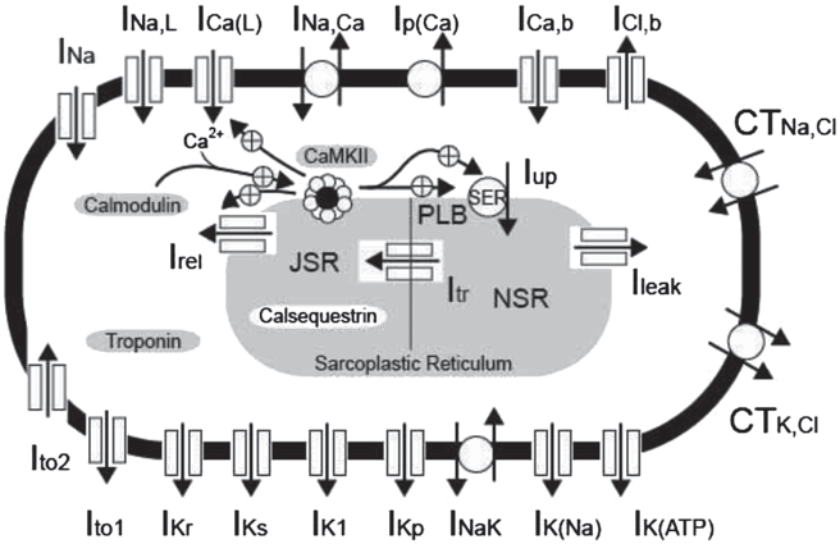

Fig. 7.3 Schematic representation of mathematical canine ventricular cell model developed by Hund and Rudy (2004). *Symbols: CaMKII* Ca^{2+}/calmodulin-dependent protein kinase, *JSR* junctional sarcoplasmic reticulum, *NSR* network sarcoplasmic reticulum, *PLB* phospholamban, CT_{NaCl} Na^{+}–Cl– cotransporter, CT_{KCl} K^{+}–Cl– cotransporter, I_{up} Ca^{2+} uptake from myoplasm to NSR, I_{leak} Ca^{2+} leak from NSR to myoplasm, I_{rel} Ca^{2+} release from JSR to myoplasm, I_x specific ion currents. (Reprinted with permission from Hund and Rudy 2004)

has been also adapted by Mirams et al. (2011). These authors used IC_{50} data from three ion channels: hERG, $I_{Na,}$ and I_{CaL} from 31 drugs to perform in silico modeling of ventricular cells and predict changes in APD. Simulations were performed for rabbit, dog, and human ventricular myocytes using various pacing protocols. The predictive power was then quantified by comparing predictions from the in silico models to the risk of TdP, using risk classification introduced by Redfern et al. (2003). These authors showed that they were able to accurately predict TdP risk for both pure hERG and multi-ion channel blockers, and demonstrated that APD prolongation correlated best with the torsadogenic risk out of all evaluated in silico markers (Mirams et al. 2011).

The examples presented above show that in silico models can be successfully used for compound selection through the assessment of the putative QT liability in early stages of drug discovery, namely during lead identification and optimization, along with the generation of the high-throughput screening of ion channel activity. Mathematical calculations can be performed in a short time, e.g., by using a distributed computing server, and thus such in silico models can be treated as an additional virtual high-throughput screen. It is clear that the use of in silico models can be highly beneficial during drug development: From an ethical point of view, it enables replacement and reduction of animals (thus addressing the 3R concept: replacement, refinement, and reduction, see for example, Fink et al. 2009 or www.nc3rs.org.uk); additionally, it can result in cost and time reduction. They can provide additional

information about cardiac liability and can therefore help select the most appropriate compounds to be taken forward to the preclinical testing. However, when using in silico methods, one should be aware of their underlying assumptions and limitations. For example, predictions are made using in vitro data from cell lines expressing cardiac ion channels, which may not always accurately reflect the native state of ion channels in vivo. Additionally, the accuracy of the in silico models to predict QT risk depends on the complexity of the mathematical model—for example on the number of ion channels used, inclusion of G-protein-coupled receptors (GPCRs), or kinases, all of which may be affected by a compound and as a consequence have an effect on the QT interval. There are also many other "in vivo modulators," i.e., factors that are present in the whole organism but are not accounted for in the in silico model. This may include, for example, hormonal regulation, signals from the nervous system, or underlying CV diseases.

7.3.2.2 Mechanism-Based Modeling Using In Vitro Data

The discovery of a link between QT prolongation and the inhibition of hERG potassium channel resulted in an establishment of an in vitro hERG assay (see Table 7.2). Currently, this screening method is widely used to detect a delayed repolarization risk (Brown 2004; Anon 2005a) and usually few ascending concentrations of NCE are tested to determine a concentration–effect relationship. Safety margins are generally calculated as a 30–40-fold difference between hERG IC_{50} and maximum free plasma concentration reached in in vivo or clinical studies (Redfern et al. 2003; Gintant 2011). Although these calculations are useful, they do not allow to quantitatively assess the extent of QT prolongation. Such assessment, i.e., a quantification of the relationship between in vitro channel inhibition and in vivo/clinical QT outcome is possible using mechanism-based PK/PD approach. In this approach, it is possible to characterize specific processes that take place between the administration of the drug and observed response, such as (1) PKs of a drug, (2) potential delays in target site distribution (hysteresis), (3) receptor binding, and (4) activation as well as (5) transduction.

With mechanism-based models, it is possible to distinguish between drug-specific (such as receptor binding) and system-specific parameters (signal transduction) and consequently to extrapolate from in vitro to in vivo as well as between species (for a review, see Danhof et al. 2005; Ploeger et al. 2009). Even though these models do not include all complexity of the actual physiological and pharmacological processes, they incorporate receptor theory concepts and thus allow predicting effects in vivo based on the parameters derived from in vitro assays.

The mechanism-based approach was used by Jonker et al., where operational model of pharmacologic agonism (Black and Leff 1983) was applied to relate the magnitude of hERG inhibition to the clinical QT response for a selective hERG blocker, dofetilide (Jonker et al. 2005). The authors linked in vitro properties of the drug, i.e., affinity and activity and the unbound plasma concentration to the QT effect by using the following operational model of agonism:

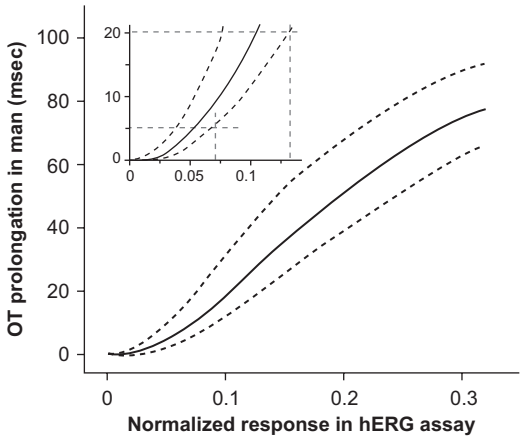

Fig. 7.4 Relationship between inhibition of in vitro hERG ion channel and absolute QT change in humans. *Solid curve* represents the median, while *dashed curves* correspond to the 95% confidence interval. The insert represents a zoomed in section of the graph, which corresponds to the change in QT interval of up to 20 ms. (Reprinted by permission from Macmillan Publishers Ltd: Clinical Pharmacology & Therapeutics (Jonker et al. 2005)

$$QT_{CF} = QT_0 + \frac{QT_m \times (\tau \times C)^n}{(K_I + C)^n + (\tau \times C)^n} \tag{7.7}$$

where QT_0 corresponds to the average QT baseline, QT_m is the maximum QT prolongation, τ is the transducer ratio, K_I is the dofetilide concentration resulting in 50% hERG current inhibition, and n represents a slope factor (Jonker et al. 2005). The dimensionless parameter τ corresponds to the half-maximum response in the hERG assay and it is defined as a ratio of the maximum current inhibition (I_{max}) to the fraction of inhibited hERG channels. The final model included additional parameters, such as system specific development of tolerance with long-term administration and the implementation of an effect compartment to account for hysteresis. The authors applied a population PK/PD approach to perform calculations and therefore were able to estimate the inter- and intraindividual variability. As a result, they were able to describe the relationship between the in vitro inhibition of hERG and the extent of the QT prolongation in human. This relationship can be seen in Fig. 7.4. According to the model, 10% inhibition of hERG corresponds to 20 ms change in QT interval. Similar relationships were reported in a presentation at the Modeling and Simulation (M&S) workshop between European Medicines Agency (EMA) regulators and European Federation of Pharmaceutical Industries and Associations industry (EFPIA; Visser et al. 2013).

Such model is an important step forward in predicting in vivo and clinical QT liabilities using parameters derived from in vitro screens. It provides a potential to quantitatively assess proarrhythmic risk in humans at relevant drug concentrations. However, since the model was developed using a pure hERG blocker, it is important to note that one should be cautious when extrapolating this model to other drugs, specifically ones that may potentially affect multiple ion channels. As it was mentioned in the previous section, and also highlighted by the authors themselves, inhibition or simulation of many channels may affect QT response. Therefore, future models need to be developed, that can relate inhibition of multiple ion channels to the clinical QT response.

7.3.2.3 Descriptive and Semi-mechanistic PK/PD Modeling Using In Vivo Data

QT interval, along with other ECG parameters and vital signs is often measured during in vivo studies using anesthetized and/or conscious animal models (see Table 7.2). Since plasma samples are also taken during the studies, it is possible to apply PK/PD modeling to describe the concentration–effect relationship. This type of analysis in preclinical studies has become increasingly popular in recent years and has been used, for example, to describe drug-induced QT changes in rats, marmosets, dogs, and monkeys (Ohtani et al. 2000; Ollerstam et al. 2006, 2007a, b; Komatsu et al. 2010; Dubois et al. 2011; van der Graaf et al. 2011; Watson et al. 2011; Chain 2012; Parkinson et al. 2013). This section will provide examples of how the application of PK/PD modeling has led to improvements in preclinical study design (Sect. 2.2.3.1) as well as development of methods to predict clinical QT outcomes based on preclinical data (Sect. 2.2.3.2).

Application to Optimal Study Design

As mentioned in Sect. 2.1, many drugs exhibit a temporal difference between plasma concentration and QT response (Le Coz et al. 1995; Hanada et al. 1999; Ohtani et al. 2000; Ollerstam et al. 2006). This situation can occur, for example, when (1) target space is in a separate compartment than plasma, (2) the response is driven by turnover, or (3) there is slow on/off target binding (Danhof et al. 2008; Gabrielsson et al. 2010). The presence of hysteresis can significantly affect the interpretation of study results. For example, if it is ignored, it may lead to incorrect calculations of safety margins and consequently incorrect predictions of safe clinical doses as illustrated by Gabrielsson et al. (2011). It is therefore necessary to account for hysteresis, for example by applying an effect compartment model or indirect response models (see Sect. 2.1). However, these models can be used only when meaningful data are available, i.e., when QT measurements are taken at informative time points after drug administration. Such meaningful data can be obtained using "time series approach," where measurements are taken during both upswing and downswing of the concentration and response time curves. It can then be used to fit a PK/PD model and fully characterize onset, intensity, and duration of response. This type of experimental design is thought to have more statistical power in terms of calculating variability and confidence intervals (Gabrielsson et al. 2010). It also allows for discrimination of system specific properties, such as turnover parameters and drug-specific properties (for example, E_{max}, EC_{50}). An example of optimizing experimental design to obtain informative data was presented by Ollerstam et al., where authors recommended the use of slow, continuous intravenous (IV) infusions followed by a wash out, instead of a rapid, stepwise infusion or a single oral dose (Ollerstam et al. 2006, 2007a). The authors showed that the concentration range produced by such slow infusions was similar to the range obtained after rapid infusions or multiple bolus injections regimen; however, in the former approach the increase in concentration

was more gradual and therefore less likely to exhibit transient fluctuations, which may result in higher variability. As a consequence, the estimation of concentration–QT effect relationship can be more precise. The authors also highlighted the need to collect measurements not only during the infusions but also during the wash-out period as these data may provide useful information in case of a delayed QT effect (Ollerstam et al. 2007a). Another advantage of using slow infusions is a reduction in the unwanted hemodynamic effects. It has been previously shown that the risk of TdP and the presence of hemodynamic effects, such as rapid increase in HR and tachycardia are related to the rate of infusion (Kleinbloesem et al. 1987; van Harten et al. 1988; Carlsson et al. 1993; Detre et al. 2005). These effects have been observed in relation to rapid-rise regiments; therefore, the use of slow infusions that produce gradual concentration increase is more favorable. Additionally, such slow and gradual rise in concentration can also be quickly terminated in cases when serious adverse effects occur.

Once the preclinical study is optimally designed and the meaningful data are collected, the next step is to perform PK/PD analysis in the most appropriate way. In another work published by Ollerstam and colleagues, the authors investigated various approaches in data processing in order to develop the most optimal method. As a result, it was recommended that QT interval should be corrected individually for HR and vehicle effects, and the linear correction was found to be most appropriate for this purpose (Ollerstam et al. 2007a). Additionally, the authors highlighted the need to exclude from the analysis the QT measurements which follow rapid increases in HR. This recommendation is associated with the fact that there is often a time delay between sudden HR changes and changes in QT interval. It was shown that it may take up to few minutes for the QT interval to adapt (Lau et al. 1988; Batchvarov et al. 2002; Malik 2004; Pueyo et al. 2004). Although the QT/RR hysteresis is a known phenomenon, it is often ignored in the analysis of QT data. This can potentially lead to an under- or overestimation of the QT response after drug administration, therefore it is important to take the abrupt HR changes into consideration. This is especially important in preclinical studies where conscious animals are used. During these studies, animals are free to move while the CV measurements are taken which can often lead to sudden changes in HR.

Application to In Vivo: Clinical Predictions

An accurate PK/PD description of drug-induced QT effect in preclinical species is a first step in translational research. It is a basis for extrapolation of preclinical PK/PD models into humans and predicting clinical effects at the intended drug exposures. The next step is to understand and quantify the translational link between two species. The rationale behind this type of translational analysis is to describe and quantify PK/PD relationship in preclinical animal and in human and then compare drug-specific PK/PD parameters between two species. For example, if both animal and human concentration–QT response relationships are described using a linear PD model (see Eq. 7.1), the resulting slope parameters can be directly compared

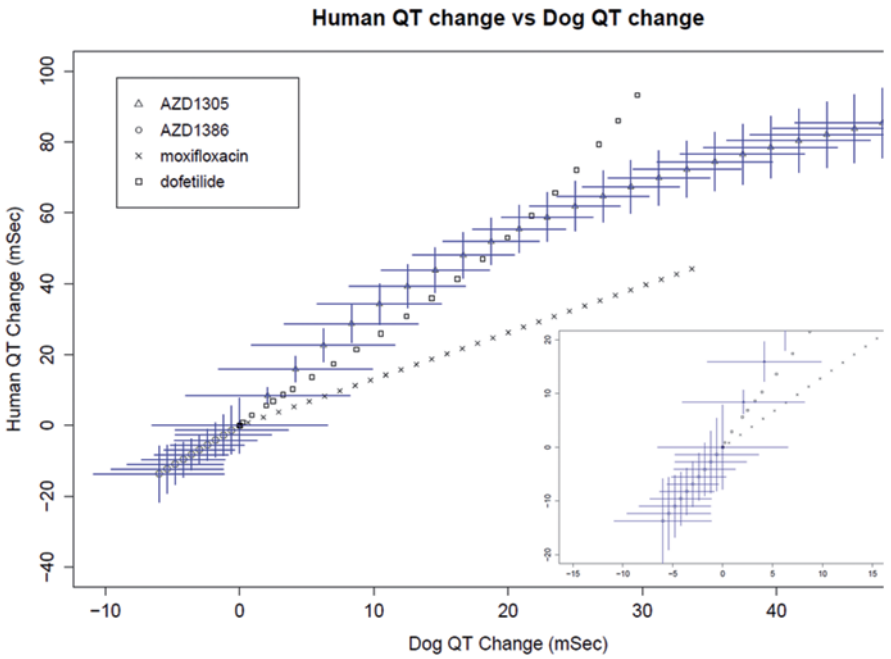

Fig. 7.5 Translational relationship between absolute QT change in dog (*x-axis*) and human (*y-axis*). Data from four compounds are plotted, and each compound is represented by a different symbol. *Lines* correspond to 95% confidence interval. The *insert* represents a zoomed in initial section of the plot. (Reprinted from Parkinson et al. 2013, with permission from Elsevier)

between two species. Similarly, if the E_{max} model is used (see Eq. 7.3), it is then possible to compare the respective EC_{50} values. Consequently, if the drug-specific parameters are consistent across two species, this knowledge can be then used to make clinical predictions for future compounds using preclinical PK/PD parameters.

An example of such translational analysis between conscious dog and human was recently presented by Parkinson et al. using four drugs—two proprietary compounds along with moxifloxacin and dofetilide (Parkinson et al. 2013). The authors used PK/PD modeling to (1) establish a relationship between QT response in dog and man at matching free concentrations of the drug and to (2) investigate whether such a relationship is consistent across all compounds or if it depends on the underlying mechanism(s) of action. The results showed that although there was high variability in the data, the translational relationship was similar for both pure hERG and multi-ion channel blockers at low delta-*QT*c intervals. The developed translational relationship between dog and human can be found in Fig. 7.5 and according to this analysis, a QT_c change of 2.5–8 ms in dog corresponds to a 10-ms change in man (Parkinson et al. 2013). Although this analysis was limited to four compounds and more examples are needed in order to fully understand the translational relationship between two species, it is nevertheless an important step forward in development of quantitative predictive method for the assessment of clinical QT liabilities.

The translation between dogs and humans was also assessed recently by Dubois et al. using moxifloxacin (Dubois et al. 2011) and by Chain et al. using moxifloxacin, sotalol, and cisapride (Chain 2012). In this work, a Bayesian PK/PD approach was used to predict clinical QT effects. Preclinical and clinical outcomes were expressed as a probability of QT prolongation greater than or equal to 10 ms at a given exposure level. Using this method, the authors showed that it was possible to distinguish between drug- and system-specific properties, which can allow direct comparison of drug-specific properties across two species. The results showed that dogs were less sensitive to the QT prolongation than humans, as judged by the slopes of their concentration–effect relationship and the concentration range of QT prolongation probability (Dubois et al. 2011).

Similar translational analyses were performed for other preclinical species. For example, Watson et al. applied PK/PD modeling to describe QT response induced by moxifloxacin in monkeys. The authors used a direct linear relationship between plasma concentration and QT response, described earlier in this chapter in Eq. (7.1), and then compared the slope of developed relationship to the slope values reported for humans in literature. The comparison revealed that although the slope of the concentration–QT response relationship in monkeys was lower than in humans, the parameters from both species were within threefold of mean estimate. Therefore, it was concluded that there is a good agreement between two species. In addition, this work confirmed the conclusion drawn earlier by Jonker et al. (2005) that 10 ms increase in QT_c can be induced by systemic exposures which give rise to less than 10% blockage of the hERG channel in vitro (van der Graaf et al. 2011; Watson et al. 2011).

When performing such translational analyses, it is important to remember that the translational relationship between preclinical animal and human may be different depending on the preclinical species used. For example, monkeys were found to be more sensitive than dogs to QT prolongation caused by moxifloxacin (Dubois et al. 2011). On the other hand, their sensitivity to QT prolongation was very similar to that of marmosets (Komatsu et al. 2010; Watson et al. 2011). Furthermore, the translational relationship between a given preclinical animal and human may also be influenced by a measurement method or other factors such as anesthesia. For example, Ollerstam et al. demonstrated that QT response in dogs may be significantly different depending on the type of dog model used. Specifically, the authors compared concentration–QT responses from three types of dog models, namely conscious, paced, and anesthetized, using four known QT prolongers (dofetilide, moxifloxacin, cisapride, and terfenadine). The analysis demonstrated that anesthetized dogs had much lower sensitivity to QT prolongation than either conscious or paced dogs. The authors suggested that these differences can be attributed to the influence of anesthesia on the metabolic processes in animals and/or a direct effect of anesthetics on the QT interval (Ollerstam et al. 2007b).

The overview presented in this section shows that there is a growing body of evidence that thorough preclinical QT (TpQT) evaluation could provide an effective and efficient quantitative decision framework for derisking of QT liability in man (van der Graaf et al. 2011). A combination of in vitro assays and in vivo studies

together with sophisticated mathematical approaches such as in silico models and PK/PD offer a comprehensive package to assess cardiac liabilities. These methods can help not only in detection and early discontinuation of potentially harmful substances before they are tested in humans but alsocan provide information about more subtle CV effects, which could potentially cause issues later in clinical development.

7.3.3 Clinical QT Modeling

7.3.3.1 QT Modeling in Clinical Studies

Given the potentially fatal consequences of QT_c prolongation, a concentration-dependent adverse drug reaction, regulatory authorities have reacted to this relatively recent "pharmacoepidemic" by denying or delaying the approval of a number of new drugs and placing severe restrictions on the use of many old and some new drugs because of concerns arising from their potential to prolong the QT/QT_c interval. For the implications for public health, scientific efforts have faced a parallel movement driven by health authorities, which have imposed the introduction of supposedly effective measures for the approval of novel compounds (Chain 2012). In 2005, the guidance introduced and mandated the performance of thorough QT (TQT) studies as the basis to systematically evaluate and demonstrate a compound's liability to cause *QT*c prolongation (ICH E14 guideline). In addition to outlining the assessment procedures for evaluating prolonged ventricular repolarization, the ICH E14 document requires the use of a positive control and supratherapeutic doses of the investigational drug to ensure accuracy and sensitivity of the experimental protocol (Anon 2005b). Suggestions are also given regarding the timing of the studies as well as the methodologies and interpretations used in the evaluation of QT measurements.

The primary analysis of a TQT study is not a pharmacometric analysis, but an analysis based on the "double-delta" method, where the time-matched mean *QT*c interval difference between active and placebo treatments, both adjusted for baseline, is taken. The result of the assessment must exclude 10 ms to be deemed safe, i.e., a negative study (Anon 2005b). Requiring that the largest time-matched mean difference between the drug and placebo QT_c interval to be around 5 ms or less implies that the one-sided 95 %-CI should exclude an effect of > 10 ms for every single measurement. This analysis has some issues, which is reviewed in more detail by Boos et al. (2007), Tsong et al. (2008), and Chain (2012). For example, the drug exposure and hence the underlying concentration–effect relationship, which determines the clinical relevance of drug-induced effects are not taken into an account (Rohatagi et al. 2009; Chain et al. 2011). Many authors have previously highlighted the importance of establishing the relationship between drug concentrations and changes in QT_c interval and provided examples that illustrate how this type of assessment has been useful during regulatory review

(Gobburu 2007; Garnett et al. 2008; Zaręba 2007; Bloomfield and Krishna 2008). Such assessment can therefore be a powerful alternative method to the double delta or any time point-based analysis. In particular, nonlinear mixed effects modeling of the concentration–QT relationship, mentioned in the previous section, allows the integration of data across all time points as well as all available treatment groups. Moreover, it relies on individual responses, instead of averaging the QT response at each time point, which enables better understanding of the uncertainty in response as well as the impact of outliers (Bloomfield and Krishna 2008).

Along with modeling and simulation techniques, one additional proposal is to consider the integration of ECG measurements in other mandatory clinical trials to generate additional evidence in support of establishing the CV safety profile of the compound. Given the statistical and scientific issues, the ethical burden and financial consequences of a TQT study, which is currently mandatory, the feasibility of using first time in human (FTIH) studies as the basis for evidence synthesis to investigate the propensity for proarrhythmic effects is a valuable alternative. FTIH studies (see Table 7.2) are a mandatory step in the drug development process. As it was reviewed by Chain (2012), in principle, the doses or dose range evaluated during escalation could enable the evaluation of the concentration–effect curve, providing evidence for drug effects not only at therapeutic level but also at supratherapeutic levels. From a safety and tolerability perspective, PD measures are monitored frequently or continuously throughout the dosing interval in parallel to PK sampling. In addition, the possibility of including a benchmark or positive control arm in a typical FTIH trial is not entirely excluded. The many historical studies with moxifloxacin (Florian et al. 2011) can be used in an integrated manner as benchmark or as priors during data analysis. Finally, in the instance where a TQT study is not feasible due to ethical considerations (see for example, Rock et al. (2009), regulatory authorities often rely heavily on FTIH studies as well as preclinical studies where QT prolongation was assessed. Thus, the limited information available can be enhanced by the incorporation of modeling and simulations results.

7.3.3.2 PK/PD Simulations in Clinical Studies

In Sect. 2.2, we have provided examples of the use of pharmacometric tools in preclinical development, where they can be applied to describe, explain, and predict clinical QT liabilities, improve decisions on compound selection during drug development, and to help design of clinical trials. Model based methods, which have increased in popularity in recent years, have also led to generation of new tools that can be used in clinical drug development. Here, modeling can be used to analyze study results, as it was mentioned in the previous section, but more importantly, it can also be applied to perform extrapolations to new situations. This can be beneficial for regulatory reviews and approvals after late phase clinical studies.

These extrapolations are possible through the computer simulations of clinical trials (CTS). In this approach, the existing knowledge of PK and PD properties of the drug is gathered and then used to simulate various hypothetical scenarios

of clinical trials (for a review, see Aarons et al. 2001; Girard 2005; Holford et al. 2010). This approach provides an opportunity to explore various study designs prior to actual experiments—for example, to investigate scenarios such as various population size with different sets of demographic features (e.g., only females, only patients at a certain age, or with a certain average HR value), various dose range and regimen, sampling scheme, etc. Additionally, it is possible to evaluate the consequences of protocol deviations, e.g., by simulating dropout and treatment compliance. In the case of QT prolongation, CTS can be valuable for a design of the most appropriate dosing regimen that may reduce drug-induced QT prolongation or to select the maximal dose at which the QT prolongation is absent. However, it is important to remember that CTS must be based on an accurate PK/PD model, supported by existing data. If the underlying model is not informative, e.g., in a case when appropriate data were not collected (for example, if there are no data available from females or elderly patients), extrapolating to many hypothetical scenarios will not be possible. The requirement for high-quality data that support CTS is emphasized by a common expression "garbage in, garbage out" and should always be remembered when performing extrapolations.

An example of application of PK/PD simulation in management of QT prolongation was presented by Isbister et al. The authors performed computer simulations using a previously developed PK/PD model, in order to establish guidelines for the management of citalopram overdose, a drug that is known to cause QT prolongation at high exposures (Isbister et al. 2006). As a result, they were able to (1) establish a minimum dose after which decontamination with single-dose activated charcoal was recommended, (2) establish a minimum dose, after which additional cardiac monitoring was needed, as well as (3) determine minimum monitoring time for patients who overdosed the drug. In addition, simulations provided information to develop guidelines for dose adjusting in elderly patients, women, and patients with underlying cardiac diseases. This study illustrated how mathematical simulations can be utilized to help clinicians to decide which patients require treatment after drug overdose, e.g., in the form of decontamination and/or additional cardiac monitoring. Similar approach was also used to establish guidelines for reducing risk of QT prolongation and TdP in methadone users (Florian et al. 2012). Simulations were proven successful in finding maximal dose below which QT interval was not prolonged above a certain threshold. It was also possible to identify factors that may contribute to the methadone-induced QT prolongation, such as gender or use of concomitant medications or substances that can additionally affect hERG channel, such as cocaine (Florian et al. 2012).

Clinical trial simulations can also be valuable in choosing the most optimal method of QT data analysis. This approach has been presented by Bonate et al., where the authors explored the power of various metrics that can be used to analyze QT data, such as maximal QT change from baseline, maximal QT interval or inclusion of QT baseline as a covariate. Simulations using different metrics revealed that area under the QT interval time curve with baseline QT interval as a covariate was the most powerful test to detect drug-induced QT changes (Bonate 2000).

7.3.3.3 Prediction of CV Risk in Patient Population

Despite numerous efforts aimed at improving signal detection of CV events for new medicines (Haverkamp et al. 2000; Netzer et al. 2001; Shah and Hondeghem 2005), none of them have focused on what actually happens after the drug has been approved and released into the general population. Although many postmarketing surveillance trials and spontaneous adverse events reporting have been used to monitor the incidence of supraventricular arrhythmias, TdP, and other safety events (Dekker et al. 1994; de Bruyne et al. 1999; Montanez et al. 2004), there is still an important advantage in knowing what can be expected so that mitigation plans can be made in advance. Furthermore, inclusion and exclusion criteria are imposed on clinical trial protocols to mitigate risk and prevent the most vulnerable patients from exposure to an experimental agent for which the risk to benefit ratio is unknown at the time of the investigation. Subsequently, however, drug prescription is not restricted or contraindicated for those patients who were excluded during the clinical development phase. Implicitly, the current practice imposes the assumption that such inclusion/exclusion criteria do not alter treatment outcome. Inferential methods offer an opportunity to address this issue in a more quantitative and systematic manner.

Many other causal factors are often present, which significantly affect the observed QT_c values in the real-life patient population. In fact, previous publications showed that heart failure, hypertension, diabetes and myocardial infarction all increase the risk of QT_c prolongation (Makkar et al. 1993; Choy et al. 1999; Nowinski et al. 2002; Torp-Pedersen et al. 1999). In addition to comorbidities, concomitant medications can also be a major contributor in prolonging the QT_c intervals. The crucial question from the regulatory perspective is "How efficient and reliable are the pre-approval clinical trials in identifying the clinical risk of TdP, given the patient population enrolled, background noise arising from spontaneous intraindividual variability in QT_c interval and the relatively low frequency of the clinically significant drug-induced effect?" (Bonate and Russell 1999).

Primarily, safety trial designs are highly efficacy oriented. The number of subjects exposed to the NCE is powered to show benefit rather than to pick up signals from rare but potentially fatal adverse events and no formal procedures exist to mitigate the impact of such differences or support the management of CV risk in the target population. Many subgroups of patients, especially those most at risk of TdP during the uncontrolled clinical use, exposed to the drug in question are usually excluded from these trials. These include: (1) females, (2) the elderly, (3) those with predisposing cardiac or noncardiac diseases associated with diminished repolarization reserve and therefore greater susceptibility to prolongation of the QT interval, (4) those with pharmacogenetic defects of drug metabolizing enzymes or pharmacological targets such as the potassium channels, (5) those susceptible to bradycardia or electrolyte imbalance, or (6) those receiving drugs with a potential for PK or PD interactions (Shah 2004, 2005). Therefore, the scope for detecting drug–drug or drug–disease interactions in clinical trials is very limited.

Given the patient population enrolled, the background noise (arising from spontaneous intraindividual variability in QT_c interval) and the relatively low frequency of clinically significant drug-induced effects, clinical trials may or may not accurately detect the frequency and intensity of QT_c interval prolongation. In fact, it is known that the proarrhythmic threshold can vary across compounds with frequency of such events ranging from approximately 1 in 100 (for halofantrine) to 1 in 50,000 (for terfenadine; Shah 2004). The evolving concepts in risk management will inevitably lead sponsors, regulatory agencies, and other stakeholders to consider how to best evaluate causality and identify the contribution of other factors determining increases in QT_c interval and consequently in CV risk in the target population. Thus, there is a need to widen the views on risk management beyond the evolving perspective from clinical pharmacology experts and regulators, i.e., that the liability for QT_c interval prolongation cannot be assessed accurately without an assessment of the concentration–effect relationships (Garnett et al. 2008). The concept of "not-in-trial simulation," in theory, enables quantitative evaluation of the implication of all factors contributing to QT_c interval prolongation in the real-life population, in addition to the observed drug effects investigated during clinical trials.

Model-based drug development (MBDD) principles offer advantages in the development and the application of pharmacostatistical models of drug efficacy and safety from preclinical and clinical data, to improve drug development knowledge management and decision making (Kola and Landis 2004; Food and Drug Administration 2004). It is also possible to utilize the techniques to make inferences about drug exposure in patients and evaluate in an integrated manner, how different covariates and sources of variability affect the observed QT_c values in real-life patients. In contrast to typical clinical trial simulations (Chan and Holford 2001; Gobburu and Marroum 2001), "not-in-trial" simulations allow the integration of PK/PD relationships. It can be applied to characterize the role of design factors, which have been omitted or excluded from a randomized trial. Thus, this novel approach will represent a natural extension of ongoing efforts within the pharmaceutical industry to improve safety signal detection where pharmacological basis is established for the assessment of causality, discriminating drug-induced from other (drug-unrelated) effects (Pater 2005; Lalonde et al. 2007; Pollard et al. 2008; DiMasi et al. 2010; Laverty et al. 2011). Specifically, safety data can be derived from epidemiological or pharmacoepidemiological studies, which are planned and performed after drug approval. It is feasible to consider integrating clinical trial and epidemiological data for the purpose of signal detection and improve risk management. As Black explained, "the false conflict between those who advocate randomized trials in all situations and those who believe observational data provide sufficient evidence needs to be replaced with mutual recognition of the complementary roles of the two approaches" (Black 1996). Others have also advocated the synergistic potential for using both kinds of data to aid decision making (Atkins 2007; Landewe and van der Heijde 2007; Hannan 2008; Yang et al. 2010).

In summary, simulation techniques can play an important role in the integration of clinical trial and epidemiological data for the prediction and interpretation of safety findings. The assessment of estimating the overall increase in QT_c intervals

must take into account different sources and contributors. Information of nondrug induced causal factors can be quantified using epidemiological techniques and incorporated with the drug-induced evaluation for the assessment of the overall effect.

7.4 Pharmacometrics in the Assessment of HR

7.4.1 Preclinical Models for Predicting Human HR Liability

Previous sections of this chapter provided multiple examples of the use of modeling and simulation in the assessment of QT prolongation in both preclinical and clinical drug development. Such extensive work resulted in great improvements in the understanding of the underlying mechanisms of QT prolongation and development of new methods in its assessment as well as in predicting the clinical outcome. Unfortunately, a lot less work has been done on other CV parameters, such as BP or HR (Howgate 2013). As a consequence, we have a limited knowledge on the mechanisms that underlie changes in these parameters and hence limited tools to assess their liability in humans. For example, it was recently highlighted that dog is a poor preclinical model for predicting changes in HR and BP in human, even though it is very valuable in predicting QT prolongation (Ewart et al. 2013).

In fact, only very recently researchers started to apply PK/PD modeling techniques to understand the concordance between preclinical species and man for HR. An example of such work was presented by Langdon et al., where authors used PK/PD modeling to describe drug-induced HR changes in dogs and humans and performed an analysis of the predictive value of the preclinical model (Langdon et al. 2010). The approach used was similar to the semi-mechanistic method described in Sect. 3.3.2—i.e., a direct linear model (Eq. 7.1) was applied along with the implementation of circadian rhythm to account for daily variation in HR. The resulting concentration–HR response profiles were then compared between two species. The analysis revealed that both dogs and humans were equally sensitive to HR changes; additionally, the authors were able to successfully predict human HR response using slope (i.e., drug-specific parameter) of the concentration–effect relationship from the dog (Langdon et al. 2010). Although this work was limited to only one compound, with unknown mechanism that underlie CV changes, it is an important step toward integrating the use of PK/PD modeling in the assessment of HR changes in preclinical species and building a translational model to predict the clinical outcome.

Other examples of the application of PK/PD modeling in the assessment of HR include the development of preclinical turnover model of biorhythms in rats published by Sällström et al. (2005). The complex model described baseline values for HR, BP, and temperature and their characteristic changes during the 24-h period, taking into account the asymmetric patterns and differences between day and night. The final model also included hypothermic response, tolerance development, and

the effects due to animal handling. Such model is of great value as it can help to separate the actual drug effect from biorhythms. This is especially important in preclinical studies, where animal handling (for example, during drug administration or while changing water bottles) can introduce disturbances in CV measurements. An understanding of asymmetric patterns and differences between day and night in biorhythms is also valuable for optimal study design, for example, when planning a dosing regimen or laboratory settings, such as 12:12 light–dark cycle (Sällström et al. 2005).

7.4.2 Application in Clinical Studies

In recent years, some effort has been made in the development of a global model that could describe basic control mechanisms and systems in the CV system, such as baroreceptor loop or systemic and pulmonary circulation. Such model could be used to simulate CV parameters—HR and BP. Complex mathematical models have been developed which includes, for example, work by Kappel and Peer (1993), Francheteau et al. (1993), Hentschel (2008), Choi and Sun (2005), and van de Vooren et al. April (2007). However, a common problem with complex models such as global models of circulatory system described above is structural identifiability of parameters. If the parameters are unidentifiable globally or locally, the model cannot be used to estimate unique parameters in the case when experimental data are available (see for example, Bellman and Åström 1970; Cobelli and DiStefano 1980). In order to apply such complex physiological models in the analysis of real data, models need to be simplified, for example, by using reparameterization techniques. An example was provided by Cheung et al., who reparameterized circulatory system model (Cheung et al. 2012). In this approach, the authors proved that it is possible to reduce number of parameters in the model and uniquely estimate them, without compromising mechanistic interpretation of the model. The parameters in their final, reparameterized model included: (1) PK parameters of the drug, such as clearance and volume of distribution, (2) PD parameters, such as *Emax* and EC_{50}, (3) physiological parameters, such as steady-state values of HR, mean arterial pressure, and total peripheral resistance, (4) parameters representing controls acting on HR, mean arterial pressure, and total peripheral resistance, and (5) time constant parameters. A schematic representation of this model can be found in Fig. 7.6. This example shows that it is possible to use even complex mechanistic models and implement them in practice.

Also, much simpler, semi-mechanistic models can be used in the clinical assessment of HR. A practical example was shown by Chaubaud et al., who used clinical trial simulation approach to assess the best design for phase III trial in patients with angina pectoris (Chabaud et al. 2002). The authors used experimental data to develop a complex PK/PD model, which included the presence of active metabolites, partial competitive agonists, and hysteresis. The final model was then used to simulate a large number of hypothetical trials. HR changes were used as simulated end

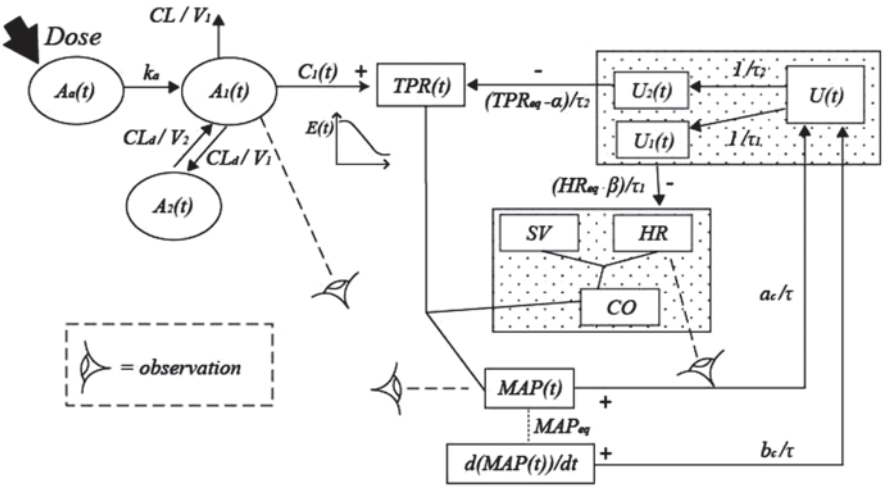

Fig. 7.6 A schematic representation of a circulatory system model. *Aa*, *A1*, *A2*, *HR*, *SV*, *CO*, *TPR* correspond to the depot, central, peripheral, HR, stroke volume, cardiac output, and total peripheral resistance, respectively. *MAP*, *HR*, *SV*, and *CO* represent mean aerial pressure, HR, stroke volume, and cardiac output, respectively. (Reprinted from Cheung et al. (2012), with permission from Elsevier)

point, and were then used to derive a binary clinical outcome—chest pain/attack of angina. The rationale behind this approach was an assumption that reduction in HR in patients with coronary artery disease will result in a decrease of angina pectoris risk. In addition, the model also included simulation of bradycardia as an unwanted adverse effect in the case when HR was below a certain threshold. The results from the simulations provided information about a minimum dose, below which no efficacy would be observed, as well as a maximum dose, above which large number of adverse effects would be present. In addition, it was also possible to recommend the most optimal dosing regimen, i.e., a single dose taken in the morning was found to be more effective when compared to twice-daily treatment. The authors suggested that this could be explained by variations of HR between day and night.

7.5 Pharmacometrics in the Assessment of BP

7.5.1 Preclinical Models for Predicting Human BP Liability

Modeling and simulation of BP is often closely connected with HR. As it was mentioned in the previous section, complex physiological models of circulatory system include BP as one of the simulated parameters. There are, however, examples where BP is the primary focus of the analysis; this is the case when changes

in BP can be linked to the underlying pharmacological mechanism. For example, it is known that the inhibition of calcium channels can produce a reduction of BP, therefore calcium agonists are used in the treatment of hypertension (Goa and Sorkin 1987; Liau 2005; Yasunari et al. 2005). In order to link this known mechanism of action to the clinical response, Shimada and coworkers performed PK/PD analysis of eight calcium channel blockers (CCB; Shimada et al. 1996). The authors successfully applied an effect compartment model to explain long lasting and slow response of several agents; they were also able to relate in vitro findings from calcium channel binding studies to the clinical effect observed in hypertensive patients. They found a significant correlation between in vitro dissociation constant and estimated in vivo EC_{50} values, which can be beneficial for future predictions (Shimada et al. 1996). Another translational study was presented by Snelder et al. (2011)—in this work, a mechanism-based PK/PD approach was used to establish a translational link between preclinical data and clinical response. It was demonstrated that changes in BP, which are regulated by the CV system can be effectively described by a mathematical model. The model included feedback between BP, cardiac output, and total peripheral resistance and was evaluated using marketed drugs with different mechanisms of action. The authors showed that their approach can be successfully used in predicting clinical response and simulation of new conditions (Snelder et al. 2011).

7.5.2 Application in Clinical Studies

In clinical studies, PK/PD modeling methods can be used to assess changes in BP, for example, in order to select the most optimal dosing regimen. Kleinbloesem et al. applied modeling techniques to demonstrate the effects of slow and rapid IV infusions of nifedipine (Kleinbloesem et al. 1987). It was shown that the rate of increase of the drug is related to the observed changes in BP; this phenomenon was also reported by others (for example, Nakaya et al. 1983; van Harten et al. 1988).

The importance of mathematical models for the assessment of BP during clinical development and regulatory submissions was also recently highlighted in a communication published by FDA which presented the impact of pharmacometrics on regulatory decisions (Lee et al. 2011). One example presented in this work included a calcium channel antagonist, which was developed for the management of BP. It was shown that the original clinical trial submitted to the FDA employed an aggressive dosing regimen which resulted in unwanted BP overshoot and its oscillations. After a regulatory enquiry into these undesired effects, a clinical trial simulation was performed, where a PK/PD model developed using experimental data from the actual clinical trial was used to explore alternative, less aggressive dosing regimens. As a result, it was possible to simulate an alternative dosing regimen, where the target BP reduction was achieved without the presence of unwanted side effects (Lee et al. 2011). Thanks to the computer simulation, it was therefore possible to address regulatory concerns without having to perform costly clinical trials.

Another example was provided by Bhattaram et al. in a similar publication from FDA (Bhattaram et al. 2005). In this case, the evaluated drug was reported to cause hypotension as a side effect. Initially the submission was not approved, partly due to the unwanted side effects on BP. Similar to the previous example, clinical trial simulations were performed in order to address the regulatory concerns. An alternative dosing regimen was explored and proved to minimize the risk of hypotension. In this case, the clinical trial simulation was followed by the actual study; however, the results from simulation were directly used to design the clinical study. The results from the study were in close agreement with the simulation and consequently, the drug was approved (Bhattaram et al. 2005).

7.6 Conclusions

This chapter provided multiple examples of the use of pharmacometric methods in the assessment of QT prolongation as well as other CV parameters, namely HR and BP. It is clear that modeling and simulation can be valuable in the assessment of CV safety during preclinical and clinical drug development as they can aid decision making (e.g., selection of compounds, go/no-go decisions), the design of clinical trials and ensure the safety of human volunteers. Additionally, they can also be beneficial in regulatory submissions—for example, the application of clinical trial simulations can result in approval of doses or dosing regimens that have not been directly assessed during the actual clinical trials. PK/PD modeling can also be valuable in providing confirmatory evidence of effectiveness or safety of tested drugs. In fact, FDA has reported recent increase in submissions where pharmacometric tools have been used and has highlighted their significance by noting that such methods were often crucial in the regulatory decision making (Bhattaram et al. 2005; Lee et al. 2011).

7.7 Summary

- CV safety is a major cause of drug attrition, with drug-induced prolongation of cardiac repolarization and proarrhythmic liabilities being the main reasons for labeling restrictions and drug withdrawals.
- The assessment of cardiac liabilities is crucial in the drug development process. It is important to detect potential liabilities early, ideally before drug is tested in humans for the first time to protect safety of human volunteers and to stop unsuccessful compounds early.
- Pharmacometric (model-based) tools can be beneficial in preclinical assessment, for example, through the use of (1) in silico APD models, (2) descriptive and semi-mechanistic PK/PD models of CV parameters (e.g., QT interval, HR, BP), or (3) mechanism-based models of QT prolongation (e.g., operational model of agonism).

- Preclinical models can be used to aid clinical trial design as well as extrapolating across different systems (e.g., from in vitro or in vivo to clinical) and hence predicting clinical outcomes. For example, it has been established that 10 ms change in QT_c in human is associated with drug exposures that give rise to:
  - ~5 % blockage of hERG in vitro assay
  - ~5 ms QT_c change in monkeys
  - ~2.5–8 ms QT_c change in dogs
- Pharmacometric tools can be used in clinical drug development, where they allow making predictions under new circumstances, for example, during new dosing regimen or in the alternative patient population (clinical trial simulations), as well as aid the design of clinical studies, or even predicting QT effects in real-life population (not-in-trial simulation).

References

Aarons L, Karlsson MO, Mentré F, Rombout F, Steimer JL, van Peer A COST B15 Experts (2001) Role of modelling and simulation in Phase I drug development. Eur J Pharm Sci 13:115–122

Abrahamsson C, Dota C, Skallefell B, Carlsson L, Halawani D, Frison L, Berggren A, Edvardsson N, Duker G (2011) DeltaT50—a new method to assess temporal ventricular repolarization variability. J Electrocardiol 44(4):477.e1–477.e9

Adesanya CO, Yousuf KA, Co C, Gaur S, Ahmed S, Pothoulakis A, Suryaprasad A, Gupta S (2008) Is wider worse? QRS duration predicts cardiac mortality in patients with right bundle branch block. Ann Noninvas Electrocardiol 13(2):165–170

Ando KHT, Kanno A, Ikeda H, Imaizumi M, Shimizu N, Sakamoto K, Shin-ichi Kitani S, Yamamoto Y, Hizume S, Nakai K, Kitayama T, Yamamoto K (2005) QT PRODACT: in vivo QT assay with a conscious monkey for assessment of the potential for drug-induced QT interval prolongation. J Pharmacol Sci 99:487–500

Anon (2005a) ICH S7B: the non-clinical evaluation of the potential for delayed ventricular repolarization (QT interval prolongation) by human pharmaceuticals. http://www.ema.europa.eu/docs/en_GB/document_library/Scientific_guideline/2009/09/WC500002841.pdf. Accessed 1 Feb 2013

Anon (2005b) International conference on harmonisation—ICH E14 clinical evaluation of QT/QTc interval prolongation and proarrhythmic potential for non-antiarrhythmic drugs. http://www.fda.gov/downloads/RegulatoryInformation/Guidances/ucm129357.pdf. Accessed 1 Feb 2013

Atkins D (2007) Creating and synthesizing evidence with decision makers in mind: integrating evidence from clinical trials and other study designs. Med Care 45(10 Suppl 2):S16–S22

Batchvarov VN, Ghuran A, Smetana P, Hnatkova K, Harries M, Dilaveris P, Camm AJ, Malik M (2002) QT–RR relationship in healthy subjects exhibits substantial intersubject variability and high intrasubject stability. Am J Physiol Heart Circ Physiol 282(6):H2356–H2363

Bazan C, Barba DT, Hawkins T, Nguyen H, Anderson S, Vazquez-Hidalgo E, Lemus R, Moore J, Mitchell J, Martinez J, Moore D, Larsen J, Paolini P (2012) Contractility assessment in enzymatically isolated cardiomyocytes. Biophys Rev 4:231–243

Bazett HC (1920) The Q–T intervals, Heart 7: 353

Bellman R, Åström KJ (1970) On structural identifiability. Math Biosci 7(3–4):329–339

Benson AP, Aslanidi OV, Zhang H, Holden AV (2008) The canine virtual ventricular wall: a platform for dissecting pharmacological effects on propagation and arrhythmogenesis. Prog Biophys Mol Biol 96(1–3):187–208

Berger RD, Kasper EK, Baughman KL, Marban E, Calkins H, Tomaselli GF (1997) Beat-to-beat QT interval variability: novel evidence for repolarization lability in ischemic and nonischemic dilated cardiomyopathy. Circulation 96(5):1557–1565

Bhattaram V, Booth B, Ramchandani R, Beasley BN, Wang Y, Tandon V, Duan J, Baweja R, Marroum P, Uppoor R, Rahman N, Sahajwalla C, Powell JR, Mehta M, Gobburu JS (2005) Impact of pharmacometrics on drug approval and labeling decisions: a survey of 42 new drug applications. AAPS J 7(3):E503–E512

Black N (1996) Why we need observational studies to evaluate the effectiveness of health care. BMJ 312:1215–1218

Black JW, Leff P (1983) Operational models of pharmacological agonism. Proc R Soc Lond Ser B Biol Sci 220(1219):141–162

Bloomfield D, Krishna R (2008) Commentary on the clinical relevance of concentration/QTc relationships for new drug candidates. J Clin Pharmacol 48(1):6–8

Bonate P (2000) Rank power of metrics used to assess QTc interval prolongation by clinical trial simulation. J Clin Pharmacol 40(5):468–474

Bonate P, Russell T (1999) Assessment of QTc prolongation for non-cardiac-related drugs from a drug development perspective. J Clin Pharmacol 39(4):349–358

Boos DD, Hoffman D, Kringle R, Zhang J (2007) New confidence bounds for QT studies. Stat Med 26(20):3801–3817

Bottino D, Penland RC, Stamps A, Traebert M, Dumotier B, Georgieva A, Helmlinger G, Lett GS (2006) Preclinical cardiac safety assessment of pharmaceutical compounds using an integrated systems-based computer model of the heart. Prog Biophys Mol Biol 90(1–3):414–443

Bril A, Gout B, Bonhomme M, Landais L, Faivre J-F, Linee P, Poyser RH, Ruffolo Jr RR (1996) Combined potassium and calcium channel blocking activities as a basis for antiarrhythmic efficacy with low proarrhythmic risk: experimental profile of BRL-32872. J Pharmacol Exp Ther 276(2):637–646

Brown AM (2004) Drugs, hERG and sudden death. Cell Calcium 35(6):543–547

Buoen C, Bjerrum OJ, Thomsen MS (2005) How first-time-in-human studies are being performed: a survey of phase I dose-escalation trials in healthy volunteers published between 1995 and 2004. J Clin Pharmacol 45(10):1123–1136

Car BD (2006) Enabling technologies in reducing drug attrition due to safety failures. Am Drug Discov 1:53–56

Carlsson L, Abrahamsson C, Andersson B, Duker G, Schiller-Linhardt G (1993) Proarrhythmic effects of the class III agent almokalant: importance of infusion rate, QT dispersion, and early afterdepolarisations. Cardiovasc Res 27(12):2186–2193

Chabaud S, Girard P, Nony P, Boissel J (2002) Clinical trial simulation using therapeutic effect modeling: application to ivabradine efficacy in patients with angina pectoris. J Pharmacokinet Pharmacodyn 29(4):339–363

Chain ASY (2012) Mind the gap: predicting cardiovascular risk during drug development. Doctoral dissertation, Universiteit Leiden

Chain ASY, Krudys KM, Danhof M, Della Pasqua O (2011) Assessing the probability of drug-induced QTc-interval prolongation during clinical drug development. Clin Pharmacol Ther 90(6):867–875

Chain ASY, Sturkenboom MCJM, Danhof M, Pasqua OED (2012) Establishing in vitro to clinical correlations in the evaluation of cardiovascular safety pharmacology. Drug Discov Today Technol. http://dx.doi.org/10.1016/j.ddtec.2012.07.001. Accessed Oct 2012

Chan PL, Holford NHG (2001) Drug treatment effects on disease progression. Annu Rev Pharmacol Toxicol 41:625–659

Chen X, Cordes JS, Bradley JA, Sun Z, Zhou J (2006) Use of arterially perfused rabbit ventricular wedge in predicting arrhythmogenic potentials of drugs. J Pharmacol Toxicol Meth 54(3):261–272

Chen MX, Helliwell RM, Clare JJ (2009) In vitro profiling against ion channels beyond hERG as an early indicator of cardiac risk. Curr Opin Mol Ther 11:269–281
Cheng S, Keyes MJ, Larson MG, McCabe EL, Newton-Cheh C, Levy D, Benjamin EJ, Ramachandran SV, Thomas JW (2009) Long-term outcomes in individuals with prolonged pr interval or first-degree atrioventricular block. JAMA 301:2571–2577
Cheung SYA, Majid O, Yates JWT, Aarons L (2012) Structural identifiability analysis and reparameterisation (parameter reduction) of a cardiovascular feedback model. Eur J Pharm Sci 46(4):259–271
Choi YH, Sun Y (2005) Modeling and simulation of baroreflex regulation of heart rate in response to respiratory fluctuations in arterial pressure. Key Eng Mater 227–279:28–32
Choy AMJ, Darbar D, Dell'Orto S Roden DM (1999) Exaggerated QT prolongation after cardioversion of atrial fibrillation. J Am Coll Cardiol 34(2):396–401
Christensen TF, Randløv J, Kristensen LE, Eldrup E, Hejlesen OK, Struijk JJ (2010) QT measurement and heart rate correction during hypoglycemia: is there a bias? Cardiol Res Prac 2010:961290
Clark M, Wiseman JS (2009) Fragment-based prediction of the clinical occurrence of long qt syndrome and torsade de pointes. J Chem Inform Model 49:2617–2626
Cobelli C, DiStefano JJ (1980) Parameter and structural identifiability concepts and ambiguities: a critical review and analysis. Am J Physiol Regul Integr Comp Physiol 239(1):7–24
Cooper CM, Skinner M, Antrobus B, Brown S, Lainee P, Valentin J (2011) Echocardiography: a sensitive, clinically translatable biomarker for cardiac contractility. J Pharmacol Toxicol Meth 64(1):29
Curran ME, Splawski I, Timothy KW, Vincen GM, Green ED, Keating MT (1995) A molecular basis for cardiac arrhythmia: HERG mutations cause long QT syndrome. Cell 80(5):795–803
Danhof M, Alvan G, Dahl S, Kuhlmann J, Paintaud G (2005) Mechanism-based pharmacokinetic-pharmacodynamic modeling: a new classification of biomarkers. Pharm Res 22(9):1432–1437
Danhof M, de Lange ECM, Della Pasqua OE, Ploeger BA, Voskuyl RA (2008) Mechanism-based pharmacokinetic-pharmacodynamic (PK-PD) modeling in translational drug research. Trend Pharmacol Sci 29(4):186–191
Darpö B (2007) Detection and reporting of drug-induced proarrhythmias: room for improvement. Europace 9(Suppl 4):iv23–iv36
Davies MR, Mistry HB, Hussein L, Pollard CE, Valentin J, Swinton J, Abi-Gerges N (2012) An in silico canine cardiac midmyocardial action potential duration model as a tool for early drug safety assessment. Am J Physiol Heart Circ Physiol 302(7):H1466–H1480
Dayneka NL, Garg V, Jusko WJ (1993) Comparison of four basic models of indirect pharmacodynamic responses. J Pharmacokinet Biopharm 21:457–478
de Bruyne MC, Hoes AW, Kors JA, Hofman A, van Bemmel JH, Grobbee DE (1999) Prolonged QT interval predicts cardiac and all-cause mortality in the elderly: the Rotterdam study. Eur Heart J 20(4):278–284
Dekker JM, Schouten EG, Klootwijk P, Pool J, Kromhout D (1994) Association between QT interval and coronary heart disease in middle-aged and elderly men. The zutphen study. Circulation 90(2):779–785
Derendorf H, Meibohm B (1999) Modeling of pharmacokinetic/pharmacodynamic (PK/PD) relationships: concepts and perspectives. Pharmaceut Res 16:176–185
Detre E, Thomsen MB, Beekman JD, Petersen K, Vos MA (2005) Decreasing the infusion rate reduces the proarrhythmic risk of NS-7: confirming the relevance of short-term variability of repolarisation in predicting drug-induced torsades de pointes. Br J Pharmacol 145(3):397–404
DiMasi JA, Feldman L, Seckler A, Wilson A (2010) Trends in risks associated with new drug development: success rates for investigational drugs. Clin Pharmacol Ther 87(3):272–277
Dota C, Skallefell B, Edvardsson N, Fager G (2002) Computer-based analysis of dynamic qt changes: toward high precision and individual rate correction. Ann Noninvasive Electrocardiol 7(4):289–301

Dubois VFS, Chain A, van de Graaf P, Leishman D, Gallacher D, McMahon N, Danhof M, Pasqua OD (2011) Interspecies comparison of moxifloxacin induced QTc-interval prolongation. Population Approach Group in Europe (PAGE) Meeting. Abstr 2226

Dumouchel W (1999) Bayesian data mining in large frequency tables, with an application to the FDA spontaneous reporting system. Am Stat 53(3):177–190

Erdemli G, Kim AM, Ju H, Springer C, Penland RC, Hoffmann PK (2012) Cardiac safety implications of hNav1.5 blockade and a framework for pre-clinical evaluation. Front Pharmacol 3:1–9

Ewart L, Aylott M, Deurinck M, Engwall M, Gallacher D, Geys H, Jarvis P, Ju H, Leishman D, Leong L, McMahon N, Mead A, Milliken P, Sherington J (2013) The animal model framework and the predictive power of the conscious telemetered dog for cardiovascular events in phase I clinical trials. Manuscript in preparation

Fink M, Noble PJ, Noble D (2009) Mathematical models in cardiac electrophysiology research—implications for the 3Rs, NC3Rs. 19:1–8. www.nc3rs.org.uk

Florian JA, Tornøe CW, Brundage R, Parekh A, Garnett CE (2011) Population pharmacokinetic and concentration–QTc models for moxifloxacin: pooled analysis of 20 thorough QT studies. J Clin Pharmacol 51(8):1152–1162

Florian J, Garnett CE, Nallani SC, Rappaport BA, Throckmorton DC (2012) A modeling and simulation approach to characterize methadone QT prolongation using pooled data from five clinical trials in MMT patients. Clin Pharmacol Ther 91(4):666–672

Food and Drug Administration (2004) Innovation or stagnation: challenge and opportunity on the critical path to new medical products. FDA Report, pp 1–38

Fox JJ, McHarg JL, Gilmour RF (2002) Ionic mechanism of electrical alternans. Am J Physiol Heart Circ Physiol 282(2):H516–H530

Francheteau P, Steimer JL, Merdjan H, Guerret M, Dubray C (1993) A mathematical model for dynamics of cardiovascular drug action: application to intravenous dihydropyridines in healthy volunteers. J Pharmacokinet Biopharmaceut 21:489–510

Fridericia LS (1920) Die Systolendauer im Elektrokardiogramm bei normalen Menschen und bei Herzkranken. Acta Med Scand 53(1):469–486

Gabrielsson JL, Weiner DL (1999) Methodology for pharmacokinetic/pharmacodynamic data analysis. Pharm Sci Technol Today 2(6):244–252

Gabrielsson J, Weiner D (2000) Pharmacokinetic and pharmacodynamic data analysis: concepts & applications (3rd edn.). Apotekarsocieteten, Swedish Pharmaceutical Society, Sweden

Gabrielsson J, Green AR, van der Graaf PH (2010) Optimising in vivo pharmacology studies—practical PKPD considerations. J Pharmacol Toxicol Meth 61(2):146–156

Gabrielsson J, Fjellstrom O, Ulander J, Rowley M, van der Graaf PH (2011) Pharmacodynamic-pharmacokinetic integration as a guide to medicinal chemistry. Curr Top Med Chem 11:404–418

Garnett CE, Beasley N, Bhattaram VA, Jadhav PR, Madabushi R, Stockbridge N, Tornøe CW, Wang Y, Zhu H, Gobburu JV (2008) Concentration–QT relationships play a key role in the evaluation of proarrhythmic risk during regulatory review. J Clin Pharmacol 48(1):13–18

Gavaghan C, Arnby C, Blomberg N, Strandlund G, Boyer S (2007) Development, interpretation and temporal evaluation of a global QSAR of hERG electrophysiology screening data. J Comput-Aided Mol Des 21(4):189–206

Gintant G (2011) An evaluation of hERG current assay performance: translating preclinical safety studies to clinical QT prolongation. Pharmacol Ther 129(2):109–119

Gintant GA, Gallacher DJ, Pugsley MK (2011) The "overly-sensitive" heart: sodium channel block and QRS interval prolongation. Br J Pharmacol 164(2):254–259

Girard P (2005) Clinical trial simulation: a tool for understanding study failures and preventing them. Basic Clin Pharmacol Toxicol 96(3):228–234

Goa K, Sorkin E (1987) Nitrendipine. A review of its pharmacodynamic and pharmacokinetic properties, and therapeutic efficacy in the treatment of hypertension. Drugs 33(2):123–155

Gobburu J (2007) PKPD modeling can be used in lieu of the endpoint definition in ICH E14. Paper presented at: Drug Information Association, Food and Drug Administration, Heart Rhythm

Society Symposium QT Issues in Drug Development: the evolving science, practical issues, and regulatory implications. Washington, DC
Gobburu JV, Marroum PJ (2001) Utilisation of pharmacokinetic–pharmacodynamic modelling and simulation in regulatory decision-making. Clin Pharmacokinet 40:883–892
Grandi E, Pasqualini FS, Bers DM (2010) A novel computational model of the human ventricular action potential and Ca transient. J Mol Cell Cardiol 48(1):112–121
Groth AV (2008) Alternative parameterisations of saturable (Emax) models allowing for nesting of non-saturable models. Population Approach Group in Europe (PAGE) Meeting. Abstr 1371
Gwathmey JK, Tsaioun K, Hajjar RJ (2009) Cardionomics: a new integrative approach for screening cardiotoxicity of drug candidates. Exp Opin Drug Metabol Toxicol 5(6):647–660
Hanada E, Ohtani H, Kotaki H, Sawada Y, Sato H, Iga T (1999) Pharmacodynamic analysis of the electrocardiographic interaction between disopyramide and erythromycin in rats. J Pharma Sci 88(2):234–240
Hannan EL (2008) Randomized clinical trials and observational studies guidelines for assessing respective strengths and limitations. JACC: Cardiovasc Interv 1(3):211–217
Harmer AR, Abi-Gerges N, Easter A, Woods A, Lawrence CL, Small BG, Valentin J, Pollard CE (2008) Optimisation and validation of a medium-throughput electrophysiology-based hNav1.5 assay using IonWorks™. J Pharmacol Toxicol Meth 57(1):30–41
Harmer A, Valentin J, Pollard C (2011) On the relationship between block of the cardiac Na+ channel and drug-induced prolongation of the QRS complex. Br J Pharmacol 164(2):260–273
Haverkamp W, Breithardt G, Camm AJ, Janse MJ, Rosen MR, Antzelevitch C, Escande D, Franz M, Malik M, Moss A, Shah R (2000) The potential for QT prolongation and pro-arrhythmia by non-anti-arrhythmic drugs: clinical and regulatory implications: report on a policy conference of the european society of cardiology. Cardiovasc Res 47(2):219–233
Heath BM, Cui Y, Worton S, Lawton B, Ward G, Ballini E, Doe CPA, Ellis C, Patel BA, McMahon NC (2011) Translation of flecainide- and mexiletine-induced cardiac sodium channel inhibition and ventricular conduction slowing from nonclinical models to clinical. J Pharmacol Toxicol Meth 63(3):258–268
Hentschel S (2008) Modeling and simulation of blood pressure in rats. Master's degree Thesis: Faculty of Mathematics and Natural Sciences. University of Oslo
Hinterseer M, Thomsen MB, Beckmann B, Pfeufer A, Schimpf R, Wichmann H-, Steinbeck G, Vos MA, Kaab S (2008) Beat-to-beat variability of QT intervals is increased in patients with drug-induced long-QT syndrome: a case control pilot study. Eur Heart J 29(2):185–190
Holford NHG, Sheiner LB (1981) Understanding the dose-effect relationship: clinical application of pharmacokinetic–pharmacodynamic models. Clin Pharmacokinet 6:429–453
Holford N, Ma SC, Ploeger BA (2010) Clinical trial simulation: a review. Clin Pharmacol Ther 88(2):166–182
Hondeghem LM, Carlsson L, Duker G (2001) Instability and triangulation of the action potential predict serious proarrhythmia, but action potential duration prolongation is antiarrhythmic. Circulation 103(15):2004–2013
Howgate EM (2013) Cross-species scaling of cardiovascular safety pharmacology using PKPD modelling and simulation. A thesis submitted to the University of Manchester for the degree of Doctor of Philosophy in the Faculty of Medical and Human Sciences
Hund TJ, Rudy Y (2004) Rate dependence and regulation of action potential and calcium transient in a canine cardiac ventricular cell model. Circulation 110(20):3168–3174
Inanobe A, Kamiya N, Murakami S, Fukunishi Y, Nakamura H, Kurachi Y (2008) In silico prediction of the chemical block of human ether-a-go-go-related gene (hERG) K+ current. J Physiol Sci 58:459–470
Isbister G, Friberg L, Duffull S (2006) Application of pharmacokinetic-pharmacodynamic modelling in management of QT abnormalities after citalopram overdose. Intensive Care Med 32(7):1060–1065
Jacobson I, Carlsson L, Duker G (2011) Beat-by-beat QT interval variability, but not QT prolongation per se, predicts drug-induced torsades de pointes in the anaesthetised methoxamine-sensitized rabbit. J Pharmacol Toxicol Meth 63(1):40–46

John AD, Fleisher LA (2006) Electrocardiography: the ECG. Anesthesiol Clin 24:697–715
Jonker DM, Kenna LA, Leishman D, Wallis R, Milligan PA, Jonsson EN (2005), A pharmacokinetic-pharmacodynamic model for the quantitative prediction of dofetilide clinical QT prolongation from human ether-a-go-go-related gene current inhibition data. Clin Pharmacol Ther 77:572–582
Jusko WJ, Ko HC (1994) Physiologic indirect response models characterize diverse types of pharmacodynamic effects. Clin Pharm Ther 56(4):406–419
Kappel F, Peer RO (1993) A mathematical model for fundamental regulation processes in the cardiovascular system. J Math Biol 31(6):611–631
Karlsson M, Beal S, Sheiner L (1995) Three new residual error models for population PK/PD analyses. J Pharmacokinet Biopharm 23(6):651–672
Kashani A, Barold SS (2005) Significance of QRS complex duration in patients with heart failure. J Am Coll Cardiol 46:2183–2192
Kleinbloesem CH, Brummelen PV, Danhof M, Faber H, Urquhart J, Breimer DD (1987) Rate of increase in the plasma concentration of nifedipine as a major determinant of its hemodynamic effects in humans. Clin Pharm Ther 41(1):26–30
Kola I, Landis J (2004) Can the pharmaceutical industry reduce attrition rates? Nat Rev Drug Discov 8:711–716
Komatsu R, Honda M, Holzgrefe HH, Kubo J, Yamada Y, Isobe T, Kimura K, Itoh T, Tamaoki N, Tabo M (2010) Sensitivity of common marmosets to detect drug-induced QT interval prolongation: moxifloxacin case study. J Pharmacol Toxicol Meth 61(3):271–276
Lainee P (2009) Incidence of cardiac contractility issues in safety pharmacology studies: is the core battery sufficient? J Pharmacol Toxicol Meth 60(2):252
Lalonde RL, Kowalski KG, Hutmacher MM, Ewy W, Nichols DJ, Milligan PA, Corrigan BW, Lockwood PA, Marshall SA, Benincosa LJ, Tensfeldt TG, Parivar K, Amantea M, Glue P, Koide H, Miller R (2007) Model-based drug development. Clin Pharmacol Ther 82(1):21–32
Landewe R, van der Heijde D (2007) Primer: challenges in randomized and observational studies. Nat Clin Pract Rheum 3(11):661–666
Langdon G, Davis JD, McFadyen LM, Dewhurst M, Brunton NS, Rawal JK, van der Graaf PH, Benson N (2010) Translational pharmacokinetic?pharmacodynamic modelling; application to cardiovascular safety data for PF-00821385, a novel HIV agent. Br J Clin Pharmacol 69(4):336–345
Lau CP, Freedman AR, Fleming S, Malik M, Camm AJ, Ward DE (1988) Hysteresis of the ventricular paced QT interval in response to abrupt changes in pacing rate. Cardiovasc Res 22(1):67–72
Laverty H, Benson C, Cartwright E, Cross M, Garland C, Hammond T, Holloway C, McMahon N, Milligan J, Park B, Pirmohamed M, Pollard C, Radford J, Roome N, Sager P, Singh S, Suter T, Suter W, Trafford A, Volders P, Wallis R, Weaver R, York M, Valentin J (2011) How can we improve our understanding of cardiovascular safety liabilities to develop safer medicines? Br J Pharmacol 163(4):675–693
Le Coz F, Funck-Brentano C, Morell TM, Ghadanfar MM, Jaillon P (1995) Pharmacokinetic and pharmacodynamic modeling of the effects of oral and intravenous administrations of dofetilide on ventricular repolarization. Clin Pharmacol Ther 57:533–542
Lee JY, Garnett CE, Gobburu JVS, Bhattaram VA, Brar S, Earp JC, Jadhav PR, Krudys K, Lesko LJ, Li F, Liu J, Madabushi R, Marathe A, Mehrotra N, Tornoe C, Wang Y, Zhu H (2011) Impact of pharmacometric analyses on new drug approval and labelling decisions: a review of 198 submissions between 2000 and 2008. Clin Pharmacokinet 50:627–635
Liau C (2005) Barnidipine: a new calcium channel blocker for hypertension treatment. Exp Rev Cardiovasc Ther 3(2):207–213
Lunn DJ, Best N, Thomas A, Wakefield J, Spiegelhalter D (2002) Bayesian analysis of population PK/PD models: general concepts and software. J Pharmacokinet Pharmacodyn 29:271–307
Mahajan A, Shiferaw Y, Sato D, Baher A, Olcese R, Xie L, Yang M, Chen P, Restrepo JG, Karma A, Garfinkel A, Qu Z, Weiss JN (2008) A rabbit ventricular action potential model replicating cardiac dynamics at rapid heart rates. Biophys J 94(2):392–410

Makkar RR, Fromm BS, Steinman RT, Meissner MD, Lehmann MH (1993) Female gender as a risk factor for torsades de pointes associated with cardiovascular drugs. JAMA 270(21):2590–2597

Malik M (2004) Errors and misconceptions in ECG measurement used for the detection of drug induced QT interval prolongation. J Electrocardiol 37(Suppl 0):25–33

Markert M, Stubhan M, Mayer K, Trautmann T, Klumpp A, Schuler-Metz A, Schumacher K, Guth B (2009) Validation of the normal, freely moving gottingen minipig for pharmacological safety testing. J Pharmacol Toxicol Meth 60(1):79–87

Martin RL, McDermott JS, Salmen HJ, Palmatier J, Cox BF, Gintant GA (2004) The utility of hERG and repolarization assays in evaluating delayed cardiac repolarization: influence of multi-channel block. J Cardiovasc Pharmacol 43(3):369–379

Mason DT, Braunwald E, Covell JW, Sonnenblick EH, Ross J (1971) Assessment of cardiac contractility: the relation between the rate of pressure rise and ventricular pressure during isovolumic systole. Circulation 44(1):47–58

Mirams GR, Cui Y, Sher A, Fink M, Cooper J, Heath BM, McMahon NC, Gavaghan DJ, Noble D (2011) Simulation of multiple ion channel block provides improved early prediction of compounds' clinical torsadogenic risk. Cardiovasc Res 91(1):53–61

Molnar J, Zhang F, Weiss J, Ehlert FA, Rosenthal JE (1996) Diurnal pattern of QTc interval: how long is prolonged? Possible relation to circadian triggers of cardiovascular events. J Am Coll Cardiol 27(1):76–83

Montanez A, Ruskin JN, Hebert PR, Lamas GA, Hennekens CH (2004) Prolonged qtc interval and risks of total and cardiovascular mortality and sudden death in the general population: a review and qualitative overview of the prospective cohort studies. Arch Intern Med 164(9):943–948

Moors J, Philip K, Harmer A, Lainee P, Valentin JP (2007) Incidence of cardiac contractility issues in safety pharmacology studies: is the core battery sufficient. The Society of Safety Pharmacology annual meeting (abstract)

Moss AJ (1999) The QT interval and torsade de pointes. Drug Safety 21:5–10

Mould D, Frame B, Taylor T (2011) Modeling and simulation in the development of cardiovascular agents. In: Kimko HHC, Peck CC (eds). Springer, New York, pp 199–226

Nagy D, DeMeersman R, Gallagher D, Pietrobelli A, Zion AS, Daly D, Heymsfield SB (1997) QTc interval (cardiac repolarization): lengthening after meals. Obes Res 5:531–537

Nakaya H, Schwartz A, Millard RW (1983) Reflex chronotropic and inotropic effects of calcium channel-blocking agents in conscious dogs. Diltiazem, verapamil, and nifedipine compared. Circ Res 52(3):302–311

Netzer R, Ebneth A, Bischoff U, Pongs O (2001) Screening lead compounds for QT interval prolongation. Drug Discov Today 6(2):78–84

Norton K, Iacono G, Vezina M (2009) Assessment of the pharmacological effects of inotropic drugs on left ventricular pressure and contractility: an evaluation of the QA interval as an indirect indicator of cardiac inotropism. J Pharmacol Toxicol Meth 60(2):193–197

Nowinski K, Gadler F, Jensen-Urstad M, Bergfeldt L (2002) Transient proarrhythmic state following atrioventricular junction radiofrequency ablation: pathophysiologic mechanisms and recommendations for management. Am J Med 113(7):596–602

Ohtani H, Taninaka C, Hanada E, Kotaki H, Sato H, Sawada Y, Iga T (2000) Comparative pharmacodynamic analysis of Q–T interval prolongation induced by the macrolides clarithromycin, roxithromycin, and azithromycin in rats. Antimicrob Agents Chemother 44(10):2630–2637

Ollerstam A, Visser SA, Persson AH, Eklund G, Nilsson LB, Forsberg T, Wiklund SJ, Gabrielsson J, Duker G, Al-Saffar A (2006) Pharmacokinetic-pharmacodynamic modeling of drug-induced effect on the QT interval in conscious telemetered dogs. J Pharmacol Toxicol Meth 53(2):174–183

Ollerstam A, Persson AH, Visser SA, Fredriksson JM, Forsberg T, Nilsson LB, Eklund G, Wiklund SJ, Gabrielsson J, Duker G, Al-Saffar A (2007a) A novel approach to data processing of the QT interval response in the conscious telemetered beagle dog. J Pharmacol Toxicol Meth 55(1)35–48

Ollerstam A, Visser SA, Duker G, Forsberg T, Persson AH, Nilsson LB, Bjorkman JA, Gabrielsson J, Al-Saffar A (2007b) Comparison of the QT interval response during sinus and paced rhythm in conscious and anesthetized beagle dogs. J Pharmacol Toxicol Meth 56(2):131–144

Olson H, Betton G, Robinson D, Thomas K, Monro A, Kolaja G, Lilly P, Sanders J, Sipes G, Bracken W, Dorato M, Van Deun K, Smith P, Berger B, Heller A (2000) concordance of the toxicity of pharmaceuticals in humans and in animals. Regul Toxicol Pharmacol 32(1):56–67

Ovsyshcher IE, Barold SS (2004) Drug induced bradycardia. Pacing Clin Electrophysiol 27(8):1144–1147

Parkinson J, Visser SAG, Jarvis P, Pollard C, Valentin JP, Yates JWT, Ewart L (2013) Translational pharmacokinetic-pharmacodynamic modeling of QTc effects in dog and human. J Pharmacol Toxicol Meth 68:357–366

Patat AA (2000) Designing and interpreting the results of first-time-to-man studies. Dialogues Clin Neurosci 2:203–12

Pater C (2005) Methodological considerations in the design of trials for safety assessment of new drugs and chemical entities. Curr Control Trials Cardiovasc Med 6:1

Pillai G, Mentra F, Steimer J (2005) Non-linear mixed effects modeling: from methodology and software development to driving implementation in drug development science. J Pharmacokinet Pharmacodyn 32(2):161–183

Piotrovsky V (2005) Pharmacokinetic-pharmacodynamic modeling in the data analysis and interpretation of drug-induced QT/QTc prolongation. AAPS 24:609–624

Ploeger BA, van der Graaf PH, Danhof M (2009) Incorporating receptor theory in mechanism-based pharmacokinetic–pharmacodynamic (PK–PD) modeling. Drug Metab Pharmacokinet 1:3–15

Pollard CE, Valentin J, Hammond TG (2008) Strategies to reduce the risk of drug-induced QT interval prolongation: a pharmaceutical company perspective. Br J Pharmacol 154(7):1538–1543

Pollard C, Abi Gerges N, Bridgland-Taylor M, Easter A, Hammond T, Valentin J (2010) An introduction to QT interval prolongation and non-clinical approaches to assessing and reducing risk. Br J Pharmacol 159(1):12–21

Prospective Studies Collaboration (2002) Age-specific relevance of usual blood pressure to vascular mortality: a meta-analysis of individual data for one milion adults in 61 prospective studies. Lancet 360:1903–1913

Pueyo E, Smetana P, Caminal P, Bayes de Luna A, Malik M, Laguna P (2004) Characterization of QT interval adaptation to RR interval changes and its use as a risk-stratifier of arrhythmic mortality in amiodarone-treated survivors of acute myocardial infarction. IEEE Trans Biomed 51:1511–1520

Redfern WS, Carlsson L, Davis AS, Lynch WG, MacKenzie I, Palethorpe S, Siegl PKS, Strang I, Sullivan AT, Wallis R, Camm AJ, Hammond TG (2003) Relationships between preclinical cardiac electrophysiology, clinical QT interval prolongation and torsade de pointes for a broad range of drugs: evidence for a provisional safety margin in drug development. Cardiovasc Res 58(1):32–45

Redfern WS, Ewart L, Hammond TG, Bialecki R, Kinter L, Lindgren S, Pollard CE, Roberts R, Rolf MG, Valentin JP (2010) Impact and frequency of different toxicities throughout the pharmaceutical life cycle. Toxicol 114:1081

Rock E, Finkle J, Fingert H, Booth B, Garnett C, Grant S, Justice R, Kovacs R, Kowey P, Rodriguez I, Sanhai W, Strnadova C, Targum S, Tsong Y, Uhl K, Stockbridge N (2009) Assessing proarrhythmic potential of drugs when optimal studies are infeasible. Am Heart J 157(5):827–836, 836.e1

Rohatagi S, Carrothers TJ, Kuwabara-Wagg J, Khariton T (2009) Is a thorough QTc study necessary? The role of modeling and simulation in evaluating the qtc prolongation potential of drugs. J Clin Pharmacol 49(11):1284–1296

Sällström B, Visser SG, Forsberg T, Peletier L, Ericson A, Gabrielsson J (2005) A pharmacodynamic turnover model capturing asymmetric circadian baselines of body temperature, heart rate and blood pressure in rats: challenges in terms of tolerance and animal-handling effects. J Pharmacokinet Pharmacodyn 32(5–6):835–859

Schmitt J, Ehrlich JR, Hohnloser SH (2008) New antiarrhythmic drugs for the treatment of atrial fibrillation. Herz Cardiovasc Dis 33:562–567
Schroeder K, Neagle B, Trezise DJ, Worley J (2003) IonWorks™ HT: a new high-throughput electrophysiology measurement platform. J Biomol Screen 8(1):50–64
Seger DL (2006) A critical reconsideration of the clinical effects and treatment recommendations for sodium channel blocking drug cardiotoxicity. Toxicol Rev 25:283–296
Shah RR (2002) The significance of QT interval in drug development. Br J Clin Pharmacol 54(2):188–202
Shah RR (2004) Drug-induced QT interval prolongation: regulatory perspectives and drug development. Ann Med 36:47–52
Shah RR (2005) Drug-induced QT interval prolongation—regulatory guidance and perspectives on hERG channel studies. In: The hERG cardiac potassium channel: structure, function and long QT syndrome. John Wiley & Sons Ltd, Chichester, pp 251–285
Shah RR, Hondeghem LM (2005) Refining detection of drug-induced proarrhythmia: QT interval and TRIaD. Heart Rhythm 2(7):758–772
Sheiner LB, Beal SL (1980) Evaluation of methods for estimating population pharmacokinetic parameters. I. Michaelis–Menten model: routine clinical pharmacokinetic data. J Pharmacokinet Biopharm 8:553–571
Sheiner LB, Beal SL (1982) Bayesian individualization of pharmacokinetics: simple implementation and comparison with non-Bayesian methods. J Pharm Sci 71:1344–1348
Shibao C, Grijalva CG, Raj SR, Biaggioni I, Griffin MR (2007) Orthostatic hypotension-related hospitalizations in the united states. Am J Med 120(11):975–980
Shimada S, Nakajima Y, Yamamoto K, Sawada Y, Iga T (1996) Comparative pharmacodynamics of eight calcium channel blocking agents in Japanese essential hypertensive patients. Biol Pharm Bull 19:430–437
Sibille M, Deigat N, Janin A, Kirkesseli S, Vital Durand D (1998) Adverse events in phase-I studies: a report in 1015 healthy volunteers. Eur J Clin Pharmacol 54(1):13–20
Snelder N, Ploeger B, Danhof M, Stanski D, Rigel D, Webb R, Feldman D, Luttringer O (2011) Quantitative understanding of drug effects on the interrelationship between mean arterial blood pressure, cardiac output and total peripheral resistance, Population Approach Group in Europe (PAGE) Meeting., Abstr 2058
Stevens JL, Baker TK (2009) The future of drug safety testing: expanding the view and narrowing the focus. Drug Discov Today 14(3–4):162–167
Sumner G, Salehian O, Yi Q, Healey J, Mathew J, Al-Merrii K, Al-Nemer K, Mann JFE, Dagenais G, Lonn E (2009) The prognostic significance of bundle branch block in high-risk chronic stable vascular disease patients: a report from the HOPE trial. J Cardiovasc Electrophysiol 20(7):781–787
Suter W (2006) Predictive value of in vitro safety studies. Curr Opin Chem Biol 10(4):362–366
Szilágyi S, Pollesello P, Levijoki J, Kaheinen P, Haikala H, Édes I, Papp Z (2004) The effects of levosimendan and OR-1896 on isolated hearts, myocyte-sized preparations and phosphodiesterase enzymes of the guinea pig. Eur J Pharmacol 486(1):67–74
Terrar D, Wilson C, Graham S, Bryant S, Heath B (2007) Comparison of guinea-pig ventricular myocytes and dog Purkinje fibres for in vitro assessment of drug-induced delayed repolarization. J Pharmacol Toxicol Meth 56(2):171–185
Tonkin A, Wing L (1992) Aging and susceptibility to drug-induced orthostatic hypotension. Clin Pharm Ther 52(3):277–285
Tornøe CW, Agersø H, Jonsson EN, Madsen H, Nielsen HA (2004) Non-linear mixed-effects pharmacokinetic/pharmacodynamic modelling in NLME using differential equations. Comput Meth Prog Biomed 76(1):31–40
Torp-Pedersen C, Møller M, Bloch-Thomsen P, Køber L, Sandøe E, Egstrup K, Agner E, Carlsen J, Videbæk J, Marchant B, Camm AJ (1999) Dofetilide in patients with congestive heart failure and left ventricular dysfunction. N Engl J Med 341(12):857–865
Tsong Y, Shen M, Zhong J, Zhang J (2008) Statistical issues of QT prolongation assessment based on linear concentration modeling. J Biopham Stat 18:564–584

Valentin J, Hoffmann P, De Clerck F, Hammond T, Hondeghem L (2004) Review of the predictive value of the Langendorff heart model (Screenit system) in assessing the proarrhythmic potential of drugs. J Pharmacol Toxicol Meth 49(3):171–181

Van de Vooren H, Gademan MGJ, Swenne CA, TenVoorde BJ, Schalij MJ, van der Wall EE (2007) Baroreflex sensitivity, blood pressure buffering, and resonance: what are the links? Computer simulation of healthy subjects and heart failure patients. J App Physiol 102(4):1348–1356

Van de Water A, Verheyen J, Xhonneux R, Reneman RS (1989) An improved method to correct the Q–T interval of the electrocardiogram for changes in heart rate. J Pharmacol Meth 22:207–217

Van der Graaf P, Gabrielsson J (2009) Pharmacokinetic–pharmacodynamic reasoning in drug discovery and early development. Future Med Chem 1:1371–1374

Van der Graaf PH, Watson KJ, Gorczyca WP, Umland J, Zhang Y, Chen X, Sun SZ, Fermini B, Holbrook M (2011) Towards a thorough preclinical QT (TpQT) study paradigm: pharmacokinetic-pharmacodynamic (PKPD) modelling of qtc effects of moxifloxacin in cynomolgus monkeys. Population Approach Group in Europe (PAGE) Meeting. Abstr IV–36

Van Harten J, van Brummelen P, Zeegers R, Danhof M, Breimer D (1988) The influence of infusion rate on the pharmacokinetics and haemodynamic effects of nisoldipine in man. Br J Clin Pharmacol 25(6):709–717

Varkevisser R, Wijers SC, van der Heyden MAG, Beekman JDM, Meine M, Vos MA (2012) Beat-to-beat variability of repolarization as a new biomarker for proarrhythmia in vivo. Heart Rhythm 9(10):1718–1726

Verhaeverbeke I, Mets T (1997) Drug-induced orthostatic hypotension in the elderly: avoiding its onset. Drug Saf Int J Med Toxicol Drug Exp 17:105–118

Visser SAG, Manolis E, Danhof M, Kerbusch T (2013) Modeling and simulation in early development. CPT Pharmacomet Sys Pharmacol. Accepted

Watson KJ, Gorczyca WP, Umland J, Zhang Y, Chen X, Sun SZ, Fermini B, Holbrook M, van der Graaf PH (2011) Pharmacokinetic–pharmacodynamic modelling of the effect of Moxifloxacin on QTc prolongation in telemetered cynomolgus monkeys. J Pharmacol Toxicol Meth 63(3):304–313

Wible BA, Kuryshev YA, Smith SS, Liu Z, Brown AM (2008) An ion channel library for drug discovery and safety screening on automated platforms. Assay Drug Dev Technol 6:765–780

Winslow RL, Rice J, Jafri S, Marbán E, O'Rourke B (1999) Mechanisms of altered excitation-contraction coupling in canine tachycardia-induced heart failure, II: model studies. Circ Res 84(5):571–586

Wu L, Shryock JC, Song Y, Li Y, Antzelevitch C, Belardinelli L 2004 Antiarrhythmic effects of ranolazine in a guinea pig in vitro model of long-QT syndrome. J Pharmacol Exp Ther 310(2):599–605

Yang W, Zilov A, Soewondo P, Bech O, Sekkal F, Home P (2010) Observational studies: going beyond the boundaries of randomized controlled trials. Diabetes Res Clin Pract 88(Suppl 1):S3–S9

Yano Y, Beal SL, Sheiner LB (2001) Evaluating pharmacokinetic/pharmacodynamic models using the posterior predictive check. J Pharmacokinet Pharmacodyn 28:171–192

Yasunari K, Maeda K, Nakamura M, Watanabe T, Yoshikawa J (2005) Benidipine, a long-acting calcium channel blocker, inhibits oxidative stress in polymorphonuclear cells in patients with essential hypertension. Hypertens Res 28(2):107–112

Zaręba W (2007) Drug induced QT prolongation. Cardiol J 14:1897–5593

Chapter 8
Pharmacometrics in Bacterial Infections

Sherwin K. B. Sy and Hartmut Derendorf

8.1 Introduction

The issue of bacterial resistance to antimicrobial agents, which is evident by a diminishing therapeutic value of many commercially available antimicrobials, has reached an alarming height of imminent danger to the general population. The rapid emergence of bacterial resistance to antimicrobial agents has rendered many of the commercially available antibiotics useless at the clinically tolerable dose. The resistance to treatment has also rapidly increased hospital mortality due to opportunistic infections (De Kraker et al. 2011). To combat this crisis, there are two options: (1) the development of new antimicrobials, which requires developing a new class of drugs and/or (2) preserving the value of existing ones by tackling bacterial resistance mechanisms. The first option can prove extremely costly and lengthy; the pharmaceutical industry has no incentive in developing new class of antibiotics due to a small return on the investment. The second option can be addressed in two ways: first, development of new drugs that counter the resistance mechanisms in bacteria for example the use of β-lactamase inhibitor in combination with a β-lactam agent; and second, optimizing treatment of existing antibiotics. The need for an optimized treatment, whether it is for new or existing drugs, in order to limit the chance of bacterial resistance, has prompted the use of quantitative approaches to guide dosing regimens.

The application of pharmacokinetic–pharmacodynamic (PKPD) modeling and simulation has been proven useful in the selection of dosing regimens that overcome resistance development and achieve the desired clinical outcome (Drusano

H. Derendorf (✉)
Department of Pharmaceutics, College of Pharmacy,
University of Florida, Gainesville, FL, USA
e-mail: hartmut@ufl.edu

Sherwin K. B. Sy
Department of Pharmaceutics, University of Florida, Gainesville, FL, USA

S. Schmidt, H. Derendorf (eds.), *Applied Pharmacometrics,* AAPS Advances
in the Pharmaceutical Sciences Series 14, DOI 10.1007/978-1-4939-1304-6_8

2004). Even with a good track record of optimizing antimicrobial dosages, however, the PKPD model and simulation is still underutilized in managing bacterial infections. This chapter focuses on the available PKPD models that were derived from *in vitro*, animal, and clinical data. The discussion separates two major modeling approaches applied to antimicrobial PKPD, namely, the minimum inhibitory concentration (MIC)-based and the *in vitro* time-course-based approaches. We explore how each approach handles monotherapy and combination therapy, as well as in the context of emergence of drug-resistant infections.

8.2 MIC-based Approaches

The PKPD properties of antibiotics to guide dosing schedules were conceived as early as the 1950s by Eagle who demonstrated the time-dependent nature of penicillin antibacterial activity, the concentration-dependent pattern for streptomycin and bacitracin, and a characteristic mixture of both patterns for tetracyclines (Eagle et al. 1950a, b; 1953a, b). With this knowledge, Eagle suggested that the efficacious way to administer penicillin was to give continuous infusion and regimens that gave the highest peak concentrations, such as an intravenous bolus, and would provide an effective cure for drugs that are concentration dependent (Eagle et al. 1950a).

It was not until much later, when Craig rediscovered and expanded the PKPD concepts in antimicrobial therapy using rodent studies (Craig 1998), that the PKPD relationship of new antibiotics was evaluated routinely. This information provides the basis for deciding the dose and dosing interval of antimicrobial agents, as well as determination of susceptibility breakpoints.

This first part of characterizing the PKPD properties of antibiotics is generally classified as the MIC-based approaches. This section will discuss how the MIC-based approaches are utilized to optimize dosing strategies, as well as their limitations.

8.2.1 In Vitro Susceptibility Tests

The MIC has been the primary tool for determining bacterial susceptibility to an antibiotic. This test is carried out by either an agar diffusion or broth dilution; both methods are most commonly used for MIC determination, since they are easy to perform (Jorgensen and Ferraro 2009). In the agar diffusion method, the bacterial culture is spread uniformly across the agar plate and then grown overnight; a rectangular strip impregnated with a gradient amount of drug is laid on top of the agar plate. This test is commonly known as the Epsilometer test (or Etest). Because MICs are typically based on twofold dilution, the drug concentrations on the Etest strip also increases exponentially. In post-24-h incubation, an elliptical zone of bacteria-free area resulted along the strip where the drug concentrations were

sufficient against the specific bacteria. The point at which the bacteria-free ellipse intersects with the Etest strip is the MIC. Older agar diffusion test utilizes disk diffusion wherein circular wafers impregnated with fixed concentrations of antibiotic are placed on a plate full of bacteria.

The broth dilution method utilizes a liquid medium usually Mueller-Hinton broth inoculated with specific bacterial colony forming unit (5×10^5 CFU/mL) and specific drug concentration is pre-added in twofold dilutions (e.g., 0.125, 0.25, 0.5,1, 2, 4, 8,…μg/mL). The mixture is incubated for 24 h at 37 °C. The lowest drug concentration of antibiotic allowing no visible bacterial growth in the media is the MIC. Positive controls containing only the bacteria and negative controls containing only MHB are observed simultaneously. Because the MIC is determined by visual inspection, it does not necessarily mean that there are no bacteria remaining in the media. Rather in most cases, the bacteria level is below a CFU size that is detectable by the human eye ($\leq 10^6$ CFU/mL). For large MIC values (MIC ≥ 100 μg/mL), it is advisable to evaluate susceptibility using a linear increase (e.g., 100, 200, 300,…μg/mL) than an exponential increase (i.e., twofold) in drug concentration.

The macrodilution and microdilution methods differ in the volume of the media wherein macrodilution method is often between 1 and 2 mL and microdilution is ≤500 μL. The bacteria inoculum should be the same for both methods. The volume of bacteria solution to add to the mixture should be adjusted to achieve a final inoculum of 5×10^5 CFU/mL.

For the past several decades, the MIC has been used extensively to define the susceptibility of a specific bacterial species or strain to an antibiotic agent. In the hospital setting where multiple strains of a specific bacterial species are available, MIC_{50} and MIC_{90}, representing the concentration of the antimicrobial agents wherein 50 and 90% of the bacterial population do not show visible growth after 24-h incubation, are often reported (Walkty et al. 2011). The ease of use, rapid turnover of results, and cost effectiveness have made the MIC approach the testing of choice in the clinical setting.

8.2.2 PKPD Indices

The current approach in the treatment of microbial infection in the clinic is primarily based on the relationships between drug exposure and MIC (Drusano 2004; Schmidt et al. 2008). The three standard PKPD indices are $fT > \text{MIC}$, fC_{max}/MIC, and $f\text{AUC}/\text{MIC}$. The duration of time in the 24-h period wherein the drug concentration is above the MIC is $fT > \text{MIC}$. The percentage of time above MIC over the 24-h period is often used instead ($\%fT > \text{MIC}$). AUC refers to the area under the drug concentration–time curve over the 24-h period and C_{max} is the peak drug concentration. The prefix *f* refers to the free drug concentration. The indices are based on the free and unbound drug concentration, as only the unbound drug can exert its pharmacological effect. If the relationship is time dependent, the dosing strategy is simply to maintain the free drug concentrations above the MIC value for an ex-

tended period of time. On the other hand, if the efficacy is concentration dependent, the goal is to attain sufficient peak drug concentrations or drug exposure above MIC (Mueller et al. 2004). The β-lactams are commonly associated with the term "concentration-independent kill" or "time-dependent kill." That is because the efficacy of the β-lactams is associated with the time that the free drug concentration of these agents is maintained above MIC. The quinolones and aminoglycosides, on the other hand, are "concentration dependent" in their effects. Whether these agents are above MIC for an extended period or not do not seem to have a significant impact on the observed antimicrobial effect but rather the magnitude of the peak concentration is associated with a more efficient bacterial kill. The third type of antibiotics which include azithromycin and vancomycin is not concentration dependent but their efficacy is linked to the *f*AUC/MIC ratio (Drusano et al. 2004; Rybak et al. 2009a, b). The 24-h exposure, measured by the AUC-to-MIC (*f*AUC/MIC) ratio, is related to the observed effect. The action of many antimicrobial agents has generally been classified based on these PKPD indices.

The determination of which indices best characterize the drug action is based on fitting a sigmoidal E_{max} model to the PD endpoint such as the bacterial $\log_{10}$ CFU/mL at 24 h or the log change in CFU/mL against the three PK/PD indices (Dudhani et al. 2010). The PD endpoint is often taken from animal studies wherein several live mouse thighs or lungs were injected with specific bacteria with predetermined MIC. The mice were then administered antibiotic at different drug doses and regimens in dose fractionation studies. The pharmacokinetic parameters ($fT>$MIC, fC_{max}/MIC, *f*AUC/MIC) were then determined for each animal. At the end of the experiments, the bacterial CFU/mL was determined from the tissues injected with bacteria. The 24-h $\log_{10}$ CFU/thigh against the PKPD indices was used to evaluate which PKPD index best characterizes the activity of the specific antimicrobial agent being tested (Dudhani et al. 2010). The relationship between the PD endpoints and PKPD indices are plotted and the best fits for the relationships were determined by R^2 (coefficient of determination). It was suggested that the PKPD index determined in mice could be extrapolated to clinical efficacy (Ambrose et al. 2007). Many of the current dosing regimens in the clinic were based on the PKPD indices determined from animal studies. Vancomycin dosing regimens, for example, were determined based on the target of AUC/MIC ratio of approximately 325 in treating ventilator-associated *Staphylococcus aureus* pneumonia (Moise-Broder et al. 2004a, b; Sakoulas et al. 2004; Rybak et al. 2009b). The vancomycin nomogram was designed to achieve a target trough concentration of 15–20 mg/L (Kullar et al. 2011).

Drusano provided an explanation of how the shape of the drug profile affects the type of cell kill for drugs that are concentration dependent versus those that are time dependent (Drusano 2004; Jumbe and Drusano 2011). The rate of kill in concentration-dependent drugs is different at each segment of the concentration–time profile and the total number of organisms killed can be approximated as an expectation which is the summation of the kill rate and time period over the specific kill rate. For time-dependent drugs, the kill rate is constant and the total

cell kill is the rate constant multiplied by the time period that the drug concentration is above the MIC.

8.2.3 Probability of Target Attainment and Clinical Breakpoints

The probability of target attainment (PTA) is often determined from simulation of 1000–10,000 individual drug concentration–time profiles using a population pharmacokinetic model and the proportion of the population above a specific target (Drusano et al. 2001; de Kock et al. 2014). The simulation generates a distribution of PKPD index (e.g., $f\text{AUC}_{24}$/MIC) which becomes the basis for determining the likelihood of achieving a certain target attainment. The $f\text{AUC}_{24}$/MIC will be used as an example because it is easier to generate than $fT > \text{MIC}$ or $f\text{C}_{max}$/MIC, as AUC can be estimated by integrating the population-PK model or estimated from the clearance values without running secondary pharmacokinetic analysis (e.g., noncompartmental analysis) of the generated profiles. The PTA is determined as the proportion of simulated individual profiles that are above a specific target, such as $f\text{AUC}_{24}$/MIC, to achieve greater than or equal to 2 $\log_{10}$ kill from animal studies, for a range of increasing MIC values and is usually evaluated using several dosing regimens in dose fractionation studies. In the study of tigecycline against *E. coli*, Ambrose et al. (2009) determined the potential tigecycline–Enterobacteriaceae susceptibility using both PTA and clinical response expectation as responses. The steady-state AUC_{24} was simulated from the distribution of clearance parameter from a population pharmacokinetic model of tigecycline. In the example in Fig. 8.1,

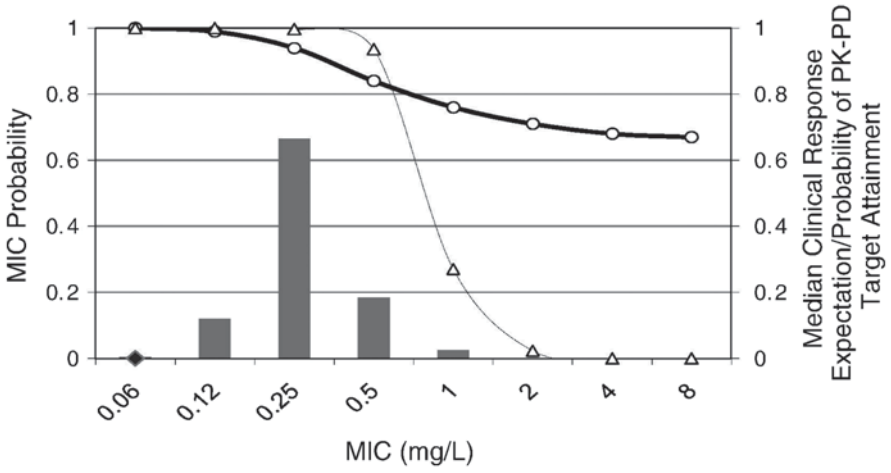

Fig. 8.1 Probability of target attainment (PTA, *open triangles*) based on $\text{AUC}_{ss,24h}$/MIC ratio, clinical response expectation (*open circles*), and tigecycline MIC distribution (*bars*), showing a trend of decreasing PTA and median clinical response expectation in increasing MIC. (Image from Ambrose et al. 2009; used with permission)

PTA is plotted as a function of MIC, represented by triangle symbols. The clinical response expectation versus MIC, represented by circular symbol, was determined from a logistic regression model that describes the PKPD relationship for efficacy in patients with complicated intra-abdominal infections (Meagher et al. 2007; Passarell et al. 2008). As shown in their study, the two metrics, namely PTA and clinical response expectation, may not necessarily correlate with each other. However, both metrics indicate a trend towards less favorable outcome with increasing MIC.

A natural extension of the PTA is to categorize the antimicrobial activity of specific treatment against a microorganism population. The European Committee on Antimicrobial Susceptibility Testing (EUCAST) has provided definitions to categorize microorganisms' antibiotic phenotype based on the quantitative antimicrobial susceptibility evaluation (Kahlmeter et al. 2003, 2006). Mouton et al. (2012) provided this categorical description:

> A microorganism is defined as susceptible by a level of antimicrobial activity associated with a high likelihood of therapeutic success. A microorganism is categorized as susceptible by applying the appropriate breakpoints in a defined phenotypic test system. Conversely, resistance is defined as a high likelihood of therapeutic failure. Ideally, clinical breakpoints should therefore distinguish between patients that are likely or unlikely to respond to antimicrobial treatment.

The clinical breakpoints are determined from (1) statistical approach such as classification and regression tree (CART) analysis or multivariate logistic regression to look for a value of PKPD index that best differentiate failures and successes in treatment outcome and (2) probabilistic approach of PTA that considers the variability in patients' pharmacokinetic and the MIC of the microorganism population. With the probabilistic approach of PTA, the microorganism with MIC values that result in the PKPD index value lower than the target are considered resistant, which translates to a lower probability of cure whereas those that result in a larger PKPD index values than a specific target are considered susceptible. This target value that separates the PKPD index for the two-microorganism phenotype is the clinical MIC breakpoint. It is noted that the clinical breakpoint may be dependent on the dosing regimen. A case is illustrated by Mouton et al. (2005, 2012) wherein the relationship between $fT>\text{MIC}$ and MIC of ceftazidime for two different dosing regimens produces two separate and distinct PTA–MIC curves as shown in Fig. 8.2. Assuming that the target is 60 % $fT>\text{MIC}$, the dosing of 500 mg thrice daily and 1 g thrice daily resulted in breakpoints of 4 and 8 mg/L MIC.

Ambrose et al. (2007) provided an excellent review to show how rodent studies translate to humans. The studies in rodent infection models showed that a total levofloxacin AUC_{24}:MIC value of 88 in immunosuppressed mice was associated with favorable microbiological response (Jumbe et al. 2003). Levofloxacin $f AUC_{24}$:MIC value of 62 determined from patients with hospital-acquired pneumonia separates those patients with 90 and 43 % response to therapy (Drusano et al. 2004).The two studies show a good correlation between rodent studies and humans, given that the PKPD indices in animal studies are closely related to that in humans.

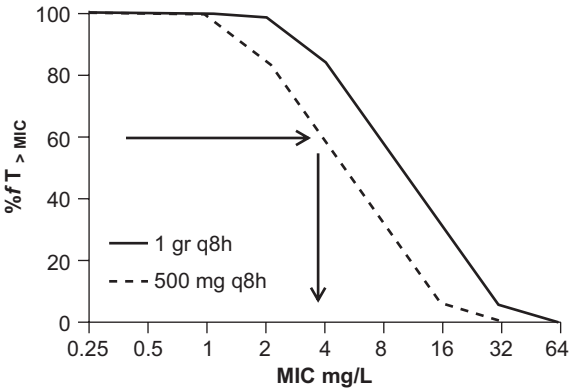

Fig. 8.2 The percent of time that the free ceftazidime concentration is above MIC (%$fT>$MIC) for two dosing regimens of ceftazidime (1 g q8h vs. 500 mg q8h) against MIC to illustrate that clinical breakpoint is dependent on the dosing regimen. *Arrows* indicate that the pharmacodynamics target corresponding to 60 %$fT>$MIC is 4 and 8 mg/L for 500 mg q8h and 1 g q8h, respectively. (Image from Mouton et al. 2012; used with permission)

8.2.4 Limitations of the MIC-based Approach

Though this approach has been used to guide dosing for various classes of antimicrobials, several shortfalls of the MIC-guided approach are discussed here. The determination of the MIC of the patient's infection often takes several days following the initial treatment and consequently the drug concentration and duration may not be optimal without the prior knowledge of the MIC, particularly when using the relationship between pharmacokinetic properties of the drug and the MIC-based PKPD indices to guide treatment. This simplification of dosing scheme is believed to potentially lead to treatment failure and may foster the emergence of resistant bacterial populations (Hoffman and Stepensky 1999).The utility of MIC assumes that this value is stationary. This is not the case because MIC within a bacteria species can change. When bacteria are exposed to a low concentration of drug, which is not enough to eradicate them, the bacteria will acquire resistance, resulting in a shift towards a higher MIC level (Tam et al. 2007a). Also depending on the species and strain of bacteria, the MIC may not be consistent across the species and strains. This scenario renders a "nonstationary" MIC. With an increasing rate of treatment failure, MIC is more likely to be changing over time due to development of resistance. For example, the AmpC β-lactamase is induced when exposed to low β-lactam concentration. The *ampC* expression is repressed by three AmpD homologues, including the previously described AmpD protein (Langaee et al. 1998, 2000) plus two additional proteins AmpDh2 and AmpDh3 (Juan et al. 2006). The two additional homologues are responsible for the stepwise *ampC* upregulation that results in hyper-expression of cephalosporinase and high level of β-lactam resistance (Juan et al. 2006).

The rate of bactericidal activity or bacteriostatic effect with different drug concentrations cannot be determined from the MIC approach. Several killing patterns can converge to the same MIC value when only the 24-h time point is measured. Relying on a "snapshot" view of MIC for defining the PKPD relationship for the entire treatment duration can be misleading.

Because only unbound drug concentration can exert its pharmacological effect, ignoring protein binding and tissue distribution of the drug can have serious implication in extrapolating *in vitro* efficacy results to human studies. When the drug enters the blood stream, it can bind to proteins such as albumin, α-, β-, or γ-globulins, α1-acid glycoprotein, lipoproteins, and/or erythrocytes (Dasgupta 2007; Treyaprasert et al. 2007; Mouton et al. 2008). The percentage of drug binding can be constant (linear) or nonconstant (nonlinear) depending on the drug concentration; characterization of protein binding across a range of drug concentrations can provide important information on its protein binding properties. Since anti-infective drugs need to get to the infection sites, for example, in skin infection, the unbound fraction of drug crosses the membrane to the infected tissue. Microdialysis procedures have been used to determine the free fraction of drug at a specific tissue (e.g., adipose and skin; Li et al. 2006). It is important to consider protein binding when translating *in vitro* results to the clinic.

8.2.5 Resistance Problem in Antimicrobial Therapy

The number of new bacterial strains with more efficient resistance mechanisms has emerged over the past decade. From the year 2000 through 2004, the percentages of methicillin susceptible and resistant *S. aureus* (MSSA and MRSA) isolates with vancomycin MIC of 1 μg/mL increased from 40 to >70% and from 10 to >60%, respectively (Wang et al. 2006). Within the span of 5 years, *S. aureus* clinical isolates have evolved towards decreasing vancomycin susceptibility. The resistance problem is not isolated to just one class of antimicrobials. Various newly discovered β-lactamases can rapidly inactivate β-lactams and some β-lactamases such as the variant of TEM-1 are resistant to β-lactamase inhibitors, for example clavulanic acid (Sideraki et al. 2001).

There are experimental evidences that the efflux pump upregulation is a first-line defense for microorganisms when challenged with antimicrobial agents (Jumbe et al. 2006; Louie et al. 2007; Drusano et al. 2009). The MexCD-OprJ, not typically expressed under noninduced conditions, exports fluoroquinolones and a number of β-lactams (Poole et al. 1996; Masuda et al. 2000b). MexXY-OprM contributes to resistance to fluoroquinolone, aminoglycoside, and some β-lactam (Aires et al. 1999; Mine et al. 1999; Masuda et al. 2000b; Sobel et al. 2003); this efflux pump is induced by tetracycline and aminoglycosides (Aires et al. 1999; Mine et al. 1999; Masuda et al. 2000a). β-Lactam resistance in clinical isolates of *Pseudomonas aeruginosa* has been shown to interplay between diminished production of OprD (an outer membrane protein that regulates the entry of carbapenems) and an increased AmpC β-lactamase activity (Quale et al. 2006).

The choice of dosing regimen affects the extent of resistance development. Tam et al. (2007a) demonstrated that the relationship between quinolone exposure and resistance amplification is characterized by an inverted U-shaped curve. This indicates that development of resistance is minimal at low antimicrobial challenge and rapidly increases over a range of drug concentration unless a sufficiently high

drug concentration kills both the susceptible and resistant populations. These results prompted recommendations for increasing doses, shorter treatment period, and combining several antimicrobials with different mechanisms of action to counter the emergence of drug-resistant bacteria (Mouton et al. 2011).

8.2.6 Combination Therapies

The resistance to treatment has also rapidly increased hospital mortality due to opportunistic infections (De Kraker et al. 2011). Administering two antibiotic drugs with different mechanisms of action can potentially restore the utilities of these agents. This approach is called combination therapy. The action of many antimicrobial agents has generally been classified based on the PKPD indices, previously described. These indices, however, are relevant primarily to monotherapy. When evaluating combination therapy that includes multiple antibiotics, the pattern may no longer be relevant. This renders the classification of combination therapy and the determination of optimal dosing strategies nontrivial.

Drugs of different mechanisms of action may act synergistically, resulting in greater than fourfold decrease in the MIC of each drug in the same pathogen *in vitro* (Paul et al. 2004). The use of aminoglycoside/β-lactam combination was practiced in the past (Piccart et al. 1984; Hoepelman et al. 1988a, b; Mondorf et al. 1989). However, the benefits from the combination were later questioned based on a meta-analysis study (Bliziotis et al. 2005). The likely reason could be that the patients who received combination therapy had a higher propensity for mortality since combination antibiotics are more commonly prescribed for the critically ill patients than the single-agent antibiotics. The one subgroup of Gram-negative pathogens, for which the question of combination therapy is currently being investigated in more and more studies, is *P. aeruginosa* (Louie et al. 2013). This bacterial species is also more common in patients who are severely ill, including the late stage of morbidity in cystic fibrosis (CF) patients (Breen and Aswani 2012). In fact, the Cystic Fibrosis Foundation guidelines recommend that an antipseudomonal β-lactam with an aminoglycoside be used in the treatment of acute pulmonary exacerbations of CF (Flume et al. 2009). CF patients were thought to have higher clearance and larger volumes of distribution, which makes dosing more challenging due to lower exposure (Spino 1991). In a matched control study, no difference was found in aztreonam volume of distribution between CF patients and matched healthy subjects but total body clearance was 30% higher in CF patients due to enhanced renal clearance as CF patients had 20% higher free fraction of the drug (Vinks et al. 2007).

The synergy of activities from combination of β-lactam and aminoglycoside would be particularly beneficial in these difficult-to-treat populations. The combination of an aminoglycoside and a β-lactam seems to be the most frequently used combination against *P. aeruginosa*. Louie et al. (2013) showed that tobramycin in combination with meropenem suppressed resistance amplification in *P. aeruginosa* at all combination regimens that were tested in the murine pneumonia model.

Safdar et al. (2004) performed a meta-analysis on combination antimicrobial therapy for bacteremia due to Gram-negative bacilli. Their overall results, combining all types of bacteria that were found in their literature search, indicated that combination therapy does not reduce mortality in patients with Gram-negative bacteremia. One limitation of their study was that the literature that they used did not stratify the outcome by the severity of illness. The patients with multiple comorbidities were also more likely to die due to their underlying conditions. In a stratified analysis, they found a significant survival benefit with combination therapy in *P. aeruginosa* bacteremia, translating to an approximately 50% mortality reduction (CI: 32–79%). This specific result provided the rationale for the hypothesis that the combination of aminoglycoside and β-lactam may provide synergism *in vivo* in a setting where the suspected infection is predominantly *P. aeruginosa* or other multiresistant Gram-negative bacilli where more than one drug would assure susceptibility to at least one of the antimicrobial agents.

The exact mechanism of action of aminoglycosides is not fully known. It was suggested that aminoglycosides could be either bacteriostatic and/or bactericidal (Bakker 1992). The bacteriostatic effect stops the growing of bacteria by inhibiting protein synthesis as the aminoglycoside binds to the 16S rRNA. The mechanism for its bactericidal effect is by disrupting the integrity of bacterial cell membrane (Shakil et al. 2008). In contrast, the mechanism of action of β-lactam antibiotics is completely known. β-Lactam antibiotics are bactericidal and act by an irreversible inhibition of the penicillin-binding proteins, which normally catalyze the cross-linking of bacterial cell walls. The drug binding to the penicillin-binding proteins kills the bacteria due to the disruption of the cell wall synthesis (Fisher et al. 2005).

The PKPD indices for combination therapy have not been explored yet. It is likely more challenging to develop since the evaluation would require a much larger set of dose fractionation studies especially combining two drugs. The *in vitro* time-course-based approach may provide a simpler methodology to evaluate dosing regimens for combination therapies than the summary PKPD variables that are MIC based.

8.3 *In Vitro* Time-Course-Based Approaches

8.3.1 Time-Kill Kinetic Studies

The advancement of PKPD modeling approach came with more defined *in vitro* methodologies. The *in vitro* time course of drug–bacterial response characterized by the kill-curve assays has been used as the basis for developing PKPD models to describe bacterial population dynamics, drug effects, and the emergence of resistance. Depending on the objective of the study, the drug concentration in these *in vitro* time-kill experiments can be relatively constant in the static situation (Garrett et al. 1966; Mielck and Garrett 1969; Garrett and Nolte 1972) or dynamically changing to mimic the *in vivo* half-life of the drug in humans (Sanfilippo and Morvillo 1968;

Sanfilippo and Schioppacassi 1973; Grasso et al. 1978). The data from static time-kill experiments are often used to develop a mathematical model that links the free drug concentrations to the bacterial response whereas dynamic time-kill data are used to validate the model and to predict the outcome in the clinic. The dynamic kill-curve provides an alternative for evaluating PKPD relationships; it simulates the time course of the unbound drug concentrations at the site of action based on a preset half-life. Using multiple pumps, the hollow fiber infection model is used to simulate concentration-time profiles of free drug concentration that mimics the *in vivo* profiles (Crandon et al. 2012). The effects of different dosing regimens, drug half-lives and even starting inocula can be simulated to study their effects on the bacterial population dynamics over a time period, for example 24 or 48 h.

8.3.2 PKPD Models of In Vitro Time-Kill Kinetics

The Logistic Growth Models The PKPD models currently used to describe the *in vitro* bacterial population dynamics came from models used to study human population dynamics. In 1838, Pierre-François Verhulst described the logistic growth model that many of the modern antimicrobial PKPD models were based on:

$$\frac{dN}{dt} = r\left(1 - \frac{N}{K}\right)N, \tag{8.1}$$

where N is the population number, r is the growth rate, and K is the carrying capacity or the maximum number of individuals that is supported by the environment (Gershenfeld 1999). The analytical solution to Eq. (8.1) is:

$$N(t) = \frac{KN_0e^{rt}}{K + N_0(e^{rt} - 1)}, \tag{8.2}$$

where N_0 is the initial population number at time $t=0$. The important property of this model is that the limit of this function as time goes to infinity is the carrying capacity: $\lim_{t\to\infty} N(t) = K$. In an *in vitro* time-kill curves of both static and dynamic systems, the bacterial CFU is restricted from growing indefinitely and usually reaches a plateau, where the net growth is zero. For this reason, the logistic growth model suitably describes this behavior.

The Compartmental Models The second type of antimicrobial PKPD model can be described in simplistic terms consisting of the natural self-replication and death of bacteria (Eq. 8.3):

$$\frac{dN}{dt} = (k_{\text{growth}} - k_{\text{death}})N, \tag{8.3}$$

where N is the bacterial population with the initial count of N_0, k_{growth} is the first-order rate constant for bacterial synthesis, and k_{death} is the first-order rate constant for bacterial death. This common structure to describe bacterial growth is also used in other disease areas such as tumor dynamic models, where a first-order self-replication rate is implemented (Jusko 1971). This model assumes that the bacteria are from a homogeneous population with the same growth and death rate constants, which may not reflect the true population of microbes, which is known to select for resistant strain in the presence of an antimicrobial challenge. The variations based on the compartmental model have improved on this limitation and will be described more thoroughly in later sections of this chapter.

The Mechanistic Models The third type of antimicrobial models considers the bacterial growth cycle, states of bacterial susceptibility, drug–receptor interaction, and the mechanisms of drug action. This type of models utilized many concepts of mathematical modeling in biology, including the two modeling approaches discussed above. Each of the mechanistic models will be discussed separately as there is no common mathematical approach across these models that can be summarized briefly.

8.3.3 Modifications on the Logistic Growth Model

To incorporate drug action to the capacity limited growth model, Eq. (8.1) can be modified to include a function to describe the drug effect:

$$\frac{dN}{dt} = k_{growth} N\left(1 - \frac{N}{N_{max}}\right) - f_{death}(\text{drug}), \tag{8.4}$$

where the added f_{death} (drug) describes the effect of an antimicrobial agent (Nolting et al. 1996; Mouton et al. 1997; Yano et al. 1998; Mouton and Vinks 2005). In this equation, as N approaches N_{max}, the growth term approaches a plateau or stationary condition, where there is no net change in the bacterial population. The drug effect is often represented by an E_{max} or a sigmoidal E_{max} model such that,

$$f_{death}(\text{drug}) = \frac{E_{max} C^{\gamma}}{EC_{50}^{\gamma} + C^{\gamma}} N, \tag{8.5}$$

where C is the drug concentration at any specific time, E_{max} is the maximum drug effect, and EC_{max} is the concentration at which the half-maximum effect is achieved. The shape parameter γ is 1 in the E_{max} model and is a parameter in the sigmoidal E_{max} model.

During the initial growth phase where $N << N_{max}$ and the growth is linear, Eq. (8.4) can be simplified to the following equation (Nolting et al. 1996):

$$\frac{dN}{dt} = \left[k_{\text{growth}} - \frac{E_{\max} C^{\gamma}}{EC_{50}^{\gamma} + C^{\gamma}} \right] N. \tag{8.6}$$

By solving for the analytical solution to Eq. (8.6), one can determine the number of bacteria at time (t) through the following equation:

$$N(t) = N_0 e^{\left(k_{\text{growth}} - \frac{E_{\max} C^{\gamma}}{EC_{50}^{\gamma} + C^{\gamma}} \right) t}. \tag{8.7}$$

Mouton and Vinks proposed that the stationary concentration (SC), which is defined as the concentration at which the growth rate equals the kill rate and is also the point at which no net change in the number of bacteria is observed, can be derived from Eq. (8.7) (Mouton and Vinks 2005). By taking the natural log of the ratio $N(t)/N_0$ divided by time, which is equivalent to $k_{\text{growth}} - \frac{E_{\max} C^{\gamma}}{EC_{50}^{\gamma} + C^{\gamma}}$, one can obtain the equation for C:

$$C = EC_{50} \left[\frac{k_{\text{growth}} - \frac{1}{t} ln \frac{N(t)}{N_0}}{E_{\max} - \left(k_{\text{growth}} - \frac{1}{t} ln \frac{N(t)}{N_0} \right)} \right]^{\frac{1}{\gamma}}. \tag{8.8}$$

When there is no net change in the number of bacteria, the term $\frac{1}{t} ln \frac{N(t)}{N_0}$ approaches 0 and the SC is defined as:

$$SC = EC_{50} \left[\frac{k_{\text{growth}}}{E_{\max} - k_{\text{growth}}} \right]^{\frac{1}{\gamma}}. \tag{8.9}$$

The SC is not to be confused with the MIC, as SC refers to the concentration where no net bacterial growth occurs. It is often assumed that bacterial growth occurs when the drug concentration is below the MIC. Mouton and Vinks had shown that a correction factor to the SC equation might be required to estimate the MIC (Mouton and Vinks 2005):

$$MIC = EC_{50} \left[\frac{k_{\text{growth}} - 0.29}{E_{\max} - (k_{\text{growth}} - 0.29)} \right]^{\frac{1}{\gamma}}. \tag{8.10}$$

The value 0.29 is obtained from the kill curves such that $N(t)$ reached 10^8 CFU/mL at 18 h, assuming an initial inoculum of 5×10^5 CFU/mL. This correction factor

is therefore dependent on the specific system that is being tested. The relationship between MIC and SC is described in greater detail in Mouton and Vinks (2005).

Tam et al. (2008) modified the logistic growth model to study the effects of gentamicin and amikacin on the *in vitro* time-kill kinetics of *P. aeruginosa* ATCC 27853 and *Acinetobacter baumannii* ATCC BAA 747, respectively, by introducing an adaptation factor to the EC_{50} parameter:

$$f_{\text{death}}(\text{drug}) = \frac{E_{\max} C^{\gamma}}{(\propto EC_{50})^{\gamma} + C^{\gamma}} N \tag{8.11}$$

α is defined as:

$$\propto = 1 + \beta(1 - e^{-C\tau t}), \tag{8.12}$$

where τ is the exponent of the adaptation factor and β is the maximal adaptation. The range of values for the function $1 - e^{-C\tau t}$ is between 0 and 1. The adaptation function α starts from a baseline EC_{50} and increases over time to a maximal value of β, if τ is positive.

Delay functions were applied to both the growth rate and the drug effect function to describe the population dynamics of *Streptococcus pneumoniae, Haemophilus influenzae,* and *Moraxella catarrhalis* in the presence of azithromycin (Treyaprasert et al. 2007). The delay function has the following form:

$$\frac{dN}{dt} = \left[k_{\text{growth}} \left(1 - \frac{N}{N_{\max}} \right) (1 - e^{-xt}) - \left(\frac{k_{\max} C}{EC_{50} + C} \right) (1 - e^{-yt}) \right] N. \tag{8.13}$$

One can see that the delay function has a similar form to the adaptation function discussed above. The two equations, $1 - e^{-xt}$ and $1 - e^{-yt}$ (Mouton et al. 1997), behave like a cumulative density function starting from 0 at $t = 0$ to a maximum value of 1 as $t \to \infty$. The delay function acts as a modulator to allow the curves to conform to the S-shaped pattern of bacterial growth which is often observed during the first couple of hours of the time-kill kinetic experiments in the presence of low antimicrobial agent concentrations. The two functions also shape the transition to plateau after a decrease then increase in bacterial population at the antimicrobial concentrations that allow for bacterial regrowth to occur. An example of model using the delay function is shown in Fig. 8.3. Another modification introduced a second compartment for the persistent bacterial population to differentiate from the first compartment of susceptible bacteria; this alteration was used to model the effect of oxazolidinone on *Staphylococcus aureus* (Schmidt et al. 2009).

Bulitta et al. (2009) linked the bacterial population dynamic to cell wall synthesis, and drug effect of ceftazidime on cell wall synthesis to describe the lag time in bactericidal effect of β-lactams. The study examines the inoculum effect of ceftazidime against *P. aeruginosa*. The natural first-order death rate was dependent on the number of existing CFU in the system and the logistic growth part of the model

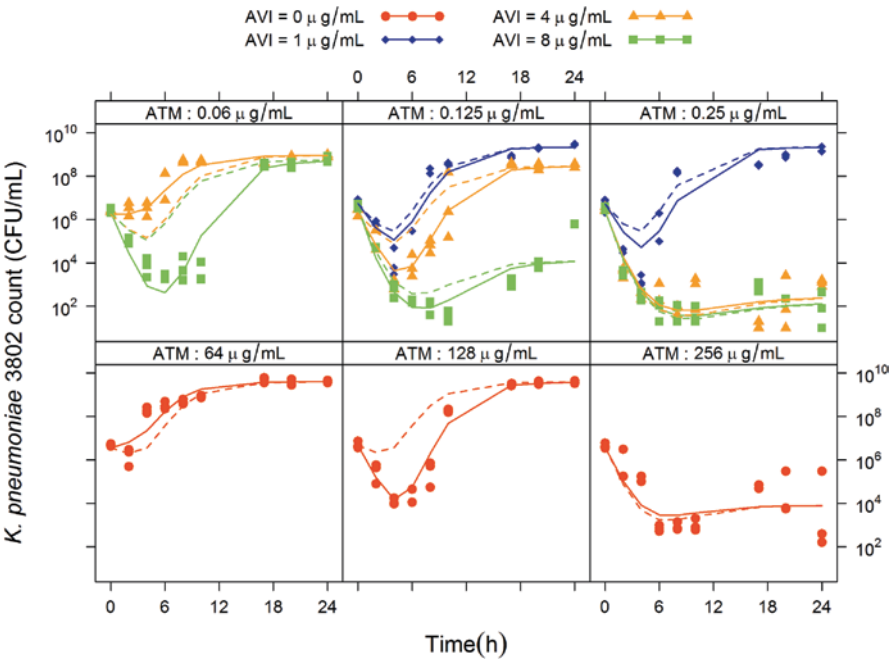

Fig. 8.3 Time-kill kinetics and model prediction of aztreonam-avibactam effect against *K. pneumoniae*

was dependent on both the cell wall synthesis and CFU. The drug effect acts on the compartment representing the cell wall dynamics, since the primary mode of action of ceftazidime is to inhibit cell wall synthesis:

$$\frac{dCW}{dt} = \left[\left(1 - \frac{C_B}{IC_{50,CW} + C_B}\right) - CW\right] \cdot k_{\text{out},CW} \tag{8.14}$$

$$\frac{dN}{dt} = \left[k_{\text{growth}}\left(1 - \frac{N}{N_{\max}}\right)CW - k_{\text{death}}\right]N, \tag{8.15}$$

where CW represents a hypothetical cell wall measurement, whose synthesis is expressed as a fraction of the baseline value. The $IC_{50,CW}$ is the concentration of ceftazidime in the broth that inhibits 50% of cell wall synthesis and $k_{\text{out},CW}$ is the first-order rate constant for the cell wall turnover. The investigators claimed that this model accounts for the slow onset due to the delay between ceftazidime binding to the penicillin-binding proteins and the depletion of cell wall components (Bulitta et al. 2009).

8.3.4 Examples of the Compartmental Model

During the linear growth phase just before reaching the plateauing phase, the population dynamics can be described by simple first-order growth and death rates that are dependent on the bacterial burden present at the specific time. In addition to the logistic growth model, other strategies had been utilized to describe the decrease in the net growth rate as the system approaches the plateau wherein the net bacterial growth is zero. One approach is to implement a phenotypic switch between susceptible and persistent population such that the persisters have a markedly reduced growth rate (Balaban et al. 2004). The overall change in the total number of bacteria would then be the sum of those in susceptible (S) and in persistent resting (R) states, such that:

$$A_{\text{total}} = S + R \tag{8.16}$$

The transition between the two states is defined by their respective rate constants. Nielsen et al. presented an example of compartmental model wherein a two-compartment model was used to describe the *in vitro* effect of a number of antibiotics, including moxifloxacin, vancomycin, benzylpenicillin, cefuroxime, and erythromycin against *Streptococcus pyogenes* (Nielsen et al. 2007). The delay in the effect of drugs was modeled using an effect compartment model for the drug. The following assumptions were made: (1) The drug effect is to increase the death rate of the susceptible state and (2) the antimicrobials have no effect on the persistent population. The differential equations for the two bacterial populations are shown in the following equations:

$$\frac{dS}{dt} = k_{\text{growth}} S - k_{\text{death}} S - k_{SR} S + k_{RS} R \tag{8.17}$$

$$\frac{dR}{dt} = k_{SR} S - k_{RS} R - k_{\text{death}} R. \tag{8.18}$$

As the persistent population is unlikely to return to the susceptible state for the duration of the experiment, the transfer rate for the return to the susceptible state was assumed to be negligible and k_{RS} was fixed to 0. The transfer rate constant that indicates the rate of change from the susceptible to the persistent states, k_{SR}, dictates the growth-limited capacity using the following equation:

$$k_{SR} = \frac{k_{\text{growth}} - k_{\text{death}}}{B_{\max}} (S + R), \tag{8.19}$$

where $B_{\max}$ is the maximum number of bacteria supported by the system.

The investigators evaluated whether the drug decreases the growth rate or increases the rate of death. The later scenario, increase in death rate, was examined as either an additive or a proportional effect. The equations to describe the three different scenarios are shown below:

$$\frac{dS}{dt} = k_{\text{growth}}(1 - f(\text{drug}))S - k_{\text{death}}S - k_{SR}S + k_{RS}R \tag{8.20}$$

$$\frac{dS}{dt} = k_{\text{growth}}S - (k_{\text{death}} + f(\text{drug}))S - k_{SR}S + k_{RS}R \tag{8.21}$$

$$\frac{dS}{dt} = k_{\text{growth}}S - k_{\text{death}}(1 + f(\text{drug}))S - k_{SR}S + k_{RS}R, \tag{8.22}$$

where $f(\text{drug})$ is a sigmoidal $E_{\max}$ model to account for the effect of various drug concentrations.

In a follow-up study, the same group described a mechanism for adaptive resistance in *E. coli* due to gentamicin by introducing two additional compartments that regulate resistance development (Mohamed et al. 2012):

$$\frac{dAR_{\text{off}}}{dt} = k_{\text{off}}AR_{\text{on}} - k_{\text{on}}AR_{\text{off}}C \tag{8.23}$$

$$\frac{dAR_{\text{on}}}{dt} = k_{\text{on}}AR_{\text{off}}C - k_{\text{off}}AR_{\text{on}}, \tag{8.24}$$

where AR_{off} represents the adaptive resistance in dormant stage and AR_{on} is for the active state; the transfer between states is represented by k_{off} and k_{on}; and C refers to gentamicin concentration. A greater flexibility was achieved by the two additional compartments as can be seen in how the model adapted to the data trend. The investigators noted that the model is suitable for gentamicin in the context of compartmental models.

8.3.5 Examples of Mechanistic Models

A similar approach to the compartment model involving three-state susceptibility was used to study colistin effect in *P. aeruginosa* (Bulitta et al. 2010). In this model, the states of susceptibility included susceptible (S), intermediate (I), and resistant (R). A fourth compartment or state ($CFU_{S,lag}$) was introduced to account for the difference between the initial total bacterial burden, CFU_{ALL}, and the initial conditions of the susceptible, intermediate and the resistant populations.

$$CFU_{\text{ALL}} = CFU_{S,lag} + CFU_S + CFU_I + CFU_R. \tag{8.25}$$

The intermediate and resistant populations were assumed to be fractions of the initial total bacterial burden, CFU_0:

$$\frac{dCFU_{S,\text{lag}}}{dt} = (-k_{\text{lag}} - INH_{\text{Kill}} \cdot \leq k_{2S} \cdot C_{\text{Colistin,eff}}) \cdot CFU_{S,\text{lag}} \tag{8.26}$$

$$\frac{dCFU_S}{dt} = \left(\frac{INH_{\text{Rep}} \cdot VG_{\max,S}}{CFU_m + CFU_{\text{ALL}}} - k_d - INH_{\text{Kill}} \cdot k_{2S} \cdot C_{\text{Colistin,eff}} \right) \cdot CFU_S + k_{\text{lag}} \tag{8.27}$$

$$\frac{dCFU_I}{dt} = \left(\frac{INH_{\text{Rep}} \cdot VG_{\max,I}}{CFU_m + CFU_{\text{ALL}}} - k_d - INH_{\text{Kill}} \cdot k_{2I} \cdot C_{\text{Colistin,eff}} \right) \cdot CFU_I \tag{8.28}$$

$$\frac{dCFU_R}{dt} = \left(\frac{INH_{\text{Rep}} \cdot VG_{\max,R}}{CFU_m + CFU_{\text{ALL}}} - k_d - INH_{\text{Kill}} \cdot k_{2R} \cdot C_{\text{Colistin,eff}} \right) \cdot CFU_R, \tag{8.29}$$

where $VG_{\max}$ refers to the maximal rate of bacterial growth in the unit of CFU/(mL.h), CFU_m is the bacterial density that produces 50% of the maximal growth rate, k_{d} is the natural death rate, k_{lag} represents the first-order growth rate constant associated with the slower initial growth phase of the susceptible population in the lag compartment, INH_{Kill} and INH_{Rep} are represented by the following equations:

$$INH_{\text{Kill}} = 1 - I_{\max,\text{Kill}} \cdot \frac{C_{\text{Signal}}}{IC_{50} + C_{\text{Signal}}} \tag{8.30}$$

$$INH_{\text{Rep}} = 1 - I_{\max,\text{Rep}} \cdot \frac{C_{\text{Signal}}}{IC_{50} + C_{\text{Signal}}}. \tag{8.31}$$

INH_{Kill} and INH_{Rep} are inhibition of killing and of replication by signal molecules, C_{signal}. The synthesis of freely diffusible signal molecules C_{Signal} by the bacteria was assumed to inhibit or to slow down the killing effects of colistin. The $I_{\max,\text{Kill}}$ and $I_{\max,\text{Rep}}$ were the maximum inhibition of killing and of replication; the concentration of signal molecules to achieve 50% of the maximum inhibition is the IC_{50}. The kinetic behavior of the hypothetical signal molecule is described by the following differential equation:

$$\frac{dC_{\text{Signal}}}{dt} = \left(CFU_{\text{ALL}} \frac{ml}{CFU} - C_{\text{Signal}} \right) k_{\text{deg}}, \tag{8.32}$$

where k_{deg} is the degradation rate constant.

The assumption was made that the effect of colistin is to displace competitively both Mg^{2+} and Ca^{2+} from the binding sites in the outer membrane and the resulting displacement is responsible for colistin killing effect. The model utilizes receptor occupancy model to describe the competitive inhibition of colistin with Mg^{2+} and Ca^{2+} for the membrane binding sites. The fractional occupancy of these cations as a function of the molar sum of Mg^{2+} and Ca^{2+} concentrations as well as colistin concentration in mg/L is defined such that:

$$Fr_{\text{Cations}} = \frac{C_{\text{Cations}}}{K_{d,\text{Cations}} + C_{\text{Cations}} + \frac{K_{d,\text{Cations}}}{K_{d,\text{Colistin}}} \cdot \frac{C_{\text{Colistin}}}{M_m}}, \tag{8.33}$$

where $K_{d,Cations}$ and $K_{d,Colistin}$ are the dissociation constants for the two cations and colistin, respectively; M_m is the average molecular mass of colistin A and B, which are the two primary components of colistin; and C refers to the concentration of the respective components in the broth. The fraction of the receptors that were not bound to Mg^{2+} or Ca^{2+} was used to compute the effective colistin concentration at the target site. The effective colistin concentration, $C_{\text{Colistin,eff}}$, was a Hill function dependent on the Fr_{Cations} and colistin concentration in broth, C_{Colistin}:

$$C_{\text{Colistin,eff}} = \frac{(1 - Fr_{\text{Cations}})^{\gamma}}{EC_{50}^{\gamma} + (1 - Fr_{\text{Cations}})^{\gamma}}. \tag{8.34}$$

An important difference between this model and the logistic growth or the compartment models is that it assumes that the drug has an effect on all types of bacteria from the susceptible to the intermediate to the resistant ones. The limitation of such a complex model is that the data from an *in vitro* time-kill study will not be sufficient to characterize the model parameters and that many of the parameter values will have to be derived from the literature.

Another compartmental-type model incorporated mechanisms involved in the life cycle of bacterial replication, autolysis, and ceftazidime effect against *P. aeruginosa* (Bulitta et al. 2009). The model utilizes a two-compartment model for the bacteria population and a turnover model to describe the time-kill behavior in the presence of antimicrobial agents. The bacterial life-cycle model utilizes two states for the susceptible population, wherein the first state, S_1, describes the cycle immediately after cell replication whereas the second state, S_2, occurs just before replication:

$$\frac{dS_1}{dt} = 2\left[1 - \frac{CFU_{\text{total}}}{CFU_{\text{total}} + CFU_{\max}}\right]\left[1 - ALys_S\right] \cdot k_{21} \cdot S_2 - Inh_{k12} \cdot k_{12} \cdot S_1 \tag{8.35}$$

$$\frac{dS_2}{dt} = -k_{21} \cdot S_2 + Inh_{k12} \cdot k_{12} \cdot S_1, \tag{8.36}$$

where k_{12} and k_{21} are first-order transition rates between the first and second states. k_{12} is determined from the mean generation time (MGT) such that $k_{12} = 1/MGT_{12}$. The MGT is discussed later in this section. Inh_{k12} is identical to Eqs. (8.30) and (8.31). The factor 2 was used to represent bacterial doubling during cell replication. The autolysin activity $ALys_S$ is stimulated by ceftazidime and is described by a turnover model:

$$\frac{dALys_S}{dt} = \left[\frac{S_{\max,S} \cdot C_B}{SC_{50} + C_B} - \left(1 + \frac{S_{\max,\text{loss}} \cdot C_{Sig1}}{C_{50,\text{Sig}} + C_{\text{Sig1}}}\right) \cdot ALys_S\right] \cdot k_{\text{out}}. \tag{8.37}$$

The $S_{\max,S}$ value limits the maximum value of $ALys_S$ to 1, indicating that a high drug concentration can completely inhibit replication. SC_{50} refers to the drug concentration at which autolysin is half maximally stimulated. $S_{\max,\text{loss}}$ represents the

maximum extent of the inoculum effect at high signal molecule concentrations. In contrast to the previous model, the current one assumes two signal molecules with the following behavior:

$$\frac{dC_{\text{Sig1}}}{dt} = (CFU_{\text{ALL}} - C_{\text{Sig1}}) \cdot k_{\text{deg}} - k_{S12} \cdot C_{\text{Sig1}} + k_{S21} \cdot C_{\text{Sig2}} \tag{8.38}$$

$$\frac{dC_{\text{Sig2}}}{dt} = k_{S12} \cdot C_{\text{Sig1}} - k_{S21} \cdot C_{\text{Sig2}},$$

where the initial conditions for C_{Sig1} and C_{Sig2} were CFU_0 and $CFU_0 \cdot k_{S12} / k_{S21}$. The role of the first signal molecule C_{Sig1} is to slow down the replication rate and C_{Sig1} is in equilibrium with C_{Sig2}.

The life-cycle growth model involving two-stage susceptibility was applied to the study of linezolid against vancomycin-resistant *enterococci* and *S. aureus* (Tsuji et al. 2012a, b). Linezolid effect was assumed to inhibit protein synthesis; a turnover-type model was used to describe its effect:

$$\frac{dP}{dt} = k_{\text{Prot}} \left[\left(1 - \frac{C_{\text{drug}}}{IC_{50} + C_{\text{drug}}} \right) - P \right], \tag{8.39}$$

where P represents the protein pool whose steady-state maximum value is 1, IC_{50} is the linezolid concentration that produces half-maximum inhibition of protein synthesis and k_{prot} is the turnover rate constant of the protein pool. The probability of death due to lack of protein represented by ($Lack = 1 - P$) was defined by the following function:

$$Prob_{\text{death}} = I_{\text{max,Rep}} \cdot Lack. \tag{8.40}$$

The E_{max}-type model was used to describe the plateau phase of the primary susceptible bacterial population. A two-state susceptibility bacterial population was described for S_1 and S_2, similar to the model described in Eqs. (8.35) and (8.36), with the function $1 - Prob_{\text{death}}$ replacing the $1 - ALys_s$ and Inh_{12} was fixed to 1. The number of sensitive alleles (N_{Sen}) was a covariate to determine the IC_{50} of linezolid in inhibiting protein synthesis:

$$IC_{50} = IC_{50\text{Sen}0} \cdot \left(1 - \frac{I_{\text{max,Sen}} \cdot N_{\text{sen}}^{\text{HSen}}}{N_{50,\text{Sen}}^{\text{HSen}} + N_{\text{sen}}^{\text{HSen}}} \right) \cdot f_{HFIM}, \tag{8.41}$$

where $IC_{50\text{Sen}0}$ refers to the IC_{50} for a strain with no sensitive alleles, $I_{\text{max,Sen}}$ refers to the maximum fractional decline for IC_{50}, f_{HFIM} refers to the ratio of IC_{50} in the hollow fiber infection model compared with the static time-kill model, and $HSen$ is the hill coefficient.

The MGT is defined as the doubling time required for the bacteria to double in number and is computed from the net growth rate, similar to the computation of half-life (Garrett 1978):

$$MGT = \frac{\ln(2)}{k_{net}}, \tag{8.42}$$

where $k_{net} = k_{growth} - k_{death}$. In the model, the number of resistant alleles (N_{res}) was used as a covariate to compute the MGT (MGT_{12}) wherein k_{12} was computed as $1/MGT_{12}$:

$$MGT_{12} = MGT_0 \cdot \left(1 + \frac{S_{max,Res} \cdot N_{res}^{HRes}}{N_{50,Res}^{HRes} + N_{res}^{HRes}}\right), \tag{8.43}$$

where $N_{50,Res}$ refers to the number of resistant alleles that produce 50% of $S_{max,Res}$, which is the maximum fractional increase in MGT_{12} due to resistant alleles, and *HRes* is the Hill coefficient.

The goal of anti-infective therapy is to administer an effective dose of drug to a patient with a high probability of achieving therapeutic success while minimizing toxicity. Mechanistic models are believed to better describe the processes and subtleties of nature that may not be apparent in an empirical model (Lo et al. 2011). Whether mechanistic models are better predictors of clinical outcome over the empirical and semi-mechanistic models is yet to be proven.

8.3.6 Models of Combination Therapy

We have recently modified the logistic growth model to study the enhanced potency of aztreonam by avibactam using a shift in EC_{50} that approximates the reduction in MIC values at increasing avibactam concentrations against *K. pneumoniae* (Fig. 8.3; Sy et al. 2013). The reduction in aztreonam EC_{50} as a function of avibactam concentration was approximated by an empirical bi-exponential decay equation. Avibactam, being a β-lactamase inhibitor, has no antimicrobial activity against *K. pneumoniae*, but rather restores the potency of aztreonam by inhibiting aztreonam removal and degradation by the β-lactamase enzymes. The advantages of this simple approach are that the model-predicted aztreonam EC_{50} closely mimicked the MIC value and the generated curves described well the observed bacterial dynamics in response to the combination therapy.

The Loewe additivity was utilized to evaluate the effect of combination therapy consisting of a novel aminoglycoside, vertilmicin, and ceftazidime on *P. aeruginosa* (Zhuang et al. 2013). The bacterial population model was based on a two-state logistic growth model. In contrast to the aztreonam–avibactam study, both agents have antimicrobial effects with different mechanisms of action. Greco et al. pro-

posed a generalized sigmoidal E_{max} equation to describe Loewe additivity of the combined effect of two agents (Greco et al. 1995):

$$1 = \frac{C_1}{EC_{50,1}\left(\frac{E_{max}}{E_{max}-k_{max}}\right)^{1/m_1}} \frac{C_2}{EC_{50,2}\left(\frac{E_{max}}{E_{max}-k_{max}}\right)^{1/m_2}} + \frac{\gamma \cdot C_1 \cdot C_2}{EC_{50,1} \cdot EC_{50,2}\left(\frac{E_{max}}{E_{max}-k_{max}}\right)^{(1/2m_1+1/2m_2)}}. \tag{8.44}$$

The additive effect of the two agents is described by the sum of the first two terms and the third term is an interaction term, wherein γ is a parameter that indicates synergism–antagonism interaction. The interaction is additive if the 95% confidence interval of the γ estimate overlaps the zero value. If $\gamma > 0$ or $\gamma < 0$, the interaction is either synergistic or antagonistic, respectively. In the model, m_1 and m_2 were assumed to be equal. An additional interaction term λ was incorporated to the effect of an initial killing rate of both agents (k_{max}) such that:

$$k_{max} = k_{max,1} + k_{max,2} + \lambda \cdot k_{max,1} \cdot k_{max,2}. \tag{8.45}$$

The resulting E_{max} model to evaluate the combination of vertilmicin and ceftazidime was:

$$E_{max} = \frac{k_{max}\left(\frac{C_1}{\alpha_1 EC_{50,1}} + \frac{C_2}{\alpha_2 EC_{50,2}} + \frac{\gamma C_1 C_2}{\alpha_1 \alpha_2 \cdot EC_{50,2} \cdot EC_{50,2}}\right)^k}{1 + \left(\frac{C_1}{\alpha_1 EC_{50,1}} + \frac{C_2}{\alpha_2 EC_{50,2}} + \frac{\gamma C_1 C_2}{\alpha_1 \alpha_2 \cdot EC_{50,2} \cdot EC_{50,2}}\right)^k}, \tag{8.46}$$

where $\propto_i$ refers to the adaptation factor mentioned in Eq. (8.12). This empirical approach described well the combined effects of an aminoglycoside and a β-lactam against *P. aeruginosa*.

8.3.7 Models Estimating Resistant Subpopulation

To quantify the resistant bacterial subpopulation in an *in vitro* time-kill experiment, one can plate the bacteria in agar plates that contained the antimicrobial agent at three times the MIC or greater. This approach ensures that susceptible bacteria are removed by the drug. The choice for at least thrice the MIC is that twice the MIC level is still within the error measurement of susceptibility determination. An alternative method to determine resistance development is to determine the MIC after the 24-h time-kill experiment.

The subpopulation of resistant bacteria is a very small fraction of the total bacterial population that is predominantly drug-susceptible wild-type population. The probability of detecting the resistant subpopulation is dependent on the inoculum size or total bacterial burden and the frequency of mutation to the drug-specific resistance (Jumbe and Drusano 2011). For a resistant subpopulation to amplify effectively, both the fitness of the mutant and the selection pressure presented by the antimicrobial agent are important determining factors. Jumbe and Drusano proposed equations that incorporate probability estimates to a general model that governs the natural replication of bacteria and the death due to antimicrobial effect (Jumbe and Drusano 2011):

$$\frac{dS}{dt} = \zeta_{G,s} \cdot E_{R,s}\left[a(t)\right] \cdot (1-P) S(t) + \zeta_{G,r} \cdot E_{R,r}\left[a(t)\right] \cdot P \cdot \Gamma \cdot R(t) - \Psi_{K,s} \cdot E_{D,s}\left[a(t)\right] \cdot S(t) \tag{8.47}$$

$$\frac{dR}{dt} = \zeta_{G,r} \cdot E_{R,r}\left[a(t)\right] \cdot (1-P) \cdot \Gamma \cdot R(t) + \zeta_{G,s} \cdot E_{R,s}\left[a(t)\right] \cdot P \cdot S(t) - \Psi_{K,r} \cdot E_{D,r}\left[a(t)\right] \cdot R(t), \tag{8.48}$$

where S and R represent susceptible and resistant bacterial population, ζ_G and Ψ_K are rates related to the natural replication and bacterial death, and $E_R a(t)$ and $E_D a(t)$ refer to antimicrobial effects on replication and death. P is the probability related to mutation occurrence and Γ determines the relative fitness of the susceptible to resistant population. This modeling strategy of estimating the proportion of each subpopulation was adopted in the model used to study colistin effect in *P. aeruginosa* that was previously discussed (Bulitta et al. 2010). Tam et al. (2005, 2007b) applied the PKPD model to describe the dynamics of garenoxacin-sensitive and -resistant subpopulations of *P. aeruginosa* and *S. aureus* in response to fluctuating concentrations of quinolone drugs. Their study showed that exposure below a specific breakpoint allowed resistant subpopulation to grow rapidly. Jumbe et al. (2003) showed the predictive value of modeling and simulation in determining the proliferation of resistant population in insufficient antimicrobial therapy.

8.3.8 Models Incorporating Host Defense

Rodent studies provide a good model to evaluate the effect of the host's immune system on the time course of antimicrobial effect by chemotherapeutic agents, as well as the antimicrobial effect imposed by the immune system. The effect of the immune system can be quantified by comparing the immune-competent mice and the neutropenic mice. To evaluate the contribution of granulocytes on bacterial kill, studies performed in the mouse thigh-infection model and the murine model of pneumonia showed that granulocytes alone are potent in eradicating bacteria at a low inoculum size whereas for bacterial burden of $\geq 10^7$ CFU/g of tissue, a net bac-

terial growth was observed after 24 h (Drusano et al. 2010, 2011a, b). The model incorporating host defense has similar mathematical form as that of drug effects and combination study (Jumbe and Drusano 2011):

$$\frac{dN}{dt} = \zeta_G \cdot E_R\left[a(t)\right] \cdot N(t) - C_K \cdot E_D\left[a(t) + E_P + E_P \cdot E_I + E_I\right] \cdot N(t), \quad (8.49)$$

where E_P and E_I refer to the humoral and cellular response of the host and the innate adaptive immunity interaction is characterized by $E_P \cdot E_I$. When the combined effect of the two host's defense processes is greater than the microorganism natural proliferation rate, $C_K >> \zeta_G$, the host immunity can remove the infection without therapeutic intervention (Jumbe and Drusano 2011).

8.3.9 Linking In Vitro Models to PKPD Indices

The concentration–effect relationship of ceftazidime established from *in vitro* time-kill curves was used to explain the PKPD index that $\%fT > \text{MIC}$ of 40 % is required for a static effect *in vivo* (Mouton et al. 2007). The logistic-growth model was used to simulate the bacterial kill over time in dosing regimens of 1 mg every 2 h to 256 mg every 8 h. The pharmacokinetic profiles were simulated using parameters for mice and humans. The dosing regimens that resulted in a predicted static effect (i.e., CFU at 24 h $\leq$ CFU at 0 h) were then evaluated and the corresponding $\%fT > \text{MIC}$ for the dosing regimen was determined. For a 2 $\log_{10}$ decrease after 24 h, the authors estimated that $\%fT > \text{MIC}$ of at least 50 % is required. Neilsen et al. (2011) used a semi-mechanistic PKPD model based on the compartment approach to predict the PKPD indices of several antibiotics. They have shown that simulation studies using the information from *in vitro* studies can be used to predict the PKPD indices of antimicrobial agents but cautioned that the determination of the suitable PKPD index for a particular drug is sensitive to the study conditions including dosing frequency as well as uncertainty in the MIC values.

8.4 Summary

Due to rapid evolution of bacterial resistance to many of the commercially available antimicrobial agents, many investigators have called for drug discovery and development programs that target suppression of resistance selection and eradication of drug-resistant infections (Jumbe and Drusano 2011; Nielsen and Friberg 2013). Pharmacometrics has an important role in developing dosing strategies to effectively achieve these two goals. The search for regimens and drug combinations in anti-infectives has benefitted tremendously from modeling and simulation. Many of the current dosing regimens were based on understanding of the PK–PD relationship between antimicrobial agents and bacterial infection.

In this chapter, we have summarized the pharmacometric models that were used to derive the current state-of-the-art treatment paradigm. More progress can still be made to maximize patients' benefits through implementing treatment programs based on sound analysis of all available information from *in vitro* studies, animal models of infections, and clinical data.

References

Aires JR, Kohler T, Nikaido H, Plesiat P (1999) Involvement of an active efflux system in the natural resistance of *Pseudomonas aeruginosa* to aminoglycosides. Antimicrob Agents Chemother 43:2624–2628

Ambrose PG, Bhavnani SM, Rubino CM, Louie A, Gumbo T, Forrest A, Drusano GL (2007) Pharmacokinetics–pharmacodynamics of antimicrobial therapy: it's not just for mice anymore. Clin Infect Dis 44:79–86

Ambrose PG, Meagher AK, Passarell JA, Van Wart SA, Cirincione BB, Rubino CM, Korth-Bradley JM, Babinchak T, Ellis-Grosse E (2009) Use of a clinically derived exposure–response relationship to evaluate potential tigecycline-Enterobacteriaceae susceptibility breakpoints. Diagn Microbiol Infect Dis 63:38–42

Bakker EP (1992) Aminoglycoside and aminocyclitol antibiotics: hygromycin B is an atypical bactericidal compound that exerts effects on cells of *Escherichia coli* characteristics for bacteriostatic aminocyclitols. J Gen Microbiol 138:563–569

Balaban NQ, Merrin J, Chait R, Kowalik L, Leibler S (2004) Bacterial persistence as a phenotypic switch. Science 305:1622–1625

Bliziotis IA, Samonis G, Vardakas KZ, Chrysanthopoulou S, Falagas ME (2005) Effect of aminoglycoside and beta-lactam combination therapy versus beta-lactam monotherapy on the emergence of antimicrobial resistance: a meta-analysis of randomized, controlled trials. Clin Infect Dis 41:149–158

Breen L, Aswani N (2012) Elective versus symptomatic intravenous antibiotic therapy for cystic fibrosis. Cochrane Database Syst Rev 7:CD002767

Bulitta JB, Ly NS, Yang JC, Forrest A, Jusko WJ, Tsuji BT (2009) Development and qualification of a pharmacodynamic model for the pronounced inoculum effect of ceftazidime against *Pseudomonas aeruginosa*. Antimicrob Agents Chemother 53:46–56

Bulitta JB, Yang JC, Yohonn L, Ly NS, Brown SV, D'hondt RE, Jusko WJ, Forrest A, Tsuji BT (2010) Attenuation of colistin bactericidal activity by high inoculum of *Pseudomonas aeruginosa* characterized by a new mechanism-based population pharmacodynamic model. Antimicrob Agents Chemother 54:2051–2062

Craig WA (1998) Pharmacokinetic/pharmacodynamic parameters: rationale for antibacterial dosing of mice and men. Clin Infect Dis 26:1–10; quiz 11–12

Crandon JL, Schuck VJ, Banevicius MA, Beaudoin ME, Nichols WW, Tanudra MA, Nicolau DP (2012) Comparative in vitro and in vivo efficacies of human simulated doses of ceftazidime and ceftazidime-avibactam against *Pseudomonas aeruginosa*. Antimicrob Agents Chemother 56:6137–6146

Dasgupta A (2007). Usefulness of monitoring free (unbound) concentrations of therapeutic drugs in patient management. Clin Chim Acta 377:1–13

De Kraker ME, Davey PG, Grundmann H (2011) Mortality and hospital stay associated with resistant *Staphylococcus aureus* and *Escherichia coli* bacteremia: estimating the burden of antibiotic resistance in Europe. PLoS Med 8:e1001104

De Kock L, Sy SK, Rosenkranz B, Diacon AH, Prescott K, Hernandez KR, Yu M, Derendorf H, Donald PR (2014) The pharmacokinetics of para-aminosalicylic acid in HIV-uninfected and HIV co-infected tuberculosis patients receiving antiretroviral therapy, managed on multi-

drug-resistant and extensively drug-resistant tuberculosis. Antimicrob Agents Chemother (pii: AAC.03073-14; epub ahead of print)
Drusano GL (2004) Antimicrobial pharmacodynamics: critical interactions of 'bug and drug'. Nat Rev Microbiol 2:289–300
Drusano GL, Preston SL, Hardalo C, Hare R, Banfield C, Andes D, Vesga O, Craig WA (2001) Use of preclinical data for selection of a phase II/III dose for evernimicin and identification of a preclinical MIC breakpoint. Antimicrob Agents Chemother 45:13–22
Drusano GL, Preston SL, Fowler C, Corrado M, Weisinger B, Kahn J (2004) Relationship between fluoroquinolone area under the curve: minimum inhibitory concentration ratio and the probability of eradication of the infecting pathogen, in patients with nosocomial pneumonia. J Infect Dis 189:1590–1597
Drusano GL, Liu W, Fregeau C, Kulawy R, Louie A (2009) Differing effects of combination chemotherapy with meropenem and tobramycin on cell kill and suppression of resistance of wild-type *Pseudomonas aeruginosa* PAO1 and its isogenic MexAB efflux pump-overexpressed mutant. Antimicrob Agents Chemother 53:2266–2273
Drusano GL, Fregeau C, Liu W, Brown DL, Louie A (2010) Impact of burden on granulocyte clearance of bacteria in a mouse thigh infection model. Antimicrob Agents Chemother 54:4368–4372
Drusano GL, Liu W, Kulawy R, Louie A (2011a) Impact of granulocytes on the antimicrobial effect of tedizolid in a mouse thigh infection model. Antimicrob Agents Chemother 55:5300–5305
Drusano GL, Vanscoy B, Liu W, Fikes S, Brown D, Louie A (2011b) Saturability of granulocyte kill of *Pseudomonas aeruginosa* in a murine model of pneumonia. Antimicrob Agents Chemother 55:2693–2695
Dudhani RV, Turnidge JD, Coulthard K, Milne RW, Rayner CR, Li J, Nation RL (2010) Elucidation of the pharmacokinetic/pharmacodynamic determinant of colistin activity against *Pseudomonas aeruginosa* in murine thigh and lung infection models. Antimicrob Agents Chemother 54:1117–1124
Eagle H, Fleischman R, Musselman AD (1950a) Effect of schedule of administration on the therapeutic efficacy of penicillin; importance of the aggregate time penicillin remains at effectively bactericidal levels. Am J Med 9:280–299
Eagle H, Fleischman R, Musselman AD (1950b) The effective concentrations of penicillin in vitro and in vivo for streptococci, pneumococci, and *Treponema pallidum*. J Bacteriol 59:625–643
Eagle H, Fleischman R, Levy M (1953a) "Continuous" vs. "discontinuous" therapy with penicillin; the effect of the interval between injections on therapeutic efficacy. N Engl J Med 248:481–488
Eagle H, Fleischman R, Levy M (1953b) On the duration of penicillin action in relation to its concentration in the serum. J Lab Clin Med 41:122–132
Fisher JF, Meroueh SO, Mobashery S (2005) Bacterial resistance to beta-lactam antibiotics: compelling opportunism, compelling opportunity. Chem Rev 105:395–424
Flume PA, Mogayzel PJ, JR, Robinson KA, Goss CH, Rosenblatt RL, Kuhn RJ, Marshall BC (2009) Cystic fibrosis pulmonary guidelines: treatment of pulmonary exacerbations. Am J Respir Crit Care Med 180:802–808
Garrett ER (1978) Kinetics of antimicrobial action. Scand J Infect Dis 14(Suppl):54–85
Garrett ER, Nolte H (1972) Kinetics and mechanisms of drug action on microorganisms. XIV. The action of fluorouracil, other uracils and derived nucleosides on the microbial kinetics of *Escherichia coli*. Chemotherapy 17:81–108
Garrett ER, Miller GH, Brown MR (1966) Kinetics and mechanisms of action of antibiotics on microorganisms. V. Chloramphenicol and tetracycline affected *Escherichia coli* generation rates. J Pharm Sci 55:593–600
Gershenfeld NA (1999) The nature of mathematical modeling. Cambridge University Press, Cambridge
Grasso S, Meinardi G, De Carneri I, Tamassia V (1978) New in vitro model to study the effect of antibiotic concentration and rate of elimination on antibacterial activity. Antimicrob Agents Chemother 13:570–576

Greco WR, Bravo G, Parsons JC (1995) The search for synergy: a critical review from a response surface perspective. Pharmacol Rev 47:331–385

Hoepelman IM, Rozenberg-Arska M, Verhoef J (1988a) Comparative study of ceftriaxone monotherapy versus a combination regimen of cefuroxime plus gentamicin for treatment of serious bacterial infections: the efficacy, safety and effect on fecal flora. Chemotherapy 34(Suppl 1):21–29

Hoepelman IM, Rozenberg-Arska M, Verhoef J (1988b) Comparison of once daily ceftriaxone with gentamicin plus cefuroxime for treatment of serious bacterial infections. Lancet 1:1305–1309

Hoffman A, Stepensky D (1999) Pharmacodynamic aspects of modes of drug administration for optimization of drug therapy. Crit Rev Ther Drug Carrier Syst 16:571–639

Jorgensen JH, Ferraro MJ (2009) Antimicrobial susceptibility testing: a review of general principles and contemporary practices. Clin Infect Dis 49:1749–1755

Juan C, Moya B, Perez JL, Oliver A (2006) Stepwise upregulation of the *Pseudomonas aeruginosa* chromosomal cephalosporinase conferring high-level beta-lactam resistance involves three AmpD homologues. Antimicrob Agents Chemother 50:1780–1787

Jumbe LNN, Drusano GL (2011) A model-based PK/PD antimicrobial chemotherapy drug development platform to simultaneously combat infectious diseases and drug resistance. In: Kimko HHC, Peck CC (eds) Clinical trial simulations. Springer, New York

Jumbe N, Louie A, Leary R, Liu W, Deziel MR, Tam VH, Bachhawat R, Freeman C, Kahn JB, Bush K, Dudley MN, Miller MH, Drusano GL (2003) Application of a mathematical model to prevent in vivo amplification of antibiotic-resistant bacterial populations during therapy. J Clin Invest 112:275–285

Jumbe NL, Louie A, Miller MH, Liu W, Deziel MR, Tam VH, Bachhawat R, Drusano GL (2006) Quinolone efflux pumps play a central role in emergence of fluoroquinolone resistance in *Streptococcus pneumoniae*. Antimicrob Agents Chemother 50:310–317

Jusko WJ (1971) Pharmacodynamics of chemotherapeutic effects: dose-time-response relationships for phase-nonspecific agents. J Pharm Sci 60:892–895

Kahlmeter G, Brown DF, Goldstein FW, Macgowan AP, Mouton JW, Osterlund A, Rodloff A, Steinbakk M, Urbaskova P, Vatopoulos A (2003) European harmonization of MIC breakpoints for antimicrobial susceptibility testing of bacteria. J Antimicrob Chemother 52:145–148

Kahlmeter G, Brown DF, Goldstein FW, Macgowan AP, Mouton JW, Odenholt I, Rodloff A, Soussy CJ, Steinbakk M, Soriano F, Stetsiouk O (2006) European Committee on Antimicrobial Susceptibility Testing (EUCAST) Technical notes on antimicrobial susceptibility testing. Clin Microbiol Infect 12:501–503

Kullar R, Leonard SN, Davis SL, Delgado G JR, Pogue JM, Wahby KA, Falcione B, Rybak MJ (2011) Validation of the effectiveness of a vancomycin nomogram in achieving target trough concentrations of 15–20 mg/L suggested by the vancomycin consensus guidelines. Pharmacotherapy 31:441–448

Langaee TY, Dargis M, Huletsky A (1998) An ampD gene in *Pseudomonas aeruginosa* encodes a negative regulator of AmpC beta-lactamase expression. Antimicrob Agents Chemother 42:3296–3300

Langaee TY, Gagnon L, Huletsky A (2000) Inactivation of the ampD gene in *Pseudomonas aeruginosa* leads to moderate-basal-level and hyperinducible AmpC beta-lactamase expression. Antimicrob Agents Chemother 44:583–589

Li Y, Peris J, Zhong L, Derendorf H (2006) Microdialysis as a tool in local pharmacodynamics. AAPS J 8:E222–E235

Lo A, Beh J, De Leon H, Hallow MK, Ramakrishna R, Rodrigo M, Sarkar A, Sarangapani R, Georgieva A (2011) Using a systems biology approach to explore hypotheses underlying clinical diversity of the renin angiotensin system and the response to antihypertensive therapies. In: Kimko HHC, Peck CC (eds) Clinical trial simulations. Springer, New York

Louie A, Brown DL, Liu W, Kulawy RW, Deziel MR, Drusano GL (2007) In vitro infection model characterizing the effect of efflux pump inhibition on prevention of resistance to levofloxacin and ciprofloxacin in *Streptococcus pneumoniae*. Antimicrob Agents Chemother 51:3988–4000

Louie A, Liu W, Fikes S, Brown D, Drusano GL (2013) Impact of meropenem in combination with tobramycin in a murine model of *Pseudomonas aeruginosa* pneumonia. Antimicrob Agents Chemother 57:2788–2792

Masuda N, Sakagawa E, Ohya S, Gotoh N, Tsujimoto H, Nishino T (2000a) Contribution of the MexX-MexY-oprM efflux system to intrinsic resistance in *Pseudomonas aeruginosa*. Antimicrob Agents Chemother 44:2242–2246

Masuda N, Sakagawa E, Ohya S, Gotoh N, Tsujimoto H, Nishino T (2000b) Substrate specificities of MexAB-OprM, MexCD-OprJ, and MexXY-oprM efflux pumps in *Pseudomonas aeruginosa*. Antimicrob Agents Chemother 44:3322–3327

Meagher AK, Passarell JA, Cirincione BB, Van Wart SA, Liolios K, Babinchak T, Ellis-Grosse EJ, Ambrose PG (2007) Exposure-response analyses of tigecycline efficacy in patients with complicated skin and skin-structure infections. Antimicrob Agents Chemother 51:1939–1945

Mielck JB, Garrett ER (1969) Kinetics and mechanisms of drug action on microorganisms. IX. Inhibitory action of lincomycin on *Escherichia coli* by microbial kinetics. Chemotherapy 14:337–355

Mine T, Morita Y, Kataoka A, Mizushima T, Tsuchiya T (1999) Expression in *Escherichia coli* of a new multidrug efflux pump, MexXY, from *Pseudomonas aeruginosa*. Antimicrob Agents Chemother 43:415–417

Mohamed AF, Nielsen EI, Cars O, Friberg LE (2012) Pharmacokinetic-pharmacodynamic model for gentamicin and its adaptive resistance with predictions of dosing schedules in newborn infants. Antimicrob Agents Chemother 56:179–188

Moise-Broder PA, Forrest A, Birmingham MC, Schentag JJ (2004a) Pharmacodynamics of vancomycin and other antimicrobials in patients with *Staphylococcus aureus* lower respiratory tract infections. Clin Pharmacokinet 43:925–942

Moise-Broder PA, Sakoulas G, Eliopoulos GM, Schentag JJ, Forrest A, Moellering RC JR (2004b) Accessory gene regulator group II polymorphism in methicillin-resistant *Staphylococcus aureus* is predictive of failure of vancomycin therapy. Clin Infect Dis 38:1700–1705

Mondorf AW, Bonsiepe C, Mondorf W (1989) Randomized multi center study comparing nephrotoxicity of ceftazidime versus the combination of piperacillin and netilmicin with and without furosemide. Adv Exp Med Biol 252:307–312

Mouton JW, Vinks AA (2005) Pharmacokinetic/pharmacodynamic modelling of antibacterials in vitro and in vivo using bacterial growth and kill kinetics: the minimum inhibitory concentration versus stationary concentration. Clin Pharmacokinet 44:201–210

Mouton JW, Vinks AA, Punt NC (1997) Pharmacokinetic-pharmacodynamic modeling of activity of ceftazidime during continuous and intermittent infusion. Antimicrob Agents Chemother 41:733–738

Mouton JW, Punt N, Vinks AA (2005) A retrospective analysis using Monte Carlo simulation to evaluate recommended ceftazidime dosing regimens in healthy volunteers, patients with cystic fibrosis, and patients in the intensive care unit. Clin Ther 27:762–772

Mouton JW, Punt N, Vinks AA (2007) Concentration–effect relationship of ceftazidime explains why the time above the MIC is 40 % for a static effect in vivo. Antimicrob Agents Chemother 51:3449–3451

Mouton JW, Theuretzbacher U, Craig WA, Tulkens PM, Derendorf H, Cars O (2008) Tissue concentrations: do we ever learn? J Antimicrob Chemother 61:235–237

Mouton JW, Ambrose PG, Canton R, Drusano GL, Harbarth S, Macgowan A, Theuretzbacher U, Turnidge J (2011) Conserving antibiotics for the future: new ways to use old and new drugs from a pharmacokinetic and pharmacodynamic perspective. Drug Resist Updates 14:107–117

Mouton JW, Brown DF, Apfalter P, Canton R, Giske CG, Ivanova M, Macgowan AP, Rodloff A, Soussy CJ, Steinbakk M, Kahlmeter G (2012) The role of pharmacokinetics/pharmacodynamics in setting clinical MIC breakpoints: the EUCAST approach. Clin Microbiol Infect 18:E37–E45

Mueller M, De La Pena A, Derendorf H (2004) Issues in pharmacokinetics and pharmacodynamics of anti-infective agents: kill curves versus MIC. Antimicrob Agents Chemother 48:369–377

Nielsen EI, Friberg LE (2013) Pharmacokinetic-pharmacodynamic modeling of antibacterial drugs. Pharmacol Rev 65:1053–1090

Nielsen EI, Viberg A, Lowdin E, Cars O, Karlsson MO, Sandstrom M (2007) Semimechanistic pharmacokinetic/pharmacodynamic model for assessment of activity of antibacterial agents from time-kill curve experiments. Antimicrob Agents Chemother 51:128–136

Nielsen EI, Cars O, Friberg LE (2011) Pharmacokinetic/pharmacodynamic (PK/PD) indices of antibiotics predicted by a semimechanistic PKPD model: a step toward model-based dose optimization. Antimicrob Agents Chemother 55:4619–4630

Nolting A, Dalla Costa T, Rand KH, Derendorf H (1996) Pharmacokinetic-pharmacodynamic modeling of the antibiotic effect of piperacillin in vitro. Pharm Res 13:91–96

Passarell JA, Meagher AK, Liolios K, Cirincione BB, Van Wart SA, Babinchak T, Ellis-Grosse EJ, Ambrose PG (2008) Exposure-response analyses of tigecycline efficacy in patients with complicated intra-abdominal infections. Antimicrob Agents Chemother 52:204–210

Paul M, Benuri-Silbiger I, Soares-Weiser K, Leibovici L (2004) Beta lactam monotherapy versus beta lactam-aminoglycoside combination therapy for sepsis in immunocompetent patients: systematic review and meta-analysis of randomised trials. Br Med J 328:668

Piccart M, Klastersky J, Meunier F, Lagast H, Van Laethem Y, Weerts D (1984) Single-drug versus combination empirical therapy for gram-negative bacillary infections in febrile cancer patients with and without granulocytopenia. Antimicrob Agents Chemother 26:870–875

Poole K, Gotoh N, Tsujimoto H, Zhao Q, Wada A, Yamasaki T, Neshat S, Yamagishi J, Li XZ, Nishino T (1996) Overexpression of the mexC-mexD-oprJ efflux operon in nfxB-type multidrug-resistant strains of *Pseudomonas aeruginosa*. Mol Microbiol 21:713–724

Quale J, Bratu S, Gupta J, Landman D (2006) Interplay of efflux system, ampC, and oprD expression in carbapenem resistance of *Pseudomonas aeruginosa* clinical isolates. Antimicrob Agents Chemother 50:1633–1641

Rybak M, Lomaestro B, Rotschafer JC, Moellering R Jr, Craig W, Billeter M, Dalovisio JR, Levine DP (2009a) Therapeutic monitoring of vancomycin in adult patients: a consensus review of the American Society of Health-System Pharmacists, the Infectious Diseases Society of America, and the Society of Infectious Diseases Pharmacists. Am J Health Syst Pharm 66:82–98

Rybak MJ, Lomaestro BM, Rotschafer JC, Moellering RC, Craig WA, Billeter M, Dalovisio JR, Levine DP (2009b) Vancomycin therapeutic guidelines: a summary of consensus recommendations from the infectious diseases Society of America, the American Society of Health-System Pharmacists, and the Society of Infectious Diseases Pharmacists. Clin Infect Dis 49:325–327

Safdar N, Handelsman J, Maki DG (2004) Does combination antimicrobial therapy reduce mortality in Gram-negative bacteraemia? A meta-analysis. Lancet Infect Dis 4:519–527

Sakoulas G, Moise-Broder PA, Schentag J, Forrest A, Moellering RC Jr, Eliopoulos GM (2004) Relationship of MIC and bactericidal activity to efficacy of vancomycin for treatment of methicillin-resistant Staphylococcus aureus bacteremia. J Clin Microbiol 42:2398–2402

Sanfilippo A, Morvillo E (1968). An experimental model for the study of the antibacterial activity of the sulfonamides. Chemotherapy 13:54–60

Sanfilippo A, Schioppacassi G (1973) New approach to the evaluation of antibacterial activity of aminosidine. Chemotherapy 18:297–303

Schmidt S, Barbour A, Sahre M, Rand KH, Derendorf H (2008) PK/PD: new insights for antibacterial and antiviral applications. Curr Opin Pharmacol 8:549–556

Schmidt S, Sabarinath SN, Barbour A, Abbanat D, Manitpisitkul P, Sha S, Derendorf H (2009) Pharmacokinetic-pharmacodynamic modeling of the in vitro activities of oxazolidinone antimicrobial agents against methicillin-resistant *Staphylococcus aureus*. Antimicrob Agents Chemother 53:5039–5045

Shakil S, Khan R, Zarrilli R, Khan AU (2008) Aminoglycosides versus bacteria—a description of the action, resistance mechanism, and nosocomial battleground. J Biomed Sci 15:5–14

Sideraki V, Huang W, Palzkill T, Gilbert HF (2001) A secondary drug resistance mutation of TEM-1 beta-lactamase that suppresses misfolding and aggregation. Proc Natl Acad Sci U S A 98:283–288

Sobel ML, Mckay GA, Poole K (2003) Contribution of the MexXY multidrug transporter to aminoglycoside resistance in *Pseudomonas aeruginosa* clinical isolates. Antimicrob Agents Chemother 47:3202–3207

Spino M (1991). Pharmacokinetics of drugs in cystic fibrosis. Clin Rev Allergy 9:169–210

Sy SK, Beaudoin ME, Schuck VJ, Derendorf H (2013) Modeling the potentiation of in vitro aztreonam activities by avibactam against four beta-lactam-resistant bacterial strains. Interscience Conference on Antimicrobial Agents and Chemotherapy, Poster A–1014

Tam VH, Louie A, Deziel MR, Liu W, Leary R, Drusano GL (2005) Bacterial-population responses to drug-selective pressure: examination of garenoxacin's effect on *Pseudomonas aeruginosa*. J Infect Dis 192:420–428

Tam VH, Louie A, Deziel MR, Liu W, Drusano GL (2007a) The relationship between quinolone exposures and resistance amplification is characterized by an inverted U: a new paradigm for optimizing pharmacodynamics to counterselect resistance. Antimicrob Agents Chemother 51:744–747

Tam VH, Louie A, Fritsche TR, Deziel M, Liu W, Brown DL, Deshpande L, Leary R, Jones RN, Drusano GL (2007b) Impact of drug-exposure intensity and duration of therapy on the emergence of *Staphylococcus aureus* resistance to a quinolone antimicrobial. J Infect Dis 195:1818–1827

Tam VH, Ledesma KR, Vo G, Kabbara S, Lim TP, Nikolaou M (2008) Pharmacodynamic modeling of aminoglycosides against *Pseudomonas aeruginosa* and *Acinetobacter baumannii*: identifying dosing regimens to suppress resistance development. Antimicrob Agents Chemother 52:3987–3993

Treyaprasert W, Schmidt S, Rand KH, Suvanakoot U, Derendorf H (2007) Pharmacokinetic/pharmacodynamic modeling of in vitro activity of azithromycin against four different bacterial strains. Int J Antimicrob Agents 29:263–270

Tsuji BT, Brown T, Parasrampuria R, Brazeau DA, Forrest A, Kelchlin PA, Holden PN, Peloquin CA, Hanna D, Bulitta JB (2012a) Front-loaded linezolid regimens result in increased killing and suppression of the accessory gene regulator system of *Staphylococcus aureus*. Antimicrob Agents Chemother 56:3712–3719

Tsuji BT, Bulitta JB, Brown T, Forrest A, Kelchlin PA, Holden PN, Peloquin CA, Skerlos L, Hanna D (2012b) Pharmacodynamics of early, high-dose linezolid against vancomycin-resistant enterococci with elevated MICs and pre-existing genetic mutations. J Antimicrob Chemother 67:2182–2190

Vinks AA, Van Rossem RN, Mathot RA, Heijerman HG, Mouton JW (2007). Pharmacokinetics of aztreonam in healthy subjects and patients with cystic fibrosis and evaluation of dose-exposure relationships using monte carlo simulation. Antimicrob Agents Chemother 51:3049–3055

Walkty A, Decorby M, Lagace-Wiens PR, Karlowsky JA, Hoban DJ, Zhanel GG (2011) In vitro activity of ceftazidime combined with NXL104 versus *Pseudomonas aeruginosa* isolates obtained from patients in Canadian hospitals (CANWARD 2009 study). Antimicrob Agents Chemother 55:2992–2994

Wang G, Hindler JF, Ward KW, Bruckner DA (2006) Increased vancomycin MICs for *Staphylococcus aureus* clinical isolates from a university hospital during a 5-year period. J Clin Microbiol 44:3883–3886

Yano Y, Oguma T, Nagata H, Sasaki S (1998) Application of logistic growth model to pharmacodynamic analysis of in vitro bactericidal kinetics. J Pharm Sci 87:1177–1183

Zhuang L, Sy SK, Xia H, Singh RP, Liu C, Derendorf H (2013) Characterization of the in vitro antimicrobial activity of vertilmicin alone and in combination with ceftazidime by using a semi-mechanistic pharmacokinetic/pharmacodynamic model. Interscience Conference on Antimicrobial Agents and Chemotherapy, Poster A-017

Chapter 9
Pharmacometrics of Viral Infections

George L. Drusano and Ashley N. Brown

9.1 Introduction

The overall goal of antiviral therapy is to reduce morbidity and mortality from viral infections by preventing viral replication and spread. Successful antiviral therapy can lead to viral eradication in afflicted patients as well as preventing long-term complications that can arise from these infections. Thus, antiviral therapy is an important tool in our therapeutic arsenal for combating and managing viral-related infections. This chapter will focus on antiviral drugs used to treat three viruses that have a significant impact on human public health: human immunodeficiency virus (HIV), influenza virus, and hepatitis C virus (HCV).

Despite the many benefits that antiviral therapy has to offer, there are several challenges associated with this form of treatment. Patient adherence to therapeutic regimens is arguably one of the greatest challenges that threatens antiviral efficacy. In order for an antiviral regimen to achieve maximal efficacy, the patient must strictly adhere to the prescribed dosage regimen. Missed doses and early cessation of treatment are two factors that lead to therapeutic failure of antiviral regimens. This is especially evident for chronic viral infections, such as HIV and HCV, which require a long duration of therapy.

Drug-related toxicities are a second barrier to antiviral success and often play a major role in patient adherence. Unfortunately, toxicity due to antiviral treatment, particularly long-term treatment, is a relatively common occurrence. Adverse side effects are typical manifestations of antiviral toxicity and can be severe. One example of antiviral-related toxicity is demonstrated by the treatment of HCV with pegylatedinterferon in combination with ribavirin, the accepted standard of care for HCV infections. This therapeutic regimen has been reported to cause depression, anemia, and influenza-like symptoms in patients throughout the course of treatment which spans 24–48 weeks (Fried 2002; Fried et al. 2002). Oftentimes the side ef-

A. N. Brown (✉) · G. L. Drusano
Research and Academic Center, Institute for Therapeutic Innovation,
University of Florida, Orlando, FL, USA
e-mail: Ashley.Brown@medicine.ufl.edu

S. Schmidt, H. Derendorf (eds.), *Applied Pharmacometrics,* AAPS Advances
in the Pharmaceutical Sciences Series 14, DOI 10.1007/978-1-4939-1304-6_9

fects from therapy are so debilitating that the patient will stop therapy all together. Similar examples of toxicity can be cited for HIV therapeutic regimens (Apostolova et al. 2011a, b; Johnson et al. 2001; Lee et al. 2003).

In addition to patient adherence and drug-related toxicity, antiviral drug resistance is a major obstacle to successful therapeutic outcomes in patients with viral infections. The emergence and spread of drug-resistant HIV, influenza, and HCV poses a significant threat to human public health. The development of drug-resistant viruses is influenced by two factors: viral replication and drug therapy. HIV, influenza, and HCV replicate rapidly to high titers in humans via virally encoded proteins, such as the RNA-dependent RNA polymerase for influenza and HCV or reverse transcriptase for HIV. Both the RNA-dependent RNA polymerase and reverse transcriptase proteins are error-prone in nature and lack a proof-reading mechanism, allowing for the frequent misincorporation of nucleotides during the robust replication of the viral genome. Mutation rates for these RNA viruses have been reported to be in the range of one nucleotide misincorporation per every 10^4–10^5 nucleotides polymerized (Drake 1993; Holland et al. 1992). These misincorporations sometimes result in amino acid changes which can affect viral susceptibility to a drug. Viruses harboring drug-resistant mutations may be selected when drug pressure is applied during therapy. Additionally, these viral mutants have great potential to amplify in the presence of suboptimal therapeutic regimens due to either inappropriate dose or dosing interval selection for a specific compound or missed doses stemming from a lack of patient adherence for a prescribed regimen.

The application of pharmacometrics to antiviral therapy can help alleviate some of the challenges associated with therapy. Pharmacometric methods can be employed to predict dosage regimens for antiviral agents that will provide optimal therapeutic outcome. In this case, therapeutic success is defined by the ability of the antiviral regimen to yield maximal inhibition of viral replication and prevent the amplification of drug-resistant mutants with minimal toxicity. In order for pharmacometrics to be used productively in the guidance of intelligent design of antiviral regimens, the pharmacokinetic (PK) and pharmacodynamic (PD) properties for each compound must be well understood. For antivirals, in vitro PD model systems have been utilized to provide valuable information regarding PK/PD interactions for antiviral agents active against HIV, influenza, and HCV (Brown et al. 2010, 2011a, b, 2012; Drusano et al. 1998, 2001, 2002a; McSharry et al. 2009b). In this chapter, we will discuss the use of in vitro PD model systems to evaluate the PDs of antiviral agents and how this information is applied to the design of optimal antiviral regimens for clinical use.

9.2 HIV PDs

Virtually, all of the bench PD studies for this virus were performed with the hollow fiber infection model (HFIM). The picture of this apparatus is provided in Fig. 9.1.

For these experiments, a mixture of infected and uninfected CEM-ss cells are placed in the extra-capillary space (ECS) of the hollow fiber unit. Medium is

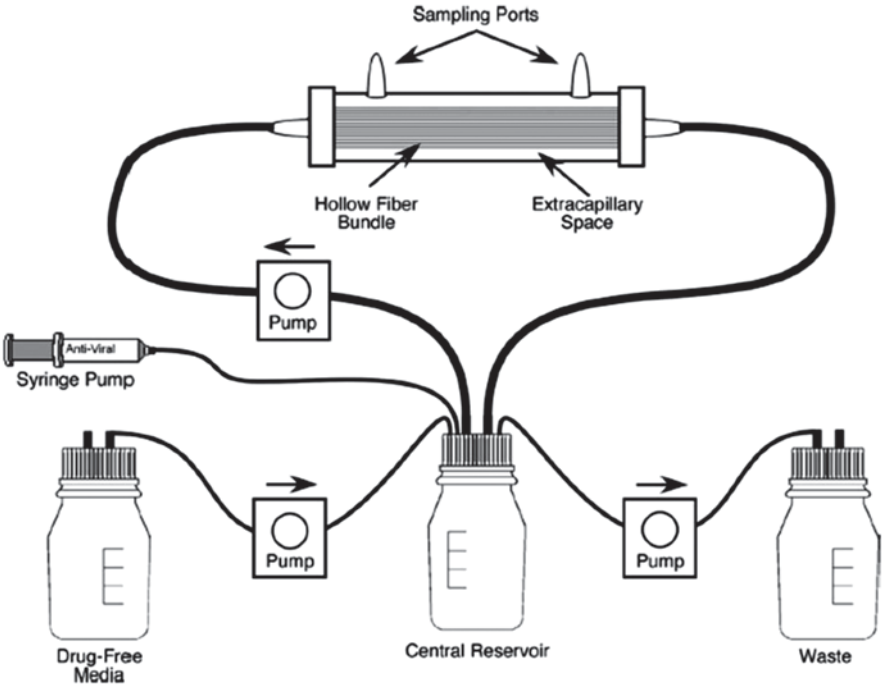

Fig. 9.1 The hollow fiber infection model (HFIM) system. (Reproduced with permission from McSharry et al. 2009a)

circulated around, allowing the cells to grow and HIV to propagate. The antiviral agent of interest is administered into the central reservoir of the system via computer-controlled syringe pumps and circulated throughout the hollow fiber cartridge. The use of programmable syringe pumps allows for the freedom to simulate any infusion rate and dosing interval desired in an in vitro setting. Antiviral-free medium is introduced in the afferent loop and an equivalent volume of antiviral-containing medium is withdrawn from the efferent part of the loop, providing a fixed volume system that is diluted at a constant rate per unit time. The ratio of dilution rate to total system volume is the rate constant of elimination. These methods permit for the simulation of any desired half-life in the HFIM system. The HFIM system can also be modified to simulate two- or three-compartment models, although this is a bit more technologically challenging. It is important to note that only free drug concentrations are simulated in HFIM system, since only free drug (drug that is not bound to human serum proteins) is efficacious in vivo. Because of the large surface area of the hollow fibers and the molecular weight cutoff of the pores (circa 20,000 Da), cells and virus (including viral proteins, such as p24 protein) are retained in the ECS. Medium containing cells and virus are harvested from the ECS through the sampling ports on the hollow fiber cartridge at various time points throughout the duration of the study and the amount of virus is quantified in these samples. Additionally, serial drug concentrations are determined from medium harvested from

the central reservoir of the HFIM system. These measurements allow for the characterization of the dose–response relationship for the antiviral agent under evaluation. Moreover, one has the ability to assess the impact of the dosing interval on the inhibition of viral replication and the emergence of resistance.

9.3 Nucleoside Analogues

The first PD studies performed with antiviral agents in the HFIM system was with the nucleoside analogue stavudine (d4T; Bilello et al. 1994). In this evaluation, the HFIM correctly predicted the clinical dose of d4t in a period of several months, whereas clinical trials required approximately 18 months to identify the appropriate dose.

The nucleoside analogue abacavir was then examined in the HFIM (Drusano et al. 2002a). The goal of these studies was to determine if 600 mg of abacavir administered once-daily (QD) was as efficacious as 300 mg given twice-daily (BID). The rationale for these experiments was based on previous findings regarding the dosing interval for the nucleoside analogue zidovudine. Initially, zidovudine was administered to patients every 4 h in the clinic. As zidovudine use progressed and further research was conducted, it was determined that longer dosing intervals, such as BID dosing, were as effective as the shorter dosing intervals (Mulder et al. 1994). Since longer dosing intervals promote better patient adherence, the sponsors for abacavir were hopeful that QD dosing would yield optimal therapeutic outcomes.

Two separate experiments were performed in the HFIM system. The first experiment was to examine the efficacy of abacavir as a continuous infusion (CI) versus daily pulse dosing every 24 h (Q24). For the Q24 dosing, abacavir was removed from the HFIM system at a rate to simulate the "correct" human half-life. The results from this study are shown in Fig. 9.2.

The second experiment was to administer the drug QD versus BID with the same half-life. The results from this experiment are shown in Fig. 9.3. It should be noted that the ultimate clinical dose for abacavir was 600 mg QD and that 300 mg BID was also being considered. At the time these experiments were performed, it was thought that the clinical dose would be 500 mg QD or 250 mg BID. Thus, these regimens were evaluated in the study.

Figures 9.2 and 9.3 both show that the dosing interval for abacavir did not influence the antiviral effect over time in the HFIM system, as viral suppression was consistent between the Q24 and CI treatment arms and the Q24 and every 12 h (Q12) treatment arms. However, the sponsor wished to prolong the experiment and to document a failure arm. Therefore, a third study was conducted. The result from this experiment, which was conducted over a course of 30 days, is displayed in Fig. 9.4.

These data were all published in Antimicrobial Agents and Chemotherapy (AAC; Drusano et al. 2002a). As shown in Fig. 9.4, the Q24 and Q12 dosage regimens consistently suppressed viral replication throughout the entire duration of the experiment. In contrast, abacavir treatment failed when the dosing interval was extended to every 48 h, as viral burden in this treatment arm was similar to that

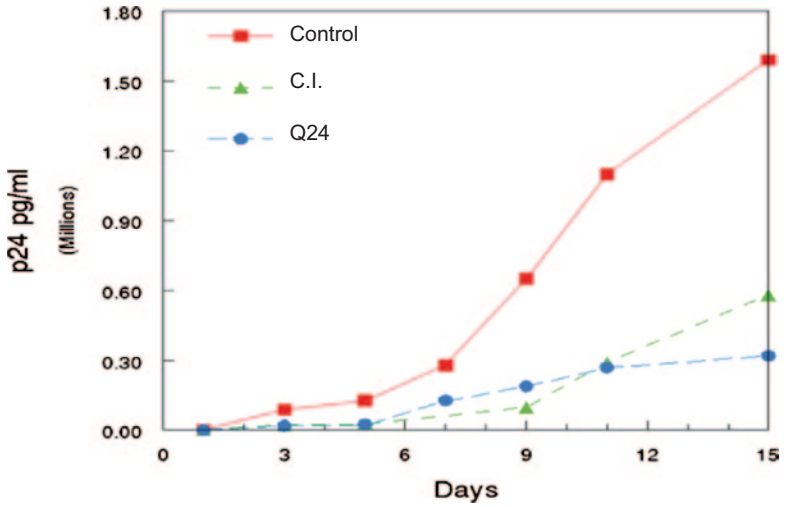

Fig. 9.2 The effect of abacavir on HIV replication in the HFIM system. Abacavir was administered into hollow fiber cartridges as a continuous infusion (CI) or as pulse dosing via computer-controlled syringe pumps once every 24 h (Q24). Hollow fiber cartridges were sampled at various times throughout the study and the amount of p24 viral antigen was quantified from sample supernatants by ELISA. (Used with permission from Drusano et al. 2002a)

reported in the no-treatment control by day 24 post exposure. These findings suggest that QD dosing for abacavir is as efficacious as BID dosing and that a QD regimen would be successful in the clinic. A clinical trial (the ZODIAC trial) was later performed to determine if abacavir administered QD in patients was noninferior to BID dosing (Moyle et al. 2005). The ZODIAC trial confirmed the findings of the HFIM system, as the QD dosage regimen for abacavir was deemed noninferior to the BID dosage regimen in HIV-infected patients (Moyle et al. 2005). This example illustrates the clinical applicability of data derived from the HFIM system.

Since QD dosing for abacavir is as efficacious as BID dosing, the sponsors wished to determine if zidovudine could also be administered once a day, as zidovudine and abacavir both belong to the nucleoside analogue drug class. Thus, a study was conducted with zidovudine in the HFIM system to answer this question. The results from this study are displayed in Fig. 9.5.

The Q12 zidovudine regimen provided continuous suppression of HIV throughout the duration of the 14-day study. The Q24 regimen, on the other hand, had significantly higher viral burden relative to the Q12 by day 10 and viral levels were similar to those of the no-treatment control by day 14. These findings show that, unlike abacavir, zidovudine Q24 is not as efficacious as the Q12 regimen in the HFIM system, suggesting that QD dosing of zidovudine will not be successful in a clinical setting. A clinical trial was later conducted in HIV-infected patients assessing the efficacy of QD versus BID dosing for zidovudine. The findings of this trial showed that QD dosing of zidovudine was in fact not as efficacious as BID dosing in infected patients (Ruane et al. 2004). These study results provide an addi-

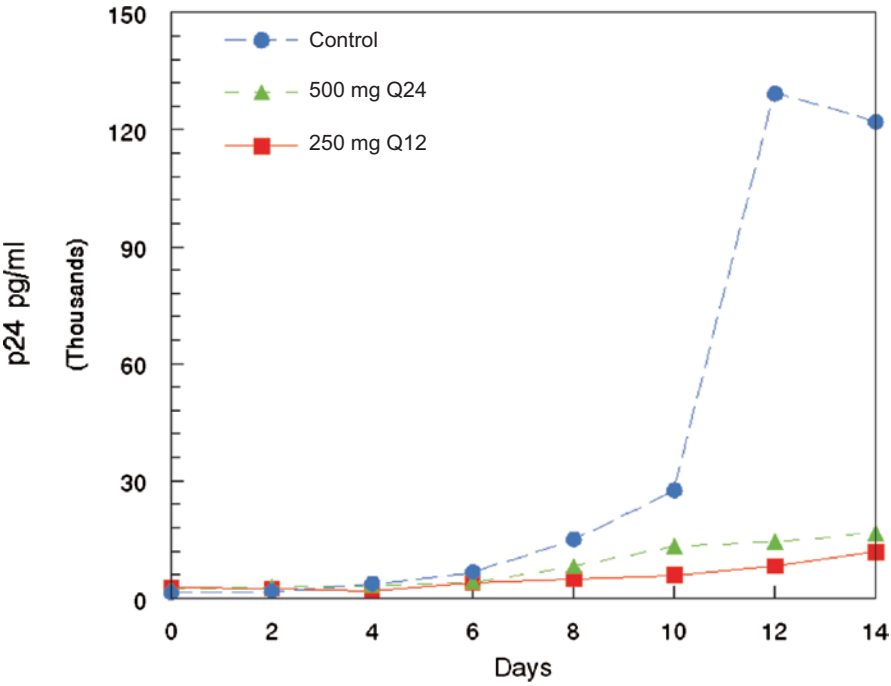

Fig. 9.3 The effect of Q24 versus Q12 dosing on the efficacy of abacavir against HIV in the HFIM system. Abacavir was administered into hollow fiber cartridges as the total daily dose once every 24 h (500 mg Q24) or half the daily dose every 12 h (250 mg Q12). Hollow fiber cartridges were sampled every other day. The amount of HIV was quantified in sample supernatants using a p24 ELISA. (Used with permission from Drusano et al. 2002a)

tional example in which predictions made by the HFIM system have been validated through human clinical trials.

The conclusions from studies performed in the HFIM system and the clinical trials clearly show that abacavir can be administered QD without compromising efficacy but zidovudine must be dosed BID, even though these two compounds belong to the same drug class. Why is this so? In an effort to answer this question, one must consider the mechanism of action for these compounds. Nucleoside analogues are prodrugs and must be triphosphorylated by host cellular enzymes to be potent. Zidovudine and abacavir, once triphosphorylated, compete with deoxynucleoside triphosphates during reverse transcription and act as chain terminators, preventing viral RNA from reverse transcribing into DNA. Thus, in order to understand the dosing interval for zidovudine or abacavir, one must analyze the PKs of the triphosphorylated active form of both compounds. Earlier, Slusher et al. (1992) examined the anabolites of zidovudine intracellularly. The data were clear-cut. There was a Michaelis–Menten step between the monophosphate and diphosphate anabolites. The importance of this is that no matter how much zidovudine is administered, only a certain amount of triphosphate anabolite (the active moiety) can be pro-

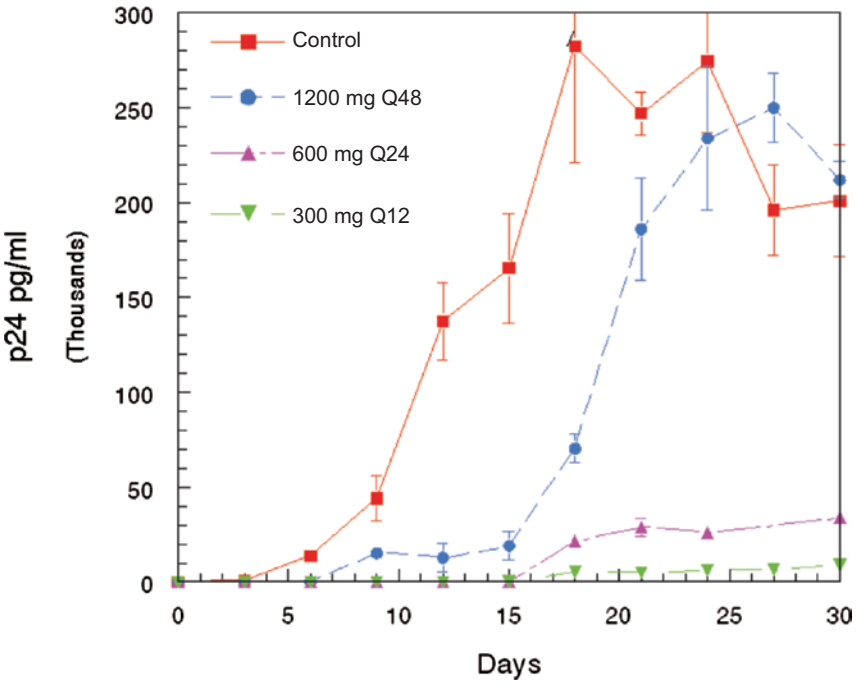

Fig. 9.4 The effect of dosing interval on the efficacy of abacavir against HIV in the HFIM system. Abacavir was administered into hollow fiber cartridges as twice the daily dose every 48 h (1200 mg Q48), the daily dose every 24 h (600 mg Q24), or half the daily dose every 12 h (300 mg Q12). Hollow fiber cartridges were sampled at various times during the study and HIV was quantified from supernatants by ELISA. (Used with permission from Drusano et al. 2002a)

duced. However, the monophosphate just keeps increasing with increasing dose. The rate of fall of the monophosphate then determines the dosing interval. As long as the amount of monophosphate is sufficient to saturate the enzyme, there will be a steady amount of triphosphate anabolite (and, hence, stable antiviral effect). If the dosing interval is too long, the monophosphate ceases to saturate the enzyme and the amount of triphosphate falls, leading to decreased antiviral effect and ultimate regimen failure. Higher dosing levels for zidovudine would not increase efficacy in this circumstance, as maximum metabolic conversion has already been reached, and would only cause increased risk of toxicity and adverse side effects. This explains the ability to prolong zidovudine's dosing interval from every 4 h to BID dosing with success, followed by the failure with the attempted extension to daily dosing. Michaelis–Menten kinetics for zidovudine are illustrated pictorially in Fig. 9.6.

When patient samples were examined, a broad range of zidovudine monophosphate concentrations were observed, spanning from 0.7 to 4.0 pmol/10^6 cells. In contrast, a very limited range of zidovudine triphosphate concentrations were seen (0.5–0.14 pmole/10^6 cells). These data are depicted in Fig. 9.7. Thus, these findings demonstrate that regardless of how much zidovudine monophosphate is inside the

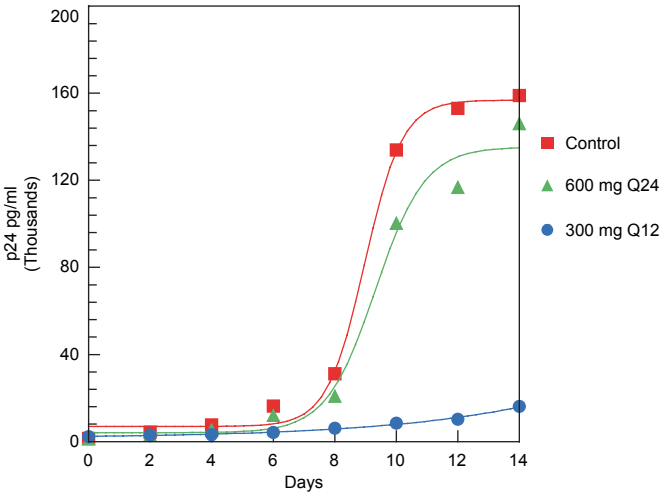

Fig. 9.5 The effect of dosing interval on the efficacy of zidovudine against HIV in the HFIM system. Zidovudine was administered into hollow fiber cartridges as the total daily dose once every 24 h (600 mg Q24) or half the daily dose every 12 h (300 mg Q12). Hollow fiber cartridges were sampled every other day. The amount of HIV was quantified in sample supernatants using a p24 ELISA

cell, only a certain amount of triphosphate will be produced. This is consistent with the hypothesis discussed above.

So what of abacavir? It has no Michaelis–Menten step, but can be administered QD without compromising efficacy. Piliero et al. (2003) examined carbovir triphosphate (active moiety of administered abacavir) in patients already receiving the drug. The PKs of intracellular carbovir triphosphate are displayed in Fig. 9.8.

The half-life of carbovir triphosphate is quite prolonged (about 20.6 h with a 95% confidence interval from 16.4–26.0 h). Consequently, the carbovir triphosphate is able to be maintained in an effective range over the full 24 h dosing interval, explaining why QD dosing for abacavir is successful in patients. These findings demonstrate that the dosing interval for nucleoside analogues can be altered by the presence or absence of a Michaelis–Menten step as well as by the terminal half-life of the triphosphate. Thus, one must consider the PKs of the active moiety of the compound when determining the appropriate dosing interval that is associated with maximal efficacy.

9.4 Aspartyl Protease Inhibitors

For nucleoside analogues, the PD index that is best linked to efficacy tends to be the free drug area under the concentration–time curve (*f*AUC), that is until the dosing interval becomes too long (i.e., Q24 for zidovudine or every 48 h (Q48) for

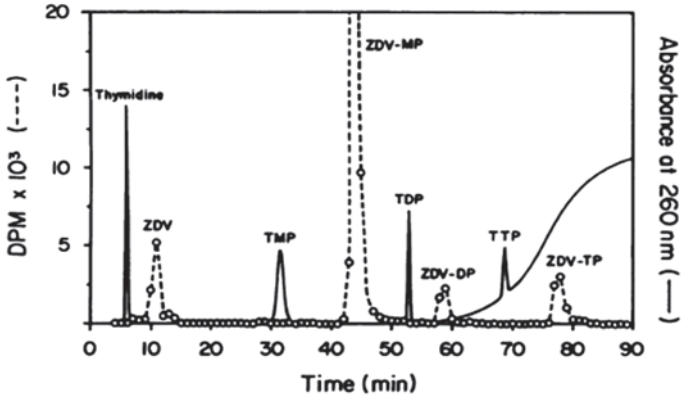

Fig. 9.6 Michaelis–Menten kinetics for zidovudine (*ZDV*). The phosphorylation kinetics for *ZDV* are illustrated by the *dashed line*. *ZDV* is phosphorylated by host cellular enzymes and converted to high levels of *ZDV*-monophosphate (*ZDV-MP*) which accumulates in the cell after administration. Despite high levels of *ZDV-MP*, only a fraction of *ZDV-MP* is converted to *ZDV*-diphosphate (*ZDV-DP*) due to the saturation of the phosphorylating enzyme, representing the Michaelis–Menten step in *ZDV* phosphorylation kinetics. *ZDV-DP* is then phosphorylated to yield the active moiety, *ZDV*-triphosphate (*ZDV-TP*). (Reproduced with permission from Slusher et al. 1992)

abacavir) resulting in treatment failure. However, for aspartyl protease inhibitors (hereafter called protease inhibitors or PIs) the PD index linked with effect was believed to be the amount of time free drug concentrations remain above a threshold (*f*Time > threshold). This difference in PD indices between these two drug classes is attributed to the limited mean residence time of the PI in the active site of the

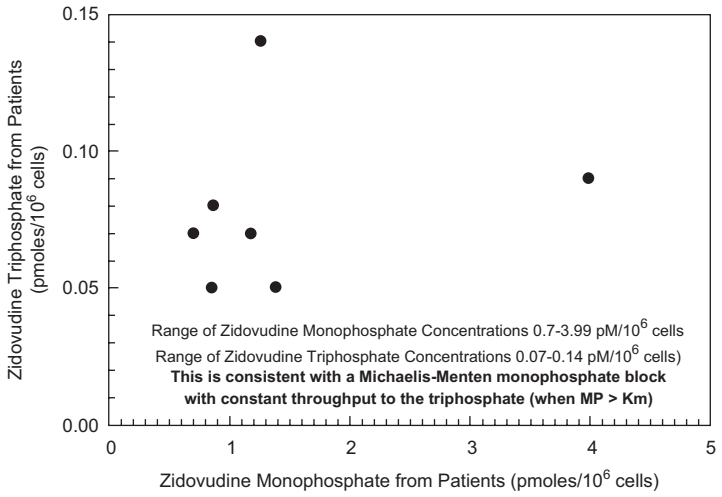

Fig. 9.7 The concentration of intracellular zidovudine monophosphate versus intracellular zidovudine triphosphate in patients treated with zidovudine. (Data from Slusher et al. 1992)

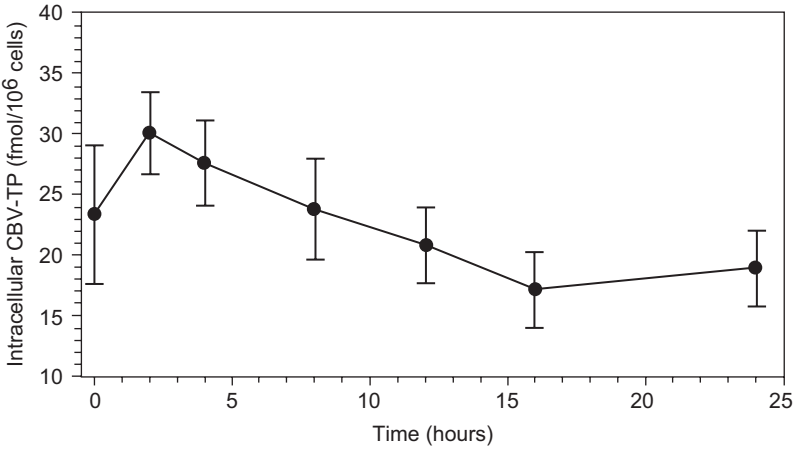

Fig. 9.8 The intracellular pharmacokinetics of carbovir triphosphate (CBV-TP; the active moiety of abacavir) in patients receiving abacavir. (Data from Piliero et al. 2003)

viral protease. PD indices offer great insight into the optimal dosing interval for a compound. For example, the efficacy of *f*AUC driven compounds is not influenced by dosing interval and, consequently, QD dosing is often employed for these compounds. In contrast, *f*Time > threshold driven drugs often require more frequent dosing intervals (i.e., CI, BID, or thrice-daily (TID) dosing) to achieve maximal effect. It is important to correctly identify the PD index of antiviral agents to guide the design of optimal dosage regimens, as a misidentification may lead to suboptimal dosing and ultimately result in therapeutic failure.

The PI amprenavir was evaluated in the HFIM system to determine the PD index linked with viral inhibition for this compound (Preston et al. 2003). The results of this study are illustrated below in Fig. 9.9. The figure shows that more frequent dosing intervals of amprenavir, including CI and every 8 h (Q8; TID) regimens, were required to maximally suppress HIV replication. The longer dosing interval (Q12) resulted in viral breakthrough as early as 7 days post therapy. These findings indicate that $f\text{Time} > EC_{95}$ is the PD index that is best linked to viral suppression for the PI amprenavir, thereby confirming the hypothesis stated above.

Consequently, the dosing interval has a major impact on the amount of viral suppression noted. In the case of amprenavir, the drug concentrations were "boosted" by the coadministration of ritonavir, which markedly lowers the clearance of amprenavir. An inhibitory sigmoid E_{max} effect model, which allows identification of an exposure target, is shown in Fig. 9.10.

It is apparent by inspection that the minimal coverage necessary to reap the full benefit of amprenavir effect is approximately 80% of the dosing interval. Using this information, a Monte Carlo simulation was performed using patient-derived PK studies with amprenavir/ritonavir to examine the impact of EC_{95} on target attainment for a fixed dose of amprenavir/ritonavir (Fig. 9.11). In this instance, the EC_{50} is plotted. It has been previously demonstrated that $EC_{95}$is approximately $4 \times EC_{50}$

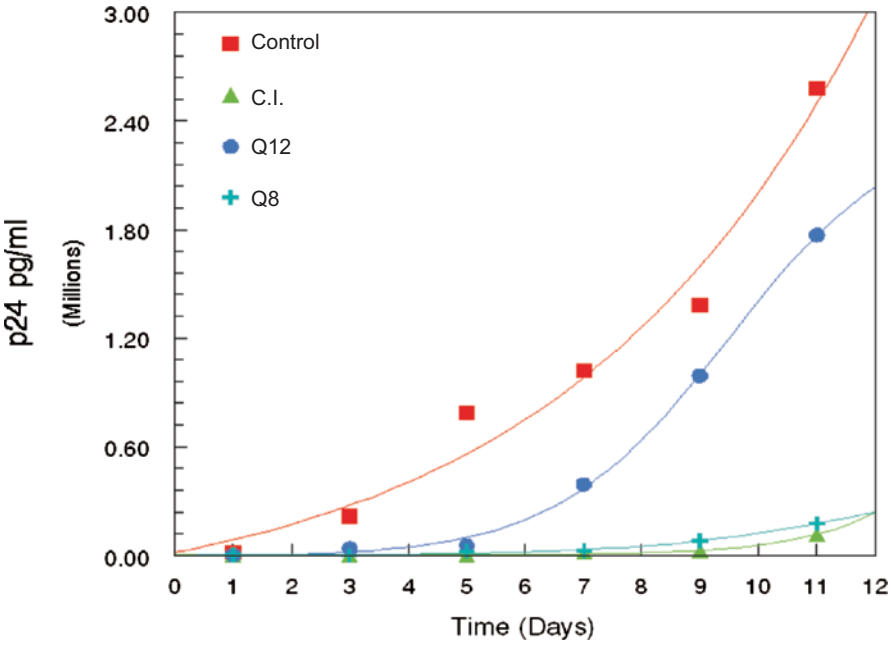

Fig. 9.9 The influence of dosing interval on the efficacy of amprenavir against HIV-1 in the HFIM system. Amprenavir was administered into hollow fiber cartridges as half the daily dose every 12 h (Q12), one third the daily dose every 8 h (Q8), or as a continuous infusion (*C.I.*). Hollow fiber cartridges were sampled every other day. The amount of HIV was quantified in sample supernatants using a p24 ELISA. (Reproduced with permission from Preston et al. 2003)

for nonprotein-bound drug. The Fig. 9.11 shows that 90 % target attainment is maintained to approximately an EC_{50} of 50 nM.

Haas et al. (2000) studied TID versus BID dosing for patients receiving the PI indinavir. They showed that of the first 87 patients reaching 24 weeks of treatment, 91 % had achieved <400 copies/ml with TID dosing versus 64 % receiving BID dosing ($p<0.01$). These clinical findings also suggest that more frequent dosing intervals are required to obtain maximal efficacy with PIs, thereby validating the results from the HFIM studies with amprenavir.

The PI Atazanavir was also examined in the HFIM system and demonstrated the same finding of $f\text{Time}>EC_{95}$ as the dynamically linked index for the nonritonavir boosted drug (Drusano et al. 2001).

9.5 Nonnucleoside Reverse Transcriptase Inhibitors

Because of the success of employing Monte Carlo simulation to identify robust doses of drug with PIs, we wished to examine this issue for a nonnucleoside reverse transcriptase inhibitor (NNRTI), GW420867X. Population PK analysis was

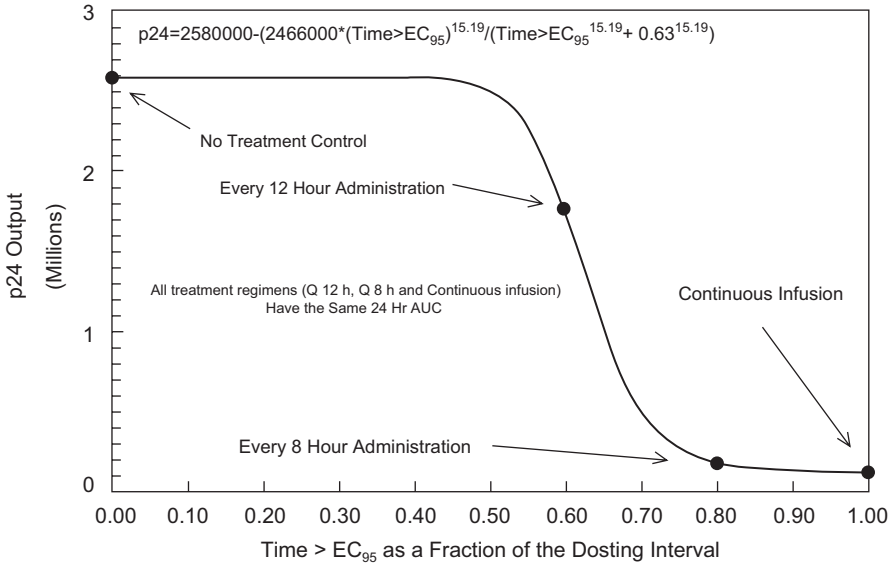

Fig. 9.10 The effect of amprenaviron HIV replication as a function of *f*Time>EC_{95}. The p24 output observed on day 11 for the control, Q12, Q8, and continuous infusion experimental arms described in Fig. 9.9 were graphed against the amount of time that the PK profiles for each dosing interval yielded concentrations that were above the EC_{95} for the HIV IIIB strain. (Reproduced with permission from Preston et al. 2003)

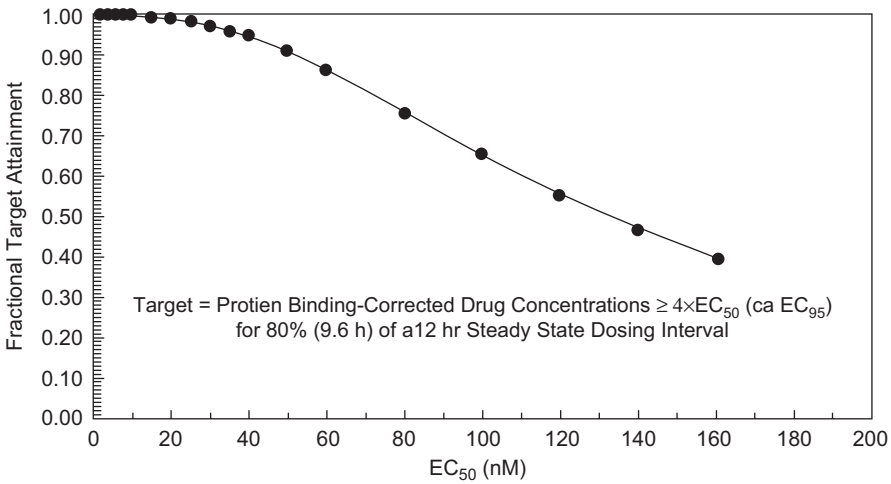

Fig. 9.11 Monte Carlo simulations for fixed doses of amprenavir and ritonavir at 600 and 100 mg, respectively. Patient-derived PK were used in the simulation to examine the impact of HIV EC_{95}, or $4\times EC_{50}$, values on the target attainment rate for the amprenavir/ritonavir dosage regimen. (Reproduced with permission from Preston et al. 2003)

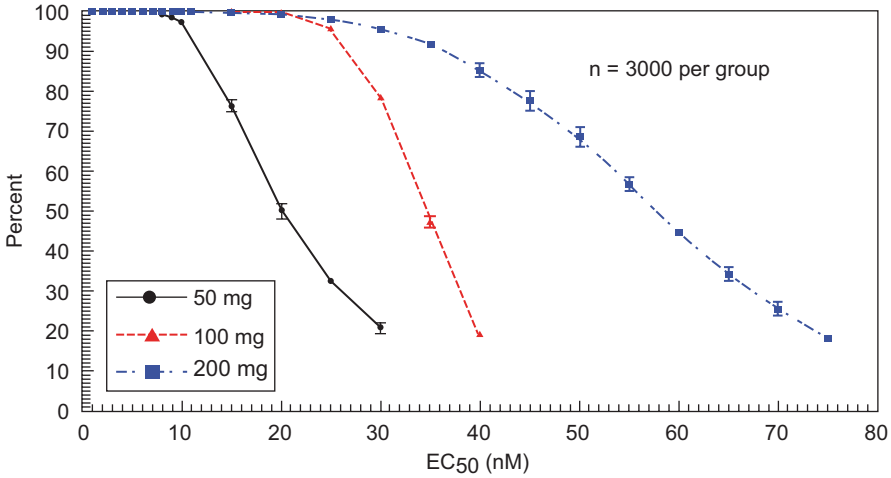

Fig. 9.12 Monte Carlo simulations for 50, 100, and 200 mg doses of GW420867X. 3000-subject Monte Carlo simulations were conducted for all three doses to determine the percentage of patients that would have free trough concentrations of GW420867X that were 10 times greater than the EC_{50} of HIV. GW420867X was administered QD by mouth. (Reproduced with permission by Drusano et al. 2002b)

performed for three doses (50–200 mg daily) of GW420867X. A 3000-subject Monte Carlo simulation was performed for each dose evaluated. EC_{50} values were corrected for protein binding and for the difference between EC_{50} and EC_{90}. The fraction of patients with free drug trough concentrations that were above the EC_{90} was determined. It should be noted that the highest EC_{50} was 7 nM in a large clinical collection (Drusano et al. 2002b). The target attainment is shown in Fig. 9.12.

Given that the highest EC_{50} value in the clinical collection of HIV was 7 nM, it is clear that a short-term clinical evaluation would not be expected to show any differences in treatment effect (resistance emergence is another issue). Figure 9.13 shows the results of a phase I/II clinical trial with these three doses of GW420867X. For the 1st week of the study, GW420867X was administered as monotherapy and combination therapy was initiated (GW420867X + zidovudine + 3TC) in the 2nd week (designated by the vertical line at day 8) of the trial.

At the end of monotherapy, as predicted, the viral load decline was essentially identical among the three arms. In the clinic, Marzolini et al. (2001) were able to demonstrate a significantly higher rate of virological failure in patients with lower concentrations of the NNRTI efavirenz, as would be predicted from this analysis.

It should be noted that for HIV, we have a number of clinically validated predictions from the HFIM: (1) d4T (dose and dosing interval), (2) abacavir (dosing interval), (3) amprenavir (dosing interval), (4) atazanavir (dose and dosing interval), and (5) zidovudine (failure of QD dosing). Monte Carlo simulation was also demonstrated to be a valuable tool for identification of a robust dose: (1) atazanavir and (2) the NNRTI GW420867X.

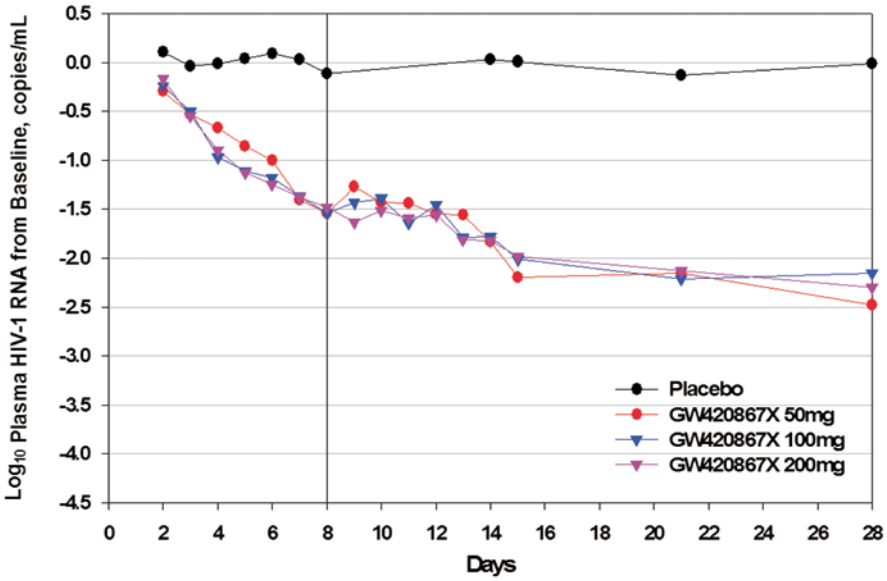

Fig. 9.13 Phase I/II clinical trial results of GW420867X. Three different doses of GW420867X (50, 100 mg, and 200 ng) were administered to patients QD orally as monotherapy for the first 8 days, followed by combination therapy with zidovudine and 3TC thereafter. The decline in viral load was determined in patients at various times throughout the study. (Reproduced with permission from Drusano et al. 2002b)

As with bacteria and fungi, it is straightforward to link a measure of drug exposure relative to a measure of potency to desired outcomes for a number of different agents against HIV.

9.6 Combination HIV Chemotherapy

As in the therapy of tuberculosis, combination chemotherapy is de rigeur for the therapy of HIV disease. Generally, selection of drugs as well as their doses and schedules of administration are empirical. By examining mathematically how drugs interact and understanding the variability of their PK profiles, it is possible to gain insight on potential clinical utility.

When one examines drug effect interaction, the first requirement is to have a definition of additivity. There are many extant in the literature, but the two most common are Loewe additivity and Bliss independence. Understanding additivity allows rational definition of synergy and antagonism, with synergy being significantly more effective than additivity and antagonism being significantly less active than additivity. This topic is well reviewed by Greco et al. (1995). Here there will be an examination of a method for evaluating drug interaction employing Loewe additivity.

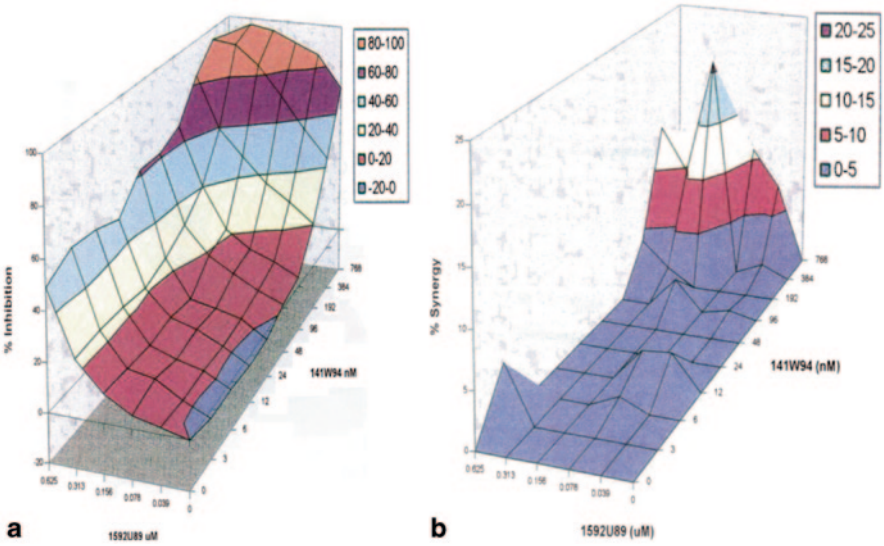

Fig. 9.14 The three-dimensional effect surface for combination therapy of abacavir (nucleoside analogue) and amprenavir (a protease inhibitor). The interaction between abacavir and amprenavir was evaluated using a 96-well format. The full effect surface (**a**) and the true effect synergy plot (**b**) are shown for the combination. (Reproduced with permission from Drusano et al. 1998)

The combination of abacavir (a nucleoside analogue) plus amprenavir (a protease inhibitor) was examined in a 96-well format (Drusano et al. 1998). The three-dimensional effect surfaces are displayed in Fig. 9.14. Figure 9.14a shows the full effect surface and in Fig. 9.14b, the theoretical additive surface has been removed and the remaining is true significant synergy.

By applying the Greco equation, we can identify a point estimate of the interaction parameter α and its 95 % confidence interval. In this case, the estimate is 1.144 with a confidence interval of 0.534–1.754. As the estimate is positive and the lower bound does not cross zero, the interaction is defined as statistically significant synergy. Because the approach is fully parametric, we can employ Monte Carlo simulation to examine the impact of dosing interval on antiviral effect. Giving both agents on a Q12 basis was compared to Q12 administration for the nucleoside analogue and Q8 administration for the PI (Drusano et al. 2000).

Figure 9.15a shows the concentration–time profiles for amprenavir and abacavir when administered on a Q8/Q12 schedule. In Fig. 9.15c, the Greco equation has been employed to turn a concentration–time triplet (time, drug1 concentration, drug2 concentration) into an effect–time doublet. Figures 9.15b and d show the same type of data, with the exception that amprenavir and abacavir are both administered as Q12.

Performing Monte Carlo simulation demonstrated that there was a significant difference between the two dosing intervals (total daily doses were identical) as shown in Table 9.1.

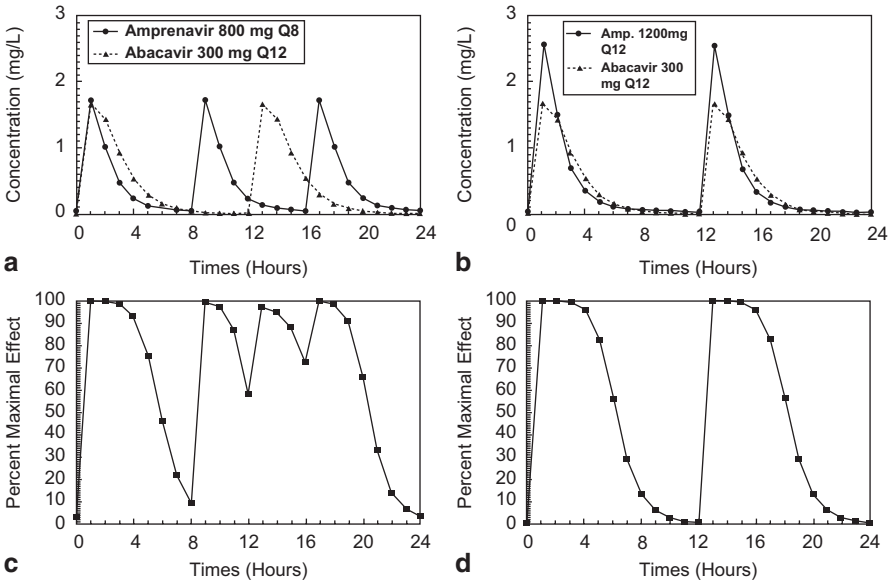

Fig. 9.15 Monte Carlo simulations of combination therapeutic regimens of amprenavir 800 mg Q8/abacavir, 300 mg Q12, or amprenavir 1200 mg Q12/abacavir 300 mg Q12. **a** Concentration–time curves for amprenavir 800 mg Q8 and abacavir 300 mg Q12 at steady state for one randomly chosen subject from the 500-patient Monte Carlo simulation. **b** Concentration–time curves for amprenavir 1200 mg Q12 and abacavir 300 mg Q12 at steady state for one randomly chosen subject from the 500-patient Monte Carlo simulation. **c** Steady-state effect–time curves for the amprenavir (800 mg Q8) and abacavir (300 mg Q12) combination therapeutic regimen. **d** Steady-state effect–time curves for the amprenavir (1200 mg Q12) and abacavir (300 mg Q12) combination therapeutic regimen. (Reproduced with permission from Drusano et al. 2000)

Thus, these findings effectively illustrate that it is quite possible to employ preclinical techniques to gain insight on how to optimize combination chemotherapy.

9.7 Influenza Virus

9.7.1 The Adamantanes

The first effective agents against influenza were amantadine and rimantadine. Influenza virus has been shown to emerge resistant to both drugs rapidly. Amantadine was studied in the HFIM against an influenza A virus and the antiviral activity as well as resistance emergence was quantified (Brown et al. 2010). In the first experiment, amantadine was administered as a CI in a dose ranging design. As can be seen in Fig. 9.16, there was modest antiviral effect, regardless of the level of exposure.

The M2 gene was sequenced from viral samples harvested between 48 and 120 h post exposure to look for emergence of resistance to amantadine. The sequencing

Table 9.1 Mean percentages of the antiviral suppressive effect and the fractions of the simulated population ($n = 500$) exceeding the 70 and 90% maximal suppressive effects over a 24-h steady-state-dosing interval for two regimens of abacavir plus amprenavir differing only in the dosing interval for amprenavir. (Reproduced with permission from Drusano et al. 2000)

Parameter	Value for regimen	
	Abacavir at 300 mg orally ql2h plus amprenavir at 800 mg orally q8h	Abacavir at 300 mg orally ql2h plus amprenavir at 1200 mg orally q12h
Mean effect ± SD (%)	90.9 ± 11.4	80.9* ± 18.6
Fraction ≥ 70% of maximal effect	459/500	354/500**
Fraction ≥ 90% of maximal effect	344/500	230/500**

*$P < 0.001$ (paired t test)
**$P < 0.001$ (Fisher exact test)

results are presented in Table 9.2. Increasing pressure from increasing drug exposure results in rapid resistance emergence. Of equal interest, differing levels of antiviral pressure selects for different resistance mutations. At a CI of 6 mg/L resistance is partially suppressed, being 70% wild type at 120 h. It is important to mention that 6 mg/L is equivalent to a supraphysiological dose in humans due to the toxicity associated with amantadine therapy. Therefore, these data show that even at toxic exposures of amantadine, the emergence of resistant viruses was not prevented.

To better mimic the clinical circumstance, orally administered profiles of amantadine were generated (66 mg daily = subtherapeutic dose; 200 mg daily = clinical daily dose; 660 mg daily = supratherapeutic regimen). Again, antiviral activity (Fig. 9.17a) and resistance emergence (Fig. 9.17b) were quantified.

As previously, it was not possible to counterselect resistance emergence. As stated above, it should be noted again that many of the exposures generated in these experiments, either as CIs or as orally administered profiles, are nontolerable, or toxic, in humans. This rapid resistance emergence has essentially wiped out the clinical utility of amantadine and rimantadine. Today, 100% of circulating influenza A viruses are resistant to the adamantanes (Bright et al. 2006; CDC 2006; Deyde et al. 2007).

The findings demonstrated by the HFIM system explain the clinical failure of amantadine as a therapeutic option against influenza. The EC_{50} values for amantadine against wild-type influenza viruses that retain susceptibility to this drug are approximately 0.05 μg/ml. However, influenza viruses that are resistant to amantadine have EC_{50} values that are greater than 10 μg/ml (Krumbholz et al. 2009). Since the clinical dose of amantadine (200 mg per day) is equivalent to a CI of 0.45 μg/ml, it is impossible to prevent the amplification of drug-resistant mutants which display EC_{50} values that are 22 times greater than the clinical exposure. Thus, it is not clinically feasible to dose amantadine at exposures high enough to suppress the viral resistant mutants due to toxicity-related issues associated with this compound. These findings clearly show that widespread amantadine resistance could not have been prevented when administered as monotherapy for the treatment of influenza, even if different doses or dosing intervals were employed.

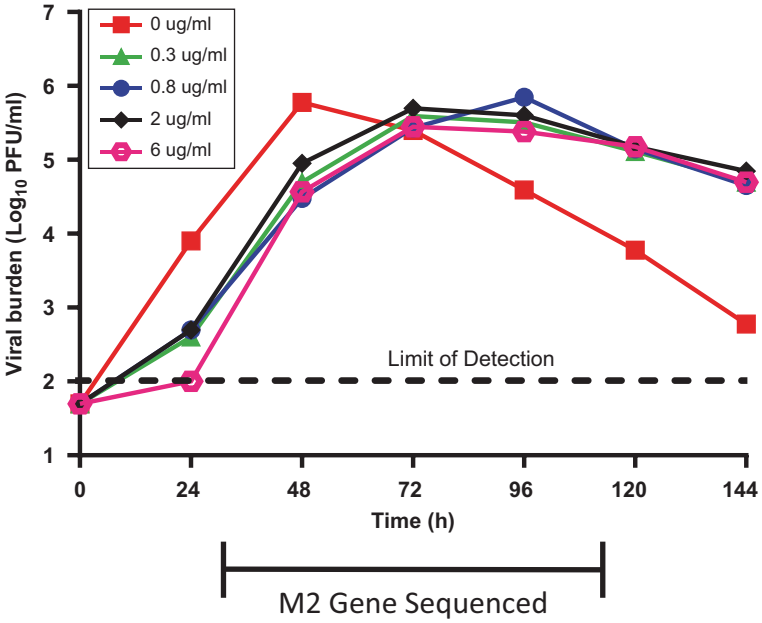

Fig. 9.16 Dose-ranging study with amantadine against an influenza A viral isolate in the HFIM system. Influenza-infected MDCK cells were mixed with uninfected MDCK cells at a ratio of $1{:}10^6$ and inoculated into the HF cartridges. Amantadine at various concentrations was administered into hollow fiber cartridges as a continuous infusion. Hollow fiber cartridges were sampled daily. Viral burden was quantified from clarified supernatants by plaque assay on MDCK cells. Viral burden determinations were performed in duplicate. The mean values are represented by the *symbols*, and *error bars* correspond to one standard deviation. (This figure contains data modified from Brown et al. 2010)

9.7.2 Neuraminidase Inhibitors

Neuraminidase inhibitors work to block the release of newly formed influenza virions from the host cell membrane. The first neuraminidase inhibitor available for oral administration was oseltamivir. Oseltamivir is a prodrug that is rapidly converted in the blood to the active form (oseltamivir carboxylate). The clinical dose of oseltamivir is 75 mg BID, but doses of 1000 mg per day have been shown to be well tolerated in people (Massarella et al. 2000). Since toxicity is not of great concern for this compound, we wished to determine if higher doses of oseltamivir would yield greater therapeutic outcomes relative to the current clinical dosage regimen and if QD dosing is as efficacious as the clinically employed BID dosing. To answer these questions, the PDs of oseltamivir were evaluated in the HFIM (McSharry et al. 2009b). For all PD studies performed in the HFIM system, the active form of oseltamivir, oseltamivir carboxylate, was employed. Dose ranging studies were conducted in which oseltamivir was administered into the HFIM system as a CI at various concentrations. The results are shown in Fig. 9.18.

Table 9.2 The influence of concentration on the percentage and type of M2 mutations selected in an influenza-A isolate under continuous amantadine pressure. (Reproduced with permission from Brown et al. 2010)

Arm	Time point (h)	Percent wild type	Mutant genotype
Control	48	100	
	120	100	
Continuous infusion			
0.3 μg/ml	48	100	
	72	80	S3IN
	96	70	S3IN
	120	80	S3IN
0.8 μg/ml	48	100	
	72	100	
	96	40	20% V27A, 40%
			A30T
	120	60	20% V27A, 20%
			A30T
2 μg/ml	48	90	I32S
	72	80	I32S
	96	60	I32S
	120	70	I32S
6 μg/ml	48	100	
	72	90	V27A
	96	100	
	120	70	V27A

A clear exposure–response relationship was observed for oseltamivir against influenza A virus. This is in contrast to the amantadine CI experiment (Fig. 9.16) where the exposure–response relationship is not evident because of different rates of outgrowth of resistant viral mutants. The clinical exposure of oseltamivir (75 mg BID) is equivalent to a CI of 400 ng/ml. From Fig. 9.18, it is evident that the maximal effect (E_{max}) of oseltamivir occurs at a CI of 100 ng/ml. Thus, these results demonstrate that higher clinical doses of oseltamivir are unlikely to be more efficacious, as E_{max} is achieved at the current clinical dosage regimen.

In order to determine if oseltamivir administered QD is as efficacious as the current clinical BID dosage regimen, a dose fractionation study was performed with oseltamivir in the HFIM system. For this experiment, oseltamivir administered as a CI, Q8h, Q12h, and Q24h dosage regimens (with the same total 24-h AUC) were contrasted. The PK profiles and the relative antiviral effect are illustrated in Figs. 9.19a and b, respectively.

There are no statistically significant differences in antiviral activity across any of the modes of administration (dosing intervals). It is important to note that these data were developed with an oseltamivir terminal half-life of 8 h. These data imply that the PD index linked to antiviral effect is $f\text{AUC}/\text{EC}_{50}$, suggesting that QD dosing for oseltamivir would not compromise efficacy in the clinic. This is an important finding as QD dosing would promote higher patient adherence, thereby minimizing

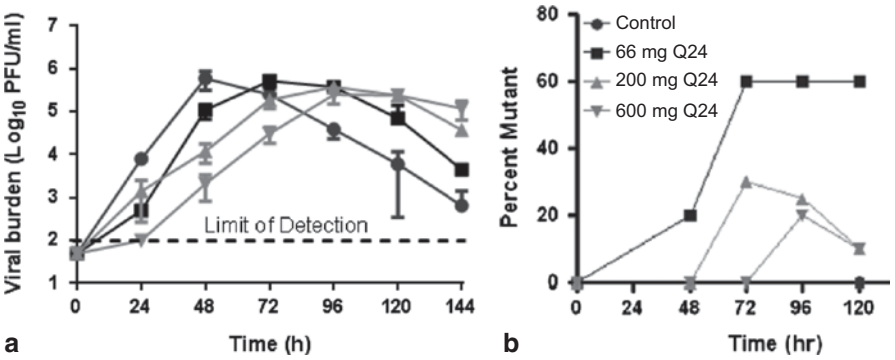

Fig. 9.17 Dose ranging study with amantadine administered Q24 against an influenza A viral isolate in the HFIM system. Influenza-infected MDCK cells were mixed with uninfected MDCK cells at a ratio of $1:10^6$ and inoculated into the HF cartridges. Amantadine at exposures equivalent to QD doses of 66, 200, or 600 mg was administered into hollow fiber cartridges as a 1-h infusion Q24. Hollow fiber cartridges were sampled daily. **a** Viral burden was quantified from clarified supernatants by plaque assay on MDCK cells. Each symbol corresponds to the mean viral titer, as viral burden quantifications were performed in duplicate. *Error bars* represent one standard deviation. **b** Viral RNA was extracted from supernatant samples harvested between 48 and 120 h post exposure and the influenza M2 gene was sequenced and the number of viral isolates harboring known amantadine-resistant mutations was determined. (Reproduced with permission from Brown et al. 2010)

the danger of suboptimal dosing stemming from missed doses of oseltamivir which could contribute to the emergence and spread of oseltamivir-resistant influenza.

Oseltamivir-resistant influenza has been well documented during seasonal and pandemic outbreaks and has been described most frequently in the pediatric population, where half-lives are considerably shorter, and in immunosuppressed patients (Besselaar et al. 2008; CDC 2009a, b, c; Collins et al. 2008; Dharan et al. 2009; Ghedin et al. 2011, 2012; Hauge et al. 2009; de Jong et al. 2005; Matsuzaki et al. 2010; Moscona 2005). Several attempts were made to identify oseltamivir-resistant mutants from both dose ranging and dose fractionation studies using Sanger sequencing and pyrosequencing methods to determine if oseltamivir exposure or dosing interval influences the emergence of drug-resistant viruses. All of these attempts were unfortunately unsuccessful. These results indicate that oseltamivir resistance is less likely to emerge relative to the adamantines. However, further studies are underway to evaluate optimal oseltamivir dosage regimens that will prevent the emergence of resistance.

Resistance to oseltamivir was described in the pandemic influenza outbreak of 2009 (CDC 2009a, b; Dharan et al. 2009; Ghedin et al. 2011). The primary isolate was influenza A/Hong Kong virus which contained a H275Y mutation in the viral neuraminidase. The EC_{50} for oseltamivir increased in excess of 200-fold with this mutation, abrogating the antiviral activity. Because of the locale of the mutation, the neuraminidase inhibitor zanamivir still retained activity against this isolate. The binding sites for zanamivir relative to oseltamivirin, the active site of the neuraminidase protein, explain this observation.

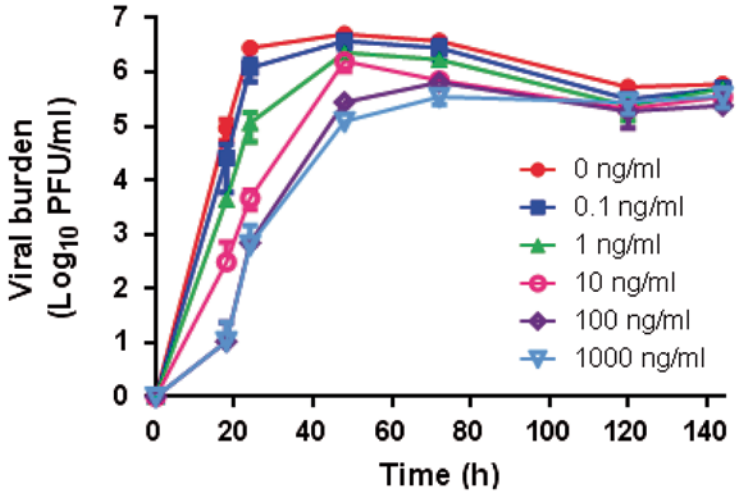

Fig. 9.18 The antiviral effect of oseltamivir, administered as a continuous infusion, on influenza A virus in the HFIM system. Influenza-infected MDCK cells were mixed with uninfected MDCK cells at a ratio of $1:10^6$ and inoculated into the HF cartridges. Oseltamivir carboxylate at various concentrations was administered into hollow fiber cartridges as a continuous infusion. Hollow fiber cartridges were sampled daily and viral burden was quantified from clarified supernatants by plaque assay on MDCK cells. Viral burden determinations were performed in duplicate. The mean values are represented by the *symbols*, and *error bars* correspond to one standard deviation. (Data modified from McSharry et al. 2009b)

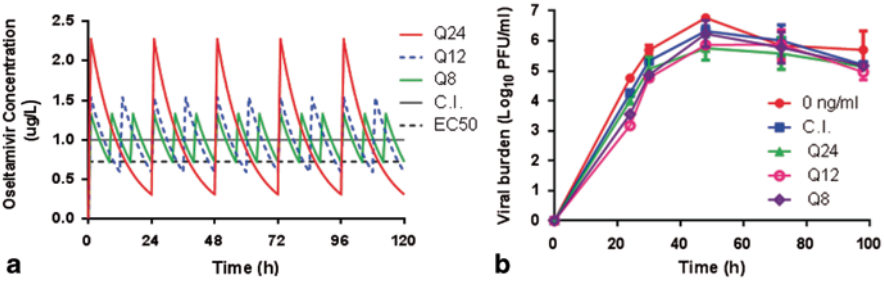

Fig. 9.19 The influence of dosing interval on the antiviral efficacy of oseltamivir against influenza A in the HFIM system. **a** The pharmacokinetic profiles simulated for oseltamivircarboxylate in the HFIM system and the EC_{50} value of the influenza A viral isolate examined in the experiment. All dosage regimens yielded a 24-h AUC value of 24 μg h/L, and a half-life of 8 h was simulated. **b** The viral burden detected in each hollow fiber cartridge over time. Viral burden in clarified supernatants harvested from hollow fiber cartridges was quantified in duplicate by plaque assay on MDCK cells. *Symbols* represent mean viral titer values and *error bars* correspond to one standard deviation. (Data modified from McSharry et al. 2009b)

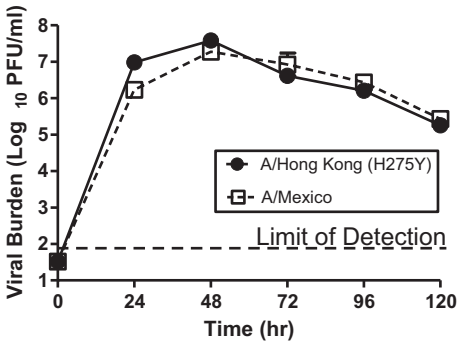

Fig. 9.20 Viral replication kinetics of A/Mexico (wild-type) and A/Hong Kong [H275Y] (oseltamivir-resistant) influenza viruses in the HFIM system. Viral burden was quantified by plaque assay on MDCK cells. Each hollow fiber unit was sampledin duplicate. *Symbols* represent mean values and *error bars* correspond to one standard deviation. (Reproduced with permission from Brown et al. 2011b)

Zanamivir was first introduced as an inhaled product. It could not be administered orally because of its low bioavailability. This limited its utility for oseltamivir-resistant influenza, especially in populations such as the very young, the elderly, and patients with severe structural lung damage. Consequently, in response to the resistance seen in the pandemic, the sponsor (Glaxo Smith-Kline) produced an intravenous (IV) formulation of zanamivir. While the H275Y mutation conferred a major shift in susceptibility to oseltamivir, there was no statistically significant change in the EC_{50} for zanamivir. Consequently, this agent was required for seriously ill patients infected with an oseltamivir-resistant isolate.

We examined zanamivir against the parent A/Mexico (wild-type) influenza strain as well as the oseltamivir-resistant mutant A/Hong Kong [H275Y] strain (Brown et al. 2011a, b). In Fig. 9.20, the growth characteristics of both isolates in the HFIM system are depicted.

The mutant isolate grew slightly better than the wild-type strain, so the H275Y mutation in the A/Hong Kong strain does not compromise viral biofitness. Zanamivir efficacy was also evaluated for both the wild-type A/Mexico and the oseltamivir-resistant A/Hong Kong [H275Y] isolates. These results are shown in Fig. 9.21. It is clear that zanamivir has a substantial inhibitory effect on both the wild-type (Fig. 9.21a) and oseltamivir-resistant (Fig. 9.21b) isolates, as viral burden in the zanamivir treatment arms were lower relative to those observed for the no-treatment control (control) arms. These results show that, in fact, the H275Y mutation does not affect viral susceptibility to zanamivir, despite conferring resistance to oseltamivir.

Since zanamivir is efficacious against both wild-type and oseltamivir-resistant influenza viral isolates, we wanted to determine if lower doses of zanamivir or less frequent dosing intervals could be administered without compromising efficacy. Thus, adose fractionation study (Q12 vs. Q24) and dose ranging study was performed simultaneously in the HFIM system with zanamivir against the oseltamivir-resistant A/Hong Kong [H275Y] isolate. The oseltamivir-resistant strain was chosen for these experiments because IV zanamivir is likely to be used only in patients exhibiting influenza infection with oseltamivir-resistant viruses. The results from these studies are shown in Fig. 9.22.

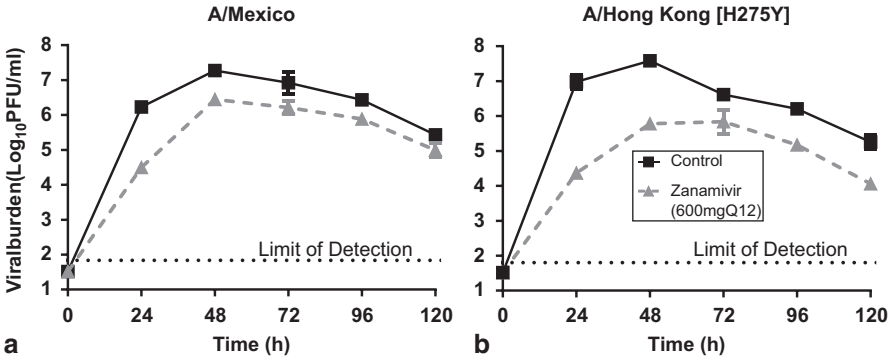

Fig. 9.21 Efficacy of the clinical IV dose of zanamivir (600 mg Q12) against **a** wild-type A/Mexico and **b** oseltamivir-resistant A/Hong Kong [H275Y] influenza in the HFIM system. Hollow fiber cartridges were sampled in duplicate and viral burden was determined from clarified viral supernatants by plaque assay. Each *symbol* represents the mean viral titer value and *error bars* correspond to one standard deviation. (Reproduced (**a**) and modified (**b**) with permission from Brown et al. 2011b)

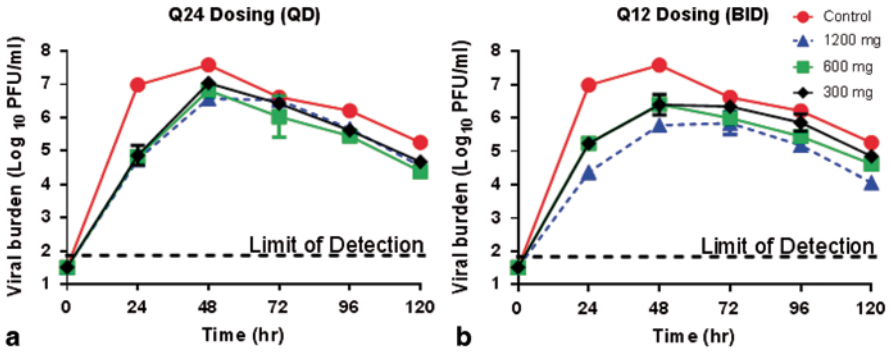

Fig. 9.22 Dose fractionation and dose-ranging studies with zanamivir against oseltamivir-resistant A/Hong Kong [H275] influenza virus in the HFIM system. Zanamivir was administered into hollow fiber cartridges at exposures equivalent to 1200, 600, or 300 mg daily doses either as **a** the total daily dose given once daily (Q24) or **b** half the daily dose administered twice daily (Q12). Hollow fiber cartridges were sampled daily in duplicate, and viral burden was quantified from clarified supernatants by plaque assay. *Symbols* correspond to mean viral titers and *error bars* represent one standard deviation. (Reproduced with permission from Brown et al. 2011b)

Greater viral inhibition resulted at all dose levels when the agent was administered Q12 versus Q24. These findings suggest that the PD index for zanamivir that is best linked with viral suppression is $f\text{Time} > EC_{50}$. This is in contrast to oseltamivir, which instead has a PD-linked index of $f\text{AUC}/EC_{50}$, as discussed above. This raises the immediate question of why the dynamic driver would be different for two agents within the same therapeutic group.

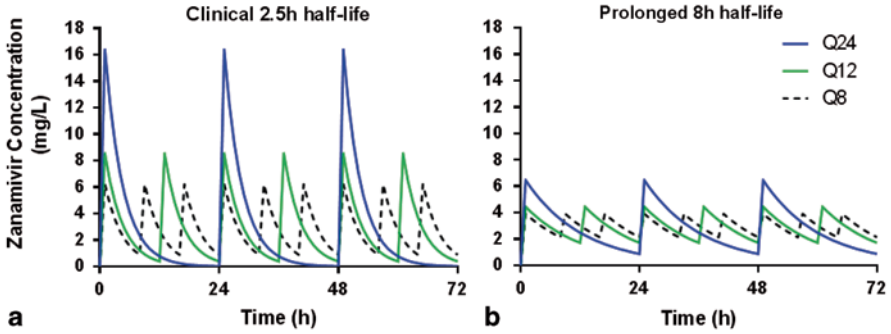

Fig. 9.23 The pharmacokinetic profiles for the study in the HFIM system evaluating the influence of half-life on the pharmacodynamic index (dosing interval) for zanamivir that is best linked to suppression of A/Hong Kong [H275Y] influenza virus. For this study, **a** the clinical 2.5-h half-life and **b** a prolonged 8-h half-life were simulated. Dosing intervals of Q24, Q12, and Q8 were evaluated at each half-life. (Data from Brown et al. 2011a)

The hypothesis set forth had to do with the different half-lives observed with these agents, with oseltamivir having an 8-h half-life and zanamivir having a 2.5-h half-life in man. To test this hypothesis, a set of experiments were performed where zanamivir was administered into hollow fiber cartridges at exposures that had the same 24-h AUC, but a 2.5-h half-life was simulated in one set of experimental arms and an 8-h half-life (the half-life reported for oseltamivir) was simulated in the other set of experimental arms. We examined the total daily dose of 1200 mg/day (the clinical dose) and fractionated it as one third the total dose Q8, one half the total daily dose Q12, and the whole dose Q24. The PK profiles of all dosage regimens evaluated in this experiment are shown in Fig. 9.23.

The PD results for this experiment are displayed in Fig. 9.24.

When the clinical 2.5 h half-life is simulated, the PD driver for zanamivir is $f\text{Time} > \text{EC}_{50}$, as greater viral suppression was observed in treatment arms with more frequent dosing intervals (Fig. 9.24a). When the half-life was prolonged to an oseltamivir-like 8 h (Fig. 9.24b), the dynamic driver switches to $f\text{AUC}/\text{EC}_{50}$. We sought to explain these findings through use of a mathematical model. The form of the model is displayed in Fig. 9.25.

This model was applied to all the data illustrated in Figs. 9.22 and 9.24 simultaneously. The individual model fits are shown in Fig. 9.26.

The fit of the model to the data was excellent, with pre-Bayesian predicted–observed plots of 0.99 for zanamivir concentrations and 0.87 for viral burden. The post-Bayesian fits were 0.99 for zanamivir concentration and 0.97 for the viral burden.

The point estimates and measures of dispersion for the parameter values are displayed in Table 9.3.

The values for the delay time to viral release, mean survival time for infected cells, and for extracellular virus are clinically plausible. Of utmost importance, the

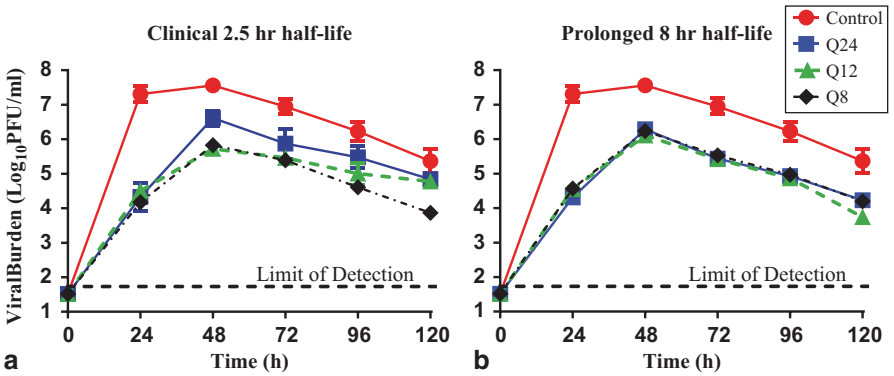

Fig. 9.24 The effect of half-life on the pharmacodynamic index of zanamivir against A/Hong Kong [H275Y]. Zanamivir, at an exposure equivalent to the total daily clinical dose of 1200 mg/day, was administered into hollow fiber cartridges as 1200 mg Q24 (Q24), 600 mg Q12 (Q12), or 400 mg Q8 (Q8) via a 1-h infusion. **a** The clinical 2.5-h half-life and **b** a prolonged 8 h half-life were simulated for each dosage regimen evaluated. Hollow fiber cartridges were sampled daily in duplicate, and viral burden was quantified from clarified supernatants by plaque assay. *Symbols* correspond to mean viral titers and *error bars* represent one standard deviation. (Reproduced with permission from Brown et al. 2011a)

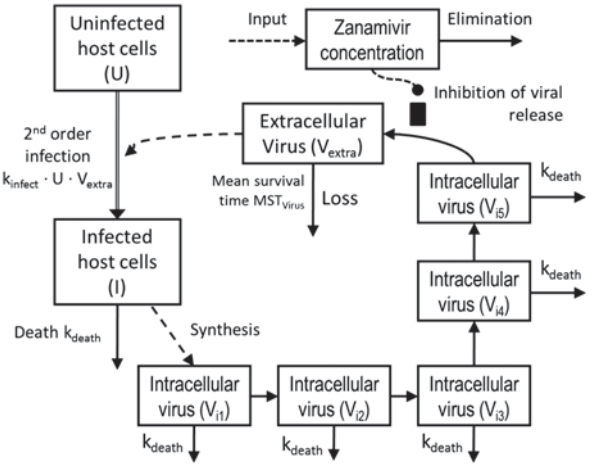

Fig. 9.25 Mathematical model for zanamivir against oseltamivir-resistant A/Hong Kong [H275Y] influenza virus. The model describes the inhibitory effect of zanamivir on the release of newly synthesized virions from the host cell over time. For enabling equations, please refer to the original publication (Brown et al. 2011a). (Reproduced with permission from Brown et al. 2011a)

maximum extent of inhibition is 99%, meaning that if enough zanamivir gets to the site of infection (in this case the lungs) it is possible to inhibit virtually all rounds (99%) of viral replication. Finally, the zanamivir concentration causing 50% of maximal inhibition is low and in accordance with other independent in vitro testing.

We employed the model to run simulations to identify the extent of viral inhibition at the end of the each dosing interval evaluated in this study. The results of the simulations are shown in Table 9.4.

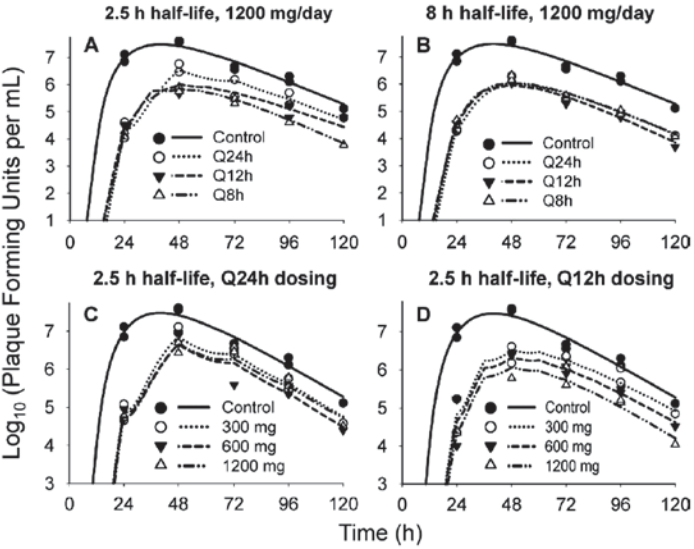

Fig. 9.26 The individual-fitted viral burdens for zanamivir against oseltamivir-resistant A/Hong Kong [H275Y] in the HFIM system, as determined by the mathematical model depicted in Fig. 9.25. **a** and **b** Graphs are based on the pharmacodynamic studies illustrated and described in Fig. 9.24. **c** and **d** Graphs are based on the dose fractionation and dose-ranging studies illustrated and described in Fig. 9.22. (Reproduced with permission from Brown et al. 2011a)

The 8-h half-life provides a high percent of maximal suppression (>96%), irrespective of the dosing interval. In contrast, when the 2.5-h half-life is simulated, the Q12 and Q8 dosing intervals provide high percent of maximal inhibition at trough (94 and 96.3%, respectively), but this is not true at the QD administration schedule (Q24), where percent of maximal inhibition shows a substantial decline (71.8%).

These findings show that the mathematical model described above (Fig. 9.25) is a powerful tool for predicting influenza viral load over time for any zanamivir dosage regimen, as the model provided physiologically plausible parameter estimates and, more importantly, explained the cause for the switch in PD-linked indices from $f\text{Time}>\text{EC}_{50}$ to $f\text{AUC}/\text{EC}_{50}$ when the half-life extends to 8 h. Since zanamivir is almost exclusively eliminated via renal excretion, such a change in half-life would likely be seen in renal failure patients. Thus, one can conclude that patients with renal failure would exhibit a PD-index of $f\text{AUC}/\text{EC}_{50}$ for zanamivir and individuals with normal renal function would have a PD-index of $f\text{Time}>\text{EC}_{50}$. These findings suggest that alternative dosing strategies for zanamivir regimens in renal failure patients may be warranted. Our model can be utilized to predict the efficacy of any desired zanamivir dosage regimen, thereby providing guidance to the selection of the most optimal regimen.

The HFIM allows insight into different drug classes to optimize dose and dosing interval in order to maximize antiviral activity and minimize the emergence of drug-resistant viruses.

Table 9.3 Parameter estimates for the population PK/PD mathematical model for zanamivir against oseltamivir-resistant A/Hong Kong [H275Y] influenza virus in the HFIM system. (Reproduced with permission by Brown et al. 2011a)

Parameter	Symbol unit	Population mean estimates		Estimate for between-curve variability	
		Mean	% CV uncertainty	Variance	% CV uncertainty
PK/PD parameters					
Log_{10} of 2nd-order infection rate constant	$Log_{10}\ K_{infect}$	−2.49	6.1	0.0834	90
Synthesis rate constant of virus	K_{syn} (1/h)	3.49	19.8	0.0045	145
Mean delay time until release of virus in the absence of reading	$MDT_{delay} = 5/K_{death}$ (h)	37.6	2.6	0.0067	82
Mean survival time of infected cells	$MST_{infected} = 1/K_{loss,\ virus}$ (h)	7.4	5.3	0.0054	74
Mean survival time for extracellular virus	$MST_{virus} = 1/K_{loss,\ virus}$ (h)	12.4	6.9	0.0183	87
Maximum extent of inhibition	I_{max} (normal scale)	0.990			
Maximum extend of inhibition (on transformed scale)	I_{max} (transformed scale)	4.6[a,b]	9.6	0.133[a,b]	140
Zanamivir concentration causing 50 % of I_{max}	IC_{50} (mg/L)	0.0168	26.1	0.0114	285
Hill coefficient	Hill	0.0885	9.7	0.0017	136
clearance	CL (L/h)	16.0	2.1	0.0041	51
Volume of distribution for 8.0-h half-life	$V1_{8\text{-h half-life}}$ (L)	170	15.0	0.0399	282
Volume of distribution for 2.5-h half-life	$V1_{2.5\text{-h half-life}}$ (L)	69.8	0.4	< 0.0001	872
Log_{10} of initial no. of uninfected cells	Log_U	8	0 (fixed)		
Log_{10} of initial no. of infected cells	Log_I	2	0 (fixed)		
Residual error parameters					
Additive error for viral load on log_{10} scale	SD_{in}	0.224	6.9		
Additive error for zanamivir concentration	PK_{in} (mg/L)	0.092	20.6		
Proportional error for zanamivir concentration	P_{ksl}	0.071	14.8		

[a] I_{max} was assumed to be normally distributed on the transformed scale ($I_{maxtransformed}$). The following logistics was used to constrain I_{max} between 0 and 1: $I_{max} = 1/[1 + \exp(-I_{maxtransformed})]$

[b] Individual I_{max} estimates (on the normal scale) ranged from 0.988 to 0.991 for all curves

Table 9.4 Percent inhibition (I_{max}) at the end of different dosing intervals with identical total daily doses (1200 mg/day). (Data from Brown et al. 2011a)

Regimen	2.5-h half-life (%)	8-h half-life (%)
Q24	71.8	96.2
Q12	94.0	97.4
Q8	96.3	97.7

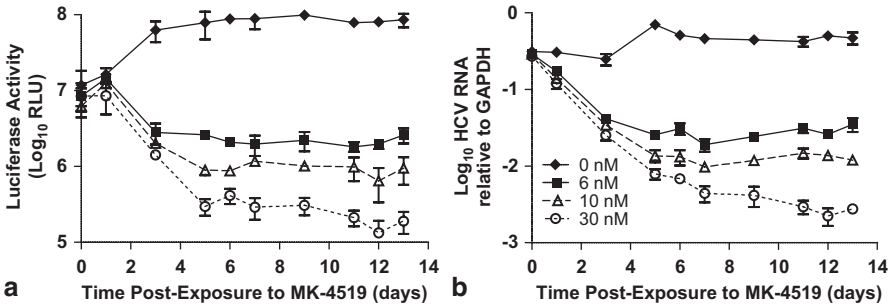

Fig. 9.27 Dose-ranging study with MK-4519 against a HCV genotype 1b replicon-bearing cell line in the BelloCell system. MK-4519 was delivered into BelloCell bottles as a continuous infusion at various concentrations. Throughout the 13-day study, six sets of six flakes were harvested from each BelloCell bottle at the time points indicated in the graph. Antiviral activity of MK-4519 was measured by **a** *Renilla* luciferase assay for three sets of six flakes and **b** real-time qRT-PCR for the three remaining sets of six flakes. Each *data point* corresponds to the mean value of the three samples measured and *error bars* represent one standard deviation. (Reproduced with permission from Brown et al. 2012)

9.8 HCV

Little has been done with PDs for HCV. The inability to grow this virus well in vitro leads to a paucity of information about optimizing therapy. We developed a new in vitro model system (BelloCell system) to examine this issue. For a more in depth description of the BelloCell system or the HCV replicon used in these studies, please refer to the original publication (Brown et al. 2012). Briefly, in the BelloCell system, HCV genotype 1b replicon-bearing cells are allowed to adhere to plastic flakes contained within each BelloCell bottle. Drug is circulated in the system. As with the HFIM, virtually any PK exposure profile can be achieved. Flakes (generally 36 per sampling time) are removed and replicon replication is quantitated by two different assays: a luciferase reporter assay and real-time quantitative reverse transcriptase PCR (qRT-PCR).

The serine protease inhibitor MK-4519 was examined in this system (Brown et al. 2012). In the first of a series of experiments, a dose ranging study was conducted in which a CI of the drug at various concentrations was administered into BelloCell bottles. The results of this dose ranging study are shown in Fig. 9.27.

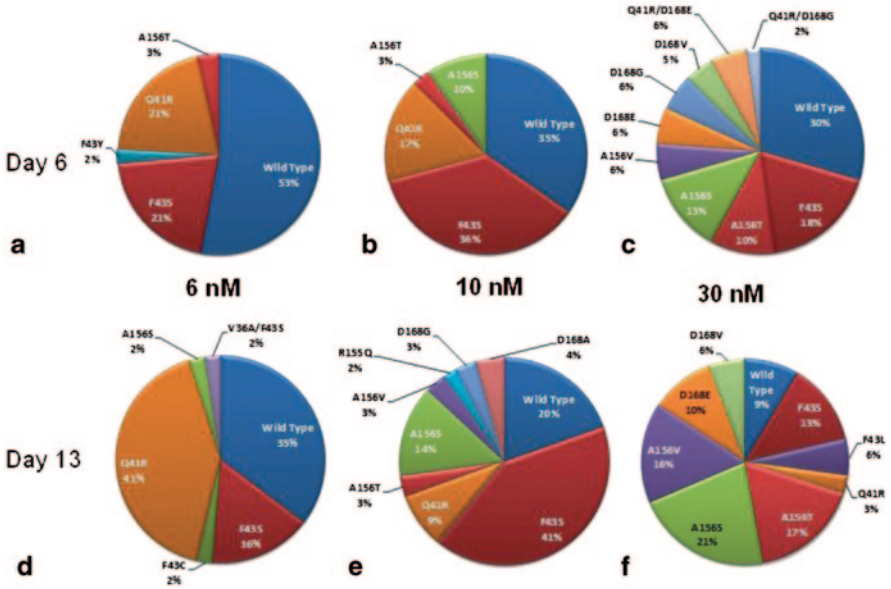

Fig. 9.28 Selection of serine protease-resistant HCV replicons as a result of MK-4519 pressure in BelloCell dose ranging studies. Cellular RNA was extracted from replicon-bearing cells harvested from BelloCell bottles in which MK-4519 was administered as a continuous infusion. The NS3/4a protein from the replicon RNA was evaluated for mutations by clonal sequencing on day 6 (*top panels*) and day 13 (*bottom panels*) post exposure. Pie charts show the genotype and frequency of mutant replicon populations for the 6-nM (**a** and **d**), 10-nM (**b** and **e**), and 30-nM (**c** and **f**) treatment arms. (Reproduced with permission from Brown et al. 2012)

These data show a clear exposure–response relationship between MK-4519 and the replicon, irrespective of the method of quantitation employed. In the clinic, use of a serine protease inhibitor as monotherapy often results in the selection and amplification of resistant HCV isolates (Sarrazin et al. 2007). We examined whether or not HCV replicons harboring known serine protease-resistance mutations were selected under the pressure of MK-4519 as a CI in the BelloCell system. These results are shown in Fig. 9.28.

These results show that drug-resistant replicons were selected for under MK-4519 pressure (essentially all the mutations have been identified in the clinic as producing drug resistance), irrespective of the intensity of the drug therapy. Indeed, the resistance emergence continuous to be a larger problem with increasing drug concentration. There is also a time dependency seen, with later times showing a higher proportion of the total population being mutants.

Since it is clear from the data above (Fig. 9.28) that drug exposure influences both the genotype and frequency of mutant populations amplified under pressure, a separate experiment was conducted to determine if dosing interval played a role in mutant amplification. For these studies, a dose fractionation was performed evaluating three different dosing intervals: CI, Q24, and Q12. For all regimens, a 24-h AUC of 240 nM h, equivalent to a CI of 10 nM (10 nM×24 h=240 nM h), was

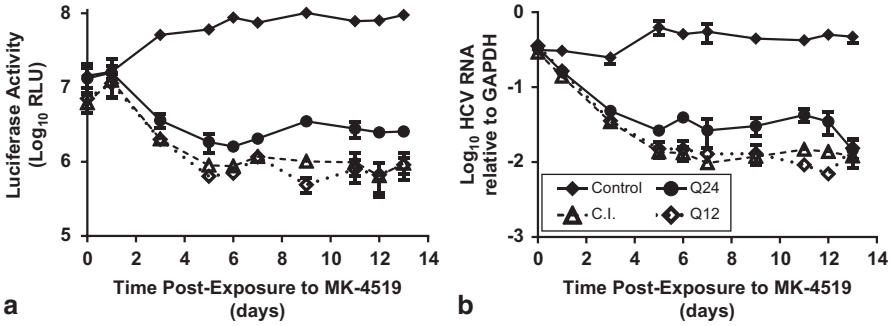

Fig. 9.29 Dose fractionation study with MK-4519 against an HCV genotype 1b replicon-bearing cell line in the BelloCell system. MK-4519 was delivered into BelloCell bottles as a continuous infusion (*C.I.*) or at dosing intervals of Q24 or Q12. All dosage regimens had a 24-h AUC of 240 nM h and a half-life of 3.6 h was simulated for MK-4519. Throughout the 13-day study, six sets of six flakes were harvested from each BelloCell bottle at the time points indicated in the graph. Antiviral activity of MK-4519 was measured by **a** *Renilla* luciferase assay for three sets of six flakes and **b** real-time qRT-PCR for the three remaining sets of six flakes. Each *data point* corresponds to the mean value of the three samples measured and *error bars* represent one standard deviation. (Reproduced with permission from Brown et al. 2012)

simulated for MK-4519. The results from this study are shown in Fig. 9.29. The outcome was clear-cut. The least amount of antiviral activity was seen with Q24 dosing, whereas the Q12 and CI dosing intervals provided significantly greater antiviral effect. This indicates that $f\text{Time} > EC_{50}$ (or EC_{90}) is the PD index most closely linked to effect for MK-4519.

Resistance emergence was also examined in replicons harvested from the dose fractionation study. As described above, a time dependency for resistance emergence was seen. For this study, a single exposure (24 h AUC = 240 nM h) was examined, albeit at three different dosing intervals. The Q24 dosing interval yielded the lowest frequency of drug resistant replicons. This is likely due to the fact that this dosage regimen produced the least amount of drug pressure over the 24 h dosing interval. Of interest, while the total antiviral activity was quite similar between CI and Q12 dosing interval, there was a significant difference in the resistance emergence, with CI causing more ultimate resistance (CI at 6 and 13 days: 35 and 20 % wild type, respectively; Q12 at 6 and 13 days: 40 and 41 % wild type, respectively). Despite the fact that the total viral decline was not different between the Q12 and CI regimens, the CI did exert more antiviral pressure, allowing for greater resistant mutant amplification over time. This provides further evidence regarding $f\text{Time} > EC_{50}$ (or EC_{90}) as being the pharmacodynamically linked index for MK-4519.

We also fit a mathematical model to all system outputs simultaneously (drug exposure, total viral burden, mutant viral burden). The equations for the model are shown below:

$$d(X_1)/dt = R(1) + B(1) - (CL/V) \times [X_1] \tag{9.1}$$

$$d(X_2)/dt = (IC_2) + K_{turn-s}x(X_2) \times \left(1.0 - \left([X_1/V]^{H-s}\right)/ \left(C_{50-s}{}^{H-s} + \left([X_1/V]^{H-s}\right)\right) \times (1 - (X_2 + X_3)/POPMAX) - K_{loss} \times X_2 \quad (9.2)$$

$$d(X_3)/dt = (IC_3) + K_{turn-r}x(X_3) \times (1.0 - ([X_1/V]^{H-r})/ \left(C_{50-r}{}^{H-r} + \left([X_1/V]^{H-r}\right)\right) \times (1 - (X_2 + X_3)/POPMAX) - K_{loss} \times X_3 \quad (9.3)$$

where X_1, X_2, and X_3 are amounts of drug, wild-type luciferase activity and mutant luciferase activity. R(1) is a piecewise input function for MK-4519. B(1) is a bolus of MK-4519. CL is the clearance of MK-4519. V is the volume of the central compartment. K_{turn-s} and K_{turn-r} are the first order turnover rate constants for wild-type and mutant replicons. C_{50-s} and C_{50-r} are the concentrations of MK-4519 for wild-type and mutant replicons at which the turnover rate constants are reduced by half. H_s and H_r are Hill's constants for the two populations. POPMAX is the maximal amount of total luciferase activity and is part of the logistic carrying function. K_{loss} is the first order rate of loss of the replicon from the cells.

It was assumed that MK-4519 did not "kill" cells or replicons, but rather decreased the rate of turnover towards zero. It was further assumed that the rate of loss of replicons from cells was the same for both wild-type and mutant replicons. The fit of the model to the data was acceptable. The simulated time profiles for the total viral burden and the mutant viral burden over time is shown below in Fig. 9.30. As can be seen, the fit of the model to the data was excellent and the model described the viral dynamics well. For the drug concentration (data not shown) the observed predicted plot had a relationship of:

Observed = 0.982 × Predicted + 0.305; $r^{2=}$0.998; $p << 0.001$

For the post-Bayesian step, the relationship was:

Observed = 0.993 × Predicted + 0.140; $r^{2=}$0.999; $p << 0.001$

The model can then be said to have accurately described all system outputs for all regimens simultaneously. The parameter values determined from the analysis are shown in Table 9.5.

There are a number of take-home messages from this analysis:

1. The mutants have a slower turnover rate.
2. The C_{50} is much higher for the mutants relative to wild type.
3. Replicon loss rate is relatively stable and independent of amount of drug pressure.

Perhaps most importantly continuous pressure with MK-4519 at more than $7 \times EC_{50}$ (30 nM) only accelerated the rate of resistance emergence. This strongly suggests that combination chemotherapy is required for therapy of Hepatitis C.

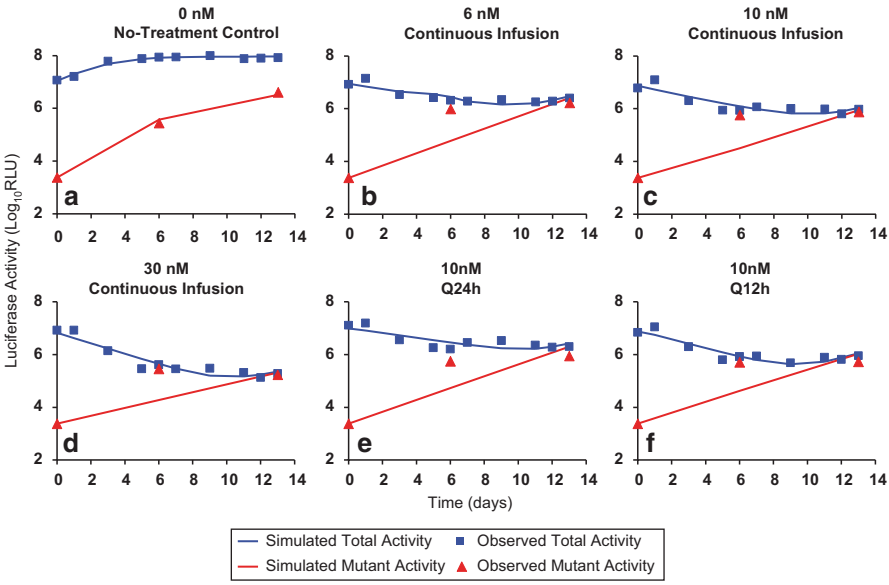

Fig. 9.30 Fitted luciferase activities for MK-4519 against a HCV genotype 1b replicon-bearing cell line in dose-ranging and dose fractionation studies conducted in the BelloCell system. **a**–**d** Luciferase activity determined from dose ranging studies in the BelloCell system described in Fig. 9.27 in which MK-4519 was administered into BelloCell bottles as a continuous infusion at various concentrations. **a**, **b**, **d**, and **f** Luciferase activity determined from dose fractionation studies in the BelloCell system described in Fig. 9.29 in which MK-4519 was administered into BelloCell bottles at a 24-h AUC exposure equivalent to 240 nM·h by Q24, Q12, or continuous infusion dosing. A half-life of 3.6 h was simulated for MK-4519. The *lines* correspond to luciferase activity simulated by the mathematical model, and the *symbols* represent the luciferase activity measured from cells harvested from the BelloCell bottles at the specified time points. *Blue* signifies total replicon activity, and *red* represents activity from only the mutant replicon population. (Reproduced with permission from Brown et al. 2012)

9.9 Conclusions

While antiviral PDs pose some challenges, it is clear that it is straightforwardly possible to perform experiments to delineate the PD index that is best linked with viral inhibition/suppression of resistance emergence (dosing interval) and optimal exposure needed to optimize antiviral therapy, as has been done for nearly three decades in the realm of bacterial and fungal therapy.

The challenge for the future, particularly for very plastic viruses like HCV and HIV is to identify optimal combination regimens that will maximize viral suppression as well as suppress resistance emergence with minimal toxicity.

Table 9.5 Mean and Bayesian estimate parameter values resulting from the mathematical analysis of dose-ranging and dose fractionation studies with MK-4519 against a HCV genotype 1b replicon-bearing cell line in the BelloCell system. (Reproduced with permission from Brown et al. 2012)

Treatment arm	$K_{turn\text{-}s}$ (day^{-1})	$K_{turn\text{-}r}$ (day^{-1})	$C_{50\text{-}s}$ (nM MK-4519)	$C_{50\text{-}r}$ (nM MK-4519)	*H-s*	*H-r*	K_{loss} (day^{-1})
0 nM	2.04	2.575	20.743	46.92	22.81	2.614	1.342
6 nM CI	1.975	2.736	19.4	55.51	6.998	19.25	2.199
10 nM CI	1.999	2.748	23.61	45.76	11.12	18.34	2.258
10 nM q24h	5.612	2.086	3.076	79.53	15.83	24.65	1.569
10 nM q12h	3.131	4.541	15.39	14.68	14.8	3.67	2.6
30 nM CI	0.242	15	2.854	21.77	23.93	5.968	0.459
Mean±SD	2.500±1.63	4.947±4.56	14.18±8.29	44.03±21.5	15.91±5.99	12.42±8.62	1.738±0.71

CI continuous infusion

9.10 Summary

- Pharmacometrics, including PK/PD principles, can be employed to guide the design of optimal dosage regimens for antiviral compounds to minimize the challenges associated with antiviral therapies.
- In vitro PD model systems are powerful tools that can be utilized to predict optimal dose(s) and dosing interval(s) for antiviral compounds that will maximize viral suppression, prevent the emergence of resistance, and minimize toxicity.
- PD data derived from in vitro PD model systems and mathematical models have been used successfully for antiviral agents to:
  - Prospectively predict optimal dosage regimens for antiviral compounds both as monotherapy and combination therapy.
  - Explain the failure of suboptimal regimens.
  - Understand resistance emergence and elucidate whether or not resistance can be counter selected.
  - Evaluate the efficacy of clinically administered dosage regimens to determine if the optimal exposure is utilized.
  - Determine whether alternative dosing intervals, such as QD dosing that promotes better patient adherence, can be administered without compromising efficacy.

References

Apostolova N, Blas-Garcia A, Esplugues J V (2011a) Mitochondrial interference by anti-HIV drugs: mechanisms beyond Pol-gamma inhibition. Trends Pharmacol Sci 32:715–725

Apostolova N, Blas-Garcia A, Esplugues JV (2011b) Mitochondrial toxicity in HAART: an overview of in vitro evidence. Curr Pharm Des 17:2130–2144

Besselaar TG, Naidoo D, Buys A, Gregory V, McAnerney J, Manamela JM, Blumberg L, Schoub BD (2008) Widespread oseltamivir resistance in influenza A viruses (H1N1), South Africa. Emerg Infect Dis 14:1809–1810

Bilello JA, Bauer G, Dudley MN, Cole GA, Drusano GL (1994) Effect of 2′,3′-didehydro-3′-deoxythymidine in an in vitro hollow-fiber pharmacodynamic model system correlates with results of dose-ranging clinical studies. Antimicrob Agents Chemother 38:1386–1391

Bright RA, Shay DK, Shu B, Cox NJ, Klimov AI (2006) Adamantane resistance among influenza A viruses isolated early during the 2005–2006 influenza season in the United States. JAMA 295:891–894

Brown AN, McSharry JJ, Weng Q, Driebe EM, Engelthaler DM, Sheff K, Keim PS, Nguyen J, Drusano GL (2010) In vitro system for modeling influenza A virus resistance under drug pressure. Antimicrob Agents Chemother 54:3442–3450

Brown AN, Bulitta JB, McSharry JJ, Weng Q, Adams JR, Kulawy R, Drusano GL (2011a) Effect of half-life on the pharmacodynamic index of zanamivir against influenza virus delineated by a mathematical model. Antimicrob Agents Chemother 55:1747–1753

Brown AN, McSharry JJ, Weng Q, Adams JR, Kulawy R, Drusano GL (2011b) Zanamivir, at 600 milligrams twice daily, inhibits oseltamivir-resistant 2009 pandemic H1N1 influenza virus in an in vitro hollow-fiber infection model system. Antimicrob Agents Chemother 55:1740–1746

Brown AN, McSharry JJ, Adams JR, Kulawy R, Barnard RJ, Newhard W, Corbin A, Hazuda DJ, Louie A, Drusano GL (2012) Pharmacodynamic analysis of a serine protease inhibitor,

MK-4519, against hepatitis C virus using a novel in vitro pharmacodynamic system. Antimicrob Agents Chemother 56:1170–1181
CDC (2006) High levels of adamantane resistance among influenza A (H3N2) viruses and interim guidelines for use of antiviral agents—United States, 2005–2006 influenza season. MMWR Morb Mortal Wkly Rep 55:44–46
CDC (2009a) Oseltamivir-resistant 2009 pandemic influenza A (H1N1) virus infection in two summer campers receiving prophylaxis—North Carolina, 2009. MMWR Morb Mortal Wkly Rep 58:969–972
CDC (2009b) Oseltamivir-resistant novel influenza A (H1N1) virus infection in two immunosuppressed patients—Seattle, Washington, 2009. MMWR Morb Mortal Wkly Rep 58:893–896
CDC (2009c) Update: drug susceptibility of swine-origin influenza A (H1N1) viruses, April 2009. MMWR Morb Mortal Wkly Rep 58:433–435
Collins PJ, Haire LF, Lin YP, Liu J, Russell RJ, Walker PA, Skehel JJ, Martin SR, Hay AJ, Gamblin SJ (2008) Crystal structures of oseltamivir-resistant influenza virus neuraminidase mutants. Nature 453:1258–1261
Deyde VM, Xu X, Bright RA, Shaw M, Smith CB, Zhang Y, Shu Y, Gubareva LV, Cox NJ, Klimov AI (2007) Surveillance of resistance to adamantanes among influenza A(H3N2) and A(H1N1) viruses isolated worldwide. J Infect Dis 196:249–257
Dharan NJ, Gubareva LV, Meyer JJ, Okomo-Adhiambo M, McClinton RC, Marshall SA, St George K, Epperson S, Brammer L, Klimov AI, Bresee JS, Fry AM (2009) Infections with oseltamivir-resistant influenza A(H1N1) virus in the United States. JAMA 301:1034–1041
Drake JW (1993) Rates of spontaneous mutation among RNA viruses. Proc Natl Acad Sci U S A 90:4171–4175
Drusano GL, D'Argenio DZ, Symonds W, Bilello PA, McDowell J, Sadler B, Bye A, Bilello JA (1998) Nucleoside analog 1592U89 and human immunodeficiency virus protease inhibitor 141W94 are synergistic in vitro. Antimicrob Agents Chemother 42:2153–2159
Drusano GL, D'Argenio DZ, Preston SL, Barone C, Symonds W, LaFon S, Rogers M, Prince W, Bye A, Bilello JA (2000) Use of drug effect interaction modeling with Monte Carlo simulation to examine the impact of dosing interval on the projected antiviral activity of the combination of abacavir and amprenavir. Antimicrob Agents Chemother 44:1655–1659
Drusano GL, Bilello JA, Preston SL, O'Mara E, Kaul S, Schnittman S, Echols R (2001) Hollow-fiber unit evaluation of a new human immunodeficiency virus type 1 protease inhibitor, BMS-232632, for determination of the linked pharmacodynamic variable. J Infect Dis 183:1126–1129
Drusano GL, Bilello PA, Symonds WT, Stein DS, McDowell J, Bye A, Bilello JA (2002a) Pharmacodynamics of abacavir in an in vitro hollow-fiber model system. Antimicrob Agents Chemother 46:464–470
Drusano GL, Moore KH, Kleim JP, Prince W, Bye A (2002b) Rational dose selection for a non-nucleoside reverse transcriptase inhibitor through use of population pharmacokinetic modeling and Monte Carlo simulation. Antimicrob Agents Chemother 46:913–916
Fried MW (2002) Side effects of therapy of hepatitis C and their management. Hepatology 36:S237–S244
Fried MW, Shiffman ML, Reddy KR, Smith C, Marinos G, Goncales FL, Jr, Haussinger D, Diago M, Carosi G, Dhumeaux D, Craxi A, Lin A, Hoffman J, Yu J (2002) Peginterferon alfa-2a plus ribavirin for chronic hepatitis C virus infection. N Engl J Med 347:975–982
Ghedin E, Laplante J, DePasse J, Wentworth DE, Santos RP, Lepow ML, Porter J, Stellrecht K, Lin X, Operario D, Griesemer S, Fitch A, Halpin RA, Stockwell TB, Spiro DJ, Holmes EC, St GK (2011) Deep sequencing reveals mixed infection with 2009 pandemic influenza A (H1N1) virus strains and the emergence of oseltamivir resistance. J Infect Dis 203:168–174
Ghedin E, Holmes EC, DePasse JV, Pinilla LT, Fitch A, Hamelin ME, Papenburg J, Boivin G (2012) Presence of oseltamivir-resistant pandemic A/H1N1 minor variants before drug therapy with subsequent selection and transmission. J Infect Dis 206:1504–1511
Greco WR, Bravo G, Parsons JC (1995) The search for synergy: a critical review from a response surface perspective. Pharmacol Rev 47:331–385

Haas DW, Arathoon E, Thompson MA, de Jesus PR, Gallant JE, Uip DE, Currier J, Noriega LM, Lewi DS, Uribe P, Benetucci L, Cahn P, Paar D, White AC, Jr, Collier AC, Ramirez-Ronda CH, Harvey C, Chung MO, Mehrotra D, Chodakewitz J, Nguyen BY (2000) Comparative studies of two-times-daily versus three-times-daily indinavir in combination with zidovudine and lamivudine. AIDS 14:1973–1978

Hauge SH, Dudman S, Borgen K, Lackenby A, Hungnes, O (2009) Oseltamivir-resistant influenza viruses A (H1N1), Norway, 2007–2008. Emerg Infect Dis 15:155–162

Holland JJ, De La Torre JC, Steinhauer DA (1992) RNA virus populations as quasispecies. Curr Top Microbiol Immunol 176:1–20

Johnson AA, Ray AS, Hanes J, Suo Z, Colacino JM, Anderson KS, Johnson KA (2001) Toxicity of antiviral nucleoside analogs and the human mitochondrial DNA polymerase. J Biol Chem 276:40847–40857

de Jong MD, Tran TT, Truong HK, Vo MH, Smith GJ, Nguyen VC, Bach VC, Phan TQ, Do QH, Guan Y, Peiris JS, Tran TH, Farrar J (2005) Oseltamivir resistance during treatment of influenza A (H5N1) infection. N Engl J Med 353:2667–2672

Krumbholz A, Schmidtke M, Bergmann S, Motzke S, Bauer K, Stech J, Durrwald R, Wutzler P, Zell R (2009) High prevalence of amantadine resistance among circulating European porcine influenza A viruses. J Gen Virol 90:900–908

Lee H, Hanes J, Johnson KA (2003) Toxicity of nucleoside analogues used to treat AIDS and the selectivity of the mitochondrial DNA polymerase. Biochemistry 42:14711–14719

Marzolini C, Telenti A, Decosterd LA, Greub G, Biollaz J, Buclin T (2001) Efavirenz plasma levels can predict treatment failure and central nervous system side effects in HIV-1-infected patients. AIDS 15:71–75

Massarella JW, He GZ, Dorr A, Nieforth K, Ward P, Brown A (2000) The pharmacokinetics and tolerability of the oral neuraminidase inhibitor oseltamivir (Ro 64-0796/GS4104) in healthy adult and elderly volunteers. J Clin Pharmacol 40:836–843

Matsuzaki Y, Mizuta K, Aoki Y, Suto A, Abiko C, Sanjoh K, Sugawara K, Takashita E, Itagaki T, Katsushima Y, Ujike M, Obuchi M, Odagiri T, Tashiro M (2010) A two-year survey of the oseltamivir-resistant influenza A(H1N1) virus in Yamagata, Japan and the clinical effectiveness of oseltamivir and zanamivir. Virol J 7:53

McSharry JJ, Deziel MR, Zager K, Weng Q, Drusano GL (2009a) Pharmacodynamics of cidofovir for vaccinia virus infection in an in vitro hollow-fiber infection model system. Antimicrob Agents Chemother 53:129–135

McSharry JJ, Weng Q, Brown A, Kulawy R, Drusano GL (2009b). Prediction of the pharmacodynamically linked variable of oseltamivir carboxylate for influenza A virus using an in vitro hollow-fiber infection model system. Antimicrob Agents Chemother 53:2375–2381

Moscona A (2005) Oseltamivir resistance—disabling our influenza defenses. N Engl J Med 353:2633–2636

Moyle GJ, DeJesus E, Cahn P, Castillo SA, Zhao H, Gordon DN, Craig C, Scott TR (2005) Abacavir once or twice daily combined with once-daily lamivudine and efavirenz for the treatment of antiretroviral-naive HIV-infected adults: results of the ziagen once daily in antiretroviral combination study. J Acquir Immune Defic Syndr 38:417–425

Mulder JW, Cooper DA, Mathiesen L, Sandstrom E, Clumeck N, Gatell JM, French M, Donovan B, Gray F, Yeo JM (1994) Zidovudine twice daily in asymptomatic subjects with HIV infection and a high risk of progression to AIDS: a randomized, double-blind placebo-controlled study. The European-Australian Collaborative Group (Study 017). AIDS 8:313–321

Piliero P, Shachoy-Clark AD, Para M, Preston S, Lou Y, Drusano GL, Stein DS, Yuen GJ (2003) A study examining the pharmacokinetics of abacavir and the intracellular carbovir triphosphate (GSK Protocol CNA10905), abstr. A-1797. Abstr 43rd Interscience Conference on Antimicrobial Agents and Chemotherapy, Chicago

Preston SL, Piliero PJ, Bilello JA, Stein DS, Symonds WT, Drusano GL (2003) In vitro-in vivo model for evaluating the antiviral activity of amprenavir in combination with ritonavir administered at 600 and 100 milligrams, respectively, every 12 hours. Antimicrob Agents Chemother 47:3393–3399

Ruane PJ, Richmond GJ, DeJesus E, Hill-Zabala CE, Danehower SC, Liao Q, Johnson J, Shaefer MS (2004) Pharmacodynamic effects of zidovudine 600 mg once/day versus 300 mg twice/day in therapy-naive patients infected with human immunodeficiency virus. Pharmacotherapy 24:307–312

Sarrazin C, Kieffer TL, Bartels D, Hanzelka B, Muh U, Welker M, Wincheringer D, Zhou Y, Chu HM, Lin C, Weegink C, Reesink H, Zeuzem S, Kwong AD (2007) Dynamic hepatitis C virus genotypic and phenotypic changes in patients treated with the protease inhibitor telaprevir. Gastroenterology 132:1767–1777

Slusher JT, Kuwahara SK, Hamzeh FM, Lewis LD, Kornhauser DM, Lietman PS (1992) Intracellular zidovudine (ZDV) and ZDV phosphates as measured by a validated combined high-pressure liquid chromatography-radioimmunoassay procedure. Antimicrob Agents Chemother 36:2473–2477

Chapter 10
Applied Antifungal Pharmacometrics: Fluconazole and Echinocandins in the Treatment of Candidemia and Invasive Candidiasis

Cornelius Joseph Clancy

10.1 Introduction

Pharmacometrics is the science of quantitative pharmacology. More specifically, it can be defined as the multidisciplinary science that facilitates drug development and identification of optimal treatment strategies by integrating pharmacology, pharmacokinetics–pharmacodynamics (PK–PD), disease pathogenesis, mathematical modeling, and statistics with patient data and outcomes. An early example of the power of pharmacometrics to improve the outcomes of infectious diseases was afforded by a clinical trial of daptomycin against complicated skin and soft tissue infections. In this study, an alteration of the daptomycin dosing schedule based on a PK–PD target identified in preclinical studies resulted in good outcomes and averted musculoskeletal toxicity (Arbeit et al. 2004).

Candida bloodstream infections (candidemia) and other forms of invasive candidiasis are the most common fungal infections among hospitalized patients in the developed world. Fluconazole revolutionized the treatment of candidiasis, offering a safe and effective alternative to the highly toxic frontline agent amphotericin B (Rex et al. 1994; Clancy and Nguyen 2012). Echinocandin antifungals are now accepted by many experts as preferred agents against most cases of candidemia and invasive candidiasis (Andes et al. 2012; Cornely et al. 2012; Ullmann et al. 2012). Despite the advantages that fluconazole and echinocandins have brought over the past two decades, treatment failures are observed in a significant minority of patients with invasive candidiasis (Andes et al. 2012), and resistance is emerging among clinical *Candida* strains (Shields et al. 2012, 2013a, b; Alexander et al. 2013). In recent years, pharmacometric principles have been applied to the study of invasive candidiasis. In this chapter, we will review the clinical manifestations and microbiology of *Candida* infections, pharmacology of fluconazole and echinocandins, PK–PD of

C. J. Clancy (✉)
Department of Medicine, Division of Infectious Diseases, University of Pittsburgh, Pittsburgh, PA, USA
e-mail: cjc76@pitt.edu

S. Schmidt, H. Derendorf (eds.), *Applied Pharmacometrics,* AAPS Advances in the Pharmaceutical Sciences Series 14, DOI 10.1007/978-1-4939-1304-6_10

the drugs against invasive candidiasis, and the application of pharmacometric data to the treatment of infected adults.

10.2 Clinical Manifestations and Microbiology of Candidiasis

Candida species (spp.) cause a wide range of human infections that necessitate antifungal therapy. Mucosal diseases include oropharyngeal, esophageal, and vulvovaginal candidiasis, which commonly manifest as "thrush"—creamy white, slightly raised, and often painful lesions that typically look like cottage cheese. Oropharyngeal and esophageal candidiasis are generally encountered among persons with immune system deficiencies, in particular AIDS or other defects in cell-mediated immunity (Egusa et al. 2008). Vulvovaginal candidiasis, on the other hand, is a common disease among healthy women, likely stemming from changes in pH, microflora, hormonal balance, and/or local host defenses (Sobel 1992). Mucosal candidiasis causes significant morbidity, especially if oral or esophageal pain limits ingestion of food, fluids, or medications, but it does not result directly in mortality. Treatment responses to antifungal agents are generally prompt, although recurrent disease occurs in about 15% of women with vulvovaginal candidiasis (Sobel 1992; Sobel et al. 1994). In the era before immune reconstitution was possible with highly active antiretroviral therapy (HAART), most persons with AIDS developed recurrent oropharyngeal candidiasis (Egusa et al. 2008).

Invasive candidiasis includes candidemia and infections of tissues beneath mucosal surfaces (deep-seated candidiasis; Clancy and Nguyen 2013). Studies suggest that about half the episodes of candidemia are complicated by deep-seated infections, as *Candida* spp. invade organs during hematogenous dissemination (Maksymiuk et al. 1984; Leroy et al. 2009). The liver, spleen, kidney, and eye are particular targets, although virtually any organ may become infected. Deep-seated candidiasis also occurs in the absence of active candidemia, as a result of either prior blood-borne seeding or direct inoculation into a sterile site. The most common portal of entry in the latter scenario is leakage or disruption of the gastrointestinal (GI) tract or hepatobiliary tree, which results in intra-abdominal diseases like peritonitis, abscesses, and cholangitis. Risk factors for invasive candidiasis include neutropenia or functional neutrophil defects, receipt of broad-spectrum antibiotics, presence of intravenous catheters, disruption of GI mucosa, hemodialysis, and *Candida* colonization of body sites (Clancy and Nguyen 2013). In contrast to mucosal candidiasis, mortality rates for invasive candidiasis are as high as 40% despite antifungal therapy (Andes et al. 2012; Clancy and Nguyen 2012). In large part, the poor outcomes stem from the severity of underlying diseases and delays in the administration of antifungal agents due to the poor sensitivity of diagnostic tests (Clancy and Nguyen 2012).

Almost all cases of mucosal and invasive candidiasis are caused by five *Candida* spp.: *C. albicans, C. glabrata, C. parapsilosis, C. tropicalis,* and *C. krusei* (Nguyen

et al. 1995, 1996). The overwhelming majority of mucosal disease is caused by *C. albicans*. *C. albicans* is also the most common cause of invasive candidiasis, although *C. glabrata* has emerged as the leading agent of candidemia at many centers (Nguyen et al. 1996).

10.3 Fluconazole and Echinocandins: Pharmacology and Roles in Treating Candidiasis

Fluconazole is a triazole agent that exerts fungistatic activity against *Candida* spp. by inhibiting 14-α-sterol-demethylase (CYP51), an enzyme in the ergosterol biosynthetic pathway (Zonios and Bennett 2008). The depletion of ergosterol and accumulation of toxic 14-α-methylsterols in the plasma membrane perturbs cell growth and division. Fluconazole is active against each of the "big 5" *Candida* spp. except *C. krusei,* which is intrinsically resistant due to diminished target enzyme affinity (Orozco et al. 1998). In the pre-HAART era, stepwise emergence of resistance was well recognized in cases of recurrent oropharyngeal candidiasis due to *C. albicans* and other spp. (White 1997). In the present era, the emergence of resistance is most common among *C. glabrata* strains causing invasive candidiasis in patients with prior fluconazole exposure (Alexander et al. 2013). Overall, about 1/3 of *C. glabrata* bloodstream isolates are fully resistant to fluconazole, and a sizeable minority exhibit diminished susceptibility (Pfaller et al. 2012a; Alexander et al. 2013). Resistance among other spp. is relatively rare. There are multiple mechanisms by which *Candida* become fluconazole resistant, several of which may interact in a given strain (Clancy and Nguyen 2011).

Fluconazole is water-soluble and available in orally administered and intravenous formulations. It is very well absorbed from the GI tract (bioavailability >90%), which is not impacted by food, gastric pH, or disease state (Bellmann 2007). As such, oral and intravenous doses are equivalent. Fluconazole exhibits highly linear plasma concentration–dose relationships (Debruyne 1997). Protein binding in serum is 12%. Eighty percent is excreted unchanged in the urine; 11% is metabolized in the liver. In general, distribution into tissue and body fluids is excellent. Cerebrospinal fluid (CSF) concentrations, for example, are 70% of serum, and urine concentrations are 10 to 20-fold higher than serum (Debruyne 1997). Terminal plasma elimination half-life following oral administration is 22–31 h, and steady-state conditions are reached on day 6 of treatment (Bellmann 2007). The recommended regimen for the treatment of candidemia and invasive candidiasis is an 800-mg loading dose, followed by 400 mg each day. Doses are reduced by 50% for creatinine clearance <50 mL/min; a full dose is administered after hemodialysis. Fluconazole inhibits hepatic CYP450 system enzymes, and interactions with agents like cisapride and antihistamines, cyclosporine, tacrolimus, sirolimus, calcium channel blockers, phenytoin, benzodiazepines, warfarin, rifabutin, statins, and steroids are important considerations (Zonios and Bennett 2008). On the whole, fluconazole is well tolerated, and serious adverse events are rare. The most severe event is liver toxicity.

Based on results from numerous clinical trials, fluconazole is the drug of choice for the treatment of oropharyngeal, esophageal, vulvovaginal, and urinary candidiasis (Pappas et al. 2009). Fluconazole demonstrated efficacy similar to echinocandins and amphotericin B deoxycholate in randomized clinical trials for the treatment of candidemia (Rex et al. 1994, 2003; Mora-Duarte et al. 2002; Reboli et al. 2007). Clinical practice guidelines from the Infectious Diseases Society of America (IDSA) recommend fluconazole or an echinocandin for nonneutropenic patients with candidemia, but favor the latter for the treatment of more severe disease, patients with neutropenia, or prior azole exposure, and *C. glabrata* or *C. krusei* infections (Pappas et al. 2009).

The echinocandin agents (anidulafungin, caspofungin, and micafungin) exert fungicidal activity against *Candida* spp. by inhibiting the synthesis of β-1.3-D-glucan, which is an essential component of the cell wall (Kauffman and Carver 2008). The target enzyme, glucan synthase, is encoded by the *FKS1, 2,* and *3* genes. The echinocandins are highly active against *C. albicans, C. glabrata, C. tropicalis,* and *C. krusei. C. parapsilosis* carries an *FKS* polymorphism that results in glucan synthase with decreased echinocandin affinity, which manifests as higher minimum inhibitory concentrations (MICs) than against other common *Candida* spp. Diminished susceptibility of *C. parapsilosis* has been corroborated in mouse models of hematogenously disseminated candidiasis (Barchiesi et al. 2006). Breakthrough *C. parapsilosis* infections among patients receiving an echinocandin are well reported (Moudgal et al. 2005; Kabbara et al. 2008), but conclusive evidence of poorer outcomes in clinical trials of treatment for invasive candidiasis is lacking.

With increased use of the echinocandins, recent reports have documented the emergence of resistance (Shields et al. 2012, 2013a, b; Alexander et al. 2013; Eschenauer et al. 2013). As for fluconazole, resistance is most common among *C. glabrata* strains, and remains rare for other spp. Diminished susceptibility is mediated by mutations in hot spots of *FKS* genes, with specific mutations conferring higher or lower levels of resistance. At some major centers, approximately 10% of *C. glabrata* strains recovered from sterile sites are *fks* mutants (Shields et al. 2012, 2013a, b; Alexander et al. 2013). Molecular resistance is seen in the setting of extensive prior echinocandin exposure (Shields et al. 2012, 2013a, b). Particularly worrisome is the emergence of *C. glabrata* that are resistant to both fluconazole and echinocandins, as recently reported for 12–14% of fluconazole-resistant strains at several centers (Pfaller et al. 2012a; Alexander et al. 2013).

Echinocandins have poor oral bioavailability, and are only available in intravenous formulations (Kauffman and Carver 2008). They exhibit linear concentration–dose relationships, although caspofungin may accumulate as doses are increased (Kofla and Ruhnke 2011). Plasma protein binding is 97 to >99% (lowest for caspofungin). Following initial distribution, caspofungin and micafungin are taken up by the liver and red blood cells (the latter for micafungin only), where they are slowly degraded to inactive metabolites that are largely excreted via bile (Kauffman and Carver 2008). Anidulafungin is degraded almost entirely in the plasma rather than liver. The agents distribute well into tissues like liver, spleen, lungs, and kidneys, but their large molecular weight and high protein-binding limit penetration into

urine, CSF, brain, and ocular fluid. Elimination half-lives range from 9 to 11 h for caspofungin, from 11 to 17 h for micafungin, and from 24 to 26 h for anidulafungin; each of the drugs is dosed once daily (Kauffman and Carver 2008). Standard dosages for the treatment of candidemia and invasive candidiasis are anidulafungin (200 mg loading dose, followed by 100 mg daily), caspofungin (70 mg loading dose, followed by 50 mg daily), and micafungin (100 mg daily). No renal dose adjustments are necessary, and the drugs are not dialyzed. Hepatic dose adjustments are not needed for anidulafungin. Dose reductions of caspofungin, but not micafungin, are recommended for moderate hepatic dysfunction; data are lacking for both agents in severe hepatic dysfunction. None of the agents are major substrates, inducers, or inhibitors of CYP450 enzymes, and drug interactions are minimal. In general, the echinocandins are well tolerated and similar in types of adverse events. Infusion-related reactions, thrombophlebitis, and mild GI symptoms may occur in $<5\%$ of patients (Kofla and Ruhnke 2011).

IDSA practice guidelines consider the echinocandins to be therapeutically equivalent (Pappas et al. 2009). All three agents achieved response rates similar to fluconazole in trials against esophageal candidiasis, but relapse rates were greater (with the exception of high-dose micafungin, which was comparable to fluconazole; Villanueva et al. 2002; de Wet et al. 2004; Krause et al. 2004). These findings and the availability of fluconazole as an oral formulation make it the preferred agent against mucosal candidiasis. The echinocandins are most useful in the treatment of candidemia and invasive candidiasis, as established in a series of randomized, blinded, controlled trials. Regardless of the comparator agent in the trials, success rates for the echinocandins were similar to each other (Mora-Duarte et al. 2002; Kuse et al. 2007; Pappas et al. 2007; Reboli et al. 2007). Individual studies, powered for noninferiority, have shown echinocandins to be comparable to fluconazole, amphotericin B deoxycholate, and liposomal amphotericin B (Mora-Duarte et al. 2002; Kuse et al. 2007; Reboli et al. 2007). More recently, a patient-level review of data pooled from seven randomized antifungal treatment trials against invasive candidiasis found that echinocandin treatment was associated with improved survival and greater clinical success rates than treatment with an azole or ampothericin B (Andes et al. 2012). In subgroup analysis, improved outcomes were evident for patients infected with *C. albicans* and non-*C. albicans* spp.

The latest clinical practice guidelines from the European Society of Clinical Microbiology and Infectious Diseases (ESCMID), which were published more recently than the IDSA guidelines, strongly recommend an echinocandin as initial treatment against most cases of candidemia (Cornely et al. 2012; Ullmann et al. 2012). If patients demonstrate a clinical response to an echinocandin, step-down therapy with fluconazole can be used to complete a treatment course. It is important to recognize that published experience with echinocandins against deep-seated candidiasis is less extensive than candidemia, and the drugs may be limited by PK considerations in the treatment of diseases like endophthalmitis, meningitis, and urosepsis (Clancy and Nguyen 2012). There is no consensus about the use of echinocandins versus fluconazole for the treatment of *C. parapsilosis* bloodstream infections.

10.4 Fluconazole and Echinocandin Pharmacometrics

A stepwise paradigm has been proposed for applying pharmacometrics to invasive fungal infections in humans (Hope and Drusano 2009), which we will use as a framework for our review. The underlying assumption in the paradigm is that antifungal exposure–response relationships are primarily shaped by the pathogen, rather than host. This assumption is reasonable because the site of antifungal activity is within the pathogen (Craig 1998). The host, of course, must be considered in assessing drug tolerance and toxicity, variations in PK, and the impact of factors such as immune function and severity of illness on outcomes. The first elements in the stepwise model are a reproducible method for measuring antifungal susceptibility of strains in vitro, and an experimental system (most often an animal model) that mimics the pathogenesis of infection in humans and provides changing antifungal exposure. Dose–responses in the animal model are used to identify PK–PD targets (area under the dose–response curve (AUC)/MIC ratio, maximum serum concentration (C_{max})/MIC ratio or time above MIC) that are associated with successful outcomes. Indeed, studies of a growing number of bacteria, viruses, and fungi have shown that PK–PD targets identified in clinically relevant animal models predict outcomes in humans, despite differences in PK between animal species (Craig 1998; Hope and Drusano 2009). With PK–PD targets defined, the likelihood of target attainment for various dosing regimens is estimated in particular patient groups by using fully parametric population PK models and Monte Carlo simulations. Finally, treatment regimens identified as optimal can be validated in clinical studies. At the same time, pharmacometric data can be used to validate interpretive breakpoint MICs and understand how they can best be incorporated into therapeutic decision making.

10.4.1 Fluconazole and Echinocandin Susceptibility Testing In Vitro

A decade of collaborative research culminated in the development of standardized macrobroth and microbroth dilution methods for measuring fluconazole MICs against *Candida* spp., which have been endorsed by the Clinical and Laboratory Standards Institute (CLSI, previously known as the National Committee for Clinical Laboratory Standards (NCCLS); Rex et al. 1997; Rex and Pfaller 2002; Pfaller et al. 2006). The reference methods distinguish between *Candida* strains with different susceptibilities to fluconazole, and demonstrate good intra-laboratory reproducibility and interlaboratory agreement. Clinical strains of spp. other than *C. krusei* exhibit a broad range of MICs, molecular mechanisms of fluconazole resistance confer higher MICs, and the accumulation of resistance mechanisms results in stepwise increases in MICs. The European Committee on Antimicrobial Susceptibility Testing (EUCAST) developed a broth microdilution reference method that generates fluconazole MICs similar to the CLSI standard (EUCAST 2008a).

Commercially available adaptations of the reference methods, such as Sensititre YeastOne and Etest, yield comparable results (Espinel-Ingroff et al. 1999; Pfaller et al. 2003). As a standardized and reproducible measure of fluconazole's potency against *Candida* strains, the MIC determined by reference and comparable methods facilitates comparisons between studies and serves as a normalizer in defining the PK–PD relationships that determine outcomes.

In contrast, the development of reproducible methods for measuring echinocandin MICs against *Candida* species has proved challenging. CLSI and EUCAST reference microbroth dilution methods are limited by significant interlaboratory variability in caspofungin MICs against *C. albicans, C. glabrata, C. tropicalis, and C. krusei* (Espinel-Ingroff et al. 2013). The reference methods have performed more reliably between laboratories when testing anidulafungin and micafungin. In general, commercialized tests like YeastOne or Etest generate echinocandin MICs that show high levels of essential agreement (defined as MICs within two doubling dilutions) with the reference methods (Arendrup and Pfaller 2012; Pfaller et al. 2012b). However, in a recent international, multicenter study of hospital clinical microbiology laboratories using the YeastOne assay, modal caspofungin MIC variability was low against each species (Eschenauer et al. 2014). The findings suggest that the shortcomings of CLSI/EUCAST reference assays may be overcome with alternative methods. Until uncertainties about caspofungin testing are resolved, researchers and EUCAST have suggested that laboratories report anidulafungin or micafungin MICs as a surrogate for the class, rather than caspofungin MICs (Arendrup et al. 2011; Shields et al. 2013a). This recommendation is less than satisfactory from clinical and scientific perspectives, as accurate caspofungin MICs are essential for determining differences in efficacy among the agents, and for performing epidemiology and PK–PD studies.

10.4.2 Defining PK–PD Targets in Animal Models of Invasive Candidiasis

A simple-to-perform and highly reproducible mouse model of hematogenously disseminated candidiasis is the standard laboratory tool for studying pathogenesis, antifungal treatment, and PK–PD. In the model, immunocompetent or immunosuppressed mice are infected with a *Candida* strain via lateral tail vein injection. The major target organ is the kidneys; invasive infections are also consistently achieved in liver, spleen, and other organs. In this regard, the disease in mice resembles candidemia in humans that is complicated by deep-seated candidiasis. There is a hierarchy of virulence among *Candida* spp. in the model (*C. albicans* > *C. tropicalis* > *C. glabrata* > *C. parapsilosis* > *C. krusei*), which does not impact PK–PD studies since each species reliably infects the kidneys of immunocompetent mice (Arendrup et al. 2002). In general, tissue burdens are preferred as the primary end point for PK–PD studies because they quantitate the effects of antimicrobial exposure on the pathogen, and yield results that are readily amenable to statistical analysis and mathematical modeling.

Table 10.1 Fluconazole pharmacokinetic–pharmacodynamic (PK–PD) targets identified by dose-ranging and dose-fractionation studies in mice with hematogenous disseminated candidiasis

Study	Design	Strain(s)	Primary end point	PK–PD target[a]	Comments
Louie et al. (1998)	Immunocompetent mice, treatment started 5 h post infection	*C. albicans* ATCC 36082 MIC: 0.5 μg/mL	ED_{50} in kidneys at 24 h of treatment	AUC/MIC: 45	Maximal suppression of tissue burden at AUC/MIC ≥75
Andes and van Ogtrop (1999)	Neutropenic mice, treatment started 2 h post infection	3 *C. albicans* clinical strains MICs: 0.5, 16, 32 μg/mL	ED_{50} in kidneys at 24 h of treatment	AUC/MIC: 24, 12, 20, respectively	Maximal suppression of tissue burden at AUC/MIC ≥100
Andes et al. (2006a, b)	Neutropenic mice, treatment started 2 h post infection	*C. albicans* clinical strain MIC: 0.5 μg/mL	Prevention of fluconazole resistance and expression of resistance genes	T MIC: ≥40% AUC> MIC: ≥32	T>MIC was most strongly correlated with end points
Gumbo et al. (2006)	Neutropenic mice, treatment started 4 h post infection	3 *C. glabrata* clinical strainsMICs: 2, 32, 128 μg/mL	ED_{max} in kidneys at 24 h of treatment	Not identified	No responses among strains against which MIC=32 or 128 μg/mL

ED_{50} effective dose required to achieve 50% of maximal suppression of kidney tissue burdens at 24 h
AUC/MIC area under the concentration curve/minimum inhibitory concentration ratio
T>MIC time above the MIC, as percentage of dosing interval
[a]PK–PD target that best correlates with primary end point. Fluconazole AUCs reflect total-drug concentrations

Two studies using the mouse model of hematogenously disseminated candidiasis were designed to specifically identify fluconazole PK–PD targets that correlated with treatment responses among *C. albicans* strains (Table 10.1; Louie et al. 1998; Andes and van Ogtrop 1999). The studies employed a classic dose-fractionation design, in which a range of doses and dosing schedules was used to optimize AUC/MIC, C_{max}/MIC, or time above MIC. AUC/MIC was the parameter that best predicted the efficacy of fluconazole among neutropenic and nonneutropenic mice, as defined by ED_{50} (effective dose that achieved 50% of the maximal drug effect, measured as *C. albicans* burdens within the kidneys after 24 h). AUC/MIC targets against individual strains ranged from 12 to 45. Reanalysis of data from earlier experiments in a nonneutropenic rat model of disseminated *C. albicans* infection found that fluconazole AUC/MIC of 18 resulted in 80% survival (Rogers and Galgiani 1986). Moreover, ED_{50}s of ravuconazole, voriconazole, and posaconazole against a wide range of *C. albicans* strains in the neutropenic mouse model were achieved at free-drug (f) AUCs/MICs of 10–36, 11–58, and 6–27, respectively (Andes et al. 2003b, c, 2004). Note that fluconazole studies measured total-drug

AUCs, which closely approximate fAUCs due to the drug's low protein binding. In contrast, fAUC was appropriate for the newer, more highly protein-bound azoles.

Across studies, a median fAUC/MIC target of approximately 20–25 was identified for the azole class. The consistency of these findings is not surprising, as numerous studies have demonstrated that PK–PD targets are similar for antimicrobials within a class, provided free-drug concentrations are considered (Andes and Craig 1998; Craig 1998). Azole PK–PD targets are comparable in immunocompetent and immunosuppressed mice infected with susceptible *C. albicans* and strains exhibiting a variety of resistance mechanisms, which is also in keeping with studies of other agents and pathogens (Craig 1998).

There are several important caveats to the fluconazole PK–PD data. First, PK–PD targets are impacted dramatically by the definition of treatment efficacy. For example, if ED_{max} was used instead of ED_{50}, the target AUC/MIC of fluconazole was ≥75 rather than 20–25. Furthermore, relative reduction of tissue burdens is not the only clinically relevant end point of fluconazole treatment. The PK–PD target that best correlated with suppression of fluconazole resistance and efflux pump expression in neutropenic mice was time above MIC ≥ 40 % (Andes et al. 2006a, b). AUC/MIC ≥ 32 was also linked with these end points, albeit less strongly. Second, fluconazole is purely fungistatic in vivo. Kidney burdens at 24 h are often higher than at the start of an experiment, even among mice treated with ED_{max}. ED end points should not be misinterpreted as signifying reductions in infectious burdens. Third, growth suppression by antifungal agents, in general, is greater in immunocompetent than neutropenic mice (Hope et al. 2007). Therefore, PK–PD targets based on ED end points may appear similar in mice with differing immune status, but the effects of a given fluconazole dose on absolute *Candida* burdens may vary significantly. Finally, PK–PD data in mice usually are based on measurements of drug exposure in serum, and they are not validated for entities other than hematogenously disseminated candidiasis. The relationships between outcomes and drug concentrations in serum and tissue subcompartments are complex and poorly understood (Warn et al. 2009); it is reasonable to be cautious in extrapolating PK–PD findings from one site of disease to another (Hope and Drusano 2009; Warn et al. 2009).

The mouse model of hematogenously disseminated candidiasis has been employed extensively to characterize echinocandin PK–PD against *C. albicans, C. glabrata, C. parapsilosis,* and *C. tropicalis* strains (Table 10.2). In comparative studies, caspofungin and anidulafungin were more active than fluconazole against the same *C. albicans* and *C. glabrata* strains, respectively (Louie et al. 2005; Gumbo et al. 2006). Across studies, C_{max}/MIC and AUC/MIC ratios were the PK–PD parameters that best predicted echinocandin efficacy. These parameters are closely related, and the identification of one versus the other in a particular study likely reflects differences in strains or experimental design. C_{max}/MIC is optimized by administering high drug doses at infrequent intervals; AUC/MIC reflects cumulative drug dose, regardless of dosing frequency. Along these lines, once-weekly dosing in mice was at least as effective as daily dosing in independent studies of different agents against different *Candida* species (Andes et al. 2003a; Gumbo et al. 2007). Due to the significant protein binding of each echinocandin, fAUC measurements are needed to

Table 10.2 Echinocandin PK–PD targets identified by dose-ranging and dose-fractionation studies in mice with hematogenous disseminated candidiasis

Study	Agent	Design	Strain(s)	Primary end point	PK–PD target[a]	Comments
Andes et al. (2003a)	HMR3270[b]	Neutropenic mice, treatment started 2 h post infection	6 *C. albicans* clinical strains MICs: 0.5 μg/mL	Fungistatic effect in kidneys over 6 days	C_{max}/MIC: 3.7 ± 1.8	AUC/MIC was also predictive. Large, infrequent dosing most effective
Louie et al. (2005)	Caspo	Immunocompetent mice, treatment started 5 h post infection	*C. albicans* ATCC 36082	Tissue burden in kidneys at 96 h	AUC/MIC (value not stated)	Caspofungin persisted within kidneys, which correlated with ongoing antifungal activity. Caspofungin was more active than fluconazole against same strains
Gumbo et al. (2006)	Anidula	Neutropenic mice, treatment started 4 h post infection	3 *C. glabrata* clinical strains MICs: 0.03 μg/mL	Tissue burden in kidneys at 24 and 96 h	AUC/MIC (value not stated)	Anidulafungin persisted within kidneys. Serum concentrations were good surrogate for tissue activity. Anidulafungin was more active than fluconazole against same strains
Gumbo et al. (2007)	Mica	Neutropenic mice, treatment started 4 h post infection	*C. glabrata* clinical strain (also included in previous study)	Fungistatic effect in kidneys at 7 days	fAUC/MIC: 23	Once-weekly dosing as effective as daily
Andes et al. (2008a)	Anidula	Neutropenic mice, treatment started 2 h post infection	4 *C. albicans*, 1 *C. tropicalis,* 10 *C. glabrata* clinical strains MICs: 0.015–2 μg/mL	Fungistatic effect in kidneys at 96 h	C_{max}/MIC: 0.26 ± 0.22 fAUC/MIC: 18 ± 15	Anidulafungin exposures associated with efficacy were similar among *Candida* spp. Some strains had fitness cost with higher MICs, but anidulafungin response was related to MIC

Table 10.2 (continued)

Andes et al. (2008b)	Mica	Neutropenic mice, treatment started 2 h post infection	4 *C. albicans,* 10 *C. glabrata* clinical strains MICs: 0.008–0.25 μg/mL	Fungistatic effect in kidneys at 96 h	fAUC/MIC: ~10	Micafungin exposures associated with efficacy were similar among *Candida* spp. Responses similar to anidulafungin against same strains
Andes et al. (2010)	Anidula Caspo Mica	Neutropenic mice, treatment started 2 h post infection	6 *C. albicans,* 9 *C. glabrata,* 15 *C. parapsilosis* clinical strains Range of MICs	Fungistatic effect in kidneys at 96 h	fAUC/MIC vs. *C. albicans:* 20.6 ± 32; *C. glabrata:* 7 ± 8.3; *C. parapsilosis:* 7.6 ± 7.1	Targets were similar for each of the agents. AUC/MIC targets were lower for *C. glabrata* and *C. parapsilosis* than *C. albicans*. Outcomes closely linked to MICs
Howard et al. (2011)	Anidula Caspo Mica	Neutropenic mice, treatment started 5 h post infection	*C. glabrata* ATCC 2001	Fungistatic effect in kidneys at 101 h	Total-drug AUC/MIC, Anidula: ~6000; Caspo: ~100–400; Mica: ~1500–3000	Targets are comparable to total-drug AUC/MIC targets identified in other studies. Exposure–response relationships for each drug partitioned into distinct fungistatic (conventional doses) and fungicidal components (high doses) of activity
Lepak et al. (2012)	Anidula Caspo Mica	Neutropenic mice, treatment started 2 h post infection	11 *fks* mutant *C. glabrata,* 8 WT *C. glabrata*	Fungistatic effect in kidneys at 96 h	*f*AUC/MIC of Anidula, Caspo, Mica vs. WT: 13.2, 2.04, 6.78; vs. mutants: 3.4, 2.7, 0.9	AUC/MIC targets roughly similar for WT and mutant strains. Higher doses needed for mutants. Outcomes closely linked to MICs

h hours, *Anidula* anidulafungin, *Caspo* caspofungin, *Mica* micafungin, *WT* wild-type

[a] Target that best correlates with primary end point. Targets reflect free-drug concentrations, unless indicated otherwise

[b] Aminocandin, an agent developed by Aventis

normalize results. fAUC/MIC targets for the class were comparable across studies, ranging from ~5 to 20. In one study, species-specific PK–PD targets were identified, as the three agents were effective against *C. glabrata* and *C. parapsilosis* at lower fAUC/MIC than *C. albicans* (~7 vs. ~20; Andes et al. 2010). The mouse data support clinical findings that echinocandins can be used to treat *C. parapsilosis* infections successfully, despite higher MICs than against other species. Moreover, echinocandins were also effective against *fks* mutant *C. glabrata* strains that exhibited elevated MICs, provided PK–PD targets were achieved (Lepak et al. 2012). On the whole, responses in mice were closely linked to MIC, even for strains in which resistance mutations conferred a fitness cost.

PK modeling in mice demonstrated that caspofungin and anidulafungin accumulated within the kidneys, which served as a reservoir from which the biologically active drug slowly returned to the bloodstream (Louie et al. 2005; Gumbo et al. 2006). Tissue persistence correlated with ongoing antifungal activity, even after serum concentrations decreased below MIC. Of course, a major advantage for echinocandins over fluconazole is the potential for fungicidal activity, which is reliably achieved in vitro (Clancy et al. 2006; Nguyen et al. 2009). In mice, however, exposure–response relationships for each echinocandin are partitioned into fungistatic and fungicidal components at lower and higher doses, respectively (Howard et al. 2011). Furthermore, dosing regimens that mimicked PK in humans receiving currently recommended treatment regimens resulted in fungistatic, rather than fungicidal activity.

Certain *Candida* clinical strains demonstrate increased growth in the presence of elevated echinocandin concentrations in vitro, a phenomenon mediated through activation of various cell wall stress response pathways (Shields et al. 2011a, b). Mouse data suggest that this paradoxical growth is of limited clinical significance, as the overwhelming majority of studies have not validated the observation. Moreover, paradoxical growth in vitro is eliminated in human serum and poorer outcomes were not reported among patients receiving higher echinocandin doses in clinical trials (Pappas et al. 2007; Betts et al. 2009; Shields et al. 2011a).

10.4.3 Cross-Validation of PK–PD Targets with Clinical Data from Humans

Fluconazole AUC/MIC ratios were estimated and correlated with outcomes in several studies of candidemia and oropharyngeal candidiasis. Mean fluconazole AUCs in healthy adults with normal renal function are virtually identical to the daily dose, a relationship that holds for dosages up to 2000 mg/day (Grant and Clissold 1990). Estimated AUC/MIC ratios or fluconazole dose/MIC associated with successful outcomes among patients with candidemia ranged from >11.5 to >75 (Table 10.3). The data are difficult to interpret conclusively due to the small numbers of strains (especially strains with higher fluconazole MCs), differences in *Candida* spp., and variations in patient populations and end points. Studies of oropharyngeal

Table 10.3 Cross-validation of fluconazole PK–PD targets with clinical data among patients with candidemia

Study	Strains (*n*)	Population	*Candida* spp. (*n*)	S-DD or R (*n*)	Primary end point (definition of treatment failure)	PK–PD target for treatment success
Clancy et al. (2005)	36	47% were neutropenic	*C. albicans* (12), *C. glabrata* (6), *C. parapsilosis* (5), *C. krusei* (4), *C. tropicalis* (3), other (2)	S-DD (5) R (6)	Persistent or breakthrough candidemia despite ≥3 days of fluconazole	Dose/MIC>50
Rodriguez-Tudela et al. (2007)	126	7% were neutropenic	*C. albicans* (73), *C. parapsilosis* (27), *C. tropicalis* (12), *C. glabrata* (9), other (2)	S-DD (4) R (0)	Persistent candidemia despite ≥4 days of fluconazole	Dose/MIC>75
Pai et al. (2007)	77	None were neutropenic	*C. albicans* (49), *C. glabrata* (11), *C. parapsilosis* (6), *C. tropicalis* (5), other (3)	S-DD (2) R (2)	In-hospital mortality	AUC/MIC 55[a] Dose/MIC 12[b]
Baddley et al. (2008)	84	11.5% were neutropenic	*C. albicans* (37), *C. glabrata* (17), *C. parapsilosis* (17), *C. parapsilosis* (10), *C. krusei* (2), other (1)	S-DD (49) R (7)	Mortality at 6 weeks after first positive blood culture	AUC/MIC>11.5[a]
Eschenauer et al. (2013)	127	2% were neutropenic	*C. glabrata* only	S-DD (49) R (17)	Composite at 14 days: lack of clinical or microbiologic (sterilization of blood cultures) responses, or mortality	Dose/MIC>12.5[c]
Lee et al. (2000)	21	10% were neutropenic	*C. albicans, C. glabrata, C. parapsilosis,* other. Spp. breakdown for candidemia not provided	S-DD (5) R (2)	Treatment failure defined as lack of clinical response at 7 days, persistent positive blood culture or drug toxicity	Dose/MIC≥50[d]

n number, *S-DD* fluconazole susceptible-dose dependent (MIC: 16–32 μg/mL), *R* fluconazole resistant: MIC≥64 μg/mL

[a] AUC estimated from daily fluconazole dose, typical fluconazole clearance, and fluconazole protein binding

[b] Dose normalized to patient weight

[c] Recorded fluconazole dose doubled in creatinine clearance was<50

[d] Based on reanalysis of published data

Table 10.4 Probability of fluconazole AUC/MIC target attainment (PTA) against invasive candidiasis in various adult patient populations

Study	Design and patient population	AUC/MIC target	Simulated PTA	Comments
Rodriguez-Tudela et al. (2007)	Fluconazole dose–AUC relationships defined by linear regression, using published data	>75	99% for daily fluconazole dose/MIC≥100	Simulated 400 mg/day dosing vs. MICs of 1–32 μg/mL
Patel et al. (2011)	Population PK study of 10 critically ill, anuric patients on CVVHD	>25	Almost 100% for dose/MIC≥50	Simulated various regimens vs. MICs of 0.06–32 μg/mL
Han et al. (2013)	Population PK study of 60 burn patients	>25 >50	Almost 100% for dose/MIC≥100 Almost 100% for dose/MIC≥200	Simulated various regimens vs. MICs of 0.25–2 μg/mL

AUC/MIC targets reflect total-drug concentrations
CVVHD continuous veno-venous hemodialysis

candidiasis are more homogeneous, since *C. albicans* is the predominant pathogen, most patients are HIV-infected, and successful clinical and microbiologic outcomes are more easily assessed (in general, resolution of oral lesions and culture-negativity, respectively). Estimated AUC/MIC targets or dose/MIC for successful outcomes of oropharyngeal candidiasis ranged from ≥25 to >75 (Rex and Pfaller 2002; Pfaller et al. 2006; Rodriguez-Tudela et al. 2007; Cuesta et al. 2009, 2010). Taken together, therefore, the human data were broadly in keeping with AUC/MIC targets identified in the animal models.

The obvious limitation of the human studies is that AUCs were extrapolated from fluconazole dose or from dose normalized by body weight, estimated protein binding, or renal function. The studies do not account for differences in drug exposure that result from PK variability among patients with invasive candidiasis, and which impact the probability that a given AUC/MIC target is attained. Population PK models use drug measurements and data from small, but carefully chosen patient cohorts to quantify expected variations in exposure at particular dosages and dosing schedules. The models can then be employed in Monte Carlo simulations, in which likelihood of PK–PD target attainment is estimated for a large population of patients by a process of random sampling from a known distribution of exposures (Hope and Drusano 2009). These powerful techniques have not been widely used to study fluconazole exposures among at-risk patient groups, but the small amount of published data from several populations suggest that there is an extremely high probability that AUC/MIC targets >25 will be achieved for fluconazole daily dose/MIC≥50–100 (Table 10.4). The data predict that fluconazole daily dose/MIC≥100 will reliably achieve AUC/MIC targets >50.

There are limited clinical data validating echinocandin PK–PD targets in humans. In one study, 493 patients enrolled in phase 3 clinical trials of micafungin for the treatment of invasive candidiasis were analyzed (Andes et al. 2011). Patients were infected with *C. albicans* (44%, $n=218$), *C. tropicalis* (20%, $n=99$), *C. parapsilosis* (16%, $n=77$), *C. glabrata* (13%, $n=62$), *C. krusei* (3%, $n=17$), and other spp. (4%, $n=20$). Micafungin exposures were estimated using a population PK model. Overall, total-drug AUC/MIC ratio ≤3000 or >12,000 was the most strongly predictive factor for treatment failure by multivariate analysis ($p=0.005$). For patients infected with *C. parapsilosis,* there was a trend toward poorer responses for total-drug AUC/MIC <285 ($p=0.11$). For patients infected with species other than *C. parapsilosis,* total-drug AUC/MIC ≤5000 or >12,000 was an independent risk factor for treatment failure ($p=0.01$).

A subsequent study assessed data from 262 patients who were treated with anidulafungin in four phase 2/3 trials (Liu 2013). A population PK model was used to fit serum drug concentration data from each of the patients. There was a trend toward an association between anidulafungin exposure and efficacy among patients with esophageal candidiasis, as stepwise improvements in response rates at 2 weeks were evident at total-drug AUC/MIC of 0–300, >300–600, and >600. Definitive targets could not be established for the smaller number of patients with invasive candidiasis/candidemia, or for the entire cohort. fAUC/MIC values were not available in either of the two studies. Based on typical protein binding for each of the agents, however, estimated fAUC/MIC targets were broadly similar to those found using the mouse model. Furthermore, the first study supported a target for *C. parapsilosis* that is lower than other species, similar to data from mice. The reasons for an association between highest AUC/MIC and poorer outcomes in the first study were not clear. The observation raises the question of possible paradoxical effects, but similar findings were not described in other echinocandin clinical studies. As mentioned earlier, the preponderance of experimental data does not support paradoxical effects in vivo; nevertheless, the issue merits further investigation.

In general, echinocandin PK is similar in patients with invasive fungal infections, bone marrow and peripheral blood stem cell transplant recipients, patients with hematologic malignancies, ICU residents, and patients undergoing continuous veno-venous hemodialysis (CVVHD; Dowell et al. 2004; Hiemenz et al. 2005; Gumbo et al. 2008; Leitner et al. 2011; Wurthwein et al. 2012; Liu et al. 2013; Maseda et al. 2014). Drug clearance may be higher in obese patients and those with candidemia or other forms of invasive candidiasis, but these covariates account for a minority of inter-patient variability in PK (Dowell et al. 2004; Nguyen et al. 2007; Hall et al. 2011). PK modeling suggests that fAUC/MIC targets will be exceeded in >90% of patients who are treated with standard micafungin dosages, if they are infected with *C. albicans* or *C. glabrata* strains against which MICs are <0.03 μg/mL (Andes et al. 2011). Comparable levels of target attainment are predicted for *C. parapsilosis* strains with MICs <0.5 μg/mL.

Table 10.5 Summary of fluconazole PK–PD data against invasive candidiasis

End point	PK–PD Target	
	Acceptable target	Optimal target
Antifungal activity in mouse model	AUC/MIC ≥ 25	AUC/MIC ≥ 75
Prevention of fluconazole resistance in mouse model	AUC/MIC ≥ 32	Time above MIC ≥ 40 %
Successful clinical outcomes in humans	Estimated AUC/MIC ≥ 25	Estimated AUC/MIC ≥ 75
Probability of PK–PD target attainment in humans	Daily dose/MIC ≥ 50 to achieve target AUC/MIC > 25	Daily dose/MIC ≥ 100 to achieve target AUC/MIC > 50

10.5 Putting It All Together: Implications for Treating Invasive Candidiasis

Data for fluconazole are synthesized in Table 10.5. In summary, mouse model and human clinical studies suggest that fluconazole AUC/MIC ≥ 25 is an acceptable, minimum target for the treatment of invasive candidiasis. This target is predicted to be reliably achieved at fluconazole daily dose/MIC ≥ 50. Fluconazole AUC/MIC ratios ≥ 75 afford optimal antifungal activity against at least some *Candida* strains in the mouse model. The clinical significance of the enhanced antifungal activity at higher AUC/MIC is not clear; however, it seems reasonable to shoot for the higher target in treating certain patients, such as those who are immunosuppressed or especially ill. Higher AUC/MIC targets and more frequent dosing intervals may also be useful in limiting emergence of fluconazole resistance in cases in which prolonged treatment is necessary, but these hypotheses are unproven in humans. Fluconazole daily dose/MIC ≥ 100 is predicted to reliably achieve higher targets. Therefore, standard dosing (800 mg loading dose, followed by 400 mg/day) is anticipated to attain the optimal and acceptable AUC/MIC targets against strains for which MICs are ≤ 4 μg/mL and ≤ 8 μg/mL, respectively (Table 10.6). For strains with higher MICs, fluconazole at dosages > 400 mg/day may achieve AUC/MIC targets. However, there are limited clinical data supporting such regimens (Rex et al. 2003; Torres et al. 2004), and the echinocandins (or amphotericin B formulations) offer clinicians fungicidal therapeutic alternatives.

Interpretive breakpoint MICs of fluconazole against *Candida* spp., as established by CLSI and EUCAST, are shown in Table 10.6. The current CLSI breakpoints were developed by applying the "90/60" rule to clinical data from patients treated with fluconazole (i.e., approximately 90 and 60 % of infections due to susceptible and resistant strains should respond to treatment, respectively; Rex et al. 1997; Rex and Pfaller 2002). Susceptibility and resistance were defined as MICs ≤ 8 μg/mL and ≥ 64 μg/mL, respectively. MICs of 16 and 32 μg/mL were assigned a novel designation as susceptible-dose dependent (S-DD), based upon observations that infections due to such strains responded to higher fluconazole dosages. Subsequently, EUCAST developed species-specific breakpoints by considering wild-type

Table 10.6 Fluconazole interpretive breakpoint MICs against *Candida* spp., and probability of PK–PD target attainment

FLU MIC (μg/mL)	*Candida* spp.	Interpretation of MIC			Daily fluconazole doses	
		CLSI BPs (current)	CLSI BPs (proposed)	EUCAST	Likely to attain AUC/MIC > 25 (mg/day)	Likely to attain AUC/MIC > 50 (mg/day)
≤2	*C. albicans*, *C. parapsilosis*, *C. tropicalis*, *C. glabrata*	S S	S S-DD	S I (S ≤ 0.002)	≥100	≥200
4	*C. albicans*, *C. parapsilosis*, *C. tropicalis*, *C. glabrata*	S S	S-DD S-DD	I I	≥200	≥400
8	*C. albicans*, *C. parapsilosis*, *C. tropicalis*, *C. glabrata*	S S	R S-DD	R I	≥400	≥800
16	*C. albicans*, *C. parapsilosis*, *C. tropicalis*, *C. glabrata*	S-DD S-DD	R S-DD	R I	≥800	≥1600
32	*C. albicans*, *C. parapsilosis*, *C. tropicalis*, *C. glabrata*	S-DD S-DD	R S-DD	R I	≥1600	Not likely to be reliably attained[a]
≥64	*C. albicans*, *C. parapsilosis*, *C. tropicalis*, *C. glabrata*	R R	R R	R R	Not likely to be reliably attained[a]	Not likely to be reliably attained[a]

BPs breakpoints, *S* susceptible, *S-DD* susceptible-dose dependent, *I* intermediate, *R* resistant
[a] AUC/MIC target not likely to be reliably attained unless daily doses significantly >2000 mg are used

MIC distributions for strains with no acquired or genetic resistance, PK–PD parameters, and correlations between MICs and clinical outcomes (EUCAST 2008b). *C. albicans, C. parapsilosis,* and *C. tropicalis* strains were defined as susceptible, intermediate, and resistant at MICs ≤ 2 μg/mL, 4 μg/mL, and >4 μg/mL, respectively. The corresponding breakpoints for *C. glabrata* strains were ≤0.002 μg/mL, 0.002–32 μg/mL, and ≥64 μg/mL, respectively. Most recently, CLSI has proposed harmonizing breakpoints with EUCAST (Pfaller et al. 2010). In effect, EUCAST and revised CLSI breakpoints define *C. albicans, C. parapsilosis,* and *C. tropicalis* strains as resistant if fluconazole is not likely to reliably achieve an optimal AUC/MIC target unless dosages ≥800 mg/day are administered (Table 10.6). For *C. glabrata* strains in which MICs are 2–32 μg/mL, EUCAST suggests that clinicians use alternative antifungal agents; if these are not options, higher dosages of fluconazole

Table 10.7 Echinocandin interpretive breakpoint MICs against *Candida* spp.

Candida spp.	Agent	CLSI breakpoint MICS			EUCAST breakpoint MICs	
		Susceptible (μg/mL)	Intermediate (μg/mL)	Resistant (μg/mL)	Susceptible (μg/mL)	Resistant (μg/mL)
C. albicans	Anidulafungin	≤0.25	0.5	>0.5	≤0.03	>0.03
	Caspofungin	≤0.25	0.5	>0.5	Not proposed	Not proposed
	Micafungin	≤0.25	0.5	>0.5	≤0.016	>0.016
C. glabrata	Anidulafungin	≤0.125	0.25	>0.25	≤0.06	>0.06
	Caspofungin	≤0.125	0.25	>0.25	Not proposed	Not proposed
	Micafungin	0.06	0.125	>0.125	≤0.03	>0.03
C. tropicalis, *C. krusei*	Anidulafungin	≤0.25	0.5	>0.5	≤0.06	>0.06
	Caspofungin	≤0.25	0.5	>0.5	Not proposed	Not proposed
	Micafungin	≤0.25	0.5	>0.5	Not proposed	Not proposed
C. parapsilosis	Anidulafungin	≤2	4	>4	≤0.002	>4
	Caspofungin	≤2	4	>4	Not proposed	Not proposed
	Micafungin	≤2	4	>4	≤0.002	>2

EUCAST has not proposed caspofungin interpretive breakpoint MICs due to interlaboratory variation in results.
EUCAST has not proposed micafungin interpretive breakpoint MICs against *C. tropicalis* or *C. krusei* due to insufficient data

may be suitable. By definition, *C. krusei* strains are fluconazole-resistant, and alternative agents are recommended for treatment.

Echinocandins are agents of choice against most cases of candidemia and invasive candidiasis, in the absence of prior drug exposure or PK concerns at particular sites of deep tissue infection. Mouse data suggest that administration of higher-than-recommended doses at less frequent intervals will optimize the probability of PK–PD target attainment, and the likelihood of achieving fungicidal activity. Pooled data from two multicenter, double-blind, randomized clinical trials of adults with esophageal candidiasis showed strong trends toward better treatment responses (87.1 vs. 78.8%; $p=0.056$) and fewer relapses (5.6 vs. 12.2%; $p=0.051$) among patients treated with 300 mg of micafungin every other day than 150 mg every day (Andes et al. 2013). Predicted median micafungin total-drug C_{max} values with the two dosing regimens were 23.5 and 14.2 μg/mL, respectively. Predicted median total-drug AUCs were almost identical (311 and 310 μg h/mL, respectively), suggesting that C_{max} was the most important PK determinant of outcome. Safety studies have not defined maximal tolerated doses of the echinocandins; in general, micafungin doses as high as 600 mg have been well tolerated (Hiemenz et al. 2005; Sirohi et al. 2006). Clinical studies of large, infrequent echinocandin dosing regimens against candidemia and other forms of invasive candidiasis are warranted.

CLSI and EUCAST interpretive breakpoint MICs of the echinocandins against *Candida* spp. are shown in Table 10.7. Both groups considered wild-type MIC distributions, PK–PD data, and published clinical experience in setting their criteria (Pfaller et al. 2011; Arendrup et al. 2014). EUCAST did not propose caspofungin breakpoints due to the interlaboratory variability in MICs obtained by the reference microbroth dilution method. For each spp., EUCAST breakpoints are lower than CLSI breakpoints. The discrepancies speak to a lack of conclusive data. In particular, clinical data about the value of MICs in guiding treatment are conflicting. In the largest study, a relationship was not apparent between caspofungin MICs and outcomes among patients with oropharyngeal or invasive candidiasis ($n=292$ and 114, respectively; Kartsonis et al. 2005). In fact, outcomes were better among the small number of patients infected with *Candida* strains for which MICs were >2 μg/mL than among those infected with strains for which MICs were <1 μg/mL. A major problem in interpreting breakpoints is that very few non-*C. glabrata* strains exhibit higher MICs. Moreover, patients with invasive candidiasis not uncommonly fail antifungal therapy despite being infected with highly sensitive strains, which is in keeping with the importance of host factors such as immune status and acuity of illness in determining outcomes. Single-center studies have demonstrated that MICs for each of the agents against *C. glabrata* strains causing invasive candidiasis correlate with outcomes, particularly among patients who had prior echinocandin exposure (Shields et al. 2012, 2013a, b). However, institution-specific breakpoints were not necessarily consistent with CLSI or EUCAST interpretive criteria. Furthermore, most hospital laboratories that offer testing do not employ the reference broth microdilution methods that were used by CLSI and EUCAST in establishing their breakpoints (Eschenauer et al. 2014). The detection of *FKS* mutations that confer higher MICs may identify strains likely to fail to respond to therapy, but molecular assays remain a research tool (Shields et al. 2012).

On balance, current data do not support the routine use of echinocandin MICs in clinical decision making. Indeed, only ~50% of major medical centers routinely perform echinocandin susceptibility testing on *Candida* strains recovered from the bloodstream or sterile sites (Eschenauer et al. 2014). Since *FKS* mutations are not detected in the absence of previous echinocandin exposure or breakthrough infections, treatment-naïve patients can be assumed to be infected with susceptible strains (Shields et al. 2012, 2013a, b; Alexander et al. 2013). In treating patients with extensive past exposure or breakthrough infections, the judicious course is to use an alternative agent.

10.6 Questions for Future Studies of Fluconazole and Echinocandins

The pharmacometrics data for fluconazole and echinocandins against invasive candidiasis raise a number of issues that merit near-term attention. Several of the most pressing clinical questions are presented in Table 10.8.

Table 10.8 Key questions about fluconazole and echinocandins

Fluconazole	Echinocandins	Fluconazole and echinocandins
What is the role of high-dose fluconazole (≥800 mg/day) in the treatment of candidemia and invasive candidiasis?	What is the role of less frequent, higher-dose echinocandin treatment regimens?	Will resistance to these agents continue to emerge (particularly among *C. glabrata*)?
Will more frequent administration of fluconazole limit the emergence of resistance among *Candida* spp.?	Is there any clinical significance to higher echinocandin MICs against *C. parapsilosis* or paradoxical effects against certain *Candida* clinical strains?	What will be the clinical impact of resistance, including multidrug resistance?
	How does limited echinocandin penetration into sites like urinary tract, central nervous system, or eye impact the treatment of invasive candidiasis?	
	Will a reproducible methodology for measuring caspofungin MICs be developed?	
	Is there a role for echinocandin susceptibility testing or *FKS* mutation detection in guiding treatment decisions?	

10.7 Conclusions

Historically, pharmacotherapy against infections has been devised in an ad hoc fashion using data from disparate laboratory studies and clinical trials. The systematic use of pharmacometrics promises more rational and efficient antimicrobial development and utilization (Ambrose et al. 2007; Hope and Drusano 2009; Davies et al. 2013). The pharmacometric paradigm employs many techniques that are currently required for the drug development process, but integrates them in a more formalized manner (Hope and Drusano 2009). The principles outlined in this chapter can be applied to other antimicrobials and infectious diseases, as well as particular subtypes of invasive candidiasis. Indeed, elegant studies have defined micafungin PK–PD in experimental hematogenous *Candida* meningoencephalitis, and demonstrated that much larger doses (10–15 mg/kg) were required than against other forms of invasive candidiasis (Hope et al. 2008; Hope et al. 2010). As a result, a randomized clinical trial of high-dose micafungin versus amphotericin B in the treatment of premature infants with hematogenous *Candida* meningoencephalitis has been initiated (Hope and Drusano 2009). This bench-to-bedside approach is the evolving model for the fields of infectious diseases and medical mycology.

10.8 Summary

- Echinocandin antifungals are increasingly recognized as agents of first choice against candidemia and many other types of invasive candidiasis in adults.
- Fluconazole is the agent of choice against mucosal candidiasis, and remains an effective alternative agent against candidemia and invasive candidiasis. In particular, fluconazole may be preferred for the treatment of patients with prior echinocandin exposure or infections in which echinocandins are limited by PK considerations (e.g., urosepsis and endophthalmitis).
- Fluconazole is also useful as a step-down agent after a clinical response to initial treatment with an echinocandin.
- Data from the mouse model of hematogenously disseminated candidiasis identify fluconazole AUC/MIC and echinocandin C_{max}/MIC as PK–PD parameters that are most closely associated with successful treatment.
- Fluconazole AUC/MIC ≥ 25 and ≥ 75 are acceptable and optimal targets, respectively, for achieving successful outcomes in mouse models and humans.
- Simulation models predict that acceptable and optimal AUC/MIC will be reliably achieved in patients if daily fluconazole dose/MIC ratio is ≥ 50 and ≥ 100, respectively.
- Echinocandins are more active than fluconazole against *C. albicans* and *C. glabrata* strains in the mouse model.
- Echinocandin MICs are higher against *C. parapsilosis* than other spp., but PK–PD targets are lower and echinocandins have been used successfully against *C. parapsilosis* candidemia in clinical trials.
- PK–PD data suggest that echinocandins will be most effective if administered infrequently at high doses, but such regimens must be validated in clinical trials and the impact on paradoxical effects, resistance, and toxicity must be defined.

References

Alexander BD, Johnson MD, Pfeiffer CD, Jimenez-Ortigosa C, Catania J, Booker R et al (2013) Increasing echinocandin resistance in *Candida glabrata*: clinical failure correlates with presence of FKS mutations and elevated minimum inhibitory concentrations. Clin Infect Dis 56:1724–1732

Ambrose PG, Bhavnani SM, Rubino CM, Louie A, Gumbo T, Forrest A et al (2007) Pharmacokinetics-pharmacodynamics of antimicrobial therapy: it's not just for mice anymore. Clin Infect Dis 44:79–86

Andes D, Craig WA (1998) In vivo activities of amoxicillin and amoxicillin-clavulanate against *Streptococcus pneumoniae*: application to breakpoint determinations. Antimicrob Agents Chemother 42:2375–2379

Andes D, van Ogtrop M (1999) Characterization and quantitation of the pharmacodynamics of fluconazole in a neutropenic murine disseminated candidiasis infection model. Antimicrob Agents Chemother 43:2116–2120

Andes D, Marchillo K, Lowther J, Bryskier A, Stamstad T, Conklin R (2003a) In vivo pharmacodynamics of HMR 3270, a glucan synthase inhibitor, in a murine candidiasis model. Antimicrob Agents Chemother 47:1187–1192

Andes D, Marchillo K, Stamstad T, Conklin R (2003b) In vivo pharmacodynamics of a new triazole, ravuconazole, in a murine candidiasis model. Antimicrob Agents Chemother 47:1193–1199
Andes D, Marchillo K, Stamstad T, Conklin R (2003c) In vivo pharmacokinetics and pharmacodynamics of a new triazole, voriconazole, in a murine candidiasis model. Antimicrob Agents Chemother 47:3165–3169
Andes D, Marchillo K, Conklin R, Krishna G, Ezzet F, Cacciapuoti A et al (2004) Pharmacodynamics of a new triazole, posaconazole, in a murine model of disseminated candidiasis. Antimicrob Agents Chemother 48:137–142
Andes D, Forrest A, Lepak A, Nett J, Marchillo K, Lincoln L (2006a) Impact of antimicrobial dosing regimen on evolution of drug resistance in vivo: fluconazole and *Candida albicans*. Antimicrob Agents Chemother 50:2374–2383
Andes D, Lepak A, Nett J, Lincoln L, Marchillo K (2006b) In vivo fluconazole pharmacodynamics and resistance development in a previously susceptible *Candida albicans* population examined by microbiologic and transcriptional profiling. Antimicrob Agents Chemother 50:2384–2394
Andes D, Diekema DJ, Pfaller MA, Prince RA, Marchillo K, Ashbeck J et al (2008a) In vivo pharmacodynamic characterization of anidulafungin in a neutropenic murine candidiasis model. Antimicrob Agents Chemother 52:539–550
Andes DR, Diekema DJ, Pfaller MA, Marchillo K, Bohrmueller J (2008b) In vivo pharmacodynamic target investigation for micafungin against *Candida albicans* and *C. glabrata* in a neutropenic murine candidiasis model. Antimicrob Agents Chemother 52:3497–3503
Andes D, Diekema DJ, Pfaller MA, Bohrmuller J, Marchillo K, Lepak A (2010) In vivo comparison of the pharmacodynamic targets for echinocandin drugs against Candida species. Antimicrob Agents Chemother 54:2497–2506
Andes D, Ambrose PG, Hammel JP, Van Wart SA, Iyer V, Reynolds DK et al (2011) Use of pharmacokinetic-pharmacodynamic analyses to optimize therapy with the systemic antifungal micafungin for invasive candidiasis or candidemia. Antimicrob Agents Chemother 55:2113–2121
Andes DR, Safdar N, Baddley JW, Playford G, Reboli AC, Rex JH et al (2012) Impact of treatment strategy on outcomes in patients with candidemia and other forms of invasive candidiasis: a patient-level quantitative review of randomized trials. Clin Infect Dis 54:1110–1122
Andes DR, Reynolds DK, Van Wart SA, Lepak AJ, Kovanda LL, Bhavnani SM (2013) Clinical pharmacodynamic index identification for micafungin in esophageal candidiasis: dosing strategy optimization. Antimicrob Agents Chemother 57:5714–5716
Arbeit RD, Maki D, Tally FP, Campanaro E, Eisenstein BI (2004) The safety and efficacy of daptomycin for the treatment of complicated skin and skin-structure infections. Clin Infect Dis 38:1673–1681
Arendrup MC, Pfaller MA (2012) Caspofungin Etest susceptibility testing of Candida species: risk of misclassification of susceptible isolates of *C. glabrata* and *C. krusei* when adopting the revised CLSI caspofungin breakpoints. Antimicrob Agents Chemother 56:3965–3968
Arendrup MC, Horn T, Frimodt-Moller N (2002) In vivo pathogenicity of eight medically relevant Candida species in an animal model. Infection 30:286–291
Arendrup MC, Rodriguez-Tudela JL, Lass-Florl C, Cuenca-Estrella M, Donnelly JP, Hope W (2011) EUCAST technical note on anidulafungin. Clin Microbiol Infect 17:E18–E20
Arendrup MC, Cuenca-Estrella M, Lass-Florl C, Hope WW (2014) Breakpoints for antifungal agents: An update from EUCAST focussing on echinocandins against Candida spp. and triazoles against Aspergillus spp. Drug Resist Updat 16:81–95
Baddley JW, Patel M, Bhavnani SM, Moser SA, Andes DR (2008) Association of fluconazole pharmacodynamics with mortality in patients with candidemia. Antimicrob Agents Chemother 52:3022–3028
Barchiesi F, Spreghini E, Tomassetti S, Della Vittoria A, Arzeni D, Manso E et al (2006) Effects of caspofungin against *Candida guilliermondii* and *Candida parapsilosis*. Antimicrob Agents Chemother 50:2719–2727
Bellmann R (2007) Clinical pharmacokinetics of systemically administered antimycotics. Curr Clin Pharmacol 2:37–58

Betts RF, Nucci M, Talwar D, Gareca M, Queiroz-Telles F, Bedimo RJ et al (2009) A Multicenter, double-blind trial of a high-dose caspofungin treatment regimen versus a standard caspofungin treatment regimen for adult patients with invasive candidiasis. Clin Infect Dis 48:1676–1684

Clancy CJ, Nguyen MH (2011) At what cost echinocandin resistance? J Infect Dis 204:499–501

Clancy CJ, Nguyen MH (2012) The end of an era in defining the optimal treatment of invasive candidiasis. Clin Infect Dis 54:1123–1125

Clancy CJ, Nguyen MH (2013) Finding the missing 50 % of invasive candidiasis: how nonculture diagnostics will improve understanding of disease spectrum and transform patient care. Clin Infect Dis 56:1284–1292

Clancy CJ, Yu VL, Morris AJ, Snydman DR, Nguyen MH (2005) Fluconazole MIC and the fluconazole dose/MIC ratio correlate with therapeutic response among patients with candidemia. Antimicrob Agents Chemother 49:3171–3177

Clancy CJ, Huang H, Cheng S, Derendorf H, Nguyen MH (2006) Characterizing the effects of caspofungin on *Candida albicans*, *Candida parapsilosis*, and *Candida glabrata* isolates by simultaneous time-kill and postantifungal-effect experiments. Antimicrob Agents Chemother 50:2569–2572

Cornely OA, Bassetti M, Calandra T, Garbino J, Kullberg BJ, Lortholary O et al (2012) ESCMID* guideline for the diagnosis and management of Candida diseases 2012: non-neutropenic adult patients. Clin Microbiol Infect 18(Suppl 7):19–37

Craig WA (1998) Pharmacokinetic/pharmacodynamic parameters: rationale for antibacterial dosing of mice and men. Clin Infect Dis 26:1–10; quiz 1–2.

Cuesta I, Bielza C, Larranaga P, Cuenca-Estrella M, Laguna F, Rodriguez-Pardo D et al (2009) Data mining validation of fluconazole breakpoints established by the European Committee on Antimicrobial Susceptibility Testing. Antimicrob Agents Chemother 53:2949–2954

Cuesta I, Bielza C, Cuenca-Estrella M, Larranaga P, Rodriguez-Tudela JL (2010) Evaluation by data mining techniques of fluconazole breakpoints established by the Clinical and Laboratory Standards Institute (CLSI) and comparison with those of the European Committee on Antimicrobial Susceptibility Testing (EUCAST). Antimicrob Agents Chemother 54:1541–1546

Davies GR, Hope W, Khoo S (2013) Opinion: the pharmacometrics of infectious disease. CPT Pharmacometrics Syst Pharmacol 2:e70

Debruyne D (1997) Clinical pharmacokinetics of fluconazole in superficial and systemic mycoses. Clin Pharmacokinet 33:52–77

de Wet N, Llanos-Cuentas A, Suleiman J, Baraldi E, Krantz EF, Della Negra M et al (2004) A randomized, double-blind, parallel-group, dose–response study of micafungin compared with fluconazole for the treatment of esophageal candidiasis in HIV-positive patients. Clin Infect Dis 39:842–849

Dowell JA, Knebel W, Ludden T, Stogniew M, Krause D, Henkel T (2004) Population pharmacokinetic analysis of anidulafungin, an echinocandin antifungal. J Clin Pharmacol 44:590–598

Egusa H, Soysa NS, Ellepola AN, Yatani H, Samaranayake LP (2008) Oral candidosis in HIV-infected patients. Curr HIV Res 6:485–499

Eschenauer GA, Carver PL, Lin SW, Klinker KP, Chen YC, Potoski BA et al (2013) Fluconazole versus an echinocandin for *Candida glabrata* fungaemia: a retrospective cohort study. J Antimicrob Chemother 68:922–926

Eschenauer GA, Nguyen MH, Shoham S, Vazquez JA, Morris AJ, Pasculle WA et al (2014) Real-world experience with Echinocandin MICs against Candida species in a multicenter study of hospitals that routinely perform susceptibility testing of bloodstream isolates. Antimicrob Agents Chemother 58:1897–1906

Espinel-Ingroff A, Pfaller M, Messer SA, Knapp CC, Killian S, Norris HA et al (1999) Multicenter comparison of the sensititre YeastOne Colorimetric Antifungal Panel with the National Committee for Clinical Laboratory standards M27-A reference method for testing clinical isolates of common and emerging Candida spp., Cryptococcus spp., and other yeasts and yeast-like organisms. J Clin Microbiol 37:591–595

Espinel-Ingroff A, Arendrup MC, Pfaller MA, Bonfietti LX, Bustamante B, Canton E et al (2013) Interlaboratory variability of Caspofungin MICs for Candida spp. Using CLSI and EUCAST

methods: should the clinical laboratory be testing this agent? Antimicrob Agents Chemother 57:5836–5842
EUCAST (2008a) Definitive document EDef 7.1: method for the determination of broth dilution MICs of antifungal agents for fermentative yeasts. Clin Microbiol Infect 14:398–405
EUCAST (2008b) Technical note on fluconazole. Clin Microbiol Infect 14:193–195
Grant SM, Clissold SP (1990) Fluconazole. A review of its pharmacodynamic and pharmacokinetic properties, and therapeutic potential in superficial and systemic mycoses. Drugs 39:877–916
Gumbo T, Drusano GL, Liu W, Ma L, Deziel MR, Drusano MF et al (2006) Anidulafungin pharmacokinetics and microbial response in neutropenic mice with disseminated candidiasis. Antimicrob Agents Chemother 50:3695–3700
Gumbo T, Drusano GL, Liu W, Kulawy RW, Fregeau C, Hsu V et al (2007) Once-weekly micafungin therapy is as effective as daily therapy for disseminated candidiasis in mice with persistent neutropenia. Antimicrob Agents Chemother 51:968–974
Gumbo T, Hiemenz J, Ma L, Keirns JJ, Buell DN, Drusano GL (2008) Population pharmacokinetics of micafungin in adult patients. Diagn Microbiol Infect Dis 60:329–331
Hall RG, Swancutt MA, Gumbo T (2011) Fractal geometry and the pharmacometrics of micafungin in overweight, obese, and extremely obese people. Antimicrob Agents Chemother 55:5107–5112
Han S, Kim J, Yim H, Hur J, Song W, Lee J et al (2013) Population pharmacokinetic analysis of fluconazole to predict therapeutic outcome in burn patients with Candida infection. Antimicrob Agents Chemother 57:1006–1011
Hiemenz J, Cagnoni P, Simpson D, Devine S, Chao N, Keirns J et al (2005) Pharmacokinetic and maximum tolerated dose study of micafungin in combination with fluconazole versus fluconazole alone for prophylaxis of fungal infections in adult patients undergoing a bone marrow or peripheral stem cell transplant. Antimicrob Agents Chemother 49:1331–1336
Hope WW, Drusano GL (2009) Antifungal pharmacokinetics and pharmacodynamics: bridging from the bench to bedside. Clin Microbiol Infect 15:602–612
Hope WW, Drusano GL, Moore CB, Sharp A, Louie A, Walsh TJ et al (2007) Effect of neutropenia and treatment delay on the response to antifungal agents in experimental disseminated candidiasis. Antimicrob Agents Chemother 51:285–295
Hope WW, Mickiene D, Petraitis V, Petraitiene R, Kelaher AM, Hughes JE et al (2008) The pharmacokinetics and pharmacodynamics of micafungin in experimental hematogenous Candida meningoencephalitis: implications for echinocandin therapy in neonates. J Infect Dis 197:163–171
Hope WW, Smith PB, Arrieta A, Buell DN, Roy M, Kaibara A et al (2010) Population pharmacokinetics of micafungin in neonates and young infants. Antimicrob Agents Chemother 54:2633–2637
Howard SJ, Livermore J, Sharp A, Goodwin J, Gregson L, Alastruey-Izquierdo A et al (2011) Pharmacodynamics of echinocandins against *Candida glabrata*: requirement for dosage escalation to achieve maximal antifungal activity in neutropenic hosts. Antimicrob Agents Chemother 55:4880–4887
Kabbara N, Lacroix C, Peffault de Latour R, Socie G, Ghannoum M, Ribaud P (2008) Breakthrough *C. parapsilosis* and *C. guilliermondii* blood stream infections in allogeneic hematopoietic stem cell transplant recipients receiving long-term caspofungin therapy. Haematologica 93:639–640
Kartsonis N, Killar J, Mixson L, Hoe CM, Sable C, Bartizal K et al (2005) Caspofungin susceptibility testing of isolates from patients with esophageal candidiasis or invasive candidiasis: relationship of MIC to treatment outcome. Antimicrob Agents Chemother 49:3616–3623
Kauffman CA, Carver PL (2008) Update on echinocandin antifungals. Semin Respir Crit Care Med 29:211–219
Kofla G, Ruhnke M (2011) Pharmacology and metabolism of anidulafungin, caspofungin and micafungin in the treatment of invasive candidosis: review of the literature. Eur J Med Res 16:159–166

Krause DS, Simjee AE, van Rensburg C, Viljoen J, Walsh TJ, Goldstein BP et al (2004) A randomized, double-blind trial of anidulafungin versus fluconazole for the treatment of esophageal candidiasis. Clin Infect Dis 39:770–775

Kuse ER, Chetchotisakd P, da Cunha CA, Ruhnke M, Barrios C, Raghunadharao D et al (2007) Micafungin versus liposomal amphotericin B for candidaemia and invasive candidosis: a phase III randomised double-blind trial. Lancet 369:1519–1527

Lee SC, Fung CP, Huang JS, Tsai CJ, Chen KS, Chen HY et al (2000) Clinical correlates of antifungal macrodilution susceptibility test results for non-AIDS patients with severe Candida infections treated with fluconazole. Antimicrob Agents Chemother 44:2715–2718

Leitner JM, Meyer B, Fuhrmann V, Saria K, Zuba C, Jager W et al (2011) Multiple-dose pharmacokinetics of anidulafungin during continuous venovenous haemofiltration. J Antimicrob Chemother 66:880–884

Lepak AJ, Marchillo K, Pichereau S, Craig WA, Andes DR (2012) Comparative pharmacodynamics of the new oxazolidinone tedizolid phosphate and linezolid in a neutropenic murine *Staphylococcus aureus* pneumonia model. Antimicrob Agents Chemother 56:5916–5922

Leroy O, Gangneux JP, Montravers P, Mira JP, Gouin F, Sollet JP et al (2009) Epidemiology, management, and risk factors for death of invasive Candida infections in critical care: a multicenter, prospective, observational study in France (2005–2006). Crit Care Med 37:1612–1618

Liu P (2013) Population pharmacokinetic-pharmacodynamic analysis of anidulafungin in adult patients with fungal infections. Antimicrob Agents Chemother 57:466–474

Liu P, Ruhnke M, Meersseman W, Paiva JA, Kantecki M, Damle B (2013) Pharmacokinetics of anidulafungin in critically ill patients with candidemia/invasive candidiasis. Antimicrob Agents Chemother 57:1672–1676

Louie A, Drusano GL, Banerjee P, Liu QF, Liu W, Kaw P et al (1998) Pharmacodynamics of fluconazole in a murine model of systemic candidiasis. Antimicrob Agents Chemother 42:1105–1109

Louie A, Deziel M, Liu W, Drusano MF, Gumbo T, Drusano GL (2005) Pharmacodynamics of caspofungin in a murine model of systemic candidiasis: importance of persistence of caspofungin in tissues to understanding drug activity. Antimicrob Agents Chemother 49:5058–5068

Maksymiuk AW, Thongprasert S, Hopfer R, Luna M, Fainstein V, Bodey GP (1984) Systemic candidiasis in cancer patients. Am J Med 77:20–27

Maseda E, Grau S, Villagran MJ, Hernandez-Gancedo C, Lopez-Tofino A, Roberts JA et al (2014) Micafungin pharmacokinetic/pharmacodynamic adequacy for the treatment of invasive candidiasis in critically ill patients on continuous venovenous haemofiltration. J Antimicrob Chemother 69:1624–1632

Mora-Duarte J, Betts R, Rotstein C, Colombo AL, Thompson-Moya L, Smietana J et al (2002) Comparison of caspofungin and amphotericin B for invasive candidiasis. N Engl J Med 347:2020–2029

Moudgal V, Little T, Boikov D, Vazquez JA (2005) Multiechinocandin- and multiazole-resistant *Candida parapsilosis* isolates serially obtained during therapy for prosthetic valve endocarditis. Antimicrob Agents Chemother 49:767–769

Nguyen MH, Peacock JE Jr, Tanner DC, Morris AJ, Nguyen ML, Snydman DR et al (1995) Therapeutic approaches in patients with candidemia. Evaluation in a multicenter, prospective, observational study. Arch Intern Med 155:2429–2435

Nguyen MH, Peacock JE Jr, Morris AJ, Tanner DC, Nguyen ML, Snydman DR et al (1996) The changing face of candidemia: emergence of non-*Candida albicans* species and antifungal resistance. Am J Med 100:617–623

Nguyen TH, Hoppe-Tichy T, Geiss HK, Rastall AC, Swoboda S, Schmidt J et al (2007) Factors influencing caspofungin plasma concentrations in patients of a surgical intensive care unit. J Antimicrob Chemother 60:100–106

Nguyen KT, Ta P, Hoang BT, Cheng S, Hao B, Nguyen MH et al (2009) Anidulafungin is fungicidal and exerts a variety of postantifungal effects against *Candida albicans*, *C. glabrata*, *C. parapsilosis*, and *C. krusei* isolates. Antimicrob Agents Chemother 53:3347–3352

Orozco AS, Higginbotham LM, Hitchcock CA, Parkinson T, Falconer D, Ibrahim AS et al (1998) Mechanism of fluconazole resistance in *Candida krusei*. Antimicrob Agents Chemother 42:2645–2649

Pai MP, Turpin RS, Garey KW (2007) Association of fluconazole area under the concentration-time curve/MIC and dose/MIC ratios with mortality in nonneutropenic patients with candidemia. Antimicrob Agents Chemother 51:35–39

Pappas PG, Rotstein CM, Betts RF, Nucci M, Talwar D, De Waele JJ et al (2007) Micafungin versus caspofungin for treatment of candidemia and other forms of invasive candidiasis. Clin Infect Dis 45:883–893

Pappas PG, Kauffman CA, Andes D, Benjamin DK Jr, Calandra TF, Edwards JE Jr et al (2009) Clinical practice guidelines for the management of candidiasis: 2009 update by the Infectious Diseases Society of America. Clin Infect Dis 48:503–535

Patel K, Roberts JA, Lipman J, Tett SE, Deldot ME, Kirkpatrick CM (2011) Population pharmacokinetics of fluconazole in critically ill patients receiving continuous venovenous hemodiafiltration: using Monte Carlo simulations to predict doses for specified pharmacodynamic targets. Antimicrob Agents Chemother 55:5868–5873

Pfaller MA, Diekema DJ, Messer SA, Boyken L, Hollis RJ (2003) Activities of fluconazole and voriconazole against 1,586 recent clinical isolates of Candida species determined by Broth microdilution, disk diffusion, and Etest methods: report from the ARTEMIS Global Antifungal Susceptibility Program, 2001. J Clin Microbiol 41:1440–1446

Pfaller MA, Diekema DJ, Sheehan DJ (2006) Interpretive breakpoints for fluconazole and Candida revisited: a blueprint for the future of antifungal susceptibility testing. Clin Microbiol Rev 19:435–447

Pfaller MA, Andes D, Diekema DJ, Espinel-Ingroff A, Sheehan D (2010) Wild-type MIC distributions, epidemiological cutoff values and species-specific clinical breakpoints for fluconazole and Candida: time for harmonization of CLSI and EUCAST broth microdilution methods. Drug Resist Updat 13:180–195

Pfaller MA, Diekema DJ, Andes D, Arendrup MC, Brown SD, Lockhart SR et al (2011) Clinical breakpoints for the echinocandins and Candida revisited: integration of molecular, clinical, and microbiological data to arrive at species-specific interpretive criteria. Drug Resist Updat 14 164–176

Pfaller MA, Castanheira M, Lockhart SR, Ahlquist AM, Messer SA, Jones RN (2012a) Frequency of decreased susceptibility and resistance to echinocandins among fluconazole-resistant bloodstream isolates of *Candida glabrata*. J Clin Microbiol 50:1199–1203

Pfaller MA, Chaturvedi V, Diekema DJ, Ghannoum MA, Holliday NM, Killian SB et al (2012b) Comparison of the Sensititre YeastOne colorimetric antifungal panel with CLSI microdilution for antifungal susceptibility testing of the echinocandins against Candida spp., using new clinical breakpoints and epidemiological cutoff values. Diagn Microbiol Infect Dis 73:365–368

Reboli AC, Rotstein C, Pappas PG, Chapman SW, Kett DH, Kumar D et al (2007) Anidulafungin versus fluconazole for invasive candidiasis. N Engl J Med 356:2472–2482

Rex JH, Pfaller MA (2002) Has antifungal susceptibility testing come of age? Clin Infect Dis 35:982–989

Rex JH, Bennett JE, Sugar AM, Pappas PG, van der Horst CM, Edwards JE et al (1994) A randomized trial comparing fluconazole with amphotericin B for the treatment of candidemia in patients without neutropenia. Candidemia Study Group and the National Institute. N Engl J Med 331:1325–1330

Rex JH, Pfaller MA, Galgiani JN, Bartlett MS, Espinel-Ingroff A, Ghannoum MA et al (1997) Development of interpretive breakpoints for antifungal susceptibility testing: conceptual framework and analysis of in vitro-in vivo correlation data for fluconazole, itraconazole, and candida infections. Subcommittee on Antifungal Susceptibility Testing of the National Committee for Clinical Laboratory Standards. Clin Infect Dis 24:235–247

Rex JH, Pappas PG, Karchmer AW, Sobel J, Edwards JE, Hadley S et al (2003) A randomized and blinded multicenter trial of high-dose fluconazole plus placebo versus fluconazole plus amphotericin B as therapy for candidemia and its consequences in nonneutropenic subjects. Clin Infect Dis 36:1221–1228

Rodriguez-Tudela JL, Almirante B, Rodriguez-Pardo D, Laguna F, Donnelly JP, Mouton JW et al (2007) Correlation of the MIC and dose/MIC ratio of fluconazole to the therapeutic response of patients with mucosal candidiasis and candidemia. Antimicrob Agents Chemother 51: 3599–3604

Rogers TE, Galgiani JN (1986) Activity of fluconazole (UK 49,858) and ketoconazole against *Candida albicans* in vitro and in vivo. Antimicrob Agents Chemother 30:418–422

Shields RK, Nguyen MH, Du C, Press E, Cheng S, Clancy CJ (2011a) Paradoxical effect of caspofungin against Candida bloodstream isolates is mediated by multiple pathways but eliminated in human serum. Antimicrob Agents Chemother 55:2641–2647

Shields RK, Nguyen MH, Press EG, Clancy CJ (2011b) Five-minute exposure to caspofungin results in prolonged postantifungal effects and eliminates the paradoxical growth of *Candida albicans*. Antimicrob Agents Chemother 55:3598–3602

Shields RK, Nguyen MH, Press EG, Kwa AL, Cheng S, Du C et al (2012) The presence of an FKS mutation rather than MIC is an independent risk factor for failure of echinocandin therapy among patients with invasive candidiasis due to *Candida glabrata*. Antimicrob Agents Chemother 56:4862–4869

Shields RK, Nguyen MH, Press EG, Updike CL, Clancy CJ (2013a) Anidulafungin and micafungin MIC breakpoints are superior to that of caspofungin for identifying FKS mutant *Candida glabrata* strains and Echinocandin resistance. Antimicrob Agents Chemother 57:6361–6365

Shields RK, Nguyen MH, Press EG, Updike CL, Clancy CJ (2013b) Caspofungin MICs correlate with treatment outcomes among patients with *Candida glabrata* invasive candidiasis and prior echinocandin exposure. Antimicrob Agents Chemother 57:3528–3535

Sirohi B, Powles RL, Chopra R, Russell N, Byrne JL, Prentice HG et al (2006) A study to determine the safety profile and maximum tolerated dose of micafungin (FK463) in patients undergoing haematopoietic stem cell transplantation. Bone Marrow Transplant 38:47–51

Sobel JD (1992) Pathogenesis and treatment of recurrent vulvovaginal candidiasis. Clin Infect Dis 14(Suppl 1):S148–S153

Sobel JD, Schmitt C, Stein G, Mummaw N, Christensen S, Meriwether C (1994) Initial management of recurrent vulvovaginal candidiasis with oral ketoconazole and topical clotrimazole. J Reprod Med 39:517–520

Torres HA, Kontoyiannis DP, Rolston KV (2004) High-dose fluconazole therapy for cancer patients with solid tumors and candidemia: an observational, noncomparative retrospective study. Support Care Cancer 12:511–516

Ullmann AJ, Akova M, Herbrecht R, Viscoli C, Arendrup MC, Arikan-Akdagli S et al (2012) ESCMID* guideline for the diagnosis and management of Candida diseases 2012: adults with haematological malignancies and after haematopoietic stem cell transplantation (HCT). Clin Microbiol Infect 18 Suppl 7:53–67

Villanueva A, Gotuzzo E, Arathoon EG, Noriega LM, Kartsonis NA, Lupinacci RJ et al (2002) A randomized double-blind study of caspofungin versus fluconazole for the treatment of esophageal candidiasis. Am J Med 113:294–299

Warn PA, Sharp A, Parmar A, Majithiya J, Denning DW, Hope WW (2009) Pharmacokinetics and pharmacodynamics of a novel triazole, isavuconazole: mathematical modeling, importance of tissue concentrations, and impact of immune status on antifungal effect. Antimicrob Agents Chemother 53:3453–3461

White TC (1997) Increased mRNA levels of ERG16, CDR, and MDR1 correlate with increases in azole resistance in *Candida albicans* isolates from a patient infected with human immunodeficiency virus. Antimicrob Agents Chemother 41:1482–1487

Wurthwein G, Young C, Lanvers-Kaminsky C, Hempel G, Trame MN, Schwerdtfeger R et al (2012) Population pharmacokinetics of liposomal amphotericin B and caspofungin in allogeneic hematopoietic stem cell recipients. Antimicrob Agents Chemother 56:536–543

Zonios DI, Bennett JE (2008) Update on azole antifungals. Semin Respir Crit Care Med 29: 198–210

Chapter 11
Pharmacometrics and Tuberculosis

Charles A. Peloquin

11.1 The Available TB Drugs

This chapter will focus on the drugs that are used to treat tuberculosis (TB), and some of the key features to using them properly. TB is a contagious, airborne bacterial disease, caused by *Mycobacterium tuberculosis* (Mtb; Peloquin and Namdar 2011). After infection, Mtb can remain dormant ("latent") for decades within an individual, only to reactivate later. Current estimates hold that one third of all the people on earth are latently infected with TB. Once reactivated from latency, TB diseases manifest most commonly as a cavitating form of pneumonia, with fever, night sweats, cough, and weight loss. The World Health Organization (WHO) estimates that there are more than 9 million incident cases of TB globally each year, leading to an estimated 1.5 million deaths annually. TB causes more deaths than HIV and malaria combined, and is the leading cause of death among HIV-infected individuals. TB is not distributed evenly across the world, with the largest concentrations of the disease found in China, India, and sub-Saharan Africa. TB is associated with poverty and crowded living conditions, and has been called "a social disease with medical consequences." Currently, the world has arrived at a tipping point. Either better procedures are implemented to deal with the emerging plaque of drug-resistant TB or we will see a dramatic reversal of the progress made against TB since the discovery of the TB drugs (Heifets 2012).

There are only a limited number of drugs that are US Food and Drug Administration (FDA) approved for treatment of TB in the USA, roughly ten old and one new (bedaquiline; Peloquin and Namdar 2011; Diacon et al. 2012). Very similar lists of drugs are available in countries around the world (see CDC treatment guidelines at http://www.cdc.gov/mmwr/PDF/rr/rr5211.pdf, and WHO treatment guidelines at http://whqlibdoc.who.int/publications/2010/9789241547833_eng.pdf). Some countries have more limited formularies, and the second-line drugs are

C. A. Peloquin (✉)
College of Pharmacy and Emerging Pathogens Institute,
University of Florida, Gainesville, FL, USA
e-mail: peloquin@cop.ufl.edu

S. Schmidt, H. Derendorf (eds.), *Applied Pharmacometrics,* AAPS Advances
in the Pharmaceutical Sciences Series 14, DOI 10.1007/978-1-4939-1304-6_11

available through programs offered by the WHO. Para-aminosalicylic acid (PAS), also known as amino-salicylate or PAS, is the oldest of the TB drugs, discovered in the early 1940s in Sweden. That discovery was followed soon thereafter by the discovery of streptomycin (SM), the first of the aminoglycosides. The third TB drug to be introduced was isoniazid (INH). With the introduction of INH, truly effective combination therapy was available for TB by the early 1950s (American Thoracic Society/Centers for Disease Control/Infectious Disease Society of America 2003). Only the more recent discovery of combination anti-HIV therapy in the mid-1990s can rival the global importance of this emerging therapy. Continuing with the list of available TB drugs, capreomycin (CM) is a polypeptide, and it is an injectable drug like SM. There are no oral dosage forms for these two drugs. Cycloserine (CS) is considered a second-line drug, as is ethionamide (ETA). In contrast, along with INH, ethambutol (EMB), pyrazinamide (PZA), rifampin (RIF), and the closely related rifapentine (RPNT) can be considered first-line TB drugs.

11.2 Alternative and Investigational TB Drugs

Other drugs that can be used for TB but that do not have FDA approval for that indication include other aminoglycosides. In particular, amikacin (AK) and kanamycin (KM) can be used in cases of SM-resistant TB. Most of the isolates that are SM resistant remain susceptible to AK and KM. Further, several of the fluoroquinolones, especially moxifloxacin (MOXI) and levofloxacin (LEVO), are the most active and the most useful for the management of TB (American Thoracic Society/Centers for Disease Control/Infectious Disease Society of America 2003; Peloquin and Namdar 2011; Loeffler et al. 2012). There are other drugs in this class, such as ciprofloxacin, that were used initially because the newer ones were not available yet. Currently, ciprofloxacin is considered a weaker drug for TB, and it is no longer recommended. LEVO is the L-isomer of ofloxacin, and it is preferred over ofloxacin, since it is more potent in vitro. Gatifloxacin (GATI) no longer is available in the USA. It is available in other countries around the world, and it could be considered a drug for the treatment of TB. It may be more likely than other "TB quinolones" to cause hypo- or hyperglycemia.

There are additional drugs that could be considered for the treatment of TB, but they also do not bear FDA approval for this indication (Loeffler et al. 2012; Dooley et al. 2013). Macrolides, and in particular, azithromycin and clarithromycin, are not very good TB drugs based upon the data available. They are used more or less in desperate cases, when one is scraping the bottom of the barrel for potentially useful drugs. It is not a class of drugs that one would consider initially for the treatment of TB. Macrolides are very good drugs for non-tuberculous mycobacteria (NTM) including *Mycobacterium avium* complex (MAC), but for TB, they are not reliable. Amoxicillin-clavulanate acid has been used sporadically for TB cases that are multidrug resistant (MDR-TB) and extremely drug resistant (XDR-TB). However, its exact role in the management of such cases has yet to be defined. Clofazimine

is a drug that is considered a leprosy drug, as we understand it right now. There are some new studies looking at clofazimine in animal models of TB, and it seems to be synergistic with a wide variety of TB drugs. Clofazimine could reenter our list of preferred TB drugs, but at this point in time, it is a reserve drug for cases of XDR-TB.

Rifabutin (RBN) is a chemical cousin of RIF and RPNT, and it is used in cases where drug–drug interactions are particularly problematic (Namdar and Peloquin 2011). Linezolid is a drug designed for Gram-positive infections. It is an oxazolidinone, as are sutezolid (PNU-100480) and AZD 5847. These drugs do seem to have a very interesting and potentially useful activity for the treatment of MDR-TB. They also have, at least in the case of linezolid, some fairly serious side effects, including bone marrow suppression, and both ocular and peripheral neuropathies (Loeffler et al. 2012; Dooley et al. 2013). Those need to be considered, and for now these drugs are reserve agents for more drug-resistant TB. Outside of the USA, prothionamide is the propyl derivative of ETA. The two drugs have similar potency and toxicity. Thiacetazone, historically used in developing countries because it was available at a very low price, also has some very serious side effects. These include Stevens–Johnson syndrome in patients who are immunocompromised, especially HIV-infected patients. Therefore, thiacetazone is no longer used. Viomycin is very similar to CM, and does not appear to have any particular advantage over CM. Much more often, CM is used as an injectable agent, as compared to viomycin (Peloquin 1991; Namdar and Peloquin 2011; Loeffler et al. 2012; Dooley et al. 2013).

PA-824 is a chemical derivative of metronidazole with a unique activity against TB (Diacon et al. 2012). It does not have activity against a wide-range of mycobacteria; rather, it is focused on TB. It appears to be bactericidal both in the mouse model and in clinical trials to date. PA-824 has a minimal inhibitory concentration (MIC) against a laboratory isolate known as H37RV that is comparable to RIF's MIC. RIF, of all the TB drugs, is the most potent from the standpoint of sterilizing activity. Sterilizing activity is a term that is relatively unique to TB, and it refers to the ability of a drug to prevent posttreatment relapses. Unlike the postantibiotic effect, which typically is measured in vitro as a lag time to bacterial regrowth, sterilizing activity is the in vivo elimination of persisters. It is hoped that PA-824 also can show that activity, but at this point, we know that it is at least bactericidal. In other words, it can kill TB in vitro, inside of a mouse model, and in humans.

OPC 67683, also known as delamanid, is chemically related to PA-824 (Lauzardo and Peloquin 2012; Skripconoka et al. 2012). In vitro, it is about 20 times more potent than PA 824. It does show cross-resistance with PA 824, so in part or in total, their mechanisms of action are very similar. At this time, delamanid also has completed phase two clinical trials. The MIC for delamanid is similar to or lower than that for INH, making it extremely potent on a milligram basis. MICs will vary from laboratory to laboratory, and they will vary depending on liquid versus solid media, and the particular type of solid media or the particular type of liquid media that is used resulting in a wide range of reported MIC values. Attention to the methodology that was used often explains why one would observe a difference. In this case, regardless of the method used, delamanid is a very potent drug, and it is hoped that

this will translate into high clinical efficacy. Delamanid also has received regulatory approval with the European Medicines Agency (EMA).

TMC207, now known as bedaquiline, is a very unique drug (Diacon et al. 2012; Lauzardo and Peloquin 2012). It is diarylquinoline, and it is chemically related to the malaria drug chloroquine. Its chlorine atom has been replaced by a bromine, which is essential for the unique properties of this molecule. The median MIC is very low, at 0.06 mcg/ml, making bedaquiline comparable in vitro to the potency of RPNT or to RBN. It has a unique target, ATP synthase, and that target is not shared by any of the other TB drugs. Bedaquiline is active against a wide variety of isolates in vitro, and clinically, good responses have been seen in phase 2 trials in patients infected with MDR-TB. This indicates that isolates resistant to other categories of TB drugs currently remain quite susceptible to bedaquiline. At the end of 2012, bedaquiline received regulatory approval from the FDA.

The ultimate goal is to develop entirely novel, multidrug regimens that can be used regardless of preexisting drug resistance. Such regimens would be the equivalent of pressing a "reset" button on the history of TB treatment. Parts of the world currently experiencing high rates of MDR- and XDR-TB would start over with a clean slate. New drugs, plus much better drug administration systems, are needed in high-burden countries in order to stem the tide of TB.

11.3 Detailed Description of TB Drug Pharmacology

INH, as mentioned, was brought into clinical practice in the early 1950s. INH is one of the two primary, first-line TB drugs, along with RIF (American Thoracic Society/Centers for Disease Control/Infectious Disease Society of America 2003; Peloquin and Namdar 2011). It is an inactive pro-drug, and its reactive intermediates are inhibitors of cell wall synthesis, specifically, the inhibitors of the formation of mycolic acids. Available data suggest that the best measure for activity is the free drug (i.e., not protein bound) area under the concentration versus time curve (AUC) divided by the MIC (*f*AUC/MIC; Gumbo et al. 2007). In some models, this PK/PD index can be rivaled by the free drug maximum concentration (*f*Cmax) divided by the MIC (*f*Cmax/MIC) as the preferred measure of INH's dose concentration–response relationship. The standard daily dose of INH is 300 mg orally. There is a dosage form available for intramuscular (i.m.) use that has been further extended for intravenous (i.v.) use, even though the package labeling does not indicate i.v. administration. Nevertheless, there is accumulated clinical experience with INH with i.v. administration of the standard 300 mg dose in about 25 ml of normal saline, as a slow bolus over about 5 min. There are oral regimens, given three times or two times weekly, where the standard adult INH dose is increased to 900 mg. The usual dose for children is 10–20 mg/kg. The excellent work done in South Africa by Peter Donald and colleagues has now shown that doses should be at the higher end of this range (Thee et al. 2011). Children tend to have lower serum concentrations and more rapid clearance of the TB drugs as compared to adults.

INH is cleared significantly more by the liver than by the kidneys, although INH metabolites are eliminated via the kidneys. There are genetic polymorphisms in N-acetyl transferase 2 (NAT2), which is the enzyme responsible for metabolizing INH to acetyl-INH. This means that there are fast acetylators and slow acetylators of INH (Peloquin 1991; Peloquin et al. 1997). The toxicities of greatest concern with INH include hepatotoxicity, which can require dose interruptions, and peripheral neuropathies (American Thoracic Society/Centers for Disease Control/Infectious Disease Society of America 2003). The latter when found, typically occur in the stocking and glove distribution. Patients often take vitamin B6 (pyridoxine) in an attempt to minimize or eliminate this particular toxicity.

RIF is the most important TB drug (American Thoracic Society/Centers for Disease Control/Infectious Disease Society of America 2003; Peloquin and Namdar 2011). The initial regimen, mentioned at the beginning of this chapter, was a three-drug regimen of PAS plus SM plus INH. That did work, but one had to take it for about 18 months for it to be reasonably effective. Shorter regimens had much higher failure rates. The introduction of RIF reduced the duration of treatment from 18 to 9 months. With the addition of PZA, the regimen could be further reduced to only 6 months. So, the current 6-month regimen is considered "short-course treatment" of TB. It is "long-course" compared to just about any other bacterial infection, but for TB, 6 months is currently the shortest regimen offering cure rates in excess of 95%. However, achieving those 95% cure rates remains a very big challenge. RIF is clearly the most important drug in the regimen. The current dose is 600 mg daily, and this dose also is used with intermittent regimens, either twice or three times weekly (American Thoracic Society/Centers for Disease Control/Infectious Disease Society of America 2003; Peloquin and Namdar 2011). RIF inhibits DNA-dependent RNA polymerase. It is generally dosed orally, although there is an i.v. dosage form available. That dosage form can be infused in 100 ml of dextrose 5% water (D5W) over about 30 min (Peloquin 1991). RIF is cleared by arylacetamide deacetylase, predominantly in the liver, with about 10% or less cleared by the kidneys (Nakajima et al. 2011). RIF can produce hepatotoxicity at a rate that appears to be less than those seen with either PZA or INH (American Thoracic Society/Centers for Disease Control/Infectious Disease Society of America 2003; Peloquin and Namdar 2011). RIF's hepatotoxicity seems to be additive with that of INH. With intermittent regimens, especially when given at higher doses (ex. 1200 mg twice weekly), flu-like symptoms can be observed. A couple of hours after the dose, the patient will start to feel nauseated, they may or may not be febrile, and in extreme cases, the patient may be hypotensive. Some flu-like syndrome patients may have anemia or renal failure, and in such extreme cases, RIF should not be reintroduced.

RBN is a cousin of RIF, and is generally used instead of RIF for HIV-positive patients (American Thoracic Society/Centers for Disease Control/Infectious Disease Society of America 2003; Namdar and Peloquin 2011; Peloquin and Namdar 2011). The reason is that, compared to RIF, RBN has less of an effect on hepatic enzyme induction, and therefore has lower extents of drug–drug interactions with the HIV drugs. RBN has the same mechanism of action as RIF, so there is no advantage against the vast majority of RIF-resistant isolates. There might be a small

number of isolates that are RBN susceptible while being RIF resistant. By and large, however, resistance is a class effect, and you will see resistance to RIF, RPNT, and RBN simultaneously. RBN currently is administered only orally. The typical dose is 300 mg. Because RBN can be the object of drug–drug interactions, in a manner not seen with RIF or RPNT, sometimes the RBN dose must either be increased or decreased to be used compatibly with some of the other drugs. This is particularly true with some of the HIV drugs. RBN is cleared, in part, by esterases, similarly to RIF. However, unlike RIF and RPNT, RBN is cleared by cytochrome P450 3A4 (CYP 3A4), and its desacetyl metabolite is completely cleared by CYP 3A4 (Namdar and Peloquin 2011). That is the reason why RBN not only is an inducer of enzymes, causing drug–drug interactions, but also can be the object of drug–drug interactions because of its clearance mechanism. Therefore, RBN is a little bit tricky to use. RBN also has concentration-related toxicities, and these further distinguish it from the other drugs in its class. RBN can produce neutropenia, thrombocytopenia, and anterior uveitis, in particular when its concentrations or the combined concentrations of the parent and desacetyl-metabolite exceed 1 mcg/ml. This is a concentration-related effect making RBN different than RIF or RPNT, and it is something that can be managed by dose reduction when it occurs.

It is possible to compare key features of the rifamycins (Burman et al. 2001; Namdar and Peloquin 2011). First, RBN and RPNT have comparable in vitro activity (MIC around 0.6 mcg/ml), and they are on the order of two to four times more potent than RIF based on mcg/ml MIC. If we look at the total (protein-bound plus protein-unbound) maximum concentration [*C*max] in plasma, both RIF and RPNT are in the teens (perhaps 12 and 16 mcg/ml, respectively). Both are much higher than the *C*max seen with RBN in humans, which is around 0.5 mcg/ml. The total drug *C*max/MIC ratio makes it appear that RPNT is substantially more potent than RIF. But this is the total drug, not the active free drug. RPNT is the highest protein-bound drug, more than 98% in the literature, and about 99% observed in our laboratory studies. RIF is about 80–85% protein bound, which may more than compensate for the higher RIF MIC when one calculates *f*Cmax/MIC. Thus, the most potent rifamycin is still a matter of debate and study (Rosenthal et al. 2007; Dutta et al. 2012).

Finally, we see differences among the rifamycin elimination half-lives (Peloquin 1991; Peloquin et al. 1997; Burman et al. 2001). RBN has biphasic elimination, and the longest terminal elimination half-life, around 36 h. RIF and RPNT generally show monophasic decays. RPNT's half-life is about five times longer than RIF's (15 h vs. ≤3 h, respectively). So, with single daily dosing of RIF, nearly all the drug is eliminated within 24 h. That is not the case for either RBN or RPNT (Weiner et al. 2004; Boulanger et al. 2009).

The rifamycins also have some unique features. Protein binding was mentioned above. The rifamycins have a varying degree of potential for hepatic enzyme induction, and in particular, the induction of CYP3A4 (Burman et al. 2001; Namdar and Peloquin 2011). As most readers know too well, CYP3A4 is responsible for the metabolism of about half of all drugs that are eliminated hepatically. So, we are particularly concerned about drug interactions at that enzyme. RIF is one of the most

potent enzyme inducers known to man, and RPNT is very similar in its potency. Whether RPNT is somewhat less potent, equally potent, or more potent than RIF depends on the dosing regimen studied for RPNT. Initially, RPNT was studied for once-weekly or twice-weekly dosing. Under those conditions, it seemed to be less potent than RIF. However, now that RPNT is being tested for daily dosing, it appears to be at least as potent as RIF as a hepatic enzyme inducer. There is no advantage of RPNT relative to RIF in that regard. However, there is an advantage with RBN, and that is why it is used (American Thoracic Society/Centers for Disease Control/Infectious Disease Society of America 2003; Namdar and Peloquin 2011; Peloquin and Namdar 2011). If you must use a rifamycin along with other drugs, be they HIV drugs or antifungal drugs or cardiovascular drugs, then there is profound potential for drug–drug interactions. Those interactions are going to affect the therapy upon which a patient is already established. RBN may be the preferred rifamycin in that case. Looking at additional unique features, we can see that, of the three drugs, the flu-like syndrome is best described with high, intermittent doses of RIF, such as 1800 mg once weekly or 1200 mg twice weekly. There is some signal for flu-like syndrome with RPNT, and that is still being studied, since there is a much smaller clinical experience with RPNT. The most important features about RBN are the concentration-related toxicities mentioned previously viz. anterior uveitis and neutropenia. These concentration-related toxicities are not seen with RIF and RPNT.

PZA was developed in the 1950s and initially used at relatively high daily doses of 50 mg/kg daily or higher (Peloquin 1991). There was a very high rate of hepatotoxicity seen at that time, and PZA was put on the shelf for a very long time. The British Medical Research Council (BMRC) pulled PZA back off the shelf in the late 1960s and early 1970s, and performed lower dose experiments with it in combination with RIF and INH. They subsequently came up with what we now consider the standard regimen for TB using at least three drugs: INH, RIF, and PZA. Typically, EMB is considered as a fourth drug (American Thoracic Society/Centers for Disease Control/Infectious Disease Society of America 2003; Peloquin and Namdar 2011). PZA can be thought of as a highly specialized drug, perhaps a ninja. The theory is that PZA interacts with microorganisms in an acidic environment, where other drugs really are not effective. PZA typically is used for the first two months of treatment, followed by the combination of INH and RIF to complete the six months of treatment. In clinical trials of patient with drug-susceptible TB, continued use of PZA beyond the first 2 months of treatment (initial phase) did not improve the outcomes achieved with INH and RIF only during the remaining four months of treatment (continuation phase; American Thoracic Society/Centers for Disease Control/Infectious Disease Society of America 2003; Peloquin and Namdar 2011). The situation can be quite different with regimens for MDR-TB, where INH and RIF are no longer effective. In such situations, PZA typically is used for the entire duration of treatment, often lasting 18–24 months. A typical PZA dose is 25–30 mg/kg, although the original study doses were somewhat higher, around 35 mg/kg daily for the treatment of TB (American Thoracic Society/Centers for Disease Control/Infectious Disease Society of America 2003; Peloquin and Namdar 2011). PZA is cleared by the liver, and PZA metabolites are excreted via the kidneys (Peloquin 1991; Peloquin et al. 1997). PZA

is known to be hepatotoxic, and its hepatotoxicity tends to last longer than that seen with INH and with RIF. If patients are being treated with PZA, they will have an elevated level of serum uric acid, not necessarily to the level that would produce gout, but it will be elevated. Thus, PZA is a great measure of adherence for patients who are not on directly observed therapy (DOT). If the patient says "oh yes, doc, I am taking those medications every day," and if he/she has normal level of serum uric acid, then the patient is not telling the truth.

EMB generally is given as the fourth drug, at the beginning of treatment, until susceptibility data are available (American Thoracic Society/Centers for Disease Control/Infectious Disease Society of America 2003; Peloquin and Namdar 2011). The initial treatment of a typical patient with TB is empiric, based on the probability of certain types of drug resistance, and that treatment usually will involve INH, RIF, PZA, and EMB. Once it is shown that the patient's isolate is fully drug susceptible, there is no need to continue the EMB treatment at that point. EMB is an inhibitor of cell wall synthesis. It is available only as an oral form in the USA; there is an i.v. form available in Europe. The typical doses are 15–25 mg/kg, though in clinical trials, doses of 12 mg/kg or less were no different from placebo. So, one may consider 25 mg/kg, especially at the initial part of therapy (Zhu et al. 2004). Caution is advised in adults and children who have renal dysfunction. While EMB does have some hepatic clearance, it is predominantly cleared by the kidneys and it can accumulate in patients with reduced renal clearance (Peloquin 1991; Zhu et al. 2004). If one provides standard daily doses to a patient with renal dysfunction, the patient may experience serious ocular toxicity. There are cases reported of patients going blind permanently because of such toxicity. It is best to check the patient's visual performance with Snellen letter charts and Ishihara color plates on a regular basis during EMB treatment as a screening test for visual function. Further, ask the patients to report if they have any difficulty in reading any kind of text, whether it is on their food packages or in newsprint, as an early warning system for visual changes (American Thoracic Society/Centers for Disease Control/Infectious Disease Society of America 2003; Peloquin and Namdar 2011).

SM was one of the first two TB drugs discovered, and for a long time was a first-line drug, with INH and PAS. Later, it was used as an alternative to EMB as the fourth drug in the initial regimen, along with INH, RIF, and PZA (American Thoracic Society/Centers for Disease Control/Infectious Disease Society of America 2003; Peloquin and Namdar 2011). Because one must give SM either intramuscularly or intravenously, it is less popular than EMB, especially in developing countries, where access to clean needles can be a challenge. In such cases, EMB, which is orally administered, would be the preferred agent. Like the other aminoglycosides, SM inhibits protein synthesis. Typical doses are 15 mg/kg daily. There are other regimens where the SM dose is 25 mg/kg given two or three times a week (Peloquin et al. 2004). Like the other aminoglycosides, SM is eliminated through the kidneys, and it will accumulate in patients who have renal dysfunction (Zhu et al. 2001b). Any patient can experience either of the two forms of ototoxicity: vestibular damage or hearing loss. Nephrotoxicity, as with the other aminoglycosides, can occur, and usually manifests as increase in serum creatinine. Since

SM is dosed daily or intermittently, nephrotoxicity generally is mild and reversible, even when continued therapy is essential. Finally, cation losses including potassium, calcium, and magnesium also can occur with the aminoglycosides. These electrolytes along with the serum creatinine should be checked periodically during treatment (Peloquin et al. 2004).

AK, KM, and CM are alternative injectable agents (American Thoracic Society/Centers for Disease Control/Infectious Disease Society of America 2003; Peloquin and Namdar 2011; Loeffler et al. 2012). These would be used when resistance to SM has been shown. AK was derived from KM, and they share very similar chemical structures. The toxicity profile and the pharmacokinetic (PK) profile of these three drugs are similar to SM. CM technically is not an aminoglycoside; it is a polypeptide. Because it so similar to the aminoglycosides in terms of dose, route of administration, PK, and toxicity, it tends to be put in the same category of "injectable agents" for TB (Peloquin 1991; American Thoracic Society/Centers for Disease Control/Infectious Disease Society of America 2003; Peloquin and Namdar 2011; Loeffler et al. 2012). These drugs are increasingly used in cases of MDR-TB (American Thoracic Society/Centers for Disease Control/Infectious Disease Society of America 2003; Peloquin and Namdar 2011). In the case of XDR-TB, by definition, resistance to at least one of the injectable agents will be observed (Peloquin and Namdar 2011; Lauzardo and Peloquin 2012; Dooley et al. 2013). It is possible to have limited, selected drug susceptibility to one injectable agent despite resistance to some of the others. In cases of MDR-TB and XDR-TB, it is highly recommended that an expert on TB is consulted as drug options are limited and careful management is necessary.

LEVO is one of two or perhaps three fluoroquinolones that typically are used when a member of this drug class is required for the treatment of drug-resistant TB (American Thoracic Society/Centers for Disease Control/Infectious Disease Society of America 2003; Johnson et al. 2006; Peloquin and Namdar 2011; Lauzardo and Peloquin 2012). The quinolones are not considered first-line agents at this time: They have not proven to be better than INH, they are more expensive than INH, and they have broader spectra of antimicrobial activity than INH and are more likely to alter the host's normal flora. As a class, they inhibit DNA gyrase. LEVO can be administered orally or intravenously, and typical doses for TB are 750–1000 mg once daily. LEVO is highly dependent on renal elimination, so caution must be exercised in patients who have renal dysfunction (American Thoracic Society/Centers for Disease Control/Infectious Disease Society of America 2003; Peloquin et al. 2008; Peloquin and Namdar 2011; Lauzardo and Peloquin 2012). In those patients, MOXI may be the preferred agent, because MOXI is not entirely dependent on renal clearance. The fluoroquinolones have a variety of toxicities, which tend to be class effects. Among those are caffeine-like stimulatory properties of the central nervous system (CNS). They also can cause nausea, vomiting, and diarrhea. Quinolones can cause tendinitis, and this is particularly a concern in older patients, or patients receiving corticosteroids. Particular caution has to be exercised in these patients, since Achilles tendon ruptures have been reported on numerous occasions with the fluoroquinolones. MOXI generally is given at a dose of 400 mg once daily.

It has been shown using in vitro and animal models that higher doses of MOXI might be more effective. However, there are concerns about concentration-related toxicities with MOXI, including corrected QT (QTc) interval prolongation. At least for the time being, the typical dose for patients who receive MOXI for TB is 400 mg once daily, and in general the drug has been used safely for TB (Takiff and Guerrero 2011; Loeffler et al. 2012). As mentioned earlier, because MOXI is cleared both hepatically and renally, it can be an alternative to patients who have renal dysfunction. The toxicity profile of MOXI is very similar to that seen with LEVO, although there is some suggestion that MOXI may have a greater effect on QTc. GATI is not available in the USA, but continues to be studied for TB outside the USA (Rustomjee et al. 2008). It can be used in cases of MDR-TB in those countries where it is available.

We will now consider some of the second-line TB drugs, and there are good reasons why these are second-line agents. ETA has a mechanism of action that is similar in some regards to that of INH. There are situations where cross-resistance is observed (Machado et al. 2013). Similar to INH, ETA is a pro-drug and undergoes bio-activation inside the mycobacteria to its active form that subsequently inhibits the processes leading up to cell wall synthesis. ETA is an oral drug. Typical doses are 250–500 mg twice daily, if possible, though if one is going to use DOT, twice daily dosing does present some difficulties (Peloquin 1991; Loeffler et al. 2012). ETA is extensively metabolized in the liver. One of the metabolites is an active sulfoxide metabolite that can interconvert with the parent drug (Jenner et al. 1984; Peloquin 1991). ETA causes profound gastrointestinal distress. It causes nausea in most patients and vomiting in some patients. ETA also is associated with significant amount of hypothyroidism, the latter is more pronounced in patients who receive both ETA and PAS together (American Thoracic Society/Centers for Disease Control/Infectious Disease Society of America 2003; Loeffler et al. 2012).

PAS was the first TB drug discovered. Its mechanism of action remains a matter of controversy, and for purposes of this discussion, it is not essential. PAS is an oral drug (Peloquin 1991; American Thoracic Society/Centers for Disease Control/Infectious Disease Society of America 2003; Peloquin and Namdar 2011; Loeffler et al. 2012). Taking the original tablet dosage form was much like high-dose aspirin. PAS is a close chemical derivative of aspirin, and it can cause stomach distress. Taking high doses, up to 12 g per day of PAS tablets causes about as much nausea, and sometimes vomiting, as seen with high doses of aspirin. There is a granule dosage form, which is an enteric-coated, sustained-release dosage form known as PASER®, and those granules generally are administered as a packet of small beads. The beads can be sprinkled into the mouth and swallowed with a beverage. Alternatively, it can be mixed with soft food and swallowed without chewing. These processes are repeated until the entire contents of the packets are consumed. Generally, twice daily dosing would be preferred, and up to three times daily dosing with PAS may be safely used (Peloquin et al. 1999). It is metabolized by NAT1, as opposed to NAT2 for INH (Peloquin 1991). PAS metabolites are cleared through the kidneys, but the parent drug appears to be cleared predominantly by the liver (Malone et al. 1999). GI upset and diarrhea may occur, and as in the case of ETA, hypothyroidism

is a concern. If one gives the two drugs together to the same patient, testing for thyroid function is required, and thyroid supplements might need to be administered to some patients.

CS is a difficult drug to for many patients to tolerate, due to its CNS toxicities (American Thoracic Society/Centers for Disease Control/Infectious Disease Society of America 2003; Loeffler et al. 2012). It inhibits cell wall synthesis upstream of the beta-lactam antibiotics' site of action in the process of producing the peptidoglycan. CS is available as an oral drug. Typical doses are similar to those for ETA: 250–500 mg once or twice daily. Twice daily may be preferred, but again, under DOT conditions, twice daily dosing can be very challenging. CS is predominantly eliminated via renal route, so it can accumulate in patients who have renal dysfunction (Peloquin 1991; Zhu et al. 2001). Such a situation would best be handled by monitoring the serum concentrations of CS. Virtually everyone who takes CS is going to have some form of CNS toxicity. The most common forms are lethargy and the inability to concentrate; sometimes, this progresses to altered behavior. Frank seizures have been described, although at least in the experience of clinicians in the USA those tend to be extremely rare. Higher incidences of seizures have been reported out of South Africa, where they also use terizidone, a derivative of CS. Because CNS toxicities are of concern with CS, and patients should be monitored closely for changes in behavior.

11.4 How Do Antibiotics Work? PK and Pharmacodynamics

Now that we have introduced the TB drugs, let us step back and consider what we are trying to accomplish with them. Here is a basic statement of how the antibiotics work: For every drug with a proven mechanism of action, this action involves the drug contacting or entering the pathogenic organism, binding physically to an intracellular target, and producing either an inhibitory or a lethal effect. This is true for all classes of antibiotics, against all classes of organisms, and is not unique to Gram-positive or Gram-negative bacteria. This also is true when we are trying to treat TB.

We acknowledge that, for every drug given either orally or parenterally, the only way for the drug to reach the pathogenic organism is through the blood stream. Unlike simple abrasions on the surface of the skin that can be addressed with topical drugs, in systemic infections such as TB, we generally cannot instill the drug directly at the site(s) of infection because the sites are not in a readily accessible. Hence, TB drugs are administered orally, intramuscularly, or intravenously. In all of these routes of administration, the drugs have to go through the blood stream to get to the site(s) of infection. Given this situation, the conclusion can be simply put: "If it isn't in the blood, it isn't in the bug." The only way to deliver the vast majority of drugs is through the blood stream. Underdosing can lead to drug resistance and clinical failures, while for some drugs, overdosing can lead to overt toxicity. Therefore, it is important to understand and use knowledge of each drug PK in the treatment of bacterial infections, including the treatment of TB (Peloquin 1991).

PK is the study of the movement of drugs through the body. In most cases, we are going to be looking at serum concentrations, because they are readily available. One can get serum concentrations much more easily than tissue or fluid concentrations at site(s) of infection. Obtaining the latter tends to be much more invasive, and in many situations, one simply cannot access those sites. We rely on the use of serum concentrations as surrogates for determining what is happening at the site of infection. We can use the serum concentration to interpret how well the PK are working in a particular patient, compared to what was anticipated based on prior experience in other patients, and we can use this kind of information to adjust doses.

Extending these concepts further, we now turn to pharmacodynamics (PD). PD is the study of the relationships between the drug concentrations and the corresponding observed physiological responses, either efficacy or toxicity (Drusano 2007; Mouton et al. 2011). When we are assessing antibiotics, we typically have three primary methods available to us for determining the PD of the drug. We have in vitro models, which tend to be the simplest and least expensive. Animal models add to that an immune system. One can study mice, guinea pigs, rabbits, or other species for TB, with and without effective immune systems. And, one can give a wider range of supraphysiological doses in these models than one might administer in the clinic. Animal models often are more expensive and more complicated than in vitro models, but they give us additional pieces of information, including activity within a mammalian system. Further modifications to the model, using knockout species or chemotherapeutic pretreatment, can explore drug activity in the model plus or minus an immune system. Finally, once we have selected a suitable range of human doses based on data from the in vitro and animal methods as well as using mathematical modeling for human dose estimation, we then proceed to clinical trials. By including dose escalation in clinical trials, we can determine the optimal dose of each drug that we want to use going forward in phase 2B or phase 3 clinical trials, and ultimately, in the clinical management of TB (Nuermberger and Grosset 2004; Davies and Nuermberger 2008).

The PK/PD relationship can best be explained by considering a graph of probability of a response on the *y* axis and increasing drug concentration on the *x* axis (Fig. 11.1). There can be two different response curves constructed—one for efficacy, and one for concentration-related toxicity (Peloquin 2001). These curves can represent an individual, or the curves can represent a typical or median response observed in subject population. We are looking for two things when we examine these curves: We want the therapeutic response curve to approach 100 %, and we want the toxicity curve to be shifted towards higher concentrations than the response curve (shifted to the right). Not all drugs show concentration-related toxicity in or near the range of clinically effective plasma concentrations, but for some drugs, there clearly is overlap of the effective and toxic ranges. While undesirable, for serious diseases with limited therapeutic options, sometimes this is the best that we can do. Nevertheless, these kinds of curves can be seen with the vast majority of drugs that we use, across all kinds of disease states. The aim is to maximize the therapeutic response while minimizing the toxic response of the drugs. In a hypothetical example, serum concentrations between 20 and 30 mcg/ml give us a high probability of the

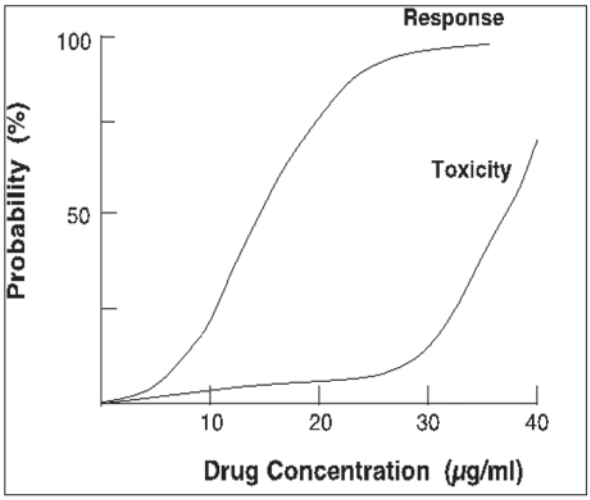

Fig. 11.1 PK/PD relationships displayed as the probability of a response (y) versus increasing drug concentration (x). (Reprinted with permission from Annals of the New York Academy of Science 2001; 953: 157–164)

desired response, while giving us a low probability of concentration-related toxicities. Certain toxicities, such as rashes, really are not concentration-related per se. If you give any therapeutic amount of the drug, allergic reactions can occur. But for other drugs such as EMB, ocular toxicity clearly increases as serum concentrations exceed normal values with daily doses. Thus, for EMB, serum concentrations can inform both efficacy and toxicity.

There are three most common PD parameters that can be used to describe the activity of antimicrobial agents. These include the free drug *C*max to the MIC ratio (*fC*max/MIC), duration of time when free concentrations remain above the MIC (*f*T > MIC), and the *f*AUC above the MIC (*f*AUC > MIC; Nuermberger 2004; Drusano 2007; Davies and Nuermberger 2008; Mouton 2011). These three parameters are used most commonly for assessing the potency of the antimicrobial agent, and this information is helpful for dosing purposes.

Figure 11.2 gives a graphical representation of the parameters just mentioned. In this hypothetical example, the gray line is the concentration versus time curve and the MIC depicted with a green line. Let us assume that this drug has very low protein binding, so the values represent free drug. The *fC*max is about 9 mcg/ml and MIC is 3 mcg/ml; therefore, the *fC*max/MIC ratio is 3. The duration of time above MIC is the time when the gray line rises above and then falls below the green MIC line, and in this case, it is about 8 h. The *f*AUC > MIC also can be calculated, and is that portion of the AUC which is above the green line. It is important to note that the concentrations described in this example are measures of in vivo drug exposure, and the MIC is an in vitro measure. So, during the construction of these relationships, it is important to bear in mind that these are distinct parameters that are estimated from two different methods. This is an imperfect approach; however, because direct in vivo MIC measurement in the patient is not feasible, one has to use the isolate taken from that patient and test it in vitro. Generally, for TB patients,

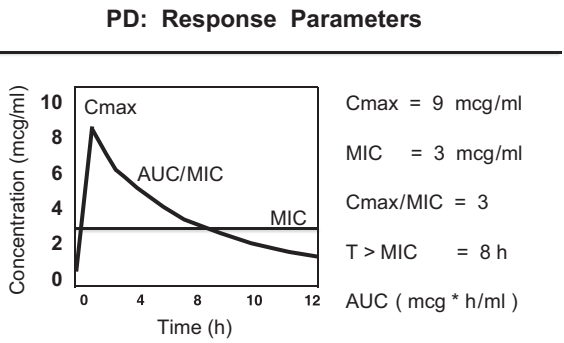

Fig. 11.2 PK/PD relationships displayed as antibiotic exposure in a patient relative to the minimal inhibitory concentration of a pathogen determined in vitro

the isolate is contained in expectorated sputum, and is evaluated in the laboratory. Ideally, we would have an MIC value to work with. Unfortunately, most clinical laboratories test a single breakpoint concentration, the so-called critical concentration, to differentiate "wild type" from "resistant" organisms. Therefore, while a TB isolate may be considered "susceptible," we typically do not know *how* susceptible. If the MICs for a given drug vary of a tenfold range, then the PD parameters above also vary widely from patient to patient. It is easy to imagine that one patient has an *f*Cmax/MIC ratio of 20, while the next patient has a ratio of 2. For most antibiotics, we would not expect the same outcome with such disparate drug potency. Unfortunately, with TB, we generally have to work in the dark regarding these factors.

11.5 Specific Examples of TB Drug PK/PD

We will apply the PK/PD concepts just presented to TB drugs. Let us take a look at INH, one of the primary drugs for the treatment of TB. With INH, there always is a high *f*Cmax/MIC ratio with normal absorption (Peloquin et al. 1997). This is true either in slow acetylators (those patients who have deficient amounts of NAT2), where the drug remains in the serum longer, or in fast acetylators. This occurs because the MIC is so low, roughly 0.01 mcg/ml (Heifets 1991). We have very good values of PD parameters with INH, whether we look at the *f*Cmax/MIC or the *f*AUC > MIC or even *f*T > MIC, particularly in the slow acetylator. So, by all of these measures, INH is a particularly potent drug.

Now let us consider ETA, a second-line drug for TB. And it is a second-line drug not only because it has a higher rate of toxicity, including nausea and hypothyroidism, but due to its undesirable PD (Jenner et al. 1984; Auclair et al. 2001). ETA serum concentrations barely get above the MIC needed for the treatment of TB, and they quickly fall below the MIC (Heifets 1991; Auclair et al. 2001). The MIC for ETA is one or two orders of magnitude higher than what is observed for INH. However, if these two drugs were reversed in their PD, such that ETA had great PD despite its toxicity, ETA would be considered a first-line agent. If INH had the low

potency seen with ETA, then INH would be considered a second line even though it is better tolerated than ETA. This is the primary complication: good or bad PK/PD. While the second-line drugs are considered as being potentially more toxic, and that is true in majority of the cases, the main point in the case of TB treatment is that the second-line drugs are less potent.

Drugs that show "concentration-dependent" antimicrobial activity are those that show increasing activity with increasing concentrations. (Drusano 2007; Mouton et al. 2011; Nuermberger and Grosset 2004; Davies and Nuermberger 2008) This might track better with *f*AUC/MIC for some, and *fC*max/MIC for others, but typically, both measures are useful for "concentration-dependent" drugs. Typically, these are drugs that we give as large, single daily doses, because we want to take advantage of *fC*max/MIC ratios. Typically, we want that ratio to be at least 10 or 12 to 1. Examples of such drugs would be the aminoglycosides. For bacterial infections, aminoglycosides now are all dosed once daily, and not every 8 h, as was done previously. This allows for better killing, and for lower trough concentrations with potentially lower nephrotoxicity. This approach of using larger, intermittent also is observed with the fluoroquinolones, and this has clearly been demonstrated in a variety of models and in the clinical setting (Drusano 2007; Mouton et al. 2011). But not commonly discussed in this context is the fact that the rifamycins show profound concentration-dependent bactericidal activity (Jayaram et al. 2003; Peloquin 2003; Lauzardo and Peloquin 2012). Unfortunately, this is not reflected in the way we currently dose these drugs.

11.6 Rifamycins and Their Concentration-Dependent Activity

Figure 11.3 provides a particular example of the "concentration-dependent" activity of RIF performed by Ludo Verbist, and published in 1969 (Verbist 1969). A standardized infectious dose of about 100×10^6 pathogenic organisms were administered to all these mice. The RIF amounts administered in mice were 5, 10, 20, and 40 mg/kg. The mice were sacrificed on week ten of treatment, and their spleens and lungs were examined to determine the number of colony forming units (CFUs) remaining. At the 5 mg/kg dose, there were a lot of TB CFUs present in these animals. But as the dose increased, the number of CFUs decreased. At 40 mg/kg, no pathogenic organisms could be cultured in vitro. Thus, it suggests that an RIF dose of 40 mg/kg would be ideal in patients. However, the current dose in humans is only 10 mg/kg.

Beginning in the early 2000s, the author and other TB researchers around the world started reexamining the older literature to see if we were actually giving the correct dose of RIF. Figure 11.4 shows some very nice work by Jayaram and colleagues from AstraZeneca (Bangalore, India; Jayaram et al. 2003). They showed similar data to that from Ludo Verbist in his 1969 paper (Verbist 1969). We have a concentration–response curve similar to what was described earlier. There is a sigmoid-shaped response curve, with low killing potency at the top left to high

PD: Sterilizing Activity of Rifampin

Week	5 mg/kg	10 mg/kg	20 mg/kg	40 mg/kg
Lung CFU week 1	100,000,000	100,000,000	100,000,000	100,000,000
Lung CFU week 10	10,000	100	10	0
% reduction	99.99000%	99.99990%	99.99999%	100.00000%

Fig. 11.3 Concentration–response relationship of rifampin, leading to sterilizing activity, from early studies of rifampin. (Data from Verbist L. Acta Tuberculosa et Phneumolgia Belgica 1969; no. 3–4:397–412)

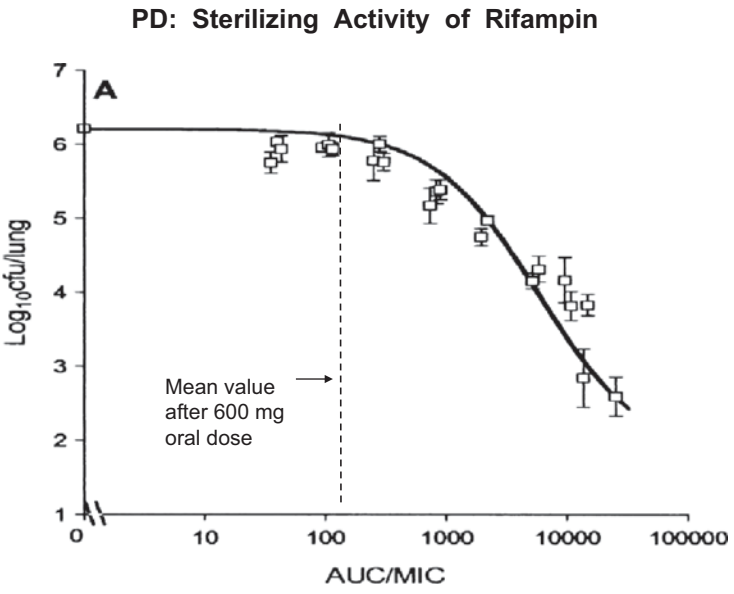

Fig. 11.4 Concentration–response relationship of rifampin, from recent studies of rifampin. (Reprinted with permission from Jayaram et al. 2003, courtesy of E. Nuermberger)

killing potency at the bottom right. Note that there is a plateau in the response at low drug concentrations, and these low drug concentrations correspond to the clinically relevant concentrations currently obtained in humans with 600 mg doses. If one were to plot the data produced by Ludo Verbist, a similar graph would be observed (Verbist 1969). Also, note that in the Jayaram mouse model, one cannot observe a clear plateau at higher AUC/MIC (Jayaram et al. 2003). The authors determined the toxicity threshold before they were able to determine the maximum effective dose.

The lesson for human dosing is that, in order to have maximum efficacy with RIF, one really needs to give much higher doses (Peloquin 2003; Mitnick et al. 2009; Lauzardo and Peloquin 2012).

Returning to the summary of PD again (Fig. 11.1), one would like to raise the response curve without any increase in the toxicity curve. Right now, it appears that we can achieve this with RIF. There are groups of researchers studying patients both in South America and in Africa to see just how high a dose of RIF can be administered in order to maximize the response without producing overt toxicity (Martin Boeree et al. 2013).

11.7 Specific Clinical Examples of Rifamycin PK/PD

The current treatment regimen for TB is based on the work done by the BMRC and colleagues (Fox et al. 1999). A key study was published in British Journal of Diseases of the Chest in 1981 (British Thoracic Association 1981). For patients who received either SM (1000 mg) or EMB (25 mg/kg) added to a core of INH, RIF, and PZA (35 mg/kg), the responses were very similar. The measure of activity or response was the percentage of patients who went from being sputum culture positive to sputum culture negative at 1, 2, and 3 months. For the two patient groups, these percentages were 35–38, 77, and 97–99 %. Note that the PZA dose was 35 mg/kg; current US guidelines from the American Thoracic Society (ATS)/Center for Disease Control (CDC)/Infectious Diseases Society of America (IDSA) often recommend smaller doses of 20–25 mg/kg, not what was studied in the original trials (American Thoracic Society/Centers for Disease Control/Infectious Disease Society of America 2003). Also, note that the EMB dose was 25 mg/kg whereas in the USA a 15 mg/kg is commonly used (American Thoracic Society/Centers for Disease Control/Infectious Disease Society of America 2003). While the intentions behind these dose reductions in the USA were good (to reduce toxicities), they are not data driven (Peloquin 1991; American Thoracic Society/Centers for Disease Control/Infectious Disease Society of America 2003; Peloquin and Namdar 2011; Lauzardo and Peloquin 2012; Martin Boeree et al. 2013). There was an assumption that one could move down the toxicity curve without affecting the response curve. Using Fig. 11.1, it is assumed that the response curve is shifted dramatically to the left, creating a near certainty of complete response at any clinically relevant concentration. Unfortunately, there is no reason to believe that is true, based on available clinical data. A more reasonable expectation is that one would be moving down both of those curves with a dose reduction.

Let us now compare the work that we just discussed from the BMRC to a paper published by Kreis and Pretet in 1976 (Kreis et al. 1976). This study used INH, RIF, and SM, but not EMB or PZA. All patients received daily SM at 1000 mg and INH 900 mg daily or every other day, which is different from the standard 300 mg of INH daily. Patients also received 1200 mg of RIF rather than the standard 600 mg daily or every other day. Responses were similar in both groups, but the response

occurred about a month earlier than those in the BMRC trial. Patients were clearing the organisms at a faster rate than they did in the BMRC study. Here, at 1, 2, and 3 months, the two groups showed the following percentages of culture-negative patients: 70–72, 93–94, and 98–100 %. Since these are two separate studies, it is not appropriate to do a direct statistical comparison of the results. Nevertheless, it is representative of what we might expect should we escalate the doses of RIF from 600 to 1200 mg. Kreis and Pretet generated these superior results even in the absence of PZA. Recall that we used PZA typically in the first two months of treatment. The addition of PZA allowed the 9-month regimen of INH and RIF to be shortened to a 6-month regimen. PZA adds about 10–13 % to the 2-month culture-negativity rate. Thus, PZA has sterilizing activity to contribute, but Kreis and Pretet did not include PZA. Based on these data, the high-dose study groups are reasonably optimistic that better results can be obtained by taking advantage of RIF's "concentration-dependent" activity in new clinical trials.

Earlier, we reviewed the fact that RIF can produce a flu-like syndrome if it is given in high intermittent doses (American Thoracic Society/Centers for Disease Control/Infectious Disease Society of America 2003; Peloquin 2003; Lauzardo and Peloquin 2012). In the study by Kreis and Pretet, by giving RIF either daily or every other day for 3 months, there were no reports of any patient experiencing flu-like syndromes. Further, in the early studies of high dose, once weekly and twice weekly RIF, the flu-like syndrome typically was not seen until 3 months or more into treatment. Thus, in at least the first 2 months of therapy, high doses of RIF probably will not produce the issue of the flu-like syndrome (Martin Boeree et al. 2013). Nevertheless, patients will be followed closely for this potential adverse drug reaction in current clinical trials of high-dose RIF (Martin Boeree et al. 2013; Trial of High-Dose Rifampin in Patients With TB 2013).

The PK/PD approach described above included finding the most important PK/PD parameter using models, followed by dose-escalation studies in humans to optimize this parameter (Drusano 2007; Davies and Nuermberger 2008). Unfortunately, that approach was not closely followed with most of the original TB drug trials (Fox et al. 1999; Iseman 2000; American Thoracic Society/Centers for Disease Control/Infectious Disease Society of America 2003). While some PK/PD data do exist, it is a challenge to clearly define the two response curves (efficacy and toxicity) for many of the TB drugs (Weiner et al. 2003, 2005). We have managed to define the usual PK for the various drugs, and we continue to strive to link this more closely to the PD of the drugs (Peloquin 2001, 2002). Current TB studies now incorporate PK and PD assessments. Data available from prior and recent clinical trials can be utilized to show that, indeed, just like other antibiotics for bacterial infections, the TB drugs truly do show definable PK/PD responses.

Let us examine one such clinical study, conducted by the CDC TB Trials Consortium (TBTC). The parent study was study 23, and study 23A was the PK sub-study. Published in 2005, this study examined the association between acquired rifamycin resistance (typically abbreviated as ARR) in the context of HIV-associated TB (Weiner et al. 2005). Specifically, it examined the association between ARR and the PK of RBN and INH among patients with both TB and HIV. ARR is the worst-case

scenario in the treatment of drug-susceptible TB. First, the patient is not cured and now requires a lengthy re-treatment. There is a risk of toxicity, a risk of losing the patient to follow-up, and a risk of continued spread of TB in the community. If that was not bad enough, we also have lost the use of the rifamycins, the drugs that make a 6-month or even a 9-month regimen possible. This is the therapeutic equivalent of MDR-TB. We may be looking at an 18-month re-treatment regimen. So, we really want to avoid the generation of ARR, and proper doses and frequencies of the drugs are critical (Peloquin 2002; Weiner et al. 2005; Boulanger et al. 2009).

In study 23A, we found the differences in responses based upon the INH AUC and *C*max. The highest AUC (52.9 mg*h/ml) values were observed in the cured, HIV-negative patients in a prior TBTC study, study 22. Lower INH AUC values (28.0 mg*h/ml) were reported for the HIV-positive patients in study 23A; these patients also were cured. Finally, six patients in study 23A not only failed treatment but did so with ARR; these patients had the lowest INH AUC (20.6 mg*h/ml; Weiner et al. 2005).

Not only did study 23A show that there was a measurable concentration response for INH at the doses we currently use clinically; it showed the same thing for RBN. Again, all of the patients in this study are HIV-positive. The 82 cured patients had higher RBN AUC values (5.1 mg*h/ml). The six patients in study 23A who failed treatment, and had ARR, showed lower RBN AUC (3.1 mg*h/ml, $p = 0.04$). While CD4 count was associated with poor outcomes in the parent study, when controlled for drug exposure, the odds ratio for ARR based on CD4 count was 1.01. In contrast, odds ratio for ARR based on RBN AUC was 23. Clearly, drug malabsorption was a key factor in the selection of ARR—a scenario that is entirely avoidable with prospective therapeutic drug monitoring (TDM) and dose adjustment.

11.8 Recap

Let us now recap what we have learned. Not all of the TB drugs are FDA approved for that indication. Some of the drugs that are used seem to have activity against TB, and there is a tradition of using them for TB, but controlled clinical trials are lacking for most second-line TB drugs (American Thoracic Society/Centers for Disease Control/Infectious Disease Society of America 2003; Loeffler et al. 2012). Further, the EMA and the FDA have not explicitly approved several of the drugs for TB. The "second-line" TB drugs have poor PK/PD profiles (Peloquin 1991, 2001, 2002). These are weak drugs, typically with high MICs, they have low concentrations relative to those MICs, and in addition, they tend to produce toxicities at rates higher than seen with the first-line TB drugs. But the driver behind their reserve status is that they have poor PK/PD profiles. To use TB drugs safely, one must understand how they are absorbed and how they are eliminated (Peloquin 1991; American Thoracic Society/Centers for Disease Control/Infectious Disease Society of America 2003; Peloquin and Namdar 2011). As mentioned in the cases of CS and EMB, those drugs are renally cleared, so patients with renal dysfunction are at risk of overt, concentration-related toxicity if they receive the standard daily doses.

We see that the rifamycins, and in particular RIF, currently are underdosed (Peloquin 2003; Martin Boeree et al. 2013). Higher doses are very likely to produce better bacteriological results. There is a lot of experience in hollow fiber models, other in vitro models, and in preclinical animal models that clearly show this to be the case. There are some human data available so far, and these data will be bolstered by two ongoing clinical trials that will give us a much better picture of how to use the rifamycins, and in particular RIF going forward (Martin Boeree et al. 2013; Trial of High-Dose 2013). There are ongoing studies of higher doses of RPNT as well. Those studies will inform us whether RIF or RPNT might be the preferred rifamycin in majority of patients treated for drug-susceptible TB (Dorman et al. 2012). For many HIV-positive patients who are going to be on antiretroviral therapy, RBN is going to be the preferred agent for the foreseeable future because of its lower drug–drug interaction profile. However, higher doses of RBN may not be possible because RBN has concentration-related toxicities not seen with RIF or RPNT (Boulanger et al. 2009).

We see that recent TB studies demonstrate that poor drug absorption (leading to poor PK/PD) is associated with poor outcomes clinically (Weiner et al. 2003, 2005; Boulanger et al. 2009). TB treatment tends to be driven by the guidelines, and the guidelines are very well written and immensely useful (American Thoracic Society/Centers for Disease Control/Infectious Disease Society of America 2003). However, the guidelines themselves state that they cannot possibly cover every conceivable situation that might arise in the clinic. Going forward, modeling and simulation, based on data acquired in the clinic, can help to fill in the missing pieces. Still, clinicians need to make good decisions going forward with the information currently available. Even though, historically, the PK/PD of the TB drugs have not been emphasized, new studies that show that PK/PD is at play just the same (Weiner et al. 2003, 2005; Boulanger et al. 2009). Just like antibiotics used for Gram-positive and Gram-negative bacteria, the antibiotics used for TB have to reach the site of infection, interact with the organism, and produce an inhibitory or lethal effect. Thus, all antibiotics including the TB drugs are entirely dependent on their PK/PD profiles (Peloquin 2001; Drusano 2007).

11.9 TDM and TB

There is a role for TDM in the treatment of TB (Peloquin 2001, 2002). Not every nation is going to have ready access to TDM for their patients with TB. But many nations do—the USA, the countries of Europe, South Korea, and South Africa have laboratories capable of performing these tests. TDM is available, at least under selected conditions, and that allows individualization of TB therapy. Now, it certainly is true that the standard doses and the standard regimens in the regulatory guidelines can be very effective (American Thoracic Society/Centers for Disease Control/Infectious Disease Society of America 2003). It

also is important to remember that the vast majority of that data come from the pre-HIV era, and also from the preobesity epidemic era (Fox et al. 1999; American Thoracic Society/Centers for Disease Control/Infectious Disease Society of America 2003). Patients in those studies weighed less than the patients of today. The doses that were highly effective for pre-HIV era patients may or may not be the right doses for patients today, since for drugs given at fixed milligram doses, the current mg/kg dose is lower. TDM allows for optimization of the PD-linked variable for each drug. In the case of rifamycins, this seems to be *f*Cmax/MIC or the *f*AUC/MIC. TDM also allows unraveling complicated multidrug interactions (Peloquin 2002; Boulanger et al. 2009). As previously mentioned, RBN is the preferred rifamycin for HIV-positive patients receiving concurrent antiretroviral therapy. However, also as mentioned, RBN is the object of multiple two-way interactions (Boulanger et al. 2009). Rifamycins also interact with drugs like voriconazole and other azole antifungal drugs (Schwiesow et al. 2008). So, if one finds that one has to use drugs that are known to interact, TDM provides the opportunity to measure those various drug interactions and adjust the doses accordingly. Thus, one can individualize patient treatment to maximize the benefit while minimizing the risks of adverse drug reactions.

Clinical data are accumulating that show that TDM could avoid some of the failures, relapses, and ARR seen in TB treatment, especially in HIV coinfected patients (Weiner et al. 2003, 2005; Boulanger et al. 2009). There are a variety of reasons why patients fail to respond to a therapy. Their immune system may not be able to contain the infection, they have very extensive disease progression, they have highly damaged lungs, and/or they may have meningitis where the drugs may not penetrate very well. There are a host of reasons beyond the drug-related reasons, which could lead to failure of therapy. However, the selection of the drugs and their doses are the only things we routinely control. So, one can argue that optimizing the doses and dosing regimen aids in optimizing the outcomes in the patients (Peloquin 1991, 2001, 2002).

The new regulatory guidelines for the treatment of opportunistic infections in patients who are HIV positive are now going to recommend a starting dose of RBN 150 mg daily.(http://www.cdc.gov/tb/publications/guidelines/TB_HIV_Drugs/default.htm) Previously, the recommendation was RBN 150 mg administered three times a week in the context of ritonavir-boosted protease inhibitor therapy for HIV. Conversely, if the patient is on efavirenz, a nonnucleoside reverse transcriptase inhibitor (NNRTI), a starting dose of 450 or even 600 mg of RBN is required. For such patients, it seems reasonable to measure the RBN concentrations early in the treatment, and also measure the concentrations of the protease inhibitors or the NNRTIs for HIV. One can adjust all of these drugs for a particular patient's ability to absorb and eliminate these drugs, and in doing so, hopefully optimize both categories of drugs so that the patients have good response for both, TB and HIV.

References

American Thoracic Society/Centers for Disease Control/Infectious Disease Society of America (2003) Treatment of tuberculosis. Am J Respir Crit Care Med 167:603–662

Auclair B, Nix DE, Adam RD, James GT, Peloquin CA (2001) Pharmacokinetics of ethionamide under fasting conditions, with orange juice, food, and antacids. Antimicrob Agents Chemother 45:810–814

Boulanger C, Hollender E, Farrell K, Stambaugh JJ, Maasen D, Ashkin D, Symes S, Espinoza LA, Rivero RO, Graham JJ, Peloquin CA (2009) Pharmacokinetic evaluation of rifabutin in combination with lopinavir-ritonavir in patients with HIV infection and active tuberculosis. Clin Infect Dis 49:1305–1311

British Thoracic Association (1981) A controlled trial of six months chemotherapy in pulmonary tuberculosis. First report: results during chemotherapy. Br J Dis Chest 75:141–153

Burman WJ, Gallicano K, Peloquin CA (2001) Comparative pharmacokinetics and pharmacodynamics of the rifamycin antibiotics. Clin Pharmacokinet 40:327–341

Davies GR, Nuermberger EL (2008) Pharmacokinetics and pharmacodynamics in the development of anti-tuberculosis drugs. Tuberc [Edinb] 88(Suppl 1):S65–S74

Diacon AH, Dawson R, von Groote-Bidlingmaier F, Symons G, Venter A, Donald PR, van Niekerk C, Everitt D, Winter H, Becker P, Mendel CM, Spigelman MK (2012) 14-day bactericidal activity of PA-824, bedaquiline, pyrazinamide, and moxifloxacin combinations: a randomised trial. Lancet 380:986–993

Dooley KE, Obuku EA, Durakovic N, Belitsky V, Mitnick C, Nuermberger EL, On behalf of the Efficacy Subgroup, RESIST-TB (2013) World health organization group 5 drugs for the treatment of drug-resistant tuberculosis: unclear efficacy or untapped potential? J Infect Dis 207:1352–1358

Dorman SE, Goldberg S, Stout JE, Muzanyi G, Johnson JL, Weiner M, Bozeman L, Heilig CM, Feng PJ, Moro R, Narita M, Nahid P, Ray S, Bates E, Haile B, Nuermberger EL, Vernon A, Schluger NW, Tuberculosis Trials Consortium (2012) Substitution of rifapentine for rifampin during intensive phase treatment of pulmonary tuberculosis: study 29 of the tuberculosis trials consortium. J Infect Dis 206:1030–1040

Drusano GL (2007) Pharmacokinetics and pharmacodynamics of antimicrobials. Clin Infect Dis 45(Suppl 1):S89–S95

Dutta NK, Illei PB, Peloquin CA, Pinn ML, Nuermberger EL, Karakousis PC (2012) Rifapentine is not more active than rifampin against chronic tuberculosis in guinea pigs. Antimicrob Agents Chemother 56:3726–3731

Fox W, Ellard GA, Mitchison DA (1999) Studies on the treatment of tuberculosis undertaken by the British Medical Research Council tuberculosis units, 1946–1986, with relevant subsequent publications. Int J Tuberc Lung Dis 3(10)(Suppl 2):S231–S279

Gumbo T, Louie A, Liu W, Brown D, Ambrose PG, Bhavnani SM, Drusano GL (2007) Isoniazid bactericidal activity and resistance emergence: integrating pharmacodynamics and pharmacogenomics to predict efficacy in different ethnic populations. Antimicrob Agents Chemother 51:2329–2336

Heifets L (ed) (1991) Drug susceptibility in the chemotherapy of mycobacterial infections. CRC Press, Boca Raton

Heifets L (2012) The second coming of the white plague. Tate Publ Enterp, Mustang

Iseman MD (2000) A clinician's guide to tuberculosis. Lippincott Williams and Wilkins, Philadelphia

Jayaram R, Gaonkar S, Kaur P, Suresh BL, Mahesh BN, Jayashree R, Nandi V, Bharat S, Shandil RK, Kantharaj E, Balasubramanian V (2003) Pharmacokinetics-pharmacodynamics of rifampin in an aerosol infection model of tuberculosis. Antimicrob Agents Chemother 47:2118–2124

Jenner PJ, Ellard GA, Gruer PJ, Aber VR (1984) A comparison of the blood levels and urinary excretion of ethionamide and prothionamide in man. J Antimicrob Chemother 13:267–277

Johnson JL, Hadad DJ, Boom WH, Daley CL, Peloquin CA, Eisenach KD, Jankus DD, Debanne SM, Charlebois ED, Maciel E, Palaci M, Dietze R (2006) Early and extended early bactericidal activity of levofloxacin, gatifloxacin and moxifloxacin in pulmonary tuberculosis. Int J Tuberc Lung Dis 10:605–612

Kreis B, Pretet S, Birenbaum J, Guibout P, Hazeman JJ, Orin E, Perdrizet S, Weil J (1976) Two three-month treatment regimens for pulmonary tuberculosis. Bull Int Union Tuberc 51(1): 71–75

Lauzardo M, Peloquin CA (2012) Anti-tuberculosis therapy for 2012 and beyond. Expert Opin Pharmacother 13:511–526

Loeffler AL, Peloquin CA, Schecter G (2012). In: AL Loeffler, G Schecter, CL Daley, JM Flood (eds) Tuberculosis drug information guide, 2nd edn. Curry Int Tuberc Cent Calif Dep Public Health

Machado D, Perdigão J, Ramos J, Couto I, Portugal I, Ritter C, Boettger EC, Viveiros M (2013) High-level resistance to isoniazid and ethionamide in multidrug-resistant Mycobacterium tuberculosis of the Lisboa family is associated with inhA double mutations. J Antimicrob Chemother [Epub ahead of print]

Malone RS, Fish DN, Spiegel DM, Childs JM, Peloquin CA (1999) The effect of hemodialysis on cycloserine, ethionamide, para-aminosalicylate, and clofazimine. Chest 116:984–990

Martin Boeree,Diacon A, Dawson R, Venter A, Bois J du, Narunsky K, Hoelscher M, Gillespie S, Phillips P, Aarnoutse R, PanACEA Consortium (2013) What Is the "Right" Dose of Rifampin? Paper #148LB. 20th Conference on Retroviruses and Opportunistic Infections [CROI], March 3–6, 2013, Atlanta, Georgia

Mitnick CD, McGee B, Peloquin CA (2009) Tuberculosis pharmacotherapy: strategies to optimize patient care. Expert Opin Pharmacother 10:381–401

Mouton JW, Ambrose PG, Canton R, Drusano GL, Harbarth S, MacGowan A, Theuretzbacher U, Turnidge J (2011) Conserving antibiotics for the future: new ways to use old and new drugs from a pharmacokinetic and pharmacodynamic perspective. Drug Resist Updat 14:107–117

Nakajima A, Fukami T, Kobayashi Y, Watanabe A, Nakajima M, Yokoi T (2011) Human arylacetamide deacetylase is responsible for deacetylation of rifamycins: rifampicin, rifabutin, and rifapentine. Biochem Pharmacol 82:1747–1756

Namdar R, Peloquin CA (2011) Drugs for tuberculosis. In: Piscitelli SC, Rodvold KA, Pai MP (eds) Drug interactions in infectious diseases, 3rd edn. Humana Press, c/o Springer Sci+Bus Media, LLC, New York, pp 401–424

Nuermberger E, Grosset J (2004) Pharmacokinetic and pharmacodynamic issues in the treatment of mycobacterial infections. Eur J Clin Microbiol Infect Dis 23:243–255

Peloquin CA (1991) Antituberculosis drugs: pharmacokinetics. In: Heifets L (ed) Drug susceptibility in the chemotherapy of mycobacterial infections. CRC Press, Boca Raton, pp 59–88

Peloquin CA (2001) Pharmacological issues in the treatment of tuberculosis. Ann N Y Acad Sci 953:157–164

Peloquin CA (2002) Therapeutic drug monitoring in the treatment of tuberculosis. Drugs 62: 2169–2183

Peloquin C (2003) What is the 'right' dose of rifampin? Int J Tuberc Lung Dis 7:3–5

Peloquin CA, Jaresko GS, Yong CL, Keung ACF, Bulpitt AE, Jelliffe RW (1997) Population pharmacokinetic modeling of isoniazid, rifampin, and pyrazinamide. Antimicrob Agents Chemother 41:2670–2679

Peloquin CA, Berning SE, Huitt GA, Childs JM, Singleton MD, James GT (1999) Once-daily and twice-daily dosing of p-aminosalicylic acid [pas] granules. Am J Respir Crit Care Med 159:932–934

Peloquin CA, Berning SE, Nitta AT, Simone PM, Goble M, Huitt GA, Iseman MD, Cook JL, Curran-Everett D (2004) Aminoglycoside toxicity: daily versus thrice-weekly dosing for treatment of mycobacterial diseases. Clin Infect Dis 38:1538–1544

Peloquin CA, Hadad DJ, Molion LPD, Palaci M, Boom WH, Dietze R, Johnson JL (2008) Population pharmacokinetics of levofloxacin, gatifloxacin, and moxifloxacin in adults with pulmonary tuberculosis. Antimicrob Agents Chemother 52:852–857

Peloquin CA, Namdar R (2011) Tuberculosis. In: DiPiro JT, Talbert RL, Yee GC, Matzke GR, Wells BG, Posey LM (eds) Pharmacotherapy: a pathophysiologic approach, 8th edn. McGraw Hill, New York, pp 1931–1949

Rosenthal I, Zhang M, Williams KN, Peloquin CA, Tyagi S, Vernon AA, Bishai WR, Chaisson RE, Grosset JH, Nuermberger E (2007) Daily dosing of rifapentine cures tuberculosis in three months or less in the murine model. PLoS Med 4:e344

Rustomjee R, Lienhardt C, Kanyok T, Davies GR, Levin J, Mthiyane T, Reddy C, Sturm AW, Sirgel FA, Allen J, Coleman DJ, Fourie B, Mitchison DA, Gatifloxacin for TB [OFLOTUB] study team (2008) A Phase II study of the sterilising activities of ofloxacin, gatifloxacin and moxifloxacin in pulmonary tuberculosis. Int J Tuberc Lung Dis 12:128–138

Schwiesow JN, Iseman MD, Peloquin CA (2008) Concomitant use of voriconazole and rifabutin in a patient with multiple infections. Pharmacotherapy 28:1076–1080

Skripconoka V, Danilovits M, Pehme L, Tomson T, Skenders G, Kummik T, Cirule A, Leimane V, Kurve A, Levina K, Geiter LJ, Manissero D, Wells CD (2012) Delamanid improves outcomes and reduces mortality for multidrug-resistant tuberculosis. Eur Respir J [Epub ahead of print]

Takiff H, Guerrero E (2011) Current prospects for the fluoroquinolones as first-line tuberculosis therapy. Antimicrob Agents Chemother 55:5421–5429

Thee S, Seddon JA, Donald PR, Seifart HI, Werely CJ, Hesseling AC, Rosenkranz B, Roll S, Magdorf K, Schaaf HS (2011) Pharmacokinetics of isoniazid, rifampin, and pyrazinamide in children younger than two years of age with tuberculosis: evidence for implementation of revised World Health Organization recommendations. Antimicrob Agents Chemother 55:5560–5567

Trial of high-dose Rifampin in patients with TB [HIRIF]. http://clinicaltrials.gov/ct2/show/NCT01408914?term=high+dose+rifampin&rank=1. Accessed 29 April 2013

Verbist L (1969) Rifampicin activity “in vitro” and in established tuberculosis in mice. Acta Tuberc Pneumo Belgica 60:397–412

Weiner M, Burman W, Vernon A, Benator D, Peloquin CA, Khan A, Weis S, King B, Shah N, Hodge T, The Tuberculosis Trials Consortium (2003) Low isoniazid concentration associated with outcome of tuberculosis treatment with once-weekly isoniazid and rifapentine. Am J Respir Crit Care Med 167:1341–1347

Weiner M, Bock N, Peloquin CA, Burman WJ, Khan A, Vernon A, Zhao Z, Weis S, Sterling T, Hayden K, Goldberg S, The Tuberculosis Trials Consortium (2004) Pharmacokinetics of rifapentine 600, 900 and 1200 mg during once-weekly tuberculosis therapy. Am J Respir Crit Care Med 169:1191–1197

Weiner M, Benator D, Burman W, Peloquin CA, Khan A, Vernon A, Jones BS, Silva-Trigo C, Zhao Z, Hodge T, The Tuberculosis Trials Consortium (2005) association between acquired rifamycin resistance and the pharmacokinetics of rifabutin and isoniazid among patients with HIV and tuberculosis. Clin Infect Dis 40:1481–1491

Zhu M, Nix DE, Adam RD, Childs JM, Peloquin CA (2001a) Pharmacokinetics of cycloserine under fasting conditions, with orange juice, food, and antacids. Pharmacotherapy 21:891–897

Zhu M, Burman WJ, Jaresko GS, Berning SE, Jelliffe RJ, Peloquin CA (2001b) Population pharmacokinetics of intravenous and intramuscular streptomycin in patients with tuberculosis. Pharmacotherapy 21:1037–1045

Zhu M, Burman WJ, Starke JR, Stambaugh JJ, Steiner P, Bulpitt AE, Ashkin D, Auclair B, Berning SE, Jelliffe RW, Jaresko GS, Peloquin CA (2004) Population-pharmacokinetic modeling of ethambutol in children and adults with tuberculosis. Int J Tuberc Lung Dis 8:1360–1367

Chapter 12
Pharmacometrics in Pulmonary Diseases

Bhargava Kandala and Günther Hochhaus

12.1 Introduction

Majority of the pharmaceutical drugs are delivered systemically, and systemic delivery has been the primary research focus of pharmaceutical industries during the past few decades. However, systemic delivery is not always a beneficial option especially with drugs having poor absorption, high first-pass metabolism, rapid systemic clearance, and causing serious systemic side effects (e.g., oral corticosteroids; Gonda 2004). In contrast, a local delivery of the drug at the site of action can alleviate some of these challenges by reducing the systemic side effects and having a slower clearance at the site of action compared to the systemic clearance of the drug. One such example of a local drug delivery method is pulmonary delivery, which is a lucrative option owing to the unique structure of the airways that enables efficient absorption of the inhaled particles into the blood, and the presence of an innate protection mechanism in the form of a mucociliary escalator to remove undissolved inhaled particles. Pulmonary drug delivery has been successfully employed for topical therapy of pulmonary diseases like asthma and chronic obstructive pulmonary disease (COPD) using drugs such as corticosteroids, anticholinergics, and short- and long-acting β-agonists. One of the primary goals of inhalation therapy is drug "targeting," i.e., achieving higher concentrations of the biologically active agent at the site of action, which is the lung compared to the concentrations in other parts of the body. This would be even more important for drugs used in treating respiratory diseases where the primary goal is lung-targeted inhalation to maximize the beneficial therapeutic effects while minimizing the systemic side effects (Hochhaus et al. 1992b). Even with targeting, the inhaled drugs are not completely devoid of side effects because of the systemic spillover of the

G. Hochhaus (✉) · B. Kandala
College of Pharmacy, University of Florida, 1345 Center Drive, P3-20 JHMHC, Gainesville, FL 32610-0494, USA
e-mail: hochhaus@cop.ufl.edu

S. Schmidt, H. Derendorf (eds.), *Applied Pharmacometrics,* AAPS Advances in the Pharmaceutical Sciences Series 14, DOI 10.1007/978-1-4939-1304-6_12

absorbed drug from the lung. First, the multitude of pharmacokinetic (PK) and pharmacodynamic (PD) factors that influence pulmonary targeting are reviewed in this chapter taking into consideration the fate of an inhaled drug in the human body. Second, PK/PD approaches modeling the systemic side effects of inhaled drugs are described. Third, pulmonary models that describe the complicated PK behavior of inhaled drugs taking into consideration the physiology of the lung, physicochemical properties of the inhaled drug, and patient-related factors are presented. Finally, a commercially available mechanistic multi-compartment physiological model of the lung describing the absorption and disposition of inhaled drug molecules is described in this chapter.

12.2 Factors Influencing Regional Lung Kinetics Following Inhalation Therapy

Prior to exploring the pathway of an inhaled drug, it is important to understand the basic anatomical features of the lung, physicochemical properties of the drug, and patient-related factors that influence the kinetics and hence the fate of an inhaled drug in the human body.

12.2.1 Physiological Aspects of Inhalation Therapy

Traditionally, the airways in the lung are categorized into two parts: the conducting or the central airways and the respiratory or the peripheral airways, as characterized by Weibel (1963). The central airways begin with the trachea and end with the terminal bronchioles, the smallest airways without the alveoli, and hence not involved in gas exchange. The central airways comprise of the first 16 generations and are the principal site for airway obstruction in diseases like asthma and COPD. On the other hand, the peripheral airways extend from the respiratory bronchioles (generation 17), all the way to the alveolar ducts and alveolar sacs, and these airways are responsible for gas exchange. To gain a better understanding of the impact of the physiological factors on the fate of an inhaled drug, it is imperative to classify the lung into central airways (trachea to the terminal bronchioles) and the peripheral airways (respiratory bronchioles and the alveolus; Byron 1986; Gonda 1988). Differences in the cellular profile and certain anatomical features between these two regions warrant such a distinction to be made. The luminal surface of the epithelium of the central airways is covered by a layer of mucus (Jeffery 1987) that facilitates the removal of undissolved drug particles from the lung by the mucociliary escalator. The removed drug is either spit out or swallowed and hence no longer available in the lung to induce pulmonary effects. Such a clearance mechanism is absent in the peripheral regions because of a dearth of mucus-secreting goblet cells

in these airways (Tyler 1983). Another important physical difference is the increase in surface area as we go down the bronchial tree. The cross-sectional area increases dramatically from terminal bronchiole (180 cm^2) to the alveoli (10,000 cm^2; Hickey and Thompson 2004). The large surface area of the alveoli coupled with the presence of thin membranes and their proximity to the blood may point toward a faster rate of absorption of drug from the alveolus than from the tracheobronchial region (Schanker et al. 1986; Brown and Schanker 1983). It is also important to state that the distribution of the metabolizing enzymes in the central and the peripheral regions maybe different (Petruzzelli et al. 1989). These differences indicate that the fate of an inhaled drug in terms of its pulmonary absorption, distribution, and clearance will vary in the two regions of the lung.

12.2.2 Physicochemical Properties of the Inhaled Drug

Drug particles are delivered to the lung using three basic inhalation drug delivery systems: nebulizers, metered-dose inhalers (MDIs), and dry powder inhalers (DPIs). In nebulizers, the drug present in the form of a solution or a suspension is nebulized by ultrasonics or an air jet and is delivered via a mouthpiece or a ventilation mask. MDIs are multidose inhalers wherein the drug is formulated in a volatile propellant such as a hydrofluoroalkane (HFA). Upon activation, a specific amount of the drug is delivered by a metered valve to the lung as the propellant evaporates. DPIs are single-dose or multidose inhalers, containing micronized drug particles, attached to larger carrier particles agglomerated into soft pellets. Most of the commercially available DPIs are passive devices, where the patient's inspiratory effort is required to disperse the drug powder and incorporate it into an inhalation airstream. Delivering an optimum respirable fraction (particles < 5 μm) is a common requirement of all inhalation dosage forms and delivery systems and is a function of the aerodynamic particle size distribution (APSD). The inhaled dose can be divided into three fractions depending upon its APSD. Particles that are greater than 5–7 μm, which are deposited predominantly in the oropharyngeal region by impaction and are swallowed; particles having a submicron size that are exhaled and do not deposit on the airways; and the fraction of particles having the ideal size range for the lung deposition, i.e., 1–5 μm (Bates et al. 1966; Weda et al. 2008). Depending upon the particle size distribution within this ideal size range, the particles can deposit either in the central airways by impaction or in the smaller airways and the alveoli by gravitational sedimentation or diffusion (Stuart 1984).

APSD is an important physicochemical property of the aerosol as it influences the degree and site of lung deposition, which are important parameters that determine the targeting and effectiveness of an inhaled therapy for respiratory diseases like asthma and COPD. Targeting pharmaceutical aerosols to the lung is important in maximizing the beneficial pulmonary effects and minimizing the systemic

side effects. Traditional pulmonary drug delivery systems deposit only about 20 % in the lung with significant loss (about 70 %) of the drug to the oropharyngeal region (Davies 1982; Thiel 1998; DeHaan and Finlay 2001). However, numerous advances in inhaler design and particle technology, like the advent of MDIs with HFA propellants (Newman et al. 2006), Respimat® soft mist™ inhaler (Boehringer Ingelheim, Ingelheim, Germany; Pitcairn et al. 2005), Pulmospheres™ (Geller et al. 2011), thermal vaporization technology with the Staccato® device (Dinh et al. 2010) have improved pulmonary targeting by decreasing oropharyngeal deposition to about 30 %. Recent body of work on controlled condensation growth techniques (Hindle and Longest 2010, 2012; Longest et al. 2010; Tian et al. 2013) has the potential to reduce the oropharyngeal deposition to less than 1 %, and hence aid in the development of highly efficient DPIs. In addition to the extent, the site of lung deposition is also important for drugs treating respiratory diseases. Autoradiographic studies (Carstairs et al. 1985) have shown a higher density of β-2 receptors in the bronchioles compared to the bronchi suggesting a targeted delivery of the β-2 agonists to the central airways for optimum bronchodilatation (Usmani et al. 2005). In contrast, since the inflammatory processes occur throughout the airways (Kraft et al. 1996; Carroll et al. 1997), it is believed that inhaled corticosteroids exert optimum anti-inflammatory activity when distributed throughout the lung. Lipophilicity (Lipworth and Jackson 2000) is another property that determines the dissolution and pulmonary absorption rates of the inhaled particles and, hence, the lung residence times.

12.2.3 Patient Factors

The interaction between a patient and the inhalation device is a significant factor in determining the lung deposition of the inhaled particle. Inhalation flow rate affects the velocity of the inhaled particles and hence their lung deposition (Martonen and Katz 1993; Borgström et al. 1994). Higher speeds increase the deposition in the throat and in the larger airways by impaction and decrease the deposition by sedimentation and diffusion by reducing the residence times. Use of spacers (Newman et al. 1989) with MDIs is an effective method to reduce the high velocity of the aerosol cloud and hence improve deposition efficiency. With breath-actuated devices like the DPI, higher inspiratory flow rates provide more energy to expel the drug from the device but increase inertial impaction of the drug in the upper and central airways. Applying a breath-holding time (Martonen and Katz 1993) after inhalation can enhance the deposition of particles, especially in the small airways and the alveoli. The delivery of the aerosols at specific points in the breathing cycle can influence the regional lung deposition (Nikander et al. 2010). Other important factors related to the patient are the anatomy of the airways and the state of the lung, whether healthy or diseased. The airway caliber of the patient influences the site and degree of deposition. Experimental studies have shown that the lung deposition

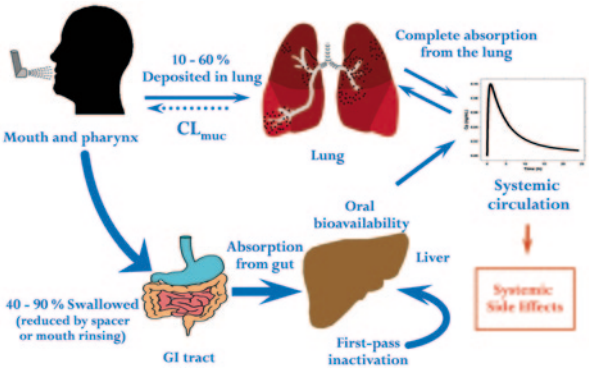

Fig. 12.1 Fate of inhaled corticosteroids

in patients with asthma or COPD is more central (Harrison and Tattersfield 2003; Singh et al. 2003), i.e., in the large airways, than in the smaller airways and the alveoli because of the decrease in airway caliber.

12.3 Fate of an Inhaled Drug in the Human Body

The schematic Fig. 12.1 shows the cascade of events that take place from the moment the drug is inhaled to the time at which it is eliminated from the human body. An inhaled particle according to its aerodynamic particle size distribution is deposited in the lung, which is the "respirable fraction" (size < 5 μm), a fraction is deposited in the oropharynx (throat), and a small fraction is exhaled. The pulmonary deposited dose can be further divided into a fraction deposited in central lung region and a fraction deposited in peripheral lung region. Solid undissolved drug particles deposited in central lung region are potentially impacted by the presence of a mucociliary clearance mechanism. Particles not removed by the mucociliary escalator will then dissolve in the bronchial fluids, pass through the pulmonary cells where they elicit the desired therapeutic effect, and are eventually absorbed into the systemic circulation. Drug particles deposited in peripheral lung regions are not subjected to mucociliary clearance because of the absence of mucus-secreting goblet cells, and hence will dissolve, pass through the pulmonary cells inducing pulmonary effects, and are absorbed into the systemic circulation. The fraction of the drug that is deposited in the oropharynx and the fraction that is removed by mucociliary clearance will be swallowed and can be absorbed systemically through the gastrointestinal tract depending upon the degree of oral bioavailability of the drug. Such a fraction of the drug will not be able to induce pulmonary effects but will contribute to systemic side effects. The total systemic bioavailability of an inhaled drug therefore, is a function of the drug available from the lung and bioavailable fraction of the swallowed dose from the gut. The amount of drug that reaches the systemic circulation will be distributed and eliminated from the body according to its PK properties.

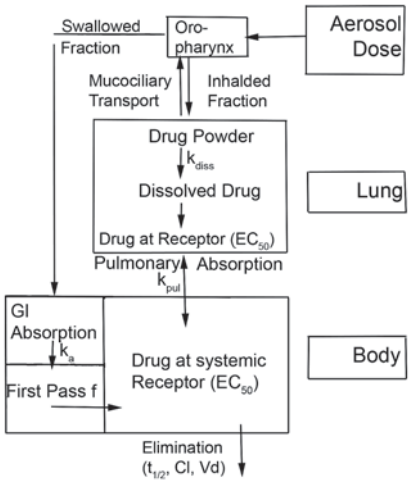

Fig. 12.2 PK/PD model for describing pulmonary targeting. (Hochhaus et al. 1997)

12.4 PK/PD Modeling of Inhaled Drugs

12.4.1 PK/PD Factors Influencing Pulmonary Targeting

The primary goal of inhalation therapy has been to achieve pronounced pulmonary selectivity by maximizing the pulmonary effects while reducing the systemic side effects. The different kinetic processes that determine the fate of an orally inhaled drug product (OIDP) point towards a range of PK and PD factors that would impact the degree of pulmonary targeting of OIDPs. Hochhaus et al. (1997), based on previously published pharmacokinetic models by Byron (1986) and Gonda (1988) provided a novel approach to evaluate the factors responsible for pulmonary targeting by integrating physiological aspects of pulmonary inhalation with PK and PD drug properties. The PK/PD model was used to evaluate pulmonary selectivity by providing a link between inhaled corticosteroid (ICS) concentrations (unbound) in the lung, and the systemic circulations with pharmacological effects using a simple E_{max} model as shown in Fig. 12.2. Simulations using this model were extended for β-2 agonists by Issar et al. (2004). An array of PK and PD properties influencing pulmonary selectivity are presented below.

12.4.1.1 Pharmacodynamic Factors

Receptor-Binding Affinity

It is widely accepted that the therapeutic effects and systemic side effects of inhalation drugs are mediated through cytosolic or membrane receptors. For example, all ICSs exert their pharmacological effects through glucocorticoid receptors within

the lungs albeit with different receptor-binding affinities/potency. These receptors are extensively present in the lungs with high density in airway epithelial cells and bronchial vascular cells. The activity of ICS at the site of action, i.e., potency, is correlated to the receptor-binding affinity of the drug (Beato et al. 1972; Dahlberg et al. 1984; Druzgala et al. 1991). Similarly, in the case of β-2 adrenergic drugs, whose therapeutic effects are mediated through the β-2 adrenergic receptor, a strong association exists between in vitro pointers of drug activity in cell culture and the pharmacological activity in vivo (Hochhaus and Möllmann 1992). Therefore, in vitro parameters and receptor-binding affinities/potency are often used as yardsticks while comparing the pharmacological effects of inhalation drugs in the lung. It is interesting to explore the role of receptor potency in pulmonary targeting using ICSs and β-2 adrenergic drugs as examples.

In the case of ICSs, wherein pulmonary effects and systemic side effects are mediated through the same glucocorticoid receptors in the lungs and systemic tissues, it has been shown that pulmonary targeting is not influenced by different receptor-binding affinities as long as the differences in affinities are adjusted by the dose of ICSs. Therefore, an ICS with a lower receptor-binding affinity is not necessarily an inferior drug. The anti-inflammatory effect of a low receptor-binding affinity ICS can be moderated by increasing its dose. On the other hand, for β-2 adrenergic drugs, the pulmonary are mediated through β-2 receptors while most of the systemic side effects are mediated through the β-1 adrenergic receptors. In such a scenario, a high binding selectivity, i.e., high binding affinity to β-2 receptors and low affinity to β-1 receptors is favorable for pulmonary selectivity.

12.4.1.2 Pharmacokinetic Factors

Oral Bioavailability

An OIDP can enter the systemic circulation via the lung as well as from the gastrointestinal (GI) tract. Sum of the fractions of the drug that is deposited in the oropharynx and swallowed, and pulmonary deposited drug removed by mucociliary clearance constitute the overall amount of drug reaching the GI tract. The oral bioavailability of the drug (F), determined by the first-pass metabolism regulates the amount of drug entering the systemic circulation via the GI tract. This GI-available fraction of OIDP will not elicit any therapeutic effect, but will contribute towards systemic side effects. Ideally F should be close to 0 to reduce the overall systemic exposure of the drug and hence the potential for adverse events. Fluticasone propionate (FP) and Ciclesonide have the lowest oral bioavailability among ICSs of 1% (Peet et al. 2005). Bioavailability estimates of current ICSs range from 0 to 40% (Ryrfeldt et al. 1982; Hochhaus et al. 1992a; Derendorf et al. 1995; Daley-Yates et al. 2001). Similarly, the bioavailability values of β-2 agonists range from 1.5 to 50%. These differences are likely to have an impact on pulmonary selectivity.

Systemic Clearance

The fraction of the inhaled drug that reaches the systemic circulation, i.e., systemically available drug, will contribute toward systemic side effects by interacting with the receptors outside the lung. Therefore, pronounced systemic clearance will reduce the systemic exposure of OIDPs and garner pulmonary selectivity. Most ICSs are extensively metabolized in the liver with clearance values close to the liver blood flow (Ryrfeldt et al. 1982; Derendorf et al. 1995; Mackie et al. 1996). An alternative approach to increase systemic clearance would be to develop ICSs with extrahepatic clearance mechanisms, for example, ICSs that are metabolized in the blood. A challenge with such an approach is to identify such enzymes that are present in high concentrations in the blood, but absent in pulmonary cells, to ensure that pulmonary efficacy is not compromised while maximizing systemic safety. Desisobutyrl-ciclesonide has an apparent clearance of 228 L/h (Winkler et al. 2004) indicating presence of extrahepatic modes of metabolism.

Plasma Protein Binding

Freely circulating unbound drug binds to receptors within and outside the lung and is responsible for both local and systemic side effects, respectively. Plasma protein binding of OIDPs (e.g., to albumin, α_1-acid glycoprotein) can decrease the potential for systemic side effects by reducing the number of pharmacologically active free drug moieties interacting with receptors outside the lung. Indeed, protein-binding rates have been utilized as valuable markers in predicting the cortisol suppression of ICSs. Ciclesonide and desisobutyryl-ciclesonide have both demonstrated protein-binding rates of ~99% (Rohatagi et al. 2005) and that may explain their minimal effect on HPA-axis function and cortisol levels.

Therefore, there has been an increased tendency to develop OIDPs that show increased plasma and tissue protein binding. Such a property not only reduces systemic side effects but also reduces the desired pulmonary effects. Systemic side effects generally show a sensitive or a steep dose–response relationship and hence are easily detected in clinical studies. On the other hand, pulmonary effects exhibit flat or insensitive dose–response relationships and are hard to detect. Therefore, such high-binding drugs when given at identical doses as their low-binding counterparts, exhibit very high safety profiles (low systemic side effects) while their pulmonary effects (anti-asthmatic effects) are not statistically significantly different, owing to insensitive pulmonary biomarkers/clinical endpoints.

Pulmonary Deposition

High pulmonary deposition is warranted for OIDPs intended for local action in the lung, as it increases the amount of drug at the site of action, and elicits the desired therapeutic effect. Increased pulmonary deposition also reduces the deposition in

the oropharynx, thus reducing the dose available for absorption from the GI tract. Pulmonary deposition varies significantly between various inhalation devices. Recent advancements in the design of delivery devices have increased the pulmonary deposition from 10–20 to 40% (Newman et al. 1998). Although higher pulmonary deposition is beneficial in general for pulmonary targeting, it has a greater upside for drugs with higher bioavailability as a lesser fraction of the dose is available for oral absorption (Hochhaus et al. 1997). For drugs with lower oral bioavailability, the drug entering the GI tract will not be able to induce systemic side effects. However, in this case, a lower dose of the OIDP can be administered. To further increase our understanding of the interplay between drug delivery device and patient characteristics (such as disease state, inhalation profile, device handling, and deposition), physiological PK/PD approaches have to be fused with computational fluid dynamics (Longest et al. 2012).

Pulmonary Residence Time

Drug particles deposited in the lung will dissolve in pulmonary fluids when released from delivery systems, such as microspheres and liposomes and diffuse to the site of action, where they exert the desired pharmacological effect, and subsequently be absorbed into the systemic circulation. Given the physiology of the lung, it seems logical to assume that the dissolution rate of the inhaled particle or the release rate of the drug from the delivery system are the rate-limiting steps that determine lung residence time.

The longer the pulmonary residence time of an OIDP, i.e., the longer it stays in the lung, the longer their therapeutic effect will be. If a drug particle is given as a solution or it dissolves quickly, it is immediately absorbed into the systemic circulation, and hence pulmonary selectivity is lost. In this case, the pulmonary effects will be accompanied by significant systemic side effects. On the other hand, lowering the pulmonary dissolution rate ensures that the drug concentrations in the lung will be greater compared to plasma levels for an extended period of time which is beneficial for pulmonary targeting. However, an optimal dissolution rate exists due to the presence of mucociliary transport in the central lung which removes undissolved drug particles leading to loss of efficacy and pulmonary targeting. A longer retention time in the lung will not reduce the overall systemic exposure of the drug, but might reduce the maximal systemic exposure of the drug.

The potential for beneficial effects has warranted the genesis of a number of approaches to improve lung residence of OIDPs (Hardy and Chadwick 2000). Examples of approaches include the use of liposomes (Suarez et al. 1998; Suntres and Shek 1998), microspheres (Edwards et al. 1997; Bot et al. 2000; Dellamary et al. 2000), ultrathin coating around dry powder formulations, and the use of excipients, such as oligolactic acid and trehalose derivatives (Hardy and Chadwick 2000), as well as use of slow-dissolving lipophilic drugs, and the formation of lipid conjugates (Tunek et al. 1997; Miller-Larsson et al. 1998; Edsbäcker and Brattsand 2002; Nave et al. 2005, 2006). Intracellular ICS conjugation to lipids prolongs the

pulmonary residence time by creating a depot of ICS that gradually is reactivated into active ICS and hence available to elicit anti-inflammatory activity. Similarly, long-acting β-2-adrenergic drugs bind tightly to pulmonary cell membranes (Green et al. 1996), creating a reservoir of the drug which slowly releases the active moiety to the receptor. This prolonged residence time might allow for once-daily dosing due to the extended therapeutic effect enhancing patient compliance.

12.4.2 PK/PD Modeling of Systemic Side Effects After Administration of Inhaled Corticosteroids

12.4.2.1 PK/PD Modeling of Cortisol Suppression After Administration of Exogenous Corticosteroids

While most of the ICSs demonstrate a series of beneficial properties, they are not completely devoid of systemic side effects. Suppression of endogenous cortisol production is one of the major side effects of corticosteroids (Koopmans et al. 1992; Wald et al. 1992). Cortisol (hydrocortisone, 11,17,21-trihydroxypreg-4-ene-3,20-dione) is the primary endogenous glucocorticoid synthesized in the human body from cholesterol via several enzyme-catalyzed steps (Chrousos and Harris 1998). Secretion of cortisol by the adrenal cortex is regulated by the adrenocorticotropic hormone (ACTH), which is produced by the anterior pituitary gland. ACTH production is in turn regulated by corticotrophin-releasing factor (CRF) produced by the hypothalamus. Finally, the circulating cortisol molecules have a negative feedback mechanism on the hypothalamus to regulate the formation of CRF and also the anterior pituitary to regulate the release of ACTH thus maintaining homeostasis. To quantify the degree of systemic steroid activity, endogenous cortisol levels are used as a suitable marker. However, due to the marked circadian rhythm (Chrousos and Harris 1998) in cortisol release and the asymmetric nature of baseline cortisol concentrations, a precise quantification of cortisol suppression becomes an intricate exercise. Cortisol reaches a peak (acrophase) in the morning (6–10 a.m.) and a trough during the night (8 p.m.–2 a.m.). Furthermore, exogenous corticosteroids can suppress the release of cortisol by a negative feedback mechanism (Slayter et al. 1996). Hence, there is a need to develop a consistent PK/PD model to characterize the effect of therapeutic corticosteroids.

The first step in modeling the steroid-induced suppression of endogenous cortisol is the characterization of the asymmetric baseline circadian concentrations of cortisol. Then by assuming that the exogenous corticosteroid inhibits the cortisol secretion rate R_C, the complete PK/PD model for cortisol suppression can be developed as an application of the k_{in}-inhibition indirect response model (Chakraborty et al. 1999). Therefore, the resulting change in cortisol concentration under baseline conditions (i.e., absence of drug) is given by:

$$\frac{dC}{dt} = R_C - k_e * C \tag{12.1}$$

where C is the cortisol concentration and k_e is the elimination rate constant for cortisol. And in the presence of corticosteroids (C_{st}) the change in cortisol concentrations can be expressed as:

$$\frac{dC}{dt} = R_C * \left(1 - \frac{I_{max} * C_{st}}{C_{st} + IC_{50}}\right) - k_e * C \tag{12.2}$$

where I_{max} is maximum fractional inhibition of R_C, IC_{50} is the concentration of steroid that causes 50 % of the maximal suppression of R_C.

Due to the circadian nature of the cortisol release rate R_C, various time-dependent 24-h periodic functions have been used to describe it. Chakraborty et al. (1999) compared several methods to model circadian cortisol concentrations. An indirect response model with six different biorhythmic functions namely, single cosine, dual ramps, dual zero order, dual cosines, and Fourier series with two and n-harmonics were evaluated to model cortisol release rate. It was shown that apart from the single cosine, all methods reasonably captured the cortisol profiles, and the inhibition data were fitted similarly by all models. Fourier analysis had the added flexibility of using the placebo data to recover equations for cortisol release rate unlike other models with preassigned functions and can be extended to other drug-induced changes in normal periodic rhythms.

Rohatagi et al. (1996a) also investigated five different models to characterize the cortisol concentrations as a function of time and concentration of the exogenous steroid triamcinolone acetonide (TCA). A cosine (Milad et al. 1994), exponential, monoexponential, and a biexponential self-suppression model were compared to a proposed linear release rate PK/PD model (Rohatagi et al. 1996a) to characterize the mean cortisol baseline data for 24 h, and the cortisol levels after single-dose administration of TCA. The linear release rate or the dual ramps model, which takes into account the elimination of cortisol, was shown to characterize the cortisol baseline and cortisol suppression in a better way compared to the other models based on certain goodness of fit and model selection criteria. After transforming the cortisol plasma levels to cortisol release rates by using PK parameters of cortisol, the linear rate model assumes a linear decrease in cortisol production during the day from the time of acrophase (with maximum release rate R_{max} (amount/time) at time t_{max}) to almost 0 at time of minimum release (t_{min}). Hence, for the time between the acrophase t_{max} to t_{min}, the decrease in release rate is modeled according to:

$$R_C = \frac{R_{max}}{V_d^{COR} * (t_{max} - t_{min} - 24)} * (t - t_{min}) \tag{12.3}$$

where t is the time after cortisol monitoring was started and V_d^{COR} is the volume of distribution of cortisol.

For the time between t_{min} and t_{max}, the increase in release rate is described by:

$$R_C = \frac{R_{max}}{V_d^{COR} * (t_{max} - t_{min})} * (t - t_{min}) \tag{12.4}$$

The resulting change in cortisol concentrations in the absence and presence of the corticosteroid are modeled using Eqs. (12.1) and (12.2). The linear release rate PK/PD model was used to study the effect of various ICS—Ciclesonide (Rohatagi et al. 2003; population approach—a sample NONMEM control stream is available in Appendix 1), FP (Xu et al. 2010), triamcinolone acetonide (Rohatagi et al. 1995), and fluocortolone (Rohatagi et al. 1996b) on cortisol suppression.

All the previously described models did not take into account the combined effect of ACTH and cortisol, though there is clearly a need for a physiologically based model to describe the system since the mechanism involves a sequential cascade of effects and circadian rhythm. Lönnebo et al. (2007) proposed a surge-based PK/PD model similar to the one developed by Nagaraja et al. (2003) to describe the effect of budesonide (BUD) on ACTH and cortisol. The release rate and the serum concentration of ACTH, and consequently cortisol were observed to fluctuate with a prominent circadian rhythm with two surges every 24 h, one a.m. surge and one p.m. surge. In the surge-based model, the circadian rhythm in hormonal production was described by a constant zero-order production coupled with surges. Also, ACTH was assumed to drive the production of cortisol, and the effect of BUD was assumed to solely effect the production of ACTH through an inhibitory $E_{\max}$ ($I_{\max}$) model. The surge-based model is described as follows:

$$\frac{dACTH}{dt} = k_{in,ACTH} * \left(1 - f_1(C_{Bud})\right) * \left(1 - f_3(C_{\mathrm{Cor}})\right) + g(clock\ time) * (1 - f_2(C_{Bud}) * \left((1 - f_4(C_{Cor})\right) - k_{out,ACTH} * ACTH \tag{12.5}$$

$$\frac{dCortisol}{dt} = h(ACTH) - k_{out,cortisol} * cortisol \tag{12.6}$$

where $k_{out,ACTH}$ and $k_{out,cortisol}$ are the first-order elimination rate constants for ACTH and cortisol, $k_{in,ACTH}$ is the baseline production rate of ACTH in the absence of surges without any drug, $k_{in,ACTH}$ is obtained as the product of the two estimated parameters $k_{out,ACTH}$ and $baseline_{ACTH}$. $f_1(C_{Bud})$ and $f_2(C_{Bud})$ are described by $I_{\max}$ models, whereas $h(ACTH)$ is a (sigmoidal) $E_{\max}$ model. Negative feedback of cortisol on ACTH production ($f_3(C_{cor})$, $f_4(C_{cor})$) was introduced in equation using $I_{\max}$ models:

$$f(C_{BUD}) = 1 - \left(\frac{I_{max} * C_{BUD}}{C_{BUD} + IC_{50}}\right) \tag{12.7}$$

$$h(ACTH) = \frac{(A_{max} * ACTH^{\gamma})}{(A_{50}^{\gamma} + ACTH^{\gamma})} \tag{12.8}$$

Surges which were characterized by the parameters SA (surge amplitude), SW (surge width), T (clock time), and PT (peak time) were used to define the function g ($clock\ time$) according to

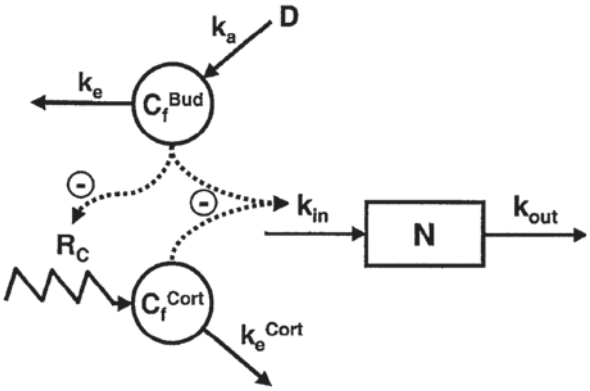

Fig. 12.3 Interplay between exogenous corticosteroid (budesonide), endogenous cortisol, and lymphocytes. (Meibohm et al. 1999)

$$g(clock\ time) = \frac{SA}{\left(\left(\frac{T - PT}{SW}\right)^4 + 1\right)} \tag{12.9}$$

The authors believe that the surge model gives a physiological description of the system and serves as a tool for further understanding of the HPA axis.

12.4.2.2 PK/PD Modeling of Systemic Corticosteroid-Induced Lymphocytopenia

In addition to cortisol suppression, the other commonly used biomarker for the systemic effects of corticosteroids is lymphocytopenia, a reduction in blood lymphocytes resulting from their redistribution into the peripheral tissues. Lymphocytopenia has been frequently used as a sensitive marker, both as a desired outcome in the treatment of allergic inflammation (Oneda 1999) and as a systemic side effect of corticosteroid therapy on the immune system during the treatment of asthma (Van Gossum et al. 1998). It has been well established that the endogenous cortisol affects the number of lymphocytes in the blood as evidenced by the circadian variation of lymphocytes (Miyawaki et al. 1984), and its subtypes in the blood (Palm et al. 1996), and its inverse correlation with the circadian rhythm of endogenous cortisol (Abo et al. 1981). Therefore, a PK/PD model for lymphocytopenia after administration of an exogenous corticosteroid should take into account the complex interplay between exogenous and endogenous corticosteroids as shown in Fig. 12.3 (Meibohm et al. 1999), modeling the decrease in blood cells as a net result of the direct inhibition of the exogenous corticosteroid, and an opposite indirect effect of the corticosteroid-induced suppression of endogenous cortisol.

A classical indirect response model was used to characterize the transient depletion of lymphocytes from the blood caused by the circadian rhythm of endogenous cortisol (Wald et al. 1992; Möllmann et al. 1998). In the model, the rate of change

in the number of lymphocytes (N) was described by a zero-order influx (k_{in}) of cells coupled with an inhibitory $E_{\max}$ model and a first-order efflux of the cells (k_{out}):

$$\frac{dN}{dt} = k_{\text{in}} * \left(1 - \frac{I_{max,L} * C_f^{Cort}}{IC_{50}^{C \to L} + C_f^{Cort}}\right) - k_{out} * N \tag{12.10}$$

The combined PD effects (Ariens 1954; Meibohm et al. 1999) of an exogenous corticosteroid and cortisol on lymphocytes was modeled by:

$$\frac{dN}{dt} = k_{in} * \left(1 - \frac{I_{max,L}\left(C_f^{St} + \frac{IC_{50}^{St \to L}}{IC_{50}^{C \to L}} * C_f^{\text{Cort}}\right)}{IC_{50}^{St \to L} + C_f^{St} + \frac{IC_{50}^{St \to L}}{IC_{50}^{C \to L}} * C_f^{\text{Cort}}}\right) - k_{out} * N \tag{12.11}$$

where $I_{max,L}$ is the maximum effect of cortisol and the exogenous steroid on the influx of lymphocytes, C_f^{Cort} and C_f^{St} are the unbound concentrations of cortisol and the exogenous steroid respectively, and $IC_{50}^{C \to L}$ and $IC_{50}^{St \to L}$ are the unbound concentrations of cortisol and the exogenous steroid that produce 50 % of $I_{max,L}$. The same PK/PD model was successfully used by Stark et al. (2006) to describe the effect–time relationships of lymphocyte subpopulations after BUD administration. Hong et al. (2007) applied a population-based PK/PD approach incorporating inter-occasion variability to model the effects of systemic corticosteroids on lymphocyte trafficking. It has been observed that the IC_{50} value for the effect of exogenous corticosteroids like BUD (Meibohm et al. 1999) and triamcinolone acetonide (Rohatagi et al. 1995) on total lymphocyte suppression is larger than that for the effect on cortisol suppression, indicating that cortisol suppression might be a more sensitive biomarker for the systemic effects of exogenous corticosteroids.

12.4.2.3 PK/PD Modeling to Study the Relationship Between Growth Velocity and Systemic Corticosteroid Exposure

Corticosteroids are essential for life as they regulate and support a variety of cardiovascular, metabolic, immunologic, and homeostatic functions. They play a major role in fetal development and are required for the maintenance of normal growth. But a deficiency or an excess of corticosteroids can lead to a reduction in growth rate. When therapeutic (exogenous) corticosteroids are given for a prolonged period of time, like in the treatment of chronic asthma, there is a risk of adrenal insufficiency and systemic adverse effects including reduced growth velocity in children (Ahmed et al. 2002). Hence, it is imperative to understand the relationship between corticosteroid exposure and growth velocity in children, simultaneously assessing the differential effects of various commercially available ICSs. This approach may assist in the selection of ICSs that maximizes the therapeutic ratio in patients. Daley-Yates and Richards (2004) consolidated data from 32 published studies of the effect of growth of inhaled, intranasal, and oral corticosteroids delivered through

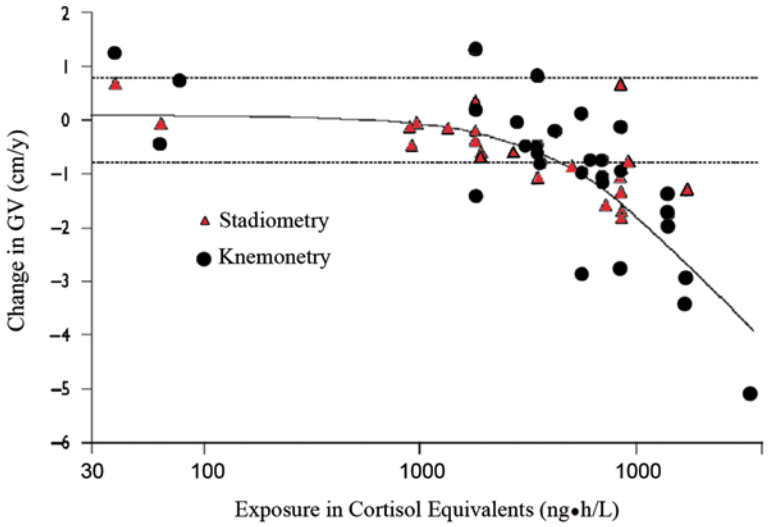

Fig. 12.4 Changes in growth velocity and exposure in cortisol equivalents. (Daley-Yates and Richards 2004)

different routes of administration using a physiologically based PK/PD approach to study the relationship between growth velocity and corticosteroid exposure. To allow the comparison between different compounds and routes of administration among these studies, corticosteroid exposure was transformed to cortisol equivalents using the following equation:

$$AUC_{ss,u} = \frac{F * dose * f_u * P_R}{CL} \tag{12.12}$$

where $AUC_{ss,u}$ is the steady-state unbound AUC in cortisol equivalents; F is the bioavailability; "dose" is the daily corticosteroid dose; f_u is the unbound fraction in plasma; P_R represents potency (glucocorticoid-receptor binding) relative to cortisol; and CL is the systemic clearance. Further, the relationship between change in growth velocity and corticosteroid exposure in cortisol equivalents was described using a nonlinear sigmoid E_{max} model, as shown in the following equation:

$$\Delta GV = \frac{E_0 - E_{max} * AUC_{ss,u}{}^{\gamma}}{AUC_{50}{}^{\gamma} + AUC_{ss,u}{}^{\gamma}} \tag{12.13}$$

where E_0 is the change in growth velocity in the absence of the drug, E_{max} is the theoretical maximum reduction in GV, AUC_{50} is the $AUC_{ss,u}$ in cortisol equivalents for 50% reduction in GV. The nonlinear relationship between annual growth velocity and exposure in cortisol equivalents for each dose group from each study is shown in Fig. 12.4. The developed model was further used to predict the annual change in

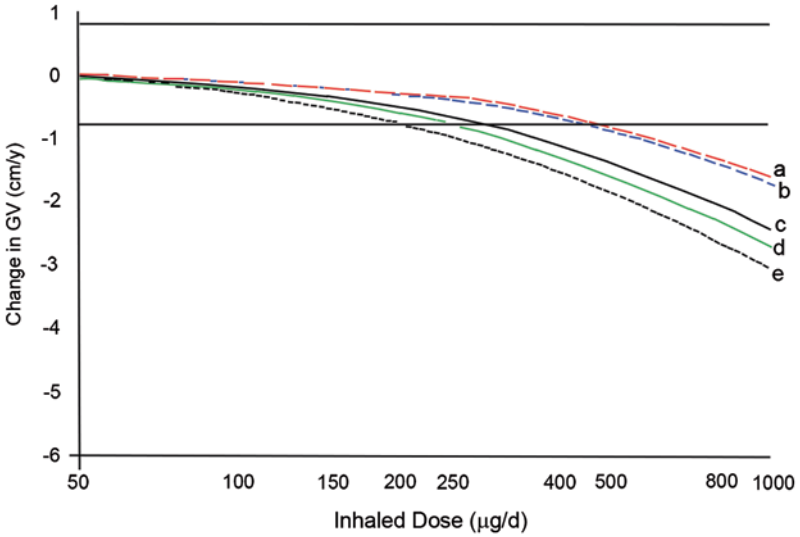

Fig. 12.5 Model-predicted changes in annual growth velocity for a range of ICS doses. (Daley-Yates and Richards 2004)

GV for different ICSs over a range of doses. Higher systemic exposures were predicted for corticosteroids with higher oral bioavailability (11–41 %)—beclamethasonedipropionate, BUD, and triamcinolone actetonide, and hence were predicted to produce systemic levels above the clinical equivalence limit for change in GV when administered at standard pediatric doses. On the other hand, corticosteroids with low oral bioavailability (< 1 %)—FP and mometasonefuroate—were predicted to show levels below the threshold (Fig. 12.5). Therefore, the model was able to establish a correlation between overall systemic bioavailability of ICSs and short-term growth effects in children.

12.4.3 PK/PD Modeling of β-2 Agonists: A Case for Lung-Targeted Therapy

β-2 Agonists like salbutamol (albuterol), terbutaline, and fenoterol have been widely used in the treatment of asthma owing to their pronounced pulmonary bronchodilatation effects mediated through the β-2 receptors and their reduced β-1-mediated cardiac effects. An increase in heart rate induced by the β-1 receptor mediated a positive ionotropic effect, and an increase in cardiac output is one of the major side effects of β-agonists besides the tremors of the skeletal muscles. PK/PD models (Hochhaus et al. 1992b; Jonkers et al. 1989) have been successfully applied in understanding the beneficial pulmonary effects and also the systemic side effects of β-agonists and thereby optimizing drug regimens.

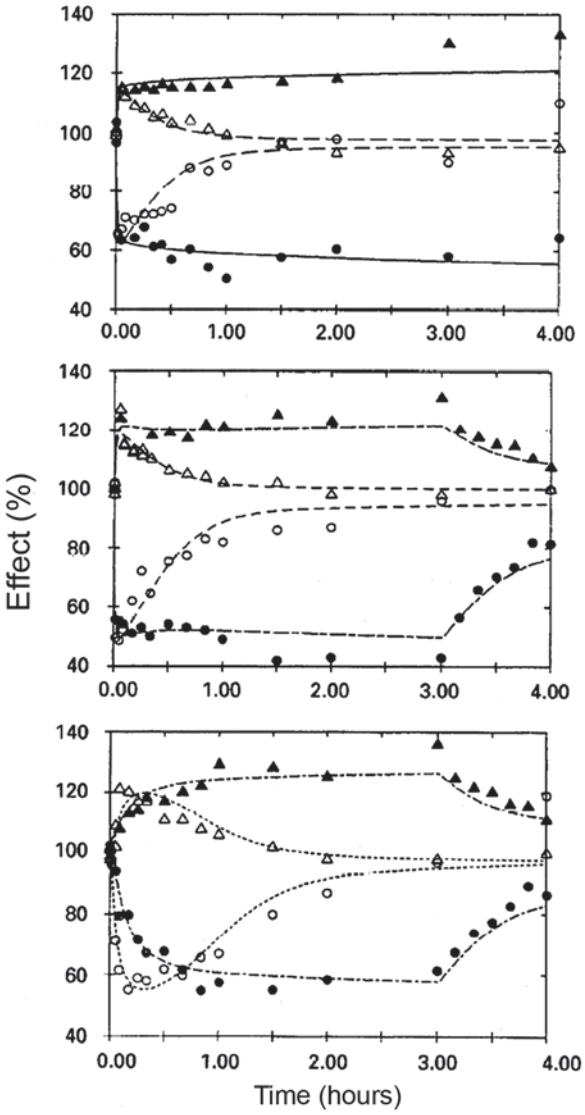

Fig. 12.6 Effect on heart rate and airway resistance after different forms of fenoterol administration. (Hochhaus and Möllmann 1992)

A PK/PD model for fenoterol developed by Hochhaus et al. (1992b) linked the drug levels in a shallow PK compartment after multiple routes of administration, to the intrathoracic gas volume, airway resistance (beneficial pulmonary effects), and heart rate (systemic side effect) via an E_{max} model. The model was able to simultaneously describe the pulmonary and cardiac effects after the administration of fenoterol, via IV injection, infusion, and nasal administration, demonstrating that the pulmonary effects after nasal administration were induced systemically and not locally (Fig. 12.6; Hochhaus and Möllmann 1992). On the other hand, with the

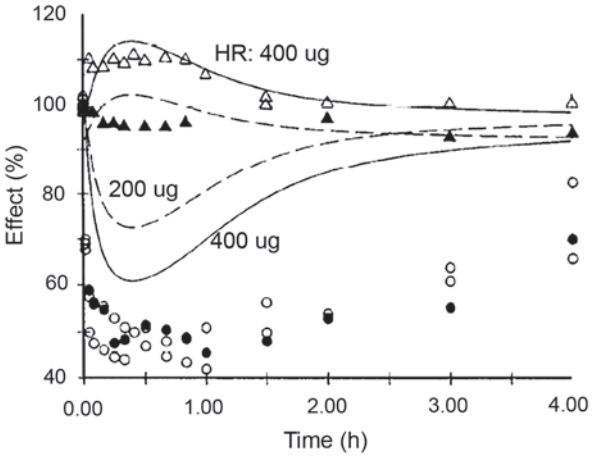

Fig. 12.7 Effect on heart rate and airway resistance after inhalation of fenoterol. (Hochhaus and Möllmann 1992)

addition of inhalation data to the model, only the cardiac effects but not the pulmonary effects were described by the model. The observed pulmonary effects after inhalation were much larger than those predicted from plasma concentrations, indicating that the pulmonary effects observed are a result of the local action of fenoterol in the lung (Fig. 12.7; Hochhaus and Möllmann 1992). Thus, this study highlights the need for lung-targeted inhalation therapy as demonstrated by an equipotent pulmonary effect with significantly smaller cardiac effects compared to other routes of administration. PK/PD modeling was also used to demonstrate the selectivity of β-2 agonists for the β-2-mediated pulmonary effects compared to the β-1-mediated cardiac effects using the relevant EC_{50} (Hochhaus et al. 1992b; Fuglsang et al. 1989) estimates.

12.4.4 PK Modeling of Inhaled Drugs: Pulmonary Models

The PK behavior of inhaled (locally acting) drugs is more complicated than that of other forms of administration (systemically acting drugs). It is imperative to acknowledge the effects of the abovementioned physiological (differences in the cellular profile and the anatomical features between the central and the peripheral lung; mucociliary escalator in the central lung region), formulation (influence of particle size distribution on the degree and site of lung deposition; particle dissolution rate), and patient factors (differences in breathing patterns and airway caliber between a healthy and a diseased lung, and its impact on the variability between and within subjects) on the systemic PK of inhaled drugs. Within the same context, a general compartment model that adequately describes the fate of an ICS by incorporating these parameters is necessary to accurately characterize the systemic PK of inhaled drugs.

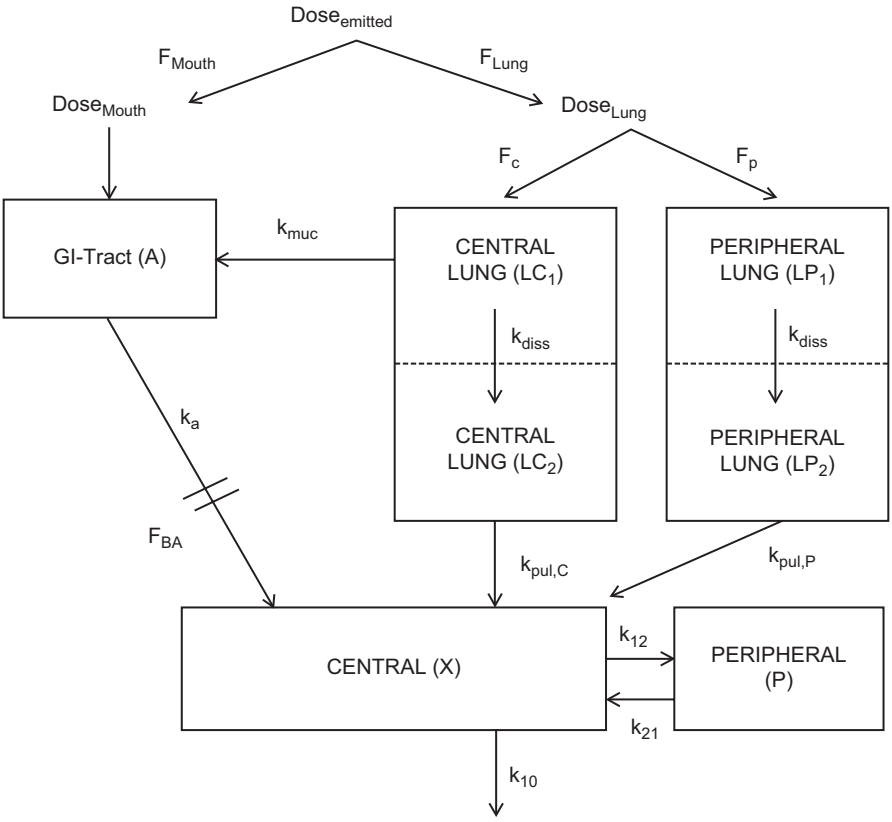

Fig. 12.8 Compartmental model for characterization of plasma concentrations after administration of ICS. (Weber and Hochhaus 2013)

Byron (1986) developed a mathematical model to predict drug residence kinetics in various regions of the human respiratory tract following inhalation of therapeutic aerosols. Gonda (1988) furthered the model incorporating release kinetics of the drug from the dosage form to study its influence on the duration of effective drug levels in the respiratory tract. But these models specifically focused on the drug kinetics in the respiratory tract and not in plasma and did not consider variability. The model by Hochhaus et al. (1997) using the abovementioned models as a basis provided a novel approach to evaluate the factors responsible for pulmonary targeting (see Section 12.4.1) by integrating physiological aspects of pulmonary inhalation with PK and PD drug properties. But the model did not distinguish between central and peripheral regions of the lung and did not have a random component to it (between and within subject variability). Weber and Hochhaus (2013) addressed the shortcomings of previously published inhalation models by developing a pharmacokinetic trial simulation tool that adequately describes the fate of ICSs (Fig. 12.8) while incorporating variability between and within subjects and

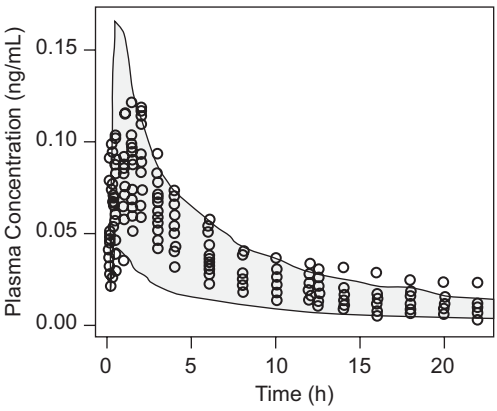

Fig. 12.9 Validation of FP module of ICS pkTS R extension package. (Weber and Hochhaus 2013)

allowing for a distinction between central and peripheral lung regions, mucociliary removal of the undissolved particles from the central lung region, and accounting for drug entering the systemic circulation via the lung and the gastrointestinal tract in the compartment model.

The primary goal of the authors was to provide a simulation tool that accurately predicts the influence of changes in relevant physiological and formulation factors on systemic PK of ICS. Furthermore, the simulation tool is provided as an extension package ("Inhaled Corticosteroids Pharmacokinetic Trial Simulation," ICSpkTS) to the statistical software R and is available for download via http://www.cop.ufl.edu/pc/research/areas-of-research/inhaled-glucocorticoids/icspkts-r-extension/. The package has in-built modules for commercially available ICS (BUD, flunisolide, FP, and triamcinolone acetonide). The performance of the BUD and FP modules was checked and hence validated by comparing the simulated PK data to data from actual studies as shown in Fig. 12.9. The package enables the users to simulate PK trials for any ICS delivered via different inhalers to healthy subjects or patients by providing the flexibility to users to specify their own model parameters. A sample NONMEM control stream for the simulation of a PK trial with FP as the model drug is presented in Appendix 2.

In spite of the stated advancements in the development of pulmonary PK models, there is still a knowledge gap regarding the quantitative mechanistic assessment of several factors impacting the PK of inhaled drugs (Labiris and Dolovich 2003). For e.g., the quantitative evaluation of the different processes that an inhaled particle is subjected to, pulmonary deposition patterns, mucociliary clearance rate, dissolution, and consequently absorption of pulmonary deposited particles using in vivo human data are rarely accomplished. In the same context, in vitro–in vivo correlation between Cascade Impactor profiles and regional lung deposition patterns, and in silico–in vivo correlations are poorly understood. Borghardt et al. (2014) developed a population PK model of Olodaterol (long-acting β-agonist with negligible oral bioavailability) to perform in silico reanalysis of previously established data to quantitatively describe the pulmonary absorption processes of a drug in solution.

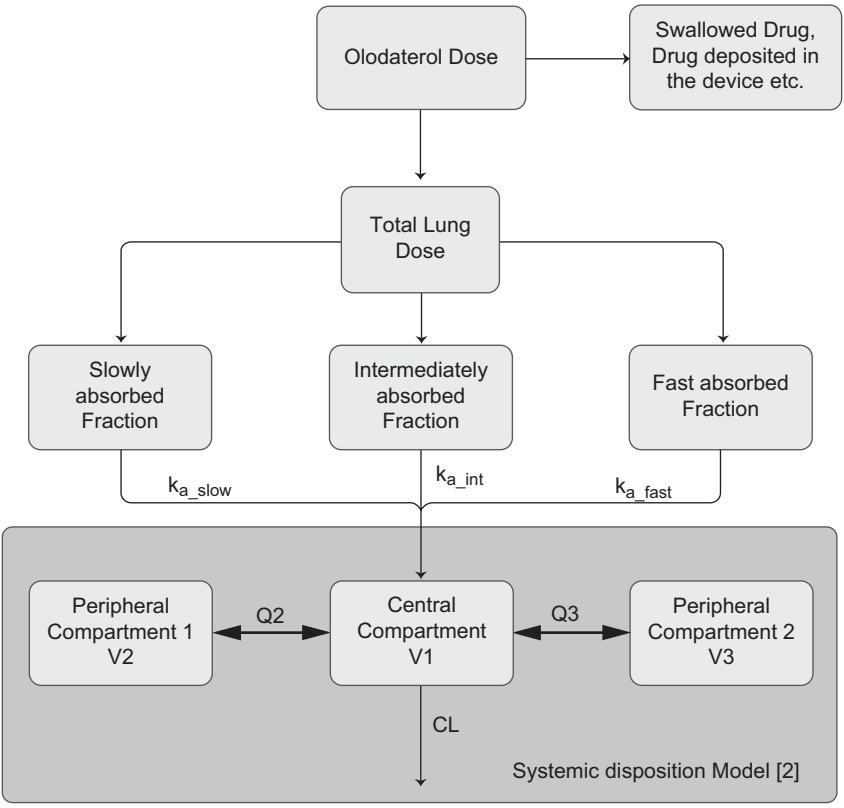

Fig. 12.10 Population PK model—three distinct pulmonary absorption processes. (Borghardt et al. 2014)

The final population PK model as shown in Fig. 12.10 consisted of three lung compartments identifying three distinct parallel pulmonary absorption processes (fast, intermediate, and slow) differing in their half-lives. The different absorption processes were linked to the absorption of the dissolved drug in different areas of the lung. The fast absorption process which contributed to the early phase of the concentration time profile (C_{max}) was linked to drug absorption from the alveoli, which is highly perfused, has a large surface area and a thin absorption barrier. Whereas the slow absorption process which had the strongest influence on the terminal phase was associated to the absorption from the central lung region with a higher amount of lung tissue where the perfusion is lower and also the drug distributes to other lung tissues before absorption to plasma. The authors opine that, even though the representation of the lung as three compartments is a strong simplification of reality, the model can be mechanistically supported as evidenced by the plausible association of the different absorption processes with the different lung regions. A sample NONMEM control stream for estimating the absorption parameters once the systemic parameters were obtained from IV data is shown in Appendix 3.

12.5 Physiologically Based Pharmacokinetic Pulmonary Models: Commercially Available Software

Physiologically based pharmacokinetic (PBPK) models can help predict the PK of drugs in humans, taking into consideration the impact of intrinsic patient factors (e.g., disease, age, genetics) and extrinsic patient factors (e.g., drug–drug interactions) on absorption, distribution, metabolism and excretion (ADME; Zhao et al. 2011). Until recently, owing to its mechanistic nature and the complexity of the mathematical models, the application of PBPK was restricted to predicting tissue exposure in toxicological and safety studies. But in the past two decades, with the advent of high-performance computing and the development of novel in vitro and in silico systems, population-based PBPK modeling and simulation has been successfully applied across various stages of drug discovery and development (Jones et al. 2012). Also, the availability of commercial PBPK packages such as GastroPlus™, SimCYP, PKSIM®, and Chloe®PK has enhanced the utility of PBPK models.

Extension of the PBPK methodology from traditional dosage forms to inhalation routes is imperative in selecting successful inhaled therapeutic agents with favorable pharmacokinetic and safety profiles. Within the same context, GastroPlus™ includes a mechanistic multi-compartment physiological model of the lung and the nose to describe the absorption and disposition of inhaled and intranasal aerosolized drug molecules (Miller et al. 2010).

This pulmonary model uses similar structure to that described in the ICRP66 model (Smith 1995) and is shown in Fig. 12.11. It describes the lung as a collection of five compartments:

- Optional nose (containing the anterior nasal passages)
- Extra-thoracic (naso- and oro-pharynx and the larynx)
- Thoracic (trachea and bronchi)
- Bronchiolar (bronchioles and terminal bronchioles)
- Alveolar–interstitial (respiratory bronchioles, alveolar ducts and sacs, and interstitial connective tissue)

The model describes the fate of an inhaled drug in the human body taking into consideration the physiological aspects of inhalation therapy, physicochemical characteristics of the drug, and patient factors. Immediately after inhalation, a fraction of the drug is exhaled and the remainder is either swallowed or deposited in the mucus layer lining the airways of the various pulmonary compartments in the model. The built-in ICRP 66 deposition model enables for the prediction of the regional lung deposition of the drug taking into consideration factors such as particle size, density, shape factor, etc. The drug deposited in the lung compartments then undergoes a myriad of processes such as removal by the mucociliary escalator, dissolution and absorption into pulmonary cells, metabolism, and transfer into the systemic circulation. The model provides flexibility in describing the dissolution rate kinetics of the drug in the pulmonary mucus by a variety of methods (e.g., Noyes Whitney equation) taking into account the solubility of the compound at a pH = 6.9 of mucus, particle size and shape, particle density, and aqueous diffusion coefficient. These physicochemical properties of the drug are obtained from in vitro measurements or in silico predictions.

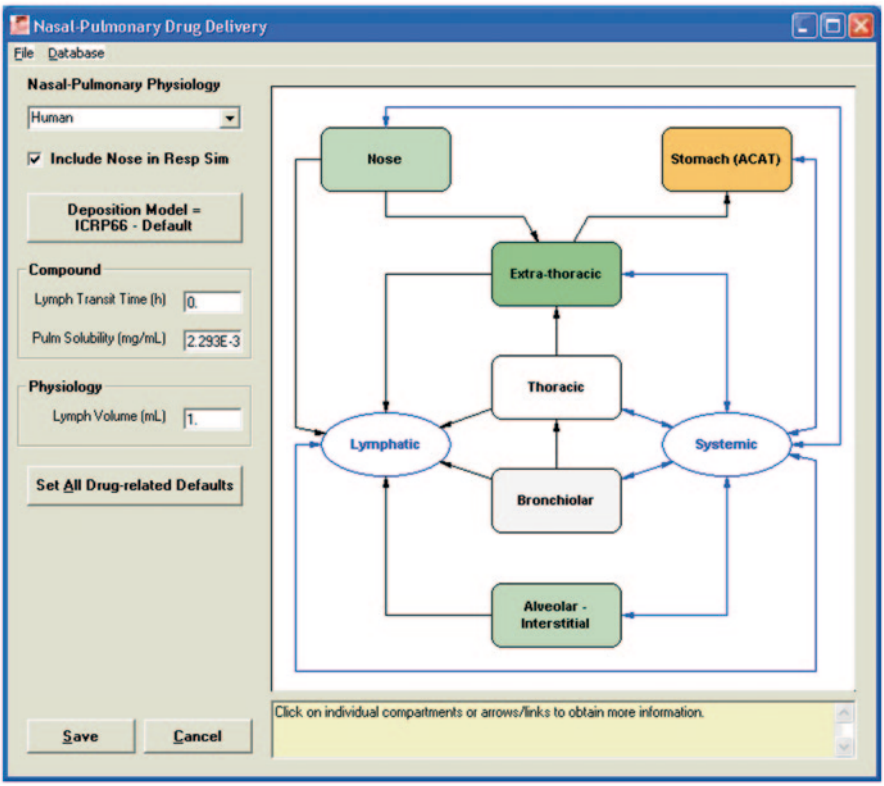

Fig. 12.11 Nasal-pulmonary drug delivery editor within the GastroPlus Additional Dosage Routes Module (ADRM). (Chaudhuri and Lukacova 2010)

The passive absorption rate of the drug is driven by concentration gradient and is dependent on the physiological and drug-dependent physicochemical properties of the drug (permeability) for each compartment. Human lung physiological parameters like surface area, thickness and volume of mucus and cell, and mucocilliary clearance rate for each compartment were obtained from literature. The drug permeability properties for each compartment are predicted from drug properties utilizing built-in models, which were generated using data obtained from literature.

The fraction of the drug deposited in oropharyngeal region and the drug removed by the mucociliary escalator and swallowed reaches the GI tract, and its kinetics is explained by advanced compartmental absorption and transit ACAT™ physiological model (Agoram et al. 2001) within GastroPlus™ connected to the lung compartments. The lung compartments are also connected to the systemic PK models to simulate drug appearance in plasma from multiple ports of entry, i.e., the GI tract and the airways.

The abovementioned pulmonary drug delivery component of the additional dosage routes module (ADRM) within GastroPlus was used to simulate absorption and PK of inhaled BUD (Miller et al. 2010) in healthy human subjects. The systemic PK parameters for BUD were obtained by fitting IV data to a three-compartmental body model using the PKPlus module and the fitted parameters were fixed to simulate

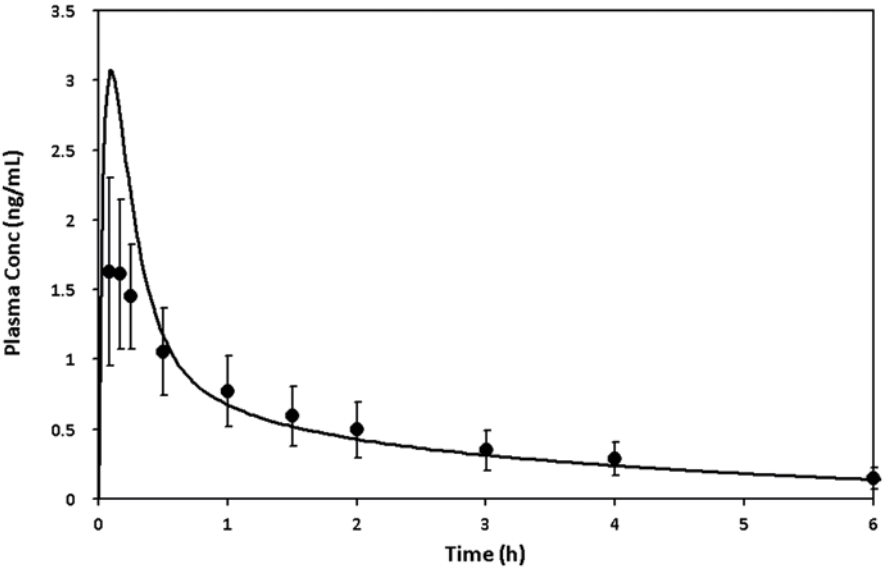

Fig. 12.12 Predicted (*line*) and observed (*circle*) plasma concentration–time profiles for inhaled administration of 0.4 mg aerosolized suspension of budesonide with no fitted parameters. (Chaudhuri and Lukacova 2010)

systemic PK for all pulmonary dosage forms. Physicochemical properties were obtained from in vitro measurements or in silico predictions. For pulmonary doses, GI physiology used the default "fasted" state human ACAT model. Deposition fractions in the lung compartment were predicted by the built-in ICRP 66 scheme. None of the parameters were fitted to the in vivo data from the pulmonary route to highlight the predictive capability of the model. The predicted plasma concentration time profile is shown in Fig. 12.12. Another example that underscores the applicability of the pulmonary model is the modeling of tobramycin (Lukacova et al. 2010) at two-dose levels and two different formulations: an aerosolized suspension (Pulmosphere, 80 mg) and a solution (TOBI, 300 mg). A similar strategy as described above was used with the only exception that, reported experimental values of deposition fractions were used in place of the ICRP 6 model. Figure 12.13 shows good agreement between the observed plasma concentration time points and the simulated profiles. Thus, this additional feature within GastroPlus serves as an invaluable tool in the development of inhaled and intranasal drug candidates.

12.6 Summary

Pharmacometrics has played a crucial role in the development of safer and more efficacious drugs during the past few years, with its enhanced utilization during various stages of drug development across therapeutic areas (Lesko et al. 2000; Gobburu and Lesko 2009; Lee et al. 2011). The role of modeling and simulation

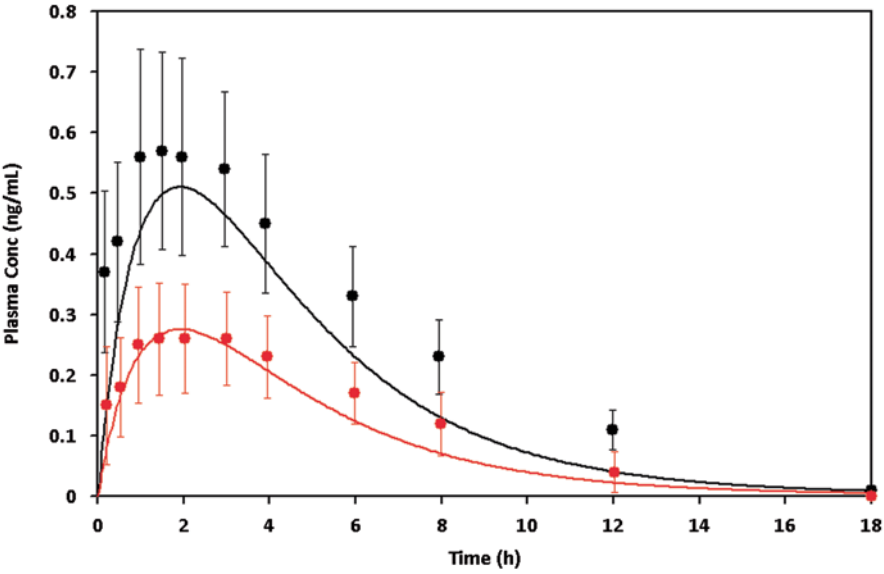

Fig. 12.13 Comparison of unfitted simulations with observed plasma concentration–time data for inhaled aerosolized administration of 80 mg suspension (*black*) and 300 mg solution (*red*) of tobramycin. *Dots* represent observed values (with *error bars*) and *lines* represent simulated profiles. (Chaudhuri and Lukacova 2010)

becomes even more important in the area of inhalation, where a plethora of factors impact the clinical performance of a drug–device combination. PK/PD models have been successfully applied in optimizing inhalation therapy by gaining a concrete understanding of the various factors that impact the targeting of the drug in the lung and also quantifying the favorable pulmonary effects and systemic side effects of locally acting inhaled drugs like corticosteroids and β-2 agonists. Advancements in computational technology and modeling software have led to the development of multi-compartment physiological and mechanistic PK models that adequately describe or predict the systemic concentration time profiles of inhaled drugs taking into consideration the physiological factors of inhalation therapy, physicochemical properties of the drug, and patient factors. Within the same context, the present chapter provides a brief summary of:

- The multitude of PK and PD factors that influence pulmonary targeting
- PK/PD approaches developed to model the systemic side effects of inhaled drugs
- Pulmonary models that explain the complicated PK behavior of inhaled drugs
- A commercially available mechanistic multi-compartment physiological model of the lung describing the absorption and disposition of inhaled drug molecules

However, there is a need to make a transition from the basic PK/PD models to enhanced PK/PD or small-to-large system models (Jusko 2013) like the corticosteroid models (Earp et al. 2008a, b), to gain a better understanding of the progression of the disease and better predict an individual's response to therapy (Vodovotz and An 2010; Iyengar et al. 2012).

Appendices

Appendix 1

```
;;1. Description: PKPD CICLESONIDE
$PROBLEM PKPD MODEL - CICLESONIDE - CORTISOL LINEAR RATE MODEL; UNITS: TIME=hour, CONC = ng/ml ; CL = l/hr, V= L
;CMT = 1 for PK, 3 for PD ;AMT=1 for CMT=3 at TIME=0 to initialize PD compartment

$INPUT  ID TIME DOSE AMT CMT DV CLI VI KAI EVID
$DATA   CIC_PKPD.csv          IGNORE = @

$SUBROUTINE  ADVAN9  TOL=11; Set up differential equation mode
$MODEL COMP(ABSORB,DEFDOSE) ;
COMP(CENTRAL)
COMP(EFFECT)

$PK
CL =      CLI                                                   ;Clearance in L/hr
V =       VI                                                    ;Central Volume of Distribution in L
KA =      KAI                                                   ;Absorption rate constant (1/hr)
RMAX = THETA(1)*EXP(ETA(1))                                     ;Max release rate at time TMAX
VDCOR = THETA(2)                                                ;Volume of distribution of cortisol
KECOR = THETA(3)                                                ;Elimination rate constant of cortisol
TMIN =  THETA(4)*EXP(ETA(2))                                    ;Time of minimum release
TMAX = THETA(5)*EXP(ETA(3))                                     ;Time of maximum release
IC50 = THETA(3)*EXP(ETA(4))                                     ;Conc of CIC causing 50% suppression of RC

F3 = RC/KECOR
K20=CL/V
S2=V2/1000

$DES
DADT(1) = -A(1)*KA ; First compartment is absorption compartment
DADT(2) = A(1)*KA -A(2)*K20
IF (TIME.LE.TMAX AND TIME.GE.TMIN) THEN
RC = ((RMAX)/(VDCOR*(TMAX-TMIN-24)))*(TIME-TMIN)
ELSE
RC = ((RMAX)/(VDCOR*(TMAX-TMIN)))*(TIME-TMIN)
ENDIF
INH = ((A(2)/S2)*IMAX)/(IC50+(A(2)/S2))                         ;INHIBITORY FUNCTION
DADT(3) = RC*(1-INH)-KECOR*A(3)                                 ;INDIRECT RESPONSE MODEL

$ERROR
IPRED = F
Y = IPRED*(1+EPS(1))+EPS(2)

$THETA
(0,3140)  ;RMAX
(33.7 FIX) ;VDCOR
(0.56 FIX) ;KECOR
(0,18)      ;TMIN
(0,22)      ;TMAX
(0,0.1)     ;IC50

$OMEGA
0.15      ;BSVRMAX
0.15      ;BSVTMIN
0.15      ;BSVTMAX
0.15      ;IC50


$SIGMA
0.2       ;ERRCV
1

$EST METHOD=COND INTERACTION MAXEVAL=9999 PRINT=5
$COV

$TABLE ID TIME DOSE AMT CMT DV IPRED PRED CWRES RMAX TMIN TMAX IC50 EVID NOPRINT ONEHEADER
        FILE = PKPDICS1_INH515_PLACEBO2
```

Appendix 2

```
;Author: user ;Description: PK Simulation Tool for ICS
$PROBLEM Pulmonary Compartment Model              ; UNITS: TIME=hour, CONC = mcg/ml ; DOSE = 5mg ; CL = l/hr, V= L
$INPUT    ID TIME CONC=DV EVID AMT CMT
$DATA     PKDATA.csv          IGNORE = C

$SUBROUTINE  ADVAN13  TOL=9 ; Set up differential equation mode
$MODEL COMP(CENTRALLUNG1,DEFDOSE)
COMP(PERIPHLUNG1)
COMP(CENTRALLUNG2)
COMP(PERIPHLUNG2)
;COMP(GUT)
COMP(CENTRAL)
COMP(PERIPH)

$PK
Kdiss = THETA(1)*EXP(ETA(1))          ; Pulmonary Dissolution Rate
Kmuc = THETA(2)*EXP(ETA(2))           ; First order Mucociliary Clearance rate
KpulC = THETA(3)                      ; Pulmonary Absorption rate (Central)
KpulP = THETA(4)                      ; Pulmonary Absorption rate (Peripheral)
CL = THETA(5)*EXP(ETA(3))             ;Clearance in L/hr
V5 = THETA(6)*EXP(ETA(4))             ;Central Volume of Distribution in L
Q  = THETA(7)*EXP(ETA(5))             ;Intercompartmental Clearance
V6 = THETA(8)*EXP(ETA(6))             ;Peripheral volume of distribution in L
F1= 0.08                              ; Central Lung Deposition (Flung*Fc = 0.16*0.5)
F2= 0.08                              ; Peripheral Lung Deposition (Flung*Fp = 0.16*0.5)
K10=CL/V5
K12=Q/V5
K21=Q/V6
S5=V5

$DES
DADT(1) = -A(1)*(Kdiss+Kmuc)          ; Central Lung Compartment Dissolution
DADT(2) = -A(2)*Kdiss                 ; Peripheral Lung Compartment Dissolution
DADT(3) = A(1)*Kdiss - A(3)*KpulC     ; Central Lung Compartment Absorption
DADT(4) = A(2)*Kdiss - A(4)*KpulP     ; Peripheral Lung Compartment Absorption
;DADT(5) = A(1)*Kmuc - A(5)*Ka        ; GI tract
DADT(5) =  A(3)*KpulC+ A(4)*KpulP - A(5)*K10 - A(5)*K12 + A(6)*K21  ; Central body Compartment
DADT(6) = A(5)*K12-A(6)*K21                    ; Peripheral body Compartment

$ERROR
IPRED = F
Y = IPRED*(1+EPS(1))+EPS(2)

$THETA
(0.189)     ;Kdiss
(0.938)     ;Kmuc
(10)        ;KpulC
(20)        ;KpulP
(73)        ;CL
(31)        ;V5
(55)        ;Q
(600)       ;V6

$OMEGA
0.09 ;BSVKdiss
0.09 ;BSVKmuc
0.09 ;BSVCL
0.09 ;BSVV5
0.09 ;BSVQ
0.09 ;BSVV6

$SIGMA
0.1 ;ERRCV Proportional
1           ;Additive
$SIM ONLYSIM (12345) NSUB=500
$TABLE ID AMT TIME DV IPRED CWRES EVID NOPRINT ONEHEADER FILE=sdtabPKMODEL1
$TABLE ID TIME AMT EVID Kdiss Kmuc KpulC KpulP CL V5 Q V6 NOPRINT ONEHEADER FILE=patabPKMODEL1
```

Appendix 3

```
;Author: user ;Description: Mechanistic Model
$PROBLEM Population PK Model for Inhaled Olodaterol  ; UNITS: TIME=hour, CONC = mcg/ml ; DOSE = X mg ; CL = l/hr, V= L

$INPUT  ID TIME CONC=DV EVID AMT CMT
$DATA   InhalDATA.csv           IGNORE = C
$SUBROUTINE  ADVAN13  TOL=9 ; Set up differential equation mode
$MODEL COMP(SLOWLUNG,DEFDOSE)
COMP(INTLUNG)
COMP(FASTLUNG)
COMP(CENTRAL)
COMP(PERIPH1)
COMP(PERIPH2)

$PK ; Define basic PK relationships
KASLOW = THETA(1)
KAINT = THETA(2)
KAFAST = THETA(3)
V4 = THETA(4)*EXP(ETA(1))
V5 = THETA(5)*EXP(ETA(2))
V6 = THETA(6)*EXP(ETA(3))
CL4 = THETA(7)*EXP(ETA(4))
CL5 = THETA(8)*EXP(ETA(5))
CL6 = THETA(9)*EXP(ETA(6))
KA = THETA(10)*EXP(ETA(7))
K40=CL4/V4
K45=CL5/V4
K46=CL6/V4
K54=CL5/V5
K64=CL6/V6
S2=V2/1000

$DES
DADT(1) = -A(1)* KASLOW                                                                    ; Slow Lung Absorption
DADT(2) = -A(2)* KAINT                                                                     ; Intermediate Lung Absorption
DADT(3) = -A(3)* KAFAST                                                                    ; Fast Lung Absorption
DADT(4) = A(1)*KASLOW+A(2)*KAINT+A(3)*KAFAST+A(5)*K54+A(6)*K64-A(4)*(K40+K45+K46) ; Central Body
DADT(5) = A(4)*K45-A(5)*K54                                                                ; Peripheral
DADT(6) = A(4)*K46-A(6)*K64                                                                ; Deep Tissue

$ERROR
IPRED = F
Y = IPRED*(1+EPS(1))+EPS(2)

$THETA
(0,0.189) ;Kdiss
(0,0.938) ;Kmuc
(10 FIX)  ;KpulC
(20 FIX)  ;KpulP
(73       FIX)      ;CL
(31       FIX)      ;V5
(55       FIX)      ;Q
(600 FIX)  ;V6

$OMEGA
0.09      ;BSVKdiss
0.09      ;BSVKmuc
0.09 FIX;BSVCL
0.09 FIX;BSVV5
0.09 FIX;BSVQ
0.09 FIX;BSVV6

$SIGMA
0.1 ;ERRCV Proportional
1           ;Additive
$EST METHOD=COND INTERACTION MAXEVAL=9999 NSIG=3 SIGL=9 PRINT=5
$COV PRINT=E
$TABLE ID AMT TIME DV IPRED CWRES EVID NOPRINT ONEHEADER FILE=sdtabPKMODEL1
$TABLE ID TIME AMT EVID Kdiss Kmuc KpulC KpulP CL V5 Q V6 NOPRINT ONEHEADER FILE=patabPKMODEL1
```

References

Abo T, Kawate T, Itoh K, Kumagai K (1981) Studies on the bioperiodicity of the immune response. I. Circadian rhythms of human T, B, and K cell traffic in the peripheral blood. J Immunol 126:1360–1363

Agoram B, Woltosz WS, Bolger MB (2001) Predicting the impact of physiological and biochemical processes on oral drug bioavailability. Adv Drug Deliv Rev 50(Suppl 1):S41–S67

Ahmed SF, Tucker P, Mushtaq T et al (2002) Short-term effects on linear growth and bone turnover in children randomized to receive prednisolone or dexamethasone. Clin Endocrinol (Oxf) 57:185–191

Ariens EJ (1954) Affinity and intrinsic activity in the theory of competitive inhibition. I. Problems and theory. Arch Int Pharmacodyn Thér 99:32–49

Bates DV, Fish BR, Hatch TF et al (1966) Deposition and retention models for internal dosimetry of the human respiratory tract. Task group on lung dynamics. Health Phys 12:173–207

Beato M, Kalimi M, Feigelson P (1972) Correlation between glucocorticoid binding to specific liver cytosol receptors and enzyme induction in vivo. Biochem Biophys Res Commun 47:1464–1472

Borghardt J, Weber B, Staab A et al (2014) Exapnding the mechanistic knowledge about pulmonary absorption processes using a population pharmacokinetic model for inhaled olodaterol. Respir Drug Deliv 2:417–422

Borgström L, Bondesson E, Morén F et al (1994) Lung deposition of budesonide inhaled via Turbuhaler: a comparison with terbutaline sulphate in normal subjects. Eur Respir J 7:69–73

Bot AI, Tarara TE, Smith DJ et al (2000) Novel lipid-based hollow-porous microparticles as a platform for immunoglobulin delivery to the respiratory tract. Pharm Res 17:275–283

Brown RA, Schanker LS (1983) Absorption of aerosolized drugs from the rat lung. Drug Metab Dispos 11:355–360

Byron PR (1986) Prediction of drug residence times in regions of the human respiratory tract following aerosol inhalation. J Pharm Sci 75:433–438

Carroll N, Cooke C, James A (1997) The distribution of eosinophils and lymphocytes in the large and small airways of asthmatics. Eur Respir J 10:292–300

Carstairs JR, Nimmo AJ, Barnes PJ (1985) Autoradiographic visualization of beta-adrenoceptor subtypes in human lung. Am Rev Respir Dis 132:541–547

Chakraborty A, Krzyzanski W, Jusko WJ (1999) Mathematical modeling of circadian cortisol concentrations using indirect response models: comparison of several methods. J Pharmacokinet Biopharm 27:23–43

Chaudhuri SR, Lukacova V (2010) Simulating delivery of pulmonary (and intranasal) aerosolised drugs, pp 26–30. ONdrugDelivery. http://www.ondrugdelivery.com/publications/OINDP%20November%202010/OINDP%20November%202010%20lo%20res.pdf. Accessed 26 Sept 2013

Chrousos GP, Harris AG (1998) Hypothalamic–pituitary–adrenal axis suppression and inhaled corticosteroid therapy. 2. Review of the literature. Neuroimmunomodulation 5:288–308

Dahlberg E, Thalén A, Brattsand R et al (1984) Correlation between chemical structure, receptor binding, and biological activity of some novel, highly active, 16 alpha, 17 alpha-acetal-substituted glucocorticoids. Mol Pharmacol 25:70–78

Daley-Yates PT, Richards DH (2004) Relationship between systemic corticosteroid exposure and growth velocity: development and validation of a pharmacokinetic/pharmacodynamic model. Clin Ther 26:1905–1919

Daley-Yates PT, Price AC, Sisson JR et al (2001) Beclomethasone dipropionate: absolute bioavailability, pharmacokinetics and metabolism following intravenous, oral, intranasal and inhaled administration in man. Br J Clin Pharmacol 51:400–409

Davies CN (1982) Deposition of particles in the human lungs as a function of particle size and breathing pattern: an empirical model. Ann Occup Hyg 26:119–135

DeHaan WH, Finlay WH (2001) In vitro monodisperse aerosol deposition in a mouth and throat with six different inhalation devices. J Aerosol Med 14:361–367

Dellamary LA, Tarara TE, Smith DJ et al (2000) Hollow porous particles in metered dose inhalers. Pharm Res 17:168–174

Derendorf H, Hochhaus G, Rohatagi S et al (1995) Pharmacokinetics of triamcinolone acetonide after intravenous, oral, and inhaled administration. J Clin Pharmacol 35:302–305

Dinh KV, Myers DJ, Noymer PD, Cassella JV (2010) In vitro aerosol deposition in the oropharyngeal region for Staccato loxapine. J Aerosol Med Pulm Drug Deliv 23:253–260. doi:10.1089/jamp.2009.0814

Druzgala P, Hochhaus G, Bodor N (1991) Soft drugs—10. Blanching activity and receptor binding affinity of a new type of glucocorticoid: loteprednol etabonate. J Steroid Biochem Mol Biol 38:149–154

Earp JC, Dubois DC, Molano DS et al (2008a) Modeling corticosteroid effects in a rat model of rheumatoid arthritis I: mechanistic disease progression model for the time course of collagen-induced arthritis in Lewis rats. J Pharmacol Exp Ther 326:532–545. doi:10.1124/jpet.108.137372

Earp JC, Dubois DC, Molano DS et al (2008b) Modeling corticosteroid effects in a rat model of rheumatoid arthritis II: mechanistic pharmacodynamic model for dexamethasone effects in Lewis rats with collagen-induced arthritis. J Pharmacol Exp Ther 326:546–554. doi:10.1124/jpet.108.137414

Edsbäcker S, Brattsand R (2002) Budesonide fatty-acid esterification: a novel mechanism prolonging binding to airway tissue. Review of available data. Ann Allergy Asthma Immunol 88:609–616. doi:10.1016/S1081-1206(10)61893-5

Edwards DA, Hanes J, Caponetti G et al (1997) Large porous particles for pulmonary drug delivery. Science 276:1868–1871

Fuglsang G, Pedersen S, Borgström L (1989) Dose–response relationships of intravenously administered terbutaline in children with asthma. J Pediatr 114:315–320

Geller DE, Weers J, Heuerding S (2011) Development of an inhaled dry-powder formulation of tobramycin using PulmoSphere™ technology. J Aerosol Med Pulm Drug Deliv 24:175–182. doi:10.1089/jamp.2010.0855

Gobburu JVS, Lesko LJ (2009) Quantitative disease, drug, and trial models. Annu Rev Pharmacol Toxicol 49:291–301. doi:10.1146/annurev.pharmtox.011008.145613

Gonda I (1988) Drugs administered directly into the respiratory tract: modeling of the duration of effective drug levels. J Pharm Sci 77:340–346

Gonda I (2004) Targeting by deposition. In: Hickey AJ (ed) Pharmaceutical inhalation aerosol technology, 2nd edn. Merckel Dekker, New York, pp 65–88

Green SA, Spasoff AP, Coleman RA et al (1996) Sustained activation of a G protein-coupled receptor via "anchored" agonist binding. Molecular localization of the salmeterol exosite within the 2-adrenergic receptor. J Biol Chem 271:24029–24035

Hardy JG, Chadwick TS (2000) Sustained release drug delivery to the lungs: an option for the future. Clin Pharmacokinet 39:1–4. doi:10.2165/00003088-200039010-00001

Harrison TW, Tattersfield AE (2003) Plasma concentrations of fluticasone propionate and budesonide following inhalation from dry powder inhalers by healthy and asthmatic subjects. Thorax 58:258–260

Hickey A, Thompson D (2004) Physiology of the airways. In: Hickey AJ (ed) Pharmaceutical inhalation aerosol technology, 2nd edn. Marcel Dekker, New York, pp 1–29

Hindle M, Longest PW (2010) Evaluation of enhanced condensational growth (ECG) for controlled respiratory drug delivery in a mouth–throat and upper tracheobronchial model. Pharm Res 27:1800–1811. doi:10.1007/s11095-010-0165-z

Hindle M, Longest PW (2012) Condensational growth of combination drug-excipient submicrometer particles for targeted high-efficiency pulmonary delivery: evaluation of formulation and delivery device. J Pharm Pharmacol 64:1254–1263. doi:10.1111/j.2042-7158.2012.01476.x

Hochhaus G, Möllmann H (1992) Pharmacokinetic/pharmacodynamic characteristics of the beta-2-agonists terbutaline, salbutamol and fenoterol. Int J Clin Pharmacol Ther Toxicol 30:342–362

Hochhaus G, Chen LS, Ratka A et al (1992a) Pharmacokinetic characterization and tissue distribution of the new glucocorticoid soft drug loteprednol etabonate in rats and dogs. J Pharm Sci 81:1210–1215

Hochhaus G, Schmidt EW, Rominger KL, Möllmann H (1992b) Pharmacokinetic/dynamic correlation of pulmonary and cardiac effects of fenoterol in asthmatic patients after different routes of administration. Pharm Res 9:291–297

Hochhaus G, Möllmann H, Derendorf H, Gonzalez-Rothi RJ (1997) Pharmacokinetic/pharmacodynamic aspects of aerosol therapy using glucocorticoids as a model. J Clin Pharmacol 37:881–892

Hong Y, Mager DE, Blum RA, Jusko WJ (2007) Population pharmacokinetic/pharmacodynamic modeling of systemic corticosteroid inhibition of whole blood lymphocytes: modeling interoccasion pharmacodynamic variability. Pharm Res 24:1088–1097. doi:10.1007/s11095-006-9232-x

Issar M, Mobley C, Khan P, Hochhaus G (2004) Pharmacokinetics and pharmacodynamics of drugs delivered to the lungs. In: Hickey A (ed) Pharmaceutical inhalation aerosol technology, 2nd edn. Marcel Dekker, New York, pp 215–252

Iyengar R, Zhao S, Chung S-W et al (2012) Merging systems biology with pharmacodynamics. Sci Transl Med 4:126ps7. doi:10.1126/scitranslmed.3003563

Jeffery PK (1987) The origins of secretions in the lower respiratory tract. Eur J Respir Dis Suppl 153:34–42

Jones HM, Dickins M, Youdim K et al (2012) Application of PBPK modelling in drug discovery and development at Pfizer. Xenobiotica 42:94–106. doi:10.3109/00498254.2011.627477

Jonkers R, van Boxtel CJ, Koopmans RP, Oosterhuis B (1989) A nonsteady-state agonist antagonist interaction model using plasma potassium concentrations to quantify the beta-2 selectivity of beta blockers. J Pharmacol Exp Ther 249:297–302

Jusko WJ (2013) Moving from basic toward systems pharmacodynamic models. J Pharm Sci 102:2930–2940. doi:10.1002/jps.23590

Koopmans RP, Braat MC, Oosterhuis B, van Boxtel CJ (1992) Time-dependent effects of dexamethasone administration on the suppression of plasma hydrocortisone, assessed with a pharmacokinetic model. J Pharmacol Exp Ther 262:503–508

Kraft M, Djukanovic R, Wilson S et al (1996) Alveolar tissue inflammation in asthma. Am J Respir Crit Care Med 154:1505–1510. doi:10.1164/ajrccm.154.5.8912772

Labiris NR, Dolovich MB (2003) Pulmonary drug delivery. Part I: physiological factors affecting therapeutic effectiveness of aerosolized medications. Br J Clin Pharmacol 56:588–599

Lee JY, Garnett CE, Gobburu JVS et al (2011) Impact of pharmacometric analyses on new drug approval and labelling decisions: a review of 198 submissions between 2000 and 2008. Clin Pharmacokinet 50:627–635. doi:10.2165/11593210-000000000-00000

Lesko LJ, Rowland M, Peck CC, Blaschke TF (2000) Optimizing the science of drug development: opportunities for better candidate selection and accelerated evaluation in humans. Pharm Res 17:1335–1344

Lipworth BJ, Jackson CM (2000) Safety of inhaled and intranasal corticosteroids: lessons for the new millennium. Drug Saf 23:11–33

Longest PW, McLeskey JT, Hindle M (2010) Characterization of nanoaerosol size change during enhanced condensational growth. Aerosol Sci Technol 44:473–483. doi:10.1080/02786821003749525

Longest PW, Tian G, Walenga RL, Hindle M (2012) Comparing MDI and DPI aerosol deposition using in vitro experiments and a new stochastic individual path (SIP) model of the conducting airways. Pharm Res 29:1670–1688. doi:10.1007/s11095-012-0691-y

Lönnebo A, Grahnén A, Karlsson MO (2007) An integrated model for the effect of budesonide on ACTH and cortisol in healthy volunteers. Br J Clin Pharmacol 64:125–132. doi:10.1111/j.1365-2125.2007.02867.x

Lukacova V, Ray Chaudhuri S, Miller N et al (2010) Simulation of tobramycin pharmacokinetics after pulmonary administration. 37th Annual Meeting & Exposition Controlled Release Society. 37th Annual Meeting and Exposition of the Controlled Release Society, Portland, OR. July 10–14, 2010.

Mackie AE, Ventresca GP, Fuller RW, Bye A (1996) Pharmacokinetics of intravenous fluticasone propionate in healthy subjects. Br J Clin Pharmacol 41:539–542

Martonen TB, Katz IM (1993) Deposition patterns of aerosolized drugs within human lungs: effects of ventilatory parameters. Pharm Res 10:871–878

Meibohm B, Derendorf H, Möllmann H et al (1999) Mechanism-based PK/PD model for the lymphocytopenia induced by endogenous and exogenous corticosteroids. Int J Clin Pharmacol Ther 37:367–376

Milad MA, Ludwig EA, Lew KH et al (1994) The pharmacokinetics and pharmacodynamics of Methylprednisolone in chronic renal failure. Am J Ther 1:49–57

Miller N, Ray Chaudhuri S, Lukacova V et al (2010) Development of physiologically-based pharmacokinetic (PBPK) model for predicting deposition and disposition following inhaled and intranasal administration. Respir Drug Deliv 2:579–584

Miller-Larsson A, Mattsson H, Hjertberg E et al (1998) Reversible fatty acid conjugation of budesonide. Novel mechanism for prolonged retention of topically applied steroid in airway tissue. Drug Metab Dispos 26:623–630

Miyawaki T, Taga K, Nagaoki T et al (1984) Circadian changes of T lymphocyte subsets in human peripheral blood. Clin Exp Immunol 55:618–622

Möllmann H, Wagner M, Meibohm B et al (1998) Pharmacokinetic and pharmacodynamic evaluation of fluticasone propionate after inhaled administration. Eur J Clin Pharmacol 53:459–467

Nagaraja NV, Pechstein B, Erb K et al (2003) Pharmacokinetic/pharmacodynamic modeling of luteinizing hormone (LH) suppression and LH surge delay by cetrorelix after single and multiple doses in healthy premenopausal women. J Clin Pharmacol 43:243–251

Nave R, Meyer W, Fuhst R, Zech K (2005) Formation of fatty acid conjugates of ciclesonide active metabolite in the rat lung after 4-week inhalation of ciclesonide. Pulm Pharmacol Ther 18:390–396. doi:10.1016/j.pupt.2005.02.012

Nave R, Fisher R, Zech K (2006) In vitro metabolism of ciclesonide in human lung and liver precision-cut tissue slices. Biopharm Drug Dispos 27:197–207. doi:10.1002/bdd.500

Newman SP, Clark AR, Talaee N, Clarke SW (1989) Pressurised aerosol deposition in the human lung with and without an "open" spacer device. Thorax 44:706–710

Newman SP, Brown J, Steed KP et al (1998) Lung deposition of fenoterol and flunisolide delivered using a novel device for inhaled medicines: comparison of RESPIMAT with conventional metered-dose inhalers with and without spacer devices. Chest 113:957–963

Newman S, Salmon A, Nave R, Drollmann A (2006) High lung deposition of 99mTc-labeled ciclesonide administered via HFA-MDI to patients with asthma. Respir Med 100:375–384. doi:10.1016/j.rmed.2005.09.027

Nikander K, Prince I, Coughlin S et al (2010) Mode of breathing-tidal or slow and deep-through the I-neb Adaptive Aerosol Delivery (AAD) system affects lung deposition of (99m)Tc-DTPA. J Aerosol Med Pulm Drug Deliv 23(Suppl 1):S37–S43. doi:10.1089/jamp.2009.0786

Oneda K (1999) Dexamethasone-induced apoptosis in peripheral T lymphocytes from patients with asthma. Arerugi 48:13–22

Palm S, Postler E, Hinrichsen H et al (1996) Twenty-four-hour analysis of lymphocyte subpopulations and cytokines in healthy subjects. Chronobiol Int 13:423–434

Peet CF, Enos T, Nave R et al (2005) Identification of enzymes involved in phase I metabolism of ciclesonide by human liver microsomes. Eur J Drug Metab Pharmacokinet 30:275–286

Petruzzelli S, De Flora S, Bagnasco M et al (1989) Carcinogen metabolism studies in human bronchial and lung parenchymal tissues. Am Rev Respir Dis 140:417–422. doi:10.1164/ajrccm/140.2.417

Pitcairn G, Reader S, Pavia D, Newman S (2005) Deposition of corticosteroid aerosol in the human lung by Respimat Soft Mist inhaler compared to deposition by metered dose inhaler or by Turbuhaler dry powder inhaler. J Aerosol Med 18:264–272. doi:10.1089/jam.2005.18.264

Rohatagi S, Hochhaus G, Mollmann H et al (1995) Pharmacokinetic and pharmacodynamic evaluation of triamcinolone acetonide after intravenous, oral, and inhaled administration. J Clin Pharmacol 35:1187–1193

Rohatagi S, Bye A, Mackie AE, Derendorf H (1996a) Mathematical modeling of cortisol circadian rhythm and cortisol suppression. Eur J Pharm Sci 4:341–350

Rohatagi S, Täuber U, Richter K, Derendorf H (1996b) Pharmacokinetic/pharmacodynamic modeling of cortisol suppression after oral administration of fluocortolone. J Clin Pharmacol 36:311–314

Rohatagi S, Arya V, Zech K et al (2003) Population pharmacokinetics and pharmacodynamics of ciclesonide. J Clin Pharmacol 43:365–378

Rohatagi S, Luo Y, Shen L et al (2005) Protein binding and its potential for eliciting minimal systemic side effects with a novel inhaled corticosteroid, ciclesonide. Am J Ther 12:201–209

Ryrfeldt A, Andersson P, Edsbäcker S et al (1982) Pharmacokinetics and metabolism of budesonide, a selective glucocorticoid. Eur J Respir Dis Suppl 122:86–95

Schanker LS, Mitchell EW, Brown RA (1986) Species comparison of drug absorption from the lung after aerosol inhalation or intratracheal injection. Drug Metab Dispos 14:79–88

Singh SD, Whale C, Houghton N et al (2003) Pharmacokinetics and systemic effects of inhaled fluticasone propionate in chronic obstructive pulmonary disease. Br J Clin Pharmacol 55:375–381

Slayter KL, Ludwig EA, Lew KH et al (1996) Oral contraceptive effects on methylprednisolone pharmacokinetics and pharmacodynamics. Clin Pharmacol Ther 59:312–321. doi:10.1016/S0009-9236(96)80009-9

Smith H (1995) Human respiratory tract model for radiological protection. ICRP Publication (1994) 66. Ann. ICRP 24:1–3

Stark JG, Werner S, Homrighausen S et al (2006) Pharmacokinetic/pharmacodynamic modeling of total lymphocytes and selected subtypes after oral budesonide. J Pharmacokinet Pharmacodyn 33:441–459. doi:10.1007/s10928-006-9013-5

Stuart BO (1984) Deposition and clearance of inhaled particles. Environ Health Perspect 55:369–390

Suarez S, Gonzalez-Rothi RJ, Schreier H, Hochhaus G (1998) Effect of dose and release rate on pulmonary targeting of liposomal triamcinolone acetonide phosphate. Pharm Res 15:461–465

Suntres ZE, Shek PN (1998) Liposomes promote pulmonary glucocorticoid delivery. J Drug Target 6:175–182. doi:10.3109/10611869808997891

Thiel CG (1998) Can in vitro particle size measurements be used to predict pulmonary deposition of aerosol from inhalers? J Aerosol Med 11(Suppl 1):S43–S52

Tian G, Longest PW, Li X, Hindle M (2013) Targeting aerosol deposition to and within the lung airways using excipient enhanced growth. J Aerosol Med Pulm Drug Deliv 26:248–265. doi:10.1089/jamp.2012.0997

Tunek A, Sjödin K, Hallström G (1997) Reversible formation of fatty acid esters of budesonide, an antiasthma glucocorticoid, in human lung and liver microsomes. Drug Metab Dispos 25:1311–1317

Tyler WS (1983) Comparative subgross anatomy of lungs. Pleuras, interlobular septa, and distal airways. Am Rev Respir Dis 128:S32–S36

Usmani OS, Biddiscombe MF, Barnes PJ (2005) Regional lung deposition and bronchodilator response as a function of beta2-agonist particle size. Am J Respir Crit Care Med 172:1497–1504. doi:10.1164/rccm.200410-1414OC

Van Gossum A, Schmit A, Peny MO (1998) Oral budesonide for lymphocytic colitis. Am J Gastroenterol 93:270. doi:10.1111/j.1572-0241.1998.270_1.x

Vodovotz Y, An G (2010) Systems biology and inflammation. Methods Mol Biol 662:181–201. doi:10.1007/978-1-60761-800-3_9

Wald JA, Law RM, Ludwig EA et al (1992) Evaluation of dose-related pharmacokinetics and pharmacodynamics of prednisolone in man. J Pharmacokinet Biopharm 20:567–589

Weber B, Hochhaus G (2013) A pharmacokinetic simulation tool for inhaled corticosteroids. AAPS J 15:159–171. doi:10.1208/s12248-012-9420-z

Weda M, Zanen P, de Boer AH et al (2008) The therapeutic index of locally acting inhaled drugs as a function of their fine particle mass and particle size distribution: a literature review. Curr Drug Deliv 5:142–147

Weibel E (1963) Morphometry of the human lung, 1st edn. Springer, New York
Winkler J, Hochhaus G, Derendorf H (2004) How the lung handles drugs: pharmacokinetics and pharmacodynamics of inhaled corticosteroids. Proc Am Thorac Soc 1:356–363. doi:10.1513/pats.200403-025MS
Xu J, Nave R, Lahu G et al (2010) Population pharmacokinetics and pharmacodynamics of inhaled ciclesonide and fluticasone propionate in patients with persistent asthma. J Clin Pharmacol 50:1118–1127. doi:10.1177/0091270009354994
Zhao P, Zhang L, Grillo JA et al (2011) Applications of physiologically based pharmacokinetic (PBPK) modeling and simulation during regulatory review. Clin Pharmacol Ther 89:259–267. doi:10.1038/clpt.2010.298

Chapter 13
State-of-the-Art Pharmacometric Models in Osteoporosis

Teun M. Post, Anna Georgieva Kondic, Antonio Cabal, Ghassan N. Fayad, Khamir Mehta and Thomas Kerbusch

13.1 Introduction

Osteoporosis is a progressive degenerative bone disease associated with an increased fracture risk. Due to the related morbidity, mortality, and costs with a general increase in life expectancy, this makes osteoporosis an important worldwide health issue.

Burge et al. (2007) conducted an epidemiology study in the USA on the burden of osteoporosis-related fractures and costs in 2005, and using a state transition Markov decision model predicted how those quantities would grow for the period of 2005–2025. Starting at 2005, the actual numbers were 2 million fractures with an associated cost of $ 19 billion. Due to aging population, the numbers are predicted to increase by 50 % by 2025 with 72 % due to hip fractures (Burge et al. 2007). Similar studies have been published in other countries (Rajagopal et al. 2008).

Due to statistical requirements and the slow progression of the disease, large clinical trials with long duration are required to establish a beneficial effect of new treatments on the reduction of fracture risk. Over time, knowledge about bone physiology and the mechanisms underlying bone diseases has increased. Furthermore, various conceptual, mathematical, statistical, and epidemiological models have been established providing further insight into the biology, mechanisms, and predictive factors of osteoporosis and corresponding fracture risk (Post et al. 2010).

T. M. Post (✉) · A. Cabal · G. N. Fayad · K. Mehta · T. Kerbusch · A. Georgieva Kondic
Quantitative Pharmacology & Pharmacometrics, Merck, Sharpe & Dohme Corp., Oss, The Netherlands
e-mail: teun.post@merck.com; teunpost@gmail.com

S. Schmidt, H. Derendorf (eds.), *Applied Pharmacometrics,* AAPS Advances in the Pharmaceutical Sciences Series 14, DOI 10.1007/978-1-4939-1304-6_13

Over the past decade, different types of mechanism-based models have had an increasing impact on drug development and none more so than models of osteoporosis. There has been an increasing body of work elucidating the mechanisms behind the (patho-)physiology of osteoporosis, including the maturation and crosstalk between osteoclasts and osteoblasts and how the balance between bone resorption and bone formation changes with age and hormonal imbalance. The intrinsic nonlinearities, feedbacks, and different time-scales present in the system may lead to counter-intuitive behavior, making mathematical modeling a useful analysis tool. Various conceptual models for bone physiology and the effects of therapies have been proposed. Data included in osteoporosis models range from pharmacokinetics (PK) of (novel) drugs, pharmacodynamics (PD) biomarkers of various time scales (peptides indicative of bone-turnover, bone mineral density), bone strength, as well as the actual clinical outcome, namely, fracture rates at various sites in the skeleton (Post et al. 2010).

Published PK-PD-disease models of osteoporosis have varying degrees of biological complexity ranging from purely descriptive of disease to detailed system models spanning various spatial scales, as well as mechanistic models of bone strength. The possible identification and estimability of parameters typically decline with complexity. Deciding between the use of descriptive, semi-mechanistic, or full mechanistic models should be driven by the drug development question at hand (model fit for purpose), the availability of data, as well as whether one needs the model for extrapolation versus interpolation. These models have been used to describe data from clinical trials, simulate new trial designs with novel mechanisms of action (e.g., what doses will result in what extent of effect on biomarkers/end points, differentiation between subpopulation of patients), simulate combination treatments (e.g., what synergy—if any—should be expected?), and how these clinical trials predict for real-life settings (e.g., prevention of fractures in elderly; Post et al. 2010).

In what follows, we start by describing the main components of bone physiology and the transition to the pathophysiology of osteoporosis. Then, we provide a general description of modeling approaches to osteoporosis, followed by a series of examples of specific model applications.

13.2 Overview of Osteoporosis Components for Modeling

13.2.1 Introduction to Bone Physiology and Pathophysiology

The biology of bone formation and resorption (a process known as bone remodeling; Fig. 13.1) and how it links to the pathophysiology of osteoporosis is progressively better understood. Bone remodeling is mainly the result of the actions of two types of cells, osteoclast and osteoblasts. In the healthy state, resorption and formation are balanced and bone remodeling leads to bone renewal. The osteoclasts

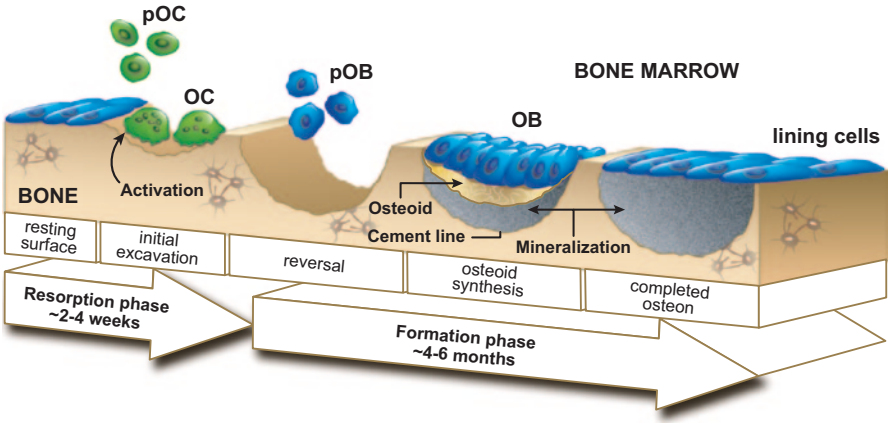

Fig. 13.1 Overview of physiological process of bone remodeling: resorption and formation

attach to the bone surface and act by removing the mineralized matrix and breaking up the organic bone component in the resorption lacuna. When resorption is complete, osteoclasts detach and die by apoptosis. In turn, the osteoblasts attach to the bone and produce a matrix of osteoid, composed predominantly of type I collagen, followed by mineralization of this matrix. The differentiation of preosteoblasts into active cells is triggered via signaling from the osteoclasts. During the mineralization process, a fraction of osteoblasts get trapped in the bone matrix, and differentiate to osteocytes (Manolagas 2000; Boyle et al. 2003).

Our current understanding is that bone remodeling is controlled through:

1. The secretion of transforming growth factor beta (TGF-β) by osteoclasts triggering the differentiation of preosteoblasts to responsive osteoblasts (early osteoblasts that are highly responsive to differentiation signals), and attenuating the differentiation of responsive osteoblasts to active osteoblasts (responsible for bone formation), controlling the build-up of a population of responsive osteoblasts that will colonize the resorption lacuna once the osteoclasts population has died out (Manolagas 2000; Boyle et al. 2003).
2. The receptor activator of nuclear factor κ B (RANK)—receptor activator of nuclear factor κ B ligand (RANKL)-osteoprotegerin (OPG) pathway, which is dedicated to the control of the osteoclasts population by osteoblasts. Schematically, active osteoblasts produce RANKL that interact with RANK located at the surface of osteoclasts precursors. Occupied RANK receptors trigger the differentiation of preosteoclasts in osteoclasts. Production of OPG that inhibits RANKL by the responsive osteoblasts ensures that the osteoclast population grows only at the end of the formation process (Aubin and Bonnelye 2000; Boyle et al. 2003).

Bone loss occurs in postmenopausal women as a result of an increase in the rate of bone remodeling and an imbalance between the activity and number of osteoclasts and osteoblasts. The bone loss occurs in two phases: (1) a rapid one, due to

predominantly estrogen deficiency and (2) a slower one, observed also in men, due to the effects of aging. While the effects of estrogen on bone are not fully understood, it is hypothesized that they may act at least partly through the osteoblasts (e.g., increased synthesis of TGF-β or decreasing OPG with decreasing estrogen), tipping the balance in bone remodeling. The effect of aging is thought to be due to a lot of factors, such as vitamin D deficiency, leading to impaired calcium absorption and increased parathyroid hormone (PTH) secretion, as well as impaired osteoblast function due to continued decline of estrogen, decreased physical activity, and decreased secretion of growth hormone (Raisz 2008).

13.2.2 Metrics of Bone Physiology

The long-term clinical end point in osteoporosis is bone fracture. Bone's material properties are assessed by a mechanical test that yields a stress–strain curve, including breaking point (Cusick et al. 2011; Lotinun et al. 2013). The linear portion of the curve, known as Young's modulus represents stiffness, while the height and inflection point are two different measures of bone strength. It has become increasingly more common to estimate bone strength through the use of finite-element analysis (FEA; Bouxsein and Seeman 2009).

Bone is categorized into two types: cortical and trabecular bone. Cortical bone, mainly the outer shell of bone, makes up about 80 % of bone mass. Trabecular bone, which accounts for only 20 % of bone mass, makes up about 80 % of bone surface. Cortical bone has a high resistance to bending and torsion and gives mechanical strength and protection. Trabecular bone is less dense than cortical bone, providing mechanical support and has a higher turnover rate than cortical bone providing a resource for calcium and phosphate for the maintenance of mineral homeostasis (Post et al. 2010).

While bone mineral density (BMD), the amount of mineral matter per square centimeter of bone is currently the best single, easy accessible, predictor of bone strength, it accounts only for 44 % of the fracture risk. Contributing to the overall bone strength are also shape, geometry, microarchitecture, bone tissue composition, mineralization, micro-damage, and the rate of bone turnover (Post et al. 2010). The most relevant areas for measuring BMD in relation to fractures are the spine (predominantly trabecular), hip (mix of trabecular and cortical), and the wrist (mainly cortical). In addition, BMD is used as a diagnostic predictor for post-menopausal osteoporosis (Melton III et al. 2003; WHO Study group 1994).

Biochemical turnover makers (BTMs) provide easily accessible information on the state of bone physiology on the shorter term. The combination of BTM and BMD has been shown to more accurately predict the risk of fracture than either marker alone, which advocates an integrated approach (Post et al. 2010). BTM can be divided into three categories: collagenous bone resorption markers, bone formation markers, and markers of osteoclast regulatory proteins (Post et al. 2010). The first are degradation products of bone collagen; most commonly used clinically are C- and N-telopeptides of collagen cross-links (CTx and NTx with existing assays in

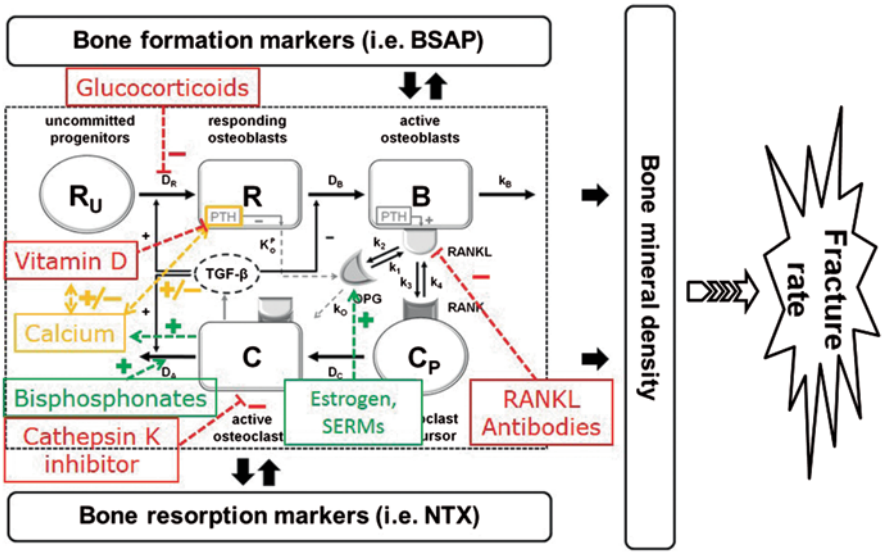

Fig. 13.2 Overview of osteoporosis mechanism of action and drug targets. (Source: Post et al. 2013, with kind permission from Springer Science+Business Media B.V.)

both serum and urine). The bone formation markers are measures of enzyme activity of osteoblasts, measures of bone protein, or measures of procollagen markers; commonly used are bone-specific alkaline phosphatase (BASP), osteocalcin (OC) and carboxy- and amino-terminal propeptide of type I collagen (procollagen type I C-terminal propeptide, PICP, and procollagen type I N-terminal propeptide, PINP). The osteoclast regulatory proteins are either markers reflecting the rate of osteoclastogenesis or the osteoclast numbers (Post et al. 2010).

13.2.3 Treatment of Osteoporosis

Various treatment paradigms have been developed that leverage the ability to influence specific components of the osteoblast–osteoclast interaction (Fig. 13.2). Treatments can be distinguished based on their differences in mechanism, site, and mode of action.

Treatments are categorized into those that (1) decrease resorption, (2) increase formation, or (3) a combination of these actions (Post et al. 2010).

13.2.3.1 Decreased Resorption

- The antiresorptive treatments include hormone replacement therapy, bisphosphonates, selective estrogen receptor modulators, and calcitonin. The bisphosphonates (e.g., alendronate, risendronate, zolendronate) act directly on the

osteoclasts' ability to resorb bone cells. This class of drugs is known to bind preferentially to calcium hydroxyapatite and can stay in the bone for years which has implications for replacement therapies.

- The RANKL inhibitor denosumab (a fully human monoclonal antibody) is a more targeted therapy, which results in osteoclast apoptosis and decreased bone resorption while avoiding some of the side effects associated with the bisphosphonate class (Baron et al. 2011). The importance of RANK–RANKL pathway was described above.
- It is recognized that estrogen, especially started soon after menopause, can maintain bone density but also leads to increased risk for blood clots, cancer, and heart disease. The selective estrogen receptor modulator (SERM) raloxifene mimics the effects of estrogen while avoiding some (but not all side effects).
- Fortical is a nasal spray that mimics the effects of calcitonin, a substance produced by the thyroid gland; it inhibits bone resorption but to a lesser degree.
- Selective and reversible inhibitors of the enzyme cathepsin K form a novel class of osteoporosis therapy. Odanacatib is currently being investigated in a phase 3 trial focused on fracture risk reduction and long-term safety. Odanacatib reduces osteoclastic bone resorption (cathepsin K-mediated) and preserves bone formation during bone remodeling (Bone et al. 2010; Langdahl et al. 2012). These actions are thought to mediate the increases in bone mineral density observed in patients with low bone mass treated with odanacatib (Bone et al. 2010; Langdahl et al. 2012). Preclinical data indicated that cathepsin K inhibition may also increase periosteal bone modeling (Cusick et al. 2011).

13.2.3.2 Increased Formation

- Injectable PTH (Forteo), which acts to preferentially increase the activity of osteoblasts. Due to the coupled mechanism of formation and resorption, the increase in formation upon continuously administered PTH leads to resorption, which presents an interesting phenomenon to be captured by modeling. The frequency of administration (daily subcutaneous injection) has largely limited the use of Forteo to severe osteoporosis patients.
- Finally, there are newer investigational medications blocking sclerostin (Amgen, Lilly, and Novartis). The full mechanism by which sclerostin causes osteoblast apoptosis is still under investigation but there is increasing evidence that sclerostin (i.e., mutations of sclerostin associated with sclerosteosis, a condition with abnormal increase in bone growth) is a promising new target for treatment of severe osteoporosis (McClung et al. 2012).

Calcium and vitamin D derivatives are important supplements that positively influence bone homeostasis and are part of the daily regimen for patients with postmenopausal osteoporosis.

Finally, there are new treatment paradigms under consideration, such as combination therapy or sequential therapy (short period with anabolic treatment, followed

by a longer maintenance with antiresorptive drug for patients with severe osteoporosis). Post et al. (2013) highlight the utility of modeling when trying to understand what the effects of such treatment regimen might be after incorporating the specific treatment effects and PK of the drug and what the effects of drug withdrawal on the bone system are.

13.3 General Pharmacometrics of Osteoporosis

Various conceptual, mathematical, statistical, and epidemiological models have been established providing insight into the biology, mechanisms, and predictive factors of osteoporosis (Post et al. 2010). In general terms, the statistical and epidemiological model provide valuable information on the correlation, predictive value, and interrelated time courses of various BTMs, BMD, and clinical outcomes and this field of research has provided valuable insight into the influences of various factors, such as age, lifestyle, and menopause, and has made it possible to evaluate, statistically confirm and compare the effects of different treatments. The conceptual mathematical models provide insight into the dynamics of the markers, the bone physiology dynamics, and are amenable for quantitative modeling purposes and are therefore the focus of this chapter. This type of modeling can be either descriptive or based on known bone physiology, i.e., more mechanistically inspired.

The benefit lies in the fact that vastly different rates of the markers or indirectly the biological system and time-variant changes in the course of the disease are incorporated. General examples of the descriptive type of modeling in osteoporosis either include single markers of bone turnover, BMD, or fracture risk or combinations of these components (Post et al. 2010).

A more integrative approach allows for a mechanism-based description of osteoporosis, and presumably other bone diseases, by explicitly including bone physiology as the underlying mechanism to which all information is linked. Various short- and long-term markers at various levels and timescales of the disease and drug action can then be combined and evaluated. The following section will describe one initial mathematical model on which two of the specific pharmacometrics of osteoporosis examples are based.

13.3.1 Bone Turnover Markers and Bone Mineral Density: Mechanism-Based Models Based on Bone Cell Interaction—Core Physiological Model

One of the first comprehensive conceptual semi-mechanistic mathematical models for bone cell interaction was published by Lemaire et al. (2004). This seminal model (Figs. 13.2 and 13.3) described pools of cells from both osteoclast and osteoblast cell lineages at different levels of maturation. Responding osteoblasts (R)

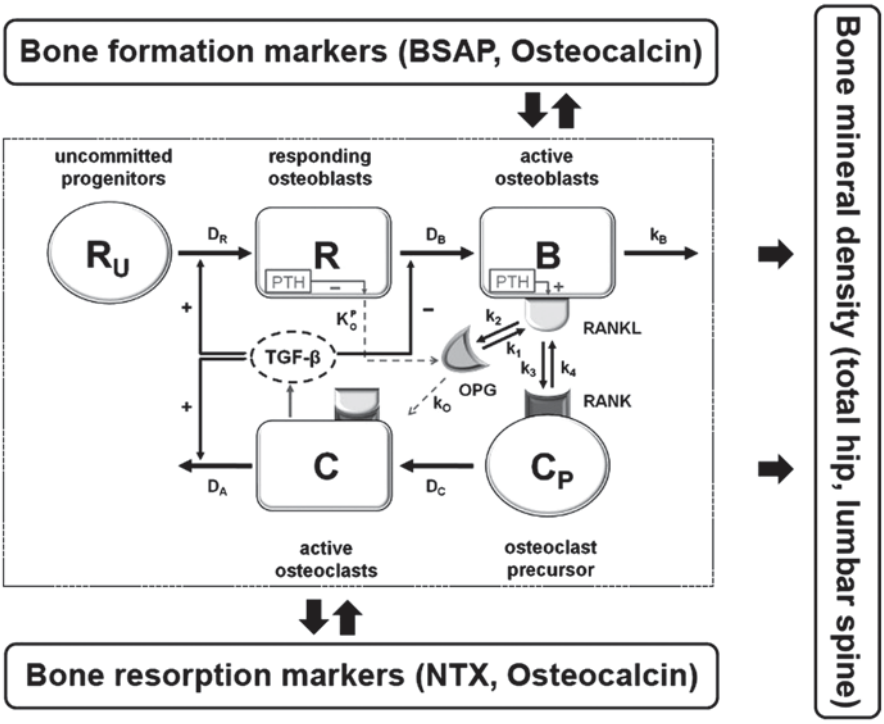

Fig. 13.3 Overview of osteoporosis mechanism of action and role of biomarkers for bone turnover and bone mineral density. (Source: Post et al. 2013, with kind permission from Springer Science+Business Media B.V.)

are recruited from a large pool of uncommitted osteoblast progenitor cells (R_u), which then differentiate into active, bone-forming osteoblasts (B). Active, bone-removing osteoclasts (C), on the other hand, are recruited from a pool of osteoclast progenitor cells (CP) upon stimulation of RANK by its ligand (RANKL). This latter process is inhibited by OPG, a soluble decoy receptor for RANKL that is formed by the responding osteoblasts. Other approaches have been published also taking into account a mathematical description of bone physiology (Komarova et al. 2003; Rattanakul et al. 2003; Moroz et al. 2006; Wimpenny and Moroz 2007; Earp et al. 2008; Pivonka et al. 2008; Peterson and Riggs 2010; Pivonka and Komarova 2010; Marathe et al. 2011; Zumsande et al. 2011; Riggs et al. 2012).

In addition, the model captures some of the postulated effects of TGF-β and PTH. In particular, TGF-β which is released from bone by active osteoclasts during bone resorption (1) stimulates the recruitment of responding osteoblasts, (2) inhibits the differentiation of responding osteoblasts into active osteoblasts, and (3) stimulates the apoptosis of active osteoclasts. On the other hand, PTH, through binding to its receptors expressed by osteoblasts, stimulates the expression of RANKL and

suppresses the secretion of OPG; we need to mention that the model by Lemaire et al. (2004) only captures the resorptive effects of PTH.

Mathematically, this translates into the following set of differential equations:

$$\begin{cases} \dfrac{dR}{dt} = D_R \pi_C - \dfrac{D_B}{\pi_C} R \\ \dfrac{dB}{dt} = \dfrac{D_B}{\pi_C} R - k_B B \\ \dfrac{dC}{dt} = D_C \pi_L(R,B) - D_A \pi_C C \end{cases}$$

in which *R, B,* and *C* denote the concentrations of responding osteoblasts, active osteoblasts, and osteoclasts, respectively, D_R, D_B, D_C represents the differentiation rates of osteoblast progenitors, responding osteoblasts, and osteoclast precursors, k_B the apoptosis rate of active osteoblasts and D_A the osteoclast apoptosis rate due to TGF-β. Finally, π_C and π_L (*R, B*) denote the TGF-β receptor occupancy and the RANK receptor occupancy. The expressions for these parameters, as well as the detailed derivations can be found in Lemaire et al. (2004).

Various extensions to the model of Lemaire were made, including explicitly incorporating calcium dynamics by Peterson and Riggs et al. and describing bone dynamics in rheumatoid arthritis by Earl et al. (Lemaire et al. 2004; Riggs et al. 2012; Earp et al. 2008; Peterson and Riggs 2010). It is worth noting that elements of this approach were also presented in Marathe et al. (2011) where the authors combined the original Lemaire et al. (2004) model and linked the number of osteoclasts to biomarkers of resorption in order to characterize the effect of the RANKL inhibitor denosumab but in multiple myeloma patients, a cancer accompanied by bone lesions. This Lemaire model forms the basis for two specific applied examples described below.

13.4 Specific Applied Examples of Pharmacometrics in Osteoporosis

13.4.1 Mechanism-Based Models of Bone Turnover Markers and Bone Mineral Density

13.4.1.1 Reduced Core Physiological Model Describing Five Biomarkers in a Population Approach

In work from Post (2009) and Schmidt et al. (2011) a way was proposed to reduce the system by Lemaire to one describing the dynamics of only osteoblasts (B) and osteoclasts (C), such that the dynamics of the system are kept and the different timescales in the system can be described as explained below:

$$\begin{cases} \dfrac{dB}{dt} = D_R \pi_C(C) - k_B B \\ \dfrac{dC}{dt} = D_C \dfrac{\alpha B}{1+\beta R} - D_A \pi_C(C) C \end{cases},$$

with the function $R = R(C)$ defined by

$$R(C) \underline{\underline{\text{def}}} \frac{D_B}{R_R} \pi_C^2(C).$$

In applying this reduced system to clinical data, Post et al. connected the dimensionless cell concentrations to the corresponding biomarkers of turnover and also to the bone mineral density measures (Post et al. 2010; Post 2009). This application of the reduced core model to clinical data was done via the population approach. To be able to include disease and treatment-related changes and to include multiple markers, the changes in B and C were related to their respective baseline values B_0 and C_0, resulting in a dimensionless system:

$$y = \frac{B}{B_0} \quad \text{and} \quad z = \frac{C}{C_0},$$

such that

$$\begin{cases} \dfrac{dy}{dt} = k_B \{\sigma(z) - y\} \\ \dfrac{dz}{dt} = D_A \pi_z(1) \left\{ \dfrac{1+b}{1+bf(t)\sigma^2(z)} y \cdot P_{Ca} \cdot E(T_i) - \sigma(z) z \right\} \end{cases},$$

$$\sigma(z) = \frac{\pi_z(z)}{\pi_z(1)},$$

where P_{Ca} and $E(T_i)$ are treatment effects of calcium and tibolone, respectively and $f(t)$ presents the disease progression related to a decline in estrogen during menopause.

This resulted in the ability to include bone turnover markers describing resorption in this system through a functional relationship of the form

$$X = X_0 p^{\rho X},$$

where the marker is linked to the dimensionless activity p, which is either z for resorption or y for formation. Biomarkers of formation (i.e., BSAP) are linked to osteoblast activity. Osteocalcin (OC) is linked to both y and z because it is produced by osteoblasts incorporated into bone and thereafter, released from bone during another resorption cycle. Markers of resorption (i.e., NTx) are linked to osteoclast activity z.

The site-specific (lumbar spine and total hip) BMD is modeled using the ratio $S = z / y$ in the following functional form:

$$\frac{dBMD}{dt} = k(1 - S^{\rho BMD}),$$

where S presents the ratio between the activities of resorption and formation, k is the turnover rate of BMD, and ρBMD is a transduction parameter relating changes in bone cells to BMD.

In this form, the reduced Lemaire model can be applied to describe the dynamics of the osteoblast/clast system under conditions of drug treatment, as it has enough granularity to capture various driving events/conditions, namely disease progression (trajectory relative to the start-of-menopause), start-of-treatment, achievement of systems (disease) steady-state, and end-of-treatment.

The system resulted in the ability to describe the effects of treatment based on clinical data within a population approach including data of NTx, BSAP, OC as bone turnover markers and lumbar spine and total hip BMD. Figure 13.4 gives the description of the model to the data by means of a predictive check (selected doses and data).

The quantitative description of the clinical biomarker data by this reduced mechanism-based core model enables the evaluation of the drug treatment effects on the various short- and long-term biomarkers. Once further developed and qualified with different biomarkers and treatments, this approach may be used to predict changes in long-term biomarkers based on short-term biomarker response. Ultimately, this model should be linked to other measures of bone strength and ultimately fracture risk (Figs. 13.2 and 13.3).

Below is an example (Fig. 13.5) which shows how to translate the estimated parameters to the course of the changes in relative osteoblasts ($z = B/B_0$) and osteoclasts ($y = C/C_0$) where the state of the RANK–RANKL–OPG system changes with each event and achieves different relative osteoblast and osteoclast turnover (z, y space) starting from healthy state (1,1). This gives a means to visualize the various changes in a two-dimensional plot. Each change in the system is defined as an orbit. The green orbit represents natural disease progression, while the blue orbit represents the addition of calcium treatment (aka placebo orbit). The solid red orbit describes the transition upon infinite tibolone treatment and the dashed red orbit represents the resetting upon treatment discontinuation after 1000 days.

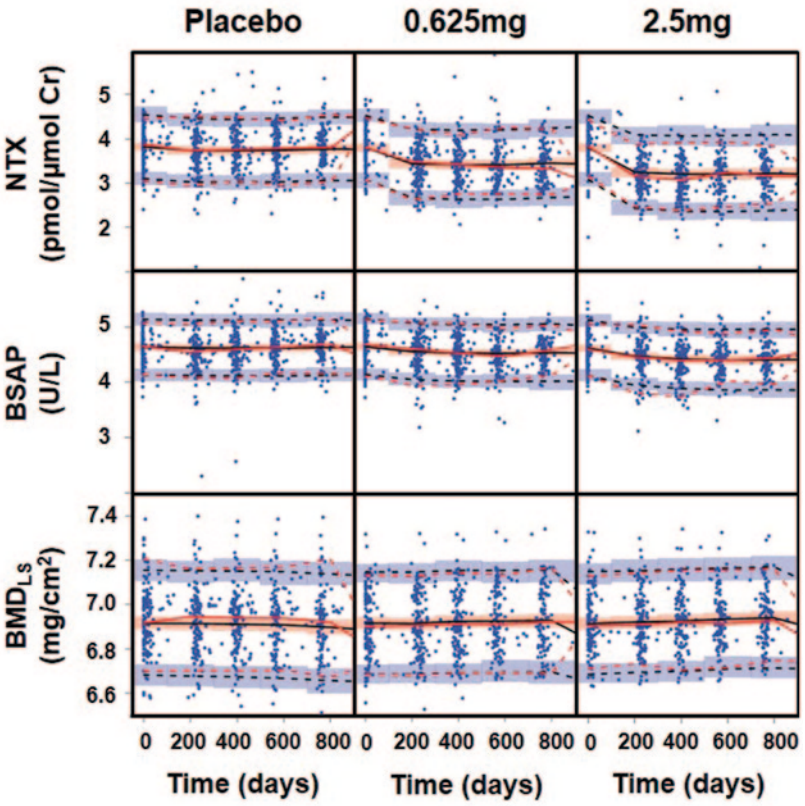

Fig. 13.4 Visual predictive check of the marker NTx, BSAP, and lumbar spine bone mineral density (*BMD*) (Post et al. 2013, with kind permission from Springer Science+Business Media B.V.). The *blue dots* represent the natural logarithms of the observations. The 5th, 50th, and 95th percentiles of the observations are presented by the *red dashed* and *red solid lines*. The 5th, 50th, and 95th percentiles of the simulated data are presented by the *black dashed* and *black solid lines.* The confidence intervals for the simulated data's 5th, 50th, and 95th percentiles are presented by the *blue, red,* and *blue area,* respectively

13.4.1.2 Extended Physiological Model in a Systems Biology Approach

Another mathematical model of dynamics of bone remodeling based on available physiological observations, specifically in the context of the mechanisms of action of available osteoporosis treatments was recently developed by Mehta et al. (2012). This work builds on prior approaches of Peterson and Riggs et al. (Peterson and Riggs 2010; Riggs et al. 2012), Marathe et al. (2008), Lemaire et al. (2004), and Komarova et al. (2003) and is novel in how it integrates known interventions in osteoporosis disease mitigation with an explicit connection to existing therapies. It also differs in the way it approaches the formulation of the model and how it retains the conceptual clarity of the relationships between the state variables and the model

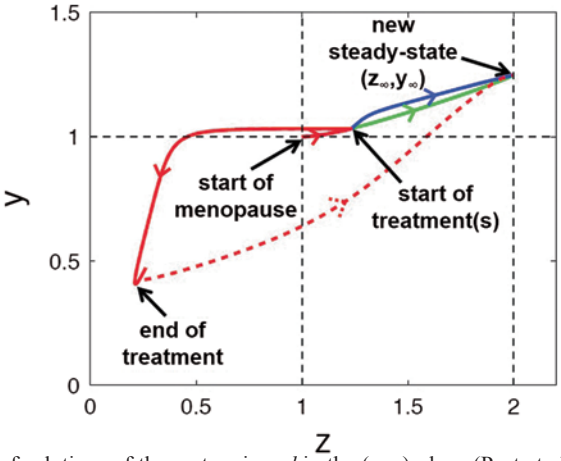

Fig. 13.5 Orbits of solutions of the system in *red* in the (z, y)-plane (Post et al. 2013, with kind permission from Springer Science+Business Media B.V.). The *green curve* is the orbit in the absence of any treatment, the *blue curve* is the orbit in the presence of calcium treatment alone and the *red curves* are orbits caused by calcium and tibolone treatment combined. The *solid red curve* is the orbit during continuous tibolone treatment, the *dashed curve* the continuation after termination and washout at $t = 1000$ days

parameters, while being parsimonious in and of itself. In contrast to the work described in the previous section, this is a deterministic and not a population model.

The extended physiological model is based on the osteoclast/osteoblast signaling model of Lemaire (Lemaire et al. 2004), the calcium sensing model of Cabal et al. (2013), a model of TGF-β signaling, and cathepsin-K (Cat K) enzymatic bone degradation, a signaling protein model of the osteoblast apoptosis regulation as suggested by Bellido (Bellido et al. 2003). The model, in the form of ordinary differential equations (ODEs), quantifies the relationships between the key molecular pathways governing bone remodeling, and links, via reasonable assumptions, the cell and molecular concentrations to the biomarkers measured in the laboratory (P1NP, CTx, and BMD). The model equations follow the interactions between the state variables of the system which are often chemical reactions following either mass-action kinetics or nonlinear hill function rates for enzymatic systems wherein the intermediate steps are excluded to preserve model simplicity.

The extended physiological model results are consistent with the known effects of PTH, bisphosphonates, and anti-RANKL treatment regimens on the bone remodeling process. Figures 13.6, 13.7 and 13.8 show the model behavior in response to the known treatment strategies for osteoporosis. Notably, it is able to predict the delicate nature of bone build up in response to PTH treatment, and the fact that the same unified model can predict treatments which differ in their mechanism of action (bisphosphonates, rPTH, and anti-RANKLs). The model allows the comparison of osteoporosis therapies already on the market and new, innovative therapies in different stages of development and lends itself as a tool to evaluate potential new therapies under various administration protocols.

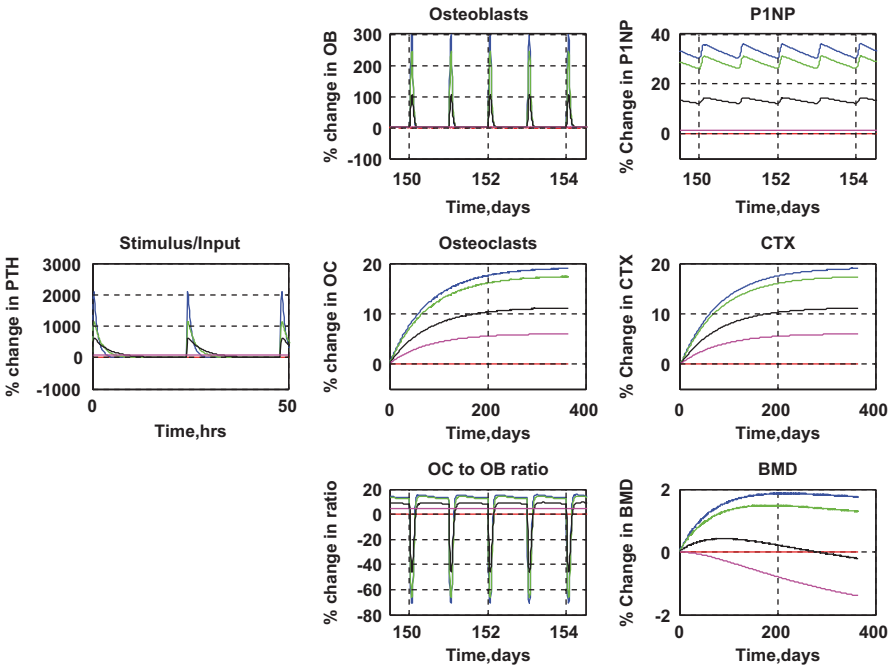

Fig. 13.6 Effect of parathyroid hormone (PTH) treatment: Simulated effect of pulse shape in the extended physiological model for five different administration profiles of PTH (*left plot:* from placebo to increasing sharper rises and declines). *Middle panel:* The shape of the PTH pulse has a nonintuitive impact on osteoblasts and progressively on bone mineral density (BMD; *right panel*). The model prediction of a sharper PTH infusion yielding improvement in BMD is consistent with results from Cosman et al. (2010). The different *colored lines* here indicate different PTH administration profiles. The total area under the curve for each of the profiles is kept similar (apart from placebo), while the pharmacokinetic profile is varied: *red*—placebo (no PTH); *magenta*—continuous administration (infusion) of PTH directly into plasma; *black*—PTH administration with slow clearance (similar to PTH secretion in response to orally administered calcilytic drugs); *green*—subcutaneous injection of PTH; and *blue*—transdermal delivery of PTH using micro-needles as per Cosman et al. (2010)

13.4.2 Finite Element Analysis

As mentioned above, the current clinical standard for diagnosing osteoporosis and assessing the risk of fracture and treatment effects is dual energy x-ray absorptiometry (DXA), which is used to measure areal BMD (aBMD) at the spine and hip. The performance of DXA-aBMD as a diagnostic, as well as a predictor of bone strength and treatment intervention are well documented (Cummings et al. 2002; Pistoia et al. 2002; Cefalu 2004; Delmas and Seeman 2004; Schuit et al. 2004; Seeman 2007). As a two-dimensional projection of three-dimensional structure, DXA-aBMD lacks the ability to interrogate the macro- and micro-architectural features of the bone that has a direct impact on its strength and ability to withstand specific

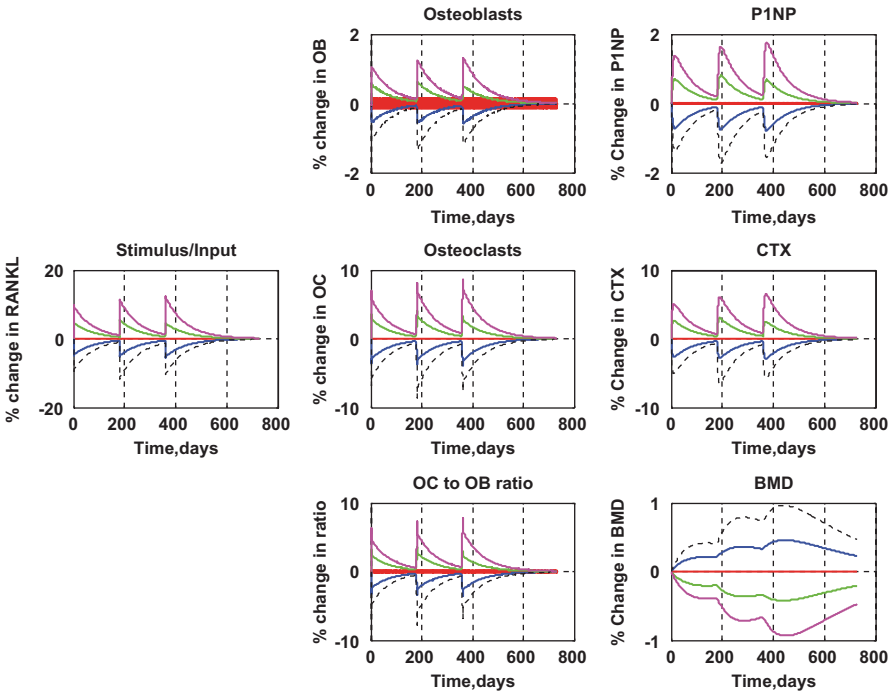

Fig. 13.7 Simulations of changing receptor activator of nuclear factor κ B ligand (RANKL) concentrations in the extended physiological model were performed as a proxy for treatment with anti-RANKL molecules like denosumab. Decreasing concentrations of RANKL resulted in a dose-dependent increase in bone mineral density (BMD), consistent with the findings of Marathe et al. (2008). The model predicts slow return to the baseline following treatment cessation after a year (three doses, at every 6 months)

loading situations. The shape and structure of bone at a macro- and micro-architectural level provide additional, independent information to better predict fracture risk, assess response to treatment, and potentially differentiate new therapies from standard of care (Homminga et al. 2002, 2004).

Computationally, this has been addressed by the use of finite element (FE) methodology, a numerical discretization procedure that has been extensively used for several decades in science and engineering to get good approximate solution of complex mathematical problems (Zienkiewicz and Taylor 2002, 2005). FEA is the most used computational analysis technique in the world today to solve solid mechanics problems and bone mechanics is no exception. Three dimensional (3D) images of bone are subdivided into a finite set of hexahedrons and tetrahedrons called elements. Applied to all nodes that form the elements, Newton's second law of motion takes the following general form:

$$\rho \frac{\partial^2 u_i}{\partial t^2} = \frac{\partial \sigma_{i,x}}{\partial x} + \frac{\partial \sigma_{i,y}}{\partial y} + \frac{\partial \sigma_{i,z}}{\partial z} + F_i$$

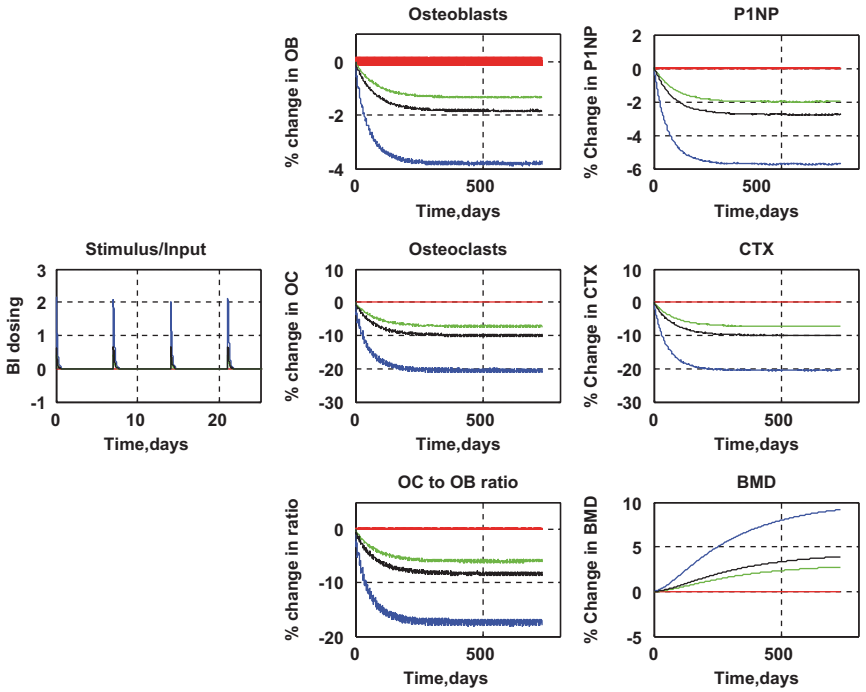

Fig. 13.8 Extended physiological model predictions of weekly dosing of bisphosphonates demonstrated a dose-dependent decrease in bone mineral density (BMD), bone biomarkers, and bone remodeling activity, which is consistent with known effects of bisphosphonates

where $i = x, y, z$ are the spatial coordinates, u_i are the coordinates of the displacement vector, F_i are the coordinates of the external body forces applied. Hooke's law yields a six-dimensional stress–strain linear relationship:

$$\begin{bmatrix} \sigma_{xx} \\ \sigma_{yy} \\ \sigma_{zz} \\ \sigma_{xy} \\ \sigma_{yz} \\ \sigma_{zx} \end{bmatrix} = \begin{pmatrix} C_{11} & C_{12} & C_{13} & C_{14} & C_{15} & C_{16} \\ C_{21} & C_{22} & C_{23} & C_{24} & C_{25} & C_{26} \\ C_{31} & C_{32} & C_{33} & C_{34} & C_{35} & C_{36} \\ C_{41} & C_{42} & C_{43} & C_{44} & C_{45} & C_{46} \\ C_{51} & C_{52} & C_{53} & C_{54} & C_{55} & C_{56} \\ C_{61} & C_{62} & C_{63} & C_{64} & C_{65} & C_{66} \end{pmatrix} \begin{bmatrix} \varepsilon_{xx} \\ \varepsilon_{yy} \\ \varepsilon_{zz} \\ \varepsilon_{xy} \\ \varepsilon_{yz} \\ \varepsilon_{zx} \end{bmatrix}$$

Various forms of this functional relationship are possible depending on the resolution of the bone 3D image available, the loads (boundary conditions) applied to the bone, and the material properties used (Young's modulus, Poisson's ratio, etc). For example, under the assumption that bone is a homogeneous isotropic material, the

above 36 coefficients are reduced to two, the Young's modulus (E) and the Poisson's ratio (g):

$$\begin{bmatrix}\sigma_{xx}\\ \sigma_{yy}\\ \sigma_{zz}\\ \sigma_{xy}\\ \sigma_{yz}\\ \sigma_{zx}\end{bmatrix} = \frac{E}{(1+\gamma)(1-2\gamma)}\begin{pmatrix}1-\gamma & \gamma & \gamma & 0 & 0 & 0\\ \gamma & 1-\gamma & \gamma & 0 & 0 & 0\\ \gamma & \gamma & 1-\gamma & 0 & 0 & 0\\ 0 & 0 & 0 & 1-2\gamma & 0 & 0\\ 0 & 0 & 0 & 0 & 1-2\gamma & 0\\ 0 & 0 & 0 & 0 & 0 & 1-2\gamma\end{pmatrix}\begin{bmatrix}\varepsilon_{xx}\\ \varepsilon_{yy}\\ \varepsilon_{zz}\\ \varepsilon_{xy}\\ \varepsilon_{yz}\\ \varepsilon_{zx}\end{bmatrix}$$

When the FE-models are generated from high-resolution micro-computed tomography (μCT) images of trabecular samples, the models accurately capture the complex morphological architecture of the structures and can be used to estimate the bone hard tissue Young's modulus (Zienkiewicz and Taylor 2002, 2005; Guo 2001). The FE model allows for computing the apparent stiffness. Physical compression experiments of trabecular bone samples provide an assessment of the experimental stiffness. The true hard tissue Young's modulus is then estimated from the ratio of the experimental and FEA-based stiffness estimates.

Animal models are a vital component of the drug discovery process and they provide an excellent opportunity to test FEA methodologies in disease models, acquiring advanced information to help design and execute clinical studies. An example of how the ovariectomized nonhuman primates osteoporosis model was used to qualify the validity of high-resolution peripheral quantitative computed tomog-

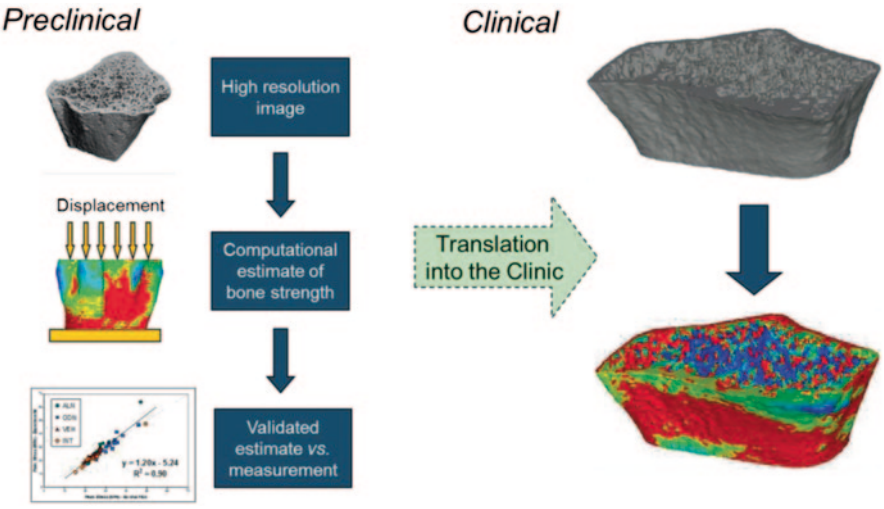

Fig. 13.9 FEA qualification and translation roadmap

raphy (HR-pQCT) based FEA estimates of bone strength was presented in (Jayakar et al. 2012). The roadmap from *ex vivo* preclinical FEA qualification to in vivo clinical translation is illustrated in Fig. 13.9.

Several clinical publications (Boutroy et al. 2008; Burghardt et al. 2010, 2011; Macdonald et al. 2011) have shown that high-resolution peripheral quantitative computer tomography (HR-pQCT)-based FEA-estimated bone strength provides information about skeletal fragility and fracture risk not assessed by BMD. A unique advantage of the preclinical FEA-estimated bone strength lies in its ability to enable in-vivo longitudinal estimates of bone strength that can be validated at the end of the study. This, in turn, provides the necessary level of confidence for the FEA predictions for the clinical estimates.

On the 3D clinical imaging technology resolution scale, the next class of lower resolution bone imaging tools is provided by QCT scanners, which can be used to scan whole bones at skeletal central sites, which are the most relevant for osteoporosis (femur and vertebra), as compared to HR-pQCT. With the lower resolution (~500 μm), the FE models generated from those images are not capable of resolving the trabecular microarchitecture at the level of a single trabecular structure. The heterogeneity of the trabecular bone is represented in the QCT-based FEA assigning different elastic properties to the different voxels of the image in correspondence to the QCT density of the given voxel (Morgan and Keaveny 2001; Crawford et al. 2003; Morgan et al. 2003).

FE models enable the testing of bone specimens in any configuration and loading conditions in silico, thus facilitating the exploration of potential treatment specific

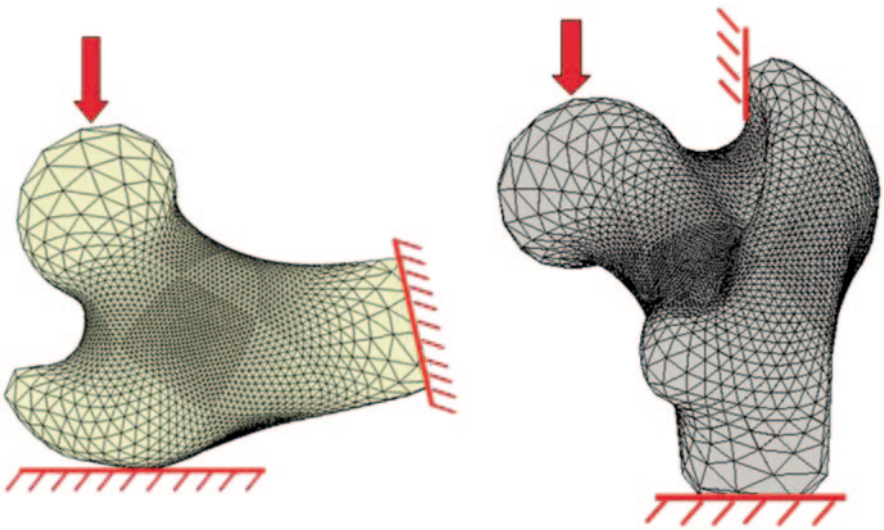

Fig. 13.10 FE-mesh of two proximal femurs under two different loading and boundary conditions

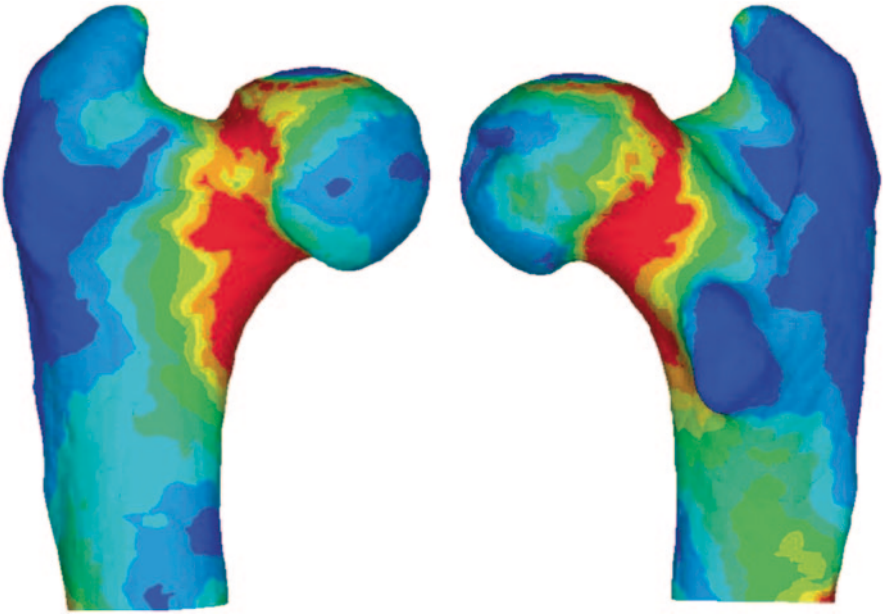

Fig. 13.11 Two different views of a rhesus monkey's right proximal femur von Mises stress spatial distribution (*red* being the highest stress and *blue* being the lowest stress)

effects. Proximal femurs could, for example, be tested in fall loading or neck shear configurations as illustrated in Fig. 13.10.

Another unique feature of the FEA is its ability to accurately estimate the spatial stress and strain distribution for any given load. This facilitates the analysis of subject specific biomechanical differences even in the cases where subjects have the same integral BMD at a given skeletal site. Some studies have been conducted to assess the ability of FE models to predict the location and type of clinically relevant fractures (Lotz et al. 1991a, b; Keyak et al. 2001). Figure 13.11 shows the spatial stress distribution on the proximal femur of a rhesus monkey subjected to a neck shear test. The location of the high stresses, in red, shows the places where the fracture is most likely to occur.

In the past decade, thanks to improvements in imaging tools and their availability, in vivo FEA have become a frequently used biomarker in phase III clinical trials for new osteoporosis therapies (Keaveny et al. 2007, 2008; Brixen et al. 2013). FEA has enabled clinical longitudinal measurements of bone strength and provided unique clinical insight into the biomechanical effects of new osteoporosis therapies.

13.5 Conclusions

During the past decade, a myriad of disease models for osteoporosis has been developed and applied to drug development questions. The current toolbox for the pharmacometricians provides state-of the-art modeling of the bone model unit including the osteoclast and osteoblast dynamics and endogenous modulator molecules, predictive biomarkers as NTx, uNTx, and bone mineral density, risk of fracture and bone strength. As a result, our understanding of mechanisms of action and (developmental) drug characteristics in osteoporosis has progressed significantly. In the future, further integration of approaches and end points will provide higher and earlier predictiveness from biomarkers to fractures and deliver on the promise of model-based drug development in osteoporosis, where the model is continuously developed in parallel with the drug. The ultimate goal is to integrate all sources of information to obtain a comprehensive description of the pathophysiology of osteoporosis, including treatment and disease. This enables the description of various treatments and their impact on clinical outcome; enabling the prediction of short-term to long-term outcome on fracture risk.

Summary and Key Aspects of the Chapter

- Due to statistical requirements and the slow progression of osteoporosis, large clinical trials with long duration are required to establish a beneficial effect of new treatments on the reduction of fracture risk.
- Over the past decade, different types of mechanism-based models have had an increasing impact on drug development.
  - Various conceptual models for bone physiology and the effects of therapies have been proposed. Data included in osteoporosis models range fromPK of (novel) drugs, PD biomarkers of various time scales (peptides indicative of bone-turnover, bone mineral density), bone strength, as well as the actual clinical outcome, namely fracture rates at various sites in the skeleton.
- Published PK–PD-disease models of osteoporosis have varying degrees of biological complexity ranging from purely descriptive of disease to detailed systems model spanning various spatial scales, as well as mechanistic models of bone strength.
  - These models have been used to describe data from clinical trials, simulate new trial designs with novel mechanisms of action, and simulate combination treatments and how these clinical trials predict for real-life settings.
- A more integrative approach allows for a mechanism-based description of osteoporosis, and presumably other bone diseases, by explicitly including bone physiology as the underlying mechanism to which all information is linked. Various short- and long-term markers at various levels and timescales of the disease and drug action can then be combined and evaluated.
- Specific applied examples of pharmacometrics in osteoporosis concern mechanism-based models based on bone cell interaction—i.e., a core physiological model.

  - Mechanism-based models of bone turnover markers and BMD.
    - Reduced core physiological model describing five biomarkers in a population approach (reduced Lemaire core model including bone turnover markers and bone mineral density).
      - Quantitative system able to describe the effects of treatment based on various short- and long-term biomarker clinical data within a population approach (treatment and disease progression).
    - Extended physiological model in a systems biology approach (extensions to the Lemaire core model).
      - Mathematical model of dynamics of bone remodeling based on available physiological observations, specifically in the context of the mechanisms of action of available osteoporosis treatments.
  - Finite element analysis
    - Describing the shape and structure of bone at a macro- and micro-architectural level provides additional, independent information to better predict fracture risk.
- The current toolbox for the pharmacometricians provides state-of the-art modeling of the bone model unit including the osteoclast and osteoblast dynamics and endogenous modulator molecules, predictive biomarkers as NTx, uNTx, and bone mineral density, risk of fracture and bone strength.
- In the future, further integration of approaches and end points will provide higher and earlier predictiveness from biomarkers to fractures and deliver on the promise of model-based drug development in osteoporosis, where the model is continuously developed in parallel with the drug. The ultimate goal is to integrate all sources of information to obtain a comprehensive description of the pathophysiology of osteoporosis, including treatment and disease. This enables the description of various treatments and their impact on clinical outcome; enabling the prediction of short-term to long-term outcome on fracture risk.

References

Aubin JE, Bonnelye E (2000) Osteoprotegerin and its ligand: a new paradigm for regulation of osteoclastogenesis and bone resorption. Osteoporos Int 11(11):905–913 (Retrieved from PM:11193242)

Baron R, Ferrari S, Russell RG (2011) Denosumab and bisphosphonates: different mechanisms of action and effects. Bone 48(4):677–692 (Retrieved from PM:21145999)

Bellido T, Ali AA, Plotkin LI, Fu Q, Gubrij I, Roberson PK et al. (2003) Proteasomal degradation of Runx2 shortens parathyroid hormone-induced anti-apoptotic signaling in osteoblasts. A putative explanation for why intermittent administration is needed for bone anabolism. J Biol Chem 278(50):50259–50272 (Retrieved from PM:14523023)

Bone HG, McClung MR, Roux C, Recker RR, Eisman JA, Verbruggen N et al (2010) Odanacatib, a cathepsin-K inhibitor for osteoporosis: a two-year study in postmenopausal women with low bone density. J Bone Miner Res 25(5):937–947 (Retrieved from PM:19874198)

Boutroy S, Van Rietbergen B, Sornay-Rendu E, Munoz F, Bouxsein ML, Delmas PD (2008) Finite element analysis based on in vivo HR-pQCT images of the distal radius is associated with

wrist fracture in postmenopausal women. J Bone Miner Res 23(3):392–399 (Retrieved from PM:17997712)
Bouxsein ML, Seeman E (2009) Quantifying the material and structural determinants of bone strength. Best Pract Res Clin Rheumatol 23(6):741–753 (Retrieved from PM:19945686)
Boyle WJ, Simonet WS, Lacey DL (2003) Osteoclast differentiation and activation. Nature 423(6937):337–342 (Retrieved from PM:12748652)
Brixen K, Chapurlat R, Cheung AM, Keaveny TM, Fuerst T, Engelke K et al (2013) Bone density, turnover, and estimated strength in postmenopausal women treated with odanacatib: a randomized trial. J Clin Endocrinol Metab 98(2):571–580 (Retrieved from PM:23337728)
Burge R, Dawson-Hughes B, Solomon DH, Wong JB, King A, Tosteson A (2007) Incidence and economic burden of osteoporosis-related fractures in the United States, 2005–2025. J Bone Miner Res 22(3):465–475 (Retrieved from PM:17144789)
Burghardt AJ, Kazakia GJ, Sode M, de Papp AE, Link TM, Majumdar S (2010) A longitudinal HR-pQCT study of alendronate treatment in postmenopausal women with low bone density: relations among density, cortical and trabecular microarchitecture, biomechanics, and bone turnover. J Bone Miner Res 25(12):2282–2295 (Retrieved from PM:20564242)
Burghardt AJ, Link TM, Majumdar S (2011) High-resolution computed tomography for clinical imaging of bone microarchitecture. Clin Orthop Relat Res 469(8):2179–2193 (Retrieved from PM:21344275)
Cabal A, Mehta K, Ross DS, Shrestha RP, Comisar W, Denker A et al (2013) A semi-mechanistic model of the time-course of release of PTH into plasma following administration of the calcilytic JTT-305/MK-5442 in humans. J Bone Miner Res. 2013 Aug;28(8):1830-6. doi: 10.1002/jbmr.1900. (Retrieved from PM:23436611)
Cefalu CA (2004) Is bone mineral density predictive of fracture risk reduction? Curr Med Res Opin 20(3):341–349 (Retrieved from PM:15025843)
Cosman F, Lane NE, Bolognese MA, Zanchetta JR, Garcia-Hernandez PA, Sees K et al (2010) Effect of transdermal teriparatide administration on bone mineral density in postmenopausal women. J Clin Endocrinol Metab 95(1):151–158 (Retrieved from PM:19858319)
Crawford RP, Cann CE, Keaveny TM (2003) Finite element models predict in vitro vertebral body compressive strength better than quantitative computed tomography. Bone 33(4):744–750 (Retrieved from PM:14555280)
Cummings SR, Karpf DB, Harris F, Genant HK, Ensrud K, LaCroix AZ et al (2002) Improvement in spine bone density and reduction in risk of vertebral fractures during treatment with antiresorptive drugs. Am J Med 112(4):281–289 (Retrieved from PM:11893367)
Cusick T, Chen CM, Pennypacker BL, Pickarski M, Kimmel D, Scott BB et al (2011) Odanacatib treatment increases hip bone mass and cortical thickness by preserving endocortical bone formation and stimulating periosteal bon formation in the ovariectomized adult rhesus monkey. J Bone Miner Res 27(3):524–537
Delmas PD, Seeman E (2004) Changes in bone mineral density explain little of the reduction in vertebral or nonvertebral fracture risk with anti-resorptive therapy. Bone 34(4):599–604 (Retrieved from PM:15050889)
Earp JC, Dubois DC, Molano DS, Pyszczynski NA, Keller CE, Almon RR et al (2008) Modeling corticosteroid effects in a rat model of rheumatoid arthritis I: mechanistic disease progression model for the time course of collagen-induced arthritis in Lewis rats. J Pharmacol Exp Ther 326(2):532–545 (Retrieved from PM:18448865)
Guo E (2001) Mechanical properties of cortical bone and cancellous bone tissue. In: Cowin S (eds) Bone biomechanics handbook, 2nd edn. CRC Press LLC, Oxford
Homminga J, McCreadie BR, Ciarelli TE, Weinans H, Goldstein SA, Huiskes R (2002) Cancellous bone mechanical properties from normals and patients with hip fractures differ on the structure level, not on the bone hard tissue level. Bone 30(5):759–764 (Retrieved from PM:11996916)
Homminga J, Van Rietbergen B, Lochmuller EM, Weinans H, Eckstein F, Huiskes, R (2004) The osteoporotic vertebral structure is well adapted to the loads of daily life, but not to infrequent "error" loads. Bone 34(3):510–516 (Retrieved from PM:15003798)
Jayakar RY, Cabal A, Szumiloski J, Sardesai S, Phillips EA, Laib A et al (2012) Evaluation of high-resolution peripheral quantitative computed tomography, finite element analysis and biome-

chanical testing in a pre-clinical model of osteoporosis: a study with odanacatib treatment in the ovariectomized adult rhesus monkey. Bone 50(6):1379–1388 (Retrieved from PM:22469953)
Keaveny TM, Donley DW, Hoffmann PF, Mitlak BH, Glass EV, San Martin JA (2007) Effects of teriparatide and alendronate on vertebral strength as assessed by finite element modeling of QCT scans in women with osteoporosis. J Bone Miner Res 22(1):149–157 (Retrieved from PM:17042738)
Keaveny TM, Hoffmann PF, Singh M, Palermo L, Bilezikian JP, Greenspan SL et al (2008) Femoral bone strength and its relation to cortical and trabecular changes after treatment with PTH, alendronate, and their combination as assessed by finite element analysis of quantitative CT scans. J Bone Miner Res 23(12):1974–1982 (Retrieved from PM:18684084)
Keyak JH, Rossi SA, Jones KA, Les CM, Skinner HB (2001) Prediction of fracture location in the proximal femur using finite element models. Med Eng Phys 23(9):657–664 (Retrieved from PM:11755810)
Komarova SV, Smith RJ, Dixon SJ, Sims SM, Wahl LM (2003) Mathematical model predicts a critical role for osteoclast autocrine regulation in the control of bone remodeling. Bone 33(2):206–215 (Retrieved from PM:14499354)
Langdahl B, Binkley N, Bone H, Gilchrist N, Resch H, Rodriguez PJ et al (2012) Odanacatib in the treatment of postmenopausal women with low bone mineral density: five years of continued therapy in a phase 2 study. J Bone Miner Res 27(11):2251–2258 (Retrieved from PM:22777865)
Lemaire V, Tobin FL, Greller LD, Cho CR, Suva LJ (2004) Modeling the interactions between osteoblast and osteoclast activities in bone remodeling. J Theor Biol 229(3):293–309 (Retrieved from PM:15234198)
Lotinun S, Kiviranta R, Matsubara T, Alzate JA, Neff L, Luth A et al (2013) Osteoclast-specific cathepsin K deletion stimulates S1P-dependent bone formation. J Clin Invest. 2013 Feb 1;123(2):666-81. doi: 10.1172/JCI64840. Epub 2013 Jan 16. (Retrieved from PM:23321671)
Lotz JC, Cheal EJ, Hayes WC (1991a) Fracture prediction for the proximal femur using finite element models: part I–linear analysis. J Biomech Eng 113(4):353–360 (Retrieved from PM:1762430)
Lotz JC, Cheal EJ, Hayes WC (1991b) Fracture prediction for the proximal femur using finite element models: part II–nonlinear analysis. J Biomech Eng 113(4):361–365 (Retrieved from PM:1762431)
Macdonald HM, Nishiyama KK, Kang J, Hanley DA, Boyd SK (2011) Age-related patterns of trabecular and cortical bone loss differ between sexes and skeletal sites: a population-based HR-pQCT study. J Bone Miner Res 26(1):50–62 (Retrieved from PM:20593413)
Manolagas SC (2000) Birth and death of bone cells: basic regulatory mechanisms and implications for the pathogenesis and treatment of osteoporosis. Endocr Rev 21(2):115–137 (Retrieved from PM:10782361)
Marathe A, Peterson MC, Mager DE (2008) Integrated cellular bone homeostasis model for denosumab pharmacodynamics in multiple myeloma patients. J Pharmacol Exp Ther 326(2):555–562 (Retrieved from PM:18460643)
Marathe DD, Marathe A, Mager DE (2011) Integrated model for denosumab and ibandronate pharmacodynamics in postmenopausal women. Biopharm Drug Dispos 32(8):471–481 (Retrieved from PM:21953540)
McClung MR, Boonen S, Brown JP, Diez-Perez A, Langdahl B, Reginster JY et al (2012) Inhibition of sclerostin with AMG 785 in postmenopausal women with low bone mineral density: phase 2 trial results. J Bone Miner Res 27(Suppl 1)
Mehta K, Cabal A, Ross SD (2012) Mathematical modeling of bone remodeling in response to osteoporosis treatments. SIAM Conference on the Life Sciences
Melton LJ III, Crowson CS, O'Fallon WM, Wahner HW, Riggs BL (2003) Relative contributions of bone density, bone turnover, and clinical risk factors to long-term fracture prediction. J Bone Miner Res 18(2):312–318 (Retrieved from PM:12568408)
Morgan EF, Keaveny TM (2001) Dependence of yield strain of human trabecular bone on anatomic site. J Biomech 34(5):569–577 (Retrieved from PM:11311697)

Morgan EF, Bayraktar HH, Keaveny TM (2003) Trabecular bone modulus-density relationships depend on anatomic site. J Biomech 36(7):897–904 (Retrieved from PM:12757797)

Moroz A, Crane MC, Smith G, Wimpenny DI (2006) Phenomenological model of bone remodeling cycle containing osteocyte regulation loop. Biosystems 84(3):183–190 (Retrieved from PM:16387419)

Peterson MC, Riggs MM (2010) A physiologically based mathematical model of integrated calcium homeostasis and bone remodeling. Bone 46(1):49–63 (Retrieved from PM:19732857)

Pistoia W, Van Rietbergen B, Lochmuller EM, Lill CA, Eckstein F, Ruegsegger P (2002) Estimation of distal radius failure load with micro-finite element analysis models based on three-dimensional peripheral quantitative computed tomography images. Bone 30(6):842–848 (Retrieved from PM:12052451)

Pivonka P, Komarova SV (2010) Mathematical modeling in bone biology: from intracellular signaling to tissue mechanics. Bone 47(2):181–189 (Retrieved from PM:20417739)

Pivonka P, Zimak J, Smith DW, Gardiner BS, Dunstan CR, Sims NA et al (2008) Model structure and control of bone remodeling: a theoretical study. Bone 43(2):249–263 (Retrieved from PM:18514606)

Post TM (2009) Disease system analysis: between complexity and (over)simplification. https://openaccess.leidenuniv.nl/handle/1887/14477. TIPharma, Division of Pharmacology, Schering-Plough, Leiden/Amsterdam Center for Drug Research, Faculty of Science, Leiden University

Post TM, Cremers SC, Kerbusch T, Danhof M (2010) Bone physiology, disease and treatment: towards disease system analysis in osteoporosis. Clin Pharmacokinet 49(2):89–118 (Retrieved from PM:20067335)

Post TM, Schmidt S, Peletier LA, de Greef R, Kerbusch T, Danhof M (2013) Application of a mechanism-based disease systems model for osteoporosis to clinical data. J Pharmacokinet Pharmacodyn. 2013 Apr;40(2):143-56. doi: 10.1007/s10928-012-9294-9. Epub 2013 Jan 12. (Retrieved from PM:23315144)

Raisz LG (2008) Overview of pathogenesis. In: Miller PD, Papapoulos S (eds) Primer on the metabolic bone disease and disorders of mineral metabolism, 7th edn. American Society for Bone and Mineral Research, Washington, DC, pp 208–212

Rajagopal V, Holroyd C, Cooper C, Dennison E (2008) Epidemiology of osteoporotic fracture. In: Clunie G, Keen RW (eds) Osteoporosis. Oxford University Press, Oxford

Rattanakul C, Lenbury Y, Krishnamara N, Wollkind DJ (2003) Modeling of bone formation and resorption mediated by parathyroid hormone: response to estrogen/PTH therapy. Biosystems 70(1):55–72 (Retrieved from PM:12753937)

Riggs MM, Peterson MC, Gastonguay MR (2012) Multiscale physiology-based modeling of mineral bone disorder in patients with impaired kidney function. J Clin Pharmacol 52(1 Suppl):45S–53S (Retrieved from PM:22232752)

Schmidt S, Post TM, Peletier LA, Boroujerdi MA, Danhof M (2011) Coping with time scales in disease systems analysis: application to bone remodeling. J Pharmacokinet Pharmacodyn 38(6):873–900 (Retrieved from PM:22028207)

Schuit SC, van der KM, Weel AE, de Laet CE, Burger H, Seeman E et al (2004) Fracture incidence and association with bone mineral density in elderly men and women: the Rotterdam study. Bone 34(1):195–202 (Retrieved from PM:14751578)

Seeman E (2007) Is a change in bone mineral density a sensitive and specific surrogate of antifracture efficacy? Bone 41(3):308–317 (Retrieved from PM:17644058)

WHO Study Group. (1994) Assessment of fracture risk and its application to screening for postmenopausal osteoporosis. Report of a WHO study group. World Health Organ Tech Rep Ser 843:1–129

Wimpenny DI, Moroz A (2007) On allosteric control model of bone turnover cycle containing osteocyte regulation loop. Biosystems 90(2):295–308 (Retrieved from PM:17070649)

Zienkiewicz OC, Taylor RL (2002) The finite element method. In: Ward JP (eds) Solid mechanics, 5th edn. Butterworth-Heinemann, Oxford

Zienkiewicz OC, Taylor RL (2005) The finite element method: its basis and fundamentals, 6th edn. Elsevier, Amsterdam

Zumsande M, Stiefs D, Siegmund S, Gross T (2011) General analysis of mathematical models for bone remodeling. Bone 48(4):910–917 (Retrieved from PM:21185412)

Chapter 14
Pharmacometrics in Psychiatric Diseases

Elizabeth C. M. de Lange

14.1 Introduction

Psychiatric disorders include a very long list of mental illnesses that have a huge impact on someone's daily behavior and functioning as well as interaction with others. Major psychiatric diseases include attention deficit hyperactivity disorder (ADHD), addiction, anxiety, bipolar disorder, depression, and schizophrenia. According to the World Health Organization (WHO), over a third of people in most countries report problems at some time in their life that meet the criteria for diagnosis of one or more of the common types of mental disorder (WHO 2000). Thereby, these diseases have a huge impact on society and health care costs. Psychiatric diseases are very complex, which makes diagnosis very difficult. In treatment, psychoactive drugs are helpful, but it is tough to measure the "true effects" at the mental and behavior level. With psychiatric diseases and drug effects both displaying high variability, there is much room for improvement of drug treatment and modalities.

For the development of better drugs and treatments there is a need for more insight into the disease processes as well as the fate of psychoactive drugs in the body, particularly the brain, and their associated effects. Also, more insight is needed into the sources of intra- and interindividual differences in the pharmacodynamic (PD) responses of psychoactive drugs. Thus, quantitative research approaches are needed on the factors that play a role in the relationship between disease conditions as well as drug dosing and ultimate effects, both at the population and individual level. To that end, pharmacometrics is needed, being the science that develops and applies mathematical and statistical methods to quantitatively characterize, understand, and predict drug's pharmacokinetic (PK), PD, and biomarker outcomes (Williams 2007). Therewith the pharmacometric approach is anticipated to contribute to improved treatment modalities, paving the way to individualized medicine in psychiatric diseases.

E. C. M. de Lange (✉)
Target Site Equilibration Group, Division of Pharmacology,
Leiden Academic Centre of Drug Research, Leiden University,
Leiden, The Netherlands
e-mail: ecmdelange@lacdr.leidenuniv.nl

S. Schmidt, H. Derendorf (eds.), *Applied Pharmacometrics*, AAPS Advances
in the Pharmaceutical Sciences Series 14, DOI 10.1007/978-1-4939-1304-6_14

In this chapter, first, the major psychiatric diseases anxiety, depression, and psychosis will be briefly introduced. Then, current available anxiolytic, antidepressants, and antipsychotic drugs used to treat such conditions will be presented. Finally, pharmacometric investigations on these drugs will be presented, with special focus on antipsychotics. It will be shown that the application of pharmacometrics in psychiatric diseases so far is scarce, but is a prerequisite to aid in further understanding of the complexity of psychiatric diseases and their drug treatments. Improvements of the quality the pharmacometric models, in the first place, lies in improvement of the quality of the data. This can be brought about by inclusion of multiple quantitative and objective measures as a composite biomarker for disease condition and treatment effects. The emphasis should lie on measures that can be obtained both preclinically and clinically, to enhance translational insights and therewith predictive power in an early stage of drug development. Then, in clinical trials, a lot can be gained by improvement of the quality of the design and explicit consideration of placebo effects and dropouts.

14.2 Psychiatric Diseases

Mental illness is a term used to describe a broad range of mental and emotional conditions. It is different from mental retardation, organic brain damage, and learning disabilities. The term "psychiatric disease" is used when mental illness significantly interferes with the performance of major life activities, such as learning, working, and communicating. Psychiatric conditions may come and go and do not always follow a regular pattern. Moreover, the type, intensity, and duration of symptoms vary from person to person. This makes it very difficult to predict when psychiatric symptoms will bristle and proper functioning will decline. Medication and psychotherapy often are helpful in the control of the symptoms. In part of the patients, the mental illness may even go into remission, while in others the illness pursues. The most common forms of psychiatric disorders are anxiety disorders, depression, and psychosis.

14.2.1 Anxiety

Anxiety (fear) is a psychological and physiological state characterized by (non)specific worries or fear(s) and avoidance behavior. Examples include panic disorder, social phobia, specific phobia, obsessive–compulsive disorder, posttraumatic stress disorder, acute stress disorder, generalized anxiety disorder, and substance-induced anxiety disorder. Anxious individuals show increased attentional capture by potential signs of danger, and interpret expressions, comments, and events in a negative manner (Bishop 2007).

14.2.2 Major Depressive Disorder

Major depressive disorder (also known as recurrent depressive disorder, clinical depression, major depression, unipolar depression, or unipolar disorder) is a mental disorder characterized by episodes of all-encompassing low mood accompanied by low self-esteem and loss of interest or pleasure in normally enjoyable activities (Weihs and Wert 2011).

14.2.3 Psychosis

Psychosis is a generic psychiatric term for a mental state often described as involving a "loss of contact with reality." It is typically characterized by radical changes in personality, impaired functioning, and a distorted or nonexistent sense of objective reality. Patients experience hallucinations and/or delusions that they believe are real, and may behave and communicate in an inappropriate and incoherent fashion. Psychosis may appear as a symptom of a number of mental disorders, including mood and personality disorders. It is also the defining feature of schizophrenia. People diagnosed with schizophrenia usually experience a combination of symptoms, including positive (i.e., hallucinations, delusions, racing thoughts), negative (i.e., apathy, lack of emotion, poor, or nonexistent social functioning), and cognitive symptoms (disorganized thoughts, difficulty concentrating and/or following instructions, difficulty completing tasks, memory problems; Andreasen and Olsen 1982).

14.2.4 Current Problems in Psychiatric Diseases

Today's lack of quantitative objective measures of psychiatric diseases is one reason that the causative factors of psychiatric diseases remain obscure (Agarwal et al. 2010; Van et al. 2008). To measure the severity of psychiatric conditions in humans, clinicians are using subjective rating scales. There are many rating scales available that provide an indication of the disease condition and guide the evaluation of recovery. For anxiety, an example of a rating scale is the Hamilton Anxiety Rating Scale (HAM-A), in the form of a psychological questionnaire (Hamilton 1959; Maier et al. 1988). For depression, the Hamilton Rating Scale for Depression (HRSD) is often used, being a multiple item questionnaire (Hamilton 1960; Hedlund and Viewig 1979). For measuring symptom severity of patients with schizophrenia, the Positive and Negative Syndrome Scale (PANSS) is widely used in the study of antipsychotic therapy (PANSS, Table 14.1; Kay et al. 1987; Marder et al. 1997). However, such scales are not truly objective because it is based on observations of a psychiatrist, primary care staff, and family members (Kay et al. 1987). The PANSS and other scoring tools can be useful in the guidance of schizophrenia treatment,

Table 14.1 The positive and negative syndrome scale (PANSS). To assess a patient using PANSS, an approximately 45-min clinical interview is conducted. The patient is rated from 1 to 7 on 30 different symptoms based on the interview as well as reports of family members or primary care hospital workers. PANSS Total score minimum = 30, maximum = 210

Positive scale: 7 items (minimum score = 7, maximum score = 49)
Delusions
Conceptual disorganization
Hallucinations
Hyperactivity
Grandiosity
Suspiciousness/persecution
Hostility
Negative scale: 7 items (minimum score = 7, maximum score = 49)
Blunted affect
Emotional withdrawal
Poor rapport
Passive/apathetic social withdrawal
Difficulty in abstract thinking
Lack of spontaneity and flow of conversation
Stereotyped thinking
General psychopathology scale: 16 items (minimum score = 16, maximum score = 112)
Somatic concern
Anxiety
Guilt feelings
Tension
Mannerisms and posturing
Depression
Motor retardation
Uncooperativeness
Unusual thought content
Disorientation
Poor attention
Lack of judgment and insight
Disturbance of volition
Poor impulse control
Preoccupation
Active social avoidance

but patient-specific factors cannot be taken into account. A more quantitative approach to determine the clinical outcome of antipsychotics is the use of biomarkers (Danhof et al. 2005). Biomarkers can also be investigated in animal models (like rats) and used to provide more mechanistic insights into the pathophysiology of the disease and prediction of treatment response in humans (Stevens et al. 2012).

Identification of the neurochemical processes in the central nervous system (CNS) associated with psychiatric disorders has led to the development of many psychoactive drugs. Psychoactive drugs can be categorized into the main categories of antidepressants, anxiolytics, mood stabilizers, antipsychotics, and stimulants. Many of these drugs are helpful to patients, but there is much room for improvement (Lader 2008).

For development of better drugs and treatments there is a need for more insight into the disease processes as well as the fate of psychoactive drugs in the body and particularly the brain and their effects measured by different biomarkers, both at the population and individual level. To that end, it is helpful to identify sources of the disease and (associated) sources of variability.

The prominent role of genetics in psychiatric diseases has been established in various family-, twin-, and adoption studies, but the identification of concrete contributing genes is difficult. This may in part be due to inconsistencies in psychiatric classification systems, complexity and heterogeneity of psychiatric disorders, genetic expression modification effects, and intervening environmental factors. Over the past years, many reliable genetic associations with complex diseases have been reported, including some associations with complex neurological and psychiatric diseases. Many of these disease associations are believed to lead to genetic variability in gene expression and splicing. The genetic epidemiology of complex psychiatric diseases has been extensively studied and it is widely believed that many genetic factors contribute to the various phenotypes and diseases, with overall contributions of a single factor being comparatively minor. More recently, the focus has shifted towards establishing endophenotypes for psychiatric diseases, including electrophysiological abnormalities and alterations in structural and functional brain imaging.

In search for contributing genetic factors, animal models with (single) gene mutation are used. However, the fact that human behavior is complex and that it cannot be easily tested in laboratories or reproduced in animal models further complicates our understanding of psychiatric diseases. Still, valuable information on mechanisms of brain dysfunction can be learned via experimental animals, like the potential impact of the P-glycoprotein (P-gp) efflux transporter at the blood–brain barrier that might influence brain distribution of part of the psychiatric drugs. That is why polymorphisms in the drug transporter gene ABCB1 encoding for P-gp is thought to account for differences in the clinical efficacy of the most drugs, most likely by influencing their access to the brain.

With overwhelming complexity of psychiatric diseases and treatment with psychoactive drugs, there is a need for quantitative description of these diseases, drug effects and variability. As a follow up of model-based drug development (Lalonde et al. 2007), pharmacometrics is the multidisciplinary science that makes use of advanced mathematical models that integrate pharmacology, physiology, and disease for quantitative analysis of interactions between drugs and biological systems, with special emphasis on sources of variability, to aid efficient drug development, regulatory decisions, and rational drug treatment in (individual) patients.

14.3 Psychoactive Drugs

14.3.1 Anxiolytics

Anxiolytics and hypnotics act on the CNS to alleviate the symptoms of anxiety and nervousness, mood stabilizing and improving sleep. Long-term use may develop psychological and physiological dependence. Fear and anxiety research to understand how to treat the potentially devastating effects of anxiety disorders in humans has utilized classical fear conditioning, a simple paradigm that has been extensively investigated in animals, helping outline a brain circuitry thought to be responsible for the acquisition, expression, and extinction of fear (Delgado et al. 2006). Categories of antianxiety drugs include benzodiazepine tranquilizers, the "new" antidepressants, and β-blockers (Kodish et al. 2011; Farach et al. 2012; Huh et al. 2011).

14.3.1.1 Benzodiazepines

Benzodiazepine tranquillizers, such as alprazolam (Xanax®), diazepam (Valium®) and lorazepam (Ativan®) fluorozapam (Dalmane®), oxazepam (Serax®), and clozapam (Klonopin®), are used to relieve the symptoms of anxiety. They also have calming and sleep-promoting effects. The actions of benzodiazepines are due to the potentiation of the neural inhibition that is mediated by gamma-aminobutyric acid (GABA). Practically, all effects of the benzodiazepines result from their actions on the ionotropic GABA(A) receptors in the CNS. Benzodiazepines do not activate GABA(A) receptors directly but they require GABA (Olkkola and Ahonen 2008).

Main effects of benzodiazepines are sedation, hypnosis, decreased anxiety, anterograde amnesia, centrally mediated muscle relaxation, and anticonvulsant activity. In addition to their action on the CNS, benzodiazepines have a dose-dependent ventilatory depressant effect and they also cause a modest reduction in arterial blood pressure and an increase in heart rate as a result of a decrease of systemic vascular resistance (Olkkola and Ahonen 2008; Vinkers et al. 2012). Side effects include dizziness, drowsiness, somnolence, fatigue, body imbalance, loss of memory, difficulty in carrying out voluntary movements, dry mouth, impaired coordination, drugs dependence and withdrawal symptoms, etc. (Vgontzas et al. 1995).

14.3.1.2 Antidepressants

The "new" antidepressants, i.e., the serotonin and noradrenaline reuptake inhibitors (SNRIs) and selective serotonin reuptake inhibitors (SSRIs) include fluvoxamine (Luvox®), venlafaxine (Effexor®), desvenlafaxine (Pristiq®), duloxetine (Cymbalta®, Yentreve®), and milnacipran (Dalcipran®, Ixel®, Savella®). These are used for the treatment of depression and other mood disorders, but also anxiety, by balancing the disorder of neurotransmitters, serotonin, and noradrenaline in the

brain to provide clinical effects. Side effects include dry mouth, gastrointestinal upsets, nausea, fatigue, and sweating. Pharmacotherapy for anxiety disorders by these drugs is effective in improving clinical symptoms, particularly in combination with psychotherapy. SSRIs are thought to be relatively safe and effective for acute treatment of several classes of anxiety disorders (Kodish et al. 2011).

14.3.1.3 Beta-blockers

The benzodiazepines have been most extensively prescribed and are still often used by many clinicians, despite the fact that it has become clear that SSRIs are better as first-choice drugs for treating anxiety disorders, alongside newer agents, such as pregabalin or SNRIs, and combined with cognitive-behavioral therapy (Lader 2008; Cloos and Ferreira 2009; Figgitt and McClellan 2000). Flumazenil is very useful in antagonizing benzodiazepine-induced sedation as well as to diagnose or treat benzodiazepine overdose (Olkkola and Ahonen 2008).

Apart from rating scales that are prone to subjectiveness, effort have been put into finding more objective measures for effectiveness of psychoactive drugs. For measurement of the effects of benzodiazepines, in healthy volunteers, measures of alertness were most sensitive to benzodiazepines. The most consistent effects were observed on saccadic peak velocity (SPV) and visual analog scores (VAS) of alertness (De Visser et al. 2003).

But, significant challenges in the field include barriers to appropriate diagnosis and treatment of anxiety disorders, failure of a significant proportion of patients to respond to first-line pharmacotherapy agents, and a limited database of efficacy or effectiveness studies to guide treatment in such cases (Koen and Stein 2011). Thus, improved treatment guidelines and algorithms are needed. More recently developed computational supports and biological markers serve as decision supports (Himmerich and Wranik 2012).

Many sources of variability in PK–PD relationships for anxiolytics are known. The SSRIs differ in their PK properties (Hiemke and Härtter 2000) and widely in their qualitative and quantitative interaction with cytochrome P450 (CYP) isozymes in the liver. CYP2D6 is inhibited by SSRIs, in order of decreasing potency paroxetine, norfluoxetine, fluoxetine, sertraline, citalopram, and fluvoxamine (Baumann 1996). Drug–drug interaction may, therefore, occur at the level of metabolism (Olkkola and Ahonen 2008; Muscatello et al. 2012; Mahmood and Sahajwalla 1999; Yuan et al. 1999; Fahey et al. 1998; Lin 2007). In addition to PK interactions, benzodiazepines have synergistic interactions with other hypnotics and opioids. Then, age is a factor in variability, and can affect PK as well as PD. In general, however, it seems that the elderly people are more sensitive to drug action, while PK remains relatively unchanged (Strawn et al. 2012; Lenze and Wetherell 2011; Klotz 1998). Genetic polymorphism also contributes to variability (Sakai and Ishizuka 2009). Furthermore, also circadian rhythm (Nagayama 1993), and pathological conditions of the liver (Mahmood and Sahajwalla 1999) and the kidneys (Baghdady et al. 2009) may affect the PK–PD relationship of anxiolytics.

14.3.2 Antidepressants

Antidepressants are the most widely prescribed therapy for depression. The exact mechanism of action of antidepressants is unknown. The prevailing theory is that antidepressants increase the concentration of one or more neurotransmitters, such as norepinephrine, serotonin, or dopamine. The different classes of antidepressants differ in the neurotransmitters they affect (Cusack et al. 1994). This determines some of their side effects and potential drug interactions. Antidepressants include:

14.3.2.1 Tricyclics

These drugs are called "tricyclics" because the drug molecules contain three rings. This class of medication is used to treat depression, and also some types of anxiety, fibromyalgia, and to control chronic pain (von Wolff et al. 2013). Tricyclics may have the following side effects: seizures, insomnia, anxiety, arrhythmia, hypertension, rash, nausea, vomiting, abdominal cramps, weight loss, constipation, urinary retention, increased pressure on the eye, and sexual dysfunction. Examples of tricyclic antidepressants are amitriptyline (Elavil®), clomipramine (Anafranil®), desipramine (Norpramin®), doxepin (Sinequan®), imipramine (Tofranil®), nortriptyline (Pamelor®), protriptyline (Vivactil®), and trimipramine (Surmontil®).

14.3.2.2 Noradrenaline and Specific Serotoninergic Antidepressants

These are a class of compounds that are used in the treatment of anxiety disorders, some personality disorders, and depression. Noradrenaline and specific serotoninergic antidepressants (NASSAs) have the following possible side effects: constipation, dry mouth, weight gain, drowsiness, sedation, blurred vision, and dizziness. More serious adverse reactions include: seizures, white blood cell reduction, fainting, and allergic reactions. Examples of NASSs include mianserin (Tolvon®) and mirtazapine (Remeron®, Avanza®, Zispin®).

14.3.2.3 SNRIs and SSRIs

SNRIs are a class of drugs used to treat major depression, mood disorders, and possibly but less commonly ADHD, obsessive compulsive disorder, anxiety disorders, menopausal symptoms, fibromyalgia, and chronic neuropathic pain. Examples of SNRIs are duloxetine (Cymbalta®), venlafaxine (Effexor®), and desvenlafaxine (Pristiq®). SNRIs raise levels of serotonin and norepinephrine that both play a key role in stabilizing mood.

Examples of SSRI antidepressants are: citalopram (Celexa®), escitalopram (Lexapro®), fluoxetine (Prozac®, Sarafem®), fluvoxamine (Luvox®), paroxetine (Paxil®), and sertraline (Zoloft®). These drugs are used to treat depression, but

some are used for anxiety, as earlier indicated (Hiemke and Härtter 2000). SSRIs will often take a month to have a noticeable effect. This is because first the brain needs to adapt to the "overflow" of serotonin by downregulating the sensitivity of the autoreceptor, which needs time (Mandrioli et al. 2012; von Wolff et al. 2013).

SSRIs and SNRIs may have the following side effects: hypoglycemia, low sodium, nausea, rashes, dry mouth, constipation, diarrhea, weight loss, sweating, tremor, sedation, sexual dysfunction, insomnia, headache, dizziness, anxiety, agitation, and abnormal thinking. Currently, the SSRIs are the most commonly prescribed antidepressants (von Wolff et al. 2013) as SSRIs are not only very effective in treating depression but are also believed that they have fewer side effects than the other types.

14.3.2.4 Monoamine Oxidase Inhibitors

Monoamine oxidase inhibitors (MAOIs) are drugs that inhibit brain metabolism and thereby increase brain levels of monoamines, such as serotonin and norepinephrine. Examples are phenelzine (Nardil®), tranylcypromine (Parnate®), isocarboxazid (Marplan®), and selegiline (EMSAM®, Eldepryl®). MAOIs are typically only used when tricyclic antidepressants or SSRIs exacerbate or fail to prevent depression. MAOIs have the following possible side effects: blurred vision, rash, seizures, edema, weight loss, weight gain, sexual dysfunction, diarrhea, nausea, constipation, anxiety, insomnia, drowsiness, headache, dizziness, arrhythmia, fainting, feeling faint when standing up (postural hypotension), and hypertension.

Antidepressants are not all the same in how they affect neurotransmitters, how they are used, and what adverse effects or drug interactions are associated with them differ (Baumann 1996). One patient may not respond to one type of antidepressant and do better with another, while another person with a similar condition might respond the other way round.

Variation in the effects of antidepressants is a problem and the relation between severity of depression and outcome is complex (Van et al. 2008). Only a small part can be related to factors know to contribute to variability. CYP450 genes play a major role in the metabolism of a substantial part of psychotropics, including antidepressants, and the first estimates of dosage adjustments for antidepressants have been provided based on metabolizer status (Spina et al. 2008; Schosser and Kasper 2009).

Two functional polymorphisms of the serotonin transporter gene, 5-HTTLPR and STin2, have been investigated in a large number of pharmacogenetic studies of depression; other candidate genes include serotonin receptor genes, brain-derived neurotrophic factor (BDNF), P-gp located in the BBB, G-proteins, TPH1 and TPH2, MAOA, the noradrenaline transporter gene, FKBP5, or cytochrome P450 (CYP450) genes (Schosser and Kasper 2009). Based on an extensive literature search, PK of antidepressants can be substantially different between women and men. Likewise, the response to antidepressants can be quite variable, including sex differences in adverse effects and time to response. Despite the many sex differences reported, there is still little published work systematically evaluating potential sex differences in antidepressant PK and PD (Bigos et al. 2009).

De Klerk et al. (2012) concluded that adverse drug effects with SSRI treatment, in particular serotonergic effects, are predicted by two common polymorphisms of the ABCB1 gene encoding for P-gp. Since P-gp is present at the BBB and (some) SSRIs display affinity as substrate for P-gp, this may affect brain distribution of SSRIs. De Klerk and colleagues found a significant association between the number of SSRI-related adverse drug effects and ABCB1 gene variants. Moreover, serotonergic effects (sleeplessness, gastrointestinal complaints, and sexual effects) were significantly predicted by these variants and haplotype.

There is an on going debate on whether or not antidepressant effects are true or the result of placebo effects. Kirsch evaluated by meta-analysis new-generation antidepressants in relation to the placebo response (Kirsch 2009). They concluded that most trials failed to show a significant advantage of SSRIs over inert placebo, and the differences between drug and placebo are not clinically significant for most depressed patients. Fountoulakis and Möller (2011) recalculated and reinterpreted the data of the Kirsch (2008) study. Their conclusion was that Kirsch et al.'s meta-analysis suffered from important flaws in the calculations; reporting of the results was selective and conclusions unjustified and overemphasized. Overall, Fountoulakis and Möller (2011) suggested that although a large percentage of the placebo response is due to expectancy, this is not true for the active drug, and effects are not additive. The drug effect is always present and is unrelated to depression severity, while this is not true for placebo.

14.3.3 Antipsychotics

Antipsychotics are drugs used to treat various symptoms of psychosis, such as those caused by psychotic disorders or schizophrenia. Antipsychotic medication is usually prescribed to bring psychotic symptoms under control and into remission. Possible side effects of antipsychotics include dry mouth, drowsiness, and Parkinson's disease like muscle stiffness and involuntary movements of the body (tardive dyskinesia) or the so-called extrapiramidal side effects (EPS; Mauri et al. 2007). The most severe side effect of antipsychotics is agranulocytosis, the destruction of white blood cells with unknown cause. It is a potentially serious but reversible health condition, and blood cell counts need to be monitored. There are two categories of antipsychotics: typical and atypical.

14.3.3.1 Typical Antipsychotics

These drugs are also called first-generation antipsychotics (FGAs) that can be categorized by inducing EPS. Most conventional antipsychotics work by blocking the D2 dopamine receptors. Side effects include muscle stiffness and shakiness, like Parkinson's disease, sluggish feeling, slow thinking, uncomfortable restlessness (akathisia), and problems with sex life. Examples of these drugs include chlorpromazine (Largactil®), haloperidol (Haldol®), pimozide (Orap®), trifluoperazine (Stelazine®), and sulpiride (Dolmatil®).

14.3.3.2 Atypical Antipsychotics

Atypical or second-generation antipsychotics (SGAs) induce significantly less EPS (Mauri et al. 2007). Atypical antipsychotics block both the D2 dopamine receptors as well as 5HT2A serotonin receptors. Compared to the older drugs they seem less likely to cause Parkinsonian side effects and tardive dyskinesia (at not too high doses), but they are more likely to produce weight gain, to produce diabetes, to give sexual problems, and to induce sleepiness and slowness. Examples of the atypical antipsychotics include amisulpride (Solian®), aripiprazole (Abilify®), chlorpromazine (Thorazine®), clozapine (Clozaril®), olanzapine (Zyprexa®), quetiapine (Seroquel®), risperidone (Risperdal®), sertindole (Serdolect®), zotepine (Zoleptil®), and paliperidone (Invega®). The atypical antipsychotics are rather expensive, but may be more effective than older medications for (negative) symptoms of schizophrenia.

Risperidone is one of the most commonly used atypical antipsychotics that can improve both the positive and the negative symptoms of schizophrenia with a low report of EPS. The pharmacological response of risperidone depends on the concentration of risperidone and its active metabolite 9-hydroxy-risperidone (9-OH-RSP), also known as paliperidone. Paliperidon was recently marketed as an independent antipsychotic drug (Invega®).

Mauri et al. (2007) provided a literature review on the relationships between plasma concentrations of SGAs and clinical responses by dividing the studies on the basis of the length of their observation periods (therapeutic ranges). The usefulness of therapeutic drug monitoring is well established. Plasma clozapine concentrations seem to be influenced by many factors, such as altered CYP450 1A4 activity, age, sex, and smoking. High plasma concentrations of clozapine can increase the risk of epileptic seizures. In use of risperidone, the metabolite 9-OH-risperidone (paliperidon) is formed, and both should be measured ("active moiety") to prevent erroneous interpretations on the pharmacological effects of risperidone. For olanzapine, the literature strongly indicates a relationship between clinical outcomes and plasma concentrations. There is little evidence in favor of the existence of a relationship between plasma quetiapine concentrations and clinical responses. Positron emission tomography (PET) studies of receptor blockade indicated a discrepancy between the time course of receptor occupancy and plasma quetiapine concentrations. There is no direct evidence concerning optimal plasma concentration ranges of ziprasidone, aripiprazole, or sertindole.

Risperidone is metabolized by CYP2D6 and CYP3A to paliperidone, indicating variability will be observed by differences in metabolism (fast and slow metabolizers). The receptor-binding affinity for the dopamine receptor and the 5HT2A receptor of paliperidone are reported to be equal to risperidone (Mauri et al. 2007). Brain distribution is another aspect that may influence PK–PD relationships of antipsychotics (and CNS drugs in general). Drugs with a poor brain distribution (risperidone) will require higher doses to be administrated to obtain similar receptor occupancy when compared to compounds with a relatively good transport (olanzap-

ine, quetiapine; Fitzgerald and Dinan 2008). Both risperidon and paliperidone are substrates for Pgp in vitro and in vivo.

Possible biomarkers for antipsychotic drugs are certain hormones, in particular prolactin (PRL). PRL is mainly associated with reproductive and metabolic functions, and is synthesized and stored in lactotrophs located in the anterior lobe of the pituitary. The release of PRL is predominantly under hypothalamic inhibitory control of dopaminergic neurons. Dopaminergic neurons project dopamine into the anterior lobe of the pituitary via several pathways. Activation of dopamine D2 receptors on the cell surface of lactotrophs inhibits the release of PRL into plasma. Likewise, blockade of D2 receptors leads to release ofPRL. Besides the dopaminergic control on PRL release, PRL concentrations in plasma are also influenced by changes in synthesis rate, lactotroph storage capacity, homeostatic feedback mechanisms and rate of plasma elimination (Freeman et al. 2000; Ben Jonathan and Hnasko 2001; Fitzgerald and Dinan 2008). Interestingly, PRL synthesis, pathways of release and homeostatic feedback and elimination half-life are similar in rats when compared to man. This makes PRL concentrations in plasma an interesting candidate for evaluation as a translational biomarker for D2 receptor activity (Ben Jonathan et al. 2008), in particular for dopamine receptor antagonists and possibly also partial agonists. Since the synthesis, pathways for release, and elimination of prolactine in humans are comparable to rats, prolactine is a good translational biomarker for the effect of dopamine receptor antagonists (Stevens et al. 2012), as will be shown in the pharmacometric section for antipsychotic drugs below.

14.4 Pharmacometric Approaches

14.4.1 Anxiolytics

Although the definition of “pharmacometrics” (quantitative pharmacology) as research field is young, approaches to that end have initiated long time ago. Especially for the group of benzodiazepines, this was possible as their effects could be well characterized from a quantitative analysis of the electroencephalogram (EEG) as a biomarker (Krijzer and Van der Molen 1987). When observed in conjunction with blood sampling, the plasma PK–PD relationships of benzodiazepines could be characterized in individual animals and humans. The EEG appeared to be an ideal biomarker of changes in CNS functionality in the sense that it can be obtained in a strict objective, continuous, sensitive, and reproducible manner in individual animals.

In the early 1990s, the first quantitative investigations on PK–PD modeling of benzodiazepines in the rat were performed in freely moving rats, using the EEG effects (Mandema and Danhof 1992). By this approach, quantitative information on the potency and intrinsic efficacy of CNS drugs could be obtained. As a measure of pharmacological effect intensity of benzodiazepines the amplitudes in the beta

frequency band of EEG signals are relevant, which reflects their affinity and intrinsic efficacy at the central GABA–benzodiazepine receptor complex.

Détári et al. (1999) studied the influence of serotonergic- and benzodiazepine-type anxiolytic drugs on the cortical activation and sleep–wakefulness cycle. The EEG signals were obtained in freely moving rats, and other measures of sleep in mice. Based on sleep quality by increasing sleep episode length and time spent in deep sleep the authors concluded that the serotonergic anxiolytic drugs seem to be superior compared to the benzodiazepine–type anxiolytic drug studied. Lau et al. (1998) published a rat study in which the possibility of both stimulation and sedation effects of midazolam were investigated by EEG effects. A stimulation–sedation model was developed suggesting that midazolam possesses both stimulatory and sedative effects in a continuous but sequential fashion, and hypothesizes the coexistence of stimulation and sedation components for midazolam. Cleton et al. (1999) showed that the rate of change in plasma concentrations is an important determinant of the EEG effects of midazolam in rats. In two groups of male volunteers with different ages (the younger ~25 years, the elderly ~75 years), Albrecht et al. (1999) investigated the pharmacologic properties of midazolam with special regard to age using EEG as a measure of the hypnotic-sedative effect. PK parameters were similar in both groups, while the PD data showed substantial hysteresis and a large difference in half-maximum concentration (EC50), being ~factor-2 lower in the elderly. So, in the elderly lower doses are needed due to increased sensitivity to midazolam action.

Acute dosing and chronic dosing might have different PK–PD relationships due to possible tolerance or other homeostatic feedback mechanisms. Laurrijssens and Greenblatt (2002) studied the influence of chronic midazolam exposure on its PK–PD relationship by EEG recordings and parallel serial blood sampling. The concentration–EEG effect relationships were consistent with a sigmoidal E_{max} (maximal effect) model. No differences in PK or PD parameters were found between day 1 and 7. However, by repeated exposure, a modest degree of tolerance to midazolam was found, the effect only being evident after correction for the fraction unbound of midazolam.

With time, the experimental approaches were refined and more statistical issues were addressed Quantitative EEG analysis and statistical procedures were applied under specific design conditions to objectively evaluate the functional bioavailability of psychotropic drugs in the human brain (Barbanoj et al. 2002a)**.** Methodological aspects were discussed (different treatments, doses, time points, states, target variables, electrodes, and even different groups). Statistical PK–PD modeling was introduced as a tool to enlarge the scope of inferences that can be derived when using "pharmaco-EEG." Statistical comparisons were discussed for making conclusions about acute, repetitive, or superimposed effects, and in relation to human psychotropic interactions (such as mechanistic drug–drug interaction descriptions, drug metabolites and enantiomers as well as the importance of acquiring drug plasma concentrations, elapse of time, and topographic distributions) to accurately identify its occurrence. Examples were presented on some anxiolytic drugs, including benzodiazepines.

Oral midazolam is widely used for preoperative sedation in children, and the contribution of the formed active 1-hydroxy metabolite 1-hydroxymidazolam (1-OHMDZ) to the EEG effects was studied (Johnson et al. 2002). Age, weight, sex, concomitant drugs, and the metabolic ratio, 1-OHMDZ/midazolam were investigated as covariates of the PK of midazolam and 1-OHMDZ. The metabolite 1-OHMDZ had approximately half the activity of the parent drug and can compensate for at least part of the decreased effect due to increased midazolam metabolism. This indicated that studies of midazolam should evaluate the contribution of 1-OHMDZ to the overall PD effect.

To place pharmaco-EEG within the clinical context, the distinction between biomarkers, surrogate end points, clinical end points, and clinical outcomes was introduced by Barbanoj et al. (2002b). State-of-the-art applications of pharmaco-EEG were discussed, together with PK–PD modeling in everyday clinical practice. For psychiatry, the applications can be used to discriminate between responders and nonresponders to pharmacological treatment using the test dose. The combination of pharmaco-EEG and PK–PD modeling, although successfully used during some drug development programs (e.g., benzodiazepines), is not widely applied in the clinical scenario where the CNS is concerned. The authors concluded that to develop fully the potentials of pharmaco-EEG together with PK–PD modeling in neuroscience therapeutics much work still needs to be done.

Using EEG, Visser et al. (2003) developed a mechanism-based PK–PD model for neuroactive steroids, comprising a separate characterization of the receptor activation process and the stimulus–response relationship was applied to various nonsteroidal GABAA receptor modulators. The model yielded estimates of both the apparent in vivo receptor affinity (KPD) and the in vivo intrinsic efficacy ePD. Significant linear correlations were observed between KPD for unbound concentrations and the affinity in an in vitro receptor bioassay and between ePD and the GABA-shift in vitro. This study showed that the in vivo effects of nonsteroidal GABAA receptor modulators and (synthetic) neuroactive steroids can be described on the basis of a single unique transducer function. Furthermore, it was found that the nonsteroidal GABAA receptor modulators behave as partial agonists relative to neuroactive steroids.

Jonker et al. (2003) investigated the PD interaction between midazolam, an allosteric modulator of the GABAA receptor, and tiagabine, an inhibitor of synaptic GABA uptake, by EEG recording and parallel plasma concentrations in the rat. They found that the in vivo PD interaction between midazolam and tiagabine is additive rather than synergistic.

14.4.2 Antidepressants

Using the rat as experimental animal, Geldof et al. (2007, 2008a, b, c) performed a series of studies that investigated different mechanisms between SSRI dosing and CNS effect in a strict quantitative manner using (semi-)mechanistic PK–PD modeling. Fluxoxamine was used as a paradigm SSRI compound. Plasma PK was

investigated by a population approach by nonlinear mixed-effects modeling (Geldof et al. 2008a). In six studies with a different experimental setup, study site and/or sampling design, rats received an intravenous infusion of a low, medium, and high dose of fluvoxamine. A population three-compartment PK model adequately described the fluvoxamine plasma concentrations. Body weight was identified as a significant covariate of the intercompartmental clearance. The PK was independent of factors, such as dose, surgery, and study site. The utility of the model in animal behavioral studies was demonstrated in a PK–PD analysis of the effects on rapid-eye-movement (REM) sleep in which a sparse PK sampling design was used. This indicates that limitations of blood sampling in particular study designs can be overcome by a mixed-effects-modeling approach.

The next study was on the kinetics of brain distribution of fluvoxamine, estimated by simultaneous analysis of plasma, free brain extracellular fluid (ECF), and total brain tissue concentrations. The PK model consisted of three compartments for fluvoxamine concentrations in plasma in combination with a catenary two compartmental model for distribution into the brain. In this catenary model, the mass exchange between a shallow perfusion-limited and a deep brain compartment was described by a passive diffusion term and a saturable active efflux term. With increasing dose, a disproportional increase in brain concentrations was observed (Geldof et al. 2008a).

The next question was how brain distribution kinetics of fluvoxamine would relate to 5-HT transporter (SERT) occupancy. SERT occupancy of fluvoxamine was determined in rat frontal cortex ex vivo. Highest SERT occupancy was at early time-points after acute administration. Duration of SERT occupancy was longer for the higher dose. The maximal SERT occupancy (B_{max}) was 95 %. SERT occupancy could be directly related to plasma, brain ECF, and brain tissue concentrations by a hyperbolic function (B_{max} model; Geldof et al. 2008c).

In the final study of this series, a mechanistic model was developed to predict the time course of the concentrations of 5-HT and its metabolite 5-hydroxyindolacetic acid (5-HIAA) in rat frontal cortex following acute administration of fluvoxamine. In the model, fluvoxamine increase synaptic 5-HT concentrations by reversible blockade of the SERT in a direct concentration-dependent manner, while the 5-HT response is attenuated by negative feedback via 5-HT autoreceptors. In principle, the model allows for the description of oscillatory patterns in the time course of 5-HT and 5-HIAA concentrations in brain ECF. The PK–PD analysis revealed that inhibition of 5-HT reuptake was directly related to the fluvoxamine concentration in plasma. The proposed mechanistic model was the first step in modeling of complex neurotransmission processes. The model constitutes a useful basis for the prediction of the time course of median 5-HT and 5-HIAA concentrations in the frontal cortex in behavioral pharmacology studies in vivo (Geldof et al. 2008b).

With a proper study design and modeling, sparse sampling may provide useful data. Feng et al. (2006) used sparse sampling to develop a population PK model to described paroxetine data in an elderly (>70 years) depressed population, with data obtained in a 5-year clinical trial investigating “maintenance therapies in late-life depression” (MTLD-2). The data indicate that female and male subjects with different CYP2D6 polymorphisms have different elimination rates and therefore may need to be dosed differently based on metabolizer genotype.

As mentioned in the introduction, disease severity measures, such as the Hamilton depression rating scale (HAM-D), are used as end points in the assessment of treatment results as well as response to newly developed drugs. Della Pasqua et al. (2010) discussed the implications of the limited sensitivity of global scales and their individual items in discriminating response, and that increasing evidence reveals that individual HAM-D items are insensitive to the mechanism of action of existing antidepressant drugs. Moreover, little distinction can be made between active treatment and placebo. They concluded that differentiation of novel compounds based on such clinical scales is unlikely and that a mechanism-based approach accounting for the multidimensional nature of symptoms and signs is required.

For improved insight into drug action in diseases as complex as psychiatric diseases, there is a need for more "composite" end points that reflect the underlying mechanisms of action need to be developed. Such was done by Zuideveld et al. (2007), who investigated hypothermia and corticosterone increase of the 5-HT(1A)-receptor agonists flesinoxan and buspiridone in the rat and mechanism-based PK–PD models were developed and characterized. Flesinoxan is a potent and selective 5-HT1A receptor partial/near-full agonist that possesses antidepressant and anxiolytic effects in animals (van Hest et al. 1992; Rodgers et al. 1994). In human clinical trials it was found to have robust efficacy with very high tolerability (but for unclear reasons development was halted and it was never marketed). In patients it enhances REM sleep latency, decreases body temperature, and increases adrenocoticotropin (ACTH), cortisol, PRL, and growth hormone secretion (Grof et al. 1993; Pitchot et al. 2004). Zuideveld et al. (2007) applied allometric scaling to predict drug effects in the human situation, on the basis of simulation, taking into account the interindividual variability and clinical study design. The model-predicted effects of both flesinoxan and buspirone were compared to those published in the literature. The main finding of this analysis was that for both hypothermia and the increase in cortisol levels, the model could predict the extent of the pharmacological response in man adequately. For the hypothermic response, the time course of the response was also predicted with a high degree of accuracy. In contrast, in the case of the cortisol response, the observed time lag was not predicted, despite the fact that it fell within the model uncertainty. All together, these results indicated that allometrically scaled mechanism-based PK–PD models are promising as a means of predicting the PD responses in man.

14.4.3 Antipsychotics

14.4.3.1 Human Studies

Human Plasma PK

Due to high interindividual variability in peripheral PK parameters, dosing of antipsychotics relies on clinical trial and error. This blind process of upward or downward clinical dose titration carries a risk of relapse and adverse effects in the

treatment of schizophrenia. Using population PK methods, insight into sources of variability has been sought for.

Mannaert et al. (2005) investigated the single-dose PK profiles of long-acting injectable risperidone and oral risperidone. Plasma concentrations of the unchanged risperidone and its metabolite 9-OH-risperidone (together referred to as the active moiety) were measured in plasma after a single oral dose of risperidone in healthy volunteers, and up to 84 days after a single intramuscular injection of long-acting injectable risperidone in schizophrenic patients. These data were projected to multiple dose regimens and average steady-state PK profiles were predicted. The most interesting results, obtained at steady state, were a lower predicted peak plasma level and a lower predicted degree of fluctuation between steady-state maximal and minimal concentrations with long-acting injectable compared to oral administration, which indicates that this long-acting injectable formulation is to be preferred.

Vermeulen et al. (2007) developed a population model to simultaneously describe risperidone and 9-hydroxyrisperidone PK, to assess information on inter- and intra-individual variability of risperidone and 9-OH-risperidone, and to evaluate the influence of patient demographic characteristics and other factors on risperidone, 9-OH-risperidone, and active moiety PK. Phase 1 (serial blood sampling) and phase 3 data (sparse sampling) were included. The PK model contained two-compartment submodels for risperidone and 9-hydroxyrisperidone disposition and a sequential zero- and first-order absorption pathway (selected based on prior knowledge). To address CYP2D6 polymorphism of risperidone conversion to 9-hydroxyrisperidone, a mixture model was incorporated. The PK model described the plasma PK for risperidone and 9-OH-risperidone reasonably well and was able to determine each patient's phenotype. Potential covariates were tested: age, sex, race, body weight, lean body mass, body mass index, creatinine clearance, liver function laboratory parameters, study, and carbamazepine comedication. Of these, carbamazepine comedication and study were significantly affecting the PK. Carbamazepine also decreased active moiety concentrations.

Using sparse sampling, Feng et al. (2008) assessed covariate effects of age (18–93 years), weight, sex, smoking status, race, and concomitant medications, on risperidone and 9-OH risperidone PK parameters. A nonlinear mixed-effects model (NONMEM) was developed to describe simultaneously the risperidone and 9-OH risperidone PK. A one-compartment mixture model with first-order absorption adequately described the risperidone and 9-OH risperidone concentrations. Age was identified as a significant covariate on 9-OH risperidone clearance in this study. Thyssen et al. (2010) studied the PK of oral risperidone in children and adolescents. The PK of oral risperidone was investigated through noncompartmental analysis and population PK analysis on a pooled database including both pediatric and adult data. Monte Carlo simulations were performed to evaluate the relevance of the effects of covariates on the plasma exposure of the active antipsychotic fraction. The PK analysis showed that, after correcting doses for bodyweight, plasma exposure was comparable between children and adolescents. None of the tested demographic or biochemical characteristics were found to have a relevant effect on any of the PK parameters of risperidone and the active antipsychotic fraction. Also, Sherwin et al.

(2012) investigated risperidone and 9-OH-risperidone PK in children and adolescents, searching for covariate effects on PK parameters. A NONMEM modeled the PKs of risperidone and 9-OH-hydroxy-risperidone; covariates included age (in contrast to Thyssen et al. 2010), weight, sex, and CYP2D6 phenotype (by metabolizer subpopulations: extensive, intermediate, and poor).

Ismail et al. (2012) studied the magnitude and variability of plasma concentrations of clozapine and norclozapine across the lifespan in a real-world clinical setting in a population PK study. “Inpatients” and “outpatients” of the Centre for Addiction and Mental Health in Toronto with schizophrenia spectrum disorders (age between 11 and 79) with clozapine (Clozaril®) treatment were included. A one-compartment model with first-order absorption and elimination best described the data. The only covariates with a significant effect on clearance were age and sex: clearance for both parent and metabolite decreased exponentially with age at least 39 years. Decreased clearance of clozapine and norclozapine with age results in increased blood concentrations and, hence, the potential for adverse drug reactions. These findings have particular clinical relevance for the dosing and safety monitoring of clozapine in older adults, highlighting a need for increased vigilance.

The PK of paliperidone was determined following intramuscular administration of its supposedly long-acting palmitate ester at various doses and at two different injection sites (deltoid and gluteal muscle) by Samtani et al. (2009). Polled patient data were used from phase 1, 2, and 3 trials. The plasma PK for paliperidone following intramuscular administration of its palmitate ester was best fitted to a one-compartment model with first-order elimination. The absorption component of the model allowed a fraction of the dose to enter relatively quickly into the central compartment via a zero-order process. After a lag time the remaining fraction entered the systemic circulation, via a first-order process (dual absorption PK). Inter individual variability was found for clearance, central volume of distribution, and the absorption rate constant. An additive-error model with log-transformed data was used to describe the residual variability. Sex, age, injection volume, injection site, body mass index, needle length, and injection volume were all influencing the PK of paliperidone after intramuscular administration, resulting in a complex dose–PK relationship.

For perphenazine, Jin et al. (2010) characterized the population PK in patients with schizophrenia from the clinical antipsychotic trials of intervention effectiveness (CATIE). Perphenazine was given daily for 14–600 days. A 1-compartment linear population PK model best described the data and race and smoking status were found to have significant impacts on perphenazine clearance estimates.

The contribution of genetic polymorphisms in the metabolizing enzyme (CYP2D6) and in the transporter (ABCB1) genes in healthy subjects was found in a population PK analysis of risperidone and 9-OH-risperidone (Yoo et al. 2012). A two-compartment model with a first-order absorption and lag time fitted well to serum concentration-time curve for risperidone. 9-OH-risperidone was well described by a one-compartment model as an extension of the parent drug (risperidone) model with first-order elimination and absorption partially from the depot. The results suggest the interplay of CYP2D6 and ABCB1 on the PK of risperidone and 9-OH-risperidone according to genetic polymorphisms.

Population PK of oral risperidone from (male) patients with schizophrenia or schizoaffective disorder maintained on risperidone was investigated by, using the mixed-effects model that was derived from the data of the clinical antipsychotic trials in intervention effectiveness study, to predict antipsychotic plasma concentrations before risperidone dose adjustment. In light of the known relationship between plasma drug concentration, dopamine D2 receptor occupancy, and clinical effects (see below), the authors concluded that individualized dosing with the measurement of antipsychotic plasma concentrations has the potential for bedside clinical application.

Human D2 Receptor Occupancy

Among various adverse reactions of atypical antipsychotics, weight gain and impaired glucose tolerance are clinically significant. Matsui-Sakata et al. (2005) analyzed the quantitative contributions of various receptors to these antipsychotics-induced adverse reactions in humans using receptor occupancy, assuming cerebrospinal fluid (CSF) concentrations to be representative for target site concentrations, which may to a certain extent be true (De Lange 2013b). Mean receptor occupancies of alpha 1 adrenergic, alpha 2 adrenergic, dopamine D2, histamine H1, muscarinic acetylcholine (mACh), serotonin 5-HT1A, 5-HT2A, and 5-HT2C receptors by antipsychotics were estimated by using the PK parameters and receptor dissociation constants. These receptor occupancy values were correlated to the extent of adverse reactions reported in literature, being two indices of antipsychotics-induced weight gain and the morbidity rate of type 2 diabetes mellitus during treatment with antipsychotics. For weight gain, the correlation between H1 and mACh receptors occupancies was significant. The morbidity rate of type 2 diabetes mellitus was highly correlated with H1, mACh, and 5-HT2C receptor occupancies. However, H1 receptor occupancy was also highly correlated with mACh receptor occupancy among antipsychotics, so that only one of them may be critically associated with the adverse reactions. As these adverse reactions have not been reported for drugs with mACh receptor antagonistic action, other than antipsychotics, the authors argued that the H1 receptor may contribute predominantly to the antipsychotics-induced weight gain and diabetes mellitus. It was concluded that model analysis based on receptor occupancy indicates that H1 receptor blockade is the primary cause of antipsychotics-induced weight gain and diabetes mellitus.

Also, using the same approach, Matsui-Sakata et al. (2005) investigated literature data on the relation between receptor occupancy and EPS induced by typical (haloperidol) and atypical (risperidone, olanzapine, and quetiapine) antipsychotics in patients. Matsui-Sakata and colleagues took five indices of EPS: (1) The ratio of patients obliged to take anticholinergic medication; (2) the occurrence rates of plural extrapyramidal symptoms (more than one of tremor, dystonia, hypokinesia, akathisia, extrapyramidal syndrome, etc.); (3) parkinsonism; (4) akathisia (inability to remain motionless); and (5) extrapyramidal syndrome (involuntary muscle spasms in the face and neck). Two models were tested. The first was a model that

incorporated endogenous dopamine release owing to 5-HT2A receptor inhibition, and the second was a model that did not consider this endogenous dopamine release. The models were used to examine the relationship between the D2 receptor occupancy of endogenous dopamine and the extent of drug-induced EPS. The model that incorporated the endogenous dopamine release better described the relationship between the mean D2 receptor occupancy of endogenous dopamine and the extent of EPS than the other model. Furthermore, the model incorporating endogenous dopamine release could appropriately predict the risks of EPS induced by two other atypical antipsychotics, clozapine, and ziprasidone, as external data that were not incorporated into the model development. It was concluded that the developed model incorporating endogenous dopamine release owing to 5-HT2A receptor inhibition may be useful for the prediction of antipsychotics-induced EPS.

Human PRL in Plasma

PRL is secreted by the anterior pituitary gland into the blood stream. It influences gonadal function in both sexes, initiates and sustains lactation in females, and controls libido in males. Secretion of PRL by the pituitary is under inhibitory control via dopamine from the hypothalamus. Dopamine acts on the pituitary as an inhibitor of PRL secretion. Blockade of dopamine D2 receptors by typical antipsychotics and risperidone can cause hyperprolactinemia in males and females, and may lead to amenorrhea, galactorrhea, infertility, loss of libido and erectile dysfunction. Increase of PRL concentrations in plasma is an unwanted effect, but can be used to have indirect information on functionality of the dopaminergic system. Movin-Osswald and Hammarlund-Udenaes (1995) were the first to develop a mechanism-based PK–PD model for the effects of remoxipride on human plasma concentrations of the biomarker PRL. The effect of remoxipride on plasma PRL levels is exterted via remoxipride preventing the inhibitory effect of dopamine D2 receptors in the anterior pituitary lactotrophs. The model described the time course of PRL plasma levels after administration of two consecutive doses of remoxipride at different time intervals, given to eight healthy non-obese volunteers in a randomized cross-over study. This design allowed the estimation of the rate of PRL synthesis in the lactotrophs. The model consists of three parts: (1) The pharmacokinetics of remoxipride, (2) a physiological substance model for PRL, incorporating the synthesis of PRL and its release into and elimination from plasma, and (3) a PD model describing the influence of remoxipride on the PRL release from the pool as an indirect response. A linear PD model gave the best description of the time course of PRL. It was shown that the limitation in the PRL release is the amount available in the pool, which takes 1–2 days to fully restore, rather than a maximal effect of remoxipride. The intra- and interindividual variability of remoxipride as well as of the PRL response was low (Fig. 14.1; Movin-Oswald and Hammarlund-Udenaes 1995).

Friberg et al. (2009b) developed a quantitative mechanism-based model to describe PRL release in patients for paliperidone and risperidone. They used data for

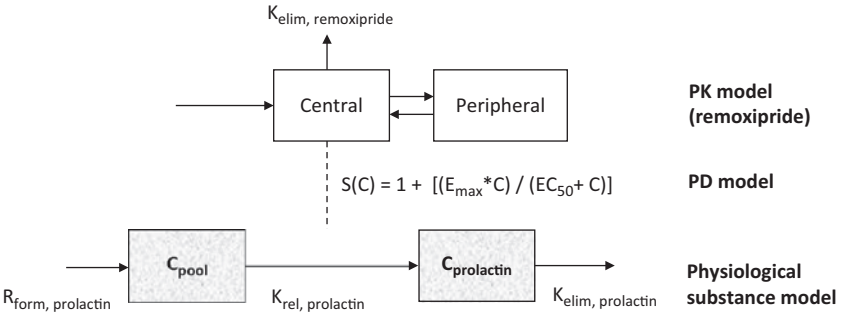

Fig. 14.1 The integrated model of neuroleptic influence on prolactin (PRL) release. (From Movin-Oswald and Hammarlund-Udenaes 1995)

the time course of PRL in healthy as well as schizophrenic subjects, following the administration of various doses and formulations of these antipsychotic drugs. A competitive agonist–antagonist interaction (AAI) model described the competition between these drugs and dopamine for the D2 receptors that regulate the PRL release. Tolerance development was explained by a feedback loop with PRL stimulating dopamine release. This feedback loop better explained the data compared with a model that included tolerance described in terms of depletion of a PRL pool. Further, the diurnal PRL rhythm was described by a two-period cosine function. Baseline PRL was health status dependent and higher in women than in men, although the drug-induced release was less than proportional to baseline. Also, the model confirmed that paliperidone and risperidone have similar potencies for PRL release.

Ma et al. (2010) evaluated tolerance to the PRL response following administration of antipsychotic drugs for the two-abovementioned models using the remoxipride data. The first was the PRL pool model (Movin-Oswald and Hammarlund-Udenaes 1995) and the second the AAI model (Friberg et al. 2009b). The remoxipride data were collected from healthy male subjects who received two remoxipride infusions on five occasions. The pool model with a circadian rhythm function fitted the data slightly better, while the AAI model was better in describing the circadian rhythm of PRL. Visual predictive checks revealed that the models predicted the PRL profiles equally well.

Clinical Trials Using Human PANSS Scores: Effects, Placebo Effects, and Dropouts

The PANSS is one of the most important rating instruments for patients with schizophrenia. All 30 items range from 1 to 7 leading to a minimum total score of 30, implying that the PANSS is an interval scale. For such interval scales, calculation of relative changes needs to be performed (which is not straightforward), and these relative (percent) changes are the widely accepted response criterion (Obermeier et al. 2011). PANSS has been used in many clinical trials to evaluate the effects of newly developed compounds.

Clinical trials aiming to prove the efficacy of newly developed molecule typically compare the effects with those observed following placebo treatment in placebo-controlled trials. However, high failure rates are encountered that are thought to be caused by considerable magnitude and variability in placebo response, high dropout rates and low sensitivity of the subjective rating scales used for assessing treatment effects. So far, non-model-based approaches make the general assumption that both placebo effect and disease progression are constant over time, which actually is not the case. This may lead to biased clinical trial outcomes. With advanced modeling and simulation approaches, one can discriminate among disease progression, placebo effects and drug effects. The use of an appropriate modeling strategy that is capable of identifying the potential sources of variable placebo responses and dropout rates is recommended for improving the sensitivity in discriminating between the effects of active treatment and placebo (Pilla Reddy et al. 2011).

The effectiveness of paliperidone extended-release (ER) tablets and olanzapine was quantified on the basis of PANSS scores in adult schizophrenia patients was modeled by Ortega et al. (2010). Patients received daily doses of paliperidone ER, olanzapine, or matched placebo for a number of weeks. An indirect response model described the time course of the PANSS. Deterioration rate was modeled as a function of baseline PANSS score, placebo, and drug effects, and the dropout effect. An exponential decrease of the placebo response was also implemented. Paliperidone ER and olanzapine treatment were characterized by a long-lasting drug effect, with a larger but short-lasting placebo effect and a notable dropout rate. The covariate exploration failed to identify any clinically relevant factors. The visual predictive check supported the model's adequacy to reproduce observed PANSS time courses. It was concluded that the population model would be useful in clinical trial simulation activities for the time course of PANSS scores in schizophrenia patients.

Large variation in placebo response within and among clinical trials can substantially affect conclusions about the efficacy of new medications in psychiatry. Developing a robust placebo model to describe the placebo response is important to facilitate quantification of drug effects, and eventually to guide the design of clinical trials for psychiatric treatment via a model-based simulation approach. In addition, high dropout rates are very common in the placebo arm of psychiatric clinical trials. While developing models to evaluate the effect of placebo response, the data from patients who drop out of the trial should be considered for accurate interpretation of the results. Better understanding of the patterns of dropout and the factors leading to dropouts are crucial in identifying the true placebo response. By modeling and simulation Friberg et al. (2009a) characterized the PK–PD relationship of sublingual asenapine in patients with schizophrenia, including placebo response and dropouts. The time course of total PANSS scores was characterized for placebo and asenapine treatments in a PK–PD model in which the asenapine effect was described by an E(max) model, increasing linearly over the study period. A logistic regression model described the time course of dropouts, with previous PANSS value being the most important predictor. The last observation carried forward (LOCF) time courses were well described in simulations from the combined

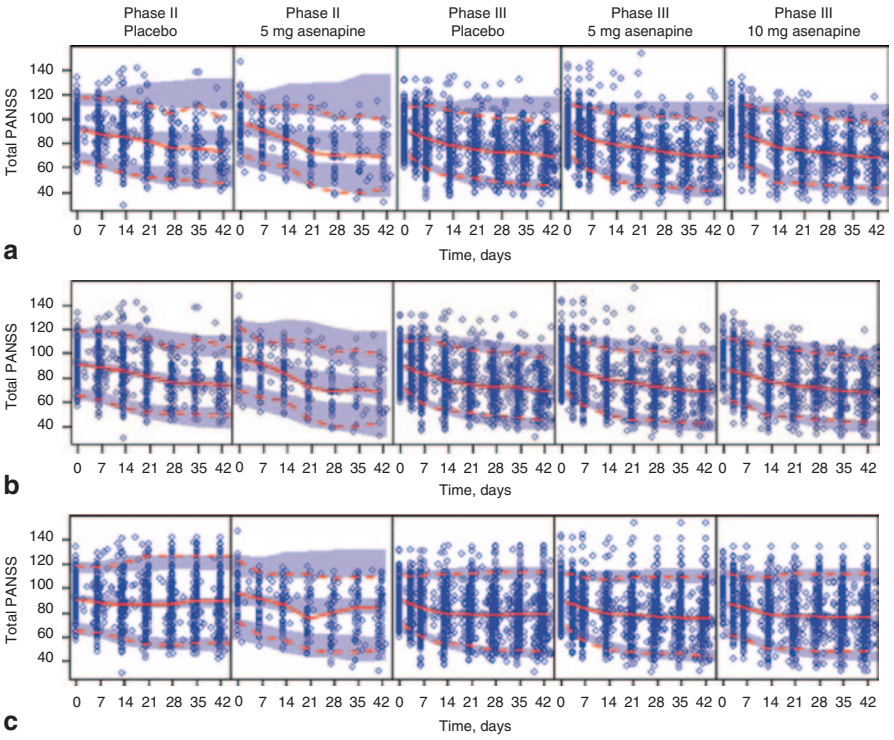

Fig. 14.2 Visual predictive checks of the final PANSS model on the PK–PD relationship of sublingual asenapine in patients with schizophrenia, including placebo response and dropouts. **a** Simulations from the realized design, **b** simulations from the combined PANSS + dropout model and all the planned visits, with PANSS score following a simulated dropout event discarded, and **c** simulations from the combined PANSS + dropout model and all planned visits, with PANSS score following a simulated dropout treated as last observation carried forward (LOCF) data. The *red lines* indicate the 5th, 50th, and 95th percentiles of the observed data or LOCF data (*blue circles*). The *shaded areas* are the 95 % confidence intervals of the corresponding percentiles of the simulated data. (From Friberg et al. 2009a)

PANSS + dropout model. The observed trial outcomes were successfully predicted for all the placebo arms and the majority of the treatment arms (Fig. 14.2).

Pilla Reddy et al. (2012) analyzed how to (1) develop a longitudinal placebo model that accounts for dropouts and predictors of the placebo effect, using the PANSS score, (2) compare the performance of empirical and semi-mechanistic placebo models, and (3) compare different time-to-event (TTE) dropout modeling approaches used to account for dropouts. Among the different tested placebo models, the Weibull model and the indirect response model adequately described the PANSS data. Covariate analysis showed that the disease condition, study duration, study year, geographic region where the trial was conducted, and route of administration were important predictors for the placebo effect. All three parametric TTE dropout models, namely the exponential, Weibull and Gompertz models, described

the probability of patients dropping out from a clinical trial equally well. The study duration and trial phase were found to be predictors for high dropout rates. Results of joint modeling of the placebo effect and dropouts indicated that the probability of patients dropping out is associated with an observed high PANSS score. Data analyses suggest that the Weibull and indirect response models are more robust than other placebo models to describe the nonlinear trends in the PANSS score. The developed placebo models accounts for dropouts and predictors of the placebo effect. This can be a useful tool in the evaluation of new trial designs and for better quantification of antipsychotic drug effects.

While the use advanced modeling the design of the trial and impact of dropouts and predictors of the placebo effects can be accounted for. However, the quality of the model also relies on the quality of the data used to develop the model. (Obermeier et al. 2011) performed a systematic review of publications in which the PANSS was used. They found that the majority of publications (62 %) actually appear to use incorrect PANSS calculations, i.e., ignoring the scale level (interval vs. ratio scale), while, moreover, in most instances the method of calculation was not even described in the manuscript. This might have led to erroneous results concerning the efficacy of the treatment. These alarming results underline the need for standardized procedures for PANSS calculations.

Apart from that, the use of rating scales such as PANSS inherently include subjectivity. It would therefore be of value to have more objective measures of mechanisms in psychosis. In that respect, preclinical research may be of added value, although it is clear that the human disease conditions cannot be reflected.

14.4.3.2 Preclinical Studies and Translational Approaches

While human studies are needed for ultimate investigation of the treatment value of antipsychotic drugs, animal studies may provide useful information as obtained under well-controlled conditions, and under well-controlled challenges, to be compared to those obtained in humans. Also, animal studies may provide mechanistic information that cannot be obtained from humans, such as drug distribution into and within the brain. The more knowledge is available on processes on the causal chain between drug dosing and effect, the better insight we will have in impact of these processes on the ultimate effect in different conditions.

Rat D2 Receptor Occupancy

In the rat, selective suppression of conditioned avoidance response has been widely reported as a test with high predictive validity for antipsychotic efficacy. Furthermore, it has been shown that the relationship between dopamine D2 receptor occupancy and the suppression of conditioned avoidance response behavior correlates well with the relationship between human dopamine D2 receptor occupancy and clinical effect. Evaluated PK–PD predictions of therapeutic effective steady-

state plasma levels by means of conditioned avoidance response behavior in rodents. Also, how this would correlate with clinically relevant plasma exposure for the classical antipsychotic drug haloperidol and four SGAs: sertindole, clozapine, risperidone, and olanzapine, including selected metabolites, like 9-OH-risperidone (paliperidone). First, the validity of the conditioned avoidance response and in vivo striatal dopamine D2 receptor occupancy was determined in parallel, using 3H-raclopride as the radioligand. The PK–PD relationship was established by modeling the time-response and time-plasma concentration data. The order of dopamine D2 receptor occupancy required to suppress conditioned avoidance response behavior according to EC50 measurements to be sertindole (+ dehydrosertindole) = dehydrosertindole = paliperidone = haloperidol = olanzapine > risperidone >> clozapine. Overall, a good agreement was observed between the rat dopamine D2 receptor occupancy levels providing 50 % response in the conditioned avoidance response test and the dopamine D2 receptor occupancy levels reported from responding schizophrenic patients treated with antipsychotics. Predictions of therapeutically effective steady-state levels for sertindole (+ dehydrosertindole) and olanzapine were three- to fourfold too high whereas for haloperidol, clozapine, and risperidone the predicted steady-state EC_{50} in conditioned avoidance responding rats correlated well with the therapeutically effective plasma levels observed in patients. This indicates that the proposed PK–PD model may serve as a guide for determining effective plasma concentrations of potential antipsychotics in the clinical setting and thereby accelerating the overall drug development process.

For rats, a mechanism-based PK–PD population model was developed to predict the time course of dopamine D2 receptor occupancy in striatum as PD biomarker following administration of olanzapine in rats by different routes (Johnson et al. 2011). A two-compartment PK model was used to describe the plasma PK. A hybrid physiology- and mechanism-based model was developed to characterize the D2 receptor occupancy in the striatum. Plasma, brain concentration profiles, and time course of D2 receptor occupancy were well described by the model. The validity of the proposed model is supported by good agreement between estimated association and dissociation rate constants and in vitro values from literature. This model includes both receptor–binding kinetics and PK as the basis for the prediction of the D2 receptor occupancy in rats. Moreover, this modeling framework can be applied to scale the in vitro and preclinical information to clinical receptor occupancy. For risperidone and paliperidone, the same approach in rats was used by Kozielska et al. (2012), now taking both dopamine D2 and serotonin 5-HT(2A) receptor occupancy as biomarkers of the PD of these drugs. The model of Johnson et al. (2011) was expanded to include metabolite kinetics, active efflux from brain, and binding to 5-HT(2A) receptors in the frontal cortex. A two-compartment model best described the plasma PK profile of risperidone and paliperidone. The expanded model described brain concentrations and D2 and 5-HT(2A) receptor occupancy well. Inclusion of binding to 5-HT(2A) receptors was necessary to describe observed brain-to-plasma ratios accurately. Interestingly, simulations showed that receptor affinity strongly influences brain-to-plasma ratio pattern. It was found that binding to both D2 and 5-HT(2A) receptors influences brain distribution of risperidone and

paliperidone. This may stem from their high affinity for D2 and 5-HT(2A) receptors. It was concluded that receptor affinities and brain-to-plasma ratios need to be considered before choosing the best PK–PD model for centrally active drugs.

To elucidate the effects of D2 receptor blockade on neurocognitive function Sakurai et al. (2013) evaluated the impact of estimated dopamine D2 receptor occupancy with antipsychotic drugs on several domains of neurocognitive function in patients with schizophrenia in the CATIE trial. Subjects treated with risperidone, olanzapine, or ziprasidone, received assessments for neurocognitive functions (verbal memory, vigilance, processing speed, reasoning, and working memory) and psychopathology. D2 receptor occupancy levels on the day of neurocognitive assessment were estimated from plasma antipsychotic concentrations, using population PK analysis and their recently developed model (Uchida et al. 2011). A multivariate general linear model was used to examine effects of clinical and demographic characteristics, including estimated D2 receptor occupancy levels, on neurocognitive functions. D2 receptor occupancy levels showed significant associations with the vigilance and the summary scores. Neurocognitive functions, including vigilance, were especially impaired in subjects who showed D2 receptor occupancy level of >77%. These findings suggest a nonlinear relationship between prescribed antipsychotic doses and overall neurocognitive function and vigilance. This study shows that D2 receptor occupancy above approximately 80% not only increases the risk for extrapyramidal side effects as consistently reported in the literature but also increases the risk for cognitive impairment. While 65–80% occupancy of dopamine D2 receptors optimizes therapeutic efficacy while minimizing risks of extrapyramidal symptoms in treating schizophrenia, it is unclear as to whether it is necessary to keep D2 receptor occupancy within this therapeutic window to maintain response. Mizuno et al. (2012) studied daily peak and trough D2 receptor occupancy levels in clinically stable patients with schizophrenia who were receiving risperidone or olanzapine. Plasma antipsychotic concentrations at peak and trough were estimated with population PK techniques. Corresponding dopamine D2 receptor occupancy levels were then estimated, using their recently developed model (Uchida et al. 2011). Of the male subjects with stable schizophrenia (Asians and Caucasians, of middle age), around 50% did not achieve a continuous blockade of ≥65%. Moreover, around 12% of the subjects did not achieve the 65% threshold at estimated peak concentrations. The results suggest that sustained D2 receptor occupancy levels of ≥65% may not always be necessary for the maintenance treatment of schizophrenia.

Translational Approach to Predict Human Effects of Antipsychotics

Stevens et al. (2012) developed a mechanism-based PK–PD model for the biological system PRL response following a dopamine inhibition challenge using remoxipride in the rat. Remoxipride concentrations were determined in plasma and in brain caudate putamen extracellular fluid (brain ECF), following a single intravenous administration of a low, medium and high dose. In these studies, PRL response was measured in plasma as well as following double dosing of the low dose with

different time intervals. Baseline variation in PRL concentrations was also assessed. The mechanistic PK–PD model consisted of: (1) a PK model for remoxipride concentrations in brain ECF; (2) a pool model incorporating PRL synthesis, storage in lactotrophs, release into- and elimination from plasma; (3) a positive feedback component interconnecting PRL plasma concentrations and PRL synthesis; and (4) a dopamine antagonism component interconnecting remoxipride brain ECF concentrations and stimulation of PRL release. The most important findings were that the brain ECF concentrations of remoxipride drive the PRL release into plasma, and the positive feedback of plasma PRL concentrations on the PRL synthesis in the lactotrophs. The latter is in contrast to the negative feedback found in the previous human models on the PK–PD correlation of remoxipride, paliperidone, and risperidone (Friberg et al. 2009b; Ma et al. 2010). An external validation of the model was performed using a dataset obtained in rats following intranasal administration of low, medium, and high doses of remoxipride. Following simulation of human remoxipride brain ECF concentrations, PD extrapolation from rat to humans was performed, using allometric scaling in combination with independent information on the values of biological system specific parameters as prior knowledge. The PK–PD model successfully predicted the system PRL response in humans as obtained by indicating that positive feedback on PRL synthesis and allometric scaling thereof could be a new feature in describing complex homeostatic mechanisms.

14.4.3.3 Summary

Psychiatric diseases are extremely complex with regard to diagnosis and treatment. This is due to the heterogeneity in the expression of the disease features and the current subjective scales used for diagnosis, the difficulties in assessment of drug treatment outcomes, and the problems in distinguishing between the "true effects from the placebo effects." The current knowledge on psychiatric diseases is largely based on empirical approaches, but it is clear that pharmacometrics in psychiatric diseases is upcoming, with the number of publications that has increased especially in the past 5 years. These publications have already aided in better understanding drug versus placebo and effects, impact of dropouts on assessment of such effects, and sources of variability. The pharmacometric models on antipsychotics so far have identified interindividual variability at the level of human plasma PK such as age (Ismail et al. 2012; Sherwin et al. 2012), sex (Ismail et al. 2012; Sherwin et al. 2012), body mass index (Sherwin et al. 2012), genetic polymorphism in CYP2D6 and ABC1 (Yoo et al. 2012), and modes of drug administration. Then, the models have improved knowledge on the relation between plasma drug concentration, human brain receptor occupancy and its, and clinical effect. H1 receptor occupancy was mostly related to anti-psychotics-induced weight gain and diabetes mellitus (Matsui-Sakata et al. 2005), and D2 receptor occupancy by endogenous dopamine released via 5-HT2A receptor inhibition mainly related to the extent of drug-induced EPS. Also, it has been concluded that sustained receptor occupancy of the D2 receptor to an extent larger than 65 % is not always necessary to maintain anti-

psychotic effects (Mizuno et al. 2012). For the effect of a number of antipsychotic drugs it should be realized that dopaminergic functionality can be reflected by PRL concentrations in plasma, but with that the rate of synthesis of PRL in the lactotroph for repetitive dosing needs to be taken into account, as has been shown for remoxipride (Movin-Osswald and Hammarlund-Udenaes 1995). Then, a very important contribution of modeling and simulation is the potential of a better distinction between drug effect and placebo effect, by inclusion of placebo and dropout models.

14.5 Discussion and Conclusions

14.5.1 Current Problems in Diagnosing and Treatment of Psychiatric Diseases

The first problem in finding good treatment for psychiatric diseases is the highly heterogeneous nature of these diseases and (therewith) the treatment outcomes (Leucht et al. 2012). The "one drug fits all" approach obviously does not work and indicates the need for personalized medicine. Second, these diseases are displayed at a behavioral and psychological level. What makes how we feel, think, and behave like we do? Human behavior and psychology is extremely complex and involve the contribution and complex interaction of a plethora of underlying mechanisms for which lots of knowledge still needs to be gained. The fact that human behavior cannot be easily tested in laboratories or reproduced in animal models further complicates our understanding of psychiatric symptoms or even diseases (Agarwal et al. 2010). Third, classification of type and severity of the diseases as well as treatment outcomes are currently still based on subjective rating scales. Fourth, in testing new treatments for psychiatric diseases, clinical trials have dealt with problems of placebo effects and dropouts during the trials that need to be taken into consideration, as otherwise in essence biased and not valid conclusions may be drawn.

14.5.2 Towards Better Treatment of Psychiatric Disorders

Nothing can be done about the heterogeneity of the psychiatric diseases, and improvements in drug treatment of psychiatric diseases must come from better diagnosis of the disease and from (more) objective assessment of drug treatment effects, as well as knowledge on sources of variability in drug treatment outcomes. Also, we need to (further) improve clinical trial design for distinction between drug effects versus placebo effects, and need to include the impact of dropouts during the trial. With such knowledge, combined with pharmacometric modeling approaches, we will be able to improve our knowledge on processes that govern our behavior and psychology, in terms of "normal" and "deviations" thereof, as well as sources of variability between "subjects" in terms of disease expression and treatment variation.

14.5.2.1 Increased Insight into Sources of Variability

Due to high interindividual variability in peripheral PK parameters, current dosing of antipsychotics relies on clinical trial and error. This "blind" process of upward or downward clinical dose titration carries a risk of relapse and adverse effects in the treatment of schizophrenia (Leucht et al. 2012). Using population PK methods, insight into sources of variability has been sought for. Pharmacometric models that have been discussed before have shown interindividual variability at the level of human plasma PK of antipsychotics include age, sex, body mass index, smoking, genetic polymorphism, and modes of drug administration, as covariates in the models.

14.5.2.2 Use of Quantitative, Objective, and Combined (Composite) Biomarkers

A pharmacometric model can never be better than the data that have been used for development of such a model. So, for that reason, here the use of different quantitative and objective types of data is recommended. A first improvement in the quality of data is to use objective biomarkers. The scores that have been used till now in essence rely on more or less extensive questionnaires (such as the PANSS score). These are highly subjective as it is about the opinion of the patient, the clinician, and possibly close relatives or friends. This is far from ideal and the search should therefore be on finding objective measures that can serve as quantitative and objective biomarkers for individual diagnosis of the disease and for individual therapeutic effects. Given the multiple processes involved in the disease, it can be seen that a single biomarker will never provide enough insights, and there is a need for a composite biomarker (combination of biomarkers) obtained at different levels of biological system functionality (for categorization see Danhof et al. 2005). Given the fact that the human brain is not really accessible for invasive measurements, information should come from accessible body compartments like blood sampling, and, if from brain, by using noninvasive techniques. These techniques can all be used in animals as well as in humans and are of high value as therefore they may be included in translational approaches, and will aid in better prediction (Stevens et al. 2012; De Lange 2013a).

Imaging Techniques

With imaging methods, brain disorders and the related occupancy of specific receptors (PET), and function of neurotransmitter pathways (magnetic resonance (MR)-based tools) can be investigated in a noninvasive way. Being noninvasive, it provides the ideal tool for translation from preclinical to clinical investigations (Klomp et al. 2012). PET studies have already been included in pharmacometric models on schizophrenia including receptor occupancy (as discussed in Sect. 14.3). Other imaging techniques can be very informative as well. During the past three decades, several MR-based tools such as MR morphometry, diffusion-tensor imaging, functional MR

imaging (fMRI) connectivity and MR spectroscopy have yielded findings that provide tangible evidence of the neurobiologic manifestations of psychiatric diseases (Agarwal et al. 2010). This holds promise to reveal more of the neurobiological underpinnings of psychiatric disorders but also enhancing our understanding of healthy (human) behavior. Structural MRI studies have indicated that patients with schizophrenia, and to some extent their unaffected relatives, have subtle deficits in several brain regions, including prefrontal and temporal lobes. Whalley et al. (2004) were curious how this inherited vulnerability leads to psychosis. They used a covert verbal initiation fMRI task that elicits frontal and temporal activity (the Hayling sentence completion task) to examine this issue. It was found that vulnerability to schizophrenia may be inherited as a disruption in a fronto-thalamic-cerebellar network, and the earliest changes specific to the psychotic state may be related to hyperactivation in the parietal lobe. Whalley et al. (2005) discussed schizophrenia from the perspective of cognitive function, along with structural and functional brain abnormalities, most notably in pre-frontal and temporal lobes. An important risk factor for developing the disorder is in the first place the inherited vulnerability. Similar deficits are apparent in relatives but less marked than those seen in patients with schizophrenia. With a hypothalamic MRI study Goldstein et al. (2007) investigated potential changes in schizophrenia with respect to supposed abnormal volumetric increases. These were indeed found, with greater severity in multiplex families (more than one ill member) compared with simplex families (one ill member). Their findings demonstrated significantly increased hypothalamic volume in psychotic cases and nonpsychotic relatives. This increase was linear from simplex to multiplex cases and positively correlated with anxiety, with a greater propensity in women. These findings suggest important implications for understanding genetic vulnerability of schizophrenia and the high rate of endocrine abnormalities. Brain MR morphometry studies on heterogeneity within the diagnostic category of schizophrenia have shown that brain structure per se is not a uniform endophenotype, but rather a combination of regional deficits highly heterogeneous in both meeting endophenotype criteria as well as in their distribution within the disease category. As fMRI brain connectivity is able to study impaired brain connectivity in schizophrenia, it also provides a tool to investigate the effect of drug treatment and challenges on the disconnectivity of functional networks in schizophrenia (Nejad et al. 2012). It can be concluded that the use of imaging methods is of great value in further investigation on schizophrenia and treatment.

Quantitative EEG, Pharmaco-EEG

Another interesting but apparently controversial technique is the quantitative electroencephalogram (QEEG; or termed pharmaco-EEG when drug treatment is evaluated). An early QEEG study was performed by Kuperman et al. (1996), who identified electrophysiological differences between children with distinct disorders of attention and/or hyperactivity and indicated that QEEG techniques may prove useful in differentiating specific subtypes of ADHD. But the introduction of pharmaco-EEG approaches into clinical practice appears problematic (Mucci et al.

2006). Prichep (2005) argued that the clinical utility of the EEG, especially in psychiatric, learning, and cognitive disorders, has been greatly enhanced by the use of quantitative analysis (QEEG), but emphasized that adequate sampling across a broad age range, inclusion/exclusion criteria, adequate sample of artifact-free data to demonstrate reliability and reproducibility of norms and specificity and sensitivity should be carefully considered. With that a normative database could be developed that allows the multivariate description of patterns of QEEG abnormalities in patients as compared to age appropriate normative values, and the exploration of neurophysiological heterogeneity within populations. They further showed the existence of the clinical significance of this approach in the scientific literature that demonstrated that QEEG provides high sensitivity and specificity to abnormalities in brain function seen in psychiatric populations. The latest publication on QEEG is a plea for this technique. According to Alhaj et al. (2011), the use of EEG offers two potential major means of addressing assessment of neurological information in psychiatric diseases. First, QEEG is able to provide direct data relating to neural activity that may be abnormal in certain disorders. With that as a given, there are opportunities for utilizing the QEEG in a variety of ways as an objective outcome measure. Second, there is growing evidence that in certain circumstances the QEEG can be used to predict which patients are likely to respond to treatment, thus potentially increasing the power of studies by decreasing non-response rates and increasing mean changes in outcome measure. It therefore seems that the QEEG approach hold promise in objective assessment of deviations in neural activity that underlies normal as well as changes in our brain functioning.

Blood Hormone Levels

Another, less expensive and more readily useful approach is (serial) blood sampling. As the brain is in constant endocrinal communication with the rest of the body, plasma may provide very useful information on brain functioning. The hypothalamus' most important function is to link the nervous system to the endocrine system, via the pituitary gland (hypophysis). Interestingly, plasma hormone levels may be assessed as well in response to administration of endogenous compounds. A very old but highly relevant study has been performed by Ferrier et al. (1983). Comparing blood sample concentrations obtained from chronic schizophrenics and controls before and after the intravenous administration of protirelin and from controls, they found reductions in basal luteinizing hormone (LH) and follicle-stimulating hormone (FSH) in the schizophrenic group. The FSH and PRL responses to the administration of protirelin and gonadorelin gonadorelin or gonadotropin releasing hormone (GnRH) were reduced in the schizophrenic group. This pattern of hypothalamic-pituitary dysfunction, which is distinct from that seen in other psychiatric and endocrinological conditions, suggests a reduction in spontaneous GnRH release from the hypothalamus in schizophrenia and may be of potential pathophysiological significance. Then, in this chapter it has already been shown that for antipsychotic drugs, PRLconcentrations in plasma may change upon administration

of antipsychotics (Movin-Osswald and Hammarlund-Udeneas 1995; Stevens et al. 2012). This is by induced changes in the hypothalamus that is taken further effect on the pituitary release, reflecting changes in dopaminergic functionality of (specific parts of) the brain. Bernstein et al. (2010) wrote a review on the hypothalamus being involved in many pathways that have been found to be disturbed in schizophrenia (hypothalamus–pituitary axis, hypothalamus–pituitary–thyroid axis, hypothalamus–pituitary–gonadal axis, metabolic syndrome, sleep–wakefulness cycle, and neuroimmune dysfunction). While it was earlier assumed that the hypothalamus plays only a subordinate role in schizophrenia, but on the basis of Bernsteins's review (Bernstein et al. 2010) the place of the hypothalamus should be reconsidered in the puzzle of schizophrenia. So, via blood sampling there is a lot to be gained in understanding the disease and effects of drugs on the disease phenotype.

14.5.2.3 Improvement in Clinical Trial Design

For the design of clinical trials also a number of issues need to be taken into consideration, which being inclusion/exclusion criteria, randomization, ethical issues, placebo effects, and dropouts.

Inclusion/Exclusion Criteria

Another consideration in clinical trial design is on selection of a representative selection of the target population as potential differences between the "ideal" and "average" patient may bias the outcomes. This is related to restrictive inclusion/exclusion criteria, ethical considerations, differences in the severity of psychopathology between clinical and trial patients, or safety issues. This was investigated by Riedel et al. (2005) using retrospective analysis of particular clinical trials. It was found that the patients included in their clinical trials were representative of the patient encountered in routine clinical practice. Their recommendations were to adhere to inclusion and exclusion criteria to prevent inclusion of severely ill (e.g. suicidal) patients requiring a more intensive treatment setting, inclusion of the more chronic, rather treatment refractory patients as this population may arguably not represent the average clinical patient either.

Randomization

Another key feature of the quality of a clinical trial is the level of randomization. Study subjects should be randomly allocated to receive one or other of the alternative treatments under study, after assessment of eligibility and recruitment but before the intervention to be studied begins (en.wikipedia.org/wiki/Randomized_controlled_trial). Random implies that each individual or unit being entered into a trial has the same chance of receiving each of the possible interventions. It also implies that the probability that an individual will receive a particular inter-

vention is independent of the probability that any other individual will receive the same intervention. After randomization, the two (or more) groups of subjects are followed in exactly the same way, and the only differences between the treatment (in terms of procedures, tests, outpatient visits, follow-up calls, etc.) should be only associated with the treatments being compared. The most important advantage of proper randomization is that it minimizes allocation bias, balancing both known and unknown prognostic factors, in the assignment of treatments. From most to least common in the medical literature, the major categories of randomized clinical study designs are: (1) Parallel-group—each participant is randomly assigned to a group, and all the participants in the group receive (or do not receive) an intervention; (2) crossover—over time, each participant receives (or does not receive) an intervention in a random sequence; (3) cluster—pre-existing groups of participants are randomly selected to receive (or not receive) an intervention; and (4) factorial—each participant is randomly assigned to a group that receives a particular combination of interventions or non-interventions (e.g. group 1 receives compound X and compound Y, group 2 receives compound X and placebo Y, group 3 receives placebo X and compound Y, and group 4 receives placebo X and placebo Y; Hopewell et al. 2010).

Ethical Issues

In addition, in clinical trials, ethical issues need to be taken into consideration. Silverman (2007) emphasized that the ethical conduct of a clinical trial does not end with the formulation of study design or the obtainment of a signature on the informed consent form. An important question is whether it is a right of investigators to have patients omitted from treatment if there is a chance that they will suffer from that. Then it is necessary to monitor responsibilities to ensure the adequate protection of the rights and welfare of human subjects and the four parties who share such responsibilities: the institutional review board, the data monitoring committee (or the data safety and monitoring board), the sponsor, and the investigator. There are numerous challenges, being associated with monitoring—such as overlapping responsibilities, communication gaps, and lack of standards—and attempts to provide recommendations to address some of these issues.

Placebo Effects

The design and conduct of clinical trials present a complex array of challenging problems, one of which is that of the placebo effect. The effect of placebo observed in schizophrenia clinical trials represents a growing problem that interferes with signal detection for treatments, increases costs of development, discourages investment in schizophrenia research, and delays the introduction of new treatments (Alphs et al. 2012). The first step in addressing the issue of placebo effect is acknowledgment of its existence. The focus should then be on its potential causes

in order to adjust clinical trial design elements. Clearly, the sources of placebo response are diverse. Understanding placebo response as a neurobiological effect is different from the sources of "placebo response" in a population that includes a much broader range of issues that relate to trial design, conduct, and factors such as ascertainment bias and regression to the mean. The latter may be associated with strong regional differences. All of these factors should be taken into consideration when interpreting results from clinical trials. Increasing placebo response is frequently associated with increased variance around study end point measurement, leading to poor signal detection. This, in turn, has led to increasing sample sizes, increasing numbers of failed studies and much higher treatment development costs. Therefore, failure to address these issues threatens the support for investments in and the success of CNS drug development.

Dropouts

Typically, high dropout rates characterize clinical trials of antipsychotic treatment and can be even higher than 50% and dropout leads to missing data that can vary so much that it affects modeling and analysis (Rabinowitz and Davido 2008a, b). Accordingly, questions have been raised about the most appropriate method for analyzing efficacy data in clinical trials of antipsychotic treatment in general, and specifically the validity of the commonly used LOCF method, mixed-effects models, and of other methods used in these trials. Three types of dropouts can be distinguished. First is the "missing completely at random" (MCAR). MCAR refers to a situation where the lack does not depend on either observed or unobserved data. MCAR can readily be handled in the analysis. Nevertheless, MCAR leads to loss of power due to diminished sample size. Second is the "missing at random" (MAR). MAR occurs if the missing data depend on variables that are observed during the trial but not on unobserved data (e.g., the increased dropout in the placebo arm of a study or high dropout rates in a particular study center). In such cases, dropout is explained by the observed data and can be accounted for in the data analysis. Third is the "missing not at random" (MNAR). MNAR occurs if the lack depends on unobserved data. For example, if a patient who was doing well but got lost to follow up because he/she had relapsed after the last observed visit and was admitted to a different hospital. Then, the observed data could not predict the missing data. The unobserved data contained information not foreseen by the observed data. MNAR cannot be corrected for without explicitly specifying a model for the missing data mechanism, which by definition cannot be observed or tested. A standard approach used in clinical trials is LOCF. LOCF uses the last completed observation while on treatment to estimate a (hypothetical) last study visit value. This is problematic because it assumes that the data are MCAR and that symptoms would remain absolutely unchanged from the last visit before dropout to the end of the study. Thereby, this approach is underestimating variability in the data. Mixed-effects models and imputation methods work if data are MCAR or MAR; however, if the data are

MNAR then inferences based on these methods will not be valid. Key to choosing an appropriate method for analyzing data in clinical trials is the extent to which dropout and outcomes are related. Rabinowitz and Davido (2008a, b) examined whether dropout is related to outcome in clinical trials of antipsychotic treatment and concluded that dropout in such clinical trials corresponds with efficacy outcomes, the dynamics of symptom change and baseline symptom severity. Therefore, methods for statistical analysis should examine both efficacy and dropout and cannot assume that missing data due to dropout are completely at random. In real life, dropout is probably often related to symptomatology and it is also an important outcome. In these situations, MNAR cannot be ruled out. Therefore, methods that can handle MNAR are needed. One such method that is not dependent on the mechanism of missing data is the composite approach that does not impute data but simultaneously tests the combined outcome of completing the trial and improvement. Because dropout corresponds with symptom severity, attention to missing data due to dropout in analyzing efficacy data in trials of antipsychotic medication is important. By meta-analysis of randomized controlled trials of antipsychotic treatment using meta-analytic random effects models Rabinowitz et al. (2009) shown that dropout was higher for first- than second-generation drugs. Mixed-effects models for meta-analysis were used to identify design features that effected dropout and to develop equations to derive expected dropout rates based on trial design features. All together, this study indicated that dropout rates are lower for second- than first-generation antipsychotic drugs and appear to be partly explained by trial design features thus providing direction for future trial design.

14.5.3 Towards a Multidisciplinary Approach

It can be seen that progress in the quality of treatment of psychiatric diseases will come from a multidisciplinary approach including (neuro)biology, (neuro)pharmacology, psychiatrists, drug companies, family and friends, regulatory agencies, and last but not least pharmacometrics. Quantitative and combined (composite) biomarkers of which most can be obtained in animals as well as humans will allow the development of translational models (Stevens et al. 2012; De Lange 2013a) and help to provide insight in the disease-related changes in schizophrenic conditions and the effects of drug treatment.

14.5.4 Conclusion

As the highest possible quality of a model is determined by the quality of the data used to develop the model (Obermeier et al. 2011; De Lange 2013a), individual diagnosis of psychiatric diseases and therapeutic effects of drugs today can, and therefore should, include quantitative and objective biomarkers at different physi-

ological levels, which can even be combined with/ compared to the PANSS score. Furthermore, pharmacometrics modeling and simulation has an important role in better selection of the right population, treatment duration, and disease conditions in clinical trials, as well as in much improved design of clinical trials, to better discriminate between drug and placebo effects. Model-based clinical trial simulation will allow reliable prediction of the outcomes of future trials, if various predictors of the placebo response and dropout are taken into consideration. Therefore, it needs to completely integrate disease-progression models, placebo models, drug-response models, covariate models, and dropout models (Pilla Reddy et al. 2011). Moreover, important additional insights can come from preclinical studies if designed according to the mastermind to allow for development of predictive translational models approach (De Lange 2013a).

Finally, it is important to realize that people suffering from psychiatric diseases need to be helped by appropriate drug treatment but also by attention and care of their surroundings.

Bullet Point Summary

- Psychiatric diseases are difficult to treat. This is due to the following issues:
  - Psychiatric diseases are highly heterogeneous and complex.
  - These diseases are displayed at a behavioral and psychological level that we do not really understand.
  - A number of drugs are available for treatment of these diseases, but there is much room for improvement.
  - Classification of type and severity of the disease and treatment outcomes are currently still based on subjective rating scales.
  - Clinical trials on testing the effects of new treatments for psychiatric diseases have dealt with problems of placebo effects and dropouts during the trial.
- Improvements in drug treatment of psychiatric diseases must come from:
  - The use of (more) objective measures and especially their combination (composite biomarkers) for better diagnosis of the disease and of drug treatment effects.
  - Inclusion of objective (composite) biomarkers that can be obtained both preclinically and clinically, to enhance translational insights.
  - More knowledge on sources of variability in disease.
  - More knowledge on sources of variability in drug treatment outcomes.
  - (Further) improvement of clinical trial design for valid distinction between drug effects versus placebo effects, the impact of dropouts during the trial on the outcome.
  - Inclusion of pharmacometric approaches, to develop and apply mathematical and statistical methods for quantitative characterization, understanding, and predicting the PK and (biomarkers of) PD of a drug, and covariates for sources of variability.

14.6 Recommendations

For improved treatment of psychiatric diseases, a highly important role has to be played by pharmacometric modeling approaches. In order to tackle practical questions in drug development in the area psychiatric disorders the following is recommended:

- The use of objective and composite biomarkers to inform on the functioning of the biological system at and treatment perturbation thereof at distinct levels/biomarker types, in a mechanistic manner.
- The use of animal studies for development of preclinical translational models, as animal research allows for obtaining more information than can be obtained from humans (although it is clear that the human disease conditions cannot be reflected).
- Inclusion of pharmacometric simulation in the design preclinical studies.
- Inclusion of model-based clinical trial simulation for reliable prediction of the outcomes of future trials (i.e., with complete integration of placebo-, dropout-, disease progression-, and drug effect models).

References

Agarwal N, Port JD, Bazzocchi M, Renshaw PF (2010) Update on the use of MR for assessment and diagnosis of psychiatric diseases. Radiology 255(1):23–41

Albrecht S, Ihmsen H, Hering W, Geisslinger G, Dingemanse J, Schwilden H, Schüttler J (1999) The effect of age on the pharmacokinetics and pharmacodynamics of midazolam. Clin Pharmacol Ther 65(6):630–639

Alhaj H, Wisniewski G, McAllister-Williams RH (2011) The use of the EEG in measuring therapeutic drug action: focus on depression and antidepressants. J Psychopharmacol 25(9):1175–1191

Alphs L, Fabrizio Benedetti F, Fleischhacker WW, Kane JM (2012) Placebo-related effects in clinical trials in schizophrenia: what is driving this phenomenon and what can be done to minimize it? Int J Neuropsychopharmacol 15(7):1003–1014

Andreasen NC, Olsen S (1982) Negative v positive schizophrenia. Definition and validation. Arch Gen Psychiatry 39(7):789–794

Baghdady NT, Banik S, Swartz SA, McIntyre RS (2009) Psychotropic drugs and renal failure: translating the evidence for clinical practice. Adv Ther 26(4):404–424

Barbanoj MJ, Riba J, Morte A, Antonijoan RM, Janı F (2002a) Basics of PK-PD using QEEG: acute/repetitive administration, interactions. Focus on anxiolytics with different neurochemical mechanisms as examples. Methods Find Exp Clin Pharmacol 24(Suppl C):67–83

Barbanoj MJ, Valle M, Kulisevsky J, Pırez V, Gambïs P (2002b) Uses of pharmaco-EEG and pharmacokinetic-pharmacodynamic modeling in the clinical scenario. Methods Find Exp Clin Pharmacol 24(Suppl D):139–144

Baumann P (1996) Pharmacokinetic-pharmacodynamic relationship of the selective serotonin reuptake inhibitors. Clin Pharmacokinet 31(6):444–469

Ben Jonathan N, Hnasko R (2001) Dopamine as a prolactin (PRL) inhibitor. Endocrin Rev 22:724–763
Ben Jonathan N, LaPensee CR, LaPensee EW (2008) What can we learn from rodents about prolactin in humans? Endocrin Rev 29:1–41
Bernstein HG, Keilhoff G, Steiner J, Dobrowolny H, Bogerts B (2010) The hypothalamus in schizophrenia research: no longer a wallflower existence. Open Neuroendocrinol J 3:59–67
Bigos KL, Pollock BG, Stankevich BA, Bies RR (2009) Sex differences in the pharmacokinetics and pharmacodynamics of antidepressants: an updated review. Gend Med 6(4):522–543
Bishop SJ (2007) Neurocognitive mechanisms of anxiety: an integrative account. Trends Cogn Sci 11(7):307–316
Cleton A, Mazee D, Voskuyl RA, Danhof M (1999) Rate of change of blood concentrations is a major determinant of the pharmacodynamics of midazolam in rats. Br J Pharmacol 127(1):227–235
Cloos JM, Ferreira V (2009) Current use of benzodiazepines in anxiety disorders. Curr Opin Psychiatry 22(1):90–95
Cusack B, Nelson A, Richelson E (1994) Binding of antidepressants to human brain receptors: focus on newer generation compounds. Psychopharmacology (Berlin) 114(4):559–565
Danhof M, Alvan G, Dahl SG, Kuhlmann J, Paintaud G (2005) Mechanism-based pharmacokinetic-pharmacodynamic modeling-a new classification of biomarkers. Pharm Res 22:1432–1437
De Klerk OL, Nolte IM, Bet PM, Bosker FJ, Snieder H, den Boer JA, Bruggeman R, Hoogendijk WJ, Penninx BW (2012) ABCB1 gene variants influence tolerance to selective serotonin reuptake inhibitors in a large sample of Dutch cases with major depressive disorder. Pharmacogenomics J. doi:10.1038/tpj.2012.16 (Epub ahead of print)
De Lange ECM (2013a) The mastermind approach to CNS drug therapy: translational prediction of human brain distribution, target site kinetics, and therapeutic effects. In: Engelhardt B, Stamirovic D, de Lange EC (eds) Fluids and barriers of the CNS, theme issue "Technique and research protocols to study brain barriers in vivo, in vitro and in situ". Fluids and Barriers CNS 10:12
De Lange ECM (2013b) Utility of cerebrospinal fluid in translational neuroscience. J Pharmacokinet Pharmacodyn. (In: Bonate P (ed) Special issue "Translational modeling in neuroscience"). 40(3):315–326
De Visser SJ, van der Post JP, de Waal PP, Cornet F, Cohen AF, van Gerven JM (2003) Biomarkers for the effects of benzodiazepines in healthy volunteers. Br J Clin Pharmacol 55(1):39–50
Delgado MR, Olsson A, Phelps EA (2006) Extending animal models of fear conditioning to humans. Biol Psychol 73(1):39–48
Della Pasqua O, Santen GW, Danhof M (2010) The missing link between clinical endpoints and drug targets in depression. Trends Pharmacol Sci 31(4):144–152
Détári L, Szentgyörgyi V, Hajnik T, Szénási G, Gacsályi I, Kukorelli T (1999) Differential EEG effects of the anxiolytic drugs, deramciclane (EGIS-3886), ritanserin and chlordiazepoxide in rats. Psychopharmacology 142(3):318–326
Fahey JM, Pritchard GA, Moltke LL, Pratt JS, Grassi JM, Shader RI, Greenblatt DJ (1998) Effects of ketoconazole on triazolam pharmacokinetics, pharmacodynamics and benzodiazepine receptor binding in mice. J Pharmacol Exp Ther 285(1):271–276
Farach FJ, Pruitt LD, Jun JJ, Jerud AB, Zoellner LA, Roy-Byrne PP (2012) Pharmacological treatment of anxiety disorders: current treatments and future directions. J Anxiety Disord 26(8):833–843
Feng Y, Pollock BG, Ferrell RE, Kimak MA, Reynolds CF 3rd, Bies RR (2006) Paroxetine: population pharmacokinetic analysis in late-life depression using sparse concentration sampling. Br J Clin Pharmacol 61(5):558–569
Feng Y, Pollock BG, Coley K, Marder S, Miller D, Kirshner M, Aravagiri M, Schneider L, Bies RR (2008) Population pharmacokinetic analysis for risperidone using highly sparse sampling measurements from the CATIE study. Br J Clin Pharmacol 66(5):629–639
Ferrier IN, Johnstone EC, Crow TJ, Rincon-Rodriguez I (1983) Anterior pituitary hormone secretion in chronic schizophrenics. Arch Gen Psychiatry 40(7):755–761
Figgitt DP, McClellan KJ (2000) Fluvoxamine. An updated review of its use in the management of adults with anxiety disorders. Drugs 60(4):925–954

Fitzgerald P, Dinan TG (2008) Prolactin and dopamine: what is the connection? A review article. J Psychopharmacol 22(2 Suppl):12–19
Fountoulakis KN, Möller HJ (2011) Efficacy of antidepressants: a re-analysis and re-interpretation of the Kirsch data. Int J Neuropsychopharmacol 14(3):405–412
Freeman ME, Kanyicska B, Lerant A, Nagy G (2000) Prolactin: structure, function, and regulation of secretion. Physiol Rev 80:1523–1631
Friberg LE, de Greef R, Kerbusch T, Karlsson MO (2009a) Modeling and simulation of the time course of asenapine exposure response and dropout patterns in acute schizophrenia. Clin Pharmacol Ther 86(1):84–91
Friberg LE, Vermeulen AM, Petersson KJ, Karlsson MO (2009b) An agonist-antagonist interaction model for prolactin release following risperidone and paliperidone treatment. Clin Pharmacol Ther 85(4):409–417
Geldof M, Freijer J, van Beijsterveldt L, Timmerman P, Ahnaou A, Drinkenburg WH, Danhof M (2007) Population pharmacokinetic model of fluvoxamine in rats: utility for application in animal behavioral studies. Eur J Pharm Sci 30(1):45–55
Geldof M, Freijer J, van Beijsterveldt L, Danhof M (2008a) Pharmacokinetic modeling of nonlinear brain distribution of fluvoxamine in the rat. Pharm Res 25(4):792–804
Geldof M, Freijer JI, Peletier LA, van Beijsterveldt L, Danhof M (2008b) Mechanistic model for the acute effect of fluvoxamine on 5-HT and 5-HIAA concentrations in rat frontal cortex. Eur J Pharm Sci 33(3):217–229
Geldof M, Freijer JI, van Beijsterveldt L, Langlois X, Danhof M (2008c) Pharmacokinetic-pharmacodynamic modelling of fluvoxamine 5-HT transporter occupancy in rat frontal cortex. Br J Pharmacol 154(6):1369–1378
Goldstein JM, Seidman LJ, Makris N, Ahern T, O'Brien LM, Caviness VS Jr, Kennedy DN, Faraone SV, Tsuang MT (2007) Hypothalamic abnormalities in schizophrenia: sex effects and genetic vulnerability. Biol Psychiatry 61(8):935–945
Grof P, Joffe R, Kennedy S, Persad E, Syrotiuk J, Bradford D (1993) An open study of oral flesinoxan, a 5-HT1A receptor agonist, in treatment-resistant depression. Int Clin Psychopharmacol 8(3):167–172
Hamilton M (1959) The assessment of anxiety states by rating. Br J Med Psychol 32:50–55
Hamilton M (1960) A rating scale for depression. J Neurol Neurosurg Psych 23:56–62
Hedlund JL, Viewig BW (1979) The Hamilton rating scale for depression: a comprehensive review. J Oper Psychiat 10:149–165
Hiemke C, Härtter S (2000) Pharmacokinetics of selective serotonin reuptake inhibitors. Pharmacol Ther 85(1):11–28
Himmerich H, Wranik DW (2012) Choice of treatment with antidepressants: influencing factors. Curr Pharm Des 18(36):5958–5975
Hopewell S, Dutton S, Yu L-M, Chan A-M, Altman DG (2010) The quality of reports of randomised trials in 2000 and 2006: comparative study of articles indexed in PubMed. BMJ 340:c723
Huh J, Goebert D, Takeshita J, Lu BY, Kang M (2011) Treatment of generalized anxiety disorder: a comprehensive review of the literature for psychopharmacologic alternatives to newer antidepressants and benzodiazepines. Prim Care Companion CNS Disord. 2011;13(2). pii: PCC.08r00709. doi: 10.4088/PCC.08r00709blu.
Ismail Z, Wessels AM, Uchida H, Ng W, Mamo DC, Rajji TK, Pollock BG, Mulsant BH, Bies RR (2012) Age and sex impact clozapine plasma concentrations in inpatients and outpatients with schizophrenia. Am J Geriatr Psychiatry 20(1):53–60
Jin Y, Pollock BG, Coley K, Miller D, Marder SR, Florian J, Schneider L, Lieberman J, Kirshner M, Bies RR (2010) Population pharmacokinetics of perphenazine in schizophrenia patients from CATIE: impact of race and smoking. J Clin Pharmacol 50(1):73–80
Johnson TN, Rostami-Hodjegan A, Goddard JM, Tanner MS, Tucker GT (2002) Contribution of midazolam and its 1-hydroxy metabolite to preoperative sedation in children: a pharmacokinetic-pharmacodynamic analysis. Br J Anaesth 89(3):428–437

Johnson M, Kozielska M, Pilla Reddy V, Vermeulen A, Li C, Grimwood S, de Greef R, Groothuis GM, Danhof M, Proost JH (2011) Mechanism-based pharmacokinetic-pharmacodynamic modeling of the dopamine D2 receptor occupancy of olanzapine in rats. Pharm Res 28(10):2490–2504

Jonker DM, Vermeij DA, Edelbroek PM, Voskuyl RA, Piotrovsky VK, Danhof M (2003) Pharmacodynamic analysis of the interaction between tiagabine and midazolam with an allosteric model that incorporates signal transduction. Epilepsia 44(3):329–338

Kay SR, Flszbein A, Opfer LA (1987) The positive and negative syndrome scale (PANSS) for schizophrenia. Schizophrenia Bull 13(2):261–276

Kirsch I (2009) Antidepressants and the placebo response. Epidemiol Psichiatr Soc 18(4):318–322

Klomp A, Tremoleda JL, Schrantee A, Gsell W, Reneman L (2012) The use of pharmacological-challenge fMRI in pre-clinical research: application to the 5-HT system. J Vis Exp pii:3956

Klotz U (1998) Effect of age on pharmacokinetics and pharmacodynamics in man. Int J Clin Pharmacol Ther 36(11):581–585

Kodish I, Rockhill C, Varley C (2011) Pharmacotherapy for anxiety disorders in children and adolescents. Dialogues Clin Neurosci 13(4):439–452

Koen N, Stein DJ (2011) Pharmacotherapy of anxiety disorders: a critical review. Dialogues Clin Neurosci 13(4):423–437

Kozielska M, Johnson M, Pilla Reddy V, Vermeulen A, Li C, Grimwood S, de Greef R, Groothuis GM, Danhof M, Proost JH (2012) Pharmacokinetic-pharmacodynamic modeling of the D2 and 5-HT (2A) receptor occupancy of risperidone and paliperidone in rats. Pharm Res 29(7):1932–1948

Krijzer FNCM, Van der Molen R (1987) Classification of psychotropic drugs by rat EEG analysis: the anxiolytic profile in comparison to the antidepressant and neuroleptic profile. Neuropsychobiology 18:51–56

Kuperman S, Johnson B, Arndt S, Lindgren S, Wolraich M (1996) Quantitative EEG differences in a nonclinical sample of children with ADHD and undifferentiated ADD. J Am Acad Child Adolesc Psychiatry 35(8):1009–1017

Lader M (2008) Effectiveness of benzodiazepines: do they work or not? Expert Rev Neurother 8(8):1189–1191

Lalonde RL, Kowalski KG, Hutmacher MM, Ewy W, Nichols DJ, Milligan PA, Corrigan BW, Lockwood PA, Marshall SA, Benincosa LJ, Tensfeldt TG, Parivar K, Amantea M, Glue P, Koide H, Miller R (2007) Model-based drug development. Clin Pharmacol Ther 82(1):21–32

Lau CE, Wang Y, Ma F (1998) Pharmacokinetic-pharmacodynamic modeling of the coexistence of stimulatory and sedative components for midazolam. Eur J Pharmacol 346(2–3):131–144

Lenze EJ, Wetherell JL (2011) A lifespan view of anxiety disorders. Dialogues Clin Neurosci 13(4):381–399

Leucht S, Tardy M, Komossa K, Heres S, Kissling W, Salanti G, Davis JM (2012) Antipsychotic drugs versus placebo for relapse prevention in schizophrenia: a systematic review and meta-analysis. Lancet 379(9831):2063–2071

Lin JH (2007) Transporter-mediated drug interactions: clinical implications and in vitro assessment. Expert Opin Drug Metab Toxicol 3(1):81–92

Ma G, Friberg LE, Movin-Osswald G, Karlsson MO (2010) Comparison of the agonist-antagonist interaction model and the pool model for the effect of remoxipride on prolactin. Br J Clin Pharmacol 70(6):815–824

Mahmood I, Sahajwalla C (1999) Clinical pharmacokinetics and pharmacodynamics of buspirone, an anxiolytic drug. Clin Pharmacokinet 36(4):277–287

Maier W, Buller R, Philipp M, Heuser I (1988) The Hamilton Anxiety Scale: reliability, validity and sensitivity to change in anxiety and depressive disorders. J Affect Disord 14(1):61–68

Mandema JW, Danhof M (1992) Electroencephalogram effect measures and relationships between pharmacokinetics and pharmacodynamics of centrally acting drugs. Clin Pharmacokinet 23(3):191–215

Mandrioli R, Mercolini L, Saracino MA, Raggi MA (2012) Selective serotonin reuptake inhibitors (SSRIs): therapeutic drug monitoring and pharmacological interactions. Curr Med Chem 19(12):1846–1863

Mannaert E, Vermeulen A, Remmerie B, Bouhours P, Levron JC (2005) Pharmacokinetic profile of long-acting injectable risperidone at steady-state: comparison with oral administration. Encephale 31(5 Part 1):609–615

Marder SR, Davis JM, Chouinard G (1997) The effects of risperidone on the five dimensions of schizophrenia derived by factor analysis: combined results of the North American trials. J Clin Psychiatry 58(12):538–546

Matsui-Sakata A, Ohtani H, Sawada Y (2005) Pharmacokinetic-pharmacodynamic analysis of antipsychotics-induced extrapyramidal symptoms based on receptor occupancy theory incorporating endogenous dopamine release. Drug Metab Pharmacokinet 20(3):187–199

Mauri MC, Volonteri LS, Colasanti A, Fiorentini A, De Gaspari IF, Bareggi SR (2007) Clinical pharmacokinetics of atypical antipsychotics: a critical review of the relationship between plasma concentrations and clinical response. Clin Pharmacokinet 46(5):359–388

Mizuno Y, Bies RR, Remington G, Mamo DC, Suzuki T, Pollock BG, Tsuboi T, Watanabe K, Mimura M, Uchida H (2012) Dopamine D2 receptor occupancy with risperidone or olanzapine during maintenance treatment of schizophrenia: a cross-sectional study. Prog Neuropsychopharmacol Biol Psychiatry 37(1):182–187

Movin-Osswald G, Hammarlund-Udenaes M (1995) Prolactin release after remoxipride by an integrated pharmacokinetic-pharmacodynamic model with intra- and interindividual aspects. J Pharmacol Exp Ther 274:921–927

Mucci A, Volpe U, Merlotti E, Bucci P, Galderisi S (2006) Pharmaco-EEG in psychiatry. Clin EEG Neurosci 37(2):81–98

Muscatello MR, Spina E, Bandelow B, Baldwin DS (2012) Clinically relevant drug interactions in anxiety disorders. Hum Psychopharmacol 27(3):239–253

Nagayama H (1993) Chronopharmacology of psychotropic drugs: circadian rhythms in drug effects and its implications to rhythms in the brain. Pharmacol Ther 59(1):31–54

Nejad AB, Ebdrup BH, Glenthøj BY, Siebner HR (2012) Brain connectivity studies in schizophrenia: unravelling the effects of antipsychotics. Curr Neuropharmacol 10(3):219–230

Obermeier M, Schennach-Wolff R, Meyer S, Möller HJ, Riedel M, Krause D, Seemüller F (2011) Is the PANSS used correctly? a systematic review. BMC Psychiatry 11:113

Olkkola KT, Ahonen J (2008) Midazolam and other benzodiazepines. Handb Exp Pharmacol (182):335–360

Ortega I, Perez-Ruixo JJ, Stuyckens K, Piotrovsky V, Vermeulen A (2010) Modeling the effectiveness of paliperidone ER and olanzapine in schizophrenia: meta-analysis of 3 randomized, controlled clinical trials. J Clin Pharmacol 50(3):293–310

Owen RT (2008) Controlled-release fluvoxamine in obsessive-compulsive disorder and social phobia. Drugs Today (Barcelona) 44(12):887–893

Pilla Reddy V, Kozielska M, Johnson M, Vermeulen A, de Greef R, Liu J, Groothuis GM, Danhof M, Proost JH (2011) Structural models describing placebo treatment effects in schizophrenia and other neuropsychiatric disorders. Clin Pharmacokinet 50(7):429–450

Pilla Reddy V, Kozielska M, Johnson M, Suleiman AA, Vermeulen A, Liu J, de Greef R, Groothuis GM, Danhof M, Proost JH (2012) Modelling and simulation of the positive and negative syndrome scale (PANSS) time course and dropout hazard in placebo arms of schizophrenia clinical trials. Clin Pharmacokinet 51(4):261–275

Pitchot W, Wauthy J, Legros JJ, Ansseau M (2004) Hormonal and temperature responses to flesinoxan in normal volunteers: an antagonist study. Eur Neuropsychopharmacol 14(2):151–155

Prichep LS (2005) Use of normative databases and statistical methods in demonstrating clinical utility of QEEG: importance and cautions. Clin EEG Neurosci 36(2):82–87

Rabinowitz J, Davido O (2008a) The association of dropout and outcome in trials of antipsychotic medication and its implications for dealing with missing data. Schizophr Bull 34(2):286–291

Rabinowitz J, Davidov O (2008b) A composite approach that includes dropout rates when analyzing efficacy data in clinical trials of antipsychotic medications. Schizophr Bull 34(6):1145–1150

Rabinowitz J, Levine SZ, Barkai O, Davidov O (2009) Dropout rates in randomized clinical trials of antipsychotics: a meta-analysis comparing first- and second-generation drugs and an examination of the role of trial design features. Schizophr Bull 35(4):775–788

Riedel M, Strassnig M, Müller N, Zwack P, Möller HJ (2005) How representative of everyday clinical populations are schizophrenia patients enrolled in clinical trials? Eur Arch Psychiatry Clin Neurosci 255(2):143–148

Rodgers RJ, Cole JC, Davies A (1994) Anti-anxiety and behavioral suppressant actions of the novel 5-HT1A receptor agonist, flesinoxan. Pharmacol Biochem Behav 48(4):959–963

Sakai N, Ishizuka M (2009) Impact of rat P450 genetic polymorphism on diazepam metabolism. Expert Opin Drug Metab Toxicol 5(11):1421–1433

Sakurai H, Bies RR, Stroup ST, Keefe RS, Rajji TK, Suzuki T, Mamo DC, Pollock BG, Watanabe K, Mimura M, Uchida H (2013) Dopamine D2 receptor occupancy and cognition in schizophrenia: analysis of the CATIE data. Schizophr Bull 39(3):564–574

Samtani MN, Vermeulen A, Stuyckens K (2009) Population pharmacokinetics of intramuscular paliperidone palmitate in patients with schizophrenia: a novel once-monthly, long-acting formulation of an atypical antipsychotic. Clin Pharmacokinet 48(9):585–600

Schosser A, Kasper S (2009) The role of pharmacogenetics in the treatment of depression and anxiety disorders. Int Clin Psychopharmacol 24(6):277–288

Sherwin CM, Saldaña SN, Bies RR, Aman MG, Vinks AA (2012) Population pharmacokinetic modeling of risperidone and 9-hydroxyrisperidone to estimate CYP2D6 subpopulations in children and adolescents. Ther Drug Monit 34(5):535–544

Silverman H (2007) Ethical Issues during the Conduct of Clinical Trials. Proc Am Thoracic Soc 4(2):180–184

Spina E, Santoro V, D'Arrigo C (2008) Clinically relevant pharmacokinetic drug interactions with second-generation antidepressants: an update. Clin Ther 30(7):1206–1227

Stevens J, Ploeger BA, Hammarlund-Udenaes M, Osswald G, van der Graaf PH, Danhof M, de Lange EC (2012) Mechanism-based PK-PD model for the prolactin biological system response following an acute dopamine inhibition challenge: quantitative extrapolation to humans. J Pharmacokinet Pharmacodyn 39(5):463–477

Strawn JR, Sakolsky DJ, Rynn MA (2012) Psychopharmacologic treatment of children and adolescents with anxiety disorders. Child Adolesc Psychiatr Clin N Am 21(3):527–539

Thyssen A, Vermeulen A, Fuseau E, Fabre MA, Mannaert E (2010) Population pharmacokinetics of oral risperidone in children, adolescents and adults with psychiatric disorders. Clin Pharmacokinet 49(7):465–478

Uchida H, Takeuchi H, Graff-Guerrero A, Suzuki T, Watanabe K, Mamo DC (2011) Predicting dopamine D2 receptor occupancy from plasma levels of antipsychotic drugs: a systematic review and pooled analysis. J Clin Psychopharmacol 31:318–325

Van Hest A, van Drimmelen M, Olivier B (1992) Flesinoxan shows antidepressant activity in a DRL 72-s screen. Psychopharmacology 107(4):474–479

Vermeulen A, Piotrovsky V, Ludwig EA (2007) Population pharmacokinetics of risperidone and 9-hydroxyrisperidone in patients with acute episodes associated with bipolar I disorder. J Pharmacokinet Pharmacodyn 34(2):183–206

Vgontzas AN, Kales A, Bixler EO (1995) Benzodiazepine side effects: role of pharmacokinetics and pharmacodynamics. Pharmacology 51(4):205–223

Vinkers CH, Tijdink JK, Luykx JJ, Vis R (2012) Choosing the correct benzodiazepine: mechanism of action and pharmacokinetics. Ned Tijdschr Geneeskd 155(35):A4900

Visser SA, Wolters FL, Gubbens-Stibbe JM, Tukker E, Van Der Graaf PH, Peletier LA, Danhof M (2003) Mechanism-based pharmacokinetic/pharmacodynamic modeling of the electroencephalogram effects of GABAA receptor modulators: in vitro-in vivo correlations. J Pharmacol Exp Ther 304(1):88–101

Von Wolff A, Hölzel LP, Westphal A, Härter M, Kriston L (2013) Selective serotonin reuptake inhibitors and tricyclic antidepressants in the acute treatment of chronic depression and dysthymia: a systematic review and meta-analysis. J Affect Disord 144(1–2):7–15

Weihs K, Wert JM (2011) A primary care focus on the treatment of patients with major depressive disorder. Am J Med Sci 342(4):324–330

Whalley HC, Simonotto E, Flett S, Marshall I, Ebmeier KP, Owens DG, Goddard NH, Johnstone EC, Lawrie SM (2004) fMRI correlates of state and trait effects in subjects at genetically enhanced risk of schizophrenia. Brain 127(Part 3):478–490

Whalley HC, Whyte MC, Johnstone EC, Lawrie SM (2005) Neural correlates of enhanced genetic risk for schizophrenia. Neuroscientist 11(3):238–249

WHO International Consortium in Psychiatric Epidemiology (2000) Cross-national comparisons of the prevalences and correlates of mental disorders. Bull World Health Organ [online] 78(4):413–426. ISSN 0042–9686

Williams PJ (2007) History of phramacometrics. In: Ette EI, Williams PJ (eds) Pharmacometrics. The science of quantitative pharmacology. Whiley, New Jersey

Yoo HD, Cho HY, Lee SN, Yoon H, Lee YB (2012) Population pharmacokinetic analysis of risperidone and 9-hydroxyrisperidone with genetic polymorphisms of CYP2D6 and ABCB1. J Pharmacokinet Pharmacodyn 39(4):329–341

Yuan R, Flockhart DA, Balian JD (1999) Pharmacokinetic and pharmacodynamic consequences of metabolism-based drug interactions with alprazolam, midazolam, and triazolam. J Clin Pharmacol 39(11):1109–1125

Zuideveld KP, Van der Graaf PH, Peletier LA, Danhof M (2007) Allometric scaling of pharmacodynamic responses: application to 5-Ht1A receptor mediated responses from rat to man. Pharm Res 24(11):2031–2039

Chapter 15
Clinical Trial Simulation in Alzheimer's Disease

Brian Corrigan, Kaori Ito, James Rogers, Daniel Polhamus, Diane Stephenson and Klaus Romero

15.1 Introduction

Alzheimer's disease (AD) affects 35 million patients worldwide, with an expected increase to 150 million within the next generation (World Alzheimer's Report 2010; Schneider and Sano 2009).

Recent late phase failures for candidate drugs for AD highlights the importance of developing more informative tools to increase the efficiency of the decision-making process (Schneider and Sano 2009). Currently available evidence suggests the initiating event in AD is related to abnormal processing of beta-amyloid (Abeta) peptide, ultimately leading to the formation of Abeta plaques in the brain. Jack et al. have proposed an overarching model that relates disease stage to AD biomarkers in which Abeta biomarkers become abnormal first, before neurodegenerative biomarkers and cognitive symptoms, and neurodegenerative biomarkers become abnormal later, and correlate with clinical symptom severity. This process can begin decades prior to any clinical signs of diminished cognition.

Ideally, a quantitative understanding of the time course of disease progression (cognitive and functional deterioration), and the relevant sources of variability would be the most useful for drug development. While the ability to detect and analyze biomarkers in the cerebrospinal fluid (CSF) related to Abeta and Tau have emerged over the past decade, limited longitudinal data are yet available to completely quantify each of the curves above. In addition, the ability of these biomarkers

K. Romero (✉)
Department Clinical Pharmacology, Critical Path Institute, Tucson, AZ 85718, USA
e-mail: KRomero@c-path.org

B. Corrigan · K. Ito
Department of Neuroscience, Pfizer, Groton, CT, USA

J. Rogers · D. Polhamus
Department of Medical-Science, Metrum Research Group LLC, Tariffville, CT, USA

D. Stephenson
Coalition Against Major Diseases, Critical Path Institute, Tucson, AZ 85718, USA

S. Schmidt, H. Derendorf (eds.), *Applied Pharmacometrics,* AAPS Advances in the Pharmaceutical Sciences Series 14, DOI 10.1007/978-1-4939-1304-6_15

(Abeta, Tau, and brain structure) to translate into clinical outcome has not yet been determined. Attempts at meta-analytics for these endpoints are further hampered by factors such as interlaboratory assay and imaging algorithm differences. On the other hand, a wealth of information is available for the clinical manifestations, especially memory or cognition. As such, the majority of work involving clinical trial simulation (CTS) on AD has involved the primary clinical outcomes typically measured in these studies—function and cognition. While various tests have been used to measure functional changes across clinical studies, the Alzheimer's disease assessment scale cognitive sub-scale (ADAS-cog) has been used almost universally in trials of mild and moderate AD patients to measure changes in cognition. As a result, the majority of CTS activities in AD have focused on variants of the ADAS-cog.

Assumptions about disease progression and the time-variant effects of placebo and existing drug treatments for AD form the basis for various decisions made in AD drug development, including decisions relating to trial design and analysis (Rogers et al. 2012). While ad hoc synthesis of estimates from a small number of trials can, in some cases, form sufficient evidence base for such assumptions, it is a generally a more informative and objective approach to concisely summarize all available and relevant data with the aid of a meta-analytic model (Rogers et al. 2012). Such a meta-analytic synthesis is particularly relevant in AD, where extensive historical data are available (Romero et al. 2009, 2011; Sheiner 1997). Moreover, models may be used to interpolate expected results and to simulate data under conditions that have not been previously studied, e.g., when sampling at different time points or when enrolling patients with a different set of covariates (Rogers et al. 2012). Such approaches also allow the incorporation of different sequences of active treatment and placebo (like staggered start or delayed withdrawal designs), while accounting for residual effects for both active treatment and placebo (Rogers et al. 2012; Holford and Peace 1992).

Standard statistical analysis methods (ANOVA, ANCOVA) are typically used for the predefined primary analysis of the results of the active treatment and control arms at the end of the randomized phase of trials in AD (Holford and Peace 1992). These approaches are also used for post-hoc subgroup analyses (mild vs. moderate ApoE4, carrier vs. noncarrier, background therapy vs. no background therapy, etc.) following large late-stage failed trials. In many cases these post-hoc analyses have lead to further development activities in these subgroups, often resulting in further failures. In addition to its role in CTS, a meta-analytic model can provide a useful informed prior consent when attempting to understand such post-hoc analyses.

This chapter describes relevant efforts in modeling and simulation-utilizing drug-disease-trial (DDT) models in AD (Gobburu and Lesko 2009), focusing on cognition. This includes data considerations and descriptions of relevant public data sources available for AD model developers. It includes a brief description of previous work in the field, along with a description of common elements contained within DDT models currently used for CTS in AD. Examples of applications for study planning and study interpretation among other potential uses are also included. It concludes with a look at potential future applications of CTS in AD and areas for growth.

15.2 Data Considerations

The data used to aid in the design of a clinical trial can come from a variety of sources. A team may use past and recent literature to inform them about expected treatment effects and current study designs in use. They may have patient-level data in their organization that informs them about expected intrasubject variability, intersubject variability, and interoccasion variability (Milligan et al. 2013). They often have past clinical trial experiences that they draw from (which varies between individuals). The team designing a clinical trial will attempt to implicitly integrate all of this information to form conclusions about what design is likely to be the best for the stage of development and the compound in question. The broader the data source(s) used with respect to patient types, study durations and designs, and patient inclusion/exclusion criteria, the more "rugged" the final model is likely to be.

Standardized quality data sources remain a significant hurdle to developing and implementing a longitudinal DDT model (Romero et al. 2009, 2011). Often, when pooling across different data sources (different studies, different programs, different sponsor), a significant amount of effort and resources are required to ensure that common standards for data collection and scoring have been adhered to (Romero et al. 2009, 2011). Small changes in something as simple as how missing scores are handled can lead to increased noise within the dataset. Often, an arduous remapping process may need to occur (if item level data are available). In addition, standards between analysts are likely to differ, making it nearly impossible to merge additional relevant datasets, without another lengthy remapping process.

In an ideal scenario, data standards would be applied a priori so that data are collected, scored, and recorded in a standardized form. The field of drug development for AD is at the forefront, being the first to have generated therapeutic area standards in this area, in a form accepted by FDA (Romero et al. 2009, 2011).

15.2.1 Relevant Data Sources for Modeling and Simulation in AD

Researchers aiming to develop a quantitative understanding of AD disease progression and drug effects, often start with data within their own organizations, or other proprietary data that have been made available to them. Often, however, they find that the data they have are limited in one or more ways, such as by limited numbers in subsets of interest (disease severity, genotype, biomarker classification). Generally, developers will utilize one or more of the number of large available data sources in AD, which may provide robust information to inform the different components of the DDT.

15.2.1.1 Literature Data

In the field of AD, a wealth of literature data from many different clinical trials and observational studies are readily available that can contribute to the development of

quantitative modeling and simulation tools. While limited in its value for determining impact of individual patient covariates of disease or drug effects, it can provide valuable estimates of drug effects (size, onset, offset), disease progression within a trial, etc.

15.2.1.2 ADNI Studies

The longitudinal Alzheimer's Disease Neuroimaging Initiative (ADNI; http://www.adni-info.org/) was launched in 2003 by the National Institute on Aging (NIA), the National Institute of Biomedical Imaging and Bioengineering (NIBIB), the US Food and Drug Administration (FDA), private pharmaceutical companies, and nonprofit organizations, initially as a 5-year public–private partnership (Weiner et al. 2012). Since 2005, the longitudinal ADNI has been validating the use of biomarkers including blood tests, tests of CSF, and magnetic resonance imaging–positron emission tomography (MRI–PET) imaging for AD clinical trials and diagnosis. Now in its third phase (ADNI, ADNI GO, and ADNI 2), ADNI 2 is studying the rate of change of cognition, function, brain structure, and biomarkers in 150 elderly controls, 450 subjects with mild cognitive impairment (MCI), 150 with mild-to-moderate AD, and a new group of 100 people with significant, yet subtle, memory complaints, referred to as the significant memory concern cohort. It has also added whole genome sequences (WGS) for 809 ADNI participants. Similar studies have also been launched in other regions, such as Japan (J_ADNI). As such, the ADNI study series will continue to be a rich and complete source of data on the natural history of AD at various stages.

15.2.1.3 The Coalition Against Major Diseases Database

Coalition Against Major Diseases (CAMD) is a formal consortium of pharmaceutical companies, research foundations, and patient advocacy/voluntary health associations, with advisors from government research and regulatory agencies including the FDA, the European Medicines Agency (EMA), the National Institute of Neurological Disorders and Stroke (NINDS), and the NIA. The CAMD is led and managed by the nonprofit Critical Path Institute (C-Path), which is funded by a cooperative agreement with the FDA (Romero et al. 2009, 2011).

The CAMD database represents patient-level data from the control arms from phase II and III clinical trials in patients with MCI as well as mild and moderate Alzheimer's dementia. As of September 2014, the CAMD database represents >6500 individual patients. Access to this database can be requested at www.codr.c-path.org. It is a rich source of control-arm data for the model developer.

In addition, CAMD partnered with the Clinical Data Interchange Standards Consortium (CDISC) to develop a standard for data collection in CDISC form. This AD standard represents the first-ever therapeutic area standards in CIDSC form. The intended advantage of such a standard is that it not only serves the purpose of

integrating data from legacy clinical trials but it is also suited for prospective data collection in new trials, foreseeing the coming FDA requirement for data to be in CDISC standard form by 2017.

15.3 Summary of Disease Progression Models for ADAS-cog to Date

15.3.1 Historical Progression of AD Models

Various disease progression models for clinical outcomes in AD have been published (Holford and Peace 1992; Chan and Holford 2001) and the methods utilized in early publications laid the groundwork for future modeling work (Mould et al. 2007). Newer work provides further improvement and increased complexity and continues to build on past researchers findings, but incorporates newer, broader data types and sources, and utilizes new modeling methodologies resulting in an evolution of models over time (Table 15.1).

Early models were based on a limited number of trials of short duration used to evaluate symptomatic agents and did not contain newer key data types such as genotype and biomarker information, now known to be important covariates in understanding the rate of disease progression (Atchison et al. 2007). Later models described utilizing a variety of data types including summary level data from literature sources, data directly from one or more of a related series of controlled clinical trials, or noninterventional natural history studies. Rogers et al. have attempted to integrate all these sources in one analysis.

Historical models primarily described AD disease progression as linear, which was sufficient for simulation of trials of the shorter durations used for the development of symptomatic agents. The Ito literature model identified that the severity of the disease itself influenced the slope, and thus the slope changed over time (introducing nonlinearity). More recent models have directly incorporated nonlinear relationships to describe the course of disease over time.

In addition, these models lacked certain structural features that would improve their use for CTS, such as constraining the limits of the ADAS-cog (0–70), and allowing for variance components to change over time (an essential feature if the model is to be used for CTS of disease progression for AD).

The models described in the literature also improved with respect to all the components typically required for a DDT model. A DDT model that includes all these components would require underlying data that can inform each of the various trial components in the model. For example, natural history data to inform underlying disease progression, placebo arm data to inform about magnitude, onset and offset of placebo response in controlled clinical trials, estimates of various drug effects (magnitude, time to onset, and durability), rate and magnitude of dropouts in the trials, and a rich source of covariates for model building. Over time, more and more of these components have been added in.

A brief description of more recent work is provided below.

Table 15.1 Relevant previous disease progression models for clinical outcomes in AD

Model	Drug effect component	Trial components	Data source	Covariates	Linearity
Holford and Peace 1992	Yes	Varied	Individual studies (tacrine)	Varied	Linear
Ito et al. 2010	Yes (symptomatic agents estimated)	Placebo (onset and magnitude)	All controlled studies in the literature 1990–2008	Baseline severity	Linear (nonlinearity introduced by baseline covariates)
Ito et al. 2011	No (NA)	No (NA)	ADNI (normal, MCI, mild AD)	Baseline severity, age, ApoE4 genotype, and sex	Linear (nonlinearity introduced by baseline covariates); fits normal MCI and mild AD
Samtani et al. 2013	No (NA)	No (NA)	ADNI mild AD	Disease onset, hippocampal volume and ventricular volume, age, total cholesterol, ApoE ε4 genotype, trail-making test (part B) score	Nonlinear; fits mild AD
William-Faltaos et al. 2013	No	Dropout No placebo		Covariates influencing the intercept were baseline ADAS-cog score (did not use data prior to 4 months) and baseline MMSE score; no covariates influenced the disease progression slope	Nonlinear (log transform not suitable for whole range of ADAS-cog scores of 0–70)
Rogers et al. 2012	Yes	Placebo dropout	Literature CAMD ADNI	Baseline MMSE; disease progression time ApoE4 status, age, gender; dropout time, baseline age, baseline MMSE	Nonlinear

MMSE mini-mental state examination

15.3.2 Model-Based AD Literature Meta-Analyses

15.3.2.1 Ito (2010)

Ito et al. (2010) applied a model-based meta-analysis to summary level data available in the literature to quantify the dependence of rates of progression on baseline ADAS-cog scores. In this analysis, a systematic literature review from 1990 to 2008 for all available AChE inhibitor studies as well as clinical studies that evaluated the rate of deterioration in AD patients was conducted. From 52 trials, which represented approximately 19,992 patients and more than 84,000 individual observations, a total of 576 mean ADAS-cog change-from-baseline data points were collected. Based on the data available from these articles, a model was developed to describe the longitudinal response in ADAS-cog (change from baseline) in mild-to-moderate severity AD patients. The model described the rate of disease progression, the placebo effect observed, and the symptomatic effect of AChE inhibitors. Baseline ADAS-cog, mini-mental state examination (MMSE), age, and publication year were tested as covariates.

Ito's model reports that disease progression in mild-to-moderate AD patients across all available and relevant literature sources was estimated at 5.5 ADAS-cog units per year. An Emax-type model best described the symptomatic drug effect for AChE inhibitors. The rate of disease progression (underlying disease progression) was not different between placebo and AChE-inhibitor-treated groups. Unlike previous modeling work, which did not include covariates, Ito's model identified baseline ADAS-cog as significant covariate on disease progression. Baseline age was also tested as a covariate on the rate of disease progression but the model was not able to describe any effect, likely due to the narrow distribution of mean age (literature-level analysis). There was no significant impact of publication year in the model.

The literature-based meta-analyses provided a useful and complete integration of the estimated natural history of AD and provided estimates of treatment effects for currently available AChE-inhibitor therapies. However, due to the nature of the literature data in that it is only study-level summary data; the model had limited ability to evaluate important individual covariates, such as age and ApoE4 genotype. Also, the meta-analysis model from the literature using study-level data neither provides intersubject variability information nor includes components for increasing variance over time.

15.3.3 Patient-Level Models

15.3.3.1 Ito ADNI Model (2011)

In 2011, Ito et al. published a patient-level model-based meta-analysis to describe the longitudinal response in ADAS-cog obtained from the ADNI (Ito et al. 2011). The model was fit to the longitudinal ADAS-cog scores from 889 patients. Risk

factors (age, ApoE4 genotype, sex, family history of AD, and years of education) and baseline severity were tested as covariates. Results indicated that rate of disease progression increased with baseline severity. Age, ApoE4 genotype, and sex were identified as potential covariates influencing disease progression. The rate of disease progression as described by the ADAS-cog in mild-to-moderate AD patients was estimated at approximately 5.5 ADAS-cog units/year, similar to that reported using literature-based analyses.

The authors concluded that a linear disease progression model adequately described the natural decline of ADAS-cog observed in ADNI over 2–3 years within the individual patients. Baseline severity, which is incorporated into the model to explain the nonlinearity of the disease progression, is an important covariate to predict a curvilinear rate of disease progression in normal elderly, mild MCI and patients with Alzheimer's dementia. Age, ApoE4 genotype, and sex also influenced the rate of disease progression.

15.3.3.2 Samtani ADNI Model (2012)

The objective of the Samtani et al. analysis was to develop a semimechanistic nonlinear disease progression model from the ADNI study, but that used an expanded set of covariates that captured the longitudinal change of ADAS-cog scores (Samtani et al. 2012). The model described the rate of progression and baseline disease severity as a function of influential covariates. The covariates that were tested fell into four categories: (1) imaging volumetric measures, (2) serum biomarkers, (3) demographic and genetic factors, and (4) baseline cognitive tests.

Covariates found to affect baseline disease status were years since disease onset, hippocampal volume, and ventricular volume. Disease progression rate in the model was influenced by age, total serum cholesterol, ApoE4 genotype, trail-making test (part B) score as well as current levels of cognitive impairment as measured by ADAS-cog. Rate of progression was slower for patients with mild and severe AD compared with moderate AD.

15.3.3.3 Faltaos Model (2013)

This research aimed to quantitatively describe the natural progression of AD based on ADAS-cog scores in patients with mild-to-moderate AD utilizing data from ten placebo-controlled clinical trials submitted to the FDA (>2600 patients) with up to 72 weeks of treatment (William-Faltaos et al. 2013). Different models describing the time course of ADAS-cog were evaluated. Patient characteristics potentially affecting score changes were assessed. Patient-dropout patterns were characterized using parametric survival models. Covariate selection was performed to identify the risk factors associated with a higher dropout rate. In this case, the ADAS-cog time course in mild-to-moderate AD patients receiving placebo was described by a log-linear model, where the intercept represents the log-transformed ADAS-cog score at week 10 , the slope is the disease progression (i.e., natural increase of ADAS-cog score) on the log scale. Covariates influencing the intercept were baseline ADAS-cog score

and baseline MMSE score. No covariates were identified that influenced the disease progression slope. A parametric log-normal model fit the dropout data best. Baseline ADAS-cog score and age were found to be significant predictors for dropout.

15.3.4 Integrative Meta-analytic Approaches

15.3.4.1 Rogers Model (2012)

This research aimed to incorporate many of the best elements of the models described above in a beta regression (BR) model (Rogers et al. 2012). The use of the BR constrained simulations to the 0–70 range of the ADAS-cog, even when residuals were incorporated. In addition, the model described the longitudinal progression of the 11 item ADAS-cog in AD patients in both natural history and randomized clinical trial settings, utilizing both individual patient and summary level literature data. Patient data from the CAMD database (3223 patients), the ADNI study database (186 patients), and summary data from 73 literature references (representing 17,235 patients) were fit to a BR DDT model. Treatment effects for currently available acetyl cholinesterase inhibitors, longitudinal changes in disease severity, dropout rate, placebo effect, and factors influencing these parameters were estimated in the model. Based on predictive checks and external validation, the researchers concluded that an adequate BR meta-analysis model for ADAS-cog using both summary-level and patient-level data was developed. Baseline ADAS-cog was estimated from baseline MMSE score. Disease progression was found to be dependent on time, ApoE4 status, age, and gender. Study dropout was a function of time, baseline age, and baseline MMSE.

The model allowed for simultaneous fitting of summary and patient-level data, allowing for integration of all information available. A further advantage of the BR model was that it constrained values to the range of the original instrument for simulation purposes, in contrast to methodologies that provide appropriate constraints only for conditional expectations.

15.4 Review of Structural Components for Models in AD

Table 15.2 lists the general basic components of a DDT model, as described by Gobburu and Lesko (2009).

15.4.1 Disease Model Components

Understanding both the placebo response and the natural underlying disease progression is crucial to designing and interpreting results from AD clinical trials, given that it is sometimes difficult to differentiate the placebo effect and underlying disease progression in longitudinal studies, resulting in misinterpretation of the study results. Several authors have proposed that the placebo response be assumed

Table 15.2 Basic components of disease-drug-trial modeling and simulation tools for drug development

Component	Quantitative description
Disease model	(1) Natural longitudinal progression, (2) relationship of biomarkers to outcome, (3) placebo effect within controlled trials
Trial model	(1) Patient population (baseline disease severity, etc.), (2) patient dropout rate and factors impacting it, (3) therapeutic adherence
Drug model	(1) Overall efficacy/effectiveness, (2) impact of patient characteristics on drug effect, (3) changes in drug effect(s) over time

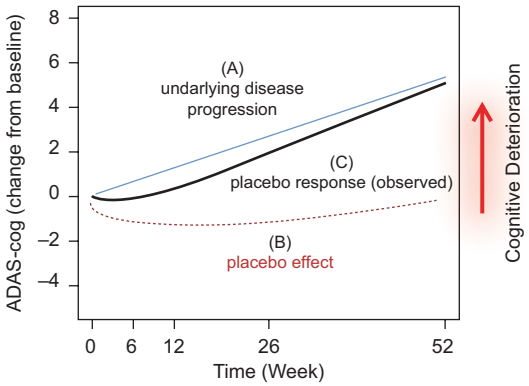

Fig. 15.1 Concept of placebo response in a disease progression scenario. *ADAS-cog* Alzheimer's disease assessment scale cognitive sub-scale

to consist of "underlying disease progression" and "placebo effect," where "underlying disease progression" describes the natural history of the disease, and the "placebo effect" represents a temporal component, i.e., such as psychological effect, or any effect derived from the conduction of and participation in clinical trials.

Figure 15.1 illustrates the concept behind the longitudinal diseases progression model, where the overall observed placebo response in a trial (C) is simply the addition of the underlying disease progression (A) and placebo effect (B). Increase in ADAS-cog score indicates cognitive deterioration over time.

In general, the shape described above, is adequate to describe both data reported from the literature and from patient-level data collected in placebo-controlled clinical trials, as shown in Fig. 15.2.

15.4.1.1 Natural Longitudinal Progression

In the case of natural history studies, such as ADNI, a placebo effect is not required, and the time course may be described by the underlying natural history of disease progression (Fig. 15.3).

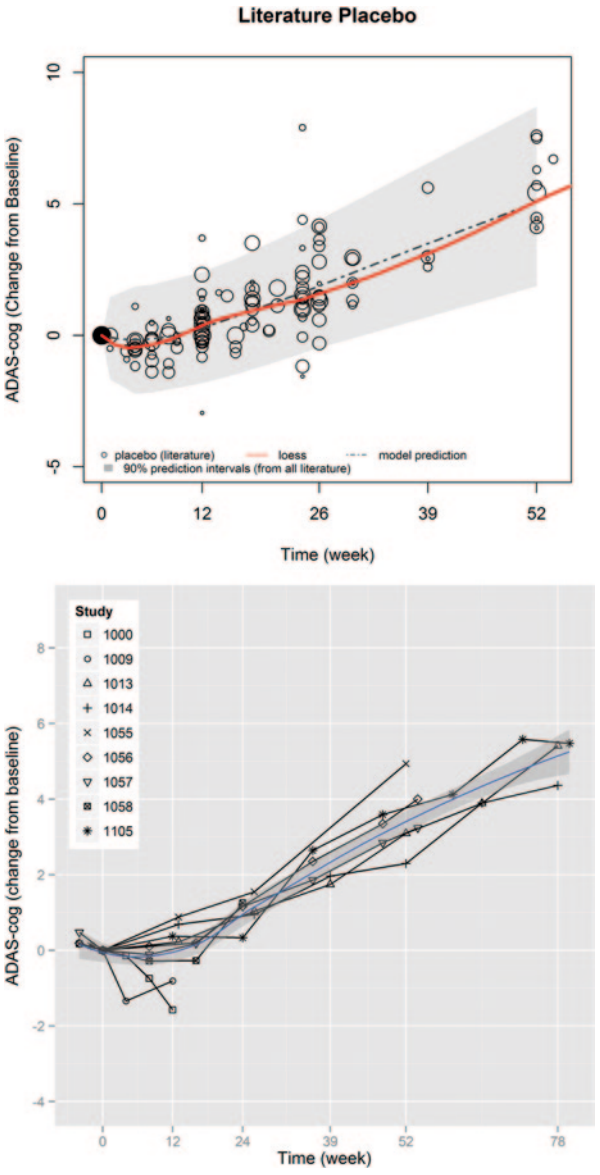

Fig. 15.2 Observed placebo response for change from baseline Alzheimer's disease assessment scale cognitive sub-scale (*ADAS-cog*) from literature, 1990–2008. (*Top:* all data with loess line and model prediction; *bottom:* CAMD studies; the *blue line* and *gray-shaded area* in the figure indicate a lowess fit line with 95 % confidential intervals)

Historically, the progression rate has been modeled as a linear function. Although the data appear linear over a short duration, given the scale is finite, and that most AD patients reach the maximum as they become more severe (requiring the use of other measures such as the severe impairment battery) the data are better described by a sigmoid-like function restricted between 0 and 70 (the limits of the ADAS-cog score; Rogers et al. 2012; Samtani et al. 2012).

Recently, different researchers (Ito et al. 2010; Samtani et al., 2012; William-Faltaos et al. 2013; Ashford and Schmitt 2001) have provided important insights

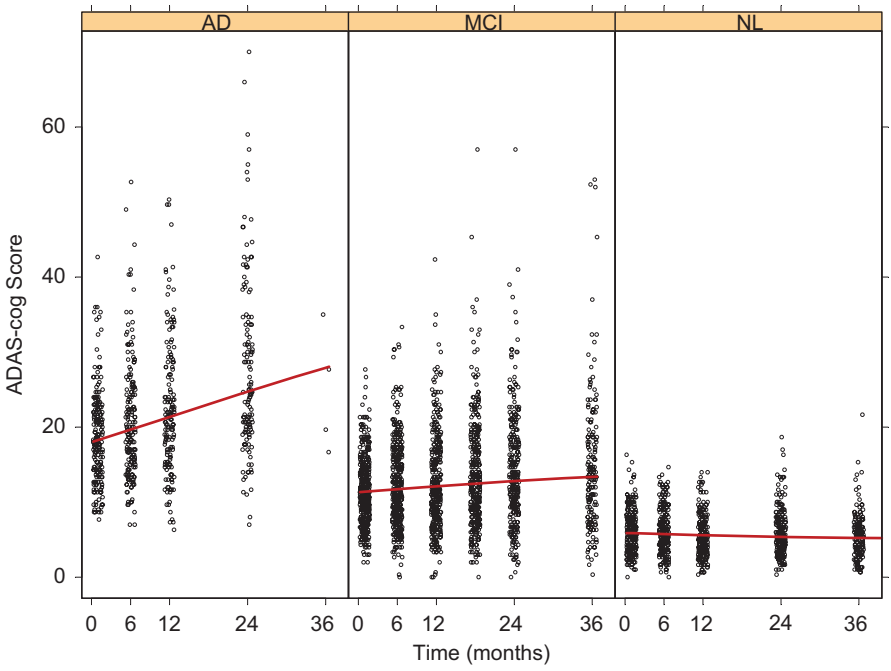

Fig. 15.3 Longitudinal Alzheimer's disease assessment scale cognitive sub-scale (*ADAS-cog*) by patient population. (Obtained from ADNI; Loess lines in red). *AD* mild AD, *MCI* mild cognitive impairment, *NL* normal elderly

into the nonlinear progression of AD. Ito et al. (2010) analyzed the ADNI data using a linear AD progression model based on a population-based mixed effects approach (with a function to introduce nonlinearity based on baseline severity), Ashford and Schmitt (2001) applied a logistic model to characterize disease progression, while Samtani et al. (2012) developed a nonlinear mixed effects model. Samtani et al. (2012) proposed a logit function that restricts the ADAS-cog scores to the test's intrinsic range of 0–70 points. Samtani's models were in turn captured using a Bayesian meta-analytic approach by Rogers et al. (2012) thus giving a comprehensive aggregation of literature- and patient-based knowledge.

In essence, the disease progression function proposed by Samtani et al. (2012) and Ito et al. (2010) has been integrated by Rogers et al. (2012), and can be described as the following logit function:

$$\theta_{ipk} = \mathrm{E}\left[{}^{ADAS_{ipk}}\!/_{70} \,\middle|\, \text{patient}_p \right]$$
$$g(\theta_{ipk}) = \eta_{pk} + \alpha_{pk} \times t_{ipk} + \varepsilon$$

Relevant covariates that affect the "intercept" (η_{pk}) that have been identified by different authors include: baseline disease severity as expressed by ADAS-cog or MMSE, baseline age, and age of onset of disease (which is usually derived from arguably unreliable data from dates of first diagnosis). ADAS_{ipk} denote the observed

ADAS-cog score on the *i*th occasion in the *p*th patient in the *k*th study. In turn, t_{ipk} represents the time of the observation relative to the randomization time for that given patient.

In line with current thinking regarding AD pathophysiology, covariates identified by several authors as affecting the rate of progression α_{pk} have included $ApoE_4$ genotype, total blood cholesterol, baseline age, gender, and baseline disease severity (baseline ADAS-cog or baseline MMSE).

15.4.1.2 Placebo Function Components

The onset, offset, and overall extent of placebo effect has been successfully estimated and described in the past by the use of a first order appearance (onset) and a first order disappearance (offset) constant, commonly known as a Bateman-type function (Holford and Peace 1992; Ito et al. 2010):

$$Pbo(t) = \beta_p \cdot (e^{-Kel_p \cdot t} - e^{-Keq_p \cdot t})$$

where β_p is a factor defining the magnitude of the placebo effect, Kel_p is the rate constant for the offset rate of the placebo effect, and Keq_p is the rate constant for the onset rate of the placebo effect.

15.4.2 Drug Model Components

The selection of drug model components and the underlying assumptions around it are highly dependent on the proposed use of the model, the mechanism(s) postulated, and information available on the compound(s) of interest. In the past, models have attempted to describe either symptomatic effects or disease-modifying effects.

15.4.2.1 Symptomatic Effect

Agents thought to have "pure symptomatic" effects can be expressed as a shift in the overall disease progression curve, without a change in the rate (slope) of progression (Holford and Peace 1992; Samtani et al. 2012; Bhattaram et al. 2009). Estimates for magnitude, onset and offset of these symptomatic effects can be estimated from data available for currently approved drugs, or from proprietary data.

It has been proposed that Emax-type models adequately describe the symptomatic drug effect for cholinesterase inhibitors, which are the main currently available symptomatic treatments for AD. For example, Ito et al. (2010, 2013) proposed the following expression:

$$E_{DRG,ipk} = (D_{ipk})^{\gamma_{d(p)}} \frac{E_{\Delta,d(p)} \times t_{ipk}}{ET_{50,d(p)} + t_{ipk}}$$

where D_{ipk} represents the dose administered to a given patient at a given occasion in a given trial, $E_{\Delta,d(p)}$ denotes the maximum symptomatic effect at a given dose for a given patient, and $ET50_{,d(p)}$ expresses the time at which 50% of the maximum symptomatic effect is achieved for a given patient at a given dose.

15.4.2.2 Disease-Modifying Effect

Agents thought to have "pure disease-modifying" effects can be expressed as a change in the rate of progression (α_{pk} in the model defined above) without a shift in the overall disease progression curve (Holford and Peace 1992; Samtani et al. 2012; Bhattaram et al. 2009). Currently, there are no FDA-approved disease-modifying treatments, which constitute a limitation in terms of available data for modeling purposes.

As mentioned previously, covariates identified by several authors as affecting the rate of progression have included $ApoE_4$ genotype, total blood cholesterol, baseline age, gender, and baseline disease severity (baseline ADAS-cog or baseline MMSE). As such, it is possible to "enrich patient populations using these factors to observe a faster rate of progression, and theoretically, to observe a disease-modifying effect in a treatment arm more easily". This has led researchers to propose the inclusion of proportional hazard functions to the rate of progression, in which a given percent modification (reduction) in the rate of progression could be incorporated into the disease progression function described before.

15.4.2.3 Dropout Component

Since the described modeling approaches aim at characterizing the complete data distribution, summary statistics based on direct simulation from the model would not correctly mimic the behavior of real summary statistics, as actual summary statistics usually are computed using incomplete data. Even in the unlikely scenario that the true missing data mechanism (MDM) is missing completely at random (MCAR), the real summary means will be based on fewer observations than their simulated counterparts, and the latter will therefore have standard errors that are unrealistically low. Accordingly, for the purpose of model validation, a MDM or "dropout model" is a reasonable component to be incorporated for simulation purposes.

Here, the work of William-Faltaos et al. (2013) constitutes an important example. As explained before, these authors identified the Weibull distribution as the one that would most adequately characterize the evolution of the dropout hazard over time, and the two most important covariates for the dropout hazard were baseline age and baseline disease severity.

As implemented in the Rogers et al. work, the fitted dropout model utilizing these two covariates exhibited a high degree of agreement with the observed dropout rates, as seen in Fig. 15.4. The model adequately captures the dropout rate both by baseline MMSE and by age in these two plots.

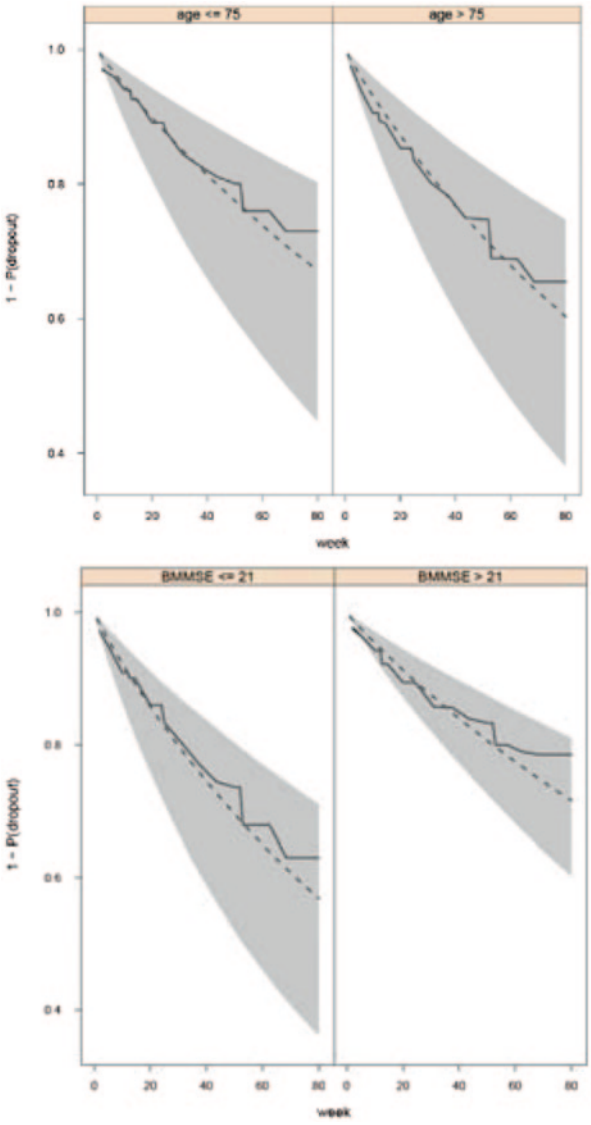

Fig. 15.4 Plot of probability (dropout) over time by baseline age (*upper panel*) and baseline mini-mental state examination (*BMMSE, lower panel*). (*Solid line* represents Kaplan–Meier (nonparametric) estimates based on observed data; *dashed line* represents model prediction; *grey* region represents 90 % credible interval for model prediction)

It is important to note that such a working model for the MDM is reasonable to employ for the purpose of model validation. However, for the purpose of model fitting, researchers can assume less restrictive conditions that are required for ignorability of the missing data mechanism, implying that posterior distribution for parameters describing the complete data distribution may be computed using the observed response and covariates.

A fully realistic MDM would be fairly complex and correspondingly would require substantial justification. Moreover, since the true MDM is never known, the issue cannot be adequately addressed without considering *several* MDMs, including

various combinations of missingness related to tolerability, missingness related to lack of efficacy, and missingness associated with disease state. While this full treatment would be a desirable research project, currently available work is only able to propose a plausible "working hypothesis" MDM based on observed associations between baseline covariates and dropout.

15.4.3 Meta-analytic Integration of Literature and Patient-Level Data

As explained before, there are a number of relevant databases for modeling and simulation in AD, which represent patient-level and study-level data from both observational studies and clinical trials. These can be combined with additional patient-level data from active treatment arms that may be available to specific researchers. However, the amount of data available from the scientific literature should not be ignored (especially when trying to incorporate drug effects into models). In order to adequately integrate those patient-level data with summary-level information, Gillespie et al. (2009) have proposed a Bayesian implementation, which allows a probabilistically correct synthesis of literature meta-data with patient-level data. Additional contributions have also been made by Rogers et al. (2012), in terms of applying β-distributed residuals in conjunction with a generalized logistic function for expected disease progression (i.e., "BR"), with the defining feature of specifying the residual scores for a given patient as following a β distribution. This results in a predictive distribution that falls entirely within the 0–70 range of the ADAS-cog, which is a valuable feature for the purpose of simulating clinical trials.

Regarding the challenge of integrating patient-level and summary-level information, Gillespie et al. (2009) propose that the summary-level data be modeled by directly specifying likelihoods based on approximate sampling distributions. As has been explained before, the model for individual ADAS-cog scores is nonlinear, and the exact sampling distributions for sample means are not available in analytical form. An elegant solution proposed by Rogers et al. (2012) concentrates on the approximate linearity of the logit function over the range of primary interest to derive the approximate distributions. These approximations can then be employed as the operational likelihoods.

15.5 Example Applications

15.5.1 Planning Prospective Trials

These models described previously have had varying degrees of applicability for CTSs, understanding CTS as a means of estimating relevant operating characteristics for essentially any clinical trial design under any hypothesized parameter

configuration for the "true" effects of a drug. It may be used to assess how different trial design and drug factors affect trial performance. These factors may be controllable trial design properties, such as the doses studied, the sampling times, the optimal study duration and sampling times, and use of washouts (Gobburu and Lesko 2009) or uncontrollable factors, such as the drug characteristics (pharmacokinetic or pharmacodynamics; Hennig et al. 2009). Other influencing factors may include the progression of disease over time or subject-specific characteristics that may be related to disease progression or treatment response.

15.5.1.1 "Super Symptomatic" Agents

"*Super symptomatic drug effect*" is conceptualized as superior clinical efficacy to currently available symptomatic therapies, either as stand-alone or as add-on therapy. Such a super symptomatic drug profile is desired for new symptomatic drugs under development for AD.

As stand-alone therapy, the drug could achieve the super symptomatic effect either by having superior acute cognitive enhancement or by having acute symptomatic benefit similar to marketed agents plus disease-stabilizing attributes. However, for compounds with new mechanisms of action, it remains unclear which of these could occur.

Given the extremely high failure rate in neurodegenerative drug development programs, it is often the goal in early development to obtain an early and cost effective read of efficacy for compounds thought to be predominantly "symptomatic" agents. In this scenario, a crossover design may provide more to detect a difference rapidly, but would underestimate the total treatment effect relative to the longer parallel trial design typically used.

Two drug profiles were studied under this scenario. In this study, the desired super symptomatic drug effect was set as 3.5 points of ADAS-cog better than placebo at week 24. For the first drug profile, it was assumed that the drug had a superior symptomatic drug effect of 3.5 points on ADAS-cog at 24 weeks but similar drug onset compared to donepezil (thus, the first profile is $E_{\text{drug,24week}} = 3.5$ and $\text{ET}_{50} = 1.62$ week). For the second drug profile, it was assumed that the drug had donepezil-like symptomatic effect ($E_{\text{drug,24week}} = 2.5$) and a moderate disease-stabilizing effect (i.e., 50% decrease on slope). In both drug scenarios, true drug effect would be 3.5 points on ADAS-cogat 24 weeks, which is the desired effect for the super symptomatic treatment.

The objectives of early studies to advance drug candidates that are expected to have a super symptomatic profile are not only to test whether the drug is better than placebo but also to obtain certain confidence that the estimated drug effect would achieve the "*target value*." Typically, this target value is defined by current standard of care, regulatory requirements or other thresholds for evidence of efficacy. The confidence level required is dependent on multiple factors, like the stage of drug development, the overall development plan and the medical need for the drug. The drug candidate in this scenario was considered to be at an early stage of development, so the confidence requirement was not as high as that for a drug in later stages of development. Herein, we defined that we would need at least 25% confidence

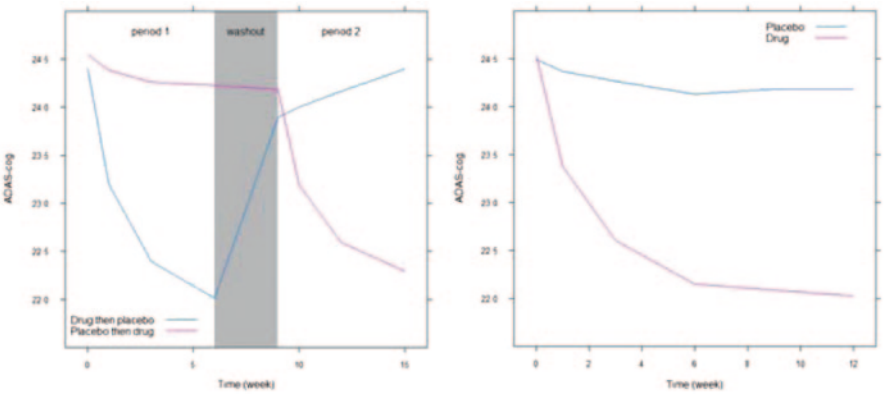

Fig. 15.5 Simulated 6-week crossover trials (*left panel*) versus 12-week parallel trials (*right panel*) for drugs with only symptomatic effects. *ADAS-cog* Alzheimer's disease assessment scale cognitive sub-scale

the drug is 3.5 points or more, better than placebo on the ADAS-cog scale after completion of the study in order to continue the drug as a potential super symptomatic treatment. Besides the 6-week crossover and 12-week parallel designs as described above (a and b), a third candidate trial design was also evaluated, which was a two-arm parallel design (75 patients per arm) with 24 week treatment duration and assessments at weeks 0, 3, 6, 9, 12, and 24. The primary analysis is based on a linear mixed-effects model with random subject effect and fixed effects for baseline ADAS-cog, visit (nominal scale), treatment, and visit by treatment interaction, with drug effect formulated as the expected difference at week 24.

Figure 15.5 displays the average simulated results for a 6-week crossover design and a 12-week parallel design using a symptomatic drug that was similar to donepezil (2.5 points superior to placebo on ADAS-cog at week 24, ET_{50} of 1.62 week and washout half-life of 1 week). In the crossover design, under these assumptions, the treatment effect (difference between placebo and treatment) at the end of each 6-week period is independent of the treatment period. Thus, in this context a crossover design has the potential to reduce the sample size while maintaining appropriate power to demonstrate the drug benefit.

The simulation results showed that approximately 89 % power was achieved with 30 patients per arm (60 patients in total) in a 6-week crossover study (Table 15.3). The power of a 12-week parallel design with 75 patients per arm (150 patients in total) was about 82 %. Meanwhile, as expected, the relative bias of the 6-week treatment in the crossover study (−17.3 %) was higher than the 12-week parallel study (−7.3 %), both of which would underestimate the true drug effect at week 24, given the achievement of a partial drug effect over the duration of the study. As also shown in Table 15.3, with a slower drug onset (e.g., ET50 of 3 weeks, two times that of donepezil), the power in a 6-week crossover study (81 %) still remained comparable to a 12-week parallel study (79 %), although the difference of the relative bias for 6-week crossover study versus 12-week parallel study significantly increased.

Table 15.3 Comparison of relative bias and power for a 6-week crossover 12-week parallel study design

	Design	Relative bias (%)	Power (α=0.05, two-sided)
Drug onset same as donepezil (ET50=1.62 weeks)	6-week crossover (n=30/arm)	−17.1	0.89
	12-week parallel (n=75/arm)	−7.9	0.81
Drug onset slower than donepezil (ET50=3 weeks)	6-week crossover (n=30/arm)	−26.8	0.81
	12-week parallel (n=75/arm)	−9.6	0.79

Table 15.4 Comparison of power to detect drug effect and to achieve target value for different study designs

Drug effect	Study design	Relative bias (%)	Power to detect drug effect (α=0.05, two-sided)	Probability to achieve 25% confidence ≥3.5
Superior acute symptomatic effect ($E_{drug,24week}$=3.5)	6-week crossover (n=30/arm)	−17.8	0.99	0.41
	12-week parallel (n=75/arm)	−7.0	0.98	0.65
	24-week parallel (n=75/arm)	−0.3	0.96	0.73
Acute symptomatic plus disease-stabilizing effect ($E_{drug,24week}$=2.5 and 50% decrease on slope)	6-week crossover (n=30/arm)	−36.7	0.92	0.11
	12-week parallel (n=75/arm)	−19.0	0.95	0.45
	24-week parallel (n=75/arm)	0.7	0.97	0.72

Depending on the primary goal of the study, the development team can use these results to determine the trade-off between the increase in bias and the gain in power. For example, when the objective of the study is to test if the drug has any effect rather than to measure the steady-state treatment effect, the crossover design would be favorable due to smaller sample size and higher power.

For super symptomatic drug scenarios, two different types of drug profiles, superior acute symptomatic drug effect ($E_{drug,24week}$=3.5) and acute symptomatic benefit plus disease-stabilizing drug effect ($E_{drug,24week}$=2.5 plus 50% decrease on slope) were assumed and studied. Three study designs of interest (6-week crossover, 12-week parallel and 24-week parallel studies) were simulated and compared for each drug profile and the results are displayed in Table 15.4.

When a drug exhibited the desired super symptomatic efficacy (3.5 points at week 24) on ADAS-cog measures, the power to detect the drug effect was high regardless of the design (≥92%) for the superior symptomatic drug profile and the symptomatic plus disease-stabilizing drug profile. However, as expected, the true

drug effect at week 24 would be underestimated in both the 6-week crossover study and, to a lesser extent, the 12-week parallel study. The bias of drug effect estimates increased remarkably for drugs with acute symptomatic plus disease-stabilizing effects compared to a drug with only superior acute symptomatic effect (−36.7 vs. −17.8 % in 6-week crossover study and −19.0 vs. −7.0 % in 12-week parallel study, respectively).

The probability for a drug to achieve the target value (3.5 points with at least 25 % confidence) in each study design is shown in Table 15.4. For a drug having superior acute symptomatic effect, the probability was 41 % in a 6-week crossover study and increased to 65 % in a 12-week parallel study while the probability was estimated as 73 % for a 24-week parallel study under the assumption that the true effect was 3.5 points at week 24. However, if a drug achieved the super symptomatic profile by having combined symptomatic and disease-stabilizing effects, the probability would be only 11 and 45 % in a 6-week crossover study and a 12-week parallel study, respectively. The probability remained the same (72 %) in a 24-week parallel trial since the true drug effect was still 3.5 points at week 24.

15.5.2 Retrospective Analyses

Given the high attrition, and often late stages of failure of compounds developed for AD, it is not surprising that following a negative trial a large number of post-hoc analyses are completed to determine if a group of responders can be identified. Typically these post-hoc analyses are data cuts done by disease severity (very mild, mild, and moderate), ApoE4 genotype (carriers vs. noncarriers) CSF Abeta or Tau cuts, gender, age, etc. Given the number of analyses involved (often without correction for multiplicity), and the smaller sample sizes, the likelihood of a false positive being identified is high.

Alternatively, a small parallel design POC trial may yield positive results in a select group of study centers or patients, but the results are not replicated in larger, multinational trials in phase III. The question then becomes which study represents the true potential of the new agent?

15.5.2.1 Using Drug Models to Facilitate Interpretation of Study Results

Figure 15.6 (upper panel) shows results from two phase-II clinical trials for two different compounds (drug A and drug B) with similar inclusion criteria. In both cases, based on change from baseline, it appears as though a treatment effect was present as compared with the placebo group in each study. However, when these two clinical trial results are compared against the historical control data overlaid along with model predictions conditioned for baseline severity, it appears that the placebo response in the drug B trial was much worse than what would be predicted (Fig. 15.6, lower panel). Conversely, the treatment arm in trial B appears to be where the expected response for placebo usually falls. Given this result, and

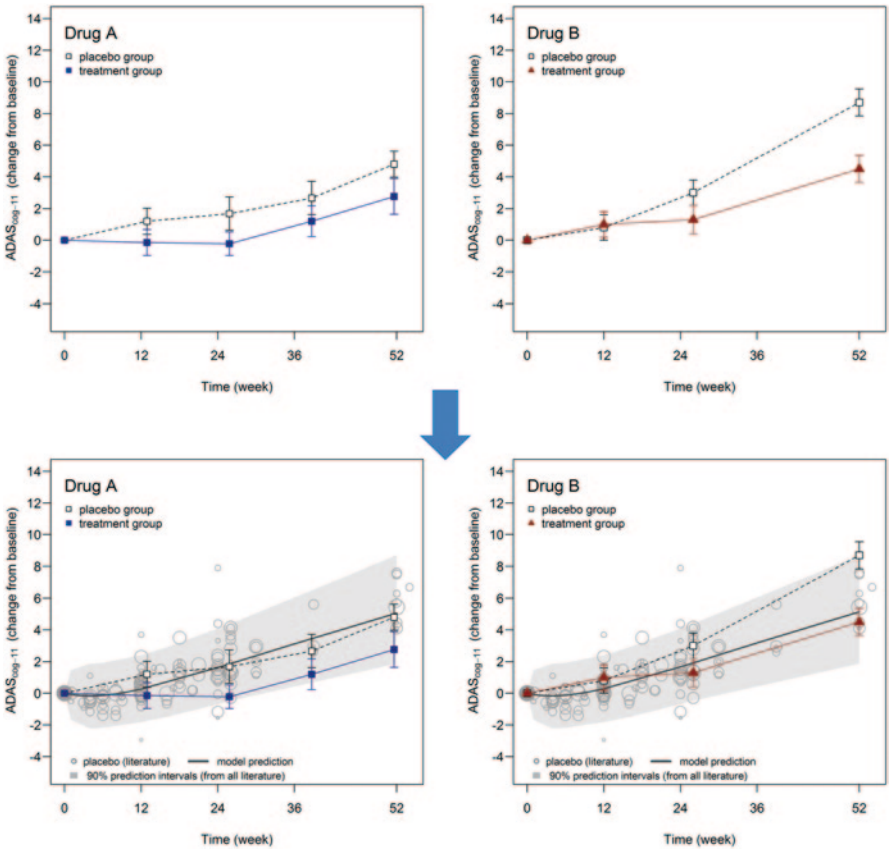

Fig. 15.6 Phase II clinical trial results from different drugs: change from baseline Alzheimer's disease assessment scale cognitive sub-scale (*ADAS-cog*, mean ± SE). *Upper panels*: The typical plot obtained after completion of the clincial trial, compared with the controlled placebo arm within the study. *Lower panels*: The same data above are overlaid with the historical data (literature) and its model prediction. (Reprinted from Ito et al. 2013, Copyright 2013, with permission from IOS Press)

without clear rationale for why a difference in placebo response would be observed, the clinical team concluded that the placebo response in the drug B study was not normal and needed more data to confirm the efficacy before taking further action (Ito et al. 2013).

15.5.2.2 Comparison of Phase II to Phase III Results

In this example, the treatment group from a 52-week, multi-center, placebo-controlled, double-blind phase-II study demonstrated a significant effect in a phase-II study, followed by a 26-week, placebo-controlled, double-blind, multi-center, global

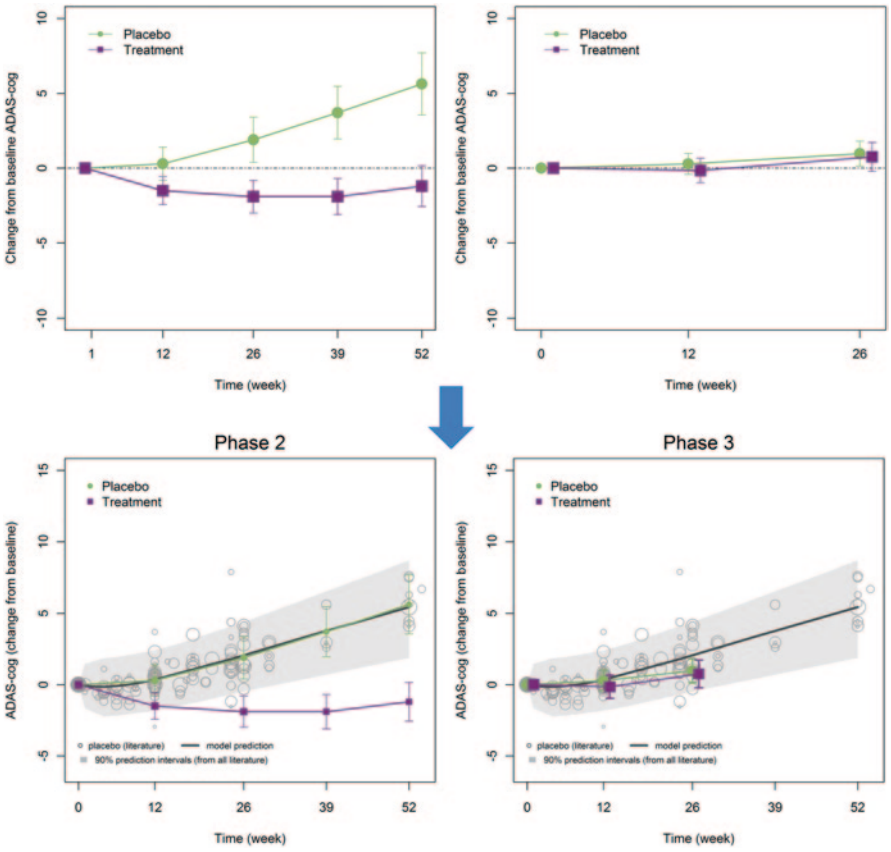

Fig. 15.7 Different results between phase-II and phase-III studies: change from baseline Alzheimer's disease assessment scale cognitive sub-scale (*ADAS-cog,* mean ± SE). (case study 2). *Upper panels:* The results obtained after completion of phase II (*left*) and phase III (*right*) studies compared with the controlled placebo arm displayed with the range of the treatment duration (52 and 26 weeks for phase II and III, respectively). *Lower panels:* The same data are overlaid with the historical data (literature) and its model prediction, using the same *x*- and *y*-axis range. The size of point is proportional to the number of patients in each treatment group. (Reprinted from Ito et al. 2013, Copyright 2013, with permission from IOS Press)

(including USA, Latin America, Europe, and Russia) phase-III study (Fig. 15.7, upper panel). The phase-III results appeared markedly different from the phase-II study, in the sense that there was no significant difference between the treatment and the placebo control groups. Unaided, by historical reference, the clinical team questioned the placebo response in the phase-III study, which appeared almost flat (Ito et al. 2013).

Phase-II and phase-III clinical trial results were then compared against the historical control data and with model predictions conditioned for baseline severity. In this case, the placebo response in phase II and III could be quantitatively assessed against historical controls and was deemed well within the normal range; it was still within the 90% prediction intervals when compared with historical placebo

response and model prediction (Fig. 15.7, lower panel). It was revealed that the placebo responses in both phase II and phase III were reasonable, and it was the treatment group that appeared different, resulting in a failed phase-III trial. Note that symbol size (points) in Fig. 15.7 (lower panel) is proportional to the sample size of the study, i.e., bigger symbols indicate larger sample studies. This method is useful when visualizing information about the size of the study and comparing different studies, as is also seen in Fig. 15.6.

15.6 Discussion and Future Perspectives

15.6.1 Moving to Early AD: Selection and Modeling of Selective Subscores of the ADAS-cog

With the understanding that AD pathology and irreversible neuronal damage are present decades before presentation of clinical symptoms, researchers are moving to study disease-modifying agents in patients at a much earlier stage of the disease. The trade-off is that in these populations, it becomes harder to measure changes in cognition and function, as the magnitude of impairment and the overall rates of change in early AD are much slower.

Although some success has been noted in modeling longitudinal changes in cognition in MCI and early AD populations with ADAS-cog, it is unlikely that the total ADAS-cog (designed for use in mild and moderate patients) will be sufficiently sensitive to be used in these populations. Other measures have been proposed for early AD Huang et al. (2014), and yet other composites, containing ADAS-cog subscales sensitive in early AD, are under development. For example, using ADNI data, Samtani et al. (2013) also identified the most informative cognitive measures from the ADAS-Cog and other available scales. Informative measures were identified based on standardized mean of 2-year change from baseline and were combined into novel composite endpoints. They assessed performance of the novel endpoints based on sample size requirements for a 2-year clinical trial. Further improvements were achieved by using cognitive-functional composites. Combining the novel composites with an enrichment strategy based on CSF beta-amyloid (A(1–42)) in a 2-year trial yielded gains in power of 20–40 % over ADAS-Cog 11, regardless of the novel measure considered.

15.6.2 Integrating Data Across the Entire AD Spectrum: the IRT Approach

As the number of tools designed for specific parts of the AD continuum continues to grow, the result is a further fragmentation of the tools used to capture the changes in the AD patient's cognition over time, and likely the need to develop new longitudinal DDT models when sufficient data becomes available.

Ueckert et al. (2014) have proposed an alternative model-based framework that maximizes the precision gained from the existing ADAS-cog assessments in any AD population, utilizing an item response theory (IRT) model for the ADAS-cog assessment. In the framework of IRT, the questions of the ADAS-cog (or any other cognitive measurement instrument now or in the future) can be described through characteristic curves, which describe the probability to answer correctly given a certain cognitive disability. This in essence, allows mapping of other instruments to a common scale. Based on a prior assumption about the distribution of cognitive disability in the population and the characteristic curves of the questions, IRT delivers an estimate of the most likely cognitive disability given a patient's response. By combining the entire knowledge gained from all questions (right or wrong; easy, hard, harder), a more precise estimate of the patients' ability can be obtained than that which would be obtained from just the simple summing of all scores typically used.

Using this approach, Ueckert et al. determined the most sensitive test subsets in MCI and mild AD populations using Fisher information. The IRT-based framework would allow use and comparison of data from any cognitive instrument (present or future), to permit instrument-independent assessment of cognition of the patient over the entire span of the disease.

15.6.3 Future

The development of models for CTS in AD have evolved continuously, as the understanding of the disease improves, and as more sophisticated modeling techniques become available. Complete DDT models require a variety of data types that support each of the components (natural progression, placebo effect, drug effects, dropouts, etc.). Obviously, no single study can provide all the relevant information for all components at once. This means that the integration of disparate data sources becomes key. Normally, literature knowledge, public access data (CAMD, ADNI), and data within one's own organization inform decision making in drug development. Rogers et al. (2012) attempted to integrate all these relevant data sources to inform each component.

While it may be that newer models have made incremental improvements in describing longitudinal changes over a longer duration, added trial execution components, such as dropout, lengthened the duration for which simulations can be completed; the key structural elements and idea behind the work remain similar in all the work reported here. At some point it may be beneficial for the field to adopt one common background model to move forward as a community. CAMD, FDA, and EMA have come together to evaluate the work of Rogers et al. as such a common background model. This CTS tool was put by CAMD through the first regulatory review process of this kind for modeling and simulation tools. As of June 12, 2013, FDA issued a regulatory letter to CAMD, regarding the Agency's decision to deem this proposed clinical trial simulator as a "fit-for-purpose" drug development tool for AD. In the Agency's opinion, this tool will assist sponsors in optimizing clinical trial

designs for AD therapies. As the first ever stand-alone CTS tool to receive a regulatory decision, this tool represents a milestone in the effort to improve the efficiency and success of future clinical trials by integrating knowledge gained from earlier studies. Moreover, since it was developed through a partnership involving multiple pharmaceutical companies, regulatory agencies, patient groups, academia, and research organizations, the tool demonstrates that stakeholders can come together precompetitively to develop tools that will benefit the entire field. In issuing a positive regulatory decision for the CAMD AD CTS tool, the FDA stated that the model can now be used to aid in the selection of clinical trial design features for mild-to-moderate AD, and that the use of this tool can facilitate the review of new drug protocols. http://www.fda.gov/AboutFDA/CentersOffices/OfficeofMedicalProductsandTobacco/CDER/ucm180485.htm. Accessed 09 Sep 2014. The FDA also recommended that sponsors help update the tool with new information about drugs under development. For example, incorporating clinical and biomarker data from patients at earlier stages of the disease could expand the usefulness of the tool in helping sponsors design appropriate clinical trials to evaluate novel therapeutic candidates.

The EMA has also endorsed the tool in Europe, through the issue of a positive qualification opinion for the CTS tool in AD drug development. http://www.ema.europa.eu/ema/pages/includes/document/open_document.jsp?webContentId=WC500146179. Accessed 09 Sep 2014

References

Ashford JW, Schmitt FA (2001) Modeling the time-course of Alzheimer dementia. Curr Psychiatry Rep 3:20–28

Atchison TB, Massman PJ, Doody RS (2007) Baseline cognitive function predicts rate of decline in basic-care abilities of individuals with dementia of the Alzheimer's type. Arch Clin Neuropsychol 22(1):99–107

Bhattaram VA, Siddiqui O, Kapcala LP, Gobburu JV (2009) Endpoints and analyses to discern disease-modifying drug effects in early Parkinson's disease. AAPS J 11:456–464

Chan PLS, Holford NHG (2001) Drug treatment effects on disease progression. Annu Rev Pharmacol Toxicol 41:625–659

Gillespie W (2009) Population dose-response model for ADAS-cog scores in patients with Alzheimer's disease by meta-analysis of a mixture of summary and individual data. American Conference on Pharmacometrics, Mashantucket, CT, 4–7 October 2009

Gobburu JV, Lesko LJ (2009) Quantitative disease, drug, and trial models. Annu Rev Pharmacol Toxicol 49:291–301

Huang Y, Ito K, Billing CB Jr, Anziano RJ (2014) For the Alzheimer's Disease Neuroimaging Initiative. Development of a straightforward and sensitive scale for MCI and early AD clinical trials. Alzheimers Dement [Epub ahead of print]

Hennig S, Nyberg J, Hooker AC et al (2009) Trial treatment length optimization with an emphasis on disease progression studies. J Clin Pharmacol 49:323–335

Holford NH, Peace KE (1992) Methodologic aspects of a population pharmacodynamic model for cognitive effects in Alzheimer patients treated with tacrine. Proc Natl Acad Sci U S A 89(23):11466–11470

Ito K, Ahadieh S, Corrigan B, French J, Fullerton T, Tensfeldt T (2010) Disease progression meta-analysis model in Alzheimer's disease. Alzheimers Dement 6(1):39–53

Ito K, Corrigan B, Zhao Q, French J, Miller R, Soares H, Katz E, Nicholas T, Billing B, Anziano R, Fullerton T (2011) Alzheimer's Disease Neuroimaging Initiative. Disease progression model for cognitive deterioration from Alzheimer's Disease Neuroimaging Initiative database. Alzheimers Dement 7(2):151–160

Ito K, Corrigan B, Romero K, Anziano R, Neville J, Stephenson D, Lalonde R (2013) Understanding placebo responses in Alzheimer's disease clinical trials from the literature meta-data and CAMD database. J Alzheimers Dis 37(1):173–183

Milligan PA, Brown MJ, Marchant B, Martin SW, van der Graaf PH, Benson N, Nucci G, Nichols DJ, Boyd RA, Mandema JW, Krishnaswami S, Zwillich S, Gruben D, Anziano RJ, Stock TC, Lalonde RL (2013) Model-based drug development: a rational approach to efficiently accelerate drug development. Clin Pharmacol Ther [Epub ahead of print]

Mould DR, Denman NG, Duffull S (2007) Using disease progression models as a tool to detect drug effect. Clin Pharmacol Ther 82(1):81–86

Rogers JA, Polhamus D, Gillespie WR, Ito K, Romero K, Qiu R, Stephenson D, Gastonguay MR, Corrigan B (2012) Combining patient-level and summary-level data for Alzheimer's disease modeling and simulation: a beta regression meta-analysis. J Pharmacokinet Pharmacodyn 39:479–498

Romero K, de Mars M, Frank D, Anthony M, Neville J, Kirby L, Smith K, Woosley RL (2009) The coalition against major diseases: developing tools for an integrated drug development process for Alzheimer's and Parkinson's diseases. Clin Pharmacol Ther 86(4):365–367

Romero K, Corrigan B, Neville J, Kopko S, Cantillon M (2011) Striving for an integrated drug development process for neurodegeneration: the coalition against major diseases. Neurodegen Dis Manage 1(5):379–385

Samtani MN, Farnum M, Lobanov V, Yang E, Raghavan N, Dibernardo A, Narayan V (2012) An improved model for disease progression in patients from the Alzheimer's disease neuroimaging initiative. J Clin Pharmacol 52:629–644

Samtani MN, Raghavan N, Shi Y, Novak G, Farnum M, Lobanov V, Schultz T, Yang E, DiBernardo A, Narayan VA, Alzheimer's disease Neuroimaging Initiative (2013) Disease progression model in subjects with mild cognitive impairment from the Alzheimer's disease neuroimaging initiative: CSF biomarkers predict population subtypes. Br J Clin Pharmacol 75(1):146–161

Schneider LS, Sano M (2009) Current Alzheimer's disease clinical trials: methods and placebo outcomes. Alzheimers Dement 5(5):388–397

Sheiner LB (1997) Learning versus confirming in clinical drug development. Clin Pharmacol Ther 61(3):275–291

Ueckert S, Plan EL, Ito K, Karlsson MO, Corrigan B, Hooker AC (2014) The Alzheimer's Disease Neuroimaging Initiative. Improved Utilization of ADAS-Cog Assessment Data Through Item Response Theory Based Pharmacometric Modeling.Pharm Res [Epub ahead of print]

Weiner MW, Veitch DP, Aisen PS, Beckett LA, Cairns NJ, Green RC, Harvey D, Jack CR, Jagust W, Liu E, Morris JC, Petersen RC, Saykin AJ, Schmidt ME, Shaw L, Siuciak JA, Soares H, Toga AW, Trojanowski JQ (2012) Alzheimer's disease neuroimaging initiative. The Alzheimer's disease neuroimaging initiative: a review of papers published since its inception. Alzheimers Dement 8(1 Suppl):S1–S68

William-Faltaos D, Chen Y, Wang Y, Gobburu J, Zhu H (2013) Quantification of disease progression and dropout for Alzheimer's disease. Int J Clin Pharmacol Ther 51(2):120–131

World Alzheimer's Report (2010) The global economic impact of dementia. Alzheimer's Disease International. http://www.alz.co.uk/research/world-report. Accessed 1 March 2012

Chapter 16
Pharmacometric Applications in Inflammation

Sujatha Menon and Sriram Krishnaswami

16.1 Introduction

A comprehensive list of inflammatory conditions would comprise over hundred diseases, including Alzheimer's disease, ankylosing spondylitis (AS), arthritis (osteoarthritis, OA, rheumatoid arthritis, RA, psoriatic arthritis, PsA), asthma, atherosclerosis, Crohn's disease, colitis, dermatitis, diverticulitis, fibromyalgia, hepatitis, irritable bowel syndrome (IBS), systemic lupus erythematosus (SLE), nephritis, Parkinson's disease (PD), ulcerative colitis, etc. (List of inflammatory diseases 2013) A brief review of the literature suggests that there are numerous successful and ongoing pharmacometric endeavors in many of these diseases. Pharmacometric applications to neurodegenerative disorders, such as Alzheimer's disease and PD, are discussed elsewhere as are applications to diseases, such as plaque psoriasis, in the dermatology area.

Numerous mathematical models have been developed to describe the disease progression and effects of anti-inflammatory drugs (Lon et al. 2012). In the excellent review by Lon et al. (2012), the authors illustrate the state of the art in modeling the effects of diverse drugs for treating inflammation, describe relevant biomarkers amenable to modeling, and summarize major advantages and limitations of the published pharmacokinetic/pharmacodynamic (PK/PD) models. The authors review the development of models ranging from direct inhibitory models to indirect response models to characterize symptoms and biomarkers. Target-mediated and transduction models as well as systems pharmacology models have been successfully applied to capture the PK/PD of many anti-inflammatory drugs and describe disease progression of inflammation. In addition, biologic treatments offer opportunities to develop different types of models due to their specific mechanisms of action, such as neutralization of specific cytokines, elimination of specific immune cells, blockade of costimulation for T-cell activation, and inhibition of cell adhesion (Lon et al. 2012). Small systems models have also been developed to describe bone formation

S. Krishnaswami (✉) · S. Menon
Department of Clinical Pharmacology, Pfizer, Groton, CT, USA
e-mail: Sriram.Krishnaswami@pfizer.com

S. Schmidt, H. Derendorf (eds.), *Applied Pharmacometrics,* AAPS Advances in the Pharmaceutical Sciences Series 14, DOI 10.1007/978-1-4939-1304-6_16

and resorption using biomarkers as well as clinical outcomes such as bone mineral density (Lemaire et al. 2004; Marathe et al. 2008, 2011; Schmidt et al. 2011).

Apart from PK/PD/disease models, large-scale systems biology models have also been developed, ranging from those describing the underlying disease process (inflammation and erosion of joints) in patients with RA (Rullmann et al. 2005) to bone homeostasis models (Peterson and Riggs 2010) to those that combine the strategies of systems biology and network pharmacology to investigate multi-targeted mechanisms of traditional Chinese medicine (Zhang et al. 2013).

Given this background, we have attempted to focus on a few documented applications in optimizing drug development strategy and/or regulatory approval. The selected case studies are by no means comprehensive or a reflection of the most influential or impactful endeavors because many successful applications are likely not in the public domain. Instead, the examples highlight some key learnings that should be broadly applicable in drug development decision making. In addition, an attempt has been made to provide a comprehensive reference list of various pharmacometric endeavors in this multifaceted therapeutic area.

16.2 Case Studies

16.2.1 Decision to Terminate Clinical Development of Canakinumab for the Treatment of RA (Demin et al. 2012)

Canakinumab (ACZ885) is a fully human monoclonal antibody that suppresses IL-1β-mediated joint inflammation and cartilage destruction in mice. A successful proof-of-concept (POC) study in patients with RA triggered a decision to conduct a dose-finding study. The key question was whether the magnitude of efficacy was sufficiently robust to warrant progression to a large phase 3 development program, which typically costs several hundreds of millions.

RA is an autoimmune disease that leads to inflammation, progressive joint damage, and disability. It affects ~1% of adults worldwide, predominantly women. Advances in understanding the pathogenesis of this highly heterogeneous disease have fostered the development of several new therapeutics with vastly improved outcomes over the past decade. Numerous cytokines, growth and differentiation factors, and intracellular signaling molecules and transcription factors have been implicated in the pathogenesis of RA (Table 16.1). However, to date, there are no reliable predictive biomarkers of prognosis, therapeutic response, or toxicities such as increased mortality, cardiovascular, and other systemic complications of the disease.

Current international treatment recommendations for the management of RA state that the treatment of RA should be aimed at reaching a target of remission or low disease activity as soon as possible in every patient; and as long as the target has not been reached, treatment should be adjusted by strict monitoring every 1–3 months (Smolen et al. 2010). Methotrexate (MTX) is part of the first treatment strategy in

Table 16.1 Key molecules and signal mediators implicated in the pathogenesis of rheumatoid arthritis

Molecule or signal mediator	Key disease relevant functions	Status[a]
Cytokines		
TNF-α	Activates leukocytes, endothelial cells, and synovial fibroblasts, inducing production of cytokines, chemokines, adhesion molecules, and matrix enzymes; suppression of regulatory T-cell function; activation of osteoclasts; and resorption of cartilage and bone; mediates metabolic and cognitive dysfunction	Approved drug
Interleukin-1α and 1β	Activate leukocytes, endothelial cells, and synovial fibroblasts; induce matrix-enzyme production by chondrocytes; activate osteoclasts; mediate fever; enhance glucose metabolism; and reduce cognitive function	Approved drug
Interleukin-6	Activates leukocytes and osteoclasts; is involved in B-lymphocyte differentiation; regulates lipid metabolism, acute-phase response, and anemia of chronic disease; and is implicated in hypothalamic–pituitary–adrenal axis dysfunction and fatigue	Approved drug
Interleukin-7 and 15	Promote and maintain T-cell and natural killer–cell activation and T-cell memory, block apoptosis, and maintain T-cell–macrophage cognate interactions	Phase 2 trial completed
Interleukin-17A and 17F	Act synergistically to enhance activation of synovial fibroblasts, chondrocytes, and osteoclasts	More than one phase 2 trial with positive results
Interleukin-18	Promotes activation of Th1, neutrophils, and natural killer cells	
Interleukin-21	Activates Th17 and B-cell subsets	
Interleukin-23	Expands Th17	
Interleukin-32	Activates cytokine production by several leukocytes and promotes osteoclast differentiation	
Interleukin-33	Activates mast cells and neutrophils	
Growth and differentiation factors		
BLyS and APRIL	Activate B cells and have a role in the maturation of B cells and enhancement of autoantibody production	In phase 2 trial

Table 16.1 (continued)

Molecule or signal mediator	Key disease relevant functions	Status[a]
GM-CSF and M-CSF	Enhance differentiation of granulocyte and myeloid-lineage cells in the bone marrow and synovium	In phase 1 trial
RANKL	Promotes maturation and activation of osteoclasts	Phase 2 trial completed
Intracellular signaling molecules and transcription factors		
JAK	Tyrosine kinase that regulates cytokine-mediated leukocyte maturation and activation, cytokine production, and immunoglobulin production	Approved drug
Syk	Tyrosine kinase that regulates immune-complex–mediated and antigen-mediated activation of B and T cells and other Fc receptor-bearing leukocytes	More than one phase 2 trial with positive results
PI3K	Mediates signals that drive proliferation and cell survival	Phase 1 trial planned
BTK	Plays an important role in the activation of B cells, macrophages, mast cells, and neutrophils, through regulation of B-cell receptor and Fc receptor signaling as appropriate	Phase 1 trial planned
NF-κB	Helps integrate inflammatory signaling and is important for cell survival	

APRIL a proliferation-inducing ligand, *BLyS* B-lymphocyte stimulator, *BTK* Bruton's tyrosine kinase, *GM-CSF* granulocyte–macrophage colony-stimulating factor, *JAK* Janus kinase, *M-CSF* macrophage colony-stimulating factor, *PI3K* phosphatidylinositol 3-kinase, *RANKL* receptor activator of NF-κB ligand, *Syk* spleen tyrosine kinase, *Th1* type 1 helper T cells

[a] Status indicates the investigational status of agents targeting the molecule or signal mediator. Approved drugs have been approved by the Food and Drug Administration and European Medicines Agency for use in patients with rheumatoid arthritis. Trials are clinical trials that are ongoing or have been completed. Reproduced with permission from McInnes and Schett (2011)

patients with active RA. However, the majority of patients experience an inadequate response to a therapeutic intervention with MTX, and many are treated with at least two nonbiologic disease-modifying antirheumatic drugs (DMARDs) before receiving a tumor necrosis factor inhibitor (TNFi). The remaining patients are treated with a biologic DMARD, especially a TNFi, typically administered in combination with MTX, which is now the standard of care (SOC). Often one or more TNFis are prescribed, but ultimately many patients move to biologic DMARDs with other mechanisms of action, and medical needs are not fully met for many patients. Thus, there remains an unmet medical need for additional therapeutic options with unique mechanisms of action, proven efficacy, and acceptable safety profiles in patients with moderate-to-severe active RA.

A systematic review of the published literature on clinical trials of biological treatments in RA was performed, using processes that have been previously

described (McDevitt et al. 2009). The majority of the trials were placebo controlled; in one trial (Schiff et al. 2008), a head-to-head comparison of two biologics (abatacept and infliximab) was performed. For the purposes of the meta-analysis, only data on approved doses and regimens were retained.

This integrated analysis included data from 37 phase 2–3 studies describing 13,474 patients. The primary end point for decision was the American College of Rheumatology (ACR)20 responder rate, which is the percentage of patients who responded to the relevant criterion based on improvements in tender or swollen joint counts and improvement in three of the following five parameters: acute phase reactant (such as sedimentation rate), patient assessment physician assessment, pain scale, and disability/functional questionnaire. Since nearly all published pivotal trials use this measure of efficacy, it provides for a standardized way to compare treatments. However, as would be expected, the ACR end point is limited by reduced precision compared to a continuous measure such as disease activity score. The final nonlinear mixed-effects model used for fitting ACR20 time course data was:

$$\text{logit}(y_{ilj}) = \text{logit}\left(\frac{\tilde{\phi}_{1k} t_{ij}^{\gamma_m \alpha}}{\exp(\theta_{2k_2})^{\gamma_m} + t_{ij}^{\gamma_m}}\right) + \varepsilon_{ilj}$$

$$\tilde{\phi}_{1k} = M\left(\frac{\exp(\phi_{1k})}{1+\exp(\phi_{1k})}\right), \quad \phi_{1k} = \theta_{1k} + \eta_{1i} + \eta_{2il},$$

$$\eta_{1i} \sim N(0, \omega_1^2), \quad \eta_{2il} \sim N\left(0, \frac{\omega_2^2}{N_{il}}\right), \quad \varepsilon_{ilj} \sim N\left(0, \frac{\sigma^2}{N_{il}}\right),$$

where i is the index over studies, l is the index for treatment arm within a study, and j is the index over time within a study. The index k represents therapies, and k_2 represents drugs. Two different γ_m values were estimated: one for biologics and one for placebo-plus-MTX and true placebo ($m=1, 2$). The E_{max} parameter $\varphi_{1,k}$ is logit transformed with $M=100$ for all treatments except certolizumab and infliximab (drugs with decreasing response at later time points), for which $M=300$. The fixed-effects θ_{1k} values represent E_{max} parameters, and fixed-effects θ_{2k2} values are time course parameters. The offset of the effect parameter α is set at 1 for all treatments except certolizumab and infliximab, for both of which $\alpha<1$. Random-effects parameters $\eta 1_i$ and $\eta 2_{il}$ represent between study variability (BSV) and between treatment arms variability (BTAV), respectively. Residual unexplained variability, ε_{ilj}, and BTAV, $\eta 2_{il}$, are adjusted according to the number of subjects in a treatment arm. The model was implemented in a Bayesian framework and coded in WinBUGS.

Figure 16.1 shows the model-based predictions of the time course of ACR20 responder rates for canakinumab in comparison to SOC treatments, etanercept and adalimumab, as well as placebo. It showed that, with the tested doses/regimens of canakinumab, there was only a low probability that this drug would be better than the most effective current treatments. At the most effective dose, the analysis predicted a very low probability (<3%) of canakinumab being better than certolizumab or infliximab, and 8% probability of being better than adalimumab, per ACR20

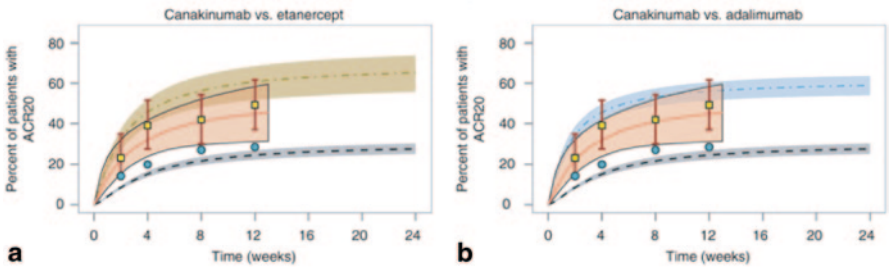

Fig. 16.1 Model-based comparison of ACR20 responder rates for canakinumab versus placebo and SOC treatments, etanercept and adalimumab. Canakinumab (both panels, *red solid lines*), etanercept (panel **a**, *brown dash-and-dot line*), adalimumab (panel **b**, *blue dash-and-dot line*), and placebo (both panels, *gray broken lines*). *Blue circles* represent placebo-plus-MTX data from the canakinumab study. *Yellow squares* represent the observed ACR20 values (with *red vertical bars* for 95% confidence intervals) for canakinumab. The shaded areas are the respective 90% Bayesian confidence intervals for model-based predictions. (Reproduced with permission from Demin et al. 2012, CPT)

scores after 12 weeks of treatment. This finding supported the decision not to continue with clinical development of canakinumab in RA.

16.2.2 Decision to Expand the Size and Scope of a Dose-Finding Study and Using Benefit and Risk Data to Select Doses for Phase 3 Testing. (Milligan et al. 2013)

This example illustrates the prospective application of model-based drug development (MBDD) concepts to the late-stage development of tofacitinib, a potent immunomodulator with a novel mechanism of action, for the treatment of RA. Results from a POC trial demonstrated a high degree of efficacy but with side effects. The challenge was to identify dose(s) of this orally administered, small molecule for pivotal registration trials that would achieve a minimally acceptable product profile of similar efficacy as biologic injectables, with acceptable safety.

Tofacitinib is a Janus kinase (JAK) inhibitor. JAK enzymes transmit the signaling of several pro-inflammatory cytokines involved in the pathogenesis of RA through pairings of JAKs (e.g., JAK1/JAK3, JAK1/JAK2) and tofacitinib works by inhibiting the activities of these combinations, resulting in modulation of cellular processes of hematopoiesis and immune cell function.

The first evidence of efficacy in RA patients was observed in a 6-week POC study of 5, 15, and 30-mg twice-daily (BID) doses of tofacitinib and placebo (Kremer et al. 2009). All doses demonstrated efficacy as measured by the ACR response criteria but were also associated with side effects, such as dose-dependent changes in laboratory markers (e.g., decreased neutrophils). The challenge was to efficiently yet comprehensively characterize dose-response relationships to identify optimal dose(s) for confirmatory trials. This process began by gaining agreement with stakeholders on the key questions and setting quantitative and action-oriented objectives for the phase 2b program, as illustrated below (Sheiner 1997).

What do we need to know? Identify the lowest dose with at least 30% difference in ACR20 response versus placebo by week 12. ACR20 response was chosen because it was the primary efficacy end point in the study to demonstrate superiority to placebo. However, the operating characteristics of the study were also verified to be reasonable with respect to ACR50 and ACR70 end points.

How sure do we want to be? Desire 80% probability that the true response for the model-estimated dose will be within ±20% of the target efficacy magnitude, i.e., 24–36%.

What are we willing to assume? A pharmacologically based, longitudinal E_{max} model will be applied; the dose range derived from the monotherapy POC study data will be applicable to combination treatment with MTX; priors for the model-based analysis will be weakly informed by the POC study data.

Various longitudinal, dose–response models were developed, including an indirect latent variable response model, relating pharmacologically based models to categorical data (Hutmacher et al. 2008). The various models gave similar predictions of the data but showed differences in their predictive performance when extrapolating to lower doses and later time points. Consequently, they were used as "data-generation" models to ensure that the design chosen had robust operating characteristics over a range of "true" relationships (Krishnaswami et al. 2009). A similar approach was implemented to characterize decreases in absolute neutrophil counts. Since the neutropenia incidence data from the POC study were too sparse, modeling efforts were focused on characterizing neutrophil counts using indirect response and semi-mechanistic models (Gupta et al. 2010) to provide a more stable basis for dose and time interpolation/extrapolation. Using clinical trial simulations, it was determined that the 10th percentile of the neutrophil count distribution was related to the risk of neutropenia and estimated with greater precision than the neutropenia incidence data, thereby providing an efficient way to eliminate doses with unacceptable neutropenia event rates predicted based on changes in continuous data.

Two 6-month, phase 2b studies were performed in which tofacitinib was administered either as monotherapy (Fleischmann et al. 2012) or in combination with MTX (Kremer et al. 2012). Both studies evaluated placebo and tofacitinib doses of 1, 3, 5, 10 and 15 mg BID. The sample sizes of these studies, totaling > 800 patients, were larger than traditional phase 2 sample sizes because they were designed to support quantitative decision criteria aimed at identifying an optimal dose rather than statistical separation from placebo. Traditional pairwise comparisons would have necessitated a 70% increase in study size (approximately 1300 patients) to achieve similar performance characteristics over a model-based approach.

Model-derived inferences, updated using Bayesian methods, were used to calculate the probability of technical success, i.e., the probability of achieving efficacy similar to that of SOC TNF inhibitor treatment (Tan et al. 2011; Tofacitinib FDA Advisory Meeting 2012). As predicted from the POC study, changes in neutrophils and predicted incidence of neutropenia were within acceptable limits and, therefore, not considered to limit the dose range under consideration for phase 3 trials. However, dose-dependent changes in hemoglobin levels were noted. A longitudinal model was applied to capture the relationship between dose and hemoglobin levels. An empirical model was applied to capture the apparent inverted U-shaped

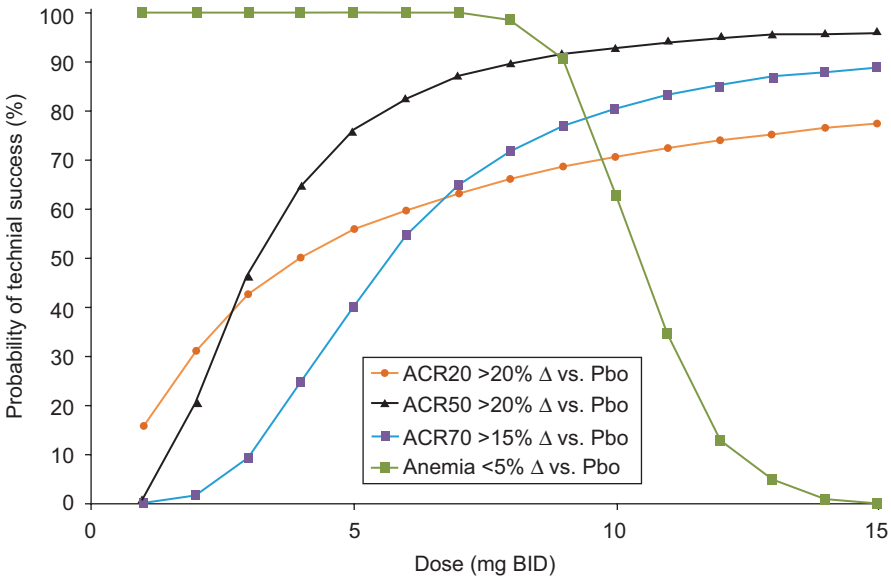

Fig. 16.2 Tofacitinib—probability of achieving targeted differences versus placebo. *Solid symbols* and *lines* represent model-based probability estimates for ACR responses and anemia. *ACR* American College of Rheumatology, *Pbo* placebo. (Reproduced with permission from Milligan et al. 2013)

relationship between dose and hemoglobin levels, possibly arising out of beneficial effects (improvement in the anemia associated with chronic disease, i.e., active RA) at lower doses and a combination of beneficial and deleterious effects (potentially due to JAK2 inhibition) at higher doses. The probability that the incidence of clinically important anemia (defined as >2 g/dl decreases from baseline in hemoglobin or absolute value <8 g/dl) will not exceed 5% above placebo over 6 months of treatment was calculated. As shown in Fig. 16.2, modeling based on the MTX combination study predicted that doses from 5 to 10 mg BID inclusive would meet both the desired efficacy and safety criteria of having approximately 50% or greater probability of achieving efficacy similar to SOC, with anemia rates <5% above placebo. In contrast, a 3-mg dose had a 10% chance of achieving the ACR70 target compared to 40% for the 5-mg dose. It is noteworthy that while the MTX combination study was designed to identify a dose that produced at least 30% difference in ACR20 rates from placebo, none of the doses in this study actually showed differences >30%, attributable to an unexpectedly high placebo rate (>40%). On the other hand, ACR50 and ACR70 response rates from the study encompassed a range of responses typically associated with TNF inhibitor treatment. As a consequence, the acceptance criteria for ACR 20 dose selection was modified to at least a 20% difference from placebo to provide better discrimination of doses between 1- and 15-mg dose range while the original criteria was retained for ACR50 and ACR70 rates.

The choice of 5- and 10-mg doses was independently verified in the monotherapy phase 2b study which became available after phase-3 dose selection was made

based on the MTX combination study. This study monotherapy showed that doses ≥5 mg provided the requisite level of efficacy, including >30% differences in ACR 20 rates from placebo, whereas a 3-mg dose was considered clinically suboptimal, even though it separated from placebo (Fleischmann et al. 2012). Thus, the totality of the data justified the choice of 5- and 10-mg BID doses for phase 3 studies.

The results from the phase 3 program were consistent with these model predictions. The efficacy of 5 mg BID was as predicted (29% difference in ACR20 rate vs. placebo across five phase 3 studies) and, more importantly, similar to that of SOC TNF inhibitor treatment (adalimumab; van Vollenhoven et al. 2012a). The rates of anemia and neutropenia were low and considered manageable with appropriate clinical monitoring.

A prospective approach to (a) designing studies to a stringent quantitative criteria, (b) characterizing exposure–response relationships using well-established clinical outcome data in patient populations representative of the phase 3 program, and (c) selecting doses based on efficacy and safety using probability of technical success as a common metric allowed demonstration of a positive benefit: risk profile with the desired product attributes. Tofacitinib 5 mg BID was approved in 2012 by the FDA for the treatment of moderately-to-severely active RA.

16.2.3 Decision to Approve a Pediatric Dose and Formulation Not Tested in a Pivotal Registration Trial (Krishnaswami et al. 2012)

Celecoxib is a nonsteroidal anti-inflammatory drug (NSAID) that exhibits anti-inflammatory, analgesic, and antipyretic activities by inhibiting prostaglandin synthesis, primarily via inhibition of cyclooxygenase-2 (COX-2) but not COX-1 at therapeutic concentrations in humans (Gierse et al. 2002). In addition to adult indications, it is currently approved for the treatment of juvenile rheumatoid arthritis (JRA), a group of disorders characterized by idiopathic inflammatory arthritis. The key question during the pediatric development program was whether an alternative dosing scheme supportable by available formulation could be derived from studies that used an investigational formulation to evaluate efficacy, safety, and PK.

Prior to and during the conduct of the efficacy/safety trial in JRA patients (Foeldvari et al. 2009), several attempts were made to develop an age-appropriate pediatric formulation, including oral suspension, orally disintegrating tablets, and chewable tablets. None of these were suitable for commercialization in a timely manner because of technical challenges. Thus, the development team was faced with the conundrum of having efficacy, safety, and PK data, in the pediatric population, but without a commercializable formulation. Thus, the overall objective of this pharmacometric endeavor was to bridge data across formulations, methods of administration, and populations to derive dosing recommendations for JRA patients. This was achieved in three steps: (1) assessing exposures in JRA and adult RA patients administered celecoxib suspension (i.e., formulation used in the efficacy trial)

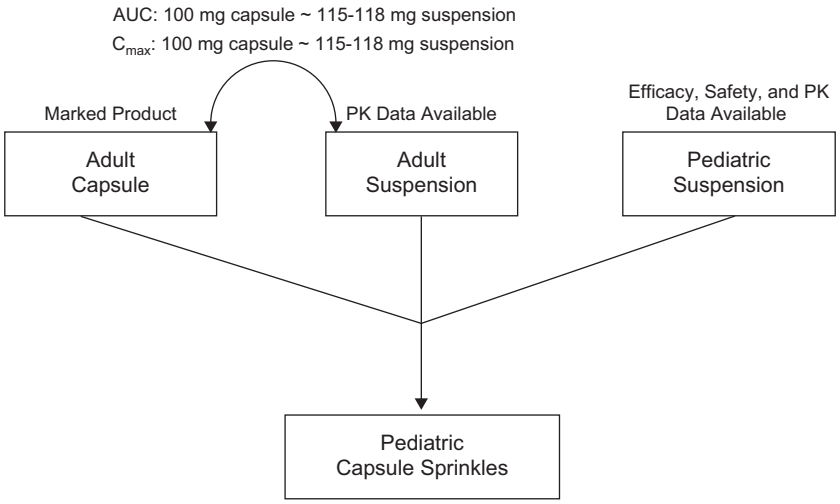

Fig. 16.3 Bridging strategy for celecoxib sprinkles in patients with JRA. (Reproduced with permission from Krishnaswami et al. 2012)

and characterizing the PK/PD relationship, (2) comparing the suspension exposures to capsule (marketed formulation) exposures, and (3) evaluating the suitability of administering celecoxib capsules as sprinkles (on applesauce) for those who may be unable or unwilling to swallow an intact capsule (Fig. 16.3).

A complicating factor in bridging capsule and suspension was that although similar AUC was expected between the two dosage forms at the same doses, C_{max} would be higher (approximately doubled) for the capsule formulation. Therefore, the rationale for the selection of capsule doses was based on achieving concentrations that do not exceed those observed in the JRA trial using the suspension formulation (safety boundary), while achieving similar overall exposures as those shown to be noninferior to naproxen (efficacy boundary), an approved drug for the treatment of JRA. Because two doses (3 and 6 mg/kg BID) of celecoxib suspension were evaluated in the efficacy trial and both were found to be noninferior to naproxen 7.5 mg/kg BID and well tolerated (Foeldvari et al. 2009), concentrations in between those of the two dose groups were targeted. The prediction of pediatric capsule PK profiles was made by combining historical capsule parameter estimates in adults and the estimated power exponents for the effect of weight on CL/F and V/F in the JRA efficacy trial. It was fortuitous that the power exponent for the weight effect on CL/F was 0.265 ± 0.074, resulting in typical oral clearance (L/h) values that were only 40 and 24% lower in patients weighing 10 and 25 kg, respectively, compared with a 70-kg patient. This allowed the potential use of a less flexible dosing form (capsule) compared to a liquid formulation.

Mechanistically, whether these results were a true reflection of the weight–clearance relationship or an artifact arising out of possible influence of collinear covariates was evaluated by fixing the weight effect to an allometric model (typical $CL/F = \theta 1 \times [weight_i/41]^{0.75}$; typical $V/F = \theta 2 \times [weight_i/41]$) and estimating the relationship between age and CL/F and age and V/F using centered power

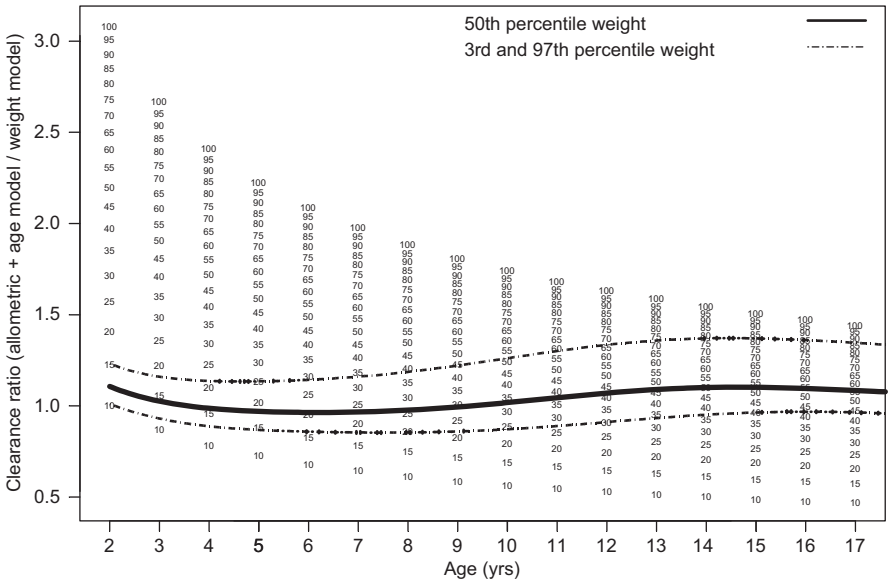

Fig. 16.4 Comparison of typical clearance estimates between allometric-plus-age model and weight-effect model. *Symbols* represent body weight; *lines* represent clearance ratios for 3rd (*lower dotted*), median (*solid*), and 97th (*upper dotted*) percentile body weights by age according to CDC weight chart. (Reproduced with permission from Krishnaswami et al. 2012)

functions. The motivation for choosing age as the second covariate was not based on the plausibility of incomplete maturation of metabolism or excretion processes, because patients typically attain full function by 2 years of age, but rather from a report showing a similar departure from allometry for another anti-inflammatory agent (leflunomide) in the JRA population (Shi et al. 2005).

Recent evidence suggests that inflammation due to underlying infectious or inflammatory conditions is associated with downregulation in the expression of several drug-metabolizing enzymes (Schmith and Foss 2010). This raised the possibility that age could be a surrogate of inflammatory burden (i.e., younger children having a lower burden of disease/inflammation compared with older children, and thus resulting in decreasing oral clearance with increasing age). Although the addition of two such parameters describing the relationship between age and CL/F and age and V/F resulted in only a 6.3-point decrease in the objective function (not statistically significant) relative to the weight-effect model (power exponent = 0.265), the parameters were estimated reasonably well (relative SE < 25 %). This suggests that caution should be exercised in interpreting the weight–clearance relationship from a mechanistic standpoint. However, the model choice or philosophy would not be expected to affect dosing decisions because the estimate of the power exponent in the weight-effect model should reflect a net effect of allometry and age. Indeed, typical clearance values calculated over a range of theoretical age (2–17 years) and weight (10–100 kg) combinations according to the 3rd, 50th, and 97th percentile Centers for Disease Control and Prevention weight charts are mostly similar between the allometric-plus-age model and the weight-effect model (Fig. 16.4). The

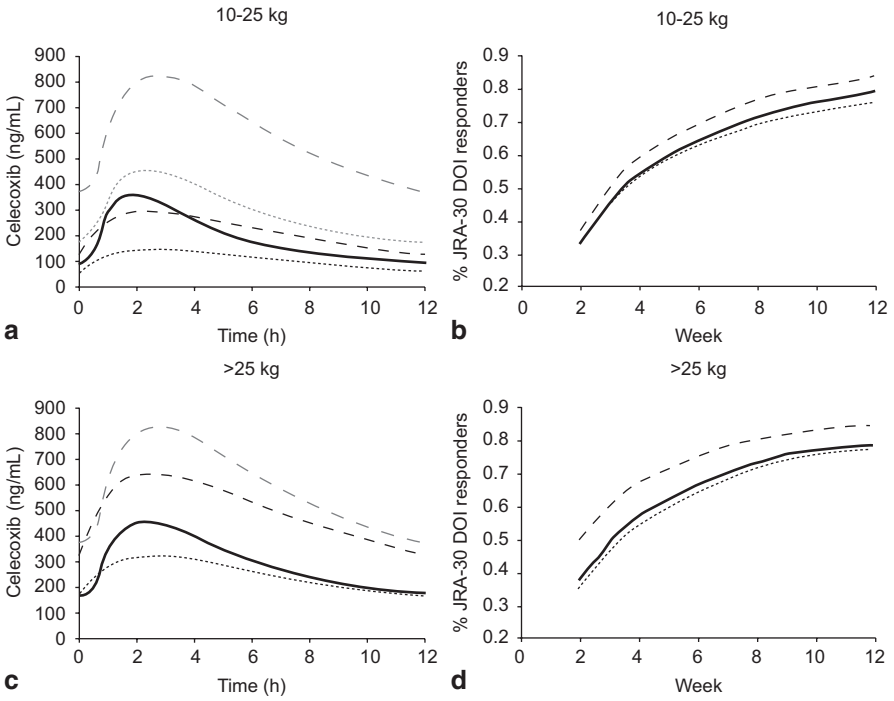

Fig. 16.5. Simulated PK/PD profiles for suspension and capsule dosing schemes of celecoxib in juvenile rheumatoid arthritis (JRA). *Black short* and *long dash lines* represent 3 and 6-mg/kg BID suspension, respectively, in JRA; *black solid line* represents (**a**, **b**) 50-mg bid or (**c**, **d**) 100-mg BID capsule in JRA; gray short and long dash lines represent 100- and 200-mg BID doses of capsule, respectively, in adult rheumatoid arthritis patients. *DOI* definition of improvement. (Reproduced with permission from Krishnaswami et al. 2012)

models diverge only under extreme scenarios (e.g., a 2-year-old child would have to weigh 40 kg to need twice the dose as compared with a 10-year-old weighing 40 kg under the allometric-plus-age model). Moreover, at younger ages, the allometric-plus-age model tends to suggest the need for higher doses under such extreme weight scenarios, making it of less utility in the absence of safety data. Thus, the simpler and more conservative weight-effect model was considered appropriate to derive dosing instructions.

Simulations supported a reduction in the number of weight-based dosing tiers employed in the JRA efficacy trial from five (10–12, 13–25, 26–37, 38–50, and >50 kg) to two (10–25 and >25 kg). An overall summary is shown in Fig. 16.5, where the simulated PK (including historical adult capsule data for reference) and efficacy profiles (percent responders) are depicted for the 10- to 25 and >25-kg weight categories for the suspension doses used in the efficacy study and for the recommended capsule doses. The results are consistent with the approach of achieving efficacy closer to that of the lower dose (3 mg/kg) tested in the efficacy study while ensuring that C_{max}, particularly in lighter patients, is not significantly greater than those of the higher dose (6 mg/kg) tested in the efficacy study (Fig. 16.5).

Finally, the interchangeability of different delivery methods (administration of the commercial capsule intact or as sprinkles) was demonstrated in adults in order to support dosing in children who are unable to swallow intact celecoxib capsules.

16.2.4 Decision to Test Higher Dose Space Based on Knowledge Derived from Totality of Internal and External Data (Kowalski et al. 2008)

SC-75416 is a benzopyran (chromene) COX-2 inhibitor, a novel class of compounds with anti-inflammatory and analgesic activity demonstrated in preclinical models of pain and inflammation. An initial dose-ranging study in post-surgical dental patients indicated that the tested doses of a capsule formulation of SC-75416 did not achieve pain relief (PR) response similar to SOC. PR scores were measured on a 5-point Likert scale (PR = 0: no pain relief; PR = 4: complete pain relief). In addition, patients receiving SC-75416 dropped out of the study and took rescue medication at a higher rate than those receiving the reference standard (rofecoxib 50 mg, currently withdrawn from the market). The key development question was whether the dose range tested was adequate to support compound termination at that point in time, or if there was a rationale to pursue higher doses that would ultimately provide efficacy differentiation from marketed products.

A modeling and simulation strategy was employed to leverage internal and external data from SC-75416, and from other products (rofecoxib, valdecoxib, and ibuprofen) to address this question. Models to characterize PR as well as dropout (time to rescue) were employed based on previously published methodology for the analysis of non-randomly censored ordered categorical data, which is typical of analgesia trials (Sheiner 1994; Mandema and Stanski 1996; Sheiner et al. 1997). A key data piece that shed light on the potential reason for the less-than-expected efficacy was the lower and more variable absorption profile of the capsule formulation of SC-75416 in the first 6 h after dosing in patients with dental pain compared to that of an oral solution (previously evaluated in healthy subjects). To assess the impact of this difference, the PR and dropout models together with the observed PK profile for the oral solution were used to predict the PR score profile for the oral solution formulation. These predictions, which are extrapolations outside of the data generated from the initial dental pain study using capsule, suggested that equivalent doses of the compound administered as an oral solution should provide higher PR response compared to those of the capsule. More importantly, higher doses of the oral solution were predicted to surpass the efficacy of an approved drug (ibuprofen 400 mg). To further increase the confidence to invest in another study to test this hypothesis, particularly to estimate the probability of success relative to ibuprofen, additional PK/PD modeling was performed pooling post-oral surgery pain data from valdecoxib studies where 400-mg ibuprofen had been used as an active comparator. The PR and dropout model parameters estimated were used to obtain two sets of population mean predictions of efficacy for SC-75416 oral solution doses ranging from 30 to 360 mg. An important assumption was made that all of these drugs can

Table 16.2 Comparison of observed and predicted TOTPAR6 responses for the SC-75416 oral solution post-oral surgery pain study. (Reproduced with permission from Kowalski et al. 2008)

Treatment group	T0TPAR6 (mean ± SE)		ΔTOTPARe[a]	
	Predicted[b]	Observed	Predicted[b]	Observed
Placebo	3.9 ± 0.9	1.4 ± 0.6	−7.1	−9.6
60 mg SC-75416	10.1 ± 1.4	9.2 ± 1.2[c]	−0.9	−1.8
180 mg SC-75416	13.0 ± 1.2	13.7 ± 1.2[c]	2	2.7[d]
360 mg SC-75416	14.2 ± 0.9	14.3 ± 0.8[c]	3.2	3.3[d]
400 mg ibuprofen	11.0 ± 0.8	11.0 ± 0.8[c]	0	0

[a] Difference in TOTPAR6 relative to 400 mg ibuprofen
[b] Predicted based on Model IIA/IIB
[c] Significantly different ($P < 0.05$) relative to placebo
[d] Significantly different ($P < 0.05$) relative to ibuprofen

achieve the same maximum drug effect, and differences in effectiveness between the compounds is dependent only on their exposure relative to their potency.

Because different data sources were used to obtain the two sets of population mean predictions of efficacy, considerable discrepancy in the dose–response predictions were noted between the two models. The predicted SC-75416 oral solution dose–response profile based on the single study was steeper compared to that predicted based on the analysis of competitor data. The parameter estimates of the PR and dropout models are less precise for the SC-75416 capsule post-oral surgery pain model because they are based on the results of a single study, and because the SC-75416 treatments had unexpectedly low exposure due to the poor absorption of the capsule formulation. For these reasons, the more conservative predictions based on the post-oral surgery pain modeling of the data from the valdecoxib studies were considered more robust and hence were used in subsequent clinical trial simulations to evaluate designs in planning the SC-75416 oral solution post-oral surgery pain study.

Based on the updated PK/PD and dropout models from the valdecoxib study and the potency (EC50) estimate for SC-75416 from the fit to the SC-75416 capsule post-oral surgery pain study, clinical trial simulations were conducted to evaluate and optimize the study design (doses and sample sizes) for a superiority trial. The design was optimized using probability of success as the metric, which was defined as a greater than 0 value for the lower bound of a 95% confidence interval of the difference in efficacy between SC-75416 and ibuprofen. Seven different design options were evaluated and the chosen design was a study with a 2:1 randomization with $N = 50$ patients per arm for the placebo and 60- and 180-mg SC-75416 oral solution treatments, and $N = 100$ patients per arm for the 360-mg SC-75416 oral solution and 400-mg ibuprofen treatments. A second post-oral surgery study was then conducted using a study design optimized to test the hypothesis that a dose of SC-75416 could achieve superior PR to 400-mg ibuprofen.

The results were remarkable, in that the observed results were consistent with model predictions and the data confirmed the hypothesis that a high dose (360 mg) of SC-75416 administered as an oral solution can achieve clinically relevant and statistically significant improvements in PR relative to 400-mg ibuprofen (Table 16.2).

16.3 Summary

The case studies presented herein highlight tangible impact (in terms of time, cost, and/or risk mitigation) achieved via the application of pharmacometric approaches to a variety of decisions that are at the core of clinical drug development. A summary of the impact of these approaches to drug development decision making is provided below:

- Case study 1: In the absence of head-to-head data, model-based meta-analysis was used to provide a quantitative basis for driving the decision to terminate the development of a compound with efficacy, but insufficient to be superior to SOC therapy. The framework is broadly applicable to support internal and external decision making at all stages of development.
- Case study 2: Use of model-based methods to design and analyze dose-finding studies resulted in efficiency gains by way of needing 437 fewer patients (~US$ 3 million in cost) compared to traditional methods. Prospective planning and pre-specification of the desired level of confidence in the magnitude of efficacy and safety resulted in larger than traditional phase 2 sample sizes, but ultimately allowed the identification of doses that produced the desired outcomes in phase 3 studies. Thus, model-based drug development should be viewed more as a risk mitigation tool than a cost-reduction tool.
- Case study 3: Use of model-based methods to bridge data across formulations and populations, along with the collection of extensive PK and PD data in the pediatric population including evaluation of the efficacy of two doses, resulted in the approval of interpolated doses and dosage forms that were not studied in the efficacy trial.
- Case study 4: Modeling and simulation providing the rationale, i.e., generated a hypothesis, for pursuing the high-dose strategy and designing a study to test the efficacy differentiation hypothesis that might not have otherwise been considered. The M and S strategy allowed progress to be made in understanding PK/PD relationships without having to wait for an improved solid dosage form to be developed, a time saving of approximately 9 months. Models that allowed predictions of clinically meaningful and statistically familiar end points were critical to gaining support to further invest in a study to evaluate the full potential of the molecule.

It must be mentioned, however, that these examples do not fully reflect the length and breadth of basic/fundamental pharmacometric research and application already demonstrated in the areas of systems biology, systems pharmacology, newer statistical methods as well as other types of applications to improve decision making in drug discovery and development (Table 16.3). The presented examples can be seen as defining the core pharmacometric activities that need to become standardized and "industrialized" so that resources can be better spent on the next frontiers of model-based development, such as characterization of drug target properties, better translation of drug attributes from preclinical to clinical space, and pharmacoeconomics.

Table 16.3 Overview of pharmacometric endeavors in inflammatory diseases

Drug	End point/disease	Model	Application(s)	Reference
Canakinumab	ACR20/RA	Longitudinal model-based meta-analysis (MBMA) model	Decision to terminate development Decision to terminate clinical development of canakinumab for the treatment of rheumatoid arthritis	Demin et al. (2012)
Biologics disease modifying anti-rheumatic drugs (DMARDs)	ACR20/RA	MBMA model	Indirect comparison of efficacy due to limited number of head-to-head trials Differences in efficacy and differential impact of dose titration were evaluated	Mandema et al. (2011)
Inhaled corticosteroids	Cortisol suppression/asthma and other conditions	Simulation using IDR model	Excel-based algorithm based on a PK/PD model to quantify and predict cumulative cortisol suppression for a variety of corticosteroids	Krishnaswami et al. (2000)
Ciclesonide and fluticasone propionate	Cortisol suppression/asthma and other conditions	Population PK/PD, IDR model	Characterization and model-based comparison of PK/PD properties of two compounds	Xu et al. (2010)
Prednisolone	PK/many conditions	Semi-mechanistic PK/PD model	Combines PK models for free prednisone and prednisolone, linear release PD model for cortisol suppression, and competitive protein binding between cortisol and prednisolone to predict total prednisolone concentrations in plasma	Xu et al. (2007)
Budesonide	Total lymphocyte and subsets and cortisol levels/asthma	IDR model with circadian rhythm	To evaluate the effect on the lymphocyte subsets relative to the effect on total lymphocytes To characterize cortisol suppression as a more sensitive marker for the systemic effect of corticosteroids	Stark et al. (2006)

Table 16.3 (continued)

Drug	End point/disease	Model	Application(s)	Reference
Certolizumab	ACR20/RA	Markov mixed-effects model	Accounts for potential serial correlation in ACR response to allow for more realistic simulations of the time course of ACR20 response	Lacroix et al. (2009)
SC-75416	Pain relief/post-oral surgery pain	PK/PD and dropout (survival) models	Provided increased confidence to pursue high-dose strategy and to test the efficacy differentiation hypothesis in a clinical trial	Kowalski et al. (2008)
Inhaled PF-00610355	Forced expiratory volume in one second (FEV1)/chronic obstructive pulmonary disease (COPD)	Longitudinal dose–response models	To characterize the dose–response relationship between two inhaled long-acting beta agonists (PF-00610355 and salmeterol) and FEV1 in order to inform dosing recommendations for future clinical trials in patients with COPD	Nielsen et al. (2012)
Tofacitinib	Health assessment questionaire (HAQ)/RA	Longitudinal dose-response model	To implement transformations of continuous bounded outcomes data A transformation strategy with a likelihood component for censoring was developed to promote the simplicity of model structures and to improve the plausibility of assumptions on the random effects	Hutmacher et al. (2011)
Celecoxib	JRA-30 definition of improvement/JRA	Mixed-effects logistic regression model	To derive dosing recommendations for the use of celecoxib in patients with juvenile rheumatoid arthritis (JRA) using PK and exposure response data	Krishnaswami et al. (2012)
Tofacitinib	ACR20/RA	Indirect latent variable response model	First application of an unobservable latent variable model, through which indirect response models can be linked with drug exposure	Hutmacher et al. (2008)

Table 16.3 (continued)

Drug	End point/disease	Model	Application(s)	Reference
Golimumab	ACR20,50,70/RA	Indirect latent variable response model	To characterize dose response using latent variable longitudinal dose response model	Hu et al. (2013)
Ciclosporine	Acute rejection/transplant	Time to event model	Describe acute rejections in pediatric renal transplant recipients treated with Ciclosporin A Optimize dose tapering	Frobel et al. (2013)
AZD-9773	Serum TNF-α/RA	IDR model	To simulate dosing options for a phase 2b study	Yates et al. (2012)
Anakinra	CIA rat model/RA	PK/PD/Disease progression	To characterize the effects of anakinra in collagen-induced arthritic (CIA) rats and explore the role of interleukin-1β (IL-1β) in rheumatoid arthritis	Liu et al. (2011)
Tocilizumab	DAS-28/RA	IDR model	Tocilizumab 8 mg/kg is more effective than 4 mg/kg in reducing disease activity	Levi et al. (2012)
RA therapies	ACR20/RA	Physiolab model platform	Deterministic simulation model to characterize life cycle of inflammatory cells, endothelium, synovial fibroblasts and chondrocytes and identify critical pathways (e.g., IL-12 and IL-15) to drive predicted disease outcome	Struemper et al. (2008)
Bone resorptive therapies	Multiple inputs, including active osteoblasts and active osteoclasts/osteoporosis and other skeletal diseases	Bone–cell interaction model/ Bone remodeling model/ RANK RANKL-OPG pathway model	To determine and evaluate potential therapies based on their efficacy using a small systems model that describes bone formation and resorption, providing insight that future models could be based on	Lemaire et al. (2004)

Table 16.3 (continued)

Drug	End point/disease	Model	Application(s)	Reference
Denosumab	NTX (a bone resorption biomarker) levels/multiple myeloma	PK/PD model using cellular bone homeostasis	To apply a cellular bone homeostasis model (a modification of the Lemaire model) to characterize the PD of denosumab in MM patients	Marathe et al. (2008)
Denosumab/Ibandronate	Levels NTX/CTX (bone resorption biomarkers) and lumbar BMD/osteoporosis	PK/PD model using cellular bone homeostasis	To characterize the PD properties of denosumab, and of ibandronate, using an integrated bone homeostasismodel in postmenopausal women To characterize the effects of these drugs on Lumbar BMD using a bone turnover model, thus providing clinical relevance	Marathe et al. (2011)
Denosumab	Multiple inputs, including active osteoblasts and active osteoclasts/various physiological and pathophysiological conditions re-bone remodeling such as osteoporosis	Reduced version of the Lemaire RANK RANKL-OPG pathway model	The conceptual bone cell interaction model by Lemaire could be reduced from a three- to a two-dimensional system. Reducing the model's complexity allowed for a transparent discussion of its dynamics and also opened the way for a geometric, two-dimensional analysis To show that on a time scale of disease progression and therapeutic intervention, the original Lemaire models and the simpler "reduced" models were found suitable for characterization of the end points tested with negligible differences in their dynamic properties	Schmidt et al. (2011)

References

Demin I, Hamrén B, Luttringer O, Pillai G, Jung T (2012) Longitudinal model-based meta-analysis in rheumatoid arthritis: an application toward model-based drug development. Clin Pharmacol Ther 92(3):352–359. doi:10.1038/clpt.2012.69. Epub 2012 Jul 4

Fleischmann R et al (2012) Phase IIb dose-ranging study of the oral JAK inhibitor tofacitinib (CP-690,550) or adalimumab monotherapy versus placebo in patients with active rheumatoid arthritis with an inadequate response to disease-modifying antirheumatic drugs. Arthritis Rheum 64:617–629

Foeldvari I, Szer IS, Zemel LS et al (2009) A prospective study comparing celecoxib with naproxen in children with juvenile rheumatoid arthritis. J Rheumatol 36(1):174–182

Frobel AK, Karlsson MO, Backman JT, Hoppu K, Qvist E, Seikku P, Jalanko H, Holmberg C, Keizer RJ, Fanta S, Jönsson S (2013) A time-to-event model for acute rejections in paediatric renal transplant recipients treated with ciclosporin A. Br J Clin Pharmacol 76:603–615

Gierse J, Kurumbail R, Walker M et al (2002) Mechanism of inhibition of novel COX-2 inhibitors. Adv Exp Med Biol 507:365–369

Gupta P, Friberg LE, Karlsson MO, Krishnaswami S, French JA (2010) A semimechanistic model of CP-690,550-induced reduction in neutrophil counts in patients with rheumatoid arthritis. J Clin Pharmacol 50:679–687

Hu C, Xu Z, Mendelsohn AM, Zhou H (2013, Feb) Latent variable indirect response modeling of categorical endpoints representing change from baseline. J Pharmacokinet Pharmacodyn 40(1):81–91

Hutmacher MM, Krishnaswami S, Kowalski KG (2008) Exposure-response modeling using latent variables for the efficacy of a JAK3 inhibitor administered to rheumatoid arthritis patients. J Pharmacokinet Pharmacodyn 35:139–157

Hutmacher MM, French JL, Krishnaswami S, Menon S (2011) Estimating transformations for repeated measures modeling of continuous bounded outcome data. Stat Med 30(9):935–949

Kowalski KG, Olson S, Remmers AE, Hutmacher MM (2008) Modeling and simulation to support dose selection and clinical development of SC-75416, a selective COX-2 inhibitor for the treatment of acute and chronic pain. Clin Pharmacol Ther 83(6):857–866

Kremer JM et al (2009) The safety and efficacy of a JAK inhibitor in patients with active rheumatoid arthritis: results of a double-blind, placebo-controlled phase IIa trial of three dosage levels of CP-690,550 versus placebo. Arthritis Rheum 60:1895–1905

Kremer JM et al (2012) A phase IIb dose-ranging study of the oral JAK inhibitor tofacitinib (CP-690,550) versus placebo in combination with background methotrexate in patients with active rheumatoid arthritis and an inadequate response to methotrexate alone. Arthritis Rheum 64:970–981

Krishnaswami S, Hochhaus G, Derendorf H (2000) An interactive algorithm for the assessment of cumulative cortisol suppression during inhaled corticosteroid therapy. AAPS PharmSci 2(3):E22

Krishnaswami S et al (2009) Modeling and clinical trial simulation to design a dose ranging study for CP-690,550 in rheumatoid arthritis patients. Clin Pharmacol Ther 85(1):PII–78

Krishnaswami S, Hutmacher MM, Robbins JL, Bello A, West C, Bloom BJ (2012) Dosing celecoxib in pediatric patients with juvenile rheumatoid arthritis. J Clin Pharmacol 52(8):1134–1149

Lacroix BD, Lovern MR, Stockis A, Sargentini-Maier ML, Karlsson MO, Friberg LE (2009) A pharmacodynamic Markov mixed-effects model for determining the effect of exposure to certolizumab pegol on the ACR20 score in patients with rheumatoid arthritis. Clin Pharmacol Ther 86(4):387–395

Lemaire V, Tobin FL, Greller LD, Cho CR, Suva LJ (2004) Modeling the interactions between osteoblast and osteoclast activities in bone remodeling. J Theor Biol 229(3):293–309

Levi M, Grange S, Frey N (2012, Feb 14) Exposure–response relationship of tocilizumab, an anti-IL-6 receptor monoclonal antibody, in a large population of patients with rheumatoid arthritis. J Clin Pharmacol 53:151–159

List of inflammatory diseases (2013). http://www.progesteronetherapy.com/list-of-inflammatory-diseases.html#ixzz2QcK2V4Ap. Accessed 4 June 2013

Liu D, Lon HK, Dubois DC, Almon RR, Jusko WJ (2011) Population pharmacokinetic-pharmacodynamic-disease progression model for effects of anakinra in Lewis rats with collagen-induced arthritis. J Pharmacokinet Pharmacodyn 38(6):769–786

Lon HK, Liu D, Jusko WJ (2012) Pharmacokinetic/pharmacodynamic modeling in inflammation. Crit Rev Biomed Eng 40(4):295–312. Review

Mandema JW, Stanski DR (1996). Population pharmacodynamic model for ketorolac analgesia. Clin Pharmacol Ther 60:619–635

Mandema JW, Salinger DH, Baumgartner SW, Gibbs MA (2011) A dose–response meta-analysis for quantifying relative efficacy of biologics in rheumatoid arthritis. Clin Pharmacol Ther 90(6):828–835

Marathe A, Peterson MC, Mager DE (2008) Integrated cellular bone homeostasis model for denosumab pharmacodynamics in multiple myeloma patients. J Pharmacol Exp Ther 326(2):555–562

Marathe DD, Marathe A, Mager DE (2011) Integrated model for denosumab and ibandronate pharmacodynamics in postmenopausal women. Biopharm Drug Dispos 32(8):471–481

McDevitt H et al (2009) Infrastructure development for building, maintaining and modeling indication-specific summary-level literature databases to support model-based drug development. PAGE Meeting 18, Abstr 1455

McInnes IB, Schett G (2011) The pathogenesis of rheumatoid arthritis. N Engl J Med 365(23):2205–2219

Milligan PA, Brown MJ, Marchant B, Martin SW, van der Graaf PH, Benson N, Nucci G, Nichols DJ, Boyd RA, Mandema JW, Krishnaswami S, Zwillich S, Gruben D, Anziano RJ, Stock TC, Lalonde R (2013) Model-based drug development: a rational approach to efficiently accelerate drug development. Clin Pharmacol Ther 93(6):502–514

Nielsen JC, Hutmacher MM, Cleton A, Martin SW, Ribbing J (2012) Longitudinal FEV1 dose-response model for inhaled PF-00610355 and salmeterol in patients with chronic obstructive pulmonary disease. J Pharmacokinet Pharmacodyn 39(6):619–634

Peterson MC, Riggs MM (2010) A physiologically based mathematical model of integrated calcium homeostasis and bone remodeling. Bone 46(1):49–63

Rullmann JAC, Meeuwisse CM, Struemper H, Defranoux NA, van Elsas A (2005) Systems biology for battling rheumatoid arthritis: application of the Entelos PhysioLab platform. IEE Proc Syst Biol 152(4):256–262

Schiff M et al (2008) Efficacy and safety of abatacept or infliximab vs placebo in ATTEST: a phase III, multi-centre, randomised, double-blind, placebo-controlled study in patients with rheumatoid arthritis and an inadequate response to methotrexate. Ann Rheum Dis 67:1096–1103

Schmidt S, Post TM, Peletier LA, Boroujerdi MA, Danhof M (2011) Coping with time scales in disease systems analysis: application to bone remodeling. J Pharmacokinet Pharmacodyn 38(6):873–900

Schmith VD, Foss JF (2010) Inflammation: planning for a source of pharmacokinetic/pharmacodynamic variability in translational studies. Clin Pharmacol Ther 87(4):488–491

Sheiner LB (1994) A new approach to the analysis of analgesic trials, illustrated with bromfenac data. Clin Pharmacol Ther 56:309–322

Sheiner LB (1997) Learning versus confirming in clinical drug development. Clin Pharmacol Ther 61:275–291

Sheiner LB, Beal SL, Dunne A (1997) Analysis of nonrandomly censored ordered categorical longitudinal data from analgesic trials. J Am Stat Assoc 92:1235–1244

Shi J, Kovacs SJ, Wang Y et al (2005) Population pharmacokinetics of the active metabolite of leflunomide in pediatric subjects with polyarticular course juvenile rheumatoid arthritis. J Pharmacokinet Pharmacodyn 32(3–4):419–439

Smolen JS, Aletaha D, Bijlsma JW, Breedveld FC, Boumpas D, Burmester G, Combe B, Cutolo M, de Wit M, Dougados M, Emery P, Gibofsky A, Gomez-Reino JJ, Haraoui B, Kalden J, Keystone EC, Kvien TK, McInnes I, Martin-Mola E, Montecucco C, Schoels M, van der Heijde D, T2T Expert Committee (2010) Treating rheumatoid arthritis to target: recommendations of an international task force. Ann Rheum Dis 69(4):631–637

Stark JG, Werner S, Homrighausen S, Tang Y, Krieg M, Derendorf H, Moellmann H, Hochhaus G (2006) Pharmacokinetic/pharmacodynamic modeling of total lymphocytes and selected subtypes after oral budesonide. J Pharmacokinet Pharmacodyn 33(4):441–459

Struemper H, Ramanujan S, Shoda LKM, Söderström K, Defranoux NA (2008) Using biosimulation to identify a biological basis for poor response to TNF-α neutralizing therapies Entelos Inc. http://wan253-192.ippl.jhu.edu/courses/540.409/docs/lit/Entelos.pdf. Accessed 11 Sept 2014

Tan H, Gruben D, French J, Thomas N (2011) A case study of model-based Bayesian dose response estimation. Stat Med 30:2622–2633

Tofacitinib Arthritis Advisory Committee Meeting (2012) FDA Advisory Committee. Washington, DC. http://www.fda.gov/downloads/AdvisoryCommittees/CommitteesMeetingMaterials/Drugs/ArthritisAdvisoryCommittee/UCM304200.pdf. Accessed 11 Sept 2014

van Vollenhoven RF, Fleischmann R, Cohen S, Lee EB, García Meijide JA, Wagner S, Forejtova S, Zwillich SH, Gruben D, Koncz T, Wallenstein GV, Krishnaswami S, Bradley JD, Wilkinson B, ORAL Standard Investigators (2012a) Tofacitinib or adalimumab versus placebo in rheumatoid arthritis. N Engl J Med 367(6):508–519

Xu J, Winkler J, Derendorf H (2007) A pharmacokinetic/pharmacodynamic approach to predict total prednisolone concentrations in human plasma. J Pharmacokinet Pharmacodyn 34(3):355–372

Xu J, Nave R, Lahu G, Derom E, Derendorf H (2010) Population pharmacokinetics and pharmacodynamics of inhaled ciclesonide and fluticasone propionate in patients with persistent asthma. J Clin Pharmacol 50(10):1118–1127

Yates JW, Das S, Mainwaring G, Kemp J (2012) Population pharmacokinetic/pharmacodynamic modelling of the anti-TNF-α polyclonal fragment antibody AZD9773 in patients with severe sepsis. J Pharmacokinet Pharmacodyn 39(6):591–599

Zhang Y, Wang D, Tan S, Xu H, Liu C, Lin N (2013) A systems biology-based investigation into the pharmacological mechanisms of wu tou tang acting on rheumatoid arthritis by integrating network analysis. Evid-based Complement Altern Med 2013:Article ID 548498

Chapter 17
Pharmacometrics in Dermatology

Vivek S. Purohit, Manisha Lamba and Pankaj Gupta

17.1 Introduction

There is a paucity of published literature on the application of pharmacometrics methods in dermatologic drug development. This can be attributed to unique challenges associated with development of new agents in this disease area as described in a review by Eaglstein et al. (2009). The market for drugs for dermatologic conditions is relatively small as compared to that for other therapeutic areas such as heart disease, neurological conditions, or cancer thus reducing the economic incentive to develop these drugs. The endpoints for assessing efficacy have a considerable subjective element involved in their quantitation. Topical agents still play a significant role in the treatment of skin diseases; newer systemic medications are usually developed after the drug has been approved for another indication that shares the underlying pathophysiology with the skin condition. This has been the case in the inflammation disease area where some of the drugs approved for the treatment of rheumatoid arthritis have been successfully developed further for the treatment of plaque psoriasis.

It can therefore be surmised that potential for pharmacometric applications in dermatology remains largely unappreciated. The commonly held belief is that there are limited opportunities to utilize model-based methods in development of dermatologic agents. Nevertheless, there are a few noteworthy examples which clearly showcase the value these methodologies bring towards optimizing the clinical development strategy and facilitating decision making. The ensuing sections will acquaint the reader with examples where quantitative methods have been successfully employed to streamline dermatologic drug development.

V. S. Purohit (✉) · P. Gupta · M. Lamba
Department of Clinical Pharmacology, Global Innovative Pharma Business,
Pfizer, Groton, CT, USA
e-mail: Pankaj.Gupta@pfizer.com

S. Schmidt, H. Derendorf (eds.), *Applied Pharmacometrics,* AAPS Advances
in the Pharmaceutical Sciences Series 14, DOI 10.1007/978-1-4939-1304-6_17

17.2 Pharmacometrics in Early Drug Development

In early stages of development, availability of richer pharmacokinetic (PK) data, biomarkers, and short-term efficacy data, allow the use of mechanistic pharmacokinetic–pharmacodynamic (PK–PD) models to characterize relationships between exposure and response variables. Such quantitative approaches can be effectively employed to establish a minimum effective dose, identify an optimal dose range, and inform futures study design. The ultimate goal at this milestone is to gain a sufficient understanding of the safety and efficacy characteristics of the drug candidate to increase the likelihood of success and minimize the chance of adverse events in the next stage in development.

17.2.1 PK–PD Targets for Antibacterial Drug Development

Infectious disease is not a disease area that one typically associates with dermatology. However, infections of skin, such as complicated skin and skin structure infections (cSSSIs) and impetigo, are very common. These infections caused by gram-positive or gram-negative pathogens can be minor in nature which can be treated with topical antibacterial products, or can be serious requiring systemic antibacterials and hospitalization. The general paradigm followed for antibacterials during early clinical development involves evaluating the PK–PD of candidates in preclinical infection models (animal (Ambrose et al. 2007) or hollow-fiber models (MacGowan et al. 2001)) where PK–PD targets or clinically meaningful thresholds are identified. The main objective of these experiments is to identify the optimal antimicrobial plasma concentration–effect curve that will provide the desired efficacy. The PD parameters usually investigated in these preclinical models are the area under the curve (AUC)/minimum inhibitory concentration (MIC), maximum plasma concentration (C_{max})/MIC and $T>$MIC (i.e., time that the serum concentrations remain above MIC; Ambrose et al. 2007). These evaluations are typically based on free drug exposures and not total exposures. Use of total exposures is usually employed for drugs which do not exhibit cross-species differences in protein binding.

Dose fractionation studies in the preclinical infection models allow for identification of the PD parameter that is best associated with the antimicrobial effect (Ambrose et al. 2007). For β-lactams (penicillins, cephalosporins, carbapenems, monobactams), $fT>$MIC has been identified as the PD parameter. For drugs like vancomycin, azithromycin, clarithromycin, linezolid, doxycycline, and tigecycline $f\text{AUC}_{0\text{-}24}$: MIC is the PD parameter. Daptomycin has both $f\text{AUC}_{0\text{-}24}$: MIC and C_{max}: MIC as PD parameter. Daptomycin is given once daily (QD) and thus $\text{AUC}_{0\text{–}24}$ and C_{max} are highly correlated, which may explain lack of differentiation between the two PD parameters.

This PD parameter is then used to define the PD threshold based on criteria such as achieving bacteriostasis or achieving at least 1-log kill. Selection of these criteria is beyond the scope of this discussion and the reader is referred to the literature for further details (MacGowan et al. 2001). Defining the PD parameters may not

Table 17.1 PD targets for evernimicin. (Adapted from Drusano et al. 2001)

Organism	AUC/MIC ratio		
	Stasis target	Log drop target[a]	90% E_{max} target
Streptococcus pneumoniae	115.7	239.4	1716.4
Staphylococcus aureus	163.4	330.1	830.8
Enterococcus faecalis	59.6	85.4	764.4

Protein binding was identical between the animal species and humans. Hence, no correction was made to the PD targets

[a] Log drop targets were 3-$\log_{10}$ unit decline for *S. pneumoniae*, 2-$\log_{10}$ unit decline for *S. aureus* and 1-$\log_{10}$ unit decline for *E. faecalis*

always be simple, especially when more than one PD parameter is associated with antimicrobial effect; more mechanistic PK–PD models may be needed to characterize the PK–PD relationships in such cases.

The PD threshold thus identified provides the dosing rationale for the design of the clinical studies. Dose selection can be based on the ability of the doses to meet the PD threshold in a target number (percent) of patients. The latter can provide the basis of conducting a dose-ranging evaluation; for instance, clinical trial simulations (CTS) based on the PK–PD model can predict the dose range that would meet the PD criteria in 80–100% of the patients to maintain maximal efficacy. Such a simulation approach has been successfully applied to several antibacterial agents for selection of doses in phase 2.

An example illustrating the application of the above approach for evernimicin was reported by Drusano et al. (2001). MIC distribution of clinical isolates, PD targets identified in animal models of infection and protein-binding characteristics of the drug were used in conjunction with the population PK model for rational dose selection for phase-2/3 trials. The PD targets (Table 17.1) were identified for three different organisms in a neutropenic mice thigh infection model.

The population PK model developed using the data from phase-1 studies in healthy volunteers was used to perform Monte Carlo simulations to obtain exposures (AUC) in subjects at each dose. The simulated exposures were then used to calculate the fraction of subjects who met the PD targets listed in Table 17.2 at each MIC; the overall response for the pathogens was calculated at a given dose using the frequency of a given MIC in the MIC distribution.

Based on the above results it is clear that a dose of 6 mg/kg would achieve stasis for all organisms given the MIC distribution typically observed. However, for enterococci, a 9 mg/kg dose would be advantageous when maximal effect is desirable.

The above strategy can be used to select doses for new candidate molecules for conducting phase–2 trials using preclinical and healthy subjects' data.

17.2.2 Target Site PK–PD

An important consideration for drugs for dermatological indications is to understand the link between local drug exposure and clinical outcome. For example, in

Table 17.2 Target achievement for evernimicin. (Adapted from Drusano et al. 2001)

Dose (mg/kg/day)	% Attainment of response (±SD)								
	Streptococcus pneumoniae			*Staphylococcus aureus*			*Enterococcus faecalis*		
	Stasis	Log drop (3 $\log_{10}$ units)	90% E_{max}	Stasis	Log drop (2 $\log_{10}$ units)	90% E_{max}	Stasis	Log drop (1 $\log_{10}$ units)	90% E_{max}
6	100	99.9	95.87	91.64	71.79	34.25	99.7	99.41	58.14
	±0.0	±0.009	±0.07	±0.2	±1.89	±0.68	±0.11	±0.11	±2.82
9	100	100	97.71	96.83	85.10	50.74	99.93	99.93	74.84
	±0.0	±0.0	±0.02	±0.08	±0.84	±0.84	±0.004	±0.004	±0.59

the case of antibacterials that treat skin infections, ability to achieve target concentrations in the skin is the key to efficacy. The PD parameters established for a candidate molecule as discussed above usually relate plasma/serum concentrations to antibacterial activity. For this correlation to be valid, it is important to establish that the ratio of drug exposure in the skin to that in serum/plasma approaches 1. The above-mentioned consideration regarding correlation between dermal availability and clinical outcome is particularly important for topically applied agents. McClain et al. (2009) evaluated cutaneous exposures of topical corticosteroids relative to that achieved by oral prednisone and concluded that their skin concentration correlated well with their efficacy.

Both local drug concentrations and the impact on disease-related biomarkers can provide valuable understanding regarding the mechanism of action as well as the exposure–response (ER) relationship in the skin. The success of this endeavor depends on quantifying concentrations in the relevant skin compartment. This is a challenging task owing to factors such as availability of a sensitive analytical method, sampling considerations and invasiveness of sampling methods, physiochemical properties of the drug, and robustness of the PD markers/biomarkers.

Dermal microdialysis is a useful minimally invasive sampling technique, which can be used to determine drug levels in the extravascular fluid in the skin. Microdialysis involves the use of a probe (a small semipermeable hollow fiber membrane) that can be inserted into tissue and perfused with a physiological solution at a constant rate. Free, unbound solutes can freely cross the membrane by passive diffusion due to a concentration gradient and can be used to sample the extravascular space continuously. The biggest advantage of this technique is the ability to measure unbound drug concentrations in the target tissue thus providing a direct correlation between the exposure driver at the site of action and the associated response. An exception to the above would be drugs which act intracellularly. The technique can be applied to both exogenous and endogenous agents in the extracellular space. For instance, microdialysis has been used to measure the baseline levels of cytokines in psoriatic plaques (IL-2, IL-6, IL-18, IL 23) and changes induced by treatment with fumaric acid derivatives (Salgo et al. 2011). However, the approach has operational limitations and may not work well for lipophilic, protein-bound, and high molecular weight drugs due to poor recoveries. A very sensitive assay capable of detecting low free drug concentrations may overcome this limitation. More recently, novel membrane-free probes and wearable multichannel pumps have overcome these limitations and have been used for prolonged sampling of lipophilic molecules in psoriatic lesional skin (Bodenlenz et al. 2012).

17.3 Population Pharmacokinetics (PK)

Collection of sparse PK samples in patients in outpatient clinical studies enables characterization of PK properties in the target population. PK analysis using a population-based approach provides an understanding of patient-specific charac-

teristic that may impact exposure and helps in deriving dosing recommendations in conjunction with exposure response (ER) analyses. Development of a population PK model also allows for simulation of different dosing regimens that can be subsequently tested in a clinical study. The typical approach for conducting population PK analyses is as follows:

- Develop a structural model that allows elucidation of concentration-time profile of the drug in the patient population.
- Incorporate random effects on structural model parameters that describe between patient/subject variability (also termed as interindividual variability), interoccasion variability, and residual variability.
- Develop a covariate model from the list of plausible patient-specific characteristics that may help explain some of the random variability in structural model parameters.

Population PK analyses for dermatologic compounds have primarily been reported in the psoriasis disease area. Plaque psoriasis is a chronic inflammatory skin disease driven by dysregulation in the immune system (Nestle et al. 2009). Cellular proliferation due to interplay of cytokines ultimately results in skin lesion formation, characterized by red, scaly, raised plaques. While no cure for psoriasis exists, symptomatic management can be achieved by therapies such as topical agents, phototherapy, systemic immunosuppressants as well as biologics. Among these, biologics have emerged as the most promising treatment options in reducing the burden of disease. These agents target cytokines such as IL-12 and IL-23 (ustekinumab), or tumor necrosis factor (TNF; etanercept, adalimumab, and infliximab). Another previously approved biologic that targets T-cells (efalizumab) has been withdrawn from the market.

The PK characteristics of biologics differ from conventional small molecules due to their unique disposition characteristics; receptor mediated clearance may lead to nonlinear PK depending on the concentration range studied. Adalimumab and infliximab are known to exhibit nonlinear PK characteristics (Nestorov 2005). However, discerning such PK attributes is usually difficult from outpatient data where factors such as the dose range studied, time points for PK sampling, and sparseness of collected data may limit the exploration of complex mechanism-based models. In such instances, a simple model may be deemed sufficient and practical to pursue future work. This is clearly evident from the example by (Nestorov et al. 2004) where a stepwise time function was modeled for apparent clearance (CL/F) and apparent volume (V/F) after attempts to fit a continuous sigmoidal function were unsuccessful for etanercept. The CL/F was found to be approximately 80 % of the steady state value before week 8 of dosing, thereafter it peaked to approximately 120 % between weeks 4 and 8 and then gradually tapered down to achieve steady state values after week 8. These time effects on clearance were postulated to be arising from the redistribution of etanercept and TNF-binding sites between the blood and the poorly perfused skin compartment (site of action).

Across the various biologic therapies, effect of body size measures such as body weight or body mass index (BMI), as clinically important determinants of drug

clearance has consistently been reported. For instance, ustekinumab exhibits a 57 % and 37 % higher CL/F and V/F, respectively, in patients weighing greater than 100 kg compared to those who weigh less than 100 kg (Zhu et al. 2009). Similarly for efalizumab, patients weighing 137 and 57 kg had a 37 % higher and 30 % lower CL/F, respectively, compared to the typical population value of 1.29 L/day (Sun et al. 2005). Such assessments are particularly relevant in psoriasis patients since they tend to have higher body weights compared to the general population. Consequently, these results can lead to clinically important implications with respect to dosing adjustments based on body size considerations. The weight-based dosing recommendations for ustekinumab were supported by the magnitude of PK change in the proposed dosing cohorts (Lebwohl et al. 2010). This example is described in detail in the next section.

Once the population PK model is finalized, it can be further used to simulate PK data under alternate dosing regimens. Such an evaluation can enable extrapolation across different dosing scenarios and provide the rationale for supporting dose modification or even a new regimen. This can be evidenced from an example by Nestorov et al. (2004), who conducted a modeling and simulation exercise to support a novel dosing regimen for etanercept. Data from three clinical studies with doses of 25 mg QW (once weekly), 25 mg BIW (twice a week), and 50 mg BIW, were used to develop a population PK model. The model included covariate effects on CL/F (gender, weight, and time) and V/F (weight). This model was used to simulate concentration–time profiles for after a new regimen involving the administration of 50 mg once a week (50 QW). The simulated steady state concentrations for this regimen demonstrated concordance with the observed profiles for 25 mg BIW. Additionally, the simulations were in good agreement with additional PK data from 84 patients receiving 50 mg QW, which provided external validation for the model. Based on these results, it was concluded that the concentration–time profile arising from 50 mg QW could be predicted with high precision; the overlap with 25 mg BIW suggested high probability of achieving consistent efficacy and safety between the two regimens.

17.4 Exposure Response (ER) Relationships

An understanding of the relationship between drug exposure (dose or summary PK measures, such as C_{max}, C_{min}, C_{avg}) and response (efficacy and safety) is critical to establishing the benefit–risk profile of a drug candidate. The food and drug administration (FDA) guidance on ER relationships (FDA 2003) highlights the utility of characterizing these relationships in drug development and also illustrates how this knowledge can facilitate regulatory decision making. ER relationships can provide support for primary evidence of efficacy or safety; they can also support benefit–risk evaluation in subpopulations or dosing adjustments (including regimens, formulations, route of administration). Characterizing ER has proven valuable in the development of new therapies in the psoriasis disease area.

17.4.1 Using ER to Understand the Impact of Patient Specific Factors on Efficacy of Psoriasis Drugs

ER assessment for psoriasis drugs has typically aimed at establishing a relationship between the measure of disease severity termed as psoriasis area and severity index (PASI) and drug exposure in patients with moderate to severe plaque psoriasis. PASI scores reflect a weighted average calculated from severity and area of psoriatic plaques. In clinical studies for psoriasis, the primary endpoint is the proportion of patients achieving $\geq 75\%$ improvement in PASI score from baseline, which is referred to as PASI 75 response. The section below presents examples where ER relationships for PASI endpoints for two approved biologics and one small molecule in development provided valuable insights into the interpretation of the efficacy profile along with elaboration of key determinants of efficacy.

Hutmacher et al. (2007) developed a population ER model for PASI 75 for etanercept with pooled data from three randomized, placebo-controlled clinical trials using a sequential PK–PD analysis approach. Predicted cumulative AUC (PCAUC) derived using the post hoc parameters from the final PK model was deemed as the most suitable exposure measure (compared to cumulative dose or predicted through concentrations) to evaluate the ER relationship. The mixed effects logistic regression model for PASI 75 is given by the following equation:

$$\text{Logit}\left[\text{P}(\text{event}=1)\right] = \textit{Intercept} + \textit{placebo time effect} + \textit{drug effect},$$

where intercept reflects the baseline probability; placebo time effect is given by the product (slope*time) and drug effect is given by the following model:

$$\text{drug effect} = E_{\max} * \frac{(\text{PCAUC}^{*})^{\gamma}}{\text{EC50}^{\gamma} + \text{PCAUC}^{*\gamma}}.$$

In the above equation, $E_{\max}$ is the maximum drug effect, EC50 is the exposure that achieves 50% of the maximum drug effect, γ is the hill coefficient, and PCAUC* is an apparent exposure expressed as PCAUC (1-exp(-keot)) to capture the delay between drug exposure and effect (characterized by rate constant keo). It should be noted that the placebo model has limited interpretation due to its simple structure, i.e., linearity with time.

Interpatient variability was allowed to change with time in the model. The final model included race and sex effects on the intercept, baseline PASI and prior systemic/phototherapy on $E_{\max}$, an age effect on keo and a weight effect on EC50. The analysis predicted a 130% increase in EC50 for a twofold weight change. Despite the variable selection algorithms selecting the weight effect on EC50, inspection of the results indicated that the model could not ascertain effectively whether difference in potency (EC50) or temporal delay (keo) was accounting for the observed weight-based trend in the data. Ultimately, it was concluded using other analyses that dose adjustment was not warranted for any subgroup of patients.

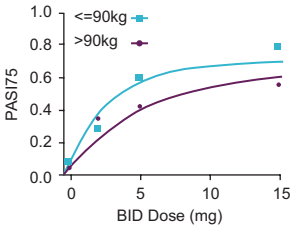

Fig. 17.1 Observed and model-predicted PASI 75 by median weight at week 12 for tofacitinib. Observed data are represented by *symbols* and model predictions by *solid lines*; data from a phase 2b dose-ranging study of tofacitinib in patients with moderate to severe chronic plaque psoriasis. (Adapted from Gupta et al. 2011)

A similar weight-based phenomenon was observed for tofacitinib an investigational psoriasis drug, in a 12-week phase 2b dose-ranging study (placebo, 2, 5, and15 mg BID) in patients with moderate to severe chronic plaque psoriasis. Longitudinal ER modeling of PASI scores revealed body weight as being a significant covariate of drug effect. Weight was found to impact pharmacodynamic potency as well as the time delay rate constant in a modified indirect response model (Gupta et al. 2011). As was found with etanercept, the model could not explain whether dose adjustment or longer trial duration was required for the heavier subgroup to achieve the same level of response as their lighter counterparts. Figure 17.1 shows the predicted PASI 75 response rate for two weight cohorts stratified by median weight (90 kg) at week 12 (time for primary endpoint evaluation).

Given the small sample size and the uncertainty associated with the ER relationship, it was proposed to continue to explore 5 and 10 mg BID as a fixed dosing regimen for a longer duration (up to 52 weeks) in the phase 3 studies in psoriasis patients. It was anticipated that the large sample size in the phase 3 program would provide an adequate number of patients to detect any significant differences in efficacy over time with respect to weight.

Another example of a population-based exposure–PASI relationship was reported for the IgG1-based monoclonal antibody-ustekinumab (Zhou et al. 2010). Data from two phase-3 studies ($n=1312$) for psoriasis patients receiving 45 or 90 mg were used to develop an indirect response model. The model assumed the formation and remission rates of the psoriatic plaques to be zero order (kin) and first order (rate constant: kout), respectively. The drug effect inhibited the formation rate as shown below:

$$\frac{\mathrm{d}(\mathrm{PASI})}{\mathrm{dt}} = kin * (1 - drug\ effect - placebo\ effect) - kout * PASI$$

$$\text{drug effect} = E_{max} * \frac{\mathrm{Cp}}{\mathrm{IC50} + \mathrm{CP}}$$

$$\text{placebo effect} = plbmax * (1 - \exp(-keo * time))$$

$$kin = kout * baseline\ PASI.$$

E_{max}, IC50, and γ have their usual interpretations as described above; *C*p represents ustekinumab serum concentrations that were derived from the final PK model (one compartment model with first order absorption and elimination). Placebo effect also inhibited the formation rate. In the above equation, plbmax describes the steady state inhibition and keo is the rate constant governing the time course of placebo effect. Interpatient variability on PD parameters (kin, kout, and IC50) was assumed to follow a log normal distribution and a combination of proportional and additive errors was used to model the residual variability. The model provided adequate fits to the observed data and was deemed acceptable by the goodness of fit plots and simulation-based diagnostics. An exhaustive pool of covariates was evaluated following the base-full-final model approach. However, since the covariates in the full model could not account for interpatient variability in the PD parameters (283, 60, and 54%, for IC50, kin, and kout, respectively), they were not retained in the final model.

The authors noted that there was a significant overlap of exposures between patients less than 100 kg receiving 45 mg and those heavier than 100 kg receiving 90 mg. This observation had previously been applied to justify the two-tiered fixed dosing regimen for ustekinumab in psoriasis patients (Lebwohl et al. 2010). The authors in this manuscript reasoned that the 100-kg weight cut point was optimal since the changes in efficacy paralleled the changes in systemic exposure, i.e., the PASI 75 response rates among heavier patients receiving 90 mg (74%) and lighter patients receiving 45 mg (77%) were comparable. The proposed regimen was:

- For patients ≤100 kg, 45 mg initial dose (and 4 weeks later) and every 12 weeks thereafter
- For patients >100 kg, 90 mg initial dose (and 4 weeks later)and every 12 weeks thereafter

However, the US FDA disagreed with this assessment and opined to the Dermatologic and Ophthalmic Drugs Advisory Committee that the dosing regimen for ustekinumab was suboptimal in terms of benefit that it yielded to heavier weight patients (FDA 2008). The FDA based their recommendation on an exposure (AUC)–PASI relationship (Fig. 17.2) developed from the two studies mentioned above which revealed that instead of a two-tiered dosing approach the patients would stand to benefit more from an alternate three-tiered regimen (<60, ≥60–<90, and ≥90 kg) that could yield PASI response rates similar to those arising from the administration of 90 mg to all subjects. Table 17.3 shows the predicted response under the different dosing scenarios based on the exposure–PASI relationship. Table 17.3 illustrates the projected improvement in clinical outcome in heavier patients receiving the alternate regimen as proposed by the FDA.

This example clearly demonstrates the successful utilization of an ER relationship to assess the impact of a key patient-specific factor (body weight) on clinical response. The example further shows how the insights gained from the ER relationship can be used to recommend dosing modifications in patient subgroups that stand to benefit from an alternate regimen.

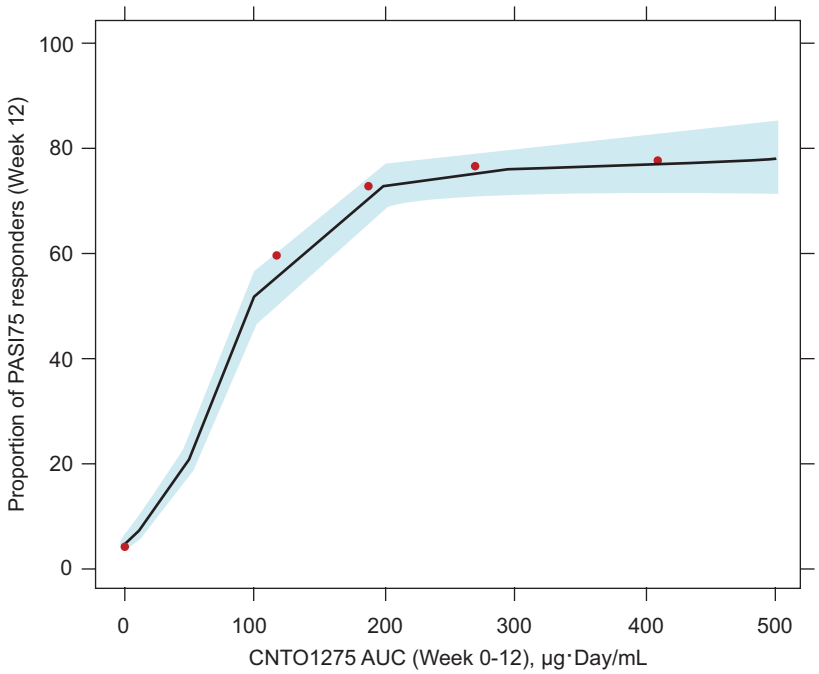

Fig. 17.2 Exposure (AUC)–response (PASI 75) relationship for ustekinumab at week 12. PASI 75 data as a function of exposure quantiles; observed (*symbols*) and predicted (*line*) medians with 95% CI (*shaded*). (Adapted from FDA 2008)

Table 17.3 Predicted response rates for ustekinumab under different dosing regimens based on the PASI75-ER model. (Adapted from FDA 2008)

Dosing strategy[a]	Dose	Proposing entity	PASI 75 response predicted from the ER model				
			Overall	By body weight quartiles			
				68 kg	84 kg	96 kg	117 kg
Two tiered	100 kg: 45 mg ≥100 kg: 90 mg	Sponsor	70	77	70	66	69
Three tiered	<60 kg: 45 mg ≥60 kg– 90 kg: 67.5 mg ≥90 kg: 90 mg	FDA	74	79	75	73	69

[a] ER model proposed by the FDA

17.4.2 Facilitating Decision Making Regarding Dose Progression to Phase 3

Pharmacometric methods can support different milestones during drug development to facilitate decision making with respect to trial design, go/no-go decisions, dose selection, and product positioning. The following section illustrates an

example where modeling and simulation were used to develop a probabilistic decision criterion for a safety laboratory endpoint to facilitate phase-3 dose selection for tofacitinib, a novel oral Janus kinase (JAK) inhibitor, currently in development for the treatment of autoimmune conditions such as psoriasis, ankylosing spondylitis, Crohn's disease, etc. Tofacitinib was recently approved for the treatment of adult patients with moderately to severely active rheumatoid arthritis (Xeljanz®).

This example is based on a 12-week phase 2b dose-ranging study evaluating tofacitinib placebo, 2, 5, and 15 mg BID in patients with moderate to severe chronic plaque psoriasis. Phase 3 dose selection was based on the probability of achieving a clinically meaningful target effect (PTE) for the selected laboratory safety and efficacy (data not shown) endpoints (Gupta et al. 2012). PTE calculation took into consideration the clinical meaningfulness of the target effect and the desired confidence in its magnitude as well as the uncertainty associated with the ER relationship(s). Doses were ranked for their performance on the PTE scale; doses achieving a 50% or higher probability were progressed for phase-3 evaluation.

Incidence of hemoglobin drop from baseline was regarded as a clinically relevant laboratory endpoint for model-based assessment. The target effect was set at a placebo-adjusted incidence rate of less than 5% for a hemoglobin change of >2 g/dL decrease from baseline through 12 weeks of treatment. The incidence of hemoglobin drop was predicted from a longitudinal, ER model for this endpoint (Gupta et al. 2012). Modeling hemoglobin levels as opposed to incidence rates offered several advantages: (a) Incidence rates were very small in the studied population and may not have allowed for dose interpolation and (b) characterizing the exposure- and time-dependent trajectories of hemoglobin levels in psoriasis patients offered greater flexibility in predicting the incidence for a trail design of interest.

An indirect response model (with stimulation of elimination (K_{out})) best described the hemoglobin time course across the studied doses. The model was used for predicting the incidence rate of >2 g/dL decrease in hemoglobin. The probability scale for the achievement of target effects was constructed and applied to identify an optimal dose range for phase-3 evaluation. Based on the PTE assessment, 5 and 10 mg BID were selected for phase 3 as they yielded PTE values of 100 and 87%, respectively (Fig. 17.3). This selection was also supported by efficacy considerations which have not been discussed here.

17.5 Integrating Knowledge from Different Sources

A very important component of pharmacometrics is integrating knowledge from other sources such as competitors and/or standard of care to inform strategy and support clinical decisions during a compound's development. Analyses of collective data across multiple studies for other drugs or therapies can provide a quantitative contextualization framework for benchmarking a compound's performance against existing treatment modalities. Prior data for the investigational drug can be used in conjunction with data available in the public domain (e.g., publications in

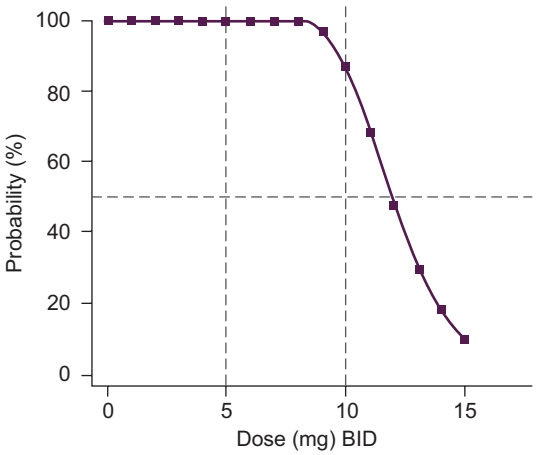

Fig. 17.3 PTE for hemoglobin change for the dose range evaluated in the phase 2b study. P (Incidence of Hgb reduction of > 2 g/dL (placebo adjusted) < 5 %). (Adapted from Gupta et al. 2012)

peer-reviewed journals, summary basis of approvals, conference posters, and abstracts, etc.) for other drugs to make a comparative assessment of the safety and efficacy profiles. Such an integrated evaluation can be further utilized to guide regulatory and commercial strategy.

17.5.1 Meta-Analysis

Meta-analysis is a method of integrating information (summary level data) from different sources to enable indirect comparisons of available treatments. Since very few clinical studies in dermatologic drug development, have undertaken a head-to-head comparison of different treatments in a randomized-controlled setting, this methodology can provide useful information regarding their comparative performance. Meta-analyses evaluating the efficacy of biologic agents in patients with chronic plaque psoriasis have been published in recent years. Most recently, Reich et al. (2012) used a network meta-analysis approach to derive the ranking of biologics, approved in Europe for the treatment of moderate to severe psoriasis (infliximab, etanercept, adalimumab, ustekinumab, and efalizumab). The analysis based on the PASI 50, 75, and 90 response rates was conducted on an ordered probit scale using a Bayesian hierarchical model. The analysis assumed consistency of treatment effects across trials (on a probit scale) and yielded the predicted ranking of different treatments based on probability of achieving the desired PASI response as well as relative risk with respect to placebo. The analysis used data from 20 trials and revealed that infliximab was the most effective treatment followed by ustekinumab, adalimumab, etanercept, and efalizumab.

Another example illustrating the successful utilization of a meta-analytic approach to answer questions pertaining to clinical usage of available atopic dermatitis treatments was reported by Sher et al. (2012). The objective of the analysis

was to compare systemic and topical therapies for their ability to reduce the pruritus associated with atopic dermatitis and to contrast these treatments against their respective controls, i.e., vehicle and placebo for topical and systemic therapies, respectively. The analysis database consisted of 42 studies (representing 7011 patients) for the topical treatment and 10 studies (representing 647 patients) for the oral treatment. An inverse variance fixed-effects model showed that after adjusting for their respective controls, topical treatments were more effective than systemic treatments. Within the topicals, calcineurin inhibitors were found to be more effective than corticosteroids. Among the systemic treatments, data deficiency prevented an evaluation of the effectiveness of antihistamines. However, immunosuppressants were found to be clinically beneficial in reducing pruritus symptoms.

17.5.2 Model-Based Meta-Analysis

Meta-analysis can also be conducted by assuming parametric regression-based models to describe the relationship between exposure (and/or time) and response. Such an analysis termed as model-based meta-analysis (MBMA) may involve assessment at a specified time point (landmark analysis) or utilize data collected over multiple time points (longitudinal analysis). The main advantage of this approach over traditional meta-analysis is the inclusion of all available data (e.g., dose levels) which may increase the precision of the estimated treatment effect (Mandema et al. 2011). Additionally, the impact of differences in patient populations on the treatment effect may be captured quantitatively by virtue of covariate models (Mandema et al. 2011). Finally, MBMA allows for prediction and simulation of data scenarios which may lend themselves quite useful towards optimizing the design of a new study. Such value additions include but are not limited to formulating criteria for proof of concept studies and design elements such as study duration, choice of an active comparator, dose levels, etc.

MBMA may be driven by a specific question of interest. For instance, Janiczek-Dolphin et al. (2010) evaluated the steady state relationship between sebum excretion and acne outcome (measures: total lesion count, acne severity grade, and inflammatory lesion count) using data from multiple studies for acne treatment. The objective of the analysis was to quantitatively characterize this relationship and assess the ability of sebum reduction in predicting acne outcome across various drug classes (retinoid, oral contraceptive, 5-lipooxygenase inhibitor, and oral contraceptive containing antiandrogen) representing patients with mild-moderate to severe disease. Both hyperbolic (E_{max}) and linear (slope–intercept) models were explored, with the latter better describing the effect (E) i.e. acne outcome as a function of reduction in sebum excretion (RSE)

The equation below shows the model used and Fig. 17.4 shows the results for the linear relationship:

$$E = baseline + slope * RSE + \varepsilon / \sqrt{N},$$

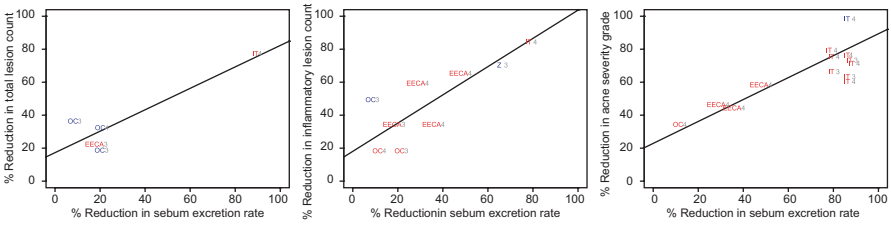

Fig. 17.4 Relationship between sebum reduction and acne outcome measures. Data points represent mean values for a treatment group in an individual study and the *line* represents the model fit. Drug class is shown by *symbols* (*OC* oral contraceptive, *IT* isotretinoin, *EECA* ethinyl estradiol/cyproterone acetate, *Z* zileuton) and duration of treatment for each data point. (Adapted from Janiczek-Dolphin et al. 2010)

where ε is the additive residual error normalized with respect to the number of patients (N).

The model used the totality of available evidence across different drug classes to quantify the association between sebum reduction and acne outcome. This relationship was used to predict the magnitude of sebum reduction required for a certain target improvement in acne outcome measures. The predicted sebum reduction to achieve a 50% improvement in total lesion count, inflammatory lesion count, and acne severity grade was (%, 95% CI): 50.3 (37.8, 75.3), 37.3 (26.6, 62.7), and 40.8 (31.4, 58.0), respectively.

This example clearly illustrates how the application of a simple model involving multiple drugs/classes allowed the quantification of the biomarker-clinical outcome relationship. The learnings from this analysis can prove useful for the development of other treatments for this indication.

17.6 Establishing Bioequivalence of Topical Corticosteroids

Bioequivalence is defined as the lack of a difference in the rate and extent of absorption between a test and a reference formulation. Typically, clinical studies that measure the drug concentration in a reference fluid (e.g., blood, urine) in healthy individuals are performed to compare these product attributes. However, for topical corticosteroid drug products, the FDA permits the use of pharmacodynamic (PD) approaches in order to establish bioequivalence (FDA 1998). The PD-based methodology relies on the vasoconstriction-induced blanching caused by topical dermatologic corticosteroids, which is known to be correlated with their potency, delivery through the stratum corneum and efficacy (Wiedersberg et al. 2008). The FDA guidance document recommends a two-stage approach for bioequivalence assessment. In the first step, a pilot study is conducted to evaluate the dose–response relationship for the corticosteroid followed by a pivotal in vivo study to compare the test and reference product for bioequivalence.

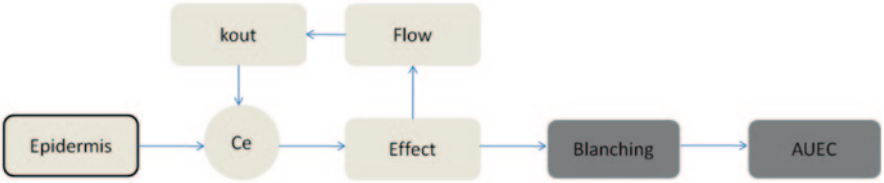

Fig. 17.5 Dermal absorption model for corticosteroids. (Adapted with permission from Holford et al. 2005).

The pilot study involves topical application of the corticosteroid for differing durations. A dose–response curve is constructed based on the increasing duration of exposure to the skin, which can be characterized by an E_{max} model that relates the area under the effect curve (AUEC) and the dose duration (effect is measured as the blanching response). The parameter ED50 reflects the dose duration that produces 50% of the maximum effect (E_{max}). The FDA guidance recommends the use of nonlinear mixed effect modeling or naïve-pooling method for model parameter estimation. The guidance suggests that the bioequivalence testing be carried out at the approximate population estimate of ED50 with two additional dose levels (durations) as half and twice ED50, respectively, also included in the assessment.

The FDA guidance was evaluated by virtue of an exploratory dose–response study comparing six dermatologic corticosteroid creams: 0.05% clobetasol propionate, 0.05% flucinonide-E, 0.5% triamcinolone acetonide, 0.1% betamethasone valerate, 0.05% alclometasonedipropionate, and 2.5% hydrocortisone (potency class: I, III, IV, V, VI, and VII, respectively; Singh et al. 1999). Incremental dosing durations (0.5–6 h) of each drug product were studied for their vasoconstrictive effect (skin blanching). Dose duration–AUEC(0–24) relationship was described by a population E_{max} model for five of the six products (except hydrocortisone) and ED50 values were estimated. Based on this study and analyzing data from a separate bioequivalence study for a potency class III product, it was concluded that the estimated application duration (ED50) provided an appropriate dose for designing the pivotal bioequivalence study.

Holford et al. (2005) challenged these findings and the agency recommendation by employing a modeling and simulation approach. The authors proposed a semi-physiological model to describe dermal absorption characteristics of corticosteroids (Fig. 17.5). In this model, drug delivery to the epidermis occurred at a constant rate (input = rate*extent); drug loss from the epidermis was a first order process governed by the rate constant k. The equation below describes the instantaneous change in drug levels "*E*" in the epidermis:

$$\frac{d\ E}{dt} = input\ -\ k.E.$$

The effective drug concentration (*C*e) which produces vasoconstriction is a function of blood flow:

$$\frac{d\ Ce}{dt} = k.E - Flow * Eff\ * \frac{Ce}{Ve}$$

$$Eff = 1 - E_{max} * \frac{Ce}{EC50 + Ce},$$

where *Flow* refers to the blood flow, *Eff* is the drug effect and *V*e is the volume of the effect compartment. Time course of skin blanching is a function of vasoconstriction produced by the corticosteroid.

AUEC was calculated by integrating the blanching effect over the period of application. The simulation study showed AUEC was not a robust measure under scenarios of rapid absorption thus suggesting that the choice of ED50 as an anchoring point for design may not always be justifiable.

As an alternative to the vasoconstrictive assay, microdialysis and dermatopharmamacokinetic (DPK) approaches have also been proposed as effective methods for BE assessment (Wiedersberg et al. 2008). The former technique has been discussed earlier; DPK involves drug extraction from the stratum corneum by virtue of repeated tape stripping and works best for quantifying the delivery of drugs such as antifungals, keratolytics, and antiseptics that act primarily in the stratum corneum (Wiedersberg et al. 2008).

17.7 Summary

- Dermatologic drug development can benefit tremendously from the advancement in pharmacometrics methods.
- As has been discussed in this chapter, the application of these methods can impart efficiencies at different junctures in development by reducing the uncertainty in the efficacy and safety profiles of the drug candidate and facilitating the progression along the development continuum.
- Ultimately, pharmacometrics techniques can provide the necessary framework for an objective evaluation of benefits versus risks with the intent of providing optimal therapy to the target patient population.

References

Ambrose PG, Bhavnani SM et al (2007) Pharmacokinetics-pharmacodynamics of antimicrobial therapy: it's not just for mice anymore. Clin Infect Dis 44(1):79–86

Bodenlenz M, Hofferer C et al (2012) Dermal PK/PD of a lipophilic topical drug in psoriatic patients by continuous intradermal membrane-free sampling. Eur J Pharm Biopharm 81(3):635–641

Drusano GL, Preston SL et al (2001) Use of preclinical data for selection of a phase II/III dose for evernimicin and identification of a preclinical MIC breakpoint. Antimicrob Agents Chemother 45(1):13–22

Eaglstein WH, Cash KR et al (2009) Challenges encountered in dermatologic drug development. Actas Dermosifiliogr 100(1):86–91

FDA (1998) Guidance for industry topical dermatological drug product, NDAs and ANDAs—in vivo, bioavailability, bioequivalence, In VitroRelease, and associated studies. Center for Drug Evaluation and Research (CDER)

FDA (2003) Guidance for industry exposure-response relationships—study design, data analysis, and regulatory applications. Office of Training and Communications, Center for Drug Evaluation and Research (CDER)

FDA (2008) Dermatologic and Ophthalmic Drugs Advisory Committee: June 17, 2008. Department of Health and Human Services Food and Drug Administration. Center for Drug Evaluation and Research

Gupta P, Hutmacher M et al (2011) The influence of body weight on the efficacy of tofacitinib (CP-690,550) in patients with plaque psoriasis. WCD, Seoul

Gupta P, Krishnaswami S et al (2012) Development and application of a model-based decision criterion for a laboratory endpoint to facilitate tofacitinib (CP-690,550) phase 3 dose selection. ASCPT, Washington

Holford N, Fleischer N et al (2005) Topical corticosteroid bioequivalence: an evaluation of the FDA guidance. PAGE, Pamplona

Hutmacher MM, Nestorov I et al (2007) Modeling the exposure-response relationship of etanercept in the treatment of patients with chronic moderate to severe plaque psoriasis. J Clin Pharmacol 47(2):238–248

Janiczek-Dolphin N, Cook J et al (2010) Can sebum reduction predict acne outcome? Br J Dermatol 163(4):683–688

Lebwohl M, Yeilding N et al (2010) Impact of weight on the efficacy and safety of ustekinumab in patients with moderate to severe psoriasis: rationale for dosing recommendations. J Am Acad Dermatol 63(4):571–579

MacGowan A, Rogers C et al (2001) In vitro models, in vivo models, and pharmacokinetics: what can we learn from in vitro models? Clin Infect Dis 33(3):S214–S220

Mandema JW, Salinger DH et al (2011) A dose-response meta-analysis for quantifying relative efficacy of biologics in rheumatoid arthritis. Clin Pharmacol Ther 90(6):828–835

McClain RW, Yentzer BA et al (2009) Comparison of skin concentrations following topical versus oral corticosteroid treatment: reconsidering the treatment of common inflammatory dermatoses. J Drugs Dermatol 8(12):1076–1079

Nestle FO, Kaplan DH et al (2009) Psoriasis. N Engl J Med 361(5):496–509

Nestorov I (2005) Clinical pharmacokinetics of TNF antagonists: how do they differ? Semin Arthritis Rheum 34(5):12–18

Nestorov I, Zitnik R et al (2004) Population pharmacokinetic modeling of subcutaneously administered etanercept in patients with psoriasis. J Pharmacokinet Pharmacodyn 31(6):463–490

Reich K, Burden AD et al (2012) Efficacy of biologics in the treatment of moderate to severe psoriasis: a network meta-analysis of randomized controlled trials. Br J Dermatol 166(1):179–188

Salgo R, Thaci D et al (2011) Microdialysis documents changes in the micromilieu of psoriatic plaques under continuous systemic therapy. Exp Dermatol 20(2):130–133

Sher LG, Chang J et al (2012) Relieving the pruritus of atopic dermatitis: a meta-analysis. Acta Derm Venereol 92(5):455–461

Singh GJ, Adams WP et al (1999) Development of in vivo bioequivalence methodology for dermatologic corticosteroids based on pharmacodynamic modeling. Clin Pharmacol Ther 66(4):346–357

Sun YN, Lu JF et al (2005) Population pharmacokinetics of efalizumab (humanized monoclonal anti-CD11a antibody) following long-term subcutaneous weekly dosing in psoriasis subjects. J Clin Pharmacol 45(4):468–476

Wiedersberg S, Leopold CS et al (2008). Bioavailability and bioequivalence of topical glucocorticoids. Eur J Pharm Biopharm 68(3):453–466

Zhou H, Hu C et al (2010) Population-based exposure-efficacy modeling of ustekinumab in patients with moderate to severe plaque psoriasis. J Clin Pharmacol 50(3):257–267

Zhu Y, Hu C et al (2009) Population pharmacokinetic modeling of ustekinumab, a human monoclonal antibody targeting IL-12/23p40, in patients with moderate to severe plaque psoriasis. J Clin Pharmacol 49(2):162–175

Chapter 18
Pharmacometrics in Pain Management

Ping Ji, Jiang Liu, Hao Zhu and Yaning Wang

18.1 Background

Pain is a dynamic phenomenon. It is defined by the International Association for the Study of Pain as "an unpleasant sensory and emotional experience associated with actual or potential tissue damage or, described in terms of such damage" (IASP 2012a, b). The sensation (perception) results from nerve impulses reaching the cerebral cortex via specific (nociceptive) neural pathways and is modulated at all levels of the peripheral and central nervous systems (Beaulieu et al. 2010). Broadly speaking, the classification of pain is based on the duration (acute, subacute, recurrent, or chronic pain) and type (nociceptive, neuropathic, or idiopathic pain; IASP 2012a, b; Australian and New Zealand College of Anaesthetists 2010). While acute pain is regarded as a symptom of disease or injury, chronic and recurrent pain is a specific health-care problem (EFIC 2010). The prevalence of chronic pain is high in industrialized countries. It has been estimated that about 100 million adults suffer from chronic pain in the USA alone, with treatment cost and loss of productivity adding up to US$ 635 billion per year (Institute of Medicine of National Academies 2011). In Canada, about 19% of adults 18 years and older suffer from chronic pain. Among them, approximately 50% experience pain for more than 10 years and about 30% rate pain intensity as very severe (Schopflocher et al. 2011). A survey in more than 1 million adult Japanese showed that lifetime and 4-week prevalence rates for low back pain were 83 and 36%, respectively (Fujii and Matsudaira 2013). Globally, about 20% of adults suffer from pain, and 10% of adults become new chronic

Opinions expressed in this chapter are those of the authors' and may not necessarily be consistent with some of the current product development standards of the regulatory agencies. To obtain the most current standards or advice for drug development for opioids or any products being developed, the reader should contact the regulatory agency.

Y. Wang (✉) · P. Ji · J. Liu · H. Zhu
Office of Clinical Pharmacology, Center for Drug Evaluation and Research,
US Food and Drug Administration, 10903 New Hampshire Ave, Room 2106,
Building 51, Silver Spring, MD 20993-0002, USA
e-mail: yaning.wang@fda.hhs.gov

S. Schmidt, H. Derendorf (eds.), *Applied Pharmacometrics*, AAPS Advances
in the Pharmaceutical Sciences Series 14, DOI 10.1007/978-1-4939-1304-6_18

pain patients each year (Goldberg and McGee 2011). The life quality of a patient with chronic pain is largely compromised because of the persistent nature of the symptom.

Pain medication management generally follows a stepwise approach as recommended by the World Health Organization guidelines (WHO 1996). When non-severe pain occurs, oral administration of nonopioid drugs should be initiated. If complete pain relief is not achieved or disease progression necessitates more aggressive treatment, a mild opioid is added to the existing nonopioid regimen. If this is or becomes insufficient, a mild opioid is replaced by a stronger opioid while continuing with nonopioid therapy, escalating opioid dose until the patient is pain free or at the maximum possible relief without intolerable side effects. If the initial presentation is severe pain, this stepping process should be skipped and a strong opioid should be started immediately in combination with a nonopioid analgesic (Schug and Auret 2008). In recent years, public health is facing the challenge of not only a lack of appropriate chronic pain management but also the increasing incidence of abuse and misuse of prescription opioid products (WHO 2008; FDA 2008). The increase in prescription opioid abuse is particularly evident among young people. In light of this, while it is important to maintain the availability of these important drug products for the millions of patients who suffer from chronic pain, FDA has encouraged drug companies to develop novel interventions to prevent opioid abuse (FDA 2008).

During drug development processes, pharmacometrics has been applied to quantify the pharmacokinetics (PK) and pharmacodynamics (PD) of the drug candidates and the disease progression at various stages to influence critical development decisions such as dosing regimen determination and evaluating abuse potential. PK characterizes drug exposure both locally and systemically. PD correlates drug concentration to physiologic effect or clinical outcome. A disease progression model refers to the evolution of pain over time. In this chapter, we review the application of pharmacometrics in pain management and its implications in affecting drug development and therapeutic decisions. This information may be useful in the design and analysis of relevant PK/PD studies, and the cited references should be consulted for more details on the application of models to specific drugs.

18.2 Model Building for Acute and Chronic Pain Relief Data

The general conceptual frame to quantitatively describe pain and therapeutic effects is similar to that in other disease areas, even though modeling strategies (e.g., mathematic equations) may vary. Several elements are considered valuable in the model-based drug development. As described by Gobburu and Lesko (2009), a standard disease-drug-trial model should include three major components—a disease model, a drug model, and a trial model. A disease model focuses on characterization of changes in clinical outcome(s) and/or biomarker(s) over time and correlations

between the clinical outcome(s) and biomarker(s). Because the placebo effect can be substantial in a clinical trial, characterization of the placebo effect is a critical component in pain disease model. For models developed based on clinical trial data, it is unnecessary or impractical to model placebo effect and disease progression separately to influence drug development decisions. Drug effect is generally described by an exposure–response (E–R) model (or a PK/PD model) that links exposure changes to efficacy and safety signals. This model is the key to determine optimal doses or dose ranges through preclinical or various phases of clinical trials. In addition to drug effects, success of a clinical trial is largely affected by patient characteristics and behaviors. Correlations among major demographic factors (e.g., gender and body weight) and/or disease severity assessments may directly affect clinical trial outcomes. Patient behaviors, such as premature discontinuation, will lead to missing data and may bias the trial results and complicate the interpretation of clinical observations. Inclusion of a quantitative model accounting for patient factors in a trial model allows a better assessment of potential trial outcomes at the trial design stage. Certain patient inclusion and exclusion criteria and trial conduct features can be enhanced based on knowledge of impact from patient factors. In recent years, attempts have been made to implement the concept of disease-drug-trial model in the clinical development of products that manage pain.

In the clinical setting, pain measurement varies and efficacy has been commonly assessed by comparisons of pain relief scores or pain intensity differences determined with visual analogue scales (VAS). Observations from the placebo arm in a clinical trial can be used to build a disease model for both acute and chronic pain. Typical clinical trials that are intended to evaluate safety or efficacy of chronic pain treatment have relatively short durations (e.g., 8–13 weeks) compared to pain histories (e.g., >0.5 years) of enrolled patients. The symptoms for most patients are considered stable (i.e., at steady state) during the trial. Therefore, in an empirical disease model, the underlying pain intensity can be assumed to be constant for a specific patient enrolled in a trial. This assumption is converted into a mathematic equation shown below (Eq. 18.1), where S_{ij} represents the pain score observed for the *i*th subject at the *j*th observation time point. S_i^0 is the estimated baseline pain score for the *i*th subject, and ε_{ij} is the random effect assumed to be normally distributed around the mean of 0 (Eq. 18.1). Placebo effects, featured by substantial improvement of pain intensity from baseline, are commonly observed in chronic pain patients. In the placebo arm, average pain scores monotonically decrease over time:

$$S_{ij} = S_i^0 + \varepsilon_{ij} \tag{18.1}$$

The reduction in the pain score appears to be fast after the trial is initiated and the pain score profile seems to approach plateau as the trial continues. Some researchers include a simple exponential term in the disease model to describe the placebo effect. Equation 18.2, derived from Eq. 18.1, can be applied to describe observations from the placebo arm. In this model, P_i is a negative ratio that represents the maximum placebo effect for the *i*th subject. K_i is a rate constant for the *i*th subject which governs how soon the placebo effect reaches the plateau, and t_j is the time for the *j*th observation:

$$S_{ij} = S_i^0[1 + P_i \cdot (1 - e^{-k_i \cdot t_j})] + \varepsilon_{ij} \tag{18.2}$$

Lockwood et al. (2003) applied this modeling approach to describe observations from clinical trials for pregabalin. The association between changes in biomarkers and pain intensity is still under investigation. Studies have shown that pain intensity can be linked to some specific substrates in preclinical chronic pain models. For instance, preclinical studies showed correlations between the maximum increase in neurokinin-1 receptor density and maximum pain intensity (Huntjens et al. 2005). However, there is rather limited information on systemic biomarkers that can predict pain response in human.

A similar modeling strategy is often applied to the acute pain placebo effect. In the postoperative pain model building, the disease progression is incorporated in the placebo effect and characterized with a time-dependent model as follows (Mandema and Stanski 1996):

$$S_{ij} = \sum_{k=1}^{m} \beta_k + PM(e^{-\gamma_1 t} - e^{-\gamma_2 t}) + \varepsilon_{ij} \tag{18.3}$$

where γ_1 and γ_2 are the first-order rate constants of the offset and onset of the placebo effect, PM determines the magnitude of the placebo effect, and β_k specifies the baseline set of probabilities of the various degrees of pain relief. This model permits the placebo effect to decrease with time.

E–R models are used to characterize drug effects. PK samples collected in a clinical trial can be linked to PD assessments (e.g., pain scores). Alternatively, simulated patient-level exposures derived from a well-established population PK model are applied to explore E–R relationships if PK samples are not available. To ensure patient-level exposures are reliably derived, the population PK model should include covariates that represent major patient characteristics. Byon et al. (2010) explored E–R relationships in fibromyalgia patients receiving pregabalin. Pregabalin exposures were simulated by using a population PK model established from more than 2000 patients enrolled in multiple clinical trials. Because pregabalin is mainly eliminated through kidney, creatinine clearance was included as the key covariate for deriving exposures. The final E–R model was established with the simulated average steady-state concentrations for each individual (i.e., C_{averg}). E_{max} and sigmoid E_{max} models are commonly used to describe therapeutic effects in drugs alleviating pain. Equation 18.4 is the sigmoid E_{max} model. In this model, γ is the hill factor that determines the steepness of the E–R curve. When γ takes the value of 1, sigmoid E_{max} model is simplified to E_{max} model. E_{ij} is the response for the ith subject at jth time point. $E_{\max,i}$ is the maximal effect for the ith subject and $EC_{50,i}$ is the exposure that yields 50 % of the maximal effect for the ith subject. C_{ij} is the exposure level for the ith subject at the jth observation. Based on the pharmacology of the compound, different exposure variables can be applied to the E_{max} model. For instance, the actions of duloxetine (Cymbalta®), a central pain inhibitor and an antidepressant, are believed to be related to serotonergic and noradrenergic

activities in the central nervous system (Eli 2004). It takes weeks before desirable efficacy can be shown in patients. Therefore, concentrations at various time points in a dosing interval might not be an appropriate exposure variable. Instead, a gross estimate of exposures (e.g., average concentrations or area under the curve at steady state) seems to be reasonable. Sometimes, the exposure range tested in the clinical trial is narrow:

$$E_{ij} = \frac{E_{\max,i} \cdot C_{ij}^{\gamma}}{EC_{50,i}^{\gamma} + C_{ij}^{\gamma}} \tag{18.4}$$

$$E_{ij} = \beta_{1,i} \cdot C_{ij} \tag{18.5}$$

$$E_{ij} = \beta_{1,i} \cdot \log\left(C_{ij}\right) \tag{18.6}$$

An E_{max} model can be simplified to a linear model (Eq. 18.5) or a log-linear model (Eq. 18.6), where $\beta_{1,i}$ is the slope for the *i*th subject. The relationships between drug response and patient characteristics are often explored to identify more subgroups of patients sensitive to the treatment. Some examples of applying E–R model in assisting decision making in acute and chronic pain treatment are illustrated in Table 18.1.

Quantification of patient characteristics and behaviors is one major component in the clinical trial model. Premature discontinuation (dropout), an important patient behavior, is commonly seen in clinical trials aiming to evaluate efficacy and safety of chronic pain treatments. For instance, only 75% of patients completed two 12-week pivotal trials intended to evaluate the efficacy of duloxetine for the treatment of diabetic peripheral neuropathic pain (Eli 2004). Likewise, about 38% of patients prematurely discontinued from the two pivotal trials intended to assess the treatment effect of duloxetine on fibromyalgia (Eli 2004). The decisions for dropout vary from patient to patient, which will lead to missing data classified by different mechanisms. Some patients randomly discontinue from the trial, independent of the pain intensity experienced. Missing data due to this type of dropout are considered as missing completely at random (MCAR). Some other patients discontinue from the trial for a reason, which is related to the observed pain intensity. However, after conditioning on the observed pain intensity, whether or not data are missing does not depend on the values of the missing data. This type of missing data is considered as missing at random (MAR). If a high pain intensity score is not recorded, and the patient decides to drop out due to this high value, i.e., missingness depends on the missing value, this type of missing data is considered as missing not at random (MNAR; Hu and Sale 2003; Panel on handling missing data in clinical trials 2010). The assumptions on missing data mechanisms affect data analyses. Characterization of patient dropout allows comparison of different data analyses and evaluation of trial success rates. Various survival functions are typically used in describing the dropout pattern. Depending on the underlying assumptions of the potential risks for patients to drop out (i.e., hazard) at a given time, different survival models can

Table 18.1 Examples of exposure–response models applied in pain treatment

Indication	Compound	E–R Model	Utility/conclusion	Reference
Postoperative pain	Ketorolac	Sigmoid E_{max}	To support the optimal dose selection for the pain relief	Mandema and Stanski 1996
Post-oral surgery pain	Fentanyl	Sigmoid E_{max}	To establish the PKPD model	Foster et al. 2008
Post-surgery pain	Acetaminophen	Sigmoid E_{max}	To support the new formulation development	Green et al. 2010
Fibromyalgia	Pregabalin	E_{max}	To support the recommended doses Greater pain reduction observed in female and older patients	Byon et al. 2010
Migraine pain	Naratriptan	E_{max}	To predict pain relief in migraine patients following naratriptan treatment	Gueorguieval et al. 2005
Acute/Chronic pain	SC-75416	E_{max}	To identify appropriate dose in future clinical trials	Kowalski et al. 2008
Neuropathic pain	Pregabalin	Sigmoid E_{max}	To identify minimum dose that led to 1-point reduction in pain score	Lockwood et al. 2003
Neuropathic pain	Gabapentin	E_{max}	To establish linkage in exposure–response relationship between two pivotal trials, which led to the final approval of the product	Miller et al. 2005
Chronic pain	Ketamine	Sigmoid E_{max}	To gain insights on complex interaction between drug and pain relief	Dahan et al. 2011
Chronic pain	Acetaminophen	Sigmoid E_{max}	To establish appropriate dosage regimen in Japanese population	Shinoda et al. 2007

be applied. A survival function, $S(t)$, describes the probability of dropping out after time t for a patient in the trial (Eq. 18.7). A hazard function, $h(t)$, describes an instantaneous rate of dropout per unit time given that a patient is still in the trial up to time t (Eq. 18.8). The relationship between a hazard function and a survival function is shown in Eq. 18.9. Based on this relationship, different survival functions can be

$$S(t) = \Pr(T > t) \tag{18.7}$$

$$h(t) = \lim_{dt \to 0} \frac{pr(t < T < t + dt \mid T > t)}{dt} \tag{18.8}$$

$$S(t) = \exp\left[-\int_0^t h(t)\cdot dt\right] \tag{18.9}$$

derived from various assumed hazard functions. For instance, Lockwood et al. (2003) applied a constant hazard model (i.e., exponential survival model) to describe the dropout pattern in a clinical trial intended to evaluate treatment effect of pregabalin for chronic neuropathic pain. The authors assumed that the dropout time follows a distribution with a constant hazard, which indicates the dropout rate is constant over time and independent of the observed pain scores. The value of the daily dropout rate was assumed to be 0.0043/day. The assumed missing data mechanism was MCAR. This dropout model provided a quantitative assessment of the potential missing data in the trial simulations. Even though the assumption of MCAR was considered unrealistically strong assumption in practice, it is commonly used at the trial planning stage to calculate the sample size for clinical trials. Kowalski et al. (2008) assumed that the missing data mechanism followed MAR. The underlying hazard is a function of the current pain score and duration of the patient in the trial. The hazard function is shown as $h(t,m) = h(m)\cdot(1+k(t-1)_+)$, where *h(m)* is the baseline hazard rate for each pain score, *m* is the pain score, *k* is the slope of change in hazard rate with time, and $k(t-1)_+$ is an indicator that equals $t-1$ if $t \geq 1$ and 0 otherwise. The author applied this model to support dose selection in clinical trials for a compound developed for pain relief.

18.3 Modeling Pain Relief in Fixed-Dose Combination Products

Attempts have been made to quantitatively characterize pain relief in subjects receiving fixed-dose combination products intended for pain management. Fixed-dose combination products, which include two or more analgesics with different pain-relief mechanisms in the same dosage form, are part of treatment strategies to control chronic or acute pain. There are several existing fixed-dose combination products. Ultracept®, a product including both tramadol hydrochloride and acetaminophen, is indicated for short-term management of acute pain. Both hydrocodone and acetaminophen are formulated into vicodin® with the approved indication of relief of moderate or moderately severe pain. More fixed-dose combination products are under clinical development for ease of pain. Quantification of pain relief following treatment of several compounds used in combination may provide important scientific merits. For example, Tröster et al. (2012) applied a sigmoid E_{max} model to describe analgesic effects in subjects receiving fentanyl and buprenorphine. The analyzed data were obtained from a crossover clinical trial in 15 healthy volunteers receiving an intravenous infusion of 1.5 μg/kg fentanyl, 1.5 μg/kg buprenorphine, a combination of 0.75 μg/kg fentanyl and buprenorphe each, or saline. As shown in Eq. 18.10, in the sigmoid E_{max} model, E represents percentage reduction in pain and

E_{max} is the maximal pain reduction. γ is the hill factor, which determines the steepness of the E–R curve. The concentration applied in the sigmoid E_{max} (i.e., C_E) is a combination of buprenorphine and fentanyl concentrations (Eq. 18.11). In the equation, $C_{E,\,Fen}$ and $C_{E,\,Bup}$ are effective concentrations of fentanyl and buprenorphine, respectively. $EC_{50,\,Fen}$ and $EC_{50,\,Bup}$ are the concentrations to generate 50% of the maximal pain reduction for fentanyl and buprenorphine, respectively. ε is the PD interaction term. If ε is zero, the two compounds demonstrate additive effect. If ε is less than zero, the two compounds show antagonistic effect. Whereas if ε is greater than zero, the two compounds show synergistic effect. The focus of this modeling approach was to determine PD interactions when the two compounds are used in combination. The authors indicated that, based on the modeling results, fentanyl and buprenorphine demonstrated additive effect:

$$E = E_{\max} \cdot \frac{C_E^{\gamma}}{1 + C_E^{\gamma}}, \text{ where } C_E = \frac{C_{E,Fen}}{EC_{50,Fen}} + \frac{C_{E,Bup}}{EC_{50,Bup}} + \varepsilon \cdot \frac{C_{E,Fen}}{EC_{50,Fen}} \cdot \frac{C_{E,Bup}}{EC_{50,Bup}} \quad (18.10)$$

One potential application of the E–R model in characterization of pain reduction in patients receiving fixed-dose combination products is to identify the contribution of each compound. However, several challenges exist, especially when the model is developed based on data from patients only receiving fixed-dose combination products. In general, significances of slope estimates of E–R models can be applied to determine whether the administered compounds are active. If *p*-values for the slope estimates are smaller than a predefined value (e.g., 0.05), the E–R relationships are significant and the specific compounds are considered pharmacologically active. Zhu and Wang (2011) have evaluated potential issues in the application of E–R models to quantify responses in patients receiving a fixed-dose combination product at various dose levels through modeling and simulation. The complications come from two sources. First, concentrations from all compounds in a fixed-dose combination product are highly correlated, because they change proportionally following the changes in doses (e.g., 50 mg A/100 mg B, 100 mg A/200 mg B). Second, the underlying E–R relationships for each compound can be nonlinear with various shapes and empirical models applied for analyses might not be able to adequately capture these shapes without prior or independent data source (e.g., data collected from patients receiving one compound at a time or receiving one compound at a fixed-dose level with changing dose levels for the other compound). As a result, a univariate E–R model is inappropriate to determine the contribution of a specific compound in a fixed-dose combination product. A multivariate E–R model, which includes concentrations from all compounds in the fixed-dose combination product, seems to be more appropriate. However, if the underlying E–R relationships (i.e., model structures) for each compound are erroneously or inadequately defined, false positive rates in determining significant E–R relationships are elevated. Therefore, the E–R analyses results based on data from fixed-dose combination products at various dose levels should be interpreted with caution.

18.4 Application of Pharmacometrics in Pediatric Pain Relief: A Case Example

Pain is a common feature of hospitalization in infants and children. Up to 80% of infants and children are reported to have pain during hospital administration (Taylor et al. 2008). Children differ from adults not only in how pain is perceived but also in PK due to ontogeny. Relative to adults, there is little research evidence to guide clinicians regarding the pain management in children. Therefore, the pain management practices in pediatric patients are mostly extrapolated from adults. Below is a brief summary of the considerations for the dosing regimen recommendation of over-the-counter (OTC) acetaminophen in pediatric patients from a PK/PD perspective.

Acetaminophen dosage schedule in pediatric patients below 12 years of age for OTC monograph is one of the many issues being evaluated and discussed in the development of the proposed rule (PR) for internal analgesic, antipyretic, and antirheumatic (IAAA) drug products. The dosage regimen based on age and weight, with instructions that weight-based dosage of 10–15 mg/kg should be used if a child's weight is known, is currently being assessed. The PK exposure of acetaminophen in pediatric patients of 6 months to 12 years of age given the proposed OTC monograph dose range of 10–15 mg/kg is within the adult exposure range at the monograph dose (Ji et al. 2012). In this dose range, the antipyretic effect of acetaminophen in pediatric patients of 6 months to 12 years of age is dose dependent and appears to be better than placebo. The PK/PD analyses of acetaminophen in pediatric patients undergoing outpatient tonsillectomy were performed by Anderson et al. (2001). In this study, the data came from three studies: 32 patients given 40 mg/kg ($n=12$) or 100 mg/kg oral dose ($n=20$) from study A, 21 patients given 40 mg/kg from study B, and 30 patients given placebo from study C. The treatment was administered between 0.5 and 1 h preoperatively to the patients. According to the authors, all three studies had similar designs. The raw data of pain score as a function of time were requested from the authors and the results were reanalyzed. High dropout rate was observed early in the placebo group as shown by the rapidly decreasing sample size over time (no scheduled pain assessment at 1 h). The last observation carried forward (LOCF) method was used to impute the missing pain scores. For those patients without first observation (0.5 h), a pain score of 10 was assigned. The analysis of variance (ANOVA) method was used to compare the two treatment groups with placebo at each time without adjusting for multiplicity. Both 40 mg/kg and 100 mg/kg achieved more pain reduction than placebo at all time points with statistical significance of 0.05 level with different effect sizes at different times. At all time points except 0.5 h, 100 mg/kg was statistically better than 40 mg/kg for pain reduction showing a clear dose–response for pain reduction. To evaluate the pain reduction for 10–15 mg/kg, an exploratory E–R modeling analysis was conducted to predict the expected pain reduction for the lower doses. Actual individual doses (0 for placebo group and 27.2–104 mg/kg for treated groups) were used to construct the E–R model. To avoid the confounding effect of time, E–R model was built at each time point with the following linear model:

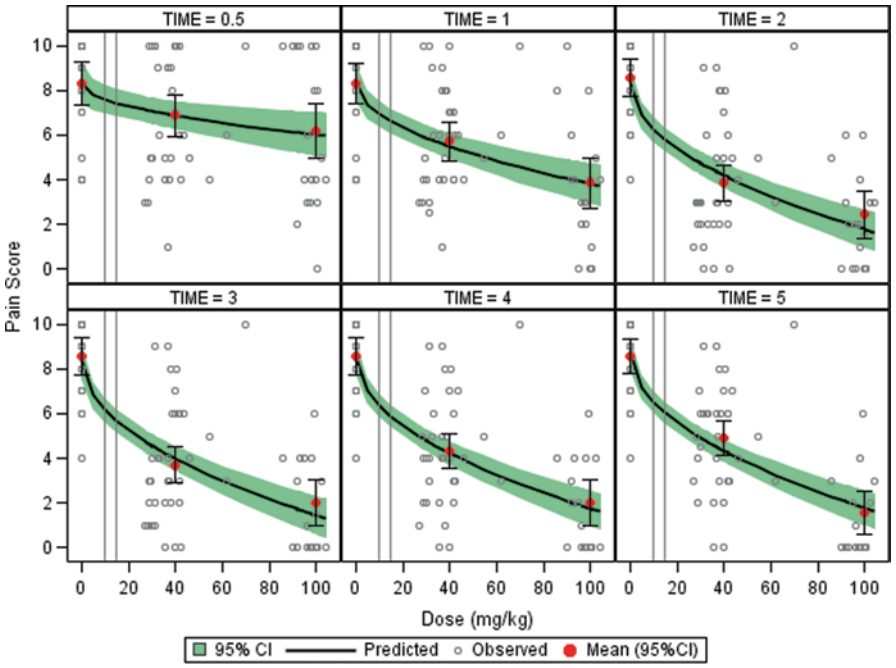

Fig. 18.1 Goodness of fit for exposure–response model (*vertical lines* are 10 and 15 mg/kg, respectively)

$$Y_i = \beta_0 + \beta_1 \cdot X_i + \varepsilon_i \tag{18.11}$$

where Y_i is the pain score for *i*th patient, X_i is the square root of dose (mg/kg) for *i*th patient, β_0 is the intercept, β_1 is the slope, and ε_i is the residual. Even though pain score ranging from 0 to 10 is not normally distributed, no extra effort was taken to transform Y into a normally distributed variable because the normal approximation was sufficient to derive a well-fitted model for each time point as shown in Fig. 18.1. Various structure models, such as linear model, log-linear model, log–log linear model, or E_{max} model, were explored and the best structure model is a linear model with dose transformed to its square root. The parameters are listed in Table 18.2, and Fig. 18.1 shows the goodness of fit. The predicted pain scores and their 95% confidence interval (CI) for 10 and 15 mg/kg are listed in Table 18.3 together with the placebo-corrected pain score changes and their 95% CI. The predicted pain score reduction ranged from 0.7 to 2.2 units for 10 mg/kg and 0.9 to 2.7 units for 15 mg/kg at various time points relative to placebo. The small normal *p*-values should be interpreted in the context of a parametric model, and the predicted pain reduction should be related to clinical relevance. Nevertheless, the E–R model provided supportive evidence for the efficacy in pain reduction for 10 and 15 mg/kg in pediatric patients (5–15 years old) undergoing outpatient tonsillectomy.

Table 18.2 Parameter estimates for exposure–response model

Time	Parameter	Estimate	95% CI	*p*-Value
0.5	Intercept	8.34	(7.4, 9.3)	<0.0001
	Slope	−0.23	(−0.4, −0.1)	0.0031
1	Intercept	8.39	(7.5, 9.2)	<0.0001
	Slope	−0.46	(−0.6, −0.3)	<0.0001
2	Intercept	8.34	(7.5, 9.2)	<0.0001
	Slope	−0.66	(−0.8, −0.5)	<0.0001
3	Intercept	8.36	(7.5, 9.2)	<0.0001
	Slope	−0.69	(−0.8, −0.6)	<0.0001
4	Intercept	8.54	(7.8, 9.3)	<0.0001
	Slope	−0.68	(−0.8, −0.6)	<0.0001
5	Intercept	8.75	(8, 9.5)	<0.0001
	Slope	−0.70	(−0.8, −0.6)	<0.0001

18.5 Pharmacometrics in the Opioid Treatment

18.5.1 Abuse Liability

The abuse liability of a drug is generally considered the degree to which repeated consumption will occur because of its positive subjective effects, reinforcing effects or to avoid negative effects (O'Connor and Mead 2010). Opioid attractiveness has been based in part on how rapidly peak plasma concentration (C_{max}) is reached (Budman et al. 2009). It may be more appropriate to think of opioids in terms of their *peak effects* and the *time to maximal effect*. Reformulation from immediate-release product to extended-release product provides patients with continuous relief from pain over a long period of time, reduces pain fluctuations, requires fewer daily doses to help patients adhere to their prescribed regimen more easily, allows them to sleep through the night, and allows a physician to increase the dose for a patient as needed to relieve pain (Zacny and Gutierrez 2003). However, it has become a target for abusers and diverters because the tablet contains larger amounts of the active ingredient and the controlled release formulation is easier for abusers to compromise. For the extended-release formulation of OxyContin, for example, both mean and individual peak exposures have been used to assess whether the extended-release characteristics of the product were compromised during manipulation (Haddox et al. 2008).

18.5.2 Opioid Tolerance

Repeated administration of opioids may lead to the development of tolerance to analgesia, as evidenced by requiring higher dose to maintain pain control. Based on the prevailing mechanism, the development of tolerance is attributed to three types:

Table 18.3 Predicted absolute pain score and placebo-corrected pain score changes for 10 and 15 mg/kg

Treatment				Treatment difference			
Time	Group (mg/kg)	Mean	95% CI	Comparison	Difference	95% CI diff	*p*-Value
0.5	10	7.6	(7, 8.2)	10 -Placebo	−0.7	(−1.2, −0.3)	0.0031
	15	7.4	(6.8, 8)	15 -Placebo	−0.9	(−1.5, −0.3)	0.0031
1	10	6.9	(6.4, 7.5)	10 -Placebo	−1.4	(−1.9, −1)	<0.0001
	15	6.6	(6.1, 7.2)	15 -Placebo	−1.8	(−2.3, −1.2)	<0.0001
2	10	6.3	(5.7, 6.8)	10 -Placebo	−2.1	(−2.5, −1.7)	<0.0001
	15	5.8	(5.3, 6.3)	15 -Placebo	−2.5	(−3.1, −2)	<0.0001
3	10	6.2	(5.6, 6.7)	10 -Placebo	−2.2	(−2.6, −1.8)	<0.0001
	15	5.7	(5.1, 6.2)	15 -Placebo	−2.7	(−3.2, −2.2)	<0.0001
4	10	6.4	(5.9, 6.9)	10 -Placebo	−2.2	(−2.5, −1.8)	<0.0001
	15	5.9	(5.4, 6.4)	15 -Placebo	−2.6	(−3.1, −2.2)	<0.0001
5	10	6.5	(6, 7)	10 -Placebo	−2.2	(−2.6, −1.8)	<0.0001
	15	6.0	(5.6, 6.5)	15 -Placebo	−2.7	(−3.2, −2.2)	<0.0001

CI confidence interval, *CI diff* confidence interval for difference

PK, PD, and learned (Dumas and Pollack 2008). PK tolerance occurs when drug disposition or metabolism is altered as a function of time. PD tolerance occurs when the intrinsic responsiveness of the receptor system diminishes over time. Learned tolerance is related to behavioral or conditional situation. Although the mechanism contributing to the tolerance development is complex, PK/PD empirical models, without incorporating specific biologic mechanisms that drive the development of tolerance, have been used to characterize and summarize the temporal loss of drug response (Ouellet and Pollack 1995, 1997; Gårdmark et al. 1993). An integrated PK/PD model for morphine tolerance was developed following morphine infusions in rats by introducing a tolerance compartment in addition to the effect compartment (Dumas and Pollack 2008). The net effect is the sum of the positive effect from the effect compartment and the negative effect from the tolerance compartment.

When the specific physiologic alterations that lead to the time-dependent loss of the pharmacologic effect are known, they can be incorporated into mechanistic PK/PD models. For example, elevated nitric oxide (NO) production has been implicated in the development of morphine antinociceptive tolerance. Heinzen evaluated the temporal relationship between morphine-induced increases in neuronal NO and the loss of pharmacologic activity (Heinzen and Pollack 2004). Antinociceptive effect was monitored at selected time points during and following infusion by electrical stimulation vocalization. The data were fitted with a PK/PD model to obtain parameters governing the morphine disposition, stimulation of NO production, antinociception, and antinociceptive tolerance development (Fig. 18.2).

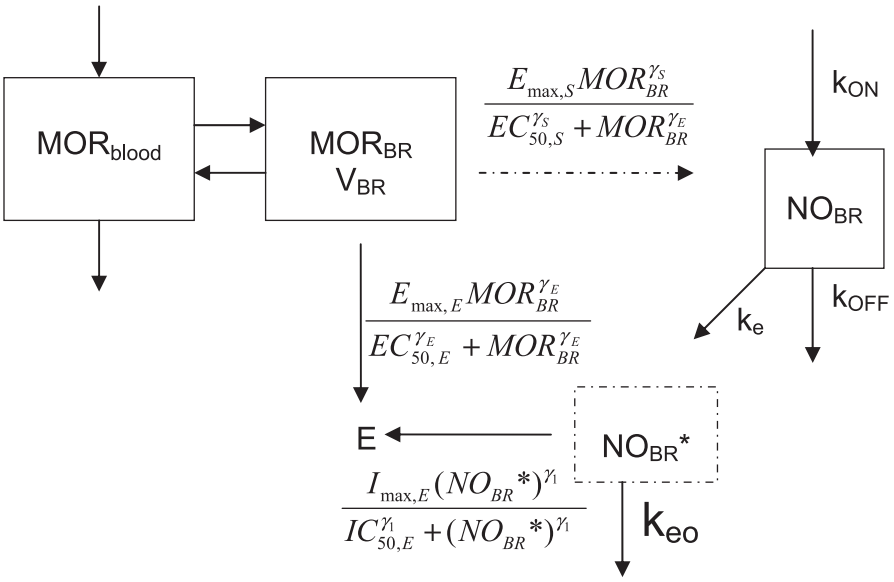

Fig. 18.2 Scheme depicting morphine antinociceptive tolerance development due to NO

In Fig. 18.2, γ_s, γ_E, and γ_I represent the shape factors, $E_{\max,s}$ is the maximum possible percent stimulation of neuronal NO production by the concentration of morphine in the brain *(MOR_{BR})*, $E_{\max,E}$ is the maximum possible antinociceptive effect produced by MOR_{BR}, $EC_{50,E}$ is the MOR_{BR} that elicits a 50% maximum response, $I_{max,E}$ is the maximum possible inverse effect produced by NO concentrations in a hypothetical compartment (NO_{BR}*), and $I_{C50,E}$ is the NO_{BR}* that produces an effect equal to 50% of the maximum possible inverse effect. The loss of antinociceptive effect due to NO_{BR}* was modeled as NO acting as an inverse agonist with the following integrated equation (Eq. 18.12):

$$E = \frac{E_{\max,E} MOR_{BR}^{\gamma_E}}{EC_{50,E}^{\gamma_E} + MOR_{BR}^{\gamma_E}} - \frac{I_{\max,E} (NO_{BR}*)^{\gamma_I}}{IC_{50,E}^{\gamma_I} + (NO_{BR}*)^{\gamma_I}} \tag{18.12}$$

These data define a strong, time-dependent relationship between morphine-induced stimulation of NO production and tolerance development, identify the specific NO-induced alterations in nociceptive processing after morphine administration, and indicate that NO is a key mediator of the antinociceptive tolerance development (Fig. 18.3).

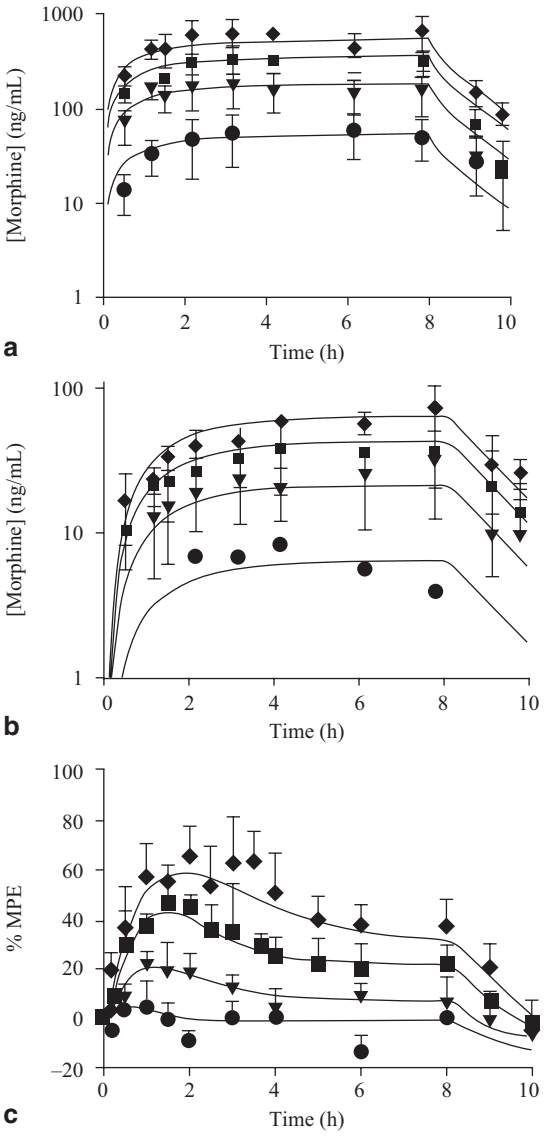

Fig. 18.3 Morphine concentration-time profiles in the **a** blood and **b** brain and **c** morphine antinociceptive effect (% MPE) during and following an 8-h morphine infusion at 0.3 (*circles*), 1 (*triangles*), 2 (*squares*), or 3 (*deltoids*) mg/kg/h. *Lines* indicate the fit of the PK/PD model to the data. (Heinzen and Pollack 2004, reprinted with permission)

18.6 Reversal of Opioid-Induced Respiratory Depression

Respiratory depression is a potentially life-threatening adverse effect of opioid therapy (Baxter 1994). Naloxone, the competitive opioid μ antagonist, is commonly used to treat and prevent recurrence of opioid-induced respiratory depression, such as fentanyl and morphine (Dahan et al. 2010). It is formulated with buprenorphine in SuboxoneÒ in an effort to dissuade patients from injecting the tablets. Yassen et al. (2007) proposed a mechanism-based PK/PD interaction model to describe and predict

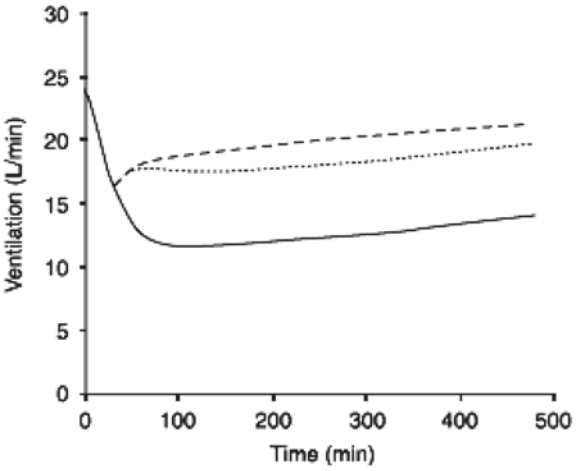

Fig. 18.4 Influence of the mode of naloxone administration on the reversibility of buprenorphine-induced respiratory depression. Buprenorphine 0.2 mg/70 kg was administered. Half of the dose was given over 90 s and the remainder over 59 min. After 30 min, naloxone was infused continuously at a rate of 0 mg/h (placebo, *solid line*), 2 mg/70 kg/h (*dotted line*), or 4 mg/70 kg/h (*dashed line*). (Yassen et al. 2007, reprinted with permission)

the time course of naloxone-induced reversal of respiratory depression after intravenous administration of buprenorphine. A combined biophase equilibration-receptor association-dissociation PD model described the competitive interaction between buprenorphine and naloxone at the opioid μ receptor as shown below (Eq. 18.13):

$$\frac{d\rho_{app(bup)}}{dt} = k_{on(bup)} \cdot \left[C_{e(bup)}\right] \cdot \left[\left(1-\rho_{app(bup)}\right) \cdot \left\{1 - \frac{C_{e(nal)}}{K_{D(nal)} + C_{e(nal)}}\right\}\right] - K_{off(bup)} \cdot \rho_{app(bup)} \tag{18.13}$$

The relationship of respiratory depressant effect to the fractional receptor occupancy is modeled as a linear function (Eq. 18.14):

$$E = E_0 \cdot (1 - \alpha \cdot \rho_{app(bup)}), \tag{18.14}$$

where ρ_{app} is the apparent fractional receptor occupancy, K_D is the equilibrium dissociation constant of naloxone and is equal to k_{off}/k_{on}, C_e is the drug concentration at the site of action, E is the ventilatory response, E_0 is the baseline ventilation, and α is the intrinsic activity, the value of which varies between 0 and 1. Due to the slow receptor kinetics of buprenorphine and the fast elimination kinetics of naloxone, the reverse of buprenorphine-induced respiratory depression requires high dose and also continuous infusion of naloxone (Fig. 18.4).

18.7 Pharmacometrics in Clinical Patient Care

Anesthesia-analgesia clinical practice generally requires a wide spectrum of pharmacological actions (e.g., analgesia, hypnosis, and suppression of somatic and autonomic responses to noxious stimuli; Kissin 1993). Therefore, a higher standard

of precision and accuracy regarding drug administration for achieving the desired therapeutic drug effect while minimizing side effects is desirable. Pharmacometric models including dose-exposure-response relationships and covariates affecting PK/PD variability have been successfully applied in this field to help optimize drug administration. One of the most important examples is the development of computer-controlled target-controlled infusion (TCI) and drug advisory displays (Syroid et al. 2002, Sahinovic et al. 2010, Struys et al. 2011). The commercially available drug advisory displays, such as the SmartPilot View (Drager Medical, Lubeck, Germany; FDA 2012) and the Navigator (GE Healthcare, Helsinki, Finland; FDA 2007), integrate real-time data from dosing history, patient monitors, and anesthesia systems to provide clinicians predicted PK/PD information at the point of care. The PK/PD models for various drugs and the combination of drugs are implemented in the algorithm of the medical device to create the predicted PK/PD profiles, which are visualized on the displays in real time. These drug advisory displays allow clinicians to visually understand the extent of synergistic effects and the predicted effects under a specific regimen.

Although there are a large number of anesthetic PK/PD modeling studies, only a small part of information is ever applied in the clinical domain (Fisher 1996). This advisory display technology brings pharmacometrics into the operating room and improves the clinical utility of anesthetic drugs' PK/PD knowledge. As shown in Fig. 18.5, the display generally consists of a drug administration history, sedation, analgesia, and relaxation response window. For the example of Navigator, the PK/PD modeling supports inhaled sedative drugs (e.g., desflurane, enflurane, isoflurane, halothane, sevoflurane, and nitrous oxide), intravenous sedative drugs (e.g., midazolam, propofol, and thiopental), analgesic drugs (e.g., alfentanil, fentanyl, remifentanil, and sufentanil), and relaxants (e.g., mivacurium, pancuronium, rocuronium, and vecuronium). The PK model is used to compute the effect-site concentration (Ce) of the drug. The effect-site concentration is normalized (or scaled) to the EC_{50} of the drug. The resulting display is a plot of $Ce(t)/EC_{50}$ over time, where $Ce(t)$ is the effect-site concentration of the drug at time t, and EC_{50} is the effect-site concentration at which 50% of the population experience the reference effect of that drug. The system also attempts to account for certain PD drug interactions when a drug with known interactive properties is administered. Various models based on response-surface methodology have been successfully developed to characterize the anesthetic drug interactions (Greco et al. 1995, Minto et al. 2000, Guan et al. 2008, Lee 2010). For the example of propofol and analgesic drug interaction (Fig. 18.6), Schnider's three-compartment PK model including age, height, weight, and lean body mass as covariates is used to describe propofol PK (Masui et al. 2010). A synergistic interaction between propofol and an analgesic drug at the hypothetical effect site could be characterized by a PD interaction model, such as a Greco's model (Greco et al. 1995):

$$E = \frac{E_{\max} \times \left(\frac{Ce_A}{EC_{50A}} + \frac{Ce_B}{EC_{50B}} + \alpha \times \frac{Ce_A}{EC_{50A}} \times \frac{Ce_B}{EC_{50B}} \right)^n}{\left(\frac{Ce_A}{EC_{50A}} + \frac{Ce_B}{EC_{50B}} + \alpha \times \frac{Ce_A}{EC_{50A}} \times \frac{Ce_B}{EC_{50B}} \right)^n + 1}, \tag{18.15}$$

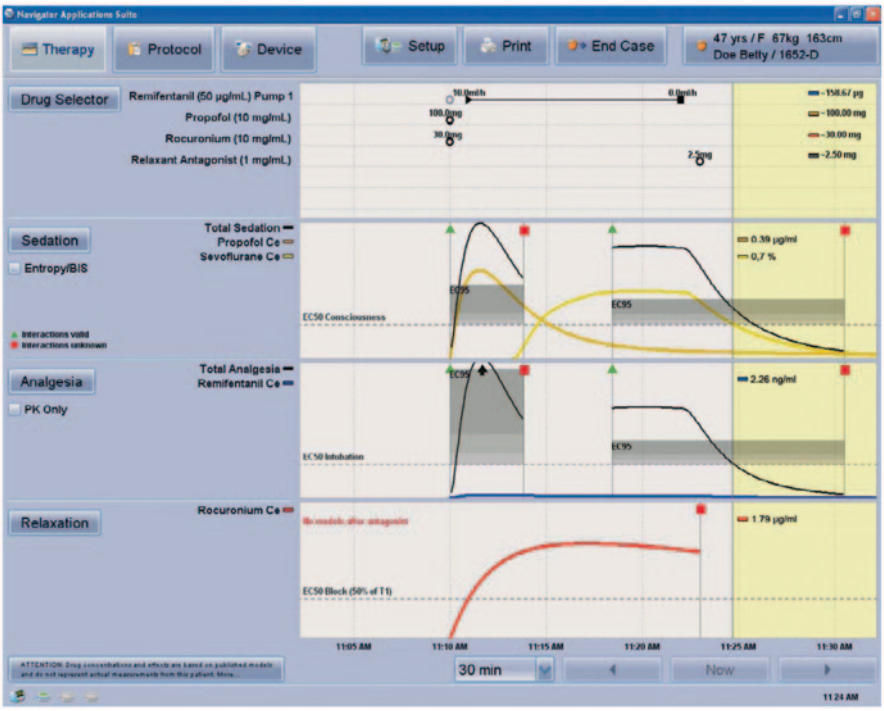

Fig. 18.5 Navigator display window visualizing PK/PD information for an individual administered remifentanil, propofol, rocuronium, and a relaxant antagonist (used with permission of GE Healthcare). The effect-site concentration is normalized to the PD parameter, the EC_{50} which is the effect-site concentration at which 50% of the population experience the reference effect of that drug. The total effect (the *black line* in the sedation and analgesia windows) visualizes the synergistic effect of the analgesic (remifentanil) and sedative drugs (propofol and sevoflurance). The models also project future effects (*right yellow panel*). (Reprinted with permission from GE Healthcare)

where $E_{\max}$ is the maximal effect of drug A and drug B, EC_{50A} and EC_{50B} are the individual drug concentrations that produce 50% of the maximal effect, n is the slope of the PD response curve, and α is a unique parameter that characterizes the nature and extent of interaction between two drugs for a particular effect measure. If $\alpha = 0$, the drug interaction is additive. If $\alpha < 0$, the drug interaction is antagonistic. If $\alpha > 0$, the drug interaction is synergistic. Ce_A and Ce_B represent the concentration at the effect site for propofol and the analgesic drug, respectively.

It is important to remember that the information on a display represents a statistical sampling of the population and is not the actual measurements from the patient undergoing anesthesia, although some patient factors affecting drug concentrations and effects may be considered in the models. The anesthesiologist is expected to compare the potential response (based on the model) and the actual patient response (based on parameters on the patient anesthesia monitor) to determine (a) what adjustments to drug dosing need to be made based on the actual patient response and (b) how well the

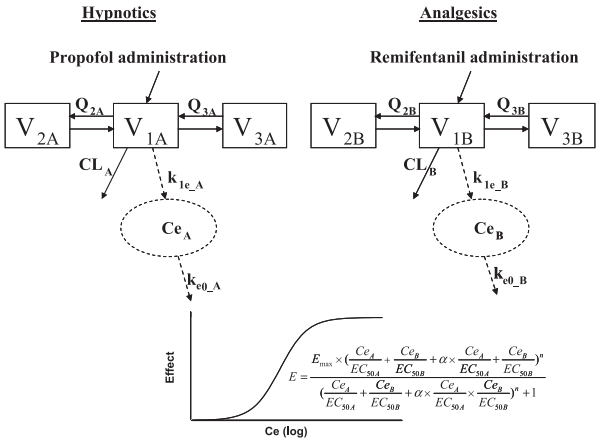

Fig. 18.6 PK and PD synergistic interaction between propofol and remifentanil at the hypothetical effect site characterized by the Greco's model

model may correlate with this patient's actual response. In addition, the models generally were established from healthy volunteers while operation procedures and other factors may affect the drug's PK and interactions. Also for the majority of published models, the key parameter k_{e0}, which is used to quantify the delay between the drug plasma concentration and the drug effect, was derived from electroencephalogram (EEG) effect data. The implicit assumption that the delay between plasma concentration and all PD effects of a drug (e.g., analgesia and hypnosis) is the same as the delay between plasma concentration and EEG effect also needs to be verified.

Drug advisory displays have been shown to be a useful tool in guiding anesthesia, resulting in adequate anesthesia and a greater safety due to a more precise titration (Cirillo et al. 2012). By applying pharmacometric technology, the anesthetists should be able to optimize anesthetic-analgesic drug administration in a more efficient manner.

18.8 Summary

- Pain models are generally developed by quantitatively integrating various aspects of information such as disease progression, placebo effect, E–R relationship, and subject-level covariates.
- Pain models are invaluable as input into clinical trial design during drug development. These models can be applied to quantify:
  - Efficacy contribution of each component in a combination product
  - Pediatric dosing recommendation
  - Abuse liability
  - Drug tolerance
  - Opioid-induced respiratory depression
  - Dropout pattern
- Pharmacometric models have been implemented in the software package for commercial medical devices for anesthesia and analgesia management.
- Pharmacometrics in pain management not only influences drug development and regulatory decision making but also facilitates patient care and therapeutic decisions.

References

Anderson BJ, Woollard GA, Holford NH (2001) Acetaminophen analgesia in pediatrics: placebo effect and pain resolution after tonsillectomy. Eur J Clin Pharmacol 57(8):559–69

Australian and New Zealand College of Anaesthetists (2010) National pain strategy. http://www.iasp-pain.org/PainSummit/Australia_2010PainStrategy.pdf. Accessed 20 March 2013

Baxter AD (1994) Respiratory depression with patient-controlled analgesia. Can J Anaesth 41:87–90

Beaulieu P, Lussier D, Porreca F, Dickenson A (2010) Pharmacology of pain. IASP Press, Seattle

Budman SH, Grimes Serrano JM, Butler SF (2009) Can abuse deterrent formulations make a difference? Expectation and speculation. Harm Reduct J 6:8. doi:10.1186/1477-7517-6-8

Byon W, Ouellet D, Chew M, Ito K, Burger P, Pauer L, Zeiher B, Corrigan B (2010) Exposure-response analyses of the effects of pregabalin in patients with fibromyalgia using daily pain scores and patient global impression of change. J Clin Pharmacol 50(7):803–815. doi:10.1177/0091270009352187

Cirillo V, Volpe ML, Iacono C, Crisconio P, De Robertis E, Tufano R (2012) Is navigator a useful tool in guiding anesthesia practice in nephropatic patients? Preliminary study: 3AP5-AP. Eur J Anaesthesiol 29:52

Dahan A, Aarts L, Smith TW (2010) Incidence, reversal, and prevention of opioid-induced respiratory depression. Anesthesiology 112(1):226–238

Dahan A, Olofsen E, Sigtermans M, Noppers I, Niesters M, Aarts L, Bauer M, Sarton E (2011) Population pharmacokinetic-pharmacodynamic modeling of ketamine-induced pain relief of chronic pain. Eur J Pain 15(3):258–267

Dumas EO, Pollack GM (2008) Opioid tolerance development: a pharmacokinetic/pharmacodynamic perspective. AAPS J 10(4):537–551

EFIC (2010) EFIC's Declaration on pain: pain is as a major health problem, a disease in its own right. http://www.efic.org/eap.htm. Accessed 20 Dec 2012

Eli L (2004) Package insert for cymbalta (Duloxetine). http://www.accessdata.fda.gov/drugsatfda_docs/label/2012/021427s040s041lbl.pdf. Accessed 20 March 2013

FDA (2007) Navigator applications suite premarket notification 510(k) summary. http://www.accessdata.fda.gov/cdrh_docs/pdf7/K071097.pdf. Accessed 20 March 2013

FDA (2008) Joint meeting of the anesthetic and life support drugs advisory committee and drug safety & risk management advisory committee. http://www.fda.gov/ohrms/dockets/ac/08/briefing/2008-4395b1-01-FDA.pdf. Accessed 20 March 2013

FDA (2012) Smartpilot view premarket notification 510(k) summary. http://www.accessdata.fda.gov/cdrh_docs/pdf10/K103035.pdf. Accessed 20 March 2013

Fisher DM (1996) (Almost) everything you learned about pharmacokinetics was (somewhat) wrong! Anesth Analg 83(5):901–903

Foster D, Upton R, Christrup L, Popper L (2008) Pharmacokinetics and pharmacodynamics of intranasal versus intravenous fentanyl in patients with pain after oral surgery. Ann Pharmacother 42(10):1380–1387. doi:10.1345/aph.1L168

Fujii T, Matsudaira K (2013) Prevalence of low back pain and factors associated with chronic disabling back pain in Japan. Eur Spine J 22(2):432–438. doi:10.1007/s00586-012-2439-0

Gårdmark M, Ekblom M, Bouw R, Hammarlund-Udenaes M (1993) Quantification of effect delay and acute tolerance development to morphine in the rat. J Pharmacol Exp Ther 267(3):1061–1067

Gobburu JV, Lesko LJ (2009) Quantitative disease, drug, and trial models. Annu Rev Pharmacol Toxicol 49:291–330. doi:10.1146/annurev.pharmtox.011008.145613

Goldberg DS, McGee SJ (2011) Pain as a global public health priority. BMC Public Health 11:770. doi:10.1186/1471-2458-11-770

Greco WR, Bravo G, Parsons JC (1995) The search for synergy: a critical review from a response surface perspective. Pharmacol Rev 47(2):331–385

Green B, Chandler S, MacDonald G, Elliott G, Roberts MS (2010) Quantifying pain relief following administration of a novel formulation of paracetamol (acetaminophen). Clin Pharmacol 50(12):1406–1413. doi: 10.1177/0091270009359181

Guan Z, Bi SS, Yang L, Zhang LP, Zhou TY, Lu W (2008) Progress in the study of response surface modeling in investigation of drug-drug interaction in anesthetic drugs. Yao Xue Xue Bao 43(12):1171–1178

Gueorguieval I, Nestorov IA, Aarons L, Rowlang M (2005) Uncertainty analysis in pharmacokinetics and pharmacodynamics: application to naratriptan. Pharm Res 22(10):1614–1626

Haddox JD, Henningfield JE, Mannion R (2008) A new formulation of OxyContin (oxycodone HCl controlled release) tablets. http://www.fda.gov/ohrms/DOCKETS/ac/08/slides/2008-4356s1-05-Purdue.pdf. Accessed 20 March 2013

Heinzen EL, Pollack EM (2004) Pharmacodynamics of morphine-induced neuronal nitric oxide production and antinociceptive tolerance development. Brain Res 1023(2):175–184

Hu C, Sale ME (2003) A joint model for nonlinear longitudinal data with informative dropout. J Pharmacokinet Pharmacodyn 30(1):83–103

Huntjens DR, Danhof M, Della Pasqua OE (2005) Pharmacokinetic-pharmcodynamic correlations and biomarkers in the development of COX-2 inhibitors. Rheumatology (Oxford) 44(7):846–859

IASP (2012a) IASP Taxonomy. http://www.iasp-pain.org/AM/Template.cfm?Section=Pain_Definitions. Accessed 20 March 2013

IASP (2012b) Pain associated with neurological disorders. http://www.iasp-pain.org/AM/Template.cfm?Section=General_Resource_Links&Template=/CM/ContentDisplay.cfm&ContentID=4174. Accessed 20 Dec 2012

Institute of Medicine of National Academies (2011) Relieving pain in America: a blueprint for transforming prevention, care, education, and research. http://www.nap.edu/catalog.php?record_id=13172. Accessed 20 Dec 2012

Ji P, Wang Y, Li Z, Doddapaneni S, Hertz S, Furness S, Sahajwalla CG (2012) Regulatory review of acetaminophen clinical pharmacology in young pediatric patients. J Pharm Sci 101(12):4383–4389. doi:10.1002/jps.23331

Kissin I (1993) General anesthetic action: an obsolete notion? Anesth Analg 76(2):215–218

Kowalski KG, Olson S, Remmers AE, Hutmacher MM (2008) Modeling and simulation to support dose selection and clinical development of SC-75416, a selective COX-2 inhibitor for the treatment of acute and chronic pain. Clin Pharmacol Ther 83(6):857–866

Lee SI (2010) Drug interaction: focusing on response surface models. Korean J Anesthesiol 58(5):421–434

Lockwood PA, Cook JA, Ewy WE, Mandema JW (2003) The use of clinical trial simulation to support dose selection: application to development of a new treatment for chronic neuropathic pain. Pharm Res 20(11):1752–1759

Mandema JW, Stanski DR (1996) Population pharmacodynamic model for ketorolac analgesia. Clin Pharmacol Ther 60(6):619–635

Masui K, Upton RN, Doufas AG, Coetzee JF, Kazama T, Mortier EP, Struys MM (2010) The performance of compartmental and physiologically based recirculatory pharmacokinetic models for propofol: a comparison using bolus, continuous, and target-controlled infusion data. Anesth Analg 111(2):368–379. doi:10.1213/ANE.0b013e3181bdcf5b

Miller R, Ewy W, Corrigan BW, Ouellet D, Hermann D, Kowalski KG, Lockwood P, Koup JR, Donevan S, El-Kattan A, Li CS, Werth JL, Feltner DE, Lalonde RL (2005) How modeling and simulation have enhanced decision making in new drug development. J Pharmacokinet Pharmacodyn 32(2):185–197

Minto CF, Schnider TW, Short TG, Gregg KM, Gentilini A, Shafer SL (2000) Response surface model for anesthetic drug interactions. Anesthesiology 92(6):1603–1616

O'Connor EC, Mead AN (2010) Tramadol acts as a weak reinforcer in the rat self-administrationmodel, consistent with its low abuse liability in humans. Pharmacol Biochem Behav 96(3):279–286. doi:10.1016/j.pbb.2010.05.018

Ouellet DM, Pollack GM (1995) A pharmacokinetic-pharmacodynamic model of tolerance to morphine analgesia during infusion in rats. J Pharmacokinet Biopharm 23(6):531–549
Ouellet DM, Pollack GM (1997) Pharmacodynamics and tolerance development during multiple intravenous bolus morphine administration in rats. J Pharmacol Exp Ther 281(2):713–720
Panel on handling missing data in clinical trials; national research council (2010) The prevention and treatment of missing data in clinical trials. http://www.nap.edu/catalog/12955.html ISBN: 0-309-15815-X. Accessed 20 March 2013
Sahinovic MM, Absalom AR, Struys MM (2010) Administration and monitoring of intravenous anesthetics. Curr Opin Anaesthesiol 23(6):734–740. doi: 10.1097/ACO.0b013e3283404579
Schopflocher D, Taenzer P, Jovey R (2011) The prevalence of chronic pain in Canada. Pain Res Manage 16(6):445–450
Schug SA, Auret K (2008) Clinical pharmacology: principles of analgesic drug management. In: Sykes N, Bennett MI, Yuan C-S (eds) Clinical pain management: cancer pain, 2nd edn. Hodder Arnold, London, pp 104–122. ISBN 978-0-340-94007–5
Shinoda S, Aoyama T, Aoyama Y, Tomioka S, Matsumoto Y, Ohe Y (2007) Pharmacokinetics/pharmacodynamics of acetaminophen analgesia in Japanese patients with chronic pain. Biol Pharm Bull 30(1):157–161
Struys M, Sahinovic M, Lichtenbelt BJ, Vereecke HEM, Absalom AR (2011) Optimizing intravenous drug administration by applying pharmacokinetic/pharmacodynamic concepts. Br J Anaesth 107(1):38–47
Syroid ND, Agutter J, Drews FA, Westenskow DR, Albert RW, Bermudez JC, Strayer DL, Prenzel H, Loeb RG, Weinger MB (2002) Development and evaluation of a graphical anesthesia drug display. Anesthesiology 96(3):565–575
Taylor EM, Boyer K, Campbell FA (2008) Pain in hospitalized children: a prospective cross-sectional survey of pain prevalence, intensity, assessment and management in a Canadian pediatric teaching hospital. Pain Res Manage 13(1):25–32
Tröster A, Ihmsen H, Singler B, Filitz J, Koppert W (2012) Interaction of fentanyl and buprenorphine in an experimental model of pain and central sensitization in human volunteers. Clin J Pain 28(8):705–711. doi: 10.1097/AJP.0b013e318241d948
World Health Organization (WHO) (1996) Cancer pain relief. With a guide to opioid availability, 2nd edn. WHO, Geneva. ISBN 92-4-154482–154481
World Health Organization (WHO) (2008) WHO treatment guidelines on chronic non-malignant pain in adults. http://www.who.int/medicines/areas/quality_safety/Scoping_WHOGuide_non-malignant_pain_adults.pdf. Accessed 20 March 2013
Yassen A, Olofsen E, van Dorp E, Sarton E, Teppema L, Danhof M, Dahan A (2007) Mechanism-based pharmacokinetic-pharmacodynamic modelling of the reversal of buprenorphine-induced respiratory depression by naloxone: a study in healthy volunteers. Clin Pharmacokinet 46(11):965–980
Zacny JP, Gutierrez S (2003) Characterizing the subjective, psychomotor, and physiological effects of oral oxycodone in non-drug abusing volunteers. Psychopharmacology (Berl) 170:242–254
Zhu H, Wang Y (2011) Evaluation of false positive rate based on exposure-response analyses for two compounds in fixed-dose combination products. J Pharmacokinet Pharmacodyn 38(6):671–696. doi:10.1007/s10928-011-9214-4

Chapter 19
Pharmacometrics of Hyperlipidemia

Maurice G. Emery, Peter C. Haughney and John P. Gibbs

19.1 Introduction

Arteriosclerosis of the coronary and peripheral vasculature is the undisputed leading cause of death worldwide resulting from cardiovascular disease, peripheral vascular disease, and stroke. Identified risk factors for cardiovascular disease and the successful mitigation of these risk factors in reducing the risk for cardiovascular disease has been the topic of recent state-of-the-art reviews (WHO et al. 2011; Smith et al. 2012; Lloyd-Jones 2010). Effective treatment of lipid disorders as a risk factor through combinations of diet and drug therapy has led to the dramatic reduction in the risk of cardiovascular disease. Despite the improvements in therapies, there is still residual cardiovascular risk which remains untreated and drives the search and development for additional treatments of these grievous illnesses.

Deposition of cholesterol into the vessel wall is a key factor in the process of arteriosclerosis. Almost all lipoproteins are an integral part of cholesterol transport processes forming the core of circulating lipids and are central in the pathogenesis of cardiovascular disease. Therefore, it is no surprise that lipoproteins represent a surrogate for cardiovascular risk, and the rich use of mathematical models describing lipoprotein kinetics have been investigated for nearly the past 50 years. These efforts represent some of the earliest applications of mathematical modeling to understand the basic physiology of lipoprotein metabolism, the influence of disease, and mechanism of action of drug treatments modifying these pathways.

J. P. Gibbs (✉)
Department of Pharmacokinetics and Drug Metabolism, Amgen Inc, Thousand Oaks, CA, USA
e-mail: gibbsj@amgen.com

M. G. Emery
Department of Pharmacokinetics and Drug Metabolism, Amgen, Inc, Seattle, WA, USA
e-mail: keokiemery@gmail.com

P. C. Haughney
Department of Pharmacokinetics and Drug Metabolism, Amgen Inc., Seattle, WA, USA
e-mail: haughney@amgen.com

S. Schmidt, H. Derendorf (eds.), *Applied Pharmacometrics,* AAPS Advances in the Pharmaceutical Sciences Series 14, DOI 10.1007/978-1-4939-1304-6_19

The application of pharmacometrics in hyperlipidemia is an emerging area. Both semi-mechanistic and empirical pharmacokinetic and pharmacodynamic (PK/PD) models have been developed to describe dose response and time course of effects for lipids. The application of pharmacometrics has been shown to effectively guide drug development decision making by accurately simulating trials, optimizing dosing regimens, and informing early termination of programs with unacceptable risk to benefit ratios. These approaches can support the development of the next wave of new treatments to meet therapeutic goals and further reduce cardiovascular risk. This chapter provides an overview of quantitative lipid metabolism, current treatments, and reviews the current state-of-the-art PK/PD modeling as applied to hyperlipidemia treatments.

19.2 Overview of Biology of Lipid Disorders

19.2.1 Lipoprotein Metabolism Overview

Lipoproteins are spherical molecules consisting of apolipoproteins, cholesterol, triglycerides, and phospholipids and serve to carry lipids with limited aqueous solubility in plasma water. They are characterized by their density, lipid composition, and the associated lipoproteins, which provide specificity with respect to functional interactions (Table 19.1).

Lipoprotein metabolism can be conveniently divided into two general pathways and are discussed in greater detail below. In healthy individuals, the first pathway functions to distribute cholesterol whereas the second pathway is often referred to as “reverse cholesterol transport” which returns cholesterol from the periphery for reuse and/or elimination. In individuals with lipid disorders, these two pathways are hypothesized to contribute to the degree of vascular pathology by either leading to deposition of excess cholesterol into or participating in removal of cholesterol from the vessel walls. Therefore, from a quantitative pharmacology perspective, the understanding of lipid and lipoprotein kinetics describes the process of lipid movement providing mechanistic insight into normal and pathological processes. In this manner, lipoprotein kinetics can help to characterize the mechanism of action and magnitude of treatment effects.

Mathematical models are applied to quantify lipoprotein metabolism. Kinetic parameters of production and elimination of circulating lipids, their precursors, and lipoproteins are obtained through direct measurement of either production or elimination of these species using tracers. These tracers can be either stable-labeled or radiolabeled molecules. The tracers can be either incorporated into lipids and lipoproteins inside the body, or labeled outside the body and then reintroduced. There are pros and cons for each approach depending on the objective of the study. The fundamental principles and major assumptions behind these quantitative tracer studies are: (1) steady-state conditions (i.e., zero-order synthesis and first-order elimination), (2) the tracer amount does not perturb the system, and (3) the tracer is

Table 19.1 Summary of major circulating lipoproteins

Lipoprotein	Density (g/dL)	Approximate molecular mass (kD)	Lipid composition (%)			Associated apolipoprotein
			TG	Chol	Phospholipid	
Chylomicron	0.95	400,000	80–95	2–7	3–9	B48, C, E, A
VLDL	0.95–1.006	10,000–80,000	55–80	5–15	10–20	B100, C, E
IDL	1.006–1.019	5000–10,000	20–50	20–40	15–25	B100, C, E
LDL	1.019–1.063	2300	5–15	40–50	20–25	B100
HDL	1.063–1.210	1700–3600	5–10	15–25	20–30	A, C, E

Chol cholesterol, *HDL* high-density lipoprotein, *IDL* intermediate-density lipoprotein, *LDL* low-density lipoprotein, *TG* triglycerides, *VLDL* very-low-density lipoprotein

representative of the disposition of the tracee. The data are fit using compartmental analyses in order to derive either the production and/or elimination rates directly or from a steady-state assumption. In older studies, exogenously radiolabeled lipoproteins were used. With the advent of sensitive mass spectrometry, incorporation of stable isotopes into proteins has been utilized with greater frequency over the past 20 years. Excellent reviews of the methodologies, models, and assumptions have been published (Barrett et al. 1996; Ji et al. 2006).

19.2.2 Production and Transport of Exogenous and Endogenous Lipids

A schematic describing the transport of exogenous or dietary lipids as well as the de novo synthesis of new lipids and their incorporation into lipoproteins is depicted in Fig. 19.1. Dietary lipids are absorbed and incorporated into nascent chylomicrons containing apo B48, apo AI, apo AII, and apo AIV. The mature chylomicron is a sphere consisting of primarily triglyceride with smaller amounts of phospholipids and free cholesterol. These particles are transported into the circulation via the thoracic duct. Once in circulation, apo C proteins are transferred from high-density lipoprotein (HDL). Apo CII appears to be responsible for the subsequent hydrolysis of triglycerides through their activation of lipoprotein lipase (LPL) residing in the capillaries of muscle and adipose tissues where the resulting fatty acids can be utilized. Once hydrolysis has occurred, apo CI and apo CII are transferred back to the surface of HDL. Apo E is then picked up by these chylomicron remnants that can be recognized by low-density lipoprotein receptors (LDLR). In this manner, the free cholesterol and phospholipids from chylomicron remnants are supplied to the liver.

Through the uptake and/or synthesis of triglycerides and cholesterol, the liver produces the majority of endogenous lipids supplying cholesterol to peripheral tissues. These lipids are combined with phospholipids and apo B100 and then secreted into the circulation as nascent very low-density lipoprotein (VLDL) particles. Other apolipoproteins (apo CI, apo CII, apo E) are inserted into VLDL particles. As with chylomicrons, VLDL is subject to action by LPL to intermediate-density lipoprotein

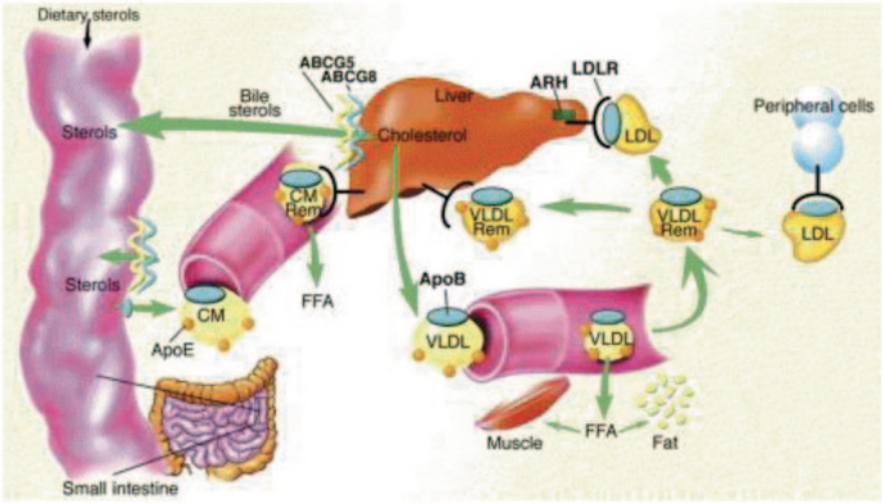

Fig. 19.1 Absorption and production of cholesterol. chylomicrons (*CM*), chylomicron remnants (*CM Rem*), VLDL remnants (*VLDL Rem*), LDL-receptor (*LDLR*), autosomal recessive hypercholesterolemia (*ARH*), ATP-binding cassette family G type 5 or 8 (*ABCG5/8*). (Reprinted from Rader DJ et al (2003) Monogenic hypercholesterolemia: new insights into pathogenesis and treatment. J Clin Invest 111/12:1796, permission conveyed through Copyright Clearance Center, Inc.)

(IDL; VLDL remnants). These particles are then converted to smaller LDL particles through the action of hepatic triglyceride lipase and apo E. The liver takes up most LDL and removal of LDL (and other apo B100 particles) occurs through the LDLR on the hepatocyte. The primary signal in the regulation of hepatic cholesterol production for secretion and hepatic cholesterol uptake by LDL and interaction with LDLR is the intracellular concentration of cholesterol. This regulation is mediated through transcription factors primarily sterol regulatory element-binding proteins (SREBP). This level of regulation has been reviewed in depth and may serve as the basis of a model-based systems biology approach to understanding the effects of dyslipidemia and treatment on circulating cholesterol. (Brown and Goldstein 2006; Dietschy 1997; van der Wulp et. al. 2012)

19.2.3 Reverse Cholesterol Transport

The concept of reverse cholesterol transport (RCT) was proposed half a century ago in describing the process of the lecithin-cholesterol acyltransferase enzyme (LCAT) activity (Glomset and Wright 1964). The role of HDL in the removal and return of excess cholesterol to the liver for reuse and efflux from the body is continuing to evolve and a current understanding is shown in Fig. 19.2.

The RCT pathway consists of lipoproteins with apo AI as their core and is believed to be protective against atherosclerosis. Pre-beta (electorphoretic mobility)

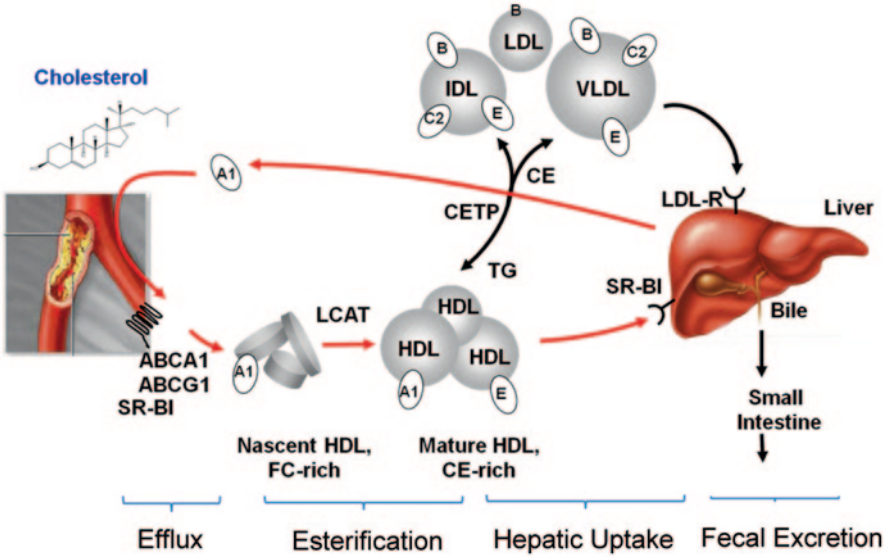

Fig. 19.2 Reverse cholesterol transport. Efflux esterification hepatic uptake fecal excretion. cholesteryl ester (*CE*), cholesteryl ester transfer protein (*CETP*), high-density lipoprotein (*HDL*), low-density lipoprotein (*LDL*), very-low-density lipoprotein (*VLDL*), LDL-receptor (*LDLR*), triglyceride (*TG*), lecithin-cholesterol acyltransferase (*LCAT*), apolipoprotein (*A1*), apolipoprotein (*B*), apolipoprotein (*C2*), apolipoprotein (*E*), scavenger receptor (*SR-BI*), free cholesterol (*FC*), ATP-binding cassette family A or G type 1 (*ABC A/G1*)

particles arise from secretion by the intestine and liver or are generated from chylomicrons which have undergone lipolysis or removal of cholesteryl ester from HDL_2 particles. The role of these discoid shaped particles is to accept unesterified cholesterol from the peripheral tissues. Cholesterol appears to be transported by members of the ATP-binding cassette transporter family from peripheral tissues including macrophages. These identified transporters include ABCA1 and ABCG1. The molecular mechanisms of HDL function and the associated cellular events by which peripheral lipid homeostasis is achieved is the subject of a recent review (Orso et al. 2011). Once the cholesterol is transferred to HDL particles, they undergo esterification through the action of lecithin-cholesterol acyltransferase (LCAT) leading to the development of spherical shaped particles. These maturing HDL particles pack cholesteryl esters into the core, and continue to grow in size while reducing their density. These particles continue to mature into HDL_2 and HDL_3 particles which constitute the largest amount of circulating HDLs. The further expansion of cholesteryl ester (CE) into the core of these HDL particles occurs as a result of apo E incorporation.

The steps in elimination of the acquired HDL cholesterol from the plasma in humans involve a number of pathways. These include the transfer of CE from HDL to VLDL/LDL particles by the action of cholesteryl ester transfer protein (CETP) and subsequent recycling to the periphery or delivery to the liver through the LDLR, di-

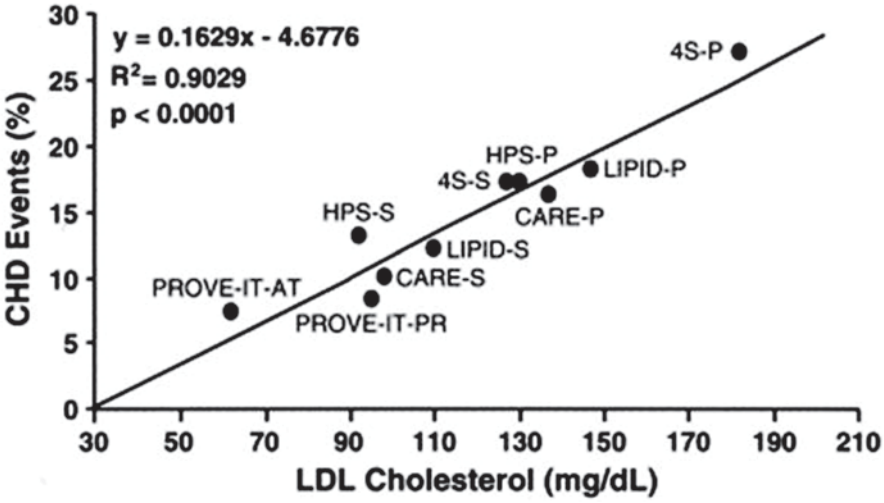

Fig. 19.3 Linkage between LDL-C and CHD events in secondary prevention trials. (Reprinted from O'Keefe et al. 2004, © 2004 by the American College of Cardiology Foundation)

rect removal of apo AI-containing particles through the hepatic scavenger receptor class B type I (SR-BI) and direct interaction of the apo E-containing HDL particles with the LDLR. Cholesterol in the liver is then subject to excretion into the bile and the feces. It is estimated that approximately 90 % of excreted cholesterol is through the formation of bile acids whose metabolic path is tightly and coordinately regulated by orphan nuclear receptors (Russell 2009; Repa and Mangelsdorf 2000). The remaining 10 % is through direct secretion into the bile by canilicular transporters and incorporation in the synthesis of biologically active steroids.

19.3 Linkage Between LDL-C and Cardiovascular Risk

A wide range of research methods including experimental animal models, laboratory investigations, epidemiology, clinical, and genetic studies indicate that elevated LDL-C is a major cause of coronary heart disease (CHD; National Heart, Lung, and Blood Institute (NHLBI) 2004). The linkage between other lipoproteins and CHD is less clear. Given the strong linkage, LDL-C is a standard primary endpoint for clinical trials evaluating the efficacy of new hypercholesterolemia drugs (European Medicines Agency 2010).

Using meta-analysis of trial level data involving ten controlled clinical studies, there was a direct relationship between on-treatment LDL-C and absolute risk of CHD in the primary and secondary prevention settings (O'Keefe et al. 2004). Figure 19.3 shows the relationship between LDL-C and CHD event rates in secondary prevention trials.

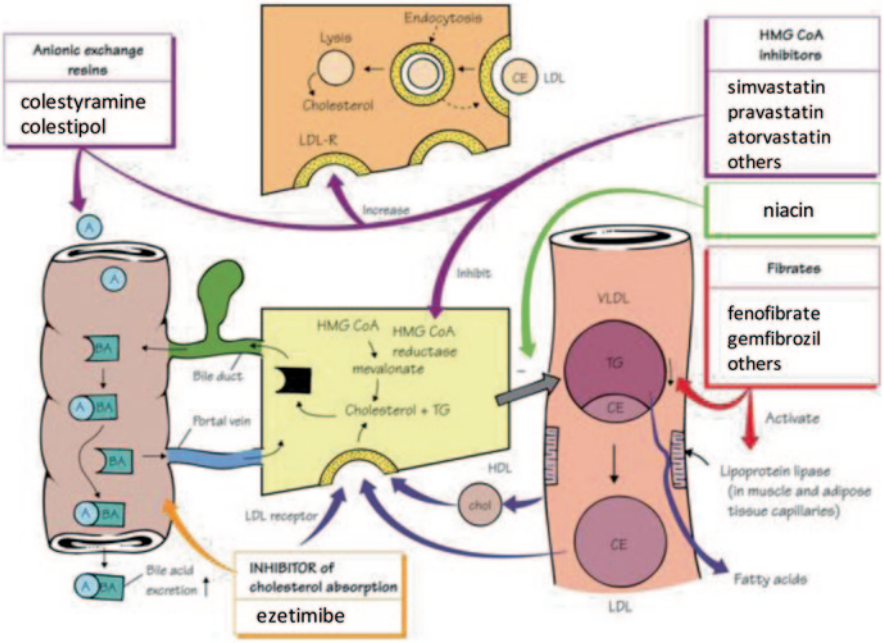

Fig. 19.4 Mechanism of action for hyperlipidemia drugs: anion exchange resins (*A*), bile acids (*BA*), cholesteryl ester (*CE*), high-density lipoprotein (*HDL*), 3-hydroxy-3-methylglutaryl coenzyme A (*HMG CoA*), low-density lipoprotein (*LDL*), LDL-receptor (*LDL-R*), very-low-density lipoprotein (*VLDL*), triglyceride (*TG*). (Reprinted from Neal MJ (2012) Medical pharmacology at a glance, 7th edn, with permission from John Wiley and Sons)

Another large-scale meta-analysis provides additional support for the linkage between LDL-C and CHD risk reduction (CTT Collaboration 2010). In a meta-analysis of individual data involving 170,000 patients participating in controlled clinical studies, relative risk reduction was calculated from studies investigating either high- versus low-dose statin or statin versus placebo. The key findings from the analysis indicated that a reduction in LDL-C of 38.6 mg/dL (or 1 mmol/L) reduced CHD risk by ~20 % for both high versus low statin and statin versus placebo trials. The authors conclude that the primary goal for patients at risk of CHD should be to achieve the largest LDL-C reduction possible.

19.4 Mechanisms of Action of Hyperlipidemia Therapies

A number of therapeutic options exist for the treatment of hyperlipidemia. All of the therapies lower cholesterol but have differential effects on lipoprotein pathways. Therapies with different mechanisms of action are often combined to achieve clinical goals. Individual classes of hyperlipidemia treatments are discussed below. Figure 19.4 highlights the mechanism of action of hyperlipidemia treatments.

Statins (including generic names of lovastatin, rosuvastatin, atorvastatin, simvastatin, pravastatin, pitavastatin, fluvastatin) inhibit 3-hydroxy-3-methylglutaryl coenzyme A (HMG-CoA) reductase. Their role in lowering LDL-C involves inhibition of HMG-CoA reductase, preventing the conversion of HMG-CoA to mevalonic acid (MVA), and further subsequent reactions involved in LDL-C synthesis in hepatocytes of the liver (Istvan and Deisenhofer 2001). Statin treatment also induces decreases in intracellular cholesterol and increased cell-surface expression of LDLR (Goldstein and Brown 2009).

Ezetimibe (Zetia) limits the absorption of dietary cholesterol across the intestine into circulation (Merck, Zetia highlights of Prescribing Information 2013; Sweeney and Johnson 2007; Van Heek et al. 2000). Limiting dietary cholesterol results in a reduced production of VLDL and LDL-C. Ezetimibe is also available in a combination product known as Vytorin (simvastatin/ezetimibe).

Fibrates are a class of drugs (such as fenofibrate, gemfibrozil, fenofibric acid, and others) that work via oxidation of fatty acids resulting in multiple pharmacological effects reducing triglycerides and LDL-C in circulation. In the nuclei of liver hepatocytes, fibrates interact with the peroxisome proliferator-activated receptor alpha (PPAR-α), a nuclear transcription factor, and induce lipoprotein lipolysis, removal of LDL-C by altering affinity for LDL-C receptor, and increasing HDL-C production (Staels et al. 1998; Caslake et al. 1993).

Niacin also works to increase HDL-C, however, the mechanism by which niacin alters lipid profiles has not been well defined (AbbVie, Niaspan Highlights of Prescribing Information 2013). The mechanism may involve several actions including partial inhibition of release of free fatty acids from adipose tissue, and increased LPL activity, which may increase the rate of chylomicron triglyceride removal from plasma. Niacin decreases the rate of hepatic synthesis of VLDL and LDL, and does not appear to affect fecal excretion of fats, sterols, or bile acids. The benefit of niacin therapy on cardiovascular risk is unclear in the current era of statins and ezetimibe as approved therapies. Investigation of niacin, prior to the availability of statins, did demonstrate a benefit (Canner et al. 1986). However, a 2011 study conducted by the NHLBI investigating adding high-dose, extended-release niacin to statin treatment was ended early. Results showed the combination treatment did not reduce the risk of cardiovascular events, including heart attacks and stroke (NHLBI 2011). Most recently, niacin failed to show an additional benefit when added to simvastatin (Merck press release 2012).

Omega-3-acid ethyl esters are also prescribed as treatment for lowering LDL-C and triglycerides. The mechanism of action of omega-3-acid ethyl esters is not well understood (Glaxo Smith Kline, Lovaza Highlights of Prescribing Information 2013). Potential mechanisms may include inhibition of acyl-CoA:1,2-diacylglycerol acyltransferase, increased mitochondrial and peroxisomal β-oxidation in the liver, decreased lipogenesis in the liver, or increased plasma LPL activity. Omega-3-acid ethyl esters also may reduce the synthesis of triglycerides in the liver.

Mipomersen (Kynamro™) is an antisense oligonucleotide inhibitor of apolipoprotein B-100 (apo B100) ribonucleic acid synthesis inhibiting apo B100 protein synthesis (Isis, Kynamro™ Highlights of Prescribing Information 2013). Reduced

protein synthesis of apo B100 results in reduced production of VLDL, LDL, and cholesterol.

Lomitapide (Juxtapid™) directly binds and inhibits microsomal triglyceride transfer protein (MTP), which resides in the lumen of the endoplasmic reticulum, thereby preventing the assembly of apo B100-containing lipoproteins in enterocytes and hepatocytes. This action inhibits the synthesis of chylomicrons and VLDL leading to reduced levels of LDL-C in circulation (Aegerion, Juxtapid Highlights of Prescribing Information 2013).

Inhibitors of CETP are being investigated for the treatment of dyslipidemia. As CETP is involved in the exchange of cholesteryl esters from HDL-C to VLDL, inhibition of CETP increases HDL-C, and may variably reduce LDL-C (Barter and Rye 2012). Preclinical efficacy studies have demonstrated that a CETP inhibitor can inhibit the progression of atherosclerosis in rabbits (Okamoto et al. 2000). This is a challenging area of investigation as two development programs have been halted due to safety outcomes or lack of efficacy (Barter and Rye 2012). Programs for at least two molecules (evacetrapib and anacetrapib) are still ongoing at this time (Nicholls et al. 2011; Bloomfield et al. 2009).

Mutations in the gene for proprotein convertase subtilisin/kexin type 9 (PCSK9) were identified as the third locus of autosomal dominant hypercholesterolemia (Abifadel et al. 2003), and inhibitors of PCSK9 are being investigated for the treatment of hyperlipidemia. PCSK9 is involved in the regulation of LDLR (Derek et al. 2007; Lambert et al. 2009). Preclinical efficacy studies have demonstrated that a PCSK9 inhibitor lowers LDL-C up to 70–80 % (Chan et al. 2009; Liang et al. 2011). Clinical studies have confirmed the effect of PCSK9 inhibition on the lowering of circulating LDL-C (Dias et al. 2012; Giugliano et al. 2012; Stein et al. 2012; Koren et al. 2012).

19.5 Drug Effect Models

19.5.1 Overview

Several types of pharmacometric analysis have been undertaken to describe the effects of hyperlipidemia drugs. In general, LDL-C has been the primary focus of these analyses, though recent examples have included MVA and HDL. A summary of drug effect models describing LDL-C is shown in Table 19.2. Models have been developed for HMG-CoA reductase inhibitors, CETP inhibitors, ezetimibe, gemcabene, and methylprednisolone. An I_{max} model was developed to characterize the steady-state drug effects. In addition, a semi-mechanistic PK/PD model was developed to capture dose response and time course of LDL-C. Models have employed dose or concentration to predict LDL-C response to treatment.

One challenge in the application of pharmacometrics in this area was the lack of a clear exposure–response relationship for statins. For example, it was reported that dose was a better predictor of LDL-C reduction than exposure (as measured

Table 19.2 Summary of drug effect models to describe LDL-C

Mechanism of action	Drug	Model	Predictor variable	Reference
HMG-CoA reductase inhibitors (Statins)	Atorvastatin, simvastatin, fluvastatin	Indirect response	Dose	Faltaos et al. 2006
	Rosuvastatin[a]	Indirect response	Concentration	Aoyama et al. 2010
	Simvastatin	Indirect response	Concentration (simvastatin acid)	Kim et al. 2011
	Rosuvastatin	I_{max}	Dose	Yang et al. 2011
	Atorvastatin	Indirect response	Dose	Oh et al. 2012
CETP inhibition	Anacetrapib[b]	I_{max}	Concentration	Krishna et al. 2011
Multiple mechanisms	Ezetimibe (cholesterol absorption inhib), gemcabene (novel mechanism), Atorvastatin (HMG-CoA)	I_{max}	Dose	Mandema et al. 2005
Glucocorticoid receptor agonist	Methylprednisolone	Indirect response	LDL receptor mRNA	Hazra et al. 2008

[a] PK/PD model was developed to predict mevalonic acid
[b] PK/PD model was developed to predict LDL-C and HDL

by C_{max} and AUC) after 2 weeks of atorvastatin treatment (Cilla et al. 1996). Challenges exist to measure active drug species which can be confounded by active metabolites and active uptake/efflux transport. However, LDL-C can be accurately measured after collection of blood samples and serves as a surrogate of efficacy. Thus, dose–response relationships can adequately characterize the drug effect after statin treatment. In addition, doses of statins can be titrated after approximately 2 weeks of treatment to optimize LDL-C reduction and minimize side effects.

19.5.2 I_{max} Models

The time course of pharmacodynamic effects can be viewed as either direct or indirect. For direct PK/PD relationships, concentrations are correlated with effects in a reversible manner with the peak pharmacodynamic effect observed at the same time as peak drug concentrations. The sigmoid I_{max} model (Hill Equation) is based on the receptor occupancy theory and used to describe the nonlinear concentration–effect relationship as shown below in Eq. 19.1:

$$E = \frac{I_{max} \cdot C^n}{IC_{50}{}^n + C^n}, \tag{19.1}$$

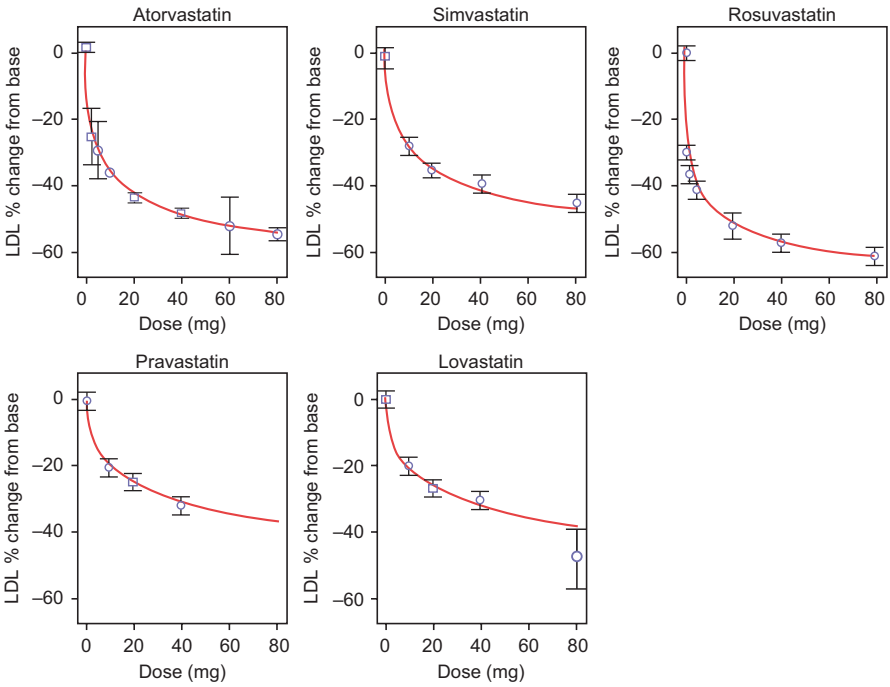

Fig. 19.5 Dose–response relationship for statins as monotherapy treatment. The *solid red line* represents the model-predicted LDL-C reduction expressed as % change from baseline in LDL-C. *Symbols* and *bars* represent the observed mean and 95% confidence interval. (With kind permission from Springer Science + Business Media: Mandema et al (2005) AAPS J 7(3):E513–522; Fig. 19.1)

where the effect of the drug (E) can be described by some maximal inhibitory effect (I_{max}) and the concentration associated with half of the maximal inhibitory effect (IC_{50}). In addition, dose–response analysis can be performed and the dose associated with the half-maximal inhibitory effect (ID_{50}) can be estimated. The Hill slope coefficient (n) increases or decreases the steepness of the concentration–effect relationship depending on whether the value of n is greater or less than 1, respectively. Alternatively, for drugs that increase the response, an alternate model can be selected with an E_{max}, EC_{50}, and n parameters in the form of Eq. 19.1.

The sigmoid I_{max} model was applied to describe the dose–response relationship of statins to facilitate drug development of gemcabene, a new chemical entity for the treatment of hypercholesterolemia (Mandema et al. 2005). The objective of the analysis was to use model-based meta-analysis to guide decision making for gemcabene, using a model of statin, ezetimibe, and gemcabene alone or in combination. Trial level data was obtained from 21 randomized clinical trials involving atorvastatin, rosuvastatin, simvastatin, lovastatin, pravastatin, and ezetimibe following multiple-dose treatment for at least 4 weeks as monotherapy. The statins shared a common I_{max} and n, and unique ED_{50} values were estimated for each drug. LDL-C

Table 19.3 Summary of PK/PD parameters (±95% confidence intervals) from I_{max} models of LDL-C response

Drug	E_0 (%)	I_{max} (%)	ID_{50} (mg)	*n*	Reference
Atorvastatin	0.802 (0.0598, 1.54)	−78.7 (−90.7, −66.7)	13.1 (6.57, 26.2)	0.451 (0.366, 0.557)	Mandema et al. 2005
Rosuvastatin			4.35 (2.19, 8.62)		
Simvastatin			30.5 (15–62.1)		
Lovastatin			82.8 (37.1–185)		
Pravastatin			97.3 (42.4, 223)		
Ezetimibe		−19.6 (−20.6, −18.6)	0.302 (0.151, 0.604)	1	Mandema et al. 2005
Rosuvastatin	0.802 (fixed)[a]	−57.0 (−61.3, −52.7)	1.74 (1.00, 2.48)	1 (fixed)	Yang et al. 2011
Anacetrapib[b]	107 (3)[c] 140(1)[d]	−80 (4)	237(25)[e]	1 (fixed)	Krishna et al. 2011

[a] Fixed value from Mandema et al. (2005)
[b] Parameter estimate (±SE)
[c] Baseline in mg/dL for healthy volunteers
[d] Baseline in mg/dL for patients
[e] IC_{50} in ng/mL

values were expressed as percentage change from baseline. Figure 19.5 shows the dose–response relationship for statins, and Table 19.3 gives a summary of the parameter estimates.

The sigmoid I_{max} model effectively described the shape of the dose–response curve for each statin. The mean response after placebo was 0.802% change from baseline indicating a small placebo response relative to the effect of statins. An estimated mean I_{max} of −78.7% change from baseline and *n* of 0.451 was observed, which is consistent with the common pharmacological mechanism of action for statins. The statin ID_{50} values varied from 4.35 to 97.3 mg reflecting in vivo potency for each statin. In addition, the I_{max}, ID_{50}, and *n* for ezetimibe and gemcabene as monotherapy were characterized.

Because gemcabene was under development for use in combination with statins, the pharmacodynamic interaction was investigated for comparison to ezetimibe, an approved therapy for use in combination with statins. The pharmacodynamic interaction model included the effect of placebo, dose response for statin or non-statin, and an interaction term to characterize the nature of the pharmacodynamic interaction. The interaction term between statin and ezetimibe was estimated to be 1, which indicated pharmacological independence. In contrast, the interaction term between statin and gemcabene was 1.69 which indicated a less than independent interaction. Moreover, limited additional LDL-C reduction was predicted when adding gemcabene to the highest doses of statins. The model-based meta-analysis supported the decision to discontinue the development of gemcabene preventing costly additional clinical studies.

Differences in the response to rosuvastatin in Western and Asian hypercholesterolemia patients were examined using a sigmoid I_{max} model (Yang et al. 2011). Trial-level data from 14 dose-ranging, and 22 one-dose trials with rosuvastatin were combined for model-based meta-analysis. The placebo response was fixed at 0.802 % change from baseline based on Mandema et al. The mean I_{max} and ID_{50} were estimated at −57 % change from baseline and 1.74 mg/day, respectively. Asian patients had a mean ID_{50} value that was approximately half (0.564) of the Western patient population estimate. The analysis supports the current dosing recommendation of 5–20 mg in Asian and 10–40 mg in Western populations which was based on bridging pharmacokinetic exposure across populations. It was reported that Asian patients have a lower oral clearance of rosuvastatin compared to Western patients (Lee et al. 2005). The resulting higher exposures may explain the lower ID_{50} in Asian populations. Results from the I_{max} model indicate that race differences in rosuvastatin pharmacodynamics were consistent with the pharmacokinetic differences, suggesting that the underlying PK/PD relationship is consistent for Asian and Western populations. A trend towards higher approved maximal doses for cardiovascular drugs has been observed for Westerners relative to Japanese and Asians in general (Liao 2007; Arnold et al. 2010).

Recently, the I_{max} model was applied to describe the effects of anacetrapib, a CETP inhibitor (Krishna et al. 2011). Because anacetrapib may be used in combination with statins, the pharmacodynamic interaction between anacetrapib and atorvastatin was characterized. Individual subject level data was obtained from phase 1 and phase 2b studies. Trough anacetrapib concentrations were found to be most predictive of HDL and LDL-C response. The effect of anacetrapib was modeled as proportional to the baseline of LDL-C. Mean baseline LDL-C values of 107 and 140 mg/dL were estimated for healthy subjects and patients, respectively, with 24 % intersubject variability in the baseline. The I_{max} and IC_{50} were −78 % and 240 ng/mL, respectively, for anacetrapib as monotherapy. Treatment with atorvastatin (20 mg/day) lowered LDL-C values by −44.5 %. The pharmacodynamic interaction term for anacetrapib and atorvastatin was estimated to be 0.99 which indicated pharmacological independence. A similar approach was applied to define the trough exposure-response for HDL. Simulations were performed using the model to predict the effect of food, patient status, and dose on LDL-C decrease and HDL increase. The I_{max} model effectively characterized the trough exposure–response relationship and provided quantitative support for phase 3 dose selection.

19.5.3 Indirect Response Models

The indirect response model has been used extensively to characterize drug effects for drugs which act on turnover processes such as production or elimination (Dayneka et al. 1993; Sharma and Jusko 1996; Mager et al. 2003). The indirect response model will describe a time delay between peak plasma concentrations and the maximal response which can be useful to help define the onset and offset of pharmacological effects. Figure 19.6 shows the compartmental model structure for the indirect response model.

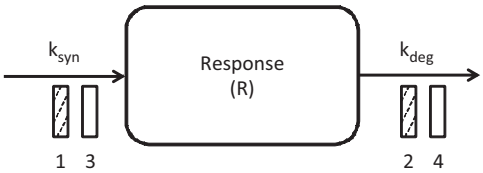

Fig. 19.6 Compartmental model structure for the indirect response model. Inhibitory effects are represented by the *shaded bar* such that models 1 and 2 represent inhibition of production rate constant (k_{syn}) or elimination rate constant (k_{deg}), respectively. Stimulatory effects are represented by the *open bar* such that models 3 and 4 represent stimulation of k_{syn} or k_{deg}, respectively

The general equation for the indirect response model is shown in Eq. 19.2:

$$\frac{dR}{dt} = k_{syn} - k_{deg} \cdot R, \tag{19.2}$$

where R is the response, k_{syn} is the zero-order synthesis rate, and k_{deg} is the first-order degradation rate. A family of four indirect effect models has been applied. Drug effects can include (1) inhibition of input, (2) inhibition of output, (3) stimulation of input, and (4) stimulation of output, where model selection is based on an understanding of the mechanism of drug action. Models 1 and 4 have been most commonly used to describe the time course of effect on LDL-C by statins.

The indirect response model was applied to characterize the hyperlipidemic effects of corticosteroids after single-dose administration in normal male Wistar rats (Hazra et al. 2008). Corticosteroids induce effects through binding to glucocorticoid receptors. Through a cascade of events, the glucocorticoid receptors modulate the expression of LDL receptors in the liver. As noted in Sect. 19.2.2, hepatocyte LDL receptors are the predominant elimination mechanism for LDL-C in humans and preclinical species, accounting for 50–80 % of the elimination of LDL-C in preclinical species (Bilheimer 1984). The authors proposed a mechanistic model where reduction in messenger RNA (mRNA) levels of the LDL receptor reduces the k_{deg} of LDL-C under the assumption that LDL receptor mRNA levels are correlated with the activity of LDL receptor. The model described the time course of LDL-C elevations after a single dose of 50 mg/kg methylprednisolone by intramuscular injection. The initial value of LDL-C was 35.8 mg/dL, and k_{deg} was 0.51 h^{-1}. The mechanistic model successfully described the time delay between methylprednisolone concentrations (t_{max} of ~1 h) and peak LDL-C response (t_{max} of ~18 h) after administration of methylprednisolone in rats giving biological insights into corticosteroid-induced hyperlipidemia.

The indirect response modeling approach was applied to simvastatin to characterize the dose–response relationship of LDL-C reduction in Koreans (Kim et al. 2011). Healthy volunteers recruited to participate in a drug–drug interaction study received simvastatin 40 mg daily for 14 days. Intensive PK measurements were obtained for simvastatin and simvastatin acid on days 1, 7, and 14, with trough measurements on days 5, 6, 12, and 13. A two-compartment model with first-order

Table 19.4 Summary of PK/PD parameters (±95% confidence intervals) from basic and precursor-pool indirect response models of LDL-C

Drug	INH	ID_{50} (mg)	k_{in} (g/L/day)	k_{out} (1/day)	BSV k_{in}	BSV ID_{50}	Reference
Atorvastatin	0.21 (0.19–0.28)	26 (19–66)	0.14 (0.10–0.24)	NR	72	160	Faltaos et al. 2006
Simvastatin		1.3 (1.0–3.7)					
Fluvastatin		15 (9–34)					
Simvastatin	NE	0.0868[a] (0.000150–0.396)	0.274 (0.208–0.346)	0.297	50.2	93.2	Kim et al. 2011
Atorvastatin	0.09	11.9 (3.8–31.8), patients 2.0 (0.2–5.9) healthy	0.15 (0.12–0.20)	0.105 (0.08–0.144)	1.6	98	Oh et al. 2012

NR not reported, *BSV* between subject variability (%)
[a] IC_{50} in ng/mL

absorption described the pharmacokinetics of simvastatin with 70% of the dose eliminated as simvastatin (central compartment), and 30% of the dose eliminated as simvastatin acid (represented as a peripheral compartment). Simvastatin acid was the active pharmacological species that inhibited k_{syn} of LDL-C in the PK/PD model. Table 19.4 gives a summary of the PK/PD parameter estimates. The system parameters baseline LDL-C and k_{syn} were 92 mg/dL and 0.274 g/L x day, respectively. Simvastatin acid had an I_{max} and IC_{50} of 0.489 and 0.0868 ng/mL, respectively. Intersubject variability was greatest for the IC_{50} with 93.2% CV, and less for I_{max}, k_{syn}, and baseline LDL-C at 15.7, 50.2, and 20.5% CV, respectively. The authors noted that the IC_{50} and intersubject variability in IC_{50} may have been poorly estimated because simvastatin acid concentrations were much higher than the IC_{50} for the 40 mg dose. A visual predictive check of concentration and LDL-C indicated that the model fit the data well and explained the observed variability, as shown in Fig. 19.7.

Simulations were performed using the PK/PD model to compare the predicted dose–response relationship with observed dose–response data. To determine if the concentration–response model could predict the effect of simvastatin on LDL-C in patients, the authors overlayed the model-predicted dose–response relationship with available data from a meta-analysis and the Zocor label. This analysis demonstrated the successful prediction of steady-state LDL-C response in patients from healthy subjects using population PK/PD modeling. Overall, the indirect response model successfully described the dose–response relationship for simvastatin in Korean patients.

The indirect response model proposed by Kim et al. was used as the basis investigating LDL-C reductions after morning or evening administration of simvastatin

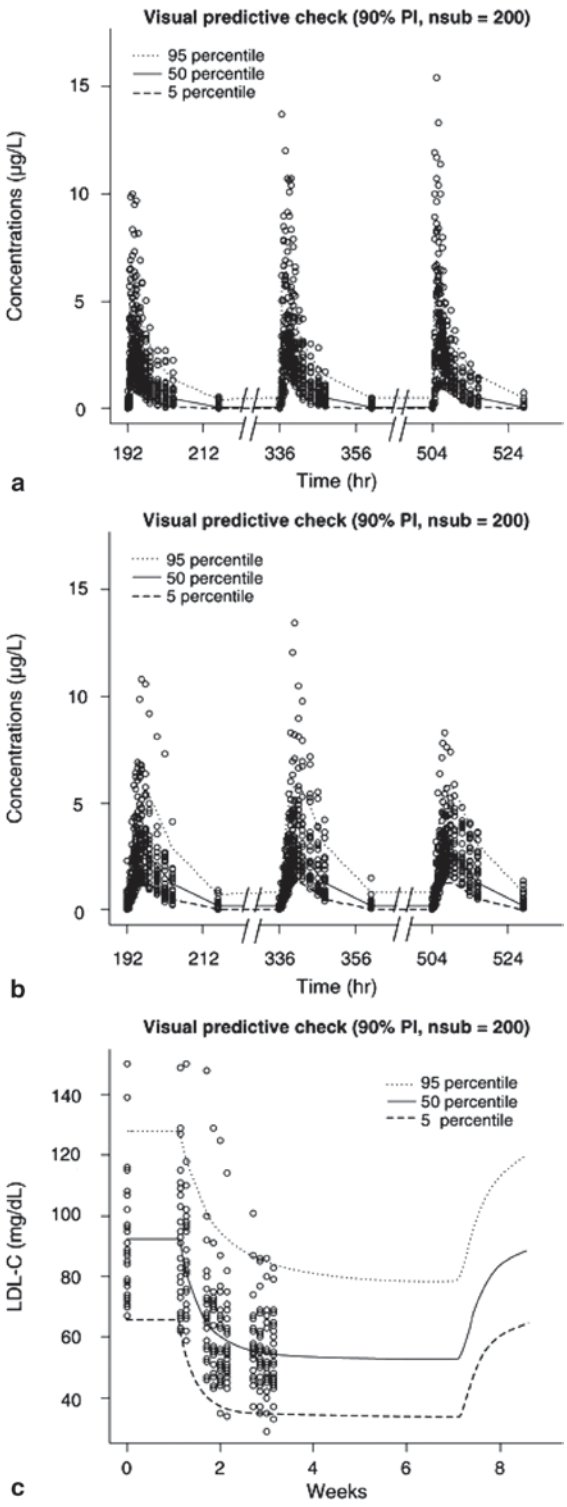

Fig. 19.7 Application of the indirect response model to LDL-C turnover after administration of simvastatin 40 mg/day for 14 days in healthy, Korean subjects. (Reprinted from Kim et al. 2011, with permission from John Wiley and Sons and © 2011 The Authors Basic & Clinical Pharmacology & Toxicology © 2011 Nordic Pharmacological Society)

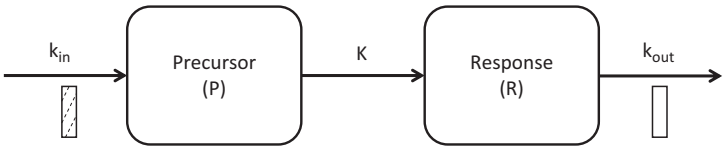

Fig. 19.8 Precursor pool indirect response model. Inhibitory effects are represented by the *shaded bar*. Stimulatory effects are represented by the *open bar*. k_{in} production rate constant, K transfer rate constant, k_{out} elimination rate constant

in a simulation study (Wright et al. 2011). It has been reported that the effects of statins are more prominent after administration in the evening, but are also associated with a 5–25% reduction in compliance relative to morning administration (Vrijens et al. 2008). The authors modified the indirect response model to include a circadian production of LDL-C, and performed simulations to compare the impact of morning versus evening administration for 10, 20, 40, and 80 mg/day simvastatin. In addition, the effect of 10% noncompliance was considered for subjects receiving the evening dose. The difference in LDL-C reduction for morning, evening, and evening with 10% noncompliance was 30.6, 33.0, and 31.6%, respectively, after 10 mg/day simvastatin. The model predictions suggested a relatively small advantage for evening administration that could be almost completely eliminated by noncompliance.

The indirect response model has been used to characterize the inhibitory effects of rosuvastatin on MVA (Aoyama et al. 2010). HMG-CoA reductase converts HMG-CoA to MVA as the rate-limiting step in de novo cholesterol biosynthesis. The data source for the modeling was based on a previously published report of the administration of 10 mg/day rosuvastatin to 24 subjects in a two-way crossover study comparing the effects of morning versus evening administration (Martin et al. 2002). The indirect response model was modified to account for the circadian production of MVA throughout the course of a day. A 7.7% reduction in the area under the effect curve over 24 h was reported for MVA for morning administration relative to evening administration. The extended indirect response model successfully described the circadian fluctuations in MVA and effects of rosuvastin after morning or evening administration. The implications of the findings with MVA on steady-state LDL-C are not entirely clear as the link between MVA and LDL-C has not been defined.

19.5.4 Precursor Pool Indirect Response Model

A modified version of the indirect response model which we refer to as the precursor pool indirect response model was proposed to describe the LDL-C reduction after multiple dose administration of atorvastatin, simvastatin, and fluvastatin in hypercholesterolemia patients (Faltaos et al. 2006). The model included a precursor compartment which represented the production of LDL-C in hepatocytes, and a response compartment which represented circulating LDL-C pool as shown in Fig. 19.8.

Distinct from the precursor-dependent indirect response model which describes tolerance and rebound phenomena (Sharma et al. 1998), the precursor pool indirect response model in this case was developed based on the known pharmacological mechanism of statins (described in Sect. 19.6.3). The general equation for the precursor pool indirect response model is shown below in Eqs. 19.3 and 19.4:

$$\frac{dP}{dt} = k_{in} \cdot (1 - INH) - K \cdot P \tag{19.3}$$

$$\frac{dR}{dt} = K \cdot P - (1 + STIM) \cdot k_{out} \cdot R, \tag{19.4}$$

where P is the precursor compartment, R is the response compartment, k_{in} is the zero-order synthesis rate, K is the transfer rate from precursor to response compartment, and k_{out} is the first-order elimination rate. INH and STIM represent the drug effects of statins, namely inhibition of synthesis and stimulation of elimination, respectively. Pharmacokinetic data were not available from the study, so the effect of each statin on k_{out} was proposed to be dose-dependent in the form of an E_{max} model while the INH function was independent of dose and/or statin. One of the limitations of the precursor pool indirect response model was reported (Kim et al. 2011), where the authors found that the model was overparameterized when applied to simvastatin data from healthy Korean subjects.

The precursor pool indirect response model was applied to describe the effect of atorvastatin, simvastatin, and fluvastatin on LDL-C in hypercholesterolemic patients (Faltaos et al. 2006). LDL-C observations ($n = 309$) were collected from 100 patients after daily administration of atorvastatin (10–40 mg/day), simvastatin (10–80 mg/day), and fluvastatin (10–80 mg/day) at different times (ranging from 14 to 150 days). Table 19.4 gives a summary of the PK/PD parameter estimates. The model described the data adequately, and suggested a k_{in} value of 0.14 g/L/day that was inhibited by 21 % by statin treatment. The potency of simvastatin, fluvastatin, and atorvastatin as measured by the ED_{50} for stimulating k_{out} was 1.3, 15, and 26 mg/day, respectively. Extensive intersubject variability in k_{in} and ED_{50} were reported (72 and 160 %, respectively). The model was one of the first examples to describe the time course of LDL-C reduction, and could be a useful platform for the design of clinical studies. Unfortunately, the authors did not provide an estimate for K or k_{out} in the publication, limiting the general application of the model by other scientists.

The precursor pool indirect response model was subsequently utilized to describe the PK/PD relationship of atorvastatin to gain insights into the dose–response relationship in Korean dyslipidemic patients and nonpatient volunteers (Oh et al. 2012). The study included 15 dyslipidemic patients that participated in a two-step dose escalation trial where the dose of atorvastatin was initiated at either 10 or 20 mg/day and escalated to 40 or 80 mg/day after 21 days of dosing. In addition, 11

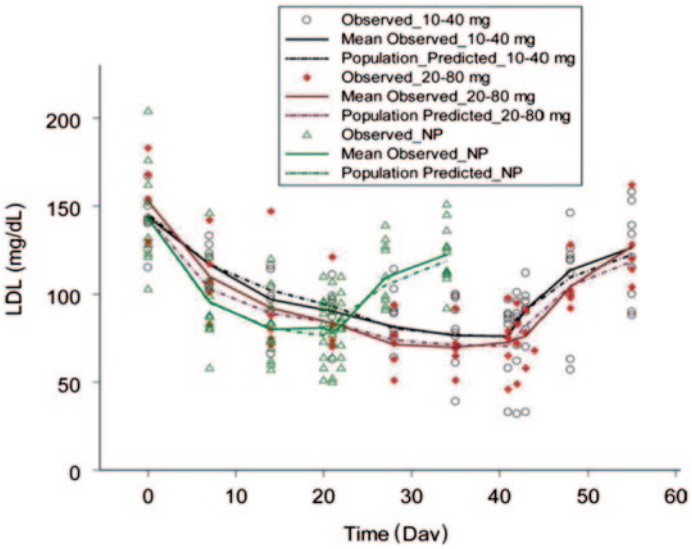

Fig. 19.9 Application of the precursor pool indirect response model to LDL-C turnover after administration of atorvastatin in Korean dyslipidemic patients and nonpatient (*NP*) volunteers. (Reprinted from Oh et al. 2012, with permission from Dustri-Verlag and © 2012 Dustri-Verlag and Dr. K Feistle)

healthy subjects were included in the study and received 10 mg/day atorvastatin for 21 days. Blood samples were collected to measure lipids for 56 days. Figure 19.9 shows the predicted and observed LDL-C reduction after administration of atorvastatin to Korean patients and healthy subjects.

Based on the analysis, the k_{in} for LDL-C was 0.15 g/L/day in the Korean subjects with a low intersubject variability of 13%. The elimination rate constant for LDL-C was 0.105 day^{-1} which suggested a half-life of 6.6 days. Atorvastatin inhibited k_{in} by 9% which was slightly less than the 21% reported by Faltaos et al. The ID_{50} in patients and healthy subjects were 11.9 and 2.0, respectively, which suggested that healthy subjects might be more sensitive to the effects of atorvastatin. However, due to the imprecision of the ID_{50} estimates, there was an overlap in the 95% confidence intervals of the ID_{50} estimates. Extensive intersubject variability in the ID_{50} of atorvastin (99% CV) was reported. The implications of a sixfold difference between patients and healthy subjects were not discussed by the authors. Because dose was the predictor of pharmacodynamic response, pharmacokinetic differences between healthy subjects and patients were not investigated. The atorvastatin ID_{50} value from Oh et al. was in close agreement to the value reported by Mandema et al. (11.9 vs. 13 mg/day atorvastatin, respectively). Application of the precursor pool indirect response model enabled the characterization of atorvastatin dose–response relationship in Korean patients and healthy subjects. The model could be used to help optimize drug therapy in dyslipidemic patients.

19.5.5 Other Applications

Examples of other applications of pharmacometrics that are not solely focused on drug effects are presented. A systems biology approach was applied to characterize the impacts of aging on LDL-C (McAuley et al. 2012). The model captured the known physiology of cholesterol metabolism, and included six compartments to describe intake, intestinal absorption, excretion, plasma, hepatic, and peripheral tissues. The influence of changes in cholesterol absorption and elimination by LDL receptors was simulated to give insights into their respective importance in cholesterol balance. Based on the simulations, a 50% reduction in hepatic clearance of LDL-C can result in a 116 mg/dL increase in plasma LDL-C. Also, increasing the bioavailability of cholesterol from 50 to 80% can increase plasma LDL-C by 34 mg/dL. The findings from a systems biology model give insights into the fundamental biology of lipoproteins, and suggest that plasma LDL-C levels were most sensitive to changes in the rate of hepatic elimination.

There may be an opportunity for pharmacometrics to guide dosing decisions in order to optimize the risk to benefit ratio of hyperlipidemia treatments. Use of high-dose simvastatin (80 mg) has been associated with an increased risk of myopathies and in rare cases rhabdomyolysis compared to lower doses (Egan and Colman 2011). In addition, the risk of myopathies can be increased with drug interactions such as coadministration of CYP3A inhibitor and/or OATP1B1 inhibitor (Neuvonen et al. 2006). Additional concentration-safety analysis may support ongoing efforts to identify intermittent dosing strategies that maintain benefit and reduce risk of myopathy with statin treatment (Keating et al. 2013).

In the area of cardiovascular disease progression, the focus of research has been on defining short-term risk estimates of cardiovascular events to define treatment algorithms (NHLBI 2004). More recently, the question of duration of LDL-C exposure as it pertains to cardiovascular risk has been raised, where it was noted that longer treatment with statins was associated with reduced risk of CHD (Brown and Goldstein 2006). In addition, it was proposed that the cumulative exposure to LDL-C may serve as surrogate of lifetime cardiovascular risk based on outcomes from human genetic observational studies (Horton et al. 2009). In the future, a pharmacometric disease progression model may serve to unify the effect of LDL-C reduction on cardiovascular risk reduction.

19.6 Summary and Conclusions

Cardiovascular disease produces significant worldwide morbidity and mortality. Lipoproteins represent a major risk factor for cardiovascular disease. Therefore, treatment of lipoproteins is important to the goal of reducing cardiovascular risk given its relationship to arteriosclerosis. PK/PD models have been used to characterize the effect on LDL-C for a wide variety of drugs including statins, CETP inhibitors, and ezetimibe. Both empirical and semi-mechanistic models have been

used to characterize dose response and the time course of effects of hyperlipidemia therapies. The application of pharmacometrics has been shown to effectively guide drug development decision making by accurately simulating trials, optimizing dosing regimens, and informing early termination of programs with unacceptable risk to benefit ratios. In conclusion, pharmacometrics will continue to be an important tool to facilitate the development of new drug therapies to alleviate the burden of cardiovascular disease.

Summary of Key Messages

- PK/PD models have been used to characterize the effect on LDL-C for hyperlipidemia drugs including statins, CETP inhibitors, and ezetimibe.
- Both empirical and semi-mechanistic models have been used to characterize dose response and the time course of effects of hyperlipidemia therapies.
- The application of pharmacometrics in the cardiovascular area has been shown to effectively guide drug development decision making by accurately simulating trials, optimizing dosing regimens, and informing early termination of programs with unacceptable risk/benefit ratios.

References

AbbVie Niaspan highlights of prescribing information (2013) http://www.rxabbvie.com/pdf/niaspan.pdf. Accessed 24 April 2013

Abifadel M, Varret M, Rabès J-P et al (2003) Mutations in PCSK9 cause autosomal dominant hypercholesterolemia. Nat Genet 34:154–156. doi:10.1038/ng1161

Aegerion Juxtapid highlights of prescribing information (2013) http://www.juxtapid.com/_pdf/Prescribing_Information.pdf. Accessed 24 April 2013

Aoyama T, Omori T, Watabe S, Shioya A, Ueno T, Fukuda N, Matsumoto Y (2010) Pharmacokinetic/pharmacodynamic modeling and simulation of rosuvastatin using an extension of the indirect response model by incorporating a circadian rhythm. Biol Pharm Bull 33:1082–1087. doi:10.1248/bpb.33.1082

Arnold FL, Kusama M, Ono S (2010) Exploring differences in drug doses between Japan and Western countries. Clin Pharmacol Ther 87:714–720. doi:10.1038/clpt.2010.31

Barrett R, Hugh P, Foster DM (1996) Design and analysis of lipid tracer kinetic studies. Curr Opin Lipidol 7:143–148

Barter PJ, Rye KA (2012) Cholesteryl ester transfer protein inhibition as a strategy to reduce cardiovascular risk. J Lipid Res 53:1755–1766. doi:10.1194/jlr.R024075

Bilheimer DW (1984) Regulation of LDL receptors *in vivo*. Agents Actions Suppl 16:191–203

Bloomfield D, Carlson GL, Sapre A, Tribble D, McKenney JM, Littlejohn TW, Sisk CM, Mitchel Y, Pasternak RC (2009) Efficacy and safety of the cholesteryl ester transfer protein inhibitor anacetrapib as monotherapy and coadministered with atorvastatin in dyslipidemic patients. Am Heart J 157:352–360. doi:10.1016/j.ahj.2008.09.022

Brown MS, Goldstein JL (2006) Lowering LDL-Not only how low, but how long? Science 311:1721–1723. doi:10.1126/science.1125884

Canner PL, Berge KG, Wenger NK, Stamler J, Friedman L, Prineas RJ, Friedewald W, Coronary Drug Project Research Group (1986) Fifteen year mortality in coronary drug project patients: long-term benefit with niacin. J Am Coll Cardiol 8:1245–1255. doi:10.1016/S0735-1097(86)80293-5

Caslake MJ, Packard CJ, Gaw A, Murray E, Griffin BA, Vallance BD, Shepherd J (1993) Fenofibrate and LDL metabolic heterogeneity in hypercholesterolemia. Arterioscler Thromb 13:702–711. doi:10.1161/01.ATV.13.5.702

Chan JCY, Piper DE, Cao Q, Liu D, King C, Wang W, Tang J, Liu Q, Higbee J, Xia Z, Di Y, Shetterly S, Arimura Z, Salomonis H, Romanow WG, Thibault ST, Zhang R, Cao P, Yang XP, Uy T, Lu M, Retter MW, Kwon G, Henne K, Pan O, Tsai MM, Fuchslocher B, Yang E, Zhou L, Lee KJ, Daris M, Sheng J, Wang Y, Shen WD, Yeh WC, Emery M, Walker NPC, Shan B, Schwarz M, Jackson SM (2009) A proprotein convertase subtilisin/kexin type 9 neutralizing antibody reduces serum cholesterol in mice and nonhuman primates. PNAS 106:9820-9825. doi: 10.1073/pnas.0903849106

Cholesterol Treatment Trialists'(CTT) Collaboration (2010) Efficacy and safety of more intensive lowering of LDL cholesterol: a meta-analysis of data from 170,000 participants in 26 randomised trials. Lancet 376:1670–1681. doi:10.1016/S0140-6736(10)61350-5

Cilla DC, Whitfield LR, Gibson DM, Sedman AJ, Posvar EL (1996) Multiple-dose pharmacokinetics, pharmacodynamics, and safety of atorvastatin, an inhibitor of HMG-CoA reductase, in healthy subjects. Clin Pharmacol Ther 60:687–695. doi:10.1016/S0009-9236(96)90218-0

Dayneka NL, Garg V, Jusko WJ (1993) Comparison of four basic models of indirect pharmacodynamic responses. J Pharmacokinet Pharmacodyn 21:457–478. doi:10.1007/BF01061691

Derek E, Piper DE, Jackson S, Liu Q, Romanow WG, Shetterly S, Thibault ST, Shan B, Walker NPC (2007) The crystal structure of PCSK9:a regulator of plasma LDL-cholesterol. Structure 15:545–552. doi:10.1016/j.str.2007.04.004

Dias CS, Shaywitz AJ, Wasserman SM, Smith BP, Gao B, Stolman DS, Crispino CP, Smirnakis KV, Emery MG, Colbert A, Gibbs JP, Retter MW, Cooke BP, Uy ST, Matson M, Stein EA (2012) Effects of AMG 145 on low-density lipoprotein cholesterol levels: results from 2 randomized, double-blind, placebo-controlled, ascending-dose phase 1 studies in healthy volunteers and hypercholesterolemic subjects on statins. J Am Coll Cardiol 60:1888–1898. doi:10.1016/j.jacc.2012.08.986

Dietschy JM (1997) Theoretical considerations of what regulates low-density-lipoprotein and high-density-lipoprotein cholesterol. Am J Clin Nutr 65(5 Suppl):1581S–1589S

Egan A, Colman E (2011) Weighing the benefits of high-dose simvastatin against risk of myopathy. N Engl J Med 365:285–287. doi:10.1056/NEJMp1106689

European Medicines Agency (2010) Guideline on lipid lowering agents. http://www.ema.europa.eu/docs/en_GB/document_library/Scientific_guideline/2010/12/WC500100189.pdf. Accessed 24 April 2013

Faltaos DW, Urlen S, Carreau V, Chauvenet M, Hulot JS, Giral P, Bruckert E, Lechat P (2006) Use of an indirect effect model to describe the LDL cholesterol-lowering effect by statins in hypercholestrerolaemic patients. Fundam Clin Pharmacol 20:321–330. doi:10.1111/j.1472-8206.2006.00404.x

Giugliano RP, Desai NR, Kohli P et al for the LAPLACE-TIMI 57 investigators (2012) Efficacy, safety, and tolerability of a monoclonal antibody to proprotein convertase subtilisin/kexin type 9 in combination with a statin in patients with hypercholesterolaemia (LAPLACE-TIMI 57): a randomised, placebo-controlled, dose-ranging, phase 2 study. Lancet 380:2007–2017. doi:10.1016/S0140-6736(12)61770-X

Glaxo Smith Kline, Lovaza highlights of prescribing information (2013) http://us.gsk.com/products/assets/us_lovaza.pdf. Accessed 18 Feb 2013

Glomset JA, Wright JL (1964) Some properties of a cholesterol esterifying enzyme in human plasma. Biochim Biophys Acta 89:266–276. doi:10.1016/0926-6569(64)90215-9

Goldstein JL, Brown MS (2009) The LDL receptor. Arterioscler Thromb Vasc Biol 29:431–438. doi:10.1161/ATVBAHA.108.179564

Hazra A, Pyszczynski NA, DuBois DC, Almon RR, Jusko WJ (2008) Modeling of corticosteroid effects on hepatic low-density lipoprotein receptors and plasma lipid dynamics in rats. Pharm Res 25:769–780. doi:10.1007/s11095-007-9371-8

Horton JD, Cohen JC, Hobbs HH (2009) PCSK9: a convertase that coordinates LDL catabolism. J Lipid Res 50:S172–S177. doi:10.1194/jlr.R800091-JLR200

Isis Kynamro™ highlights of prescribing information (2013) http://www.kynamro.com/~/media/Kynamro/Files/KYNAMRO-PI.pdf. Accessed 24 April 2013

Istvan E, Deisenhofer J (2001) Structural mechanism for statin inhibition of HMG-CoA reductase. Science 292:1160–1164. doi:10.1126/science.1059344

Ji J, Watts GF, Johnson AG et al (2006) High-density lipoprotein (HDL) transport in the metabolic syndrome: application of a new model for HDL particle kinetics. J Clin Endocrinol Metab 91:973–979. doi:10.1210/jc.2005-1895

Keating AJ, Bova Campbell K, Guyton JR (2013) Intermittent nondaily dosing strategies in patients with previous statin-induced myopathy. Ann Pharmacother 47:398–404. doi:10.1345/aph.1R509

Kim J, Ahn B-J, Chae H-S, Han S, Doh K, Choi J, Jun YK, Lee YW, Yim D-S (2011) A population pharmacokinetic-pharmacodynamic model for simvastatin that predicts low-density lipoprotein-cholesterol resduction in patients with primary hyperlipidemia. Basic Clin Pharmacol Toxicol 109:156–163. doi:10.1111/j.1742-7843.2011.00700.x

Koren MJ, Scott R, Kim JB, Knusel B, Liu T, Lei L, Bolognese M, Wasserman SM (2012) Efficacy, safety, and tolerability of a monoclonal antibody to proprotein convertase subtilisin/kexin type 9 as monotherapy in patients with hypercholesterolaemia (MENDEL): a randomised, double-blind, placebo-controlled, phase 2 study. Lancet 380:1995–2006. doi:10.1016/S0140-6736(12)61771-1

Krishna R, Bergman AJ, Green M, Dockendorf MF, Wagner JA, Dykstra K (2011) Model-based development of anacetrapib, a novel cholesteryl ester transfer protein inhibitor. AAPS J 13:179–190. doi:10.1208/s12248-011-9254-0

Lambert G, Charlton F, Rye K-A, Piper DE (2009) Molecular basis of pcsk9 function. Atherosclerosis 203:1–7. doi:10.1016/j.atherosclerosis.2008.06.010

Lee E, Ryan S, Birmingham B, Zalikowski J, March R, Ambrose H et al (2005) Rosuvastatin pharmacokinetics and pharmacogenetics in white and asian subjects residing in the same environment. Clin Pharmacol Ther 78:330–341. doi:10.1016/j.clpt.2005.06.013

Liang H, Chaparro-Riggers J, Strop P et al (2011) Proprotein convertase substilisin/kexin type 9 antagonism reduces low-density lipoprotein cholesterol in statin-treated hypercholesterolemic nonhuman primates. J Pharmacol Exp Ther 340:228–236. doi:10.1124/jpet.111.187419

Liao JK (2007) Safety and efficacy of statins in Asians. Am J Cardiol 99:410–414. doi:10.1016/j.amjcard.2006.08.051

Lloyd-Jones DM (2010) Cardiovascular risk prediction: basic concepts, current status, and future directions. Circulation 121:1768–1777. doi:10.1161/Circulationha.109.849166

Mager DE, Wyska E, Jusko WJ (2003) Diversity of mechanism-based pharmacodynamic models. Drug Metab Dispos 31:510–519. doi:10.1124/dmd.31.5.510

Mandema JW, Hermann D, Wang W, Sheiner T, Milad M, Bakker-Arkema R, Hartman D (2005) Model-based development ofgemcabene, a new lipid-altering agent. AAPS J 7:E513–E522. doi:10.1208/aapsj070352

Martin PD, Mitchell PD, Schneck DW (2002) Pharmacodynamic effects and pharmacokinetics of a new HMG-CoA reductase inhibitor, rosuvastatin, after morning or evening administration in healthy volunteers. Br J Clin Pharmacol 54:472–477. doi:10.1046/j.1365-2125.2002.01688.x

McAuley M, Wilkinson DJ, Jones JJL, Kirkwood TBL (2012) A whole-body mathematical model of cholesterol metabolism and its age-related dysfunction. BMC Syst Biol 6:130. doi:10.1186/1752-0509-6-130

Merck press release (December 20, 2012) http://www.mercknewsroom.com/press-release/prescription-medicine-news/merck-announces-hps2-thrive-study-tredaptive-extended-relea. Accessed 24 April 2013

Merck, Zetia highlights of prescribing information. http://www.merck.com/product/usa/pi_circulars/z/zetia/zetia_pi.pdf. Accessed 24 April 2013

National Heart, Lung, and Blood Institute (2004) Third report of the expert panel on detection, evaluation, and treatment of high blood cholesterol in adults (Adult treatment panel III). http://www.nhlbi.nih.gov/guidelines/cholesterol/. Accessed 24 April 2013

National Heart, Lung, and Blood Institute (2011) NIH stops clinical trial on combination cholesterol treatment. http://www.nih.gov/news/health/may2011/nhlbi-26.htm. Accessed 11 March 2013

Neuvonen PJ, Niemi M, Backman JT (2006) Drug interactions with lipid-lowering drugs: mechanisms and clinical relevance. Clin Pharmacol Ther 80(6):565–581. doi:10.1016/j.clpt.2006.09.003

Nicholls SJ, Brewer HB, Kastelein JJP, Krueger KA, Wang MD, Shao M, Hu Bo, McErlean BE, Nissen SE (2011) Effects of the CETP inhibitor evacetrapib administered as monotherapy or in combination with statins on HDL and LDL cholesterol: a randomized controlled trial. JAMA 306:2099–2109. doi:10.1001/jama.2011.1649

Oh ES, Lee S-H, Park MS, Park K, Chung J-Y (2012) Modeling of the LDL cholesterol-lowering effect of atorvastatin in Korean dyslipidemic patients and non-patient volunteers. Int J Clin Pharmacol Ther 50:647–656. doi:10.5414.CP201699

Okamoto H, Yonemori F, Wakitani K, Minowa T, Maeda K, Shinkai H (2000) A cholesteryl ester transfer protein inhibitor attenuates atherosclerosis in rabbits. Nature 406:203–207. doi:10.1038/35018119

O'Keefe JH, Cordain L, Harris WH, Moe RM, Vogel R (2004) Optimal low-density lipoprotein is 50 to 70 mg/dL Lower is better and physiologically normal. J Am Coll Cardiol 43:2142–2146. doi:10.1016/j.jace.2004.03.046

Orso E, Grandl M, Schmitz G (2011) Oxidized LDL-induced endolysosomal phospholipidosis and enzymatically modified LDL-induced foam cell formation determine specific lipid species modulation in human macrophages. Chem Phys Lipids 164:479–487. doi:10.1016/j.chemphyslip.2011.06.001

Repa JJ, Mangelsdorf DJ (2000) The role of orphan nuclear receptors in the regulation of cholesterol homeostasis. Annu Rev Cell Dev Biol 16:459–481. doi:10.1146/annurev.cellbio.16.1.459

Russell DW (2009) Fifty years of advances in bile acid synthesis and metabolism. J Lipid Res 50:S120–S125. doi:10.1194/jlr.R800026-JLR200

Sharma A, Jusko WJ (1996) Characterization of four basic models of indirect pharmacodynamic responses. J Pharmacokinet Biopharm 24:611–635. doi:10.1007/BF02353483

Sharma A, Ebling WF, Jusko WJ (1998) Precursor-dependent indirect pharmacodynamic response model for tolerance and rebound phenomena. J Pharm Sci 87:1577–1584. doi:10.1021/js98017q

Smith SC, Collins A, Ferrari R et al (2012) Our time: a call to save preventable death from cardiovascular disease (heart disease and stroke). J Am Coll Cardiol 60:2343–2348. doi:10.1016/j.jacc2012.08.962

Staels B, Dallongeville J, Auwerx J, Schoonjans K, Leitersdorf E, Fruchart J-C (1998) Mechanism of action of fibrates on lipid and lipoprotein metabolism. Circulation 98:2088–2093. doi:10.1161/01.CIR.98.19.2088

Stein EA, Mellis S, Yancopoulos GD et al (2012) Effect of a monoclonal antibody to PCSK9 on LDL cholesterol. N Engl J Med 366:1108–1118. doi:10.1056/NEJMoa1105803

Sweeney ME, Johnson RJ (2007) Ezetimibe: an update on the mechanism of action, pharmacokinetics and recent clinical trials. Expert Opin Drug Metab Toxicol 3:441–450. doi:10.1517/17425255.3.3.441

van der Wulp MY, Verkade HJ, Groen AK (2012) Regulation of cholesterol homeostasis. Mol Cell Endocrinol 368:1–16. doi:10.1016/j.mce.2012.06.007

Van Heek M, Farley C, Compton DS, Hoos L, Alton KB, Sybertz EJ, Davis HR Jr (2000) Comparison of the activity and disposition of the novel cholesterol absorption inhibitor, SCH58235, and its glucuronide, SCH60663. Br J Pharmacol 129:1748–1754. doi:10.1038/sj.bjp.0703235

Vrijens B, Vincze G, Kristanto P, Urquhart J, Burnier M (2008) Adherence to prescribed antihypertensive drug treatments: longitudinal study of electronically compiled dosing histories. Br Med J 336:1114–1117. doi:10.1136/bmj.39553.670231.25

WHO (World Health Organization), World Heart Federation, and World Stroke Organization (2011) Global atlas on cardiovascular disease prevention and control. http://whqlibdoc.who.int/publications/2011/9789241564373_eng.pdf. Accessed 11 March 2013

Wright DFB, Kumar VVP, Al-Sallami HS, Duffull SB (2011) The influence of dosing time, variable compliance and circadian low-density lipoprotein production on the effect of simvastatin: simulations from a pharmacokinetic–pharmacodynamic model. Basic Clin Pharmacol Toxicol 109:494–498. doi:10.1111/j.1742-7843.2011.00757.x

Yang J, Li LJ, He YC, Sheng YC, Xu L, Huang XH, Guo F, Zheng QS (2011) Race differences: modeling the pharmacodynamics of rosuvastatin in Western and Asian hypercholesterolemia patients. Acta Pharmacol Sin 32:116–125. doi:10.1038/aps.2010.169

Index

S. Schmidt, H. Derendorf (eds.), *Applied Pharmacometrics,* AAPS Advances in the Pharmaceutical Sciences Series 14, DOI 10.1007/978-1-4939-1304-6